Bis(tridentate) Polypyridyl Transition Metal Complexes for DSSC and LEC Applications

Dissertation

zur Erlangung des Grades

„Doktor der Naturwissenschaften"

Im Promotionsfach Chemie

am Fachbereich Chemie, Pharmazie und Geowissenschaften

der Johannes Gutenberg-Universität Mainz

<u>Andreas</u> Karl Christoph Mengel

geboren in Witzenhausen

Mainz, 2017

Die vorliegende Arbeit wurde in der Zeit von Januar 2013 bis Mai 2017 am Institut für Anorganische und Analytische Chemie der Johannes Gutenberg-Universität Mainz unter Anleitung von ████████████ angefertigt.

Hiermit erkläre ich an Eides statt, dass ich die vorliegende Arbeit selbstständig und ohne unerlaubte Hilfsmittel durchgeführt habe.

_____

(Andreas) Karl Christoph Mengel)

Mainz, Mai 2017

Dekanin: ████████████

1. Berichterstatter: ████████████

2. Berichterstatter: ████████████

Tag der mündlichen Prüfung: _____

„Wirkliches Neuland in einer Wissenschaft kann wohl nur gewonnen werden, wenn man an einer entscheidenden Stelle bereit ist, den Grund zu verlassen, auf dem die bisherige Wissenschaft ruht, und gewissermaßen ins Leere zu springen.

- Werner Heisenberg -

Zusammenfassung

Tridentate Polypyridin-Komplexe von Übergangsmetallen bieten eine Vielzahl möglicher Anwendungen in zukunftsweisenden Technologien wie Solarzellen und Emittern. Das vorrangige Ziel, teure und seltene Edelmetalle durch günstiges, in großen Mengen vorhandenes Eisen zu ersetzen, spielt dabei in der aktuellen und zukünftigen Forschung eine große Rolle, weit über den Bereich der Chemie hinaus.

Das Hauptziel dieser Arbeit ist die Darstellung und Charakterisierung von *push-pull* Eisen(II) Komplexen mit Liganden, die sich für den potenziellen Einsatz als Farbstoff-Sensibilisatoren in Solarzellen (DSSC) und als Emitter in lichtemittierenden Zellen (LEC) eignen. Durch ein elektronenreiches R_2tpda-Rückgrat (*N,N'*-Di"R"-*N,N'*-di(pyridin-2-yl)pyridin-2,6-diamin; R = H, Me, *n*Pr, *n*Hex), sowie durch einen stark elektronenziehenden dcpp-Liganden (2,6-Bis(2-carboxypyridyl)pyridin) wird eine Verzerrung der Elektronendichte am Metallzentrum erreicht. Die dabei vorrangigen Schwierigkeiten inerte, stabile Komplexe zu gewinnen, werden vorgestellt, sowie das Erreichen der zur Anwendung wichtigen Eigenschaften einer breiten Absorption im sichtbaren Bereich, eines starken *push-pull* Charakters durch die Liganden und einer starken Ligandenfeldaufspaltung. Es wird gezeigt, dass kleine Änderungen der Substitution am Liganden die Stabilität der Komplexe erheblich beeinflusst. Die Änderung der Elektronendichte am Liganden mittels Deprotonierung verdeutlicht, wie man gezielt Einfluss auf das Ligandenfeld und die bei optischer Anregung stattfindenden eletronischen Übergänge nehmen kann. Die erhöhte Elektronendichte am Donor-Liganden führt zu einem LL'CT- anstatt zu einem MLCT-Übergang. Des Weiteren bietet die einseitige Deprotonierung des Systems einen Weg zur Verringerung der elektronischen Symmetrie, worüber direktionale Übergänge zwischen den Liganden beeinflusst werden können.

Die erwünschten Eigenschaften werden experimentell nachgewiesen und durch dichte-funktional theoretische Methoden bestätigt. Das ferne Ziel einen durch niedrig liegende ^{3}MLCT-Zustände emittierenden Fe(II)-Komplex zu erhalten wird noch nicht erreicht, jedoch wird gezeigt, dass durch das *push-pull*-Konzept und durch einen großen Bisswinkel von 90° der Einfluss auf die Ligandenfeldaufspaltung so groß ist, dass die Energie des ^{5}MC-Zustandes ($^5T_2$, $(t_{2g})^4(e_g^*)^2$) nahe an das Energieniveau des ^{3}MC-Zustands ($^3T_1$, $(t_{2g})^5(e_g^*)^1$) angehoben wird. Dadurch ist man dem ersten Schritt auf dem Weg zu emittierenden Eisenkomplexen, einen ^{3}MLCT als niedrigstergetischsten, metastabilen Zustand nach Anregung vorliegen zu haben, ein ganzes Stück näher gekommen.

Des Weiteren wird ein auf Me$_2$tpda basierender Cobalt-Redoxmediator [Co(Me$_2$tpda)$_2$]$^{2+/3+}$ [Me$_2$tpda= *N,N'*-dimethyl-*N,N'*-di(pyridin-2-yl)pyridin-2,6-diamin] vorgestellt. Dieser wird an kationischen und neutralen tridentaten *push-pull* Ruthenium(II) Sensibilisatoren [Ru(Me$_2$tpda){tpy(COOH)$_3$}]$^{2+}$, (tpy(COOH)$_3$ = 2,2'6,2''-Terpyridin-4,4',4''-tricarbonsäure) in DSSC-Applikationen getestet. Ziel dieser Arbeit ist es mit den neuen Redoxmediator und mit gängigen Systemen wie [Co(bpy)$_3$]$^{2+/3+}$ (bpy= (2,2'-bipyridin) die Leistung der Zellen zu verbessern und I^-/I_3^- zu vergleichen. Dabei werden Additive wie LiClO$_4$, 4-*tert*-Butylpyridin und als Coadsorber Chenodesoxycholsäure verwendet. Der größere Fotostrom und die längere Rekombinationsdauer bei Anwendungen mit dem [Co(ddpd)$_2$]$^{2+/3+}$ Mediator lassen darauf schließen, dass die Elektronenrekombination an der TiO$_2$-Oberfläche durch die höher liegenden π*-Orbitale der Me$_2$tpda Liganden langsamer vonstatten geht, als bei dem [Co(bpy)$_3$]$^{3+}$ mit den bpy Liganden, da bei diesem die π*-Orbitale niedriger liegen. Dadurch erreicht der neue Cobalt-Elektrolyt die beste Leistung in diesen Systemen.

Zuletzt werden cyclometallierte Polypyridin *push-pull* Ruthenium(II)-Komplexe mit unterschiedlichen Donor-Substituenten [Ru(dbp-X)(tctpy)]$^{2-}$ (H$_3$tctpy=2,2';6',2''-Terpyridin-4,4',4''-tricarbonsäure; dpbH=1,3-Dipyridylbenzol; X= *N*(4-C$_6$H$_4$OMe)$_2$, *N*Ph$_2$, *N*-carbazolyl) vorgestellt (aus Arbeiten von Dr. C. Kreitner), deren Leistung in DSSCs mit verschiedenen Redoxmediatoren und Additiven im

Vergleich zum Referenzfarbstoff N719 getestet wurden. Unter Standardbedingungen kann keiner der hergestellten Farbstoffe dieselbe Performance mit I^-/I_3^- Elektrolyten wie N719 erreichen. Allerdings liefert der carbazolyl-substituierte Farbstoff bei verringerter Konzentration des I^-/I_3^- Elektrolyten vergleichbare Effizienzen wie der Standard-Farbstoff N719. In Gegenwart von Cobalt Elektrolyten sinken alle Effizienzen, wobei der carbazolyl-substituierte Farbstoff sogar bessere Ergebnisse als N719 erzielt.

Abstract

Tridentate polypyridine complexes of transition metals represent a wide range of applications in future-oriented technologies such as solar cells and emitters. The primary goal of replacing expensive and rare precious metals with inexpensive, naturally abundant iron, plays an important role in current and future research even beyond the chemical field.

The main goal of this work is the preparation and characterization of *push-pull* iron(II) complexes for potential use as dye sensitizers in solarcells (DSSC) and as emitters in light-emitting cells (LEC). Electron-rich R_2tpda (*N*, *N'*-di "R" -*N*, *N'*-di- (pyridin-2-yl) pyridine-2,6-diamine, R = H, Me, *n*Pr, *n*Hex) and a strongly electron-withdrawing Dcpp (dcpp, 2,6-bis (2-carboxypyridyl) pyridine) ligand leads to a distortion of the electron density at the metal center. The main difficulties in obtaining stable complexes are shown, as well as maintaining the properties important for application, e.g. a broad absorption in the visible region, a strong *push-pull* character by the ligands and a strong ligand field splitting. It is illustrated that small changes in the substitution at the ligand significantly affect the stability of the iron(II) complexes. The change in the electron density at the ligand by deprotonation demonstrates how to selectively influence the transitions occurring during excitation. The increased electron density at the donor ligand leads to an LL'CT instead of an MLCT transition as transition with lowest energy. It also shows how electronic symmetry can be reduced by partial deprotonation and offers the control above directional transitions between the ligands.

The desired properties are confirmed experimentally as well as theoretical by density functional theory calculations. The remote target of obtaining a low-lying ^{3}MLCT state for an emitting iron(II) complex could not be achieved yet. However, using the *push-pull* concept and a large bite angle of 90°, the influence on the ligand field splitting was significant enough to raise the energy energy of the ^{5}MC state ($^5T_2$, $(t_{2g})^4(e_g*)^2$) close to the energy level of the ^{3}MLCT state ($^3T_1$, $(t_{2g})^5(e_g*)^1$). As a result, one has come closer to achieve a ^{3}MC as a low-energy metastable state after excitation, which is the first step on the way towards emitting iron complexes.

In addition, a Me$_2$tpda-based cobalt redox mediator [Co(Me$_2$tpda)$_2$]$^{2+/3+}$ is presented in combination with a cationic and neutral tridentate push-pull ruthenium (II) sensitizers [Ru(ddpd) {tpy(COOH)}]$^{2+}$ (Me$_2$tpda = *N*, *N'*-dimethyl-*N*, *N'*-di-(pyridin-2-yl)pyridine-2,6-diamine, tpy (COOH)$_3$ = 2,2'6,2 " terpyridines -4,4 ', 4' '- tricarboxylic acid) from our group in DSSC applications. The aim of this work is to improve the performance of the dye and to compare the novel redox mediator with common systems such as [Co(bpy)$_3$]$^{2+/3+}$ (bpy = (2,2'-bipyridine) and I^-/I_3^-. The higher short-circuit photocurrent and the higher electron recombination time of the electrolyte suggest that electron recombination on the TiO$_2$ surface with [Co(Me$_2$tpda)$_2$]$^{3+}$ complex proceeds slower by the higher-energy π^* orbitals of the Me$_2$tpda ligands than [Co(bpy)$_3$]$^{3+}$ with far lower-energy π^* orbitals of the bpy ligands. The [Co(ddpd)$_2$]$^{2+/3+}$-electrolytes achieved the best performance on this system.

Finally, cyclometallated polypyridyl push-pull ruthenium(II) complexes with different donor substituents ([Ru(dbp-X) (tctpy)]$^{2-}$ ((H$_3$tctpy=2,2';6',2''-terpyridine-4,4',4''-tricarboxylic acid; dpbH=1,3-dipyridylbenzene; X= *N*(4-C$_6$H$_4$OMe)$_2$, *N*Ph$_2$, *N*-carbazolyl) from Dr. C. Kreitner are analysed. Their performance in DSSCs were tested with different redox mediators and additives

compared to the reference dye N719. Nevertheless, this also led to an increased resonance stabilization, which made the regeneration of the dyes more difficult, resulting in a poor performance of the cells with I^-/I_3^- electrolytes compared to N719. However, under certain conditions the *N*-carbazolyl substituted dye with I^-/I_3^- electrolytes shows comparable efficiencies to N719. In the presence of cobalt electrolytes, all efficiencies decrease, wherein the cabarzolyl-substituted dye outperforms N719 under these conditions in terms of efficiency and fill factor.

Table of Contents

°C	degree Celsius
ΔR	bond length difference
δ	chemical shift (NMR) [ppm]
ε	exctinction coefficient [M^{-1} cm^{-1}]
λ	wavelength [nm]
η	efficiency
τ	lifetime
$\tilde{v}$	wavenumber [cm^{-1}]
Φ	quantum yield
10 Dq	ligand field splitting
A	coupling constant (EPR) [G]
Ac	acetyl
a.u.	arbitrary units or atomic units
B	magnetic field (EPR) [mT]
BARF	tetrakis(pentafluorophenyl)borate
bpy	2,2'-bipyridine
calcd.	calculated (MS)
Cp	cyclopentadienyl
CV	cyclic voltammetry
d	day
DFT	densitiy functional theory
dcpp	2,6-bis(2-carboxypyridyl)pyridine
ddpd	N,N'-dimethyl-N,N'-dipyridine-2yl-pyridine-2,6-diamine ≡ Me_2tpda
DSSC	dye sensitized solar cell
$E_{1/2}$	half wave potential
ET	electron transfer
eq.	equivalent
EQE	external quantum efficiency
ESI	electron spray ionization (MS)
EPR	electron paramagnetic resonance
EtOAc	ethylacetate
EtOH	ethanol
exc	excitation
exp.	experimental
FcH	ferrocene
FD	field desorption (MS)
ff	fill factor
fs	femtosecond
FTO	fluorine doped tin oxide
g	g-value (EPR)
G	Gauß
GS	ground state
h	hour
h	Planck constant
H_2tpda	2,6-Bis(2'-pyridylamino)pyridine
hex$_2$tpda	N,N'-dihexyl-N,N'-dipyridine-2yl-pyridine-2,6-diamine
HOMO	highest occupied molecular orbital
HMBC	heteronuclear multiple bond coherence (NMR)

hs	high spin
HSQC	heteronuclear single quantum coherence (NMR)
I	nuclear spin
IPCE	incident photon-to-current conversion efficiency
IR	infrared
ISC	intersystem crossing
ITO	indium doped tin oxide
IVCT	intervalence charge transfer
J	coupling constant (NMR) [Hz]
KHMDS	potassium bis(trimethylsilyl)amide
LEC	light-emitting electro chemical cell
LED	light-emitting diode
LL'CT	ligand-to-ligand charge transfer
LIESST	light induced excited spin state trapping
LMCT	ligand-to-metal charge transfer
LUMO	lowest unoccupied molecular orbital
ls	low spin
MC	metal-centered
MLCT	metal-to-ligand charge transfer
m	milli
M	molar [mol^{-1}]
max	maximum
min	minute
MS	mass spectrometry
m/z	mass per charge
NMR	nuclear magnetic resonance spectroscopy
NHE	standard hydrogen electrode
NIR	near infrared
ns	nanosecond
O_h	point group symbol for octrahedral
OLED	organic light-emitting diode
P	spin paring energy
pcm	polarizable continuum model
ps	picosecond
pr$_2$tpda	N,N'-dipropyl-N,N'-dipyridine-2yl-pyridine-2,6-diamine
P$_1$-^{t}Bu	$tert$-butylimino-tris(dimethylamino)phosphorane
phen	1,10-phenanthroline
R	substituent
RT	room temperature
SEC	spectro-electro chemistry
sim.	simulated
SCO	spin-cross over
T	temperature [K]
t	time
TAS	transient absorption spectroscopy
TBAF	tetrabutylammonium fluoride
TBP	$tert$-butylpyridine
TFA	trifluoroacetic acid
THF	tetrahydrofurane

IV ABBREVIATIONS

TLC	thin layer chromatography
tpy	2,6-bis(2-pyridyl)pyridine
UV	ultraviolet
Vis	visible
XANES	x-ray absorption near-edge structure

1 Introduction: State of the Art

In our highly engineered society we are interested in cost-effective, mobile, environment-friendly and efficient solutions to meet and reduce our energy needs to operate our electrical equipment. Solar cells play a decisive role in the mobilization of energy. Since Bequerel unknowingly described the photovoltaic effect in 1837, the development of the solar cell took its course.[1] Nowadays a large number of different types of solar cells exist. In general there is to name the inorganic silicon semiconductors in several variations by doping materials and aggregation/manufactoring (e.g. microcrystalline, amorphous, GaAs, CdTe), organic solarcells (e.g. polymer, organic thin-film), the perowskite and thin-film solar cells like the dye sensitized solar cell.[2] The National Renewable Energy Laboratory (NREL) occasionally publishes the performance of all known solar cell types in a chart showing the development of the efficiencies (Figure 1).
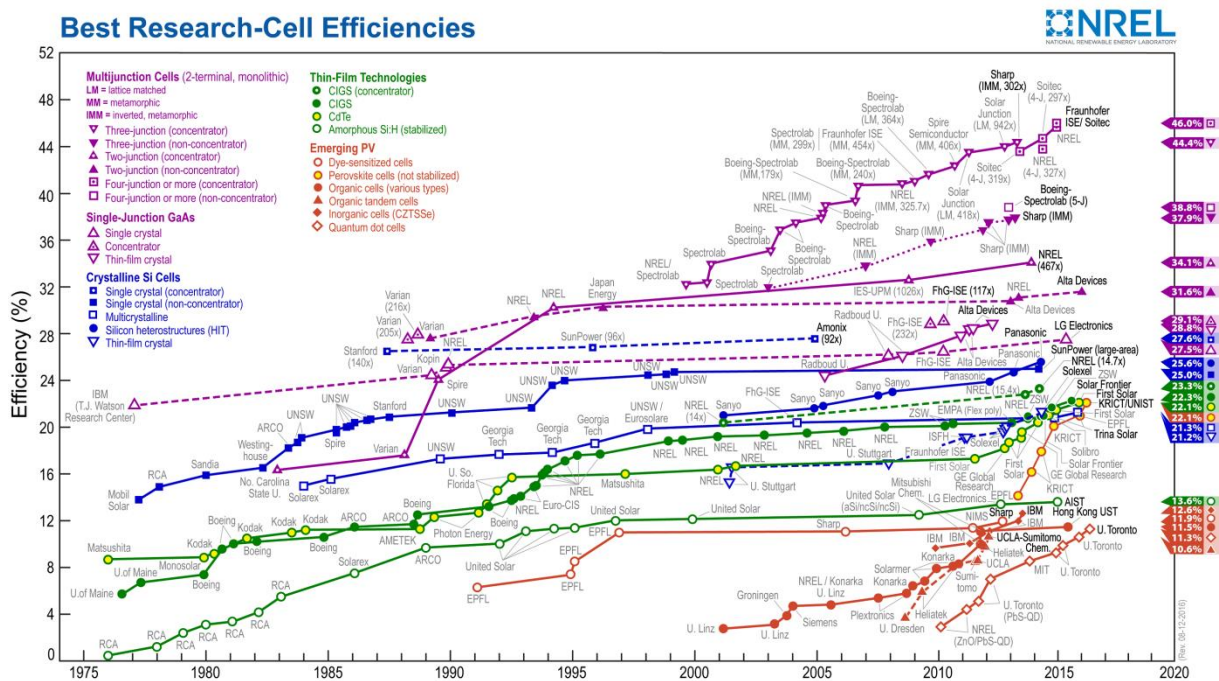

Figure 1. Conversion efficiencies of best research solar cells woldiwde for various photovoltaic technologies since 1976 (status: 12 august 2016; public domain).[3]

Despite this diversity, mainly the inorganic silicon semiconductor solar cell is being used commerically, as it combines the most important properties like longevity, mass producabitlity and average efficiency. However, these cells have various disadvantages, particularly the energy-intensive production, high weight and low flexibility.

Thin film solar cells developed by Grätzel and O'Regan in 1991 provide therefore a good alternative. In particular, the "dye sensitized solar cell" (DSSC) is distinguished by low cost

and less energy consumption in manufactoring, low weight and flexibilty.[4] Yet, DSSCs are rarely applied, because previous systems of this type are very limited in their durability. In addition, expensive 4d and 5d transition metals like ruthenium complexes are preferred utilized in this devices because of their high efficiencies.

Iron(II)-based dyes are intended to provide an alternative to 4d and 5d metals. Yet, the difficulties with iron(II)-based complexes starts with the synthesis and stability. Moreover, some iron(II) complexes show spin crossover (SCO), which occurs in first row transition metal complexes with a d^4 through d^7 electron configuration in an octahedral ligand geometry and would be a highly perturbing property for use in DSSCs. However, work on such systems opens up the perspective on iron emitters because similar problems must be solved. Especially in light-emitting electrochemical cells (LEC) an emitting iron complex would be of great interest, as explained in detail in the following sections.[5]

Further aspects in the research of DSSC applications is the tuning of the efficiency by optimization of the setup of the cell. Therefore, novel redox mediators based on cobalt(II,III) are in the focus of research. Additionally, the electrolyte soltuions can be tuned by addition of additives.

1.1 Polypyridyl Iron Complexes and their Ruthenium Analogues

There is a large number of polypyridyl iron(II) complexes for several applications, such as catalysis or molecular switches.[6,7] On the other side, only a small number of dyes for sensitized solar cells with poor performances and emitting iron(II) complexes are unknown. Analogous structures with ruthenium provide good results in the field of DSSCs and emitters (Scheme 1). For example, the ruthenium-based dye **N3** (**1**) features efficiencies up to 10 %, while the iron-based dye **2** does not reach a significant value.[8,9,10] The same phenomena are found for bis(4'-carboxy-2,2':6',2''-terpyridine) coordinated metal complexes. The ruthenium based complex $[\mathbf{3}]^{2+}$ reaches efficiencies up to $\eta = 0.77$ % and a fill factor *ff* of 0.56. under standard conditions concerning the $\mathrm{I^-}/\mathrm{I_3^-}$ electrolyte (0.5 M LiI, 0.05 M I_2, CH_3CN), while the iron based complex $[\mathbf{4}]^{2+}$ only achieves $\eta=0.01\%$ and a fill factor $ff = 0.50$.[11,12]
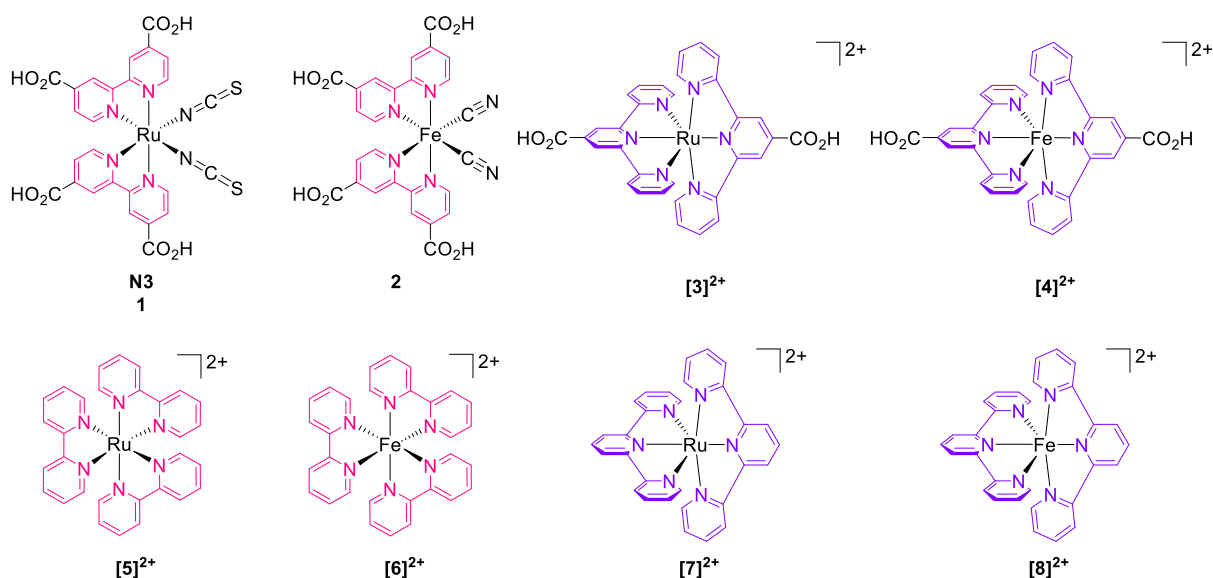
Scheme 1. Iron complexes and their ruthenium analogues potential for DSSC and LEC applications.

In case of emitter materials one finds the same tendency. While the $[\mathbf{Ru(bpy)_3}]^{2+}$ complex $[\mathbf{5}]^{2+}$ is used as a standard reference in terms of emission, with a quantum efficiency of $\Phi_{rt} \approx 6$ % and a lifetime of the ^{3}MLCT-state of $\tau_{rt} \approx 1000$ ns at room temperature (MLCT = metal-to-ligand-charge-transfer; Figure 2a), $[\mathbf{Fe(bpy)_3}]^{2+}$ $[\mathbf{6}]^{2+}$ does not show any kind of emission even at low temperatures (**bpy** = 2,2'-bipyridine).[13,14,15,16] The ruthenium(II) terpyridine (**tpy** = 2,6-bis(2-pyridyl)pyridine) complex $[\mathbf{7}]^{2+}$ suffers from an effective radiationless deactivation pathway via ^{3}MC states, which can be thermally populated from ^{3}MLCT states (MC = metal-centered; Figure 2). This fast internal conversion results in a quantum yield of $\Phi_{rt} \leq 0.0007$ % and a ^{3}MLCT lifetime of $\tau_{rt} \approx 0.1 - 0.2$ ns, which is still much

longer than that of the non-emissive homologous iron congener **[8]**$^{2+}$ with MLCT lifetimes in the femtosecond region.[17,18,19]

If one looks at the occupation in a perfect octahedral field of these two systems in the d^6 configuration, they have the same electronic character in the ground state. All 6d electrons are paired in the t_{2g} level which represents a low spin (ls) configuration (Figure 2a). However, the ligand field splitting energy (10 Dq) between the t_{2g} and e_g^* level of iron is significantly lower than that of ruthenium (Figure 2b).
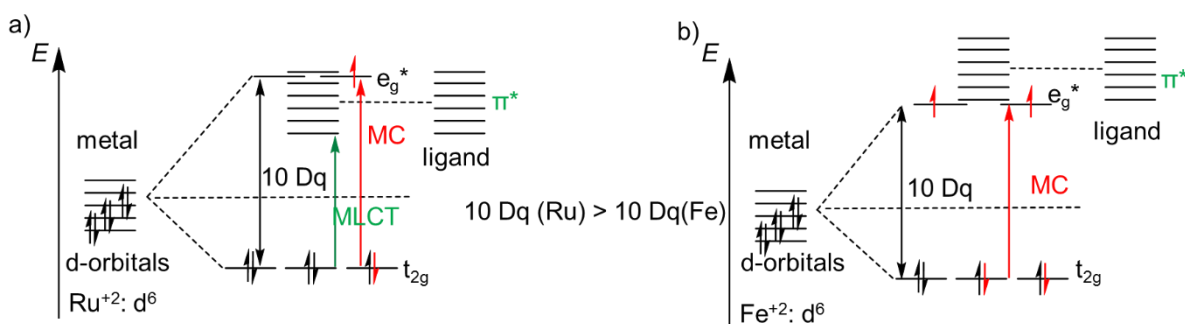

Figure 2: Ligand field splitting of a) ruthenium(II): all electron spins located at the t_{2g} level present the ^{1}GS; S = 1. The red electrons indicate possible MC transitions towards ^{3}MC state. The green arrows indicate MLCT transitions. b) iron(II): all electron spins located at the t_{2g} level present the ^{1}GS; S = 1. The red electron spins indicates two possible MC transitions towards ^{5}MC state.

As a result, iron(II) compounds exhibit several metal-centered transitions and can end up due to a spin-crossover (SCO; chapter 1.1.1) in a high spin (hs) state (Figure 2b). More states exist which are preferred over a MLCT state. In comparison, only ^{3}MC- and ^{3}MLCT-states in ruthenium complexes in the lowest energetic state are accessible. The following Tanabe Sugano diagram shows the difference between a ruthenium- and iron-based complex, using the compounds **[6]**$^{2+}$ compared to **[5]**$^{2+}$ (Figure 3a).[20,21,22]
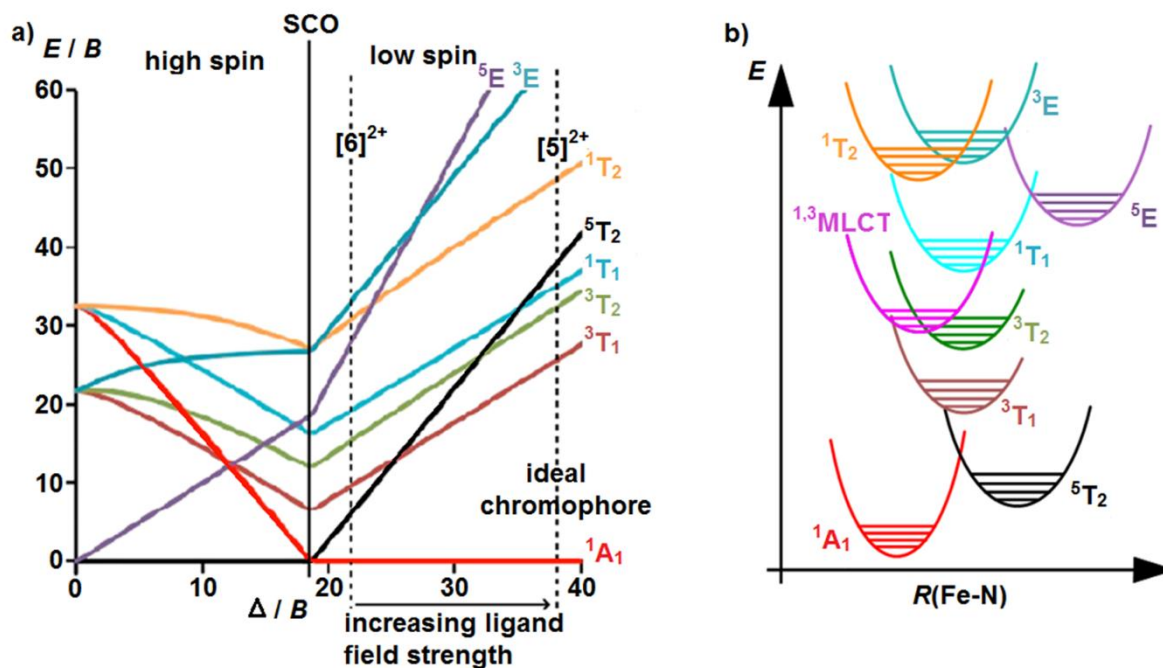
Figure 3: a) Tanabe Sugano diagram of d^6 metals including ligand field strengths of [Fe(bpy)$_3$]$^{2+}$ ([6]$^{2+}$) and [Ru(bpy)$_3$]$^{2+}$ ([5]$^{2+}$)complexes.[20] b) Possible energy states of an iron complex [6]$^{2+}$ in relation to the Fe-N bond length.[21] (adopted from literature Ref20 and Ref 21).

The influence of the ligand field strength on the number and kind of possible intersections towards metal centered transition states is clearly illustrated in the Figure 3b. In case of [6]$^{2+}$ the ligand splitting energy 10 Dq is close to the hs /ls crossing point, the SCO line. As a result, the lowest excited state is the $^5T_2$ (^5MC, black line), followed by the $^3T_1$ (brown line) and the $^3T_2$ (green line); (^3MC-states). Several crossing points of these electronic symmetries are shown. The ruthenium complex [5]$^{2+}$ has only one ^3MC-state, the $^3T_1$ as lowest excited energy level without any crossing points (Figure 4a). This changes the energetic pathway considerably when the complex is electronically excited and applies for nearly all ruthenium complexes. Here, only the ^3MLCT and ^3MC are in competition. The ^3MLCT-state can either relax to the GS via emission or populates the ^3MC state which relaxes radiationless into the GS. Therefore, mainly two excited states are important for emissive ruthenium(II) complexes. In contrast, iron(II) possesses two MC states, the ^3MC- and the ^5MC-state. The ^3MC states are described as two spectroscopic terms, the $^3T_1$ and the $^3T_2$ term, through which relaxation occurs radiationless after excitation. Generally these states are lower in energy than the MLCT-states and appear in the order demonstrated in Figure 4b.
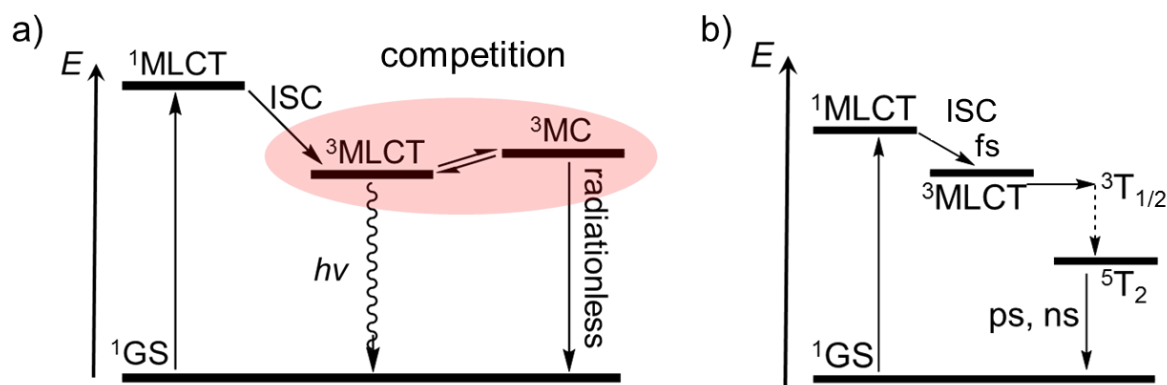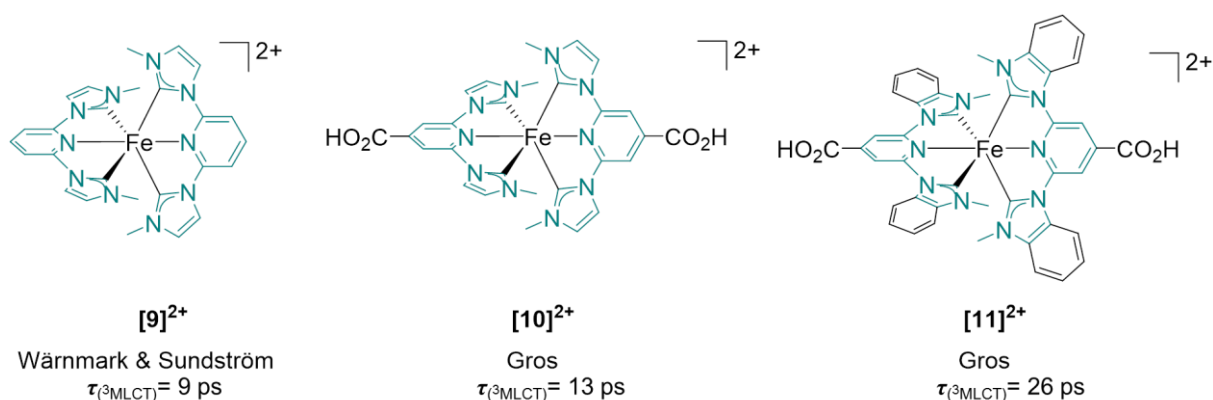
Figure 4: Jablonski state diagrams: a) ruthenium complexes; Here the emissive ^{3}MLCT and the radiationless ^{3}MC are in competition. b) Iron complexes: Here the femtosecond short living MLCT ends via an intermediate ^{3}MC state in a long-living ^{5}MC state (ps, fs), which relaxes radiation less into the ^{1}GS.

Due to this situation, further problems arise for the use with iron. The low ligand field strength has a great influence with respect to the synthesis and the stability of the desired complexes. To obtain a heteroleptic bis(tridentate) ruthenium(II) complex one need to do the reaction under heating and the synthesis can be done stepwise towards a bis(tridentate) complex.[23,24] In case of iron(II), it is more difficult to control the kinetics of the reaction. For example in reactions with terpyridine units and an iron salt the control over a stepwise reaction is impossible. Even with low equivalents of this five-membered chelate ligand, the reaction delivers the bis(tridentate) complex **[8]$^{2+}$**.[25] Furthermore, the stability of the complexes suffers from the existing hs states. Polypyridyl ruthenium complexes are more stable in presence of water or other nucleophiles e.g. OH$^-$ or CN$^-$ compared to their iron(II) congeners.[26] These small anions irreversible replace the polypyridyl ligands.[27,28,29,30,31,32,33] Nevertheless, due to economic and ecological aspects the use of iron would provide more benefits than using these expensive 4d (or 5d) noble metals and opens a wide understanding to influence excited states. The relatively occurrence of ruthenium is 0.02 ppm in the earth's crust or 1 ppb on earth, comparable to rhodium, iridium and rhenium.[34] In contrast, iron is the fourth most common element on earth and accounts for 4.7 % of the earth's crust. As result, the price of iron is less than 1 % of the price of ruthenium. If iron-based complexes can be optimized in such a manner to be efficient sensitizers, the overall costs of the already economical dye sensitized solar cell could be reduced even further.

Experimental approaches by Sundström and Wärnmark demonstrated the possibility of higher ^{3}MLCT lifetimes ($\tau = 9$ ps) based on a tridentate strong-field C^N^C complex **[9]$^{2+}$** with NHC and pyridyl donor ligands (Scheme 2).[35] This long ^{3}MLCT lifetime was achieved by slowing

down the deactivation via increasing the energy of the ^{3}MC state and inducing a large structural rearrangement during the ^{3}MLCT to ^{3}MC transition.[36]

Functionalization by carboxylic acid moieties afforded a tetracarbene iron complex **[10]**$^{2+}$ with excited state properties that allow efficient conversion of light to electrons with 92 % yield in a DSSC and an extended ^{3}MLCT lifetime of 13 ps. Modification of this complex by introduction of benzimidazolylidene-based ligands led to the champion complex with a 26 ps ^{3}MLCT state lifetime (Scheme 2).[37,38,39]

[9]$^{2+}$
Wärnmark & Sundström
$\tau_{(^3MLCT)}$= 9 ps

[10]$^{2+}$
Gros
$\tau_{(^3MLCT)}$= 13 ps

[11]$^{2+}$
Gros
$\tau_{(^3MLCT)}$= 26 ps

Scheme 2. Tetracarbene iron(II) complex **[9]**$^{2+}$ from Wärnmark and Sundström and enhancements **[10]**$^{2+}$ and **[11]**$^{2+}$ from Gros. Their ^{3}MLCT lifetimes are marked below.[35,37,38]

1.1.1 Spin Crossover

The first reports on spin crossover (SCO) were published in 1931 by L. Cambi and L. Szegö, who observed a change in magnetic susceptibility in various compounds of transition metals with Fe, Co and Ni.[40] The thermally induced SCO was first studied and investigated in 1964 by W.A. Baker and H.M. Bobonich with various **[Fe(phen)$_2$X$_2$] 12**, Scheme 5) and **[Fe(bpy)$_2$X$_2$]** compounds (phen = 1, 10-phenanthrolines, X$^-$ = Cl$^-$, Br$^-$, I$^-$, N$_3^-$, SCN$^-$, SeCN$^-$).[41]
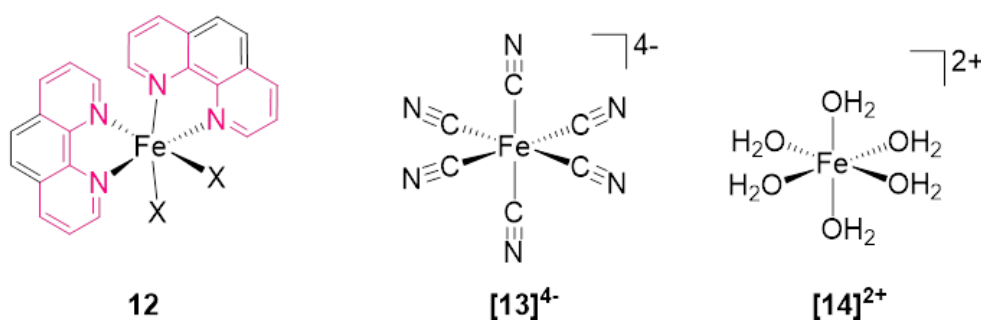
Scheme 3. Established iron(II) complexes for SCO **12**, complex in low spin configuration **[13]$^{4-}$** and in high spin configuration **[14]$^{2+}$** in their ground states. [41]

When metals of the electron configuration 3d^n (n = 4-7) are in an octahedral ligand field, the degenerated five d orbitals split into the antibonding e$_g$* and the nonbonding t$_{2g}$ orbital energy states.[42,43,44]. The energy difference between these two orbital sets is described as 10 Dq. If 10 Dq is far greater than the spin-pairing energy P, all electrons are in the lowest spin state, the so-called ls state, and provide the least number of unpaired electrons. If P is greater 10 Dq, then the d electrons obey the Hund's first rule and the metal complex adopts the hs state, and thus has the highest number of unpaired electrons.[45] Because of the unpaired electrons, the hs state then exhibits paramagnetic behavior, while the ls state in the case of d^6 iron(II)-complexes is diamagnetic. The differences are depicted for the d^6-ions ruthenium(II) and iron(II) in Figure 2.

Thus, the spin state depends on the strength of the ligand field splitting, which is strongly influenced by the coordination sphere of the metal, as well as by the nature of the metal itself. The spectrochemical series of the ligands indicates whether the ligand field splitting of the metal will be strong or weak and provides information about the 10 Dq of the metal ions. For example **[Fe(CN)$_6$]$^{4-}$** (**[13]$^{4-}$**) exists in the ls, while **[Fe(H$_2$O)$_6$]$^{2+}$** (**[14]$^{2+}$**) exists in the hs configuration (Scheme 3). The different influences on 10 Dq via the ligands are caused by their binding character. Strong-field ligands, i.e. cyanides, exhibit a strong σ-donating and

strong π-backbonding character. Because of their high electronegativity, halides have only weak π backbonding character and present weak-field ligands. Water and ammonia belong to the threshold region and result in hs configuration in combination with iron(II) metal centers at room temperature. Furthermore, the spin configuration has a great influence on the bond lengths between the metal and the ligand. In Fe-N complexes the bond length change ΔR (Fe-N) between the ls and the hs state can be up to $\Delta R \approx 0.2$ Å.[46] In the transition from the ls state to the hs state, an extension of the bond length between the coordinating atom and the metal center occurs. The reason for this is that all d-electrons in the nonbonding t_{2g} orbitals are in the $((t_{2g})^6(e_g)^0)$ configuration in the ls and thus have little influence on the length of the bond. In the hs state, however, the $((t_{2g})^4(eg)^2)$ configuration is present, and the antibinding eg* orbitals are occupied, which increases the bond length (Figure 5). If the difference between 10 Dq and P is very small, and the two lowest vibronic states are close to one another, the corresponding SCO may occur and the electron configuration changes from ls to hs. Two types of SCO exist: the thermal and light-induced SCO.

The thermally induced SCO, as the name suggests, is achieved by a change in the temperature. If the energy difference between the two vibrionic states $^1A_1$ (ls) and $^5T_2$ (hs) is in the order of thermal energies $\Delta E(HL) \cong k_b T$ (Figure 5), the SCO can be effected by a temperature change.

The coordinating anions have a great influence on thermally induced SCO. Studies have shown that an exchange of anions results in a different behavior of the complexes with respect to changes in their magnetic behavior, due to modifications in the packing of the complexes.[41,47]
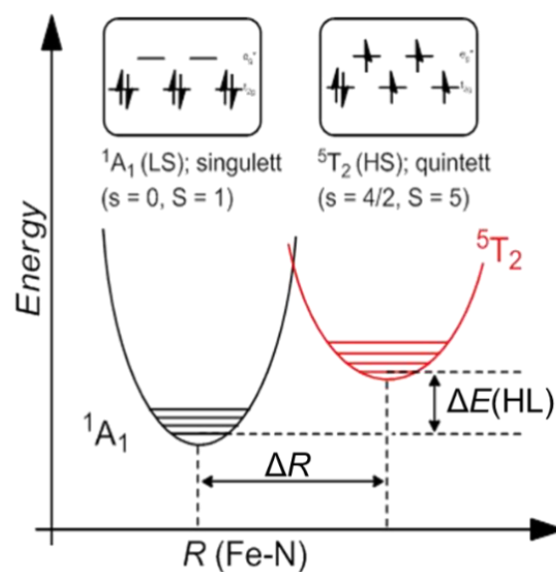

Figure 5. General potential energy diagram of a low spin to high spin transition. $\Delta E(HL)$ describes the difference in energy between the hs and the ls state, ΔR the distance between Fe and coordinating N.[46] (adopted from literature Ref 46)

1.1.2 Light-Induced Spin-Crossover

More than 30 years ago McGravey and Lawthers reported the light induced SCO for the first time and it was well demonstrated experimentally by the groups around Hauser and Gütlich.[48,49,50] They observed a $[Fe(ptz)_6](BF_4)_2$ ($[15]^{2+}$) complex at a temperature of 15 K by using Mössbauer spectroscopy (Figure 6).
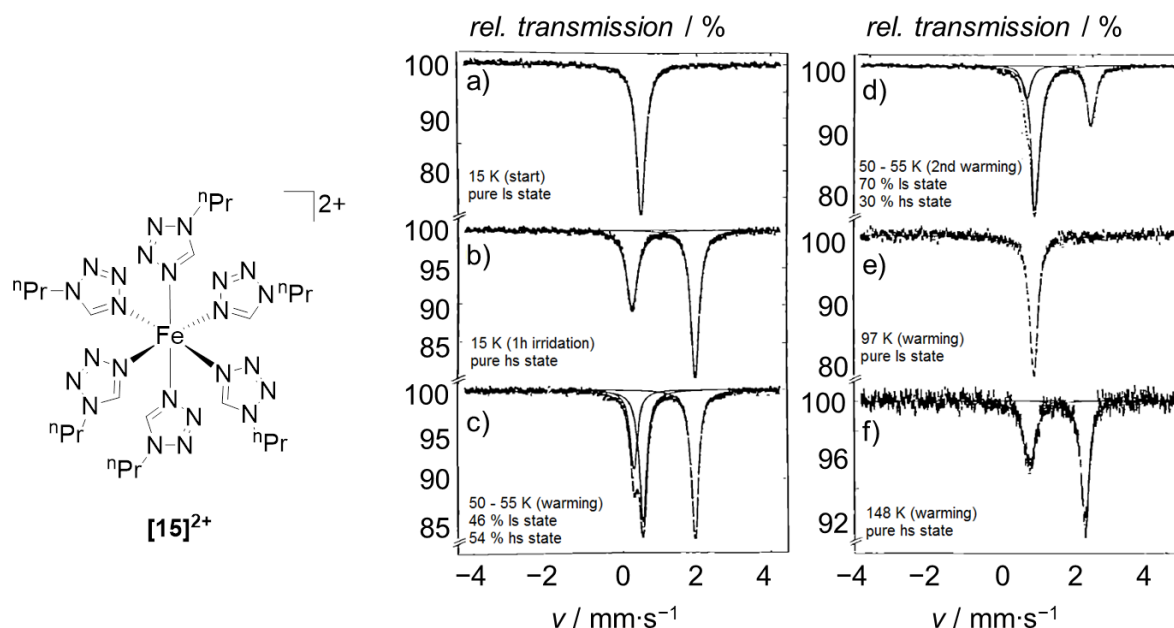

Figure 6: Structure and Mössbauer spectra of $[Fe(ptz)_6](BF_4)_2$ $[15]^{2+}$ (a) Before irradiation (measuring temperature $T_M = 15$ K); (b) after irradiation for 1 h at 15 K ($T_M = 15$ K); (c) after warming to 50-55 K and cooling to $T_M = 15$ K; (d) after second warming to 50-55 K and cooling to $T_M = 15$ K; (e) after warming to 97 K ($T_M = 97$ K); (f) after warming to 148 K ($T_M = 148$ K). [49] (adopted from literature Ref 49)

In the beginning they found a singulet state and a low spin configuration. After an irradiation of 1 h, they noticed a change of the spin towards a dublett resonance which means that the complex is in compliance with a high spin configuration. This metastable state could be found up to a temperature of 50 K, afterwards it switched again into the low spin configuration. This effect is called the light induced excited spin state trapping (LIESST) effect.[48] In contrast to the thermal SCO, the LIESST-effect is mostly independent from the anion packing effects and is solely triggered by absorption of light.[51] Furthermore, the lifetimes of the metastable states depend on the temperature in respect of the coordinating ligands. The higher the temperature is, the shorter are the excited state lifetimes, but higher denticity of the ligand results in larger lifetime of the excited state.[52,53]

The detailed exploration of the LIESST effect required techniques of spectral analysis. Norrish, Eigen and Porter did the first step by developing the flash photolysis, in which a laser pulse produces highly excited short living species such as free radicals.[168] The principle is a pump-probe technique, in which a strong, short laser pulse excites a sample. In the case of SCO complexes the pump pulse leads to an increased population of higher energy levels above the ground state within a sample of atoms or molecules. Immediately after exposure to the pulse laser, the optical absorption of the excited sample changes so that the subsequent reactions in the system are determined by measuring the intensity with a further pulsed laser, the so-called probe pulse. Therefore, the spectrum is recorded in a function of time showing the change of the absorption at different wavelengths. Most compounds observed by this technique have excited state lifetimes in a sub millisecond regime. This methode is called transient absorption spectroscopy (TAS). Initially, this method could only measure processes up to a resolution just below the millisecond scale, but nowadays resolutions up to a few femtoseconds (to attoseconds) are possible.[169] Especially in terms of iron complex chemistry, this is important because most of these complexes have lifetimes in the picosecond region and below.

A further possibility to determine individual states in a SCO system, especially in iron complexes, is the femtosecond optical pump/x-ray probe technique based on the x-ray absorption near-edge structure (XANES) method presented by Chergui et al..[21] Therein, the intensity of a characteristic XANES feature as a function of laser pump/x-ray probe time delay is recorded. They investigated the ultrafast formation of the lowest quintet state upon excitation of the ^{1}MLCT state of complex **[6]$^{2+}$** in aqueous solution and found that the quintet state is populated in about 150 fs. These results confirmed a long-standing issue about the population mechanism of quintet states in iron(II)-based complexes. Gaffney and co workers identified a ^{1}MLCT$\rightarrow^3$MLCT$\rightarrow^3$T$_2\rightarrow^5$T$_2$ cascade as a dominating pathway from the initial excited state.[54] The time scale of the ^{3}MLCT$\rightarrow^5$T relaxation corresponds to the period of the iron-nitrogen stretching vibration.

1.1.3 Ultrafast Spin-Crossover

Owing to high-resolution ultrafast spectroscopy, it is possible to perform detailed pump-probe measurements on pseudo-octahedral polypyridyl iron coordination complexes. It turned out that MLCT excited states undergo internal conversion and intersystem crossing from the MLCT state to the ^{5}MC excited state on a sub-picosecond time scale.[7,15,29] The well examined **[6]**$^{2+}$ provides ^{5}MC lifetimes at room temperature with 665 ps which is a typical region for iron(II) complexes of bidentate chelates (Figure 7). In contrast to common tridentate SCO complexes like **[8]**$^{2+}$ with ^{5}MC lifetimes more than 1 ns, novel studies of iron complexes **[9]**$^{2+}$, **[10]**$^{2+}$ and **[17]**$^{2+}$ showed ultra-short living metal-centered transition states in the picosecond regime.[35,36,37,55,56]
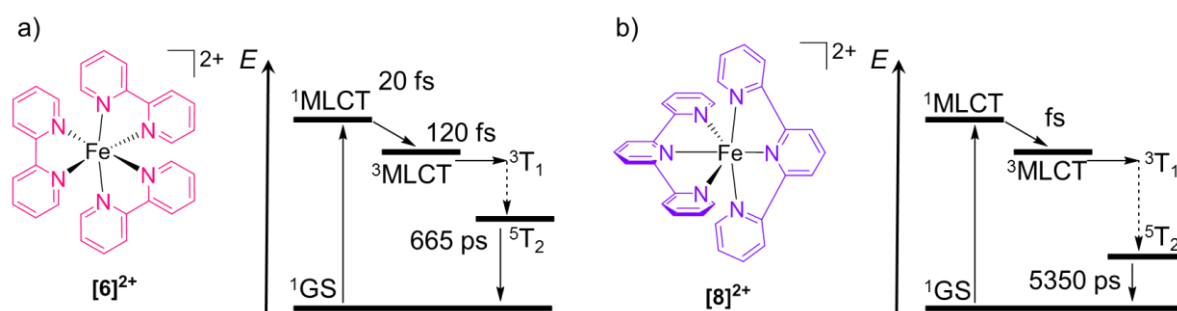

Figure 7. Jablonski state diagram for a) **[6]**$^{2+}$ as example for bidentate and b) **[8]**$^{2+}$ as example for tridentate chelates.[56]

McCusker and co-workers published a novel high-symmetry tridentate iron(II) polypyridyl complex **[17]**$^{2+}$ based on **dcpp** ligand **16** with a deep blue color and a broad absorption from 425 to 650 nm with maximum at $\lambda_{max} = 610$ nm, resulting from a strong ^{1}A$_1 \rightarrow ^1$MLCT transition.[56,57] Using TAS a fast decay of the excited state with a ground state recovery time of $\tau = 280$ ps could be observed suggesting two possible explanations (Figure 8). The first one is the reorganization energy associated with the ^{5}T$_2 \rightarrow ^1$A$_1$ relaxation which is significantly different for complex **[17]**$^{2+}$ than it is for other typical tridentate compounds with lifetimes in the nanosecond region. Another explanation is that different excited electronic states are involved in the relaxation dynamics. Variable temperature time-resolved absorption measurements have demonstrated that the reorganization energy associated with a ^{5}T$_2 \rightarrow ^1$A$_1$ relaxation in the **[Fe(tren(py)$_3$−x(6-Me-py)x)]**$^{2+}$ class of spin-crossover complexes are in the range of 1.0 eV.[56] For **[17]**$^{2+}$ the energy is significantly larger which brings a further more intriguing explanation for the fast ground-state recovery. The enhanced ligand-field strength

due to the **dcpp** ligand has pushed this system past the $^5T_2/^3T_1$ crossing point, thus results in a ^{3}MC as lowest-energy excited energy state (Figure 8b).
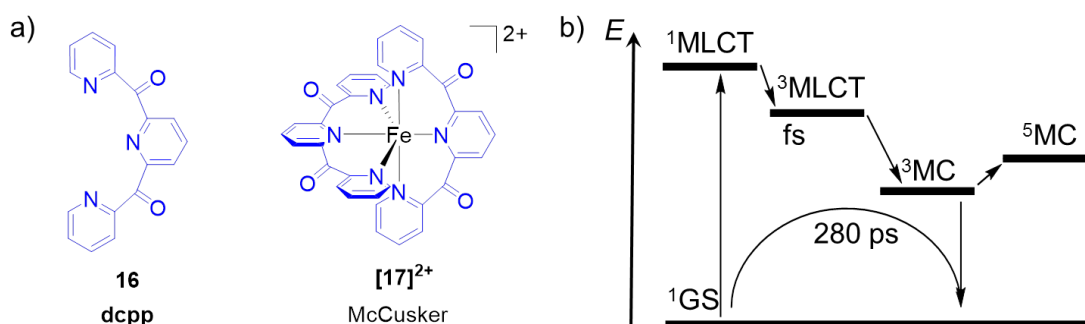
Figure 8. a) Structures of electron-withdrawing **dcpp 16** and complex **[17]$^{2+}$**. b) excited state lifetimes suggest the ^{5}MC state higher in energy than the ^{3}MC state.[56,57]

As mentioned before, Sundström and Wärnmark synthesized and characterized a series of tetracarbene complexes with interesting behavior in their excited state dynamics. Complex **[9]$^{2+}$** has a ^{3}MLCT lifetime of 9 ps and MC state lifetimes of less than 2 ps. Modifications of these systems by Gros and co-workers yielded even longer ^{3}MLCT lifetimes. The explanation for these findings is based on the destabilization of the ^{3}MC state and removing the ^{5}MC states efficiently from the easily accessible energy regions through the strongly σ-donating tetracarbene ligand.[36] This assumption can be confirmed by DFT calculations of the excited states (Figure 9). Here the ^{3}MC and the ^{5}MC state possess the same energy and the potential energy surface of the ^{3}MC is crossing the potential energy surface of the GS before the ^{5}T state.

Figure 9. Plot of calculated potential energy curves vs the bond length Fe-N of complex **[9]$^{2+}$**. The ^{3}MC and the ^{5}MC state are nearly at the same energy level (blue marked area).[36] (adopted from literature Ref 36)

Studies on ruthenium bis(tridentate) and tris(bidentate) polypyridine complexes proved the effective destabilization of the ^{3}MC state through the introductio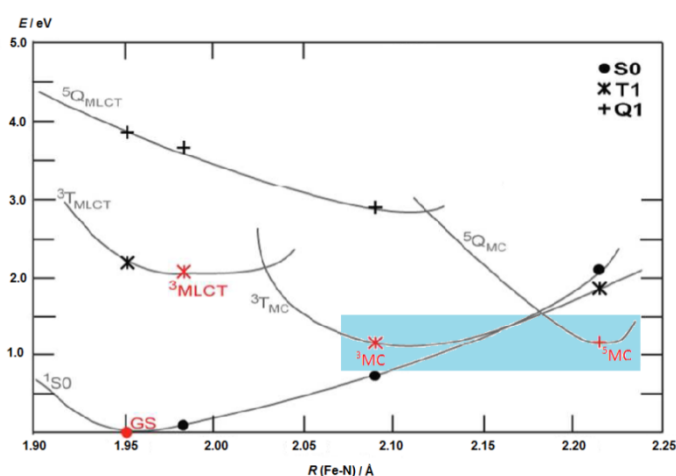n of a strongly σ-donating ligand in the first coordination sphere, likely resulting in an increased t_{2g}/e_g orbital splitting.[58,59,60] Additionally, the ^{3}MLCT lifetime can be increased by an enhanced charge-transfer character through implementation of a carboxylic acid of the acceptor ligand.

Besides the improved ^{3}MLCT lifetime, the parent structure **[9]$^{2+}$** demonstrates the crucial impact of the ligand design (Figure 10). Changing the methyl group by a *tert*-butyl moiety the lifetimes of the excited states and their energy levels change considerably. Due to the repulsion between the *tert*-butyl moiety and the pyridine ring of the second ligand all coordinating bonds are elongated. The Fe-N(NHC) bond is stretched by 0.13 Å without changing the C(NHC)-Fe-N(py) bite angle, which weakens the σ-donating capability of the *tert*-butyl substituted ligand.[35]
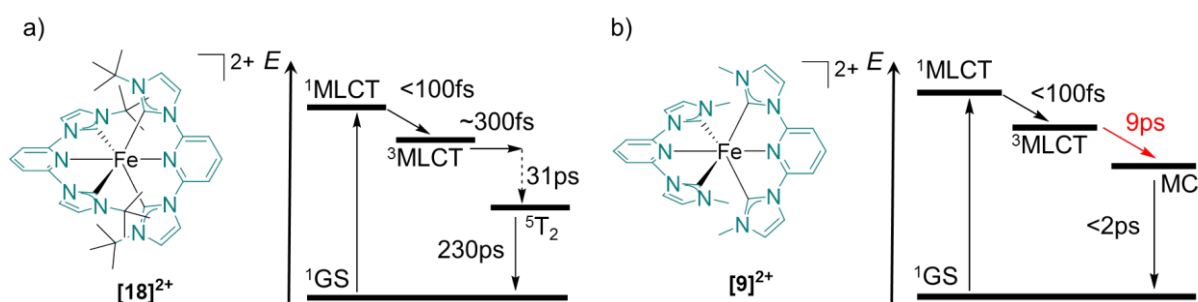
Figure 10. Impact of side chain substituents illustrated by a) Jablonski diagram of ^{i}Pr substituted tetracarbene **[18]$^{2+}$** and b) the tetracarbene role model **[9]$^{2+}$**.[35] (adopted from literature Ref 35)

This effect occurs not only in tridentate systems, but also in systems with monodentate and bidentante ligands. Gaffney and co-workers revitalized a 30-year-old synthetic strategy to extend the MLCT lifetime by synthesis of a mixed ligand iron complexes with four CN$^-$ and one bpy ligand **[Fe(CN)$_4$(bpy)]$^{2-}$** (**[19]$^{2-}$**).[61] By combination of X-ray free-electron laser (XFEL) kβ hard X-ray fluorescence spectroscopy with femtosecond time-resolved UV-visible absorption spectroscopy the electronic excited state dynamics initiated by MLCT excitation of **[19]$^{2-}$** were characterized. The lifetimes of complex **[19]$^{2-}$** is determined with roughly 20 ps (Figure 11).
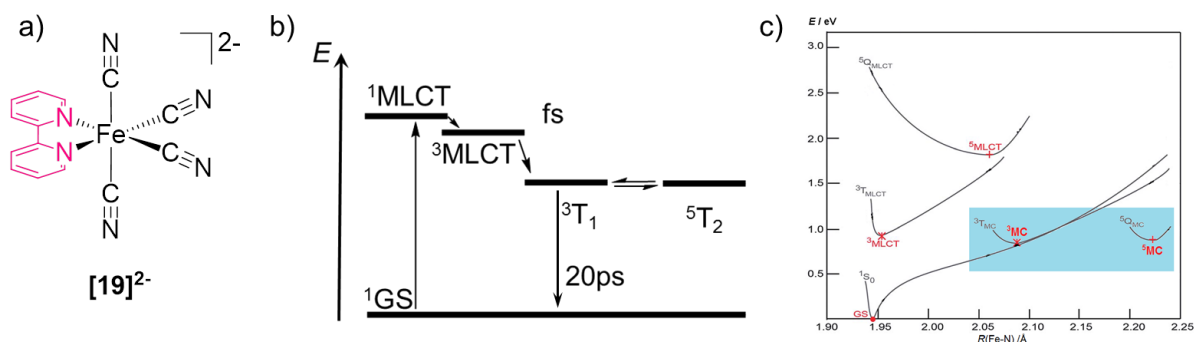
Figure 11. a) Structure of complex **[19]**$^{2-}$ b) Jablonski state diagram of **[19]**$^{2-}$ shows relaxation to the ^{1}GS via the ^{3}MC state and c) the potential energy surfaces of **[19]**$^{2-}$. ^{3}MC and ^{5}MC are similar in energy (blue marked area). (chart c) is adopted from literature Ref 61)

DFT-calculations suggest that the ^{3}MC and ^{5}MC state of **[19]**$^{2-}$ are located at the same energy level (Figure 11c) similar to the results of **[9]**$^{2+}$ in Figure 9. There the potential energy surface of the GS is crossing that of the ^{3}MC at a lower energy than that of the ^{5}MC surface. This leads to the conclusion that in the relaxation pathway of the complex **[19]**$^{2-}$ the ^{5}MC state is avoided (Figure 11b).

In combination with the results of the tetracarbene iron complexes of Gros, Wärnmark and Sundström the existence of iron(II) complexes having ^{3}MC as the lowest excited state are verified. Using carbene-coordinating ligands is one possibility to obtain low-lying ^{3}MLCT states one day.

1.2 Dye Sensitized Solar Cell

Since Grätzel and O'Regan reported the first DSSCs in 1991, efforts were made around the world to optimize them for daily application requirements, as they represent a favorable alternative to the current silicon-based solar cells.[4,58,62,63]

Such a cell consists of two electrodes, the transparent anode and cathode, which are lined on their inside with an electrically conductive material (Figure 12a). They are in general made of ITO or FTO, i.e. indium doped or fluorine doped tin oxide (SnO_2). On the working electrode (anode) nanoporous titanium oxide (TiO_2) is applied, which offers a large surface due to its structure. The sensitizing dye is then located on the TiO_2. These are surrounded by an electrolyte solution containing the redox mediator, which is required for charge transport and dye regeneration. The most common electrolyte is the iodide/triiodide (I^-/I_3^-) redox mediator containing some additives. Through the nanoporous structure of the TiO_2 the electrolyte can penetrate the sensitizer adequately. The setting is completed with the counter electrode (cathode), often made out of silver or platinum.[58,62]
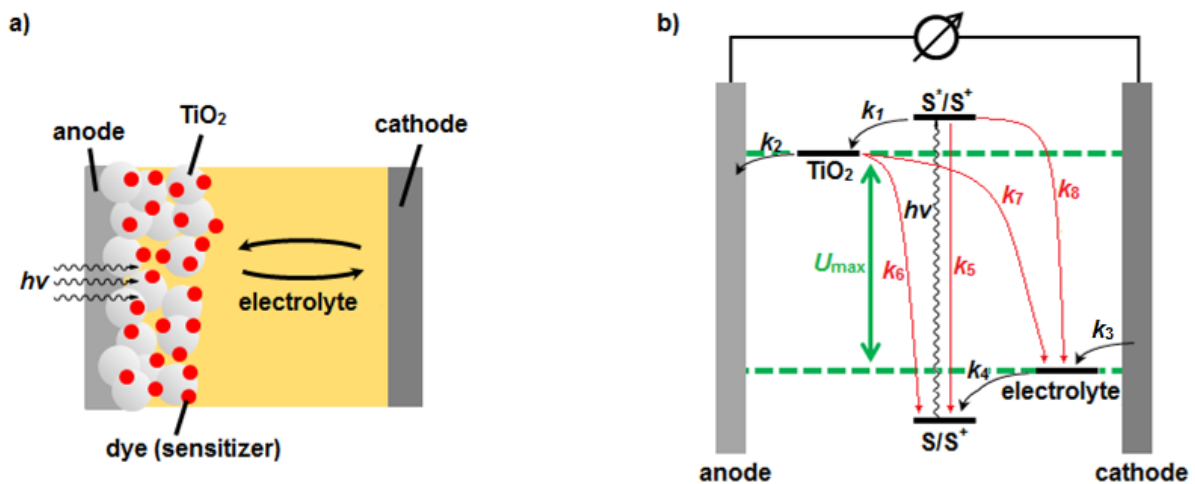
Figure 12. a) Structure of a dye-sensitized solar cell. b) Working principle of a DSSC. Green line marks the boarders of the maximum voltage, black arrows indicate productive transfer steps, and red arrows indicate detrimental back-electron transfer processes.[58,62]

In Figure 12b the working principle of a DSSC is described in detail. If the cell is irradiated with light (hv) of the absorbing wavelength of the dye, it is excited and injects electrons into the conduction band of the TiO_2 (k_1). For this process to take place, the lowest unoccupied molecular orbital (LUMO) of the dye sensitizer must be energetically higher than the conducting band of the TiO_2. The electron reaches the working electrode via the TiO_2 (k_2) and is transferred back to the counter electrode via the load. Afterwards the electron is released to

the electrolyte (k_3). The electrolyte subsequently regenerates the dye due to its reducing properties (k_4), but only if the highest occupied molecular orbital (HOMO) of the dye is below the lowest unoccupied molecular orbital (LUMO) of the redox mediator. The highest possible achievable voltage V_{OC} is determined by the potential difference between the Fermi level of the TiO$_2$ and the redox potential of the electrolyte (U_{max}).

The quality of a cell is given by its efficiency η, described by equation Eq. 1. For this purpose, the ratio of the solar cell performance obtained (P_{out}) is determined against the maximum energy input into the system (P_{in}) (Eq. 1).[87]

$$\text{Eq. 1: } \eta = \frac{P_{out}}{P_{in}} = \frac{U_{mpp} \cdot I_{mpp}}{P_{in}}$$

As shown in Figure 13, the output power P_{out} results from the product of maximum usable current I_{mpp} and the maximum usable photovoltage U_{mpp}.
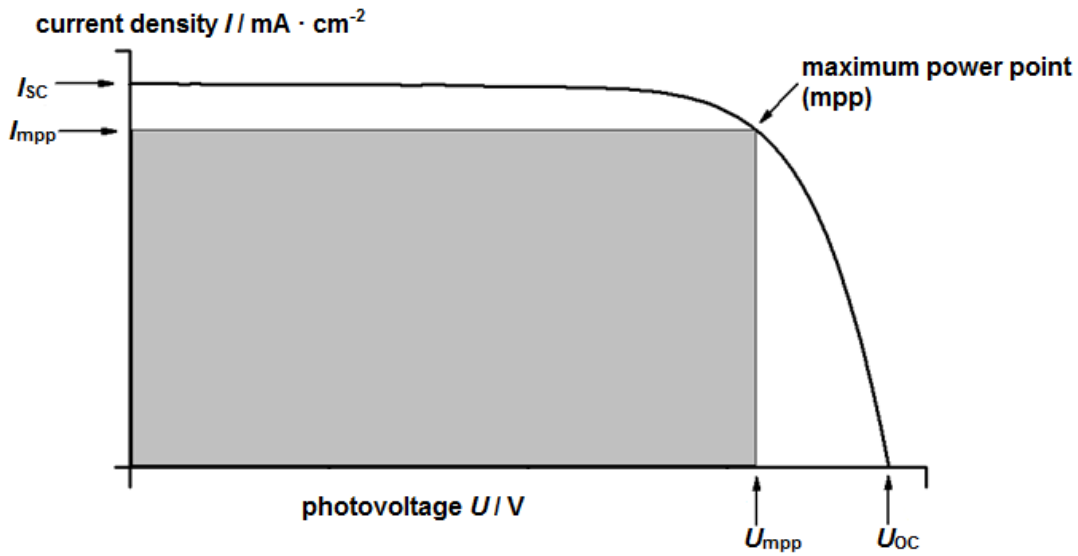
Figure 13. Current density-voltage plot (*I-U*-curve) of a DSSC indicating the short circuit current (I_{SC}), the current density at maximum power point (I_{mpp}), the open circuit voltage (U_{OC}) and the voltage at the maximum power point (U_{mpp}). The grey area marks the usable maximum output power P_{out}.

The second parameter to determine the quality of a DSSC is given by the fill factor in equation Eq. 2. Here the ratio between the maximum utilized power $P_{out} = U_{mpp} \cdot I_{mpp}$ in relation to the product of the open circuit voltage and the short circuit current describes the shape of the *I-U*-curve:

$$\text{Eq. 2: } ff = \frac{U_{mpp} \cdot I_{mpp}}{U_{OC} \cdot I_{SC}}$$

The third quality mark is given by the incident photo-to-current efficiency (IPCE). The IPCE is determined by the number of collected electrons per number of photons irradiated at a given wavelength.[87]

$$\text{Eq. 3: } IPCE = \frac{I_{SC}(\lambda)}{P_{in}(\lambda)} \cdot \frac{1}{\lambda} \cdot \frac{hc}{e};$$

with h = Planck constant, c = velocity of light and e = elementary charge

All these characteristics were obtained under standard conditions with normalized solar light irradiation of 1.5 air mass (AM) and P_{in} = 1000 W m^{-2} (Figure 14a). The number of 1.5 AM means, that the solar light has to pass the thickness of 1.5 atmospheres and corresponds to a situation when the angle of incidence is 48.2°. At a zenith angle of 0° the light would travel through 1.0 AM (Figure 14b).[64]
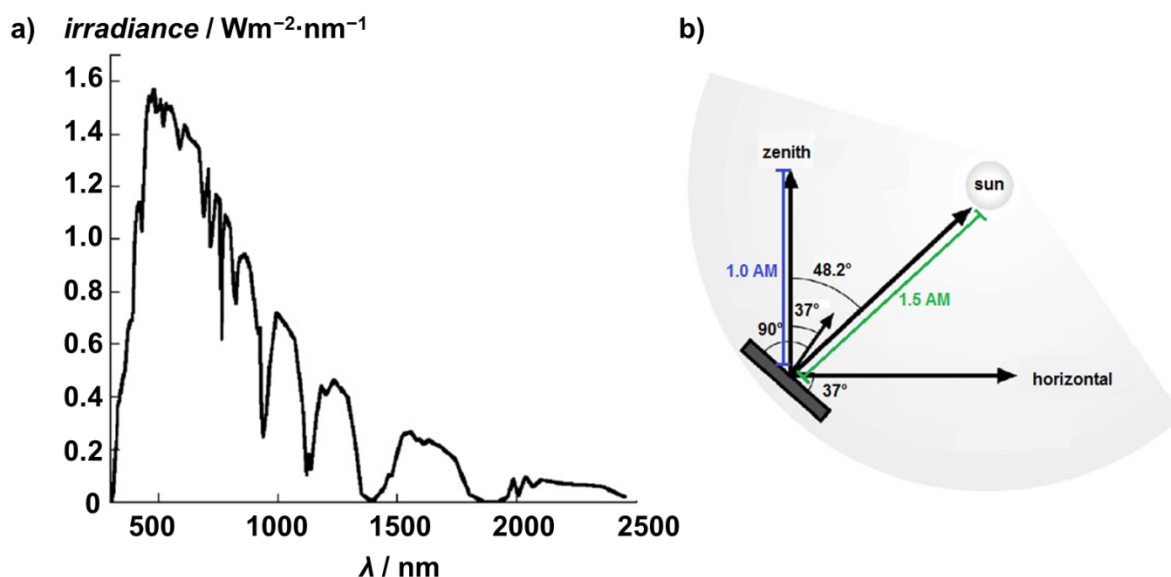
Figure 14. a) The solar spectral irradiance. b) Configuration for 1.5 AM (distance marked by the green line) solar illumination. Distance for 1.0 AM is marked by the blue line. [64] (adopted from literature Ref 64)

Although these key figures classify every DSSC obtained under standardized conditions of 1.5 AM, the cells are often not directly comparable to each other. All laboratories work with different setups of the cells. Starting with different electrode materials, preparation of the TiO$_2$ blades, including thickness and morphology, different electrolytes in respect to the concentration of the redox mediator and ionic liquids or even different redox mediators. Indications for the quality of the cell-setup, standard dyes like **N719** (**[26]$^{2-}$**) in combination with iodide/triiodide (I$^-$/I$_3^-$) electrolyte or **YD-2** (**22**) for examination of cells with cobalt

redox couple were used (Scheme 5 and 6). Besides the development of a potentially good dye and the appropriate redox mediator, the greatest challenge in the assembly of a DSSC is the coordination of the components. In some cases high concentrated electrolyte solutions promote recombination processes or solvent mixtures improve besides a better solubility also a better conductivity. The redox potentials of all compounds must match to one another in order to ensure the regeneration of the dye, but in the case of the redox mediator also be high enough to obtain the highest possible open circuit voltage. The dipping time of the TiO_2 beads in the dye solution can have influence on the efficiency too. To get the most accurate performance and quality of a DSSC multiple measurements should be done. The variation of results can be more than $\eta = 1$ % in the same setup.

1.2.1 Dye Sensitizers – Common Design and Novel Concepts

Mainly organic dyes and coordination compounds are used in DSSCs. The dye structure comprises an electron-rich moiety (donor), an electron-poor moiety (acceptor), and a small linker such as a conjugated bridge or metal center that can transfer the electrons. Furthermore, an anchoring unit is important for fixation of the dye onto the TiO_2 surface, enabling the injection of electrons into the TiO_2 conducting band. Therefore, carboxylic acids were used, but sulfonic acids, amines and other TiO_2-coordinating substituents are also possible.[65] In most structures the anchor group also performs as the acceptor. For some dyes it can be shown that sterically demanding groups like alkyl chains lead to an increased cell efficiency, because these moieties fill space between the dyes and act as an insulator to the TiO_2 surface, therefore preventing recombination processes.[66]

An important property for a dye is a wide absorption in the visible region of light with a high extinction coefficient ε. Furthermore, the LUMO of the dye must be higher in energy than the conducting band of the TiO_2. In addition, the lifetime of the excited state is important. The injection of the electron into the conduction band of the TiO_2 is rapid with 100 fs, which causes problems with the use of some iron complexes with MLCT lifetimes of less than 100 fs.[8,67,68,69] Finally, a long-term stability under thermal stress and irradiation, in the presence of oxygen, water and small anions is indispensable. There are many ways to obtain a structure having the before mentioned properties. In the following, some examples of common dyes (organic-, porphyrin-, ruthenium(II)- and iron(II)-based dyes) are discussed and the special needs in their application and their performances are pointed out (Table 1).

The most common metal-free dye is **MK-2** (**20**) (Scheme 4).[70] This dye reached efficiencies over $\eta = 8.3$ % and offers the basic scaffold of thiophene, which is easily modified by donors and acceptors. Additionally, these dyes can operate with I^-/I_3^- solution as well as with cobalt redox mediators. The highest efficiency achieved by an all-organic dye was **C219** (**21**) with $\eta = 10.1$ %.[71]
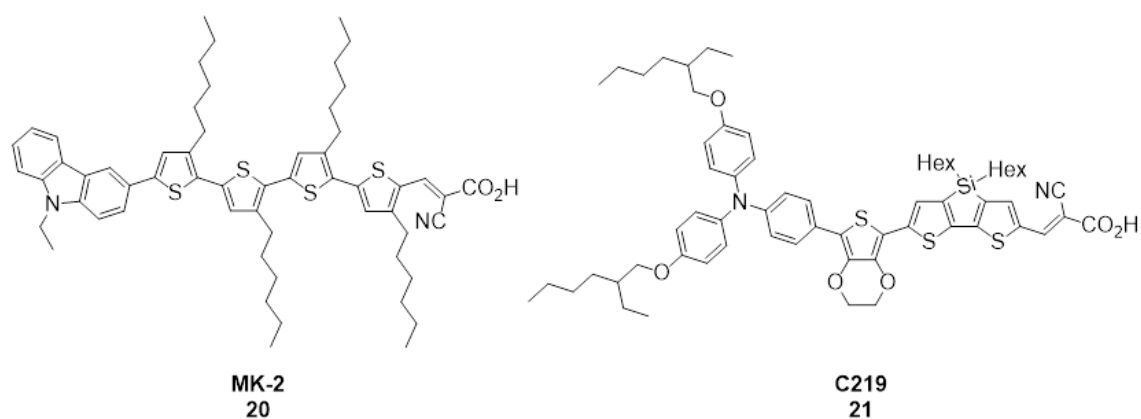
Scheme 4. Common organic dyes **MK-2** and high performing dye **C219**.[70,71]

Although porpyhrine dyes like **YD-2** (**22**) with analogous structures like the champion dye **SM315** (**24**) provide record efficiencies of up to 13% in combination with cobalt electrolyte but the effort to produce these porphyrin complexes is far greater (Scheme 5).[72,73] Nevertheless, a derivative of **YD-2** , **YD-2-o-C8** (**23**) with OC_8H_{17} moieties shows the impact of a further strategy: the use of co-sensitizers. In combination with **Y123** (**25**), **YD-o-C8** delivers efficiencies up to 12.3 %. The advantage of such a combination is that via the principle of co-sensitization the whole spectrum of light between 350−940 nm can be harvested, because finding a single dye that adsorbs strongly over this vast range is extremely difficult.[66]
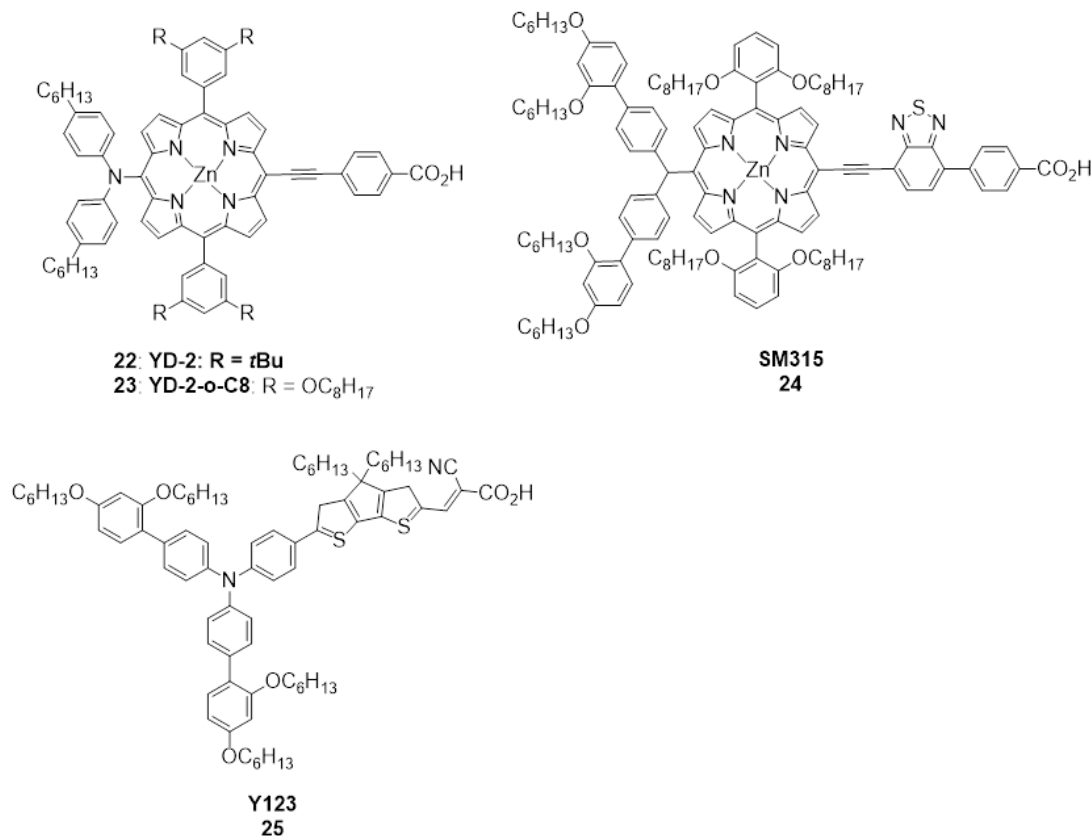
Scheme 5. Reference porphyrin dye **YD-2 22**, **YD2-o-C8 23**, champion dye **SM315 24** and co-absorbent **Y123 25**.[72,72]

From the variety of dyes, ruthenium(II)-based sensitizers seem to be a good entry to offer stable and efficient solar cells.[74,75,76,77,78] A representative ruthenium(II) complex is the bis(4,4'-dicarboxy-2,2'-bipyridine)ruthenium(II) dye also known as **N719** (**[26]$^{2-}$**), which has the best properties in terms of absorption and high efficiencies up to $\eta = 11$ % (Scheme 6).[8,79] It is based on the structure of the **N3** (**1**) dye which delivers in its best setup efficiencies of $\eta = 10.0$ %.[80] The difference between between **N719** and **N3** is in the number of protonated carboxylic acids. **N3** is completely protonated, **N719** is half protonated which causes 1 % difference in efficiency. Based on the scaffold of **N3** further successful ruthenium(II) derivatives were developed like **KD1** (**28**), **Z907** (**29**) and **C106** (**[30]$^-$**).[62,81] These three dyes show the positive effect of addition of an alkyl chain or with thiophene alkylated moieties (**KD1** $\eta = 4.5$ %, **Z907** $\eta = 8.4$ %, **C106** $\eta = 11.3$ %).[58,82]
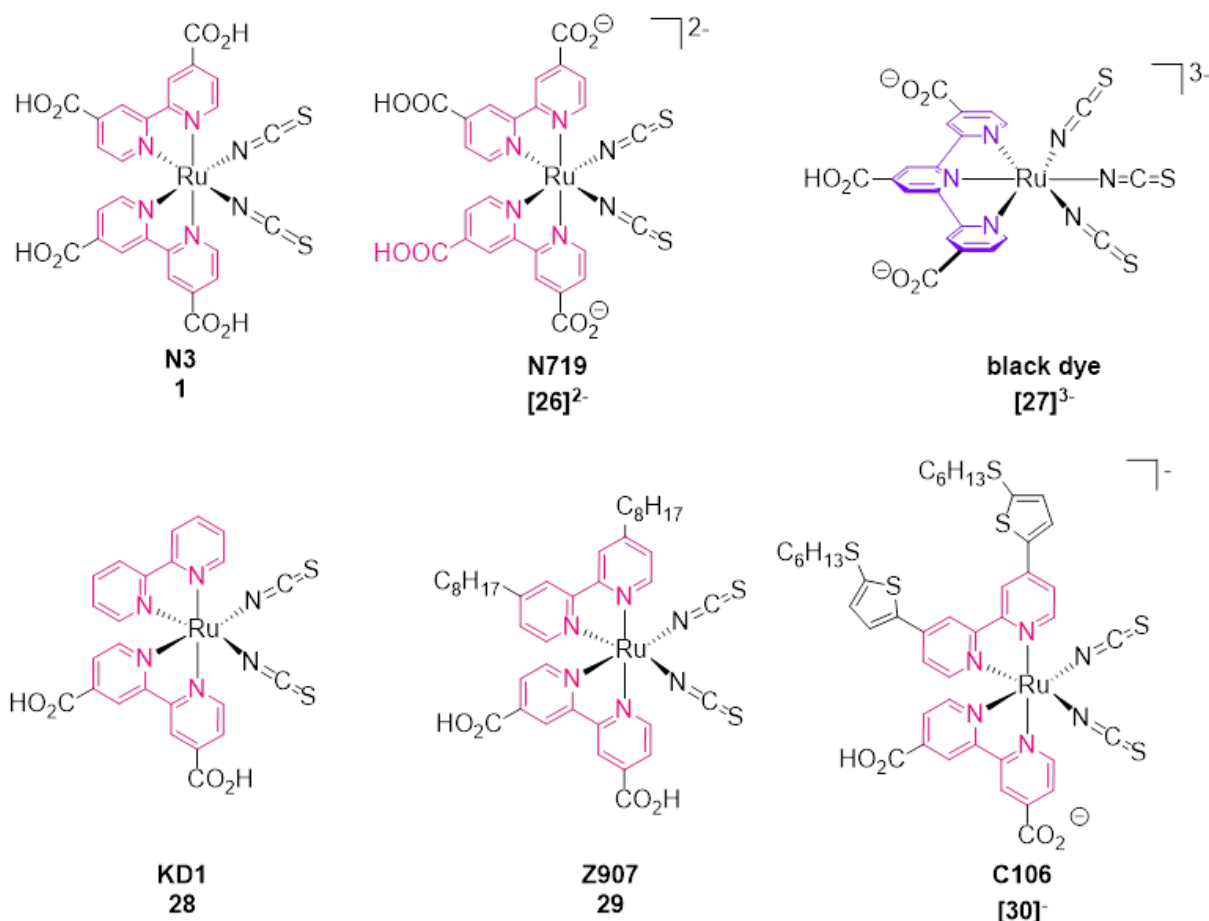
Scheme 6. Upper row shows the most famous dyes **N3**, **N719** and the "**black dye**".[83] Lower row shows the extension of the bpy-SCN **KD1** scaffold via alkylation to **Z907** and addition of alkylated thiophene complex **C106**.[58,62,81,82]

One monodentate complex is outstanding in the group of dyes with SCN⁻ ligands. The **black dye [27]³⁻** has a tridentate ligand and monodentate SCN⁻ ligands, reaching efficiencies of more than $\eta = 10$ % with an excellent $I_{SC} = 20.53$ mA·cm⁻².[58,83] However, such a monodentate binding pattern as SCN⁻ has significant disadvantages concerning long-term stability by thermal- or photo-induced isomerization or ligand exchange reactions.[84,85,86,87,88,89,90,91]

To solve this problem, the mono- and bidentate ligands were completely replaced by carboxylic acid functionalized tpy ligands **[3]²⁺**, but this system showed poor results (Scheme 8).[11] Heinze and Breivogel investigated novel tridentate heteroleptic push-pull complexes like **[32]²⁺**, containing the electron-rich **Me₂tpda** ligand **31** (Scheme 7), and studied these dyes with respect to their optical properties, long-term stability and their photovoltaic performance using a DSSC setup with the
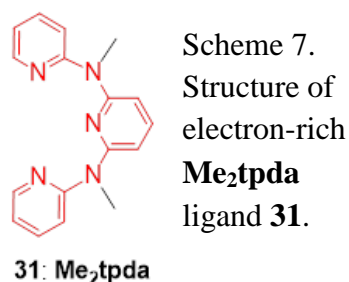
Scheme 7. Structure of electron-rich **Me₂tpda** ligand **31**.

31: Me₂tpda

I⁻/I₃⁻ redox couple through mixing 1-methyl-3-propylimidazolium iodide (**MPII**) and

iodide.[92,93] Nevertheless, the performance of these dyes is a bit higher than that of $[3]^{2+}$, but still showed poor photovoltaic properties measured against **N719**, even though the complexes have an intense and broad absorption in the visible region and adequate redox potentials.

The thermal and photochemical stability however, could be greatly increased and the synthesis compared to mono- and bidentate compounds is easier. A possible explanation may be the positive charge of these complexes, which draws the I^-/I_3^- electrolyte to the dye and increases the I_3^- concentration near the TiO_2 electrode. Consequently, this inhibits eletron-recombination between the surface and the electrolyte.[94,95]
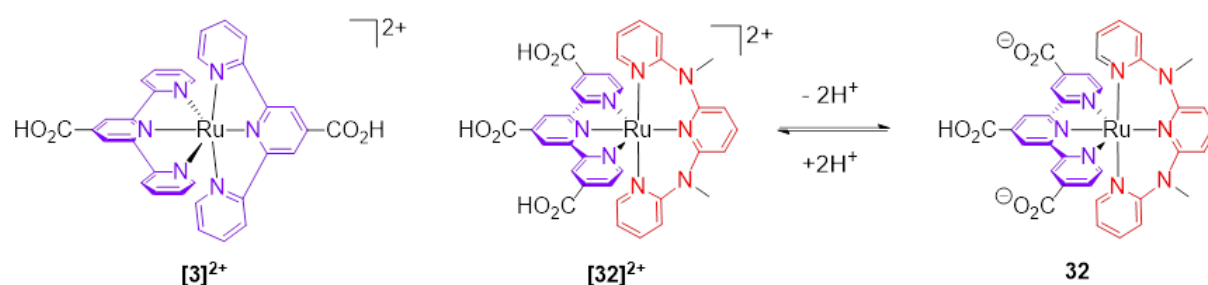
Scheme 8. Anchor functionalized polypyridyl bis(tridentate) ruthenium(II) complexes $[3]^{2+}$ and with *push-pull* and bite-angle tuned models charged $[32]^{2+}$ and uncharged **32**.[11,92,96]

A common approach to reduce the total charge in such complexes is the abstraction of protons. Mengel and Heinze showed that by deprotonation of complex $[32]^{2+}$ and therefore the reduction of its overall charge to zero, the electrostatic attraction and fast electron recombination at the TiO_2-surface can be avoided (Scheme 8).[96]

A common strategy to block the interactions of the electrolyte and the TiO_2-surface is to close holes in the dye coating on the surface by addition of a co-adsorbent. The most prominent co-adsorbent is the chenodeoxycholic acid (**CDCA**) (Figure 15).[97] A co-adsorbent molecule forms a barrier between the TiO_2 surface and the electrolyte. Free space between the dyes or π-π-stacking of the molecules at the surface decreases the efficiency immense through charge recombining processes. Therefore, the
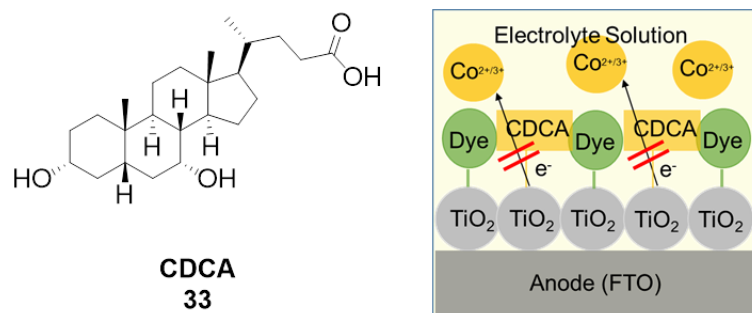
Figure 15. Structure of prominent co-adsorber **CDCA** and its working principle.[97]

work on co-adsorbent molecules is going forward.[98]

Due to the poor efficiencies due to the tridentate coordination, the search for an alternative way is still ongoing. A promising way towards higher efficiencies is the implementation of cyclometalated ligands (Scheme 9). A prominent example of these types of structures is the dye **YE05** (**[34]**$^+$) with an efficiency of $\eta = 10.1\ \%$.[58] Using the advantages of tridentate coordination, the group of Berlinguette published a series of cyclometalated complexes (**[35]**$^+$, **[36]**$^+$, **[37]**$^+$, **[38]**$^+$) with efficiencies from $\eta = 3.36\ \%$ up to 8.0 % with variation in donor units and positions of the C-Ru coordination.[99] With the same basic structure (**[39]**$^+$, **[40]**$^+$, **[41]**$^+$) but without a large donor unit and addition of 20 mM **CDCA**, the working group of Singh reached efficiencies between $\eta = 3.1\ \%$ and $\eta = 7.1\ \%$, depending on the alkyl substituent.[100] Heinze and co-workers showed with a cyclometalated complex invented by Zhong (**[42]**$^-$) that a lower concentration of I^-/I_3^- electrolyte can deliver better performances ($\eta = 3.3\ \%$) than higher concentrations.[101,102]
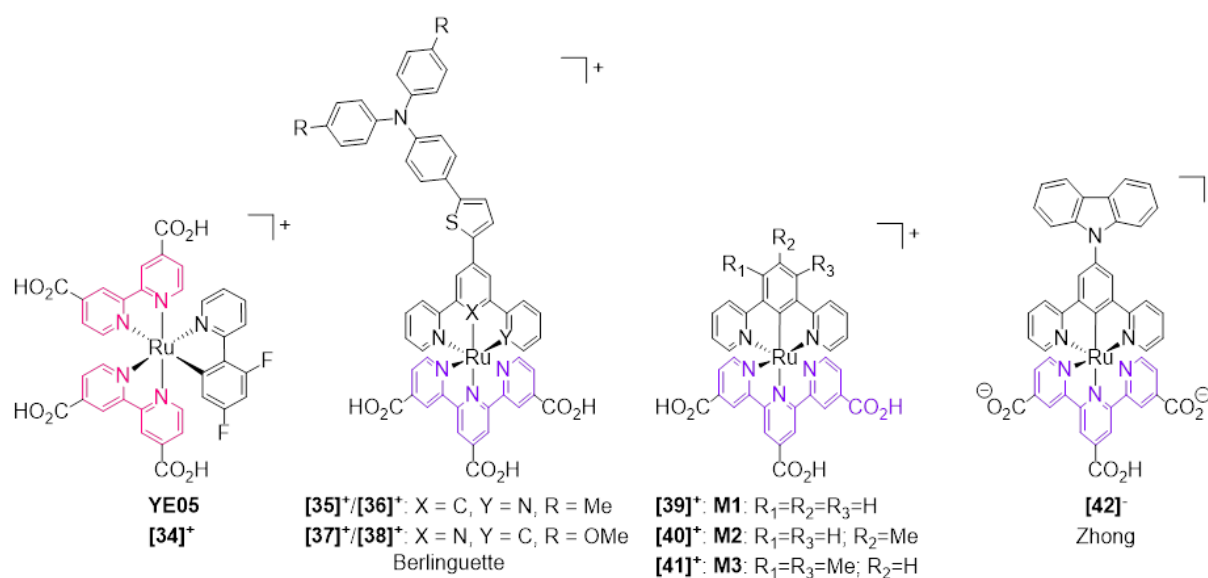
Scheme 9. Cyclometalated dyes for DSSC applications.[58,99,100,101]

The best performances in key figures under optimized conditions of all mentioned dyes found in the literature are reported in the following Table 1.

1.2.2 Iron Sensitizers

As mentioned before, iron is the most available metal in the earth's crust but in the application of DSSC iron based sensitizers have poor photophysical properties due to the low-lying MC-states that deactivate the MLCT-states within less than 100 fs.[21,22,103] Therefore, the challenge for iron polypyridine complexes is to modify the structure in a way that the energy-state diagram is similar to that of analogous ruthenium compounds in the end.[12] Attempts based on successful concepts of homologous ruthenium(II) complexes unfortunately have not brought any success so far in the discipline of an efficient dye though the iron(II) complexes have a proper absorption. Prominent examples are the studies of Meyer or Ferrere who determined the **N3** and analogue scaffolds of iron with poor photovoltaic performance.[9,10,107,108] Although the energetic position of the ^{1}MLCT energy state is above that of the conduction band of TiO_2, the MLCT lifetime of most iron complexes appears to be too short for the injection into the conduction band.

Recent studies on iron complexes have provided detailed insights into the lifetime of excited states. Studies of complex **[19]$^{2-}$** showed that a lifetime of roughly 20 ps of intramolecular electronic excited states, is sufficient to perform completion of typical interfacial charge injection in dye sensitized solar cells.[60,104,105,106] As a reason for the low efficiencies, the effect of ultrafast SCO was ruled out as well as thermodynamic driving forces.[107,108]
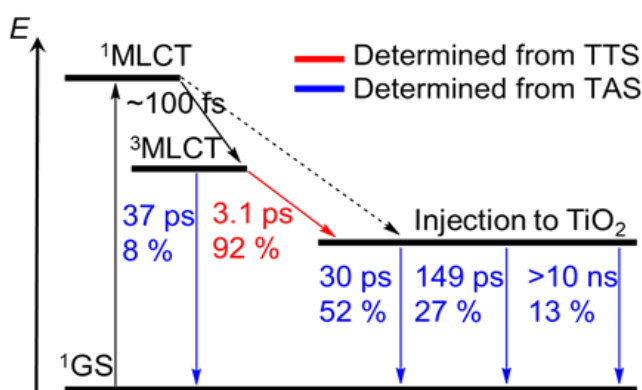
Figure 16. Jablonski diagram of the electronic states involved in photoinduced electron transfer between **10** and TiO_2, including time constants and quantum yields (in %).[109] The lifetime of the ^{3}MLCT with $\tau = 3.1$ ps and the 92 % conversion into the TiO_2 band were determined by TTS (red). All recombination processes were measured by TAS (red). (adopted from literature Ref 109)

These suggestions were confirmed by detailed studies of energy states with a carboxylic acid group functionalized tetracarbene iron complex **[10]$^{2+}$**.[12,37] By using techniques of TAS, DFT-calculations and transient terahertz spectroscopy (TTS), injection of photo generated electrons from the ^{3}MLCT into the conduction band of TiO_2 with a quantum yield of 92 % was proven (Figure 16).[109]

These findings led to the idea that the low performance of iron-based sensitizer may be limited due to

fast charge recombination as seen in the iron-carbene sensitized solar cells and therefore still offers the opportunity for development of dyes based on earth abundant metals for energy conversion. The MLCT lifetimes of iron(II) complexes like $[19]^{2-}$ are long enough for injection into the conduction band of TiO$_2$. Nevertheless, regeneration of the dyes and the long-term stability have to be improved.

The group of Jakubikova et al. calculated the properties of iron-based sensitizer for DSSC applications.[110,111] Their calculations on iron-based systems confirmed the suggestion of a competitive lifetime of MLCT- to MC-states that allows a charge injection into the TiO$_2$ conduction band. In addition, their studies showed that an iron complex with carbene-units could lead to long-living MLCT states.[20]

Table 1. List of key figures of prominent and presented dyes in DSSC applications under optimized conditions.

Dye	V_{OC} / V	I_{SC} / mA·cm^{-2}	ff	η / %
MK-2 (20)[70]	0.73	15.22	0.75	8.30
C219 (21)[71]	0.77	17.94	0.73	10.10
YD-2 (22)[72]	0.81	8.00	0.76	9.50
YD-2-o-C8 (23)[72]	0.94	17.66	0.74	12.30
SM315 (24)[72]	0.91	18.10	0.78	13.00
N719 ($[26]^{2-}$)[79]	0.85	17.73	0.72	11.20
N3 (1)[8]	0.72	18.20	0.73	10.00
black dye ($[27]^{3-}$)[58]	0.72	20.53	0.70	10.40
KD1 (28)[100]	0.53	10.40	0.62	4.50
Z907 (29)[63]	0.74	16.00	0.67	8.40
C106 ($[30]^{-}$)[62]	0.78	19.20	0.76	11.30
$[3]^{2+}$ [11]	0.49	0.48	0.62	0.15
YE05 ($[34]^{+}$)[58]	0.80	17.00	0.74	10.10
$[38]^{+}$ [99]	0.68	16.74	0.71	8.02
M3 ($[41]^{+}$)[100]	0.62	16.78	0.69	7.10
$[42]^{-}$ [101]	0.70	6.74	0.70	3.30
$[4]^{2+}$ [38]	0.25	0.02	0.50	0.01
$[10]^{2+}$ [38]	0.46	0.41	0.68	0.13

1.2.3 Electrolyte Tuning by Cobalt Complexes and Additives

The electrolyte plays a central role for the performance of a DSSC. Containing the redox mediator it is responsible for the regeneration of the dye and the transport of electrons from the cathode to the sensitizer. [112] The conditions for a good redox mediator are given by a low to no absorption in the visible light regime, high stability, a low redox potential, less to no interaction with the TiO_2 surface, slow recombination processes and environmental-compatibility. Ideally, the potential of the redox shuttle matches the dye ground state potential in order to regenerate the dye with minimal over potential, thus maximizing the photovoltage. [113] Additives like *tert*-butylpyridine (**TBP**), **LiClO4**, guanidine thiocyanate and many others can influence the performance of the electrolyte by decreasing the recombination rates between the redox couples or acting like co-adsorber by coordinating on the TiO_2 surface. Due to acid / base properties, such additives like **TBP** also have influence on the conductivity of the electrolyte. The concentrations of all involved compounds play a major role in the performance of the electrolyte and in the whole cell. A high concentrated redox mediator in the electrolyte does not always yield the best performance in a DSSC.

The most common redox mediator is the I^-/I_3^- redox couple. It is well soluble, has a low exctinction coeffiecent in the visible region, a suitable redox potential (I^-/I_3^- ($E_{1/2} = 0.32$ V vs NHE)), and provides rapid dye regeneration. With ruthenium dyes like **N719** or **C106** best performances were achieved. The redox chemistry of this redox couples is a complex system consisting of a number of one-electron processes and different kinetics (Figure 17). [112]

V vs NHE

$$I_3^- + e^- = I_2^{-\cdot} + I^-$$
$$E^0(I_3^-/I_2^{-\cdot}) > -0.35 \text{ V}$$

$$I_2 + e^- = I_2^{-\cdot}$$

$$I_3^- + 2\,e^- = 3\,I^-$$
$$E^0(I_3^-/I^-) = 0.35 \text{ V}$$

$$I_2 + 2\,e^- = 2\,I^-$$
$$E^0(I_2^-/I^-) = 0.93 \text{ V}$$

$$3\,I_2 + 2\,e^- = 2\,I_3^-$$

$$I_2^{-\cdot} + e^- = 2\,I^-$$

$$I^{\cdot} + e^- = I^-$$
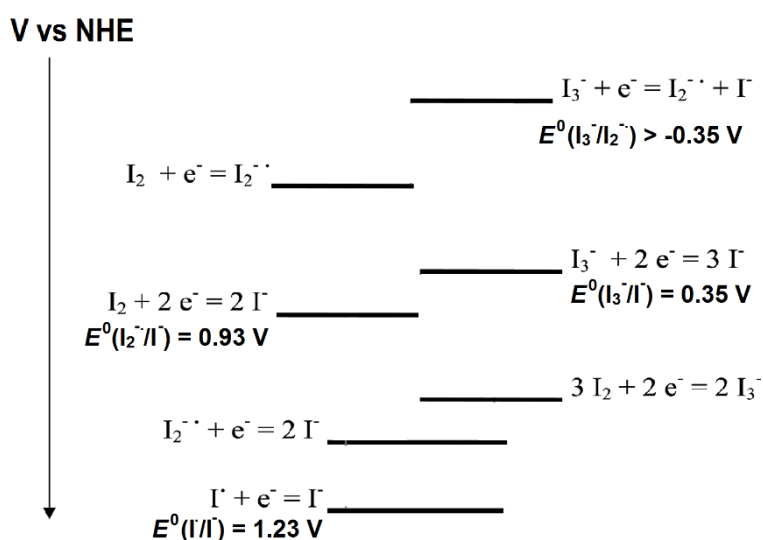$$E^0(I^{\cdot}/I^-) = 1.23 \text{ V}$$

Figure 17. Redox reactions of iodide system and their relative redox potentials. Potential values for some important reactions are given for measurements in acetonitrile. [112] (adopted from literature Ref 112)

Despite its good properties, this redox couple has some disadvantages. First to mention is its corrosive attributes and the aggressiveness especially towards silver which is often-used as cathode. This prevents the use of I^-/I_3^- redox mediator in combination with silver. When employed in high concentrations the absorption in the visible range of $\lambda = 350{-}400$ nm of iodide/triiodide is quite high compared to other redox mediators like cobalt complexes.[96,114] By using positively charged sensitizers, the negatively charged redox couple interacts with the dye and provides charge recombining processes via electrostatic attraction.[115] In addition, the low redox potential limits the open-circuit voltage to a maximum of only 1 V.

In order to avoid the negative aspects of the iodide redox mediator, cobalt complexes offer an interesting alternative.[115,116,114] In contrast to the two electron transfer processes of iodide/triiodide, cobalt complexes have simple single electron processes, which may require less effort for the dye regeneration and reduces the loss in the open-circuit voltage. The SCO behavior of the cobalt(II,III) complexes enables four different electronic configurations. For each oxidation state two spin states are possible. In principle, both hs and ls Co^{+II} species can regenerate the dye. The self-exchange through these different high-spin and low-spin states can slow down the recombination between the Co^{+II} and Co^{+III} species and restricts the kinetics of the regeneration process.[117] Thereby the most attractive feature of cobalt redox shuttles is the tunability via ligand design with electron rich/poor building blocks to influence their redox potential or the ligand field strength through bite-angle tuning which influences the internal electron conversion (SCO) (Scheme 10). Addition of sterically demanding groups at the cobalt complex decreases charge recombining processes by less interaction between the TiO_2 surface and affects the solubility as well as the anion exchange. The larger the complexes are, the slower are the kinetic processes of the electrolyte and the recombination time.[118,119]

$[43]^{2+/3+}$ $[44]^{2+/3+}$ $[45]^{2+/3+}$

$E_{1/2}= 0.65$ V $E_{1/2}= 0.86$ V $E_{1/2}= 0.52$ V
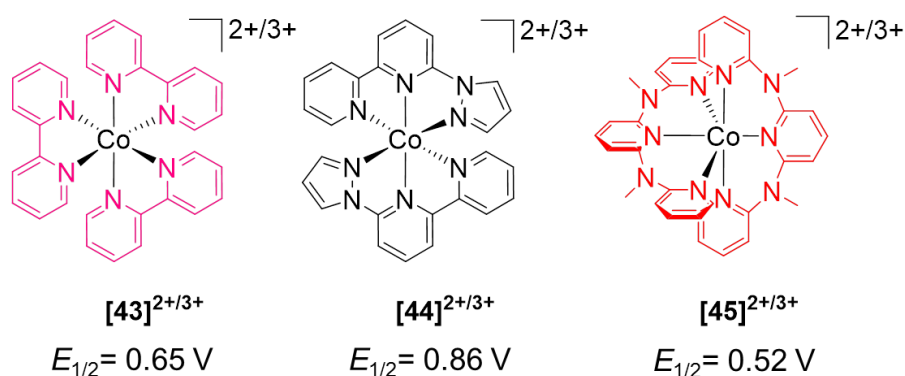
Scheme 10. Cobalt(II,III) redox mediators and their redox potentials. (References vs NHE)[73,102,116]

The currently best performance of 13 % efficiency of a DSSC was achieved by using
$[Co(bpy)_3]^{2+/3+}$ ($[43]^{2+/3+}$) with a redox potential of $E_{1/2} = 0.65$ V vs NHE in combination with
a porphyrin dye. [73] Although some ruthenium dyes, e.g. **Z907** provide similar efficiencies
with cobalt ($\eta = 6.5$ %) as iodide I_3^-/I^- redox couples ($\eta = 7.7$ %), most applications with
ruthenium-based dyes show poorer performances.[120,121]

In addition to the above mentioned redox mediators, there is still a large number of further
compounds, which are briefly summarized below. First to mention are bromide/tribromide
and pseudohalides (SCN^-/SCN_3^-, $SeCN^-/SeCN_3^-$), which have similar chemistry and
drawbacks as I^-/I_3^-.[122,123,124] A $SeCN^-$-based ionic liquid electrolyte delivered an impressive
performance in terms of stability and efficiency.[124]

Beside cobalt complexes other one-electron redox systems like copper complexes and organic
mediators are also possible alternatives.[125,126] Ferrocene offers a possibility for dyes which
require rapid recombination, but passivation of the TiO_2 surface by polysiloxane is needed. [127]
Besides these approaches many other compounds were tested as redox couples like
$[Fe(CN)_6]^{3-}/[Fe(CN)_6]^{4-}$ ($[13]^{3-/4-}$) but resulted in poor performances.[128] Nonetheless, all
these applications showed that it is possible to construct simple DSSCs with low efficiencies
but without the need of expensive components.

The most important approach to get rid of the problems involved in liquid containing
applications was to replace the liquid electrolyte by a solid-state organic hole conductor, such
as 2,2′,7,7′-tetrakis-(*N*,*N*-di-*p*-methoxyphenylamine) 9,9′-spirobifluorene (spiro-MeOTAD)
shown by Grätzel and co-workers.[129] This approach should solve a serious problem for
DSSCs. Having a fluid inside, the cells are susceptible for many defects like a change of the
aggregation due to freezing or evaporation under thermal conditions or draining of the
electrolyte by structural defects. Especially, the corrosive I^-/I_3^- solution or the toxic properties
of cobalt compounds are not favorable.

However, the implementation of the cobalt redox couple in a polymer may also be an
adequate key to get rid of numerous problems. This approach replaces the liquid component
in the application and reduces degradation processes in the cell.

1.3 Light-Emitting Electrochemical Cell (LEC)

The light-emitting electrochemical cell provides a low cost approach to achieving light emission from semiconducting, luminescent polymers and metalorganic emitters.[5,130,131] The LEC was invented 1995 by Pei and co-workers, when they mixed an inorganic salt to a mixture of a conjugated luminescent polymer and an ionic conductive polymer.[130] It combines the electrochemical properties of conjugated polymers with the ionic conductivity of polymer electrolytes.[132] In contrast to conventional organic light-emitting diodes (OLEDs) the architecture of LECs is much simpler and does not rely on air-sensitive charge-injection layers or metals for electron injection. While the OLED is based on a multi-layer structure with up to 15 layers and includes high costs, a LEC can consist of only three to five layers (Figure 18a).[133] The emitting-layer of OLEDs is neutral and in LEC it is ionic. This is caused by the fact, that the working principle of OLEDs is quite different to that of LECs. For OLEDs every layer has one specific function such as electron injection, transport, emitting layer, hole transport, etc.. LECs combine these number of processes fixed in one layer with thickness between 100 and 200 nm, which is sandwiched between two electrodes. One advantage is that airstable electrodes like gold, silver or aluminum can be used.[134] To enable light output, the material of the anode must be a transparent conductor, so ITO or FTO are commonly used.
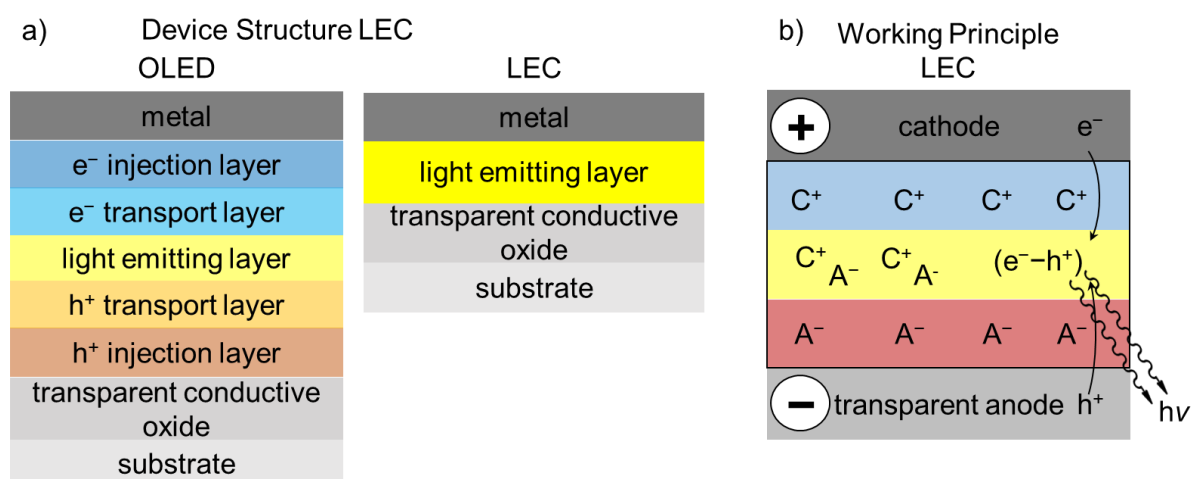
Figure 18. a) Schemtatic representation of a conventional OLED (left) and LEC (right). b) Working principle of a LEC. The light-emitting layer is divided into the cation C^+ (blue), anion A^- (red) and recombination (yellow) area.[5] (adopted from literature Ref5)

Conventional metal/polymer/metal light-emitting diodes (LEDs) are dual carrier devices in which electrons and holes are injected at the cathode and anode, respectively, into the undoped semiconducting polymer.[135] LEC applications follow nearly the same principle. In

the emitting-layer, the cations C^+ and the anions A^- are mixed up but start to separate by applying a voltage. The positively charged cations migrate towards the cathode, the negatively charged anions towards the anode. Thanks to this charge separation, electrons and holes can move easily through the layer, which allows a lower operating voltage. When electrons and holes meet, recombination occurs via excited electron-hole pairs, so-called exitons. The relaxation of these excited species results in photon emission (Figure 18b).[140]

Another difference between LECs and OLEDs is in the theoretical limit of quatum efficiency. While organic emitters only harvest singlet excitons and convert them into photons, triplet excitons only produce heat. Simple spin statistics predict that 25 % of the excitons are singlet excitons and 75 % are triplet excitons.[136,137] LECs generate light from both triplet and singlet excitons, allowing the internal quantum efficiency of such devices to reach nearly 100 %.[138]

The quality of an emitter for a light-emitting device is determined by the internal quantum efficiency (IQE), which is the ratio of the number of electron-hole pairs generated by light to the number of photons absorbed in the cell given by equation 4:[139]

$$\text{Eq. 4: } IQE = \frac{\#generated\ hole-pairs}{\#number\ of\ absorbed\ photons}$$

Since not all photons generated from the emitter can emerge from the cell due to various factors such as reabsorption, reflection at the anode and substrate, or other reasons, the external quantum efficiency (EQE) is determined to specify the quality of a whole cell by the following equation 5:[140]

$$\text{Eq. 5: } EQE = \frac{\#photons\ out}{\#electrons}$$

One of the first emitter and often used as a reference in LEC applications was the ruthenium(II) complex **[5]$^{2+}$** with an impressive efficiency of 10 lm·W^{-1}, which was the highest efficiency reported in a single layer electroluminescent device at that time.[140] Nowadays iridium(III) based emitters like **[Ir(ppy)$_2$(bpy)]$^+$** complexes are used in the majority of LECs, OLEDs and PHOLEDs (phosphorescence organic light-emitting diode).[134] This is reasoned by the fact that the ligand field splitting in 5d metals is much higher whereby the accessibility of ^{3}MC-states is remarkably reduced and not in competition to the ^{3}MLCT-state which increases emissive relaxations into the ground state. Furthermore, ^{3}MC states have a dissociative characteristic, so the photostabilities of these emitters are increased too. This larger ligand-field splitting enables even more tuning possibilities to control the lowest excited state by modifying the symmetry and inductive influence of a ligand with different substituents, thus achieves more colors of emission.[141]

1.3.1 The First Emitting Iron Complex

However, in contrast to iron metals like ruthenium, iridium or rhenium are very expensive and rare, which is why iron is an ideal substitute. In 2017, Wärnmark, Persson and Sunström published an iron(III) complex which emitts in the visible region at room temperature.[142] Their attempt to achieve a bidentate homoleptic iron(II) complex based on carbene donor atoms from the **btz** ligand [btz = 3,3′-dimethyl-1,1′-bis(p-tolyl)-4,4′-bis(1,2,3-triazol-5-ylidene)] (**46^{2+}**) resulted in an oxidation to iron(III) reasonable by its low half potential of $E_{1/2}$= −0.58 V vs FcH/FcH$^+$ (Figure 19a). The **btz** ligand features σ-donor and π-acceptor electron properties and causes the the low redox potential of the iron center by its strong electron-donating nature. The **[Fe(btz)$_3$]$^{3+}$** (**[47]$^{3+}$**) complex has a rose red colors by weak absorptions in the visible region at λ_{max}= 384, 528, 558 nm with exctinction coefficients lower than $\varepsilon = 2000$ M^{-1}·cm^{-1} in CH$_3$CN. The lowest energy bands are ascribed to a LMCT transition from the iron(III) GS. The lifetime of this ^{2}LMCT state is determined as $\tau = 100$ ps. **[47]$^{3+}$** is able to weakly emit light via an excitation in the lowest band (λ_{exc}= 558 nm) at λ_{em}= 600 nm (quantum yield $\Phi = (3 \pm 0.5)\cdot10^{-4}$) in CH$_3$CN at room temperature. Only a few complexes containing metals rhenium(II) and technetium(II) display LMCT emission.[143,144]
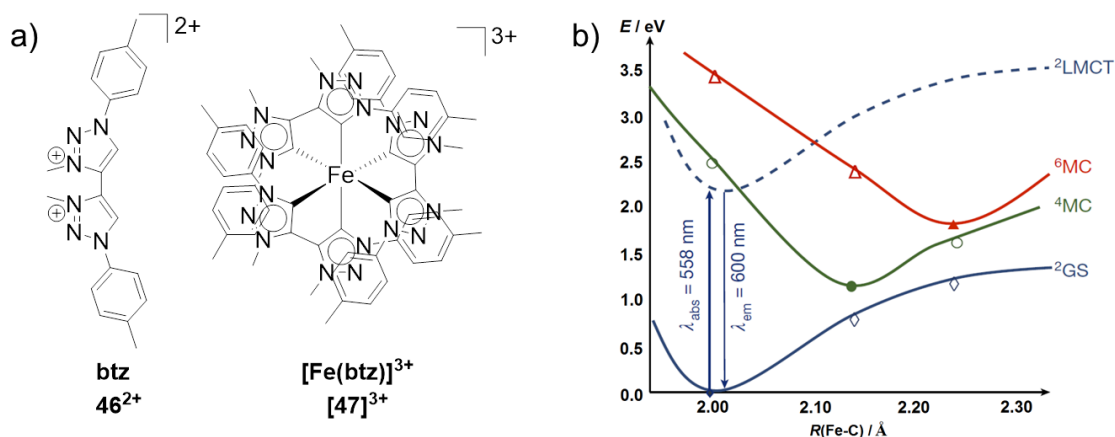
Figure 19. a) Structures of the **btz 46^{2+}** ligand and the **[Fe(btz)$_3$]$^{3+}$** complex **[47]$^{2+}$**. b) Calculated potential energy state diagram of **[47]$^{3+}$**.[142] (adopted from literature Ref 144)

The rigid structure and electronic properties provided by the carbene ligands prevent intersystem crossing to ground state or excited states and prohibits the large energy-reducing metal-centered transitions. This enables the observation of spin-allowed ^{2}LMCT emission directly to the ls iron(III) ground state and could be exploited in photochemical reactions on surfaces (hole injection into semiconductors). So this air and moisture stable

compound constitutes a new class of emitting compounds and starts the run on further iron-based complexes for use as light emitters and photosensitizers.

1.4 Push-Pull Concept, Bite-Angle Tuning and Symmetry Effects

As we can see from the previous chapters, the design of the complex is decisive for its properties as a chromophore. Especially when focusing on iron(II) complexes all concepts must fit. The most important property is long-term stability, which can be increased by the use of tridentate ligands. This reduces substitutent reactions by nucleophiles or degradation by irradiation.[92] Furthermore, tridentate coordination of C_2-symmetric ligands simplifies the synthesis giving bis(tridentate) achiral complexes which prevents isomers in case of different functionalized C_2-symmetric ligands.[145,146] However, it is found that these can also have negative effects on the properties as chromophore. This was demonstrated clearly by examples of ruthenium chemistry in the comparison of **N719** and a dye with a tridentate ligand **[32]**$^{2+}$ with respect to the DSSC application, as well as in the area of the emitters, where the bpy-complex **[5]**$^{2+}$ yields far better quantum yields ($\Phi = 6.4$ %) and excited state lifetimes ($\tau = 1.1$ µs) than its **[7]**$^{2+}$ tpy-analogues ($\Phi = 0.005$ %; $\tau = 0.1 - 0.2$ ns) (Scheme 1).[17,147,148,149,150]

Three strategies are particularly effective to improve the properties of emissive excited states with tridentate ligands.

1. Increasing the metal-ligand orbital overlap by adjusting the bite-angles L-M-L to ~90° via an enlargement of the five-membered chelate ring to a six-membered one.
2. Use of a heteroleptic complex with an electron-rich (donor) and an electron-poor (acceptor) ligand to create a push-pull system.
3. Reducing the symmetry of the complex to stabilize the MLCT states.

To obviate the negative properties of tpy ligands, Hammarström presented a strategy of increasing the ligand field strength and the energy of the ^{3}MC state by making the complex more octahedral.[151] By inserting of a methylene group between two pyridine rings in the tpy ligand six-membered chelate was formed. An increasing of the N-Ru-N bite-angle from 78° (**tpy**) to ~91° at the methylene-bridged coordination was achieved resulting in much longer excited state lifetimes ($\tau = 15$ ns) compared to **[7]**$^{2+}$.[152] Further development delivered a near octahedral homoleptic bis(tridentate) ruthenium complex with only six-membered chelates through a 2,6-bis(8'-quinolinyl)pyridine ligand. Owing to the bite-angles of ~90°, an excited state lifetime in oxygen-free environment of $\tau = 3$ µs ($\Phi = 2$ %) at room temperature was achieved. Studies on two cyclometalated heteroleptic ruthenium complexes, one with a five-membered ($\tau = 1.8$ ns) and one with a six-membered ($\tau = 16$ ns) ligand finally evidenced the advantages of complete octahedral coordination.[153]

Similar to the mentioned iron(II) complex of McCusker ([**17**]$^{2+}$), the working group of Ruben synthesized a homoleptic bis(tridentate) ruthenium complex with the **dcpp** ligand.[56,57,154] Due to carbonyl bridged pyridine rings, which decreases the energy of the π^* orbital of the ligand (LUMO), and a large bite angle of ~90°, this six-membered chelate complex achieves a quantum yield of 13% and emission lifetimes of $\tau = 1.36$ μs at room temperature and in the presence of oxygen.[154] In an oxygen-free environment this complex has a long lived ^{3}MLCT state of $\tau = 3.3$ μs and the highest room temperature quantum yield ($\Phi = 30\%$) reported to date among bis(tridentate) ruthenium(II) complexes. Nevertheless, the iron(II) congener mentioned before was not emissive so further tuning techniques to achieve emitting iron complexes are required.

Fine-tuning of HOMO and LUMO energies in the complexes systems seems to be an adequate answer. Attaching an electron withdrawing substituent lowers the energy of the ligand π^*-orbitals and thus the energy of the MLCT states relative to the deactivating MC states. Several approaches showed increased lifetimes and quantum yields compared to unsubstituted congeners.[149,155,156,157]

On the other hand, implementation of an electron-donating substituent at the second chelate ligand raises the energy of the HOMO-level of the complex. In combination with an electron withdrawing ligand a *push-pull* system is created, in which the energy gap between the HOMO, t_{2g} of the metal or π-orbitals of the electron donating ligand, and the LUMO, π^*-orbitals of the electron accepting ligand, is decreased. When the t_{2g} level is the HOMO, a transition from the metal to the acceptor ligand results, the *pull* effect. This MLCT state is stabilized by the electron-donating ligand due to its high electron density, the *push* effect. If the HOMO results from π-orbitals of the electron donating ligand the charge transfer would be a ligand-to-ligand charge transfer (LL'CT). In summary, the *push-pull* concept means that the electron-withdrawing ligand pulls the electrons towards itself and the electron-donating ligand pushes the electrons to the areas with the missing electron density. As result, the MLCT- or LL'CT-lifetimes should increase. For completely five-membered **tpy** systems, Heinze et al. improved the emission properties of ruthenium(II) chromophores using the *push-pull* concept (Figure 20a and b).[158,159]
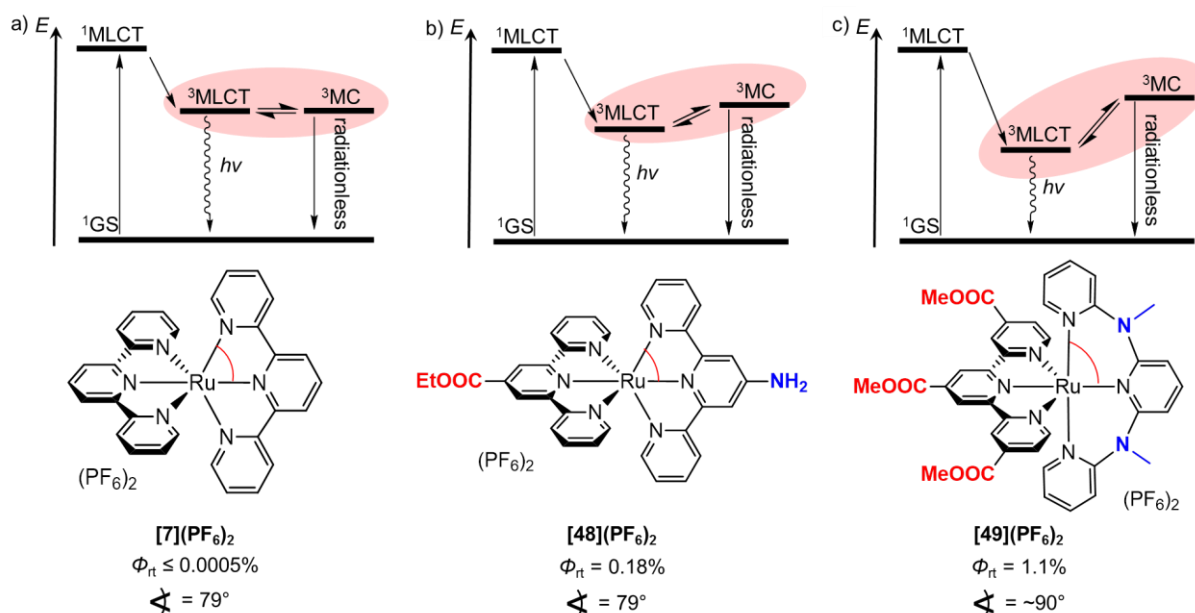
Figure 20. a) shows complex **[7]**(PF$_6$)$_2$. The small bite angle of 79° (marked red) and missing *push-pull* effect result in a low quantum efficiency. The ^{3}MLCT and ^{3}MC are in competition b) shows **[48]**(PF$_6$)$_2$. The structure is similar to **[7]**$^{2+}$ but is *push-pull* substituted by electron-rich NH$_2$ and electron- withdrawing COOEt moieties which results in a higher quantum yield due to the higher energy gap between ^{3}MLCT and ^{3}MC. c) shows complex **[49]**(PF$_6$)$_2$. The push-pull effect is even stronger due to more electron-rich and electron-withdrawing moieties. Additionally, the larger bite angle of 90° enlarges the energy gap between ^{3}MLCT and ^{3}MC and leads to the highest quantum yield in this series.[158,160]

Breivogel and Heinze demonstrated that the combination of bite angle tuning (~90°) due to the six-membered chelate **Me$_2$tpda 31** ligand and *push-pull* effects leads to favorable separation of ^{3}MLCT- and ^{3}MC-states providing useful photophysical properties in **[Ru(Me$_2$tpda)(tpyX)]** complexes (X = COOR) like **[49]**$^{2+}$ (Figure 20c) .[160] Similar to the carbonyl-bridged **dcpp** ligand, the large bite angle at the **Me$_2$tpda** system is achieved by methylamine bridged pyridine rings which leads to a six-membered chelate. Additionally, the amine units are electron-rich providing electron-donating character and a *push*-effect. Via carboxylic acids, the **tpy** ligand gets its electron-withdrawing properties and provides the *pull*-effect.[160]

Based on this work, Mengel and Heinze presented a heteroleptic iron(II) complex with the strongly electron withdrawing **dcpp** and electron-donating **Me$_2$tpda** ligand. The complex features a broad absorption in the visible spectra region combined with high stability and a strong ligand field splitting and a short ground state recovery after excitation of $\tau = 548$ ps.[161] DFT calculations predicted a large energy difference of 280 kJ·mol^{-1} between excited ^{1}MLCT

and [1]LF states, but no emission was noted. Obviously, the difference between [3]MLCT, [3]MC and [5]MC states are smaller.

Alternative ways by tuning of the ligands were suggested by a series of theoretical studies.[20,110,111] These DFT-calculations on iron(II)-based systems confirm the correctness of the approaches of bite angle tuning and the introduction of *push-pull* systems.[20,92] Dixon et. al. pointed out that a bridged biscarbene should deliver low-lying [3]MLCT states.[162] Additionally they showed the possibility of low-lying [3]MLCT states by cyclometalation of polypyridyl iron(II) complexes.[163,164] In such systems, the excited states can be influenced by a corresponding reduction of the geometry in favor of a low-energy [3]MLCT state (Figure 21).[165]
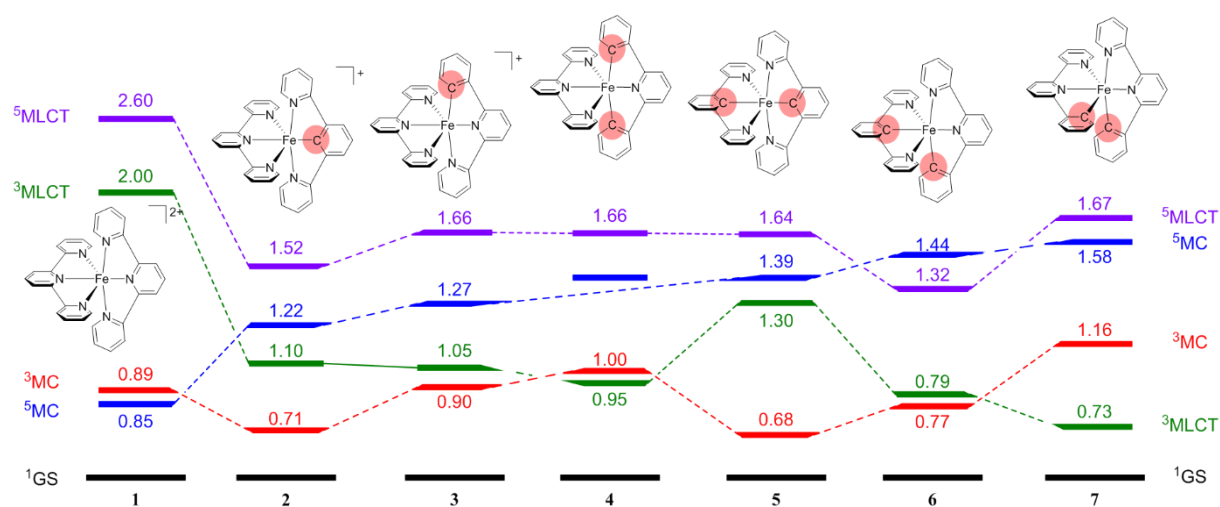
Figure 21. The Jablonski diagram shows the energy of important excited states when the geometry is changed. The [1]GS energies are set at zero for all complexes.[165] (adopted from literature Ref 165)

2 Aim of the Work

Primary aim of the work is to find strategies for 3d metal chromophores based on iron(II). As shown in the literature, the design to emissive iron polypyridyl complexes is challenging. Several approaches give ideas for concepts yielding a low-lying [3]MLCT. A strong ligand field stabilized by a suitable push-pull system, optimized bite angle of 90° and long-term stability are basic conditions for a successful application. To achieve these properties, the design of the ligand plays an important role. In a number of polypyridyl ruthenium(II) complexes, our group could prove the tunability of excited states by these concepts.

Wärnmark & Sundström $[9]^{2+}$

McCusker $[17]^{2+}$

Heinze $[32]^{2+}$
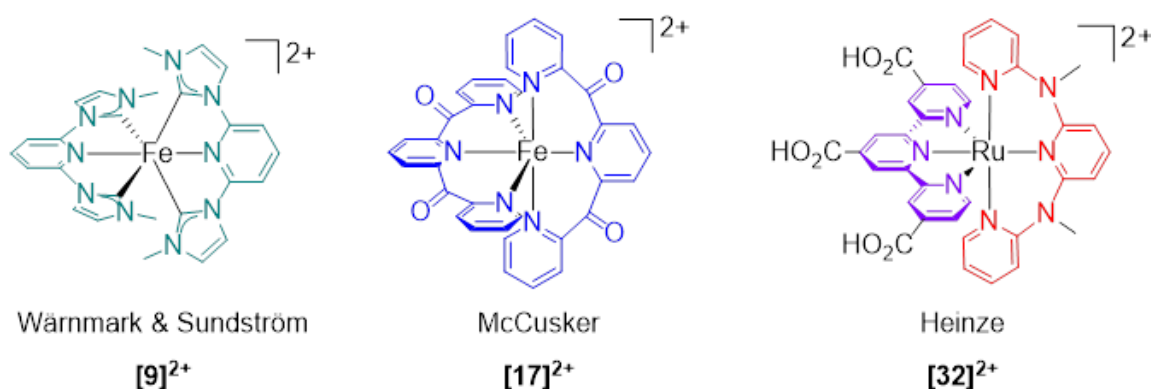
Scheme 11. Different popular concepts (carbene ligand, bite angle, push-pull) towards long-lived [3]MLCT states.[35,56,92]

Using density functional theories, several studies suggested the possibility of low-lying [3]MLCT states in iron(II) complexes by employing a lower symmetry, implementation of push-pull systems and the concept of bite angle tuning. Hereby, a series of novel polypyridyl iron(II) complexes based on the **Me₂tpda** ligand backbone were developed (Scheme 12). The nature of these promising iron chromophores will be presented in detail in chapter 3.1 and 3.2.

50: **H₂tpda**: R = H
31: **Me₂tpda**: R = Me
51: **Pr₂tpda**: R = nPr
52: **Hex₂tpda**: R = nHex

Scheme 12. Variation of ligand **31** for different aims.

The second aspect of this work is the application and tuning of DSSCs via suitable electrolytes and dyes. Most ruthenium(II) dyes in combination with cobalt(II,III) electrolytes showed poor efficiencies. Our aim was to replace the corrosive I_3^-/I^- redox couple by a cobalt(II,III) based redox mediator invented by Mack and Heinze (Scheme 13). The lower absorption and the higher redox potential of cobalt(II,III) should deliver better performances in application of DSSCs.

Previously used ruthenium dyes published by Breivogel and Heinze evidenced poor efficiencies in DSSC applications using standard setup like I^-/I_3^- electrolytes. One of these dyes ($[32]^{2+}$) was modified through deprotonation and tested in combination with different electrolyte mixtures of additives such as TBP or $LiClO_4$ and a common cobalt(II,III) redox shuttle. Addition of a co-adsorber should prevent charge recombination processes through possible interaction between electrolyte and TiO_2 (Scheme 13). The results of this work will be presented in chapter 3.3.

$[43]^{2+/3+}$ $[45]^{2+/3+}$ BARF [54]⁻   CDCA 33
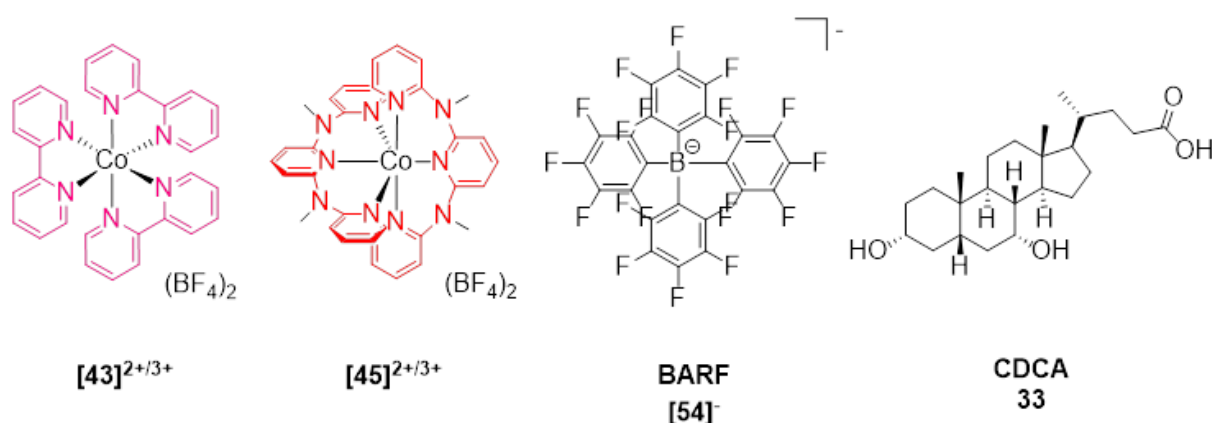
Scheme 13. Common and novel cobalt redox shuttles, weak coordinating anion BARF and co-adsorber CDCA for different DSSC setups.

Furthermore, the concept of cyclometalation gave impressive performances in DSSC applications. A number of cyclometalated ruthenium(II) dyes published by Zhong and co-workers seemed to be a promising alternative to common dyes. These dyes are based on the same poylpyridyl scaffold, but the donating substituents are different. The performance of the different donor abilities in DSSCs will be studied and discussed in chapter 3.4. The influence of replacing the BF4-anion by the weak coordinating anion tetrakis(pentafluorophenyl)borate (**BARF**) on the performance of the DSSC will be investigated.

3 Results and Discussion

The results of my doctoral thesis have been published as scientific articles in peer-reviewed journals. These articles will be reprinted under permission of the respective publishers. The publications are listed from chapter 3.1 to 3.4, the supporting information can be found in chapter 5.1 to 5.4. To clarify which parts stem from collaborators and which contributions stem from my own work, I listed the contributions of the authors in front of the publications.

3.1 RESULTS AND DISCUSSION: A HETEROLEPTIC PUSH–PULL SUBSTITUTED
IRON(II) BIS(TRIDENTATE) COMPLEX WITH LOW-ENERGY CHARGE-
TRANSFER STATES

43

3.1 "A Heteroleptic Push–Pull Substituted Iron(II) Bis(tridentate) Complex with Low-Energy Charge-Transfer States"

Andreas K. C. Mengel, Christoph Förster, Aaron Breivogel, Katharina Mack, Julian R. Ochsmann, Frédéric Laquai, Vadim Ksenofontov and Katja Heinze

Chem. Eur J. **2015**, *21*, 704–714.
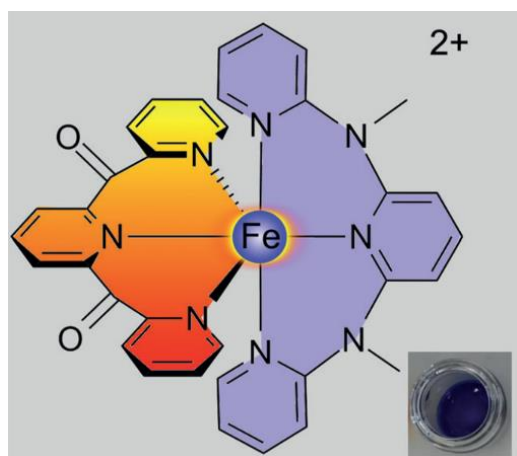
All iron complexes were synthesized and spectroscopically and analytically characterized by Andreas K. C. Mengel. The DFT calculations were conducted by A. K. C. Mengel and ███████████████. The manuscript was written by ████████████████. ████████████████ developed the ddpd-ligand in his PhD theses (████████: *Ruthenium-based Light Harvesting Complexes.* Mainz, **2014**) and ████████████ synthesized the homoleptic $[Fe(ddpd)_2]^{2+}$ complex in her diploma theses (██████: *Neue Übergangsmetall-Komplexe des N,N´-dimethyl-N,N´-dipyridin-2-ylpyridin-2,6-diamins.* Mainz, **2012**). ██ ████████████ solved the crystal structures. ████████████████ measured the Mössbauer spectra. Transient absorption spectroscopy was measured ████████████████████ (group of ████████████████ Mainz).

3.1 RESULTS AND DISCUSSION: A HETEROLEPTIC PUSH–PULL SUBSTITUTED
IRON(II) BIS(TRIDENTATE) COMPLEX WITH LOW-ENERGY CHARGE-
TRANSFER STATES

44

■ **Iron Complexes**

A Heteroleptic Push–Pull Substituted Iron(II) Bis(tridentate) Complex with Low-Energy Charge-Transfer States

Andreas K. C. Mengel,[a] Christoph Förster,[a] Aaron Breivogel,[a] Katharina Mack,[a] Julian R. Ochsmann,[b] Frédéric Laquai,[b] Vadim Ksenofontov,[a] and Katja Heinze*[a]

Abstract: A heteroleptic iron(II) complex $[Fe(dcpp)(ddpd)]^{2+}$ with a strongly electron-withdrawing ligand (dcpp, 2,6-bis(2-carboxypyridyl)pyridine) and a strongly electron-donating tridentate tripyridine ligand (ddpd, N,N'-dimethyl-N,N'-dipyridine-2-yl-pyridine-2,6-diamine) is reported. Both ligands form six-membered chelate rings with the iron center, inducing a strong ligand field. This results in a high-energy, high-spin state ($^5T_2$, $(t_{2g})^4(e_g{}^*)^2$) and a low-spin ground state ($^1A_1$, $(t_{2g})^6(e_g{}^*)^0$). The intermediate triplet spin state ($^3T_1$, $(t_{2g})^5(e_g{}^*)^1$) is suggested to be between these states on the basis of the rapid dynamics after photoexcitation. The low-energy π^* or-bitals of dcpp allow low-energy MLCT absorption plus additional low-energy LL'CT absorptions from ddpd to dcpp. The directional charge-transfer character is probed by electrochemical and optical analyses, Mößbauer spectroscopy, and EPR spectroscopy of the adjacent redox states $[Fe(dcpp)(ddpd)]^{3+}$ and $[Fe(dcpp)(ddpd)]^+$, augmented by density functional calculations. The combined effect of push–pull substitution and the strong ligand field paves the way for long-lived charge-transfer states in iron(II) complexes.

Introduction

The photophysics and photochemistry of six-coordinate d⁶ metal complexes with oligopyridine ligands has been studied intensively in recent years, especially with respect to excited-state dynamics.[1] There is a fundamental difference between iron(II) (3d metal) and ruthenium(II) (4d metal) complexes, namely, the magnitude of the ligand field strength.[2] As the ligand field splitting in complexes of first-row metals is generally significantly smaller than in homologous second-row metal complexes of the same ligand set, iron(II) complexes with an appropriate ligand environment can display spin-crossover (SCO) behavior between low-spin $(t_{2g})^6(e_g{}^*)^0$ and high-spin $(t_{2g})^4(e_g{}^*)^2$ states ($^1A_1$ and $^5T_2$ in octahedral symmetry),[3] whereas the ground state of ruthenium(II) complexes is always low-spin ($^1A_1$). Triplet terms arising from the $(t_{2g})^5(e_g{}^*)^1$ electron configuration ($^3T_1$ and $^3T_2$) appear as additional levels, for example, in reverse-LIESST processes from $^5T_2 \rightarrow {}^5E$ excitations in SCO complexes (LIESST = light-induced excited spin state trap-ping).[4] Furthermore, these metal-centered triplet states play a decisive role in the radiationless deactivation of metal-to-ligand charge transfer states (^{3}MLCT), diminishing (Ru) or impeding (Fe) emissive processes (phosphorescence) from ^{3}MLCT states.[5] Hence, iron(II) complexes have attracted considerable interest with respect to their magnetic properties, especially in thermal or optical switching processes, whereas ruthenium(II) complexes dominate the field with respect to photoinduced electron transfer and energy transfer, leading to applications in photocatalysis and light-to-energy as well as energy-to-light conversion schemes.

For Ru^{II} complexes, large bite angles and electronically distinct push–pull substituted ligands have been successful in increasing the ^{3}MLCT/$^3T_1$ energy gap (the high-spin state $^5T_2$ plays no role in Ru^{II} complexes because of its high energy), elongating the ^{3}MLCT lifetime, and culminating in long-lived room-temperature phosphorescence.[6–8] Conceptually, our group has focused on the combined action of lowering the ^{1,3}MLCT states by employing ligands with push–pull character, and of raising the energy of ligand field states $^3T_1/^3T_2$ by using stronger donors and large bite angles to increase the ligand field splitting.[8] This has led to (photo)substitutionally stable heteroleptic ruthenium(II) complexes with two tridentate ligands featuring low-energy phosphorescence up to $\lambda_{max} =$ 788 nm and ^{3}MLCT lifetimes up to $\tau = 841$ ns.[8,9] Light-emitting electrochemical cells using these complexes indeed display red to near-infrared electroluminescence.[10]

Room-temperature phosphorescent iron(II) complexes are so far unknown owing to the ultrafast departure from the ^{3}MLCT state probably to ^{3}T states[11] and finally to the $^5T_2$ state. In the $[Fe(bpy)_3]^{2+}$ complex (bpy = 2,2′-bipyridine) the ^{1}MLCT $\rightarrow$

[a] A. K. C. Mengel, Dr. C. Förster, Dr. A. Breivogel, K. Mack, Dr. V. Ksenofontov, Prof. Dr. K. Heinze
Institute of Inorganic Chemistry and Analytical Chemistry
Johannes Gutenberg-University of Mainz
Duesbergweg 10-14, 55128 Mainz (Germany)
Fax: (+49)6131-39-27-277
E-mail: katja.heinze@uni-mainz.de

[b] J. R. Ochsmann, Dr. F. Laquai
Max Planck Research Group for Organic Optoelectronics
Max Planck Institute for Polymer Research
Ackermannweg 10, 55128 Mainz (Germany)

Supporting information for this article is available on the WWW under
http://dx.doi.org/10.1002/chem.201404955.

3.1 RESULTS AND DISCUSSION: A HETEROLEPTIC PUSH–PULL SUBSTITUTED
IRON(II) BIS(TRIDENTATE) COMPLEX WITH LOW-ENERGY CHARGE-
TRANSFER STATES

45

[3]MLCT intersystem crossing (ISC) has been shown to be ultra-fast ($\tau < 20$ fs) in the non-Born–Oppenheimer regime, and the lifetime of the [3]MLCT state amounts to only $\tau = 120$ fs.[12] In the classical SCO complex [Fe(ptz)$_6$](BF$_4$)$_2$ (ptz = 1-propyl tetrazole), the [3]T$_1$ state has recently been addressed by reverse-LIESST ([5]T$_2\rightarrow$[5]E excitation and ISC to [3]T$_1$). Its lifetime at 125 K in a crystalline zinc host was reported as $\tau = 39$ ps.[4]

So far, the design of a ligand set that places the [3]MLCT states below the ligand field states [3]T$_1$/[3]T$_2$ in iron(II) complexes has not yet been achieved, although a record [3]MLCT lifetime of $\tau = 9$ ps has been reported for an octahedral tetracarbene [Fe(CNC)$_2$][2+] complex (CNC = 2,6-bis(imidazol-2-ylidene)pyridine).[13] DFT calculations predict a [3]T$_{1/2}$ state below the [5]T$_2$ state in neutral [Fe(NCN)$_2$] complexes with tridentate cyclometalating ligands (NCN = 2,5-dipyridylbenzene).[14] With the use of large bite angles of the electron-poor 2,6-bis(2-carboxypyridyl)pyridine ligand (dcpp), the homoleptic [Fe(dcpp)$_2$][2+] complex **3[2+]** has been suggested to be close to the [3]T$_1$/[5]T$_2$ crossing point, that is, the [3]T$_1$ state is similar to or indeed even lower than the [5]T$_2$ state in energy, preventing an arrival at the [5]T$_2$ state.[15] This has been proposed on the basis of the small time constant ($\tau = 280$ ps) for the ground-state recovery after 620 nm excitation, which has been attributed to a low barrier for the [3]T$_1\rightarrow$[1]A$_1$ relaxation. This low [3]T$_1\rightarrow$[1]A$_1$ barrier is opposed to the typically observed larger barrier for the [5]T$_2\rightarrow$[1]A$_1$ relaxation in oligopyrine iron(II) complexes with its associated higher net spin change, for example, in [Fe(tpy)$_2$][2+] ($\tau = 5350$ ps, tpy = 2,2′;6′,2″-terpyridine).[15] In addition, with the dcpp ligand set, the corresponding [Ru(dcpp)$_2$][2+] complex has been reported to feature low-energy [1]MLCT absorptions, exceptionally long [3]MLCT lifetimes, and high quantum yields.[7]

Although the initial excited-state deactivation in diimine iron(II) complexes occurs on an ultrafast timescale, electron transfer from excited Fe[II] complexes (presumably from hot [1/3]MLCT states) has been reported: interfacial electron injection into TiO$_2$ seems to occur from MLCT states in Fe(4,4′-bpy-(COOH)$_2$)$_2$(CN)$_2$ near the sub-picosecond regime.[16] Photosensitization of TiO$_2$ has also been reported for [Fe(CN)$_6$][4−]@TiO$_2$.[17,18] Even bimolecular oxidative photoinduced electron transfer to *N*-ethyl pyridinium has been proposed for [Fe(diimine)$_3$][2+] complexes in AlCl$_3$/*N*-ethyl pyridinium chloride melts, probably by static quenching.[19]

Here, we describe our attempts to lower the [1/3]MLCT-state energies of an iron(II) complex by a push–pull ligand set, and concomitantly, to raise the energy of [3/5]T states through increased metal–ligand orbital overlap by using tridentate ligands with large bite angles. In contrast to previously described or suggested iron(II) complexes featuring a single type of tridentate ligand (CNC,[13] NCN,[14] or dcpp[15]), this approach requires the selective formation of heteroleptic iron(II) complexes [Fe(L^1)(L^2)][2+]. Owing to the lability of Fe—N bonds, this is a challenging task, even in complexes of tridentate ligands such as tpy.[20,21]

We had previously introduced the ddpd ligand (*N,N*′-dimethyl-*N,N*′-dipyridine-2-yl-pyridine-2,6-diamine) as a tridentate electron-donating ligand with large bite angles in homoleptic Cu[II] complexes showing dynamic Jahn–Teller distortions in the solid state,[22] in redox-active Co[II/III] complexes,[23] and in heteroleptic [Ru[II](ddpd)(tpy-EWG)][2+] complexes with low [1/3]MLCT energies and long excited-state lifetimes.[8] As a strongly electron-accepting ligand with large bite angles we decided to employ the dcpp ligand,[7,15,24] and hence, the push–pull substituted heteroleptic iron(II) complex [Fe(dcpp)(ddpd)][2+] **2[2+]** was targeted. Such a directional complex should be highly amenable for selective functionalization at a single ligand suited for attachment to surfaces such as TiO$_2$ in dye-sensitized solar cells. This is, of course, one of the prominent long-term goals of these studies.

We report the synthesis, structure, and spectroscopic and photophysical properties of the novel heteroleptic iron(II) complex [Fe(dcpp)(ddpd)](PF$_6$)$_2$ [**2(PF$_6$)$_2$**]. For comparison, its corresponding homoleptic complexes [Fe(ddpd)$_2$](PF$_6$)$_2$ [**1(PF$_6$)$_2$**] and [Fe(dcpp)$_2$](PF$_6$)$_2$ [**3(PF$_6$)$_2$**] were also prepared and studied by NMR, IR, UV/Vis, and Mößbauer spectroscopy, as well as by electrochemistry. The latter complex has been reported recently by McCusker et al., and characterized structurally as well as spectroscopically.[15] Here, we add Mößbauer spectral data of this complex as well as the X-ray crystal structure determination of its CH$_3$CN solvate [**3(PF$_6$)$_2$·^{1}/$_2$ CH$_3$CN**]. To gain an insight into the excited charge-transfer states, we probe the electronics of the iron(III) complexes **1[3+]** and **2[3+]** prepared by chemical oxidation of **1[2+]** and **2[2+]** by UV/Vis, Mößbauer, and EPR spectroscopy, and the radicals **2[+]** and **3[+]** derived from the reduction of **2[2+]** and **3[2+]** are investigated by EPR spectroscopy. The excited-state dynamics of the heteroleptic complex **2[2+]** are studied by picosecond transient-absorption (TA) spectroscopy. DFT calculations are employed to elucidate the electronic structure of the redox triple **2[+]/2[2+]/2[3+]** and of the lowest-energy triplet state of **2[2+]**.

Results and Discussion

Synthesis of iron(II) complexes 1[2+]–3[2+]

Homoleptic iron(II) complexes with two identical tridentate ligands, such as [Fe[II](tpy-R)$_2$][2+], are well known and typically straightforward to prepare.[20,25] On the other hand, the selective synthesis of heteroleptic iron(II) complexes [Fe[II](L^1)(L^2)][2+] with two different tridentate ligands is more challenging because of the labile Fe—N bonds.[21]

The lability allows for facile ligand exchange compared with the homologous kinetically robust [Ru[II](L^1)(L^2)][2+] complexes. Owing to ligand scrambling, thermodynamic mixtures of [Fe[II](L^1)(L^2)][2+], [Fe[II](L^1)$_2$][2+], and [Fe[II](L^2)$_2$][2+] are often obtained, especially when L^1 and L^2 are similar in their coordination properties.[20] Indeed, the homoleptic complexes **1[2+]** and **3[2+]** are prepared straightforwardly from the respective tridentate ligand and FeBr$_2$ or Fe(BF$_4$)$_2$·6 H$_2$O followed by counter-ion exchange with (NH$_4$)(PF$_6$) if desired. The formation of orange–brown **1[2+]** is typically completed within a few minutes, whereas double coordination of dcpp to Fe[II] to give dark blue **3[2+]** requires several hours to be quantitative. Gratifyingly, no stereoisomers (*mer*, *trans-fac*, *cis-fac*) are observed, which is possible in principle owing to the flexible six-membered chelate

46

3.1 RESULTS AND DISCUSSION: A HETEROLEPTIC PUSH–PULL SUBSTITUTED IRON(II) BIS(TRIDENTATE) COMPLEX WITH LOW-ENERGY CHARGE-TRANSFER STATES

rings.[6,8a] The bright blue heteroleptic complex 2^{2+} is synthesized from dcpp, ddpd, and FeBr$_2$ in a 1:1:1 ratio (Scheme 1). Interestingly, only two complexes form under these conditions, namely 1^{2+} and 2^{2+}, as judged from TLC control (Figure 1), and some dcpp remains uncoordinated. From integration of proton resonances (H15) after precipitating all complexes with diethyl ether and redissolving the solid material in CD$_3$CN, the 1^{2+}:2^{2+} ratio is determined as 1:12 (see Supporting Information, Figure S1). Hence, the purification problem reduces to the separation of 2^{2+} from 1^{2+}, which is easily achieved by column chromatography (Scheme 1). Final counter-ion exchange with (NH$_4$)(PF$_6$) gives spectroscopically and analytically pure **2(PF$_6$)$_2$**. Again, only the meridional isomer **mer-2^{2+}** is formed selectively.
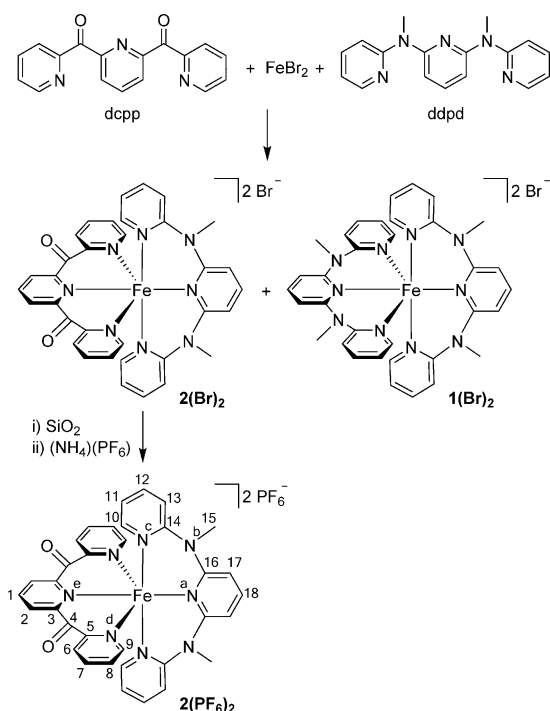
Scheme 1. Synthesis of **2(PF$_6$)$_2$** and atom numbering used for NMR assignments.
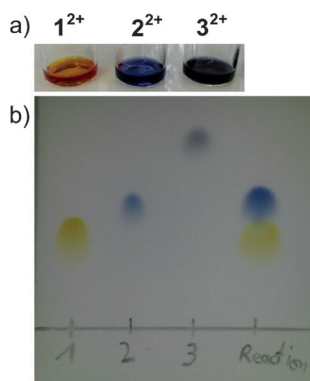
Figure 1. a) Photograph of solutions of 1^{2+}, 2^{2+}, and 3^{2+} in CH$_3$CN, and b) photograph of TLC plate (SiO$_2$, CH$_3$CN/KNO$_3$(sat., aq.) = 1:4) of 1^{2+}, 2^{2+}, and 3^{2+}, as well as of the initial reaction mixture of dcpp, ddpd, and FeBr$_2$.

As expected, all complexes 1^{2+}–3^{2+} are diamagnetic (low-spin configuration, (t$_{2g}$)^6(e$_g$*)^0), giving well-resolved NMR spectra. As judged from the unchanged color of a CH$_3$CN solution of **2(PF$_6$)$_2$**, the complexes do not undergo a thermal SCO to the ^{5}T$_2$ state (high-spin configuration, (t$_{2g}$)^4(e$_g$*)^2) up to 70 °C, suggesting that the ^{5}T$_2$ state is too high in energy. At temperatures above 70 °C in CH$_3$CN, the blue color of the solution of 2^{2+} fades. However, this thermochromism is not based on SCO, but caused by decomposition through dissociation of the ddpd ligand (TLC control) similar to the thermochromic behavior of 1^{2+} (dissociation of ddpd around 60 °C) and 3^{2+} (decomposition in boiling CH$_3$CN). The complexes [Fe(bpy)$_3$]$^{2+}$ and [Fe(tpy)$_2$]$^{2+}$ with five-membered chelate rings are found to be thermally stable under our conditions, whereas [Fe(L)$_2$]$^{2+}$ complexes with L = 2,6-dipyridyl-4-phenyltriazine have been reported to be prone to thermal ligand substitution in DMSO.[26] In fact, the addition of tpy to an orange solution of 1^{2+} at room temperature results in the formation of purple [Fe(tpy)$_2$]$^{2+}$ and the release of ddpd according to TLC, whereas the addition of dcpp to 1^{2+} gives neither 2^{2+} nor 3^{2+} but 1^{3+} by the oxidation of 1^{2+} instead (see below).

Spectroscopic and structural properties of 1^{2+}–3^{2+}

In the IR spectra of **1(PF$_6$)$_2$**–**3(PF$_6$)$_2$**, the characteristic PF stretching vibration of the hexafluorophosphate counter ion is observed around 841 cm^{-1}, substantiating the successful counter-ion exchange. The absorption band for the C=O stretching vibration of the dcpp ligands in **3(PF$_6$)$_2$** is found at 1680 cm^{-1}, whereas that of the dcpp ligand of **2(PF$_6$)$_2$** is shifted to slightly lower energy (1674 cm^{-1}), which can be attributed to the electron-donating character of ddpd resulting in increased π-back-bonding to dcpp in **2(PF$_6$)$_2$**. DFT (B3LYP, LANL2DZ, IEFPCM CH$_3$CN) geometry optimizations (see Supporting Information, Figure S2) and harmonic frequency calculations of 3^{2+} and 2^{2+} revealed a similar shift from 1648 to 1638 cm^{-1} (unscaled[27]) for the asymmetric CO stretch, respectively. The electronic asymmetry of 2^{2+} also manifests itself in the Mößbauer spectral data (see Supporting Information, Figure S3), especially in the increased quadrupole splitting of $\Delta E_Q = 0.456$ mm s^{-1} (2^{2+}) compared with those of the homoleptic complexes 1^{2+} and 3^{2+} (0.403 and 0.322 mm s^{-1}, respectively).

In the DFT calculated structures, the FeN$_6$ polyhedra are essentially of D_{4h} symmetry for the homoleptic complexes 1^{2+} and 3^{2+}, that is, compressed octahedra with short Fe–N bond lengths to the central pyridines of the tridentate ligands thanks to the chelate-ligand-induced compression (see Supporting Information, Figure S2).[22] This high symmetry of the FeN$_6$ polyhedron is reduced to C_{4v} for 2^{2+}, featuring a short Fe–N bond to the central pyridine of dcpp (1.997 Å) and a long one to the central pyridine of ddpd (2.003 Å), giving a bond-length difference of $\Delta_{FeN} = 0.006$ Å.

Single crystals of **1(PF$_6$)$_2$·CH$_3$CN**, **1(BF$_4$)$_2$·2 CH$_3$CN**, **2(PF$_6$)$_2$·CH$_3$CN**, and **3(PF$_6$)$_2$·^{1}/$_2$ CH$_3$CN** suitable for X-ray diffraction studies were obtained (Figure 2). All complex cations exhibit almost perfect 90° and 180° N–Fe–N bond angles (approximate local D_{4h} symmetry with respect to angles), with

3.1 RESULTS AND DISCUSSION: A HETEROLEPTIC PUSH–PULL SUBSTITUTED
IRON(II) BIS(TRIDENTATE) COMPLEX WITH LOW-ENERGY CHARGE-
TRANSFER STATES

47
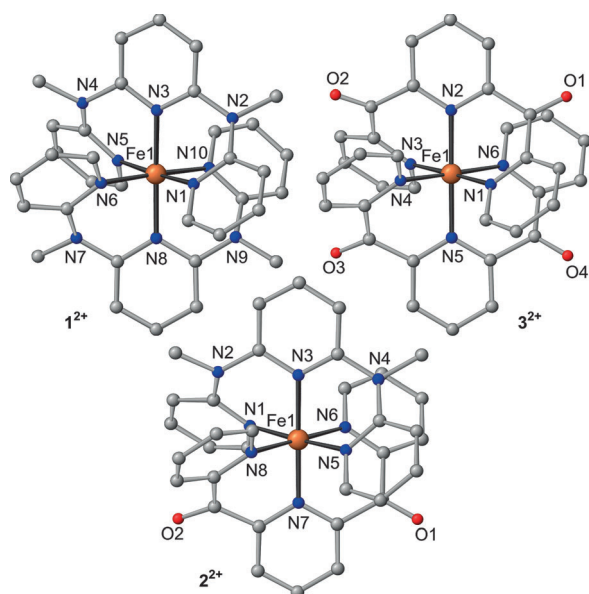
Figure 2. Molecular structures and atom numbering of 1^{2+}–3^{2+} in their respective crystals $1(PF_6)_2 \cdot CH_3CN$, $2(PF_6)_2 \cdot CH_3CN$ and $3(PF_6)_2 \cdot \frac{1}{2} CH_3CN$ as obtained by XRD; hydrogen atoms omitted.

angles of $177.33 \pm 1.05°/90.02 \pm 1.75°$ [$1(PF_6)_2 \cdot CH_3CN$], $176.97 \pm 2.62°/90.03 \pm 2.05°$ [$1(BF_4)_2 \cdot 2 CH_3CN$], $178.40 \pm 1.43°/90.00 \pm 1.23°$ [$2(PF_6)_2 \cdot CH_3CN$], and $178.49 \pm 0.38°/90.00 \pm 1.56°$ [$3(PF_6)_2 \cdot \frac{1}{2} CH_3CN$], respectively, similar to the reported structure of $3(PF_6)_2$.[15] With respect to bond lengths, the local FeN_6 symmetry of 2^{2+} is reduced, with a short Fe–N bond to the central pyridine of dcpp (Fe1–N7 1.929(4) Å) and a long one to the central pyridine of ddpd (Fe1–N3 1.953(4) Å; Δ_{FeN} = 0.024 Å; Figure 2), similar to the DFT-calculated structure (see Supporting Information, Figure S2). In contrast, in the experimentally determined structures of the homoleptic complexes 1^{2+} and 3^{2+}, the bond lengths to the central pyridine of ddpd are slightly shorter than those to the central pyridine of dcpp, possibly owing to the stronger *trans* influence of dcpp in 3^{2+}. For $1(PF_6)_2 \cdot CH_3CN$ and $1(BF_4)_2 \cdot 2 CH_3CN$, the corresponding Fe–N bond lengths to ddpd amount to 1.959(2)/1.966(2) Å (Δ_{FeN} = 0.007 Å) and 1.963(2)/1.963(2) Å (Δ_{FeN} = 0 Å), respectively. For the homoleptic dcpp complex $3(PF_6)_2$, values of 1.974(2)/1.974(2) Å (Δ_{FeN} = 0 Å) have been reported,[15] and we find 1.966(5)/1.970(5) Å (Δ_{FeN} = 0.004 Å) for the solvated crystal $3(PF_6)_2 \cdot \frac{1}{2} CH_3CN$. Hence, we ascribe the asymmetric bonding situation in 2^{2+} mainly to a strong intrinsic push–pull effect of the different tridentate ligands, which is naturally absent in the homoleptic complexes 1^{2+} and 3^{2+}. The environmental effects of lower crystal symmetry and asymmetric counter-ion and crystal solvent distributions seem to play only a minor role, because the experimentally determined bond-length differences in the homoleptic complexes are much smaller (Δ_{FeN} = 0.007 Å) than those found for 2^{2+} (Δ_{FeN} = 0.024 Å). Furthermore, the intrinsic bond-length asymmetry of 2^{2+} is also corroborated by DFT calculations (see above) using an Integral Equation Formalism Polarizable Continuum Model (IEFPCM).

All the six-membered chelate rings in 2^{2+} adopt boat conformations, and hence, the pyridine rings within a tridentate

ligand are not coplanar. This results in a twisted wrapping of the two tridentate ligands around the metal center, as illustrated in Figure 3.

The NMR spectra of 2^{2+} (^{1}H, ^{13}C, ^{15}N) are essentially a superposition of the spectra of the homoleptic complexes 1^{2+} and
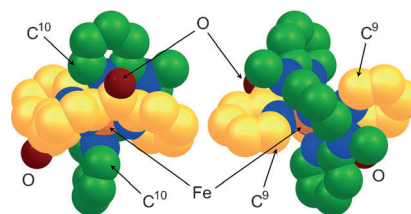
Figure 3. DFT (B3LYP, LANL2DZ, IEFPCM CH_3CN) calculated front and back views of a van der Waals representation of 2^{2+} illustrating the nonplanar nature of the two tridentate ligands. Hydrogen atoms omitted, carbon atoms of the dcpp ligand in yellow, carbon atoms of the ddpd ligand in green, nitrogen atoms in blue, oxygen atoms in red (atom numbering as for the NMR assignments).

3^{2+} (see Supporting Information, Table S1), with the notable exception of H^{10} of the ddpd ligand. Compared with 1^{2+}, the resonance is shifted to a higher field in 2^{2+} by $\Delta\delta = 0.51$ ppm. Indeed, H^{10} points approximately to the center of the central electron-deficient pyridine (distance 3.1 Å) of the dcpp ligand, experiencing a different ring current in 2^{2+} from that in 1^{2+} with an electron-rich central pyridine (see Figure 3 for the location of the corresponding carbon atom C^{10} in the DFT-optimized structure). Hence, the chemical shift of H^{10} of ddpd represents a local probe of the electronic situation in the other tridentate ligand. A less pronounced shift is found for the inverse situation (H^9 of dcpp, $\Delta\delta = 0.16$ ppm).

The ^{15}N resonances of the coordinated pyridines reflect the electron-donating and electron-withdrawing characters of ddpd ($\delta = 222.9$, 229.2 ppm) and dccp ($\delta = 247.9$, 256.2 ppm), respectively. This effect is even more pronounced in the mixed-ligand complex 2^{2+} ($\delta = 210.9$, 214.8 ppm and $\delta = 261.5$, 272.2 ppm).

Redox properties of the iron(II) complexes

The redox properties of $1(PF_6)_2$–$3(PF_6)_2$ were recorded in 0.1 M (nBu$_4$N)(PF$_6$)/CH$_3$CN solution. Our data for 3^{2+} fully confirm the reported values.[15] The cyclic voltammogram of 2^{2+} is depicted in Figure 4. The iron(II) centers of all complexes 1^{2+}–3^{2+} can be oxidized reversibly to the iron(III) state with the potential of 2^{2+} ($E_{1/2} = 0.84$ V vs. Fc/Fc$^+$) being intermediate between those of 1^{2+} ($E_{1/2} = 0.33$ V vs. Fc/Fc$^+$) and 3^{2+} ($E_{1/2} = 1.29$ V vs. Fc/Fc$^{+[15]}$). The two dcpp ligands in 3^{2+} can accept four electrons at $E_{1/2} = -0.92$, -1.21, -1.53, and -1.81 V (vs. Fc/Fc$^+$), whereas the ddpd ligands in 1^{2+} are only irreversibly reduced at $E_p = -2.33$ V (vs. Fc/Fc$^+$). In addition, the ddpd ligands in 1^{2+} are oxidized irreversibly at $E_p = 1.63$ V (vs. Fc/Fc$^+$). The dcpp ligand in 2^{2+} can be reduced twice at $E_{1/2} = -1.21$ and -1.60 V, whereas the ddpd ligand of 2^{2+} is reduced irreversibly at $E_p = -2.22$ V, similarly to 1^{2+} (Figure 4). These data reflect the excel-

48

3.1 RESULTS AND DISCUSSION: A HETEROLEPTIC PUSH–PULL SUBSTITUTED IRON(II) BIS(TRIDENTATE) COMPLEX WITH LOW-ENERGY CHARGE-TRANSFER STATES
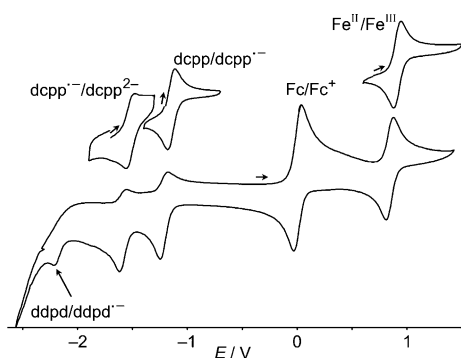
Figure 4. Cyclic voltammogram of **2(PF$_6$)$_2$** in 0.1 M (nBu$_4$N)(PF$_6$)/CH$_3$CN; potentials are given relative to the ferrocene/ferrocenium couple.

lent electron-accepting properties of dcpp and the pronounced electron-donating properties of ddpd.

Consistent with the redox data, DFT calculations of the low-spin iron(III) complexes **1^{3+}**–**3^{3+}** ((t_{2g})^5(e_g*)^0) reveal that the spin density is delocalized onto the electron-donating ddpd ligand, and especially onto the N–Me groups, but negligibly onto the electron-accepting dcpp ligand (see Supporting Information for a graphical representation of the spin densities, Figure S4). The calculated Mulliken spin density on iron in **2^{3+}** (1.08) is hence between that of **1^{3+}** (1.04) and **3^{3+}** (1.11).

The iron(III) complexes **1^{3+}** and **2^{3+}** were prepared by chemical oxidation using ceric ammonium nitrate [CAN, (NH$_4$)$_2$Ce(NO$_3$)$_6$] in 0.5 M TFA in CH$_3$CN ($E_{1/2}$ = 1.30 V vs. Fc/Fc$^+$ in HClO$_4$[28]), whereas **3^{2+}** could not be oxidized using CAN. EPR (X-band, 77 K, CH$_3$CN glass, Figure 5) and Mößbauer spectra (295 K, powder, see Supporting Information, Figure S5) of **1^{3+}** and **2^{3+}** confirm the low-spin configurations of the iron(III) centers. Use of the as-prepared solution of **2^{2+}**/CAN for the EPR measurement reveals an additional resonance at $g_{1,2}$ = 4.330, 4.020, which is assigned to a high-spin iron(III) complex[29] probably formed by dissociation of the dcpp ligand. The larger asymmetry of **2^{3+}** is reflected in its higher g-anisotropy $\Delta g = g_1 - g_3 = 1.26$ ($g_1 = 2.821$, $g_2 = 2.247$, $g_3 = 1.561$) as compared to **1^{3+}**, with $\Delta g = 0.675$ ($g_1 = 2.490$, $g_2 = 2.296$, $g_3 = 1.815$). Axial EPR spectra have been obtained for [Fe(bpy)$_3$]$^{3+}$ ($g_\perp = 2.61$,
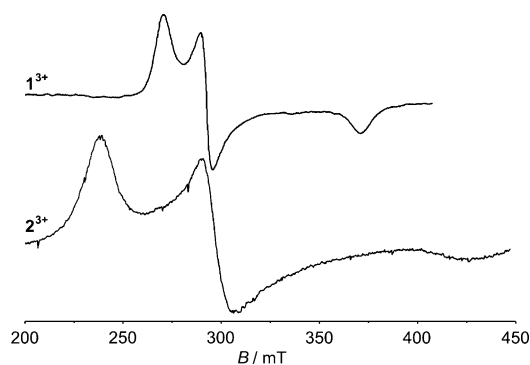
$g_{||} = 1.61$ in a Co^{III} host[30]) and [Fe(bzimpy)$_2$]$^{3+}$ ($g_\perp = 2.242$, $g_{||} = 1.915$ in a methanol:DMF glass matrix at 100 K; bzimpy = 2,6-bis(benzimidazoly-2-yl)pyridine)[31]). Interestingly, in the room-temperature Mößbauer spectra, the quadrupole splitting is larger for **1^{3+}** ($\Delta E_Q = 1.973$ mm s^{-1}) than for **2^{3+}** ($\Delta E_Q = 1.584$ mm s^{-1}). However, as nothing is known about the crystal structures of **1^{3+}** and **2^{3+}**, the powder Mößbauer data could also reflect a lower crystal symmetry and asymmetric anion distribution.

UV/Vis monitoring of the Fe^{II}→Fe^{III} oxidation by CAN in CH$_3$CN/TFA reveals an MLCT band bleach with the concomitant appearance of two new absorption bands at 619/1013 nm (**1^{3+}**, measured in H$_2$O for solubility reasons) and 772/1277 nm (**2^{3+}**, in CH$_3$CN/TFA, see Supporting Information, Figures S6 and S7). All these bands are straightforwardly assigned to ddpd→Fe^{III} LMCT excitations on the basis of time-dependent DFT calculations on the iron(III) complexes **1^{3+}** (λ_{max} = 540, 702, 770 nm) and **2^{3+}** (λ_{max} = 667, 959 nm) (see Supporting Information, Figures S8 and S9).

The radicals **2$^+$** and **3$^+$**, which were stable in the electrochemical experiment, were also prepared by chemical reduction of **2^{2+}** and **3^{2+}** with decamethylcobaltocene ($E_{1/2}$ = −1.94 V vs. Fc/Fc$^+$ in CH$_2$Cl$_2$[28]) in CH$_3$CN, respectively. X-band EPR spectra of the corresponding frozen solutions are depicted in Figure 6. The g-values near g = 2.0 with a rather small g-anisotropy confirm essentially ligand-centered reductions.[32] Hyperfine couplings to ^{14}N and ^{1}H nuclei are also observed, but not fully resolved. This assignment is further corroborated by DFT calculations localizing the spin density essentially on the C=O units of the dcpp ligands (see Supporting Information for spin-density plots of **2$^+$** and **3$^+$**, Figure S10).
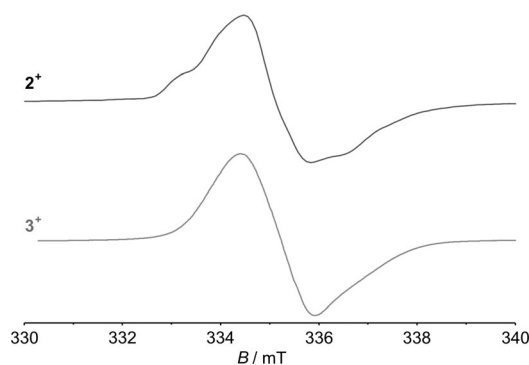
Figure 6. X-band EPR spectra of **2$^+$** (9.3843 GHz) and **3$^+$** (9.4173 GHz) in CH$_3$CN at 77 K.

Optical properties of the iron(II) complexes

The UV/Vis spectra of **1(PF$_6$)$_2$**–**3(PF$_6$)$_2$** recorded in CH$_3$CN at room temperature are collected in Figure 7. The orange–brown ddpd complex **1^{2+}** shows a medium intense absorption band at λ_{max} = 395 nm, which can be ascribed to MLCT and ligand-field transitions according to time-dependent DFT (TD-DFT) calculations (λ_{max} = 389, 393, 398 nm of mixed d$_{yz}$→ddpd and d$_{xz}$→d$_{x2-y2}$/d$_{z2}$ character). The rather high energy is consistent with the electron-donating character of ddpd and the

Figure 5. X-band EPR spectra of **1^{3+}** (9.4197 GHz) and **2^{3+}** (9.3840 GHz) in CH$_3$CN/TFA at 77 K.

3.1 RESULTS AND DISCUSSION: A HETEROLEPTIC PUSH–PULL SUBSTITUTED
IRON(II) BIS(TRIDENTATE) COMPLEX WITH LOW-ENERGY CHARGE-
TRANSFER STATES

49
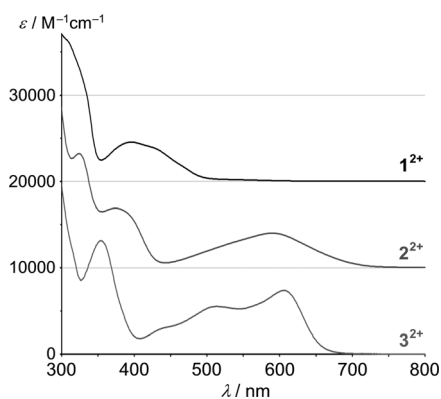
Figure 7. UV/Vis spectra of **1(PF$_6$)$_2$**–**3(PF$_6$)$_2$** in CH$_3$CN at room temperature (spectra of **1^{2+}** and **2^{2+}** are offset vertically by 20000 and 10000, respectively).

Figure 9. Relevant Kohn–Sham molecular orbitals of **2^{2+}** involved in the indicated charge-transfer transitions (isosurface value 0.1 a.u.).

analogous results for the homologous ruthenium(II) complex [Ru(ddpd)$_2$]$^{2+}$.[8a] The dcpp complexes **2^{2+}** and **3^{2+}**[15] are intense blue, with the lowest-energy absorption maxima found at 592 nm (**2^{2+}**) and 610 nm (**3^{2+}**),[15] respectively. For **2^{2+}**, the absorption reaches further into the NIR spectral region than observed for **3^{2+}** (Figure 7). According to TD-DFT calculations, the relevant absorption bands of **2^{2+}** are composed of several allowed charge-transfer transitions, with the band envelope dominated by five transitions, namely $\lambda_{max}=585$, 559, 518, 490, and 445 nm (Figure 8). Interestingly, the two lowest-energy bands at $\lambda_{max}=585$ and 559 nm are of mixed MLCT (Fe-d→dcpp) and LL'CT (ddpd →dcpp) character, involving the molecular orbitals 159→160/157→160 and 158→160/156→160 (Figure 9). The transitions at 518 nm (158→161/158→174) and 445 nm (156→161/156→174) comprise some additional ligand field character involving the d$_{z2}$ orbital of Fe (174, Figure 9).

The stabilities of **1^{2+}**–**3^{2+}** as well as [Fe(bpy)$_3$]$^{2+}$ with respect to photosubstitution (anation and aquatization) were probed through irradiation of the complexes at the high-energy side of the visible spectrum (400 nm; dissolved in 0.1 M (nBu$_4$N)Cl CH$_3$CN/H$_2$O (98:2) to give isoabsorptive solutions at 400 nm) and monitoring of the optical changes with irradiation time (Figure 10). Under these conditions, complex **3^{2+}** precipitates probably as a **3(Cl)$_2$** salt, and hence, its stability cannot be ac-

cessed. The half-lives of **1^{2+}**, [Fe(bpy)$_3$]$^{2+}$, and **2^{2+}** increase in that order, with values of 53, 257, and 1733 min, respectively. The higher stability of **2^{2+}** with respect to **1^{2+}** might be ascribed to the favorable push–pull situation in **2^{2+}** strengthening all the Fe–N (central pyridine) bonds (see above) and preventing ligand substitution. With respect to [Fe(bpy)$_3$]$^{2+}$, **2^{2+}** is kinetically stabilized thanks to the tridentate nature of its chelate ligands. Hence, the higher photostability of ruthenium(II) complexes with tridentate ligands including push–pull character[9] is also found for comparable iron(II) complexes, which is certainly beneficial for any future photo-applications of iron(II) complexes.

Excited-state dynamics occurring shortly after excitation to a Franck–Condon CT state were probed by picosecond transient absorption spectroscopy for **2^{2+}** at 298 K in CH$_3$CN (pulse $\lambda_{exc}=500$ nm, Figure 11), showing a prompt ground-state bleach around the 600 nm MLCT/LL'CT absorptions. The recovery of the ground state occurs with a time constant of $\tau=$

Figure 8. TD-DFT-derived UV/Vis stick spectrum of **2^{2+}** accounting for the bands in the near-UV and visible regions.

Figure 10. Normalized decay curves of **1^{2+}**, **2^{2+}**, and [Fe(bpy)$_3$]$^{2+}$ under 400 nm irradiation in 0.1 M (nBu$_4$N)Cl CH$_3$CN/H$_2$O (98:2) solution.

3.1 RESULTS AND DISCUSSION: A HETEROLEPTIC PUSH–PULL SUBSTITUTED
IRON(II) BIS(TRIDENTATE) COMPLEX WITH LOW-ENERGY CHARGE-
TRANSFER STATES

50

Figure 11. Transient absorption spectra of 2^{2+} ($\lambda_{exc} = 500$ nm) in CH$_3$CN at 295 K.

Figure 12. DFT-calculated lowest-energy singlet, triplet, and quintet states and spin densities (isosurface value 0.07 a.u.) of 2^{2+} with relevant Fe–N bond lengths in Å; hydrogen atoms omitted for clarity.

548 ps. Typically, after excitation, rapid ISC to triplet states and to the final $^5T_2$ state occurs. The rate-determining step back to the ground state is the $^5T_2 \rightarrow {}^1A_1$ relaxation, typically occurring within $\tau = 40$–200 ns at room temperature for iron(II) polypyridine complexes.[33–39] Recently, McCusker et al. observed an unusual fast relaxation to the ground state for 3^{2+} with $\tau = 280$ ps. This fast process has been ascribed to the possibility that the $^5T_2$ state is similar or even higher in energy than the $^3T_1$ ligand field term, and hence, relaxation to the $^1A_1$ ground state occurs rapidly from the $^3T_1$ state instead of from the $^5T_2$ state.[15] Indeed, the ground-state recovery (≈ 600 nm) from the TA spectra of the heteroleptic complex 2^{2+} is similarly rapid and monoexponential ($\tau = 548$ ps). Hence, a similar explanation to that for 3^{2+} might be invoked for 2^{2+}. If this explanation holds both for 2^{2+} and 3^{2+}, the former has a l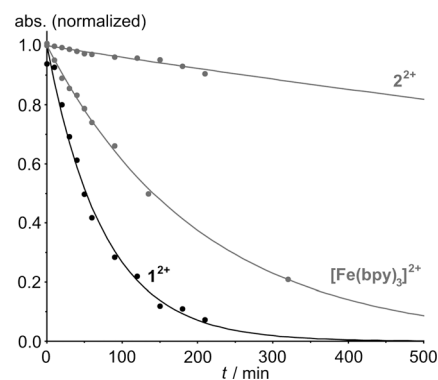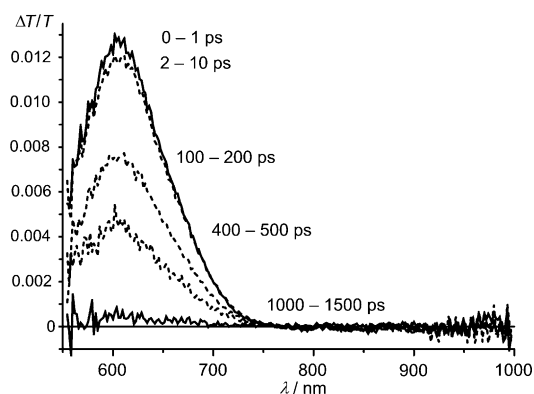onger $^3T_1$ lifetime compared with [Fe(ptz)$_6$](BF$_4$)$_2$ (39 ps at 125 K)[4] and 3^{2+} (280 ps at room temperature).[15] This could be attributed to a larger reorganization barrier for 2^{2+} than for 3^{2+}, arising from either increased inner sphere or increased solvent reorganization. The contribution of the solvent reorganization for the $^3T_1 \rightarrow {}^1A_1$ relaxation is expected to be similar for 2^{2+} and 3^{2+}. However, the ligand field splitting might be larger in 3^{2+} than in 2^{2+} owing to the two strongly electron-accepting dcpp ligands lowering the iron t$_{2g}$ orbitals. Hence, the energy difference, that is, the driving force, between the $^3T_1$ and $^1A_1$ terms is lower for 2^{2+} than for 3^{2+}, raising the inner sphere barrier for the $^3T_2 \rightarrow {}^1A_1$ relaxation. The inner sphere reorganization energy essentially comprises changes in the Fe–N bonds. The geometries of the $^1A_1$, $^3T_1$, and $^5T_2$ states of 2^{2+} have been calculated by using DFT methods at the B3LYP level of theory. As it is clear that energies of different spin states are poorly reproduced by the B3LYP functional,[40–43] we refrain from discussing energy aspects. However, geometric distortions should be well reproduced qualitatively,[26] and these are given in Figure 12. In particular, the Fe–N bond lengths to the ddpd ligand in the triplet state differ from the ground-state bond lengths (Figure 12). In the quintet state, the remaining Fe–N(dcpp) distances are elongated (Figure 12).

No excited-state absorption features were observed up to 1500 nm upon excitation at 500 nm (data not shown). For an
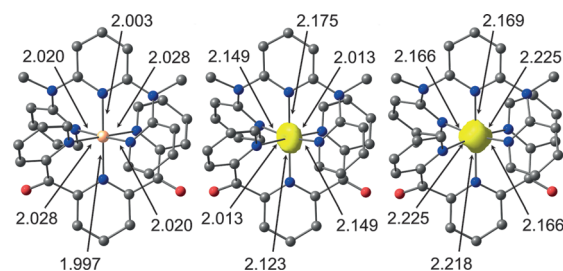
MLCT or LL'CT excited state, an absorption should be expected, for example, around 775 and 1280 nm, similarly to the iron(III) complex 2^{3+} (see above). Hence, no CT state was observed with our temporal resolution, in contrast to the tetracarbene Fe(CNC)$_2$]$^{2+}$ complex of Wärnmark et al., which showed a 9 ps lifetime based on an excited state absorption at approximately 525 nm attributed to the ^{3}MLCT state.[13]

In essence, the excited-state dynamics of 2^{2+} can be described by the following processes (Figure 13). After excitation
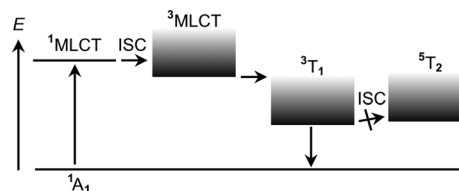
Figure 13. Proposed qualitative Jablonski diagrams of 2^{2+} and 3^{2+}.

into a CT state, the heteroleptic complex 2^{2+} undergoes rapid ISC to the $^3T_1$ ligand field state. The high-spin ligand field state $^5T_2$ is not reached, and relaxation to the $^1A_1$ ground state from $^3T_1$ is quite rapid. Compared with the homoleptic bis(dcpp) complex 3^{2+}, the latter process is slower for 2^{2+}. This can be ascribed to the weaker ligand field of 2^{2+}, and hence, the back relaxation process features a smaller driving force and a larger barrier (Figure 13). The increased photostability of 2^{2+} (see above) might in part be caused by the avoided (dissociative?) high-spin state with labile Fe–N bonds. To lower the MLCT states further with respect to the dd states, with the aim of obtaining emissive iron(II) complexes, the electron-accepting capability of dcpp and the electron-donating power of ddpd need to be increased further, for example, by substituent push–pull effects.[8] An inverse process in [Ru(bpy)$_3$]$^{2+}$ chemistry, namely, decreasing the energy of dd states relative to the MLCT states, has been achieved through alkylation of bpy adjacent to the coordinating nitrogen atoms reducing the ligand field strength.[44]

3.1 RESULTS AND DISCUSSION: A HETEROLEPTIC PUSH–PULL SUBSTITUTED IRON(II) BIS(TRIDENTATE) COMPLEX WITH LOW-ENERGY CHARGE-TRANSFER STATES

51

Conclusion

A heteroleptic iron(II) complex 2^{2+} with two push–pull substituted tridentate oligopyridine ligands was prepared. The low-lying π^* orbitals of the electron-accepting dcpp ligand allow low-energy metal-to-ligand charge transfer ($\lambda_{max} = 592$ nm). Thanks to the electron-donating ddpd ligand, the absorptions extend into the near-infrared region owing to transitions with considerable LL'CT character from ddpd to dcpp. Both charge-transfer excitations are highly directional. One-electron oxidation reveals an essentially metal-centered electron process (plus some ddpd character), giving the low-spin Fe^{III} complex 2^{3+}, whereas one-electron reduction to 2^+ is essentially centered on the dcpp ligand, in agreement with the optical data.

With the interpretation of McCusker et al. of the excited-state dynamics of the homoleptic bis(dcpp) complex 3^{2+} being correct, complex 2^{2+} represents a second member of an emerging new class of iron(II) complexes with strong ligand fields, in which the $^5T_2$ state is close in energy or possibly even higher in energy than the $^3T_1$ state, a situation typically found in second- and third-row metal complexes. Hence, the high-spin state is not populated significantly by MLCT excitation, and the rate-determining step back to the ground state is assigned to the $^3T_1 \rightarrow {}^1A_1$ relaxation ($\tau = 548$ ps) instead of the slow $^5T_2 \rightarrow {}^1A_1$ relaxation observed in other iron(II) polypyridine complexes (nanoseconds). Thus, future objectives are to push the ligand field limit even further, and finally, to arrive at low-cost photoactive complexes with earth-abundant metal centers, which are applicable to energy-conversion schemes such as dye-sensitized solar cells and light-emitting devices.

Experimental Section

General procedures

CH_3CN and THF were distilled under an argon atmosphere from calcium hydride and potassium, respectively. All reagents were used as received from commercial suppliers (Acros, Apollo Scientific, and Sigma–Aldrich). The syntheses of the ligands ddpd[8a] and dcpp[24] as well as of $3(PF_6)_2$[15] have been reported previously. NMR spectra were recorded on a Bruker Avance DRX 400 spectrometer at 400.31 MHz (^{1}H), 100.66 MHz (^{13}C{^{1}H}), and 40.56 MHz (^{15}N). All resonances are reported in ppm versus the solvent signal as an internal standard [CD$_3$CN (^{1}H, $\delta = 1.94$; ^{13}C, $\delta = 1.24$ ppm); [D$_6$]DMSO (^{1}H, $\delta = 2.50$); ^{13}C, $\delta = 39.43$ ppm)] or versus external CH$_3$NO$_2$ (90 % in CDCl$_3$ $\delta = 380.23$ ppm vs. NH$_3$(l)) and referenced to NH$_3$ (^{15}N, $\delta = 0$ ppm). IR spectra were recorded with a BioRad Excalibur FTS 3100 spectrometer with KBr disks. Electrochemical experiments were performed on a Bio Logic SP-50 voltammetric analyzer using platinum wires as counter and working electrodes and 0.01 M Ag/AgNO$_3$ as the reference electrode. The measurements were made at a scan rate of 100 mV s^{-1} for cyclic voltammetry experiments using 0.1 M (nBu$_4$N)(PF$_6$) as the supporting electrolyte and a 10^{-3} M solution of the sample in dry and degassed CH$_3$CN. Potentials are referenced to the ferrocene/ferrocenium couple ($E_{1/2} = 85 \pm 5$ mV under the experimental conditions). UV/Vis/NIR spectra were recorded on a Varian Cary 5000 spectrometer using 1.0 cm cells (Hellma, Suprasil). Transient absorption measurements were performed with a home-built pump–probe setup. For measurements in the time range 1–4 ns with a resolution of approximately 100 fs,

the output of a commercial titanium:sapphire amplifier (Coherent LIBRA HE, 3.5 mJ, 1 kHz, 100 fs) was split, with one portion used to generate a 500 nm excitation pulse (output of an optical parametric amplifier (Coherent OPerA Solo)) and another used to generate a white light probe, using a home-built two-stage broadband (480–850 nm) noncollinear optical parametric amplifier (NOPA) for white light generation and amplification in the visible region and a c-cut (3 mm thick) sapphire window for white light generation in the visible to near-infrared spectral range. The variable delay of up to 4 ns between pump and probe was introduced by a broadband retroreflector mounted on a mechanical delay stage. Only reflective optics were used to guide the probe beam to the sample to minimize chirp. The excitation pulse was chopped at 500 Hz, and the white light pulses were dispersed onto a linear photodiode array, which was read out at 1 kHz. Adjacent diode readings corresponding to the transmission of the sample after an excitation pulse and without an excitation pulse were used to calculate $\Delta T/T$. The complex was dissolved in degassed CH$_3$CN ($c = 2.48 \times 10^{-3}$ M) under a nitrogen atmosphere and measured in a quartz cuvette with 1 mm optical path length. ESI mass spectra were recorded on a Micromass Q-TOF-Ultima spectrometer. X-band CW ESR spectra were measured on a Miniscope MS 300 (Magnettech GmbH, Germany). The g values are referenced to external Mn^{2+} in ZnS ($g = 2.118$, 2.066, 2.027, 1.986, 1.946, 1.906). Measurements were conducted at 77 K, and simulations were performed with the program package Easy-Spin.[45] ^{57}Fe Mößbauer measurements of powder samples were performed in transmission geometry using a constant-acceleration spectrometer and the source ^{57}Co(Rh). The Recoil 1.03 Mößbauer Analysis Software was used to fit the experimental spectra with Lorentzian peaks.[46] Isomer shift values are quoted relative to α-Fe at 295 K. Photostability measurements were conducted at room temperature under an Ar atmosphere in 0.1 M (nBu$_4$N)Cl in CH$_3$CN/H$_2$O (98:2, v/v) at $\lambda_{exc} = 400$ nm. The concentrations of the solutions were adjusted to ensure the same absorptivity at the excitation wavelength $\lambda_{exc} = 400$ nm. The concentrations of $1(PF_6)_2$, $2(PF_6)_2$, $3(PF_6)_2$, and [Fe(bpy)$_3$](PF$_6$)$_2$ were 2.17×10^{-4}, 1.86×10^{-4}, 4.75×10^{-4}, and 6.06×10^{-4} M, respectively. As light sources, Bivar LEDs (108 A-713–5059, 400 nm) were used in combination with a 40 W supply. Elemental analyses were performed at the microanalytical laboratory of the chemical institutes of the University of Mainz.

Crystal structure determinations

Intensity data were collected with a Bruker AXS Smart 1000 CCD diffractometer with an APEX II detector and an Oxford cooling system, and corrected for absorption and other effects using MoK$_\alpha$ radiation ($\lambda = 0.71073$ Å) at 173(2) K. The diffraction frames were integrated using the SAINT package, and most were corrected for absorption with MULABS.[47,48] The structures were solved by direct methods and refined by the full-matrix method based on F^2 using the SHELXTL software package.[49,50] All nonhydrogen atoms were refined anisotropically, and the positions of all hydrogen atoms were generated with appropriate geometric constraints and allowed to ride on their respective parent carbon atoms with fixed isotropic thermal parameters. See Tables S2 and S3 for crystal and structure refinement data.

CCDC 1016551 [$1(BF_4)_2 \cdot 2$ CH$_3$CN], 1016552 [$1(PF_6)_2 \cdot$CH$_3$CN], 1016553 [$2(PF_6)_2 \cdot$CH$_3$CN] and 1016554a[$3(PF_6)_2 \cdot {}^1/_2$ CH$_3$CN] contain the supplementary crystallographic data for this paper. These data can be obtained free of charge from The Cambridge Crystallographic Data Centre via www.ccdc.cam.ac.uk/data_request/cif.

52

3.1 RESULTS AND DISCUSSION: A HETEROLEPTIC PUSH–PULL SUBSTITUTED IRON(II) BIS(TRIDENTATE) COMPLEX WITH LOW-ENERGY CHARGE-TRANSFER STATES

DFT calculations

DFT calculations were performed with the Gaussian09/DFT[51] series of programs. The B3LYP formulation of DFT was used, employing the LANL2DZ basis set.[51] No symmetry constraints were imposed on the molecules. The presence of energy minima was checked by analytical frequency calculations. The integral-equation-formalism polarizable continuum model (IEFPCM, CH_3CN) was employed for solvent modeling. All calculations were performed without explicit counterions and solvent molecules.

Synthesis of 1(PF6)2

A solution of ddpd (176 mg, 0.60 mmol, 2.0 equiv.) in ethanol (10 mL) was added to a solution of $FeBr_2$ (65.0 mg, 0.30 mmol, 1.0 equiv.) in ethanol (10 mL). The solution turned brown immediately. The mixture was stirred at room temperature for 24 h. A brown solid precipitated, which was filtered off, washed with Et_2O (30 mL), and dried under reduced pressure. The brown bromide salt was dissolved in a mixture of CH_3CN (5 mL) and water (10 mL). Addition of solid $(NH_4)(PF_6)$ in excess resulted in the precipitation of a brown solid (86.0 mg, 0.09 mmol, 30%). Crystals suitable for single-crystal X-ray diffraction were obtained by slow diffusion of diethyl ether into a solution of **1(PF$_6$)$_2$** in CH_3CN. R_f (SiO$_2$, KNO$_{3(aq)}$:CH_3CN 4:1) = 0.25; MS (ESI$^+$): m/z (%): 292.14 (60) [ddpd + H]$^+$, 319.08 (64) [M−ddpd−2PF$_6$]$^{2+}$, 366.06 (100) [M−ddpd−2PF$_6$+ F]$^+$, 657.24 (45) [M−2PF$_6$+F]$^+$, 783.22 (29) [M−PF$_6$]$^+$, 951.18 (7) [M+Na]$^+$; UV/Vis (CH_3CN): λ_{max} (ε) = 395 (4570), 290 (17695), 243 nm (15525 M^{-1}cm^{-1}); IR (KBr): $\tilde{\nu}$ = 3485 (br, m, crystal water), 3119 (w), 2925 (w), 1600 (s), 1580 (s), 1570 (m), 1495 (s), 1455 (s), 1435 (s), 1345 (m), 1304 (s), 1170 (m), 950 (s), 840 (vs, PF), 795 (s), 775 (s), 750 (s), 560 cm^{-1} (s); Mößbauer (295 K): δ = 0.388 mm s^{-1}, ΔE_Q = 0.403 mm s^{-1}; CV (CH_3CN): $E_{1/2}$ = −2.33 (irrev.), 0.33 (rev.), 1.63 (irrev.) V vs. Fc/Fc$^+$; elemental analysis calcd (%) for $C_{34}H_{34}F_{12}FeN_{10}P_2$ (928.16)·H_2O: C 43.15, H 3.83, N 14.80; found: C 43.32, H 3.65, N 14.77.

Synthesis of 1(BF4)2

A solution of Fe(BF$_4$)$_2$·6 H$_2$O (308 mg, 0.91 mmol, 1.0 equiv.) in ethanol (10 mL) was added to a solution of ddpd (585.0 mg, 2.01 mmol, 2.2 equiv.) in ethanol (8 mL). The solution turned orange–brown immediately, and dark red within a few minutes. The mixture was stirred at room temperature for 50 min, and Et_2O (75 mL) was added. A brown solid precipitated, which was filtered off, washed with Et_2O (80 mL), and dried under reduced pressure. Upon recrystallization from ethanol, **1(BF$_4$)$_2$** was obtained (427.0 mg, 0.52 mmol, 58%). Crystals suitable for single-crystal X-ray diffraction were obtained by slow diffusion of diethyl ether into a solution of **1(BF$_4$)$_2$** in CH_3CN. MS (ESI$^+$): m/z (%): 319.11 (4) [M−2BF$_4$]$^{2+}$, 366.08 (100) [M−ddpd−2BF$_4$+F]$^+$, 751.16 (3) [2(M−2BF$_4$+F)+F]$^+$; IR (KBr): $\tilde{\nu}$ = 3485 (br, m, crystal water), 3074 (w, CH), 2922 (w, CH), 1643 (w), 1599 (s), 1582 (s), 1493 (s), 1450 (s), 1437 (vs), 1364 (s), 1344 (s), 1304 (w), 1285 (w), 1236 (s), 1138 (s), 1097 (s), 1065 (vs), 1032 (s, BF), 949 (w), 864 (w), 800 (m), 777 (m), 748 (m), 671 cm^{-1} (w); ^{1}H NMR (CD$_3$CN, 400 MHz): δ = 7.96 (2 H, t, $^3J_{HH}$ = 8.0 Hz, H18), 7.80 (4 H, m, H12), 7.12 (4 H, d, $^3J_{HH}$ = 8.0 Hz, H17), 7.11 (4 H, m, H13), 7.08 (4 H, m, H10), 6.75 (4 H, m, H11), 2.98 ppm (12 H, s, H15); ^{13}C NMR (CD$_3$CN, 100 MHz): δ = 162.5 (C14), 159.4 (C16), 155.7 (C10), 141.0 (C18), 140.3 (C12), 120.9 (C11), 113.2 (C13), 112.3 (C17), 39.8 ppm (C15).

Synthesis of 2(PF6)2

A solution of dcpp (1.36 g, 4.7 mmol, 1.0 equiv.) and ddpd (1.37 g, 4.7 mmol, 1.0 equiv.) in ethanol (80 mL) was added to a solution of $FeBr_2$ (1.02 g, 4.7 mmol, 1.0 equiv.) in ethanol (20 mL). The solution turned black immediately. The mixture was stirred at room temperature for 24 h. TLC control indicated a mixture of two complexes. Dilution with Et_2O (100 mL) led to precipitation of a blue solid. The solid was filtered off and washed with Et_2O (50 mL). The product was purified by column chromatography (SiO$_2$, CH_3CN/KNO$_{3(sat,aq)}$ 4:1). The solvent was removed under reduced pressure and the dark blue solid was washed with a mixture of CH_3CN/THF (1:15 v/v). The pure bromide salt **2(Br)$_2$** (1.15 g, 1.4 mmol, 30%) was dissolved in CH_3CN (30 mL), and solid $(NH_4)(PF_6)$ was added in excess. Addition of water (100 mL) resulted in the precipitation of dark blue **2(PF$_6$)$_2$** (0.65 g, 0.7 mmol, 15%). Crystals suitable for single-crystal X-ray diffraction were obtained by slow diffusion of diethyl ether into a solution of **2(PF$_6$)$_2$** in CH_3CN. R_f (SiO$_2$, KNO$_{3(aq)}$/CH_3CN 4:1) = 0.35; MS (ESI$^+$): m/z (%): 318.48 (95) [M−2PF$_6$]$^{2+}$, 366.06 (100) [M−dcpp−2PF$_6$+F]$^+$, 655.16 (57) [M−2PF$_6$+F]$^+$, 781.13 (29) [M−PF$_6$]$^+$, 1244.68 (14) [3M<M−>2PF$_6$]$^{2+}$, 1708.21 (15) [2M<M−>PF$_6$]$^+$; UV/Vis (CH_3CN): λ_{max} (ε) = 592 (4035), 374 (6905), 324 (13230), 295 (20215), 269 (25315), 240 nm (18630 M^{-1}cm^{-1}); IR (KBr): $\tilde{\nu}$ = 3443 (br, m, crystal water), 3091 (m, CH), 1674 (s), 1599 (s), 1493 (s), 1450 (s), 1435 (s), 949 (vs), 842 (s, PF), 804 (s), 667 cm^{-1} (s); Mößbauer (295 K): δ = 0.319 mm s^{-1}, ΔE_Q = 0.456 mm s^{-1}; CV (CH_3CN): $E_{1/2}$ = −2.22 (irrev.), −1.60 (rev.), −1.21 (rev.), 0.84 (rev.) V vs. Fc/Fc$^+$; elemental analysis calcd (%) for $C_{34}H_{28}F_{12}FeN_8O_2P_2$ (926.10)·3 H$_2$O: C 42.43, H 3.35, N 11.64; found: C 42.14, H 3.22, N 11.63.

Synthesis of 3(PF6)2

Dcpp (205 mg, 0.71 mmol, 2.0 equiv.) was added to a solution of Fe(BF$_4$)$_2$·6 H$_2$O (122 mg, 0.36 mmol, 1.0 equiv.) in CH_3CN (15 mL). The solution turned black immediately. After stirring at room temperature for 24 h, the mixture was diluted with Et_2O (30 mL), and a dark blue solid precipitated. The solid was filtered off, washed with Et_2O (30 mL), and dried under reduced pressure. The dark blue complex was dissolved in CH_3CN (10 mL), and $(NH_4)(PF_6)$ was added in excess. Et_2O (30 mL) was added, and resulted in the precipitation of a dark blue solid (250 mg, 0.27 mmol, 54%). Crystals suitable for single-crystal X-ray diffraction were obtained by slow diffusion of diethyl ether into a solution of **3(PF$_6$)$_2$** in CH_3CN. R_f (SiO$_2$, KNO$_{3(aq)}$/CH_3CN 4:1) = 0.55; MS(ESI$^+$): m/z (%): 317.02 (45) [M−2PF$_6$]$^{2+}$, 364.02 (17) [M−dcpp−PF$_6$+F]$^+$, 653.09 (100) [M−2PF$_6$+F]$^+$, 779.08 (18) [M−PF$_6$]$^+$; UV/Vis (CH_3CN): λ_{max} (ε) = 606 (7380), 514 (5520), 354 (13145), 275 nm (44040 M^{-1}cm^{-1}); IR (KBr): $\tilde{\nu}$ = 3337 (br, m, crystal water), 3132 (br), 3035 (m), 1680 (s, CO), 1595 (m), 1430 (s), 1403 (s), 842 (vs, PF), 738 (vs), 559 (m), 482 cm^{-1} (s); Mößbauer (295 K): δ = 0.318 mm s^{-1}, ΔE_Q = 0.322 mm s^{-1}; CV (CH_3CN): $E_{1/2}$ = −1.81 (rev.), −1.53 (rev.), −1.21 (rev.), −0.92 (rev.), 1.29 (rev.) V vs. Fc/Fc$^+$; elemental analysis calcd (%) for $C_{34}H_{22}F_{12}FeN_6O_4P_2$ (924.03)·4 CH$_3$CN·1 Et$_2$O: C 47.52, H 3.81, N 12.05; found: C 47.80, H 3.46, N 12.06.

Oxidation of 1(PF6)2

1(PF$_6$)$_2$ (222 mg, 0.24 mmol, 1.0 equiv.) was dissolved in a 0.5 M TFA/CH_3CN solution (20 mL) and $(NH_4)_2$Ce(NO$_3$)$_6$ (210 mg, 0.38 mmol, 1.6 equiv.) was added as a solid. The solvent was removed under reduced pressure and the residue was suspended in CH_3CN (50 mL). The remaining green solid was collected by filtration, washed with CH_3CN (50 mL), and dried under reduced pres-

3.1 RESULTS AND DISCUSSION: A HETEROLEPTIC PUSH–PULL SUBSTITUTED IRON(II) BIS(TRIDENTATE) COMPLEX WITH LOW-ENERGY CHARGE-TRANSFER STATES

53

sure to give **1(X)₃** (190 mg), which was used for Mößbauer measurements. Mößbauer (295 K): $\delta = 0.105$ mm s^{-1}, $\Delta E_Q = 1.973$ mm s^{-1}; EPR (0.5 M TFA/CH₃CN, 77 K): $g_1 = 2.490$, $g_2 = 2.295$, $g_3 = 1.810$; UV/Vis (H₂O): $\lambda_{max} = 1013$, 619, 457, 426 nm.

Oxidation of 2(PF6)2

2(PF₆)₂ (270 mg, 0.29 mmol, 1.0 equiv.) was dissolved in a 0.5 M TFA/CH₃CN solution (10 mL) and (NH₄)Ce(NO₃)₆ (255 mg, 0.47 mmol, 1.6 equiv.) was added as a solid. A brown solid precipitated, which was collected by filtration and dried under reduced pressure to give **2(X)₃** (218 mg), which was used for Mößbauer measurements. The counter ions have not yet been identified because upon washing with organic solvents, the brown precipitate turns blue, indicating the re-formation of **2²⁺**. For EPR measurements, a solution of **2(PF₆)₂** (8.0 mg, 8.6 µmol, 1.0 equiv.) in a 0.5 M TFA/CH₃CN solution (0.5 mL) was added to a solution of (NH₄)Ce(NO₃)₆ (7.6 mg, 13.8 µmol, 1.6 equiv.) in 0.5 M TFA/CH₃CN (0.5 mL) in an EPR tube. The EPR tube was immersed quickly in liquid nitrogen and the EPR spectrum was recorded. The UV/Vis spectrum of **2³⁺** was obtained by titration of **2(PF₆)₂** with (NH₄)Ce(NO₃)₆ in 0.5 M TFA/CH₃CN. Mößbauer (295 K): $\delta = 0.099$ mm s^{-1}, $\Delta E_Q = 1.584$ mm s^{-1}; EPR (0.5 M TFA/CH₃CN, 77 K): $g_1 = 2.821$, $g_2 = 2.247$, $g_3 = 1.561$; UV/Vis (CH₃CN/TFA): λ_{max} (ε) = 1280 (410), 775 (315), 545 nm (245 M^{-1}cm^{-1}).

Reduction of 2(PF6)2

A solution of **2(PF₆)₂** (10.3 mg, 0.01 mmol, 1.0 equiv.) in CH₂Cl₂ (1 mL) was added to a solution of CoCp*₂ (3.28 mg, 0.01 mmol, 1.0 equiv.) in CH₂Cl₂ (1 mL) under an inert atmosphere. An aliquot was placed in an EPR tube. The EPR tube was immersed quickly in liquid nitrogen and the EPR spectrum was recorded. EPR (CH₂Cl₂, 77 K): $g_{av} = 2.0008$.

Reduction of 3(PF6)2

A solution of **3(PF₆)₂** (10.0 mg, 0.01 mmol, 1.0 equiv.) in CH₂Cl₂ (1 mL) was added to a solution of CoCp*₂ (3.22 mg, 0.01 mmol, 1.0 equiv.) in CH₂Cl₂ (1 mL) under an inert atmosphere. An aliquot was placed in an EPR tube. The EPR tube was immersed quickly in liquid nitrogen and the EPR spectrum was recorded. EPR (CH₂Cl₂, 77 K): $g_{av} = 2.0073$.

Acknowledgements

[1] a) C. Balzani, S. Campagna, *Top. Curr. Chem., Vol. 280: Photochemistry and Photophysics of Coordination Compounds I*, Springer, Berlin, **2007**; b) C. Balzani, S. Campagna, *Top. Curr. Chem., Vol. 281: Photochemistry and Photophysics of Coordination Compounds II*, Springer, Berlin, **2007**.

[2] Y. Tanabe, S. Sugano, *J. Phys. Soc. Jpn.* **1954**, *9*, 766–779.

[3] General SCO: a) P. Gütlich, H. A. Goodwin, *Top. Curr. Chem., Vol. 233: Spin Crossover in Transition Metal Compounds I*, Springer, Berlin, **2004**; b) P. Gütlich, H. A. Goodwin, *Top. Curr. Chem., Vol. 234: Spin Crossover in Transition Metal Compounds II*, Springer, Berlin, **2004**; c) P. Gütlich, H. A. Goodwin, *Top. Curr. Chem., Vol. 235: Spin Crossover in Transition Metal Compounds III*, Springer, Berlin, **2004**; d) O. Kahn, C. Jay Martinez, *Science* **1998**, *279*, 44–48; e) P. Gütlich, Y. Garcia, T. Woike, *Coord. Chem. Rev.* **2001**, *219–221*, 839–879; f) J.-F. Létard, P. Guionneau, L. Goux-Capes, *Top. Curr. Chem.* **2004**, *235*, 221–249; g) A. Bousseksou, G. Molnar, L. Salmon, W. Nicolazzi, *Chem. Soc. Rev.* **2011**, *40*, 3313–3335; h) Special issue: *Spin-Crossover Complexes*, *Eur. J. Inorg. Chem.* **2013**, 574–1067.

[4] A. Marino, P. Chakraborty, M. Servol, M. Lorenc, E. Collet, A. Hauser, *Angew. Chem. Int. Ed.* **2014**, *53*, 3863–3867; *Angew. Chem.* **2014**, *126*, 3944–3948.

[5] S. Campagna, F. Puntoriero, F. Nastasi, G. Bergamini, V. Balzani, *Top. Curr. Chem.* **2007**, *280*, 117–214.

[6] a) L. Hammarström, O. Johansson, *Coord. Chem. Rev.* **2010**, *254*, 2546–2559; b) M. Abrahamsson, M. Jäger, T. Österman, L. Eriksson, P. Persson, H.-C. Becker, O. Johansson, L. Hammarström, *J. Am. Chem. Soc.* **2006**, *128*, 12616–12617; c) M. Abrahamsson, M. Jäger, R. J. Kumar, T. Österman, P. Persson, H.-C. Becker, O. Johansson, L. Hammarström, *J. Am. Chem. Soc.* **2008**, *130*, 15533–15542; d) R. J. Kumar, S. Karlsson, D. Streich, A. R. Jensen, M. Jäger, H.-C. Becker, J. Bergquist, O. Johansson, L. Hammarström, *Chem. Eur. J.* **2010**, *16*, 2830–2842.

[7] F. Schramm, V. Meded, H. Fliegl, K. Fink, O. Fuhr, Z. Qu, W. Klopper, S. Finn, T. E. Keyes, M. Ruben, *Inorg. Chem.* **2009**, *48*, 5677–5684.

[8] a) A. Breivogel, C. Förster, K. Heinze, *Inorg. Chem.* **2010**, *49*, 7052–7056; b) A. Breivogel, M. Meister, C. Förster, F. Laquai, K. Heinze, *Chem. Eur. J.* **2013**, *19*, 13745–13760; c) A. Breivogel, C. Kreitner, K. Heinze, *Eur. J. Inorg. Chem.* **2014**, DOI: 10.1002/ejic.201402466.

[9] A. Breivogel, S. Wooh, J. Dietrich, T. Y. Kim, Y. S. Kang, K. Char, K. Heinze, *Eur. J. Inorg. Chem.* **2014**, 2720–2734.

[10] A. Breivogel, M. Park, D. Lee, S. Klassen, A. Kühnle, C. Lee, K. Char, K. Heinze, *Eur. J. Inorg. Chem.* **2014**, 288–295.

[11] C. Sousa, C. de Graaf, A. Rudavskyi, R. Broer, J. Tatchen, M. Etinski, C. M. Marian, *Chem. Eur. J.* **2013**, *19*, 17541–17551.

[12] W. Gawelda, A. Cannizzo, V.-T. Pham, F. van Mourik, C. Bressler, M. Chergui, *J. Am. Chem. Soc.* **2007**, *129*, 8199–8206.

[13] Y. Liu, T. Harlang, S. E. Canton, P. Chábera, K. Suárez-Alcántara, A. Fleckhaus, D. A. Vithanage, E. Göransson, A. Corani, R. Lomoth, V. Sundström, K. Wärnmark, *Chem. Commun.* **2013**, *49*, 6412–6414.

[14] I. M. Dixon, F. Alary, M. Boggio-Pasqua, J.-L. Heully, *Inorg. Chem.* **2013**, *52*, 13369–13374.

[15] L. L. Jamula, A. M. Brown, D. Guo, J. K. McCusker, *Inorg. Chem.* **2014**, *53*, 15–17.

[16] S. Ferrere, B. A. Gregg, *J. Am. Chem. Soc.* **1998**, *120*, 843–844.

[17] W. Macyk, Gr. Stochel, K. Szaciłowski, *Chem. Eur. J.* **2007**, *13*, 5676–5687.

[18] M. Yang, D. W. Thompson, G. J. Meyer, *Inorg. Chem.* **2002**, *41*, 1254–1262.

[19] H. Li Chum, D. Koran, R. A. Osteryoung, *J. Am. Chem. Soc.* **1978**, *100*, 310–312.

[20] R.-A. Fallahpour, M. Neuburger, M. Zehnder, *New J. Chem.* **1999**, *23*, 53–61.

[21] I. M. Henderson, R. C. Hayward, *J. Mater. Chem.* **2012**, *22*, 21366–21369.

[22] K. Mack, A. Wünsche von Leupoldt, C. Förster, M. Ezhevskaya, D. Hinderberger, K. W. Klinkhammer, K. Heinze, *Inorg. Chem.* **2012**, *51*, 7851–7858.

[23] C. Förster, K. Mack, L. M. Carrella, V. Ksenofontov, E. Rentschler, K. Heinze, *Polyhedron* **2013**, *52*, 576–581.

[24] C. R. Goldsmith, T. D. P. Stack, *Inorg. Chem.* **2006**, *45*, 6048–6055.

[25] U. S. Schubert, H. Hofmeier, G. R. Newkome, *Modern Terpyridine Chemistry*, Wiley-VCH, Weinheim, **2006**.

[26] S. K. Hain, F. W. Heinemann, K. Gieb, P. Müller, G. Hörner, A. Grohmann, *Eur. J. Inorg. Chem.* **2010**, 221–232.

[27] W. Koch, M. C. Holthausen, *A Chemist's Guide to Density Functional Theory*, Wiley-VCH, Weinheim, **2001**.

[28] N. G. Connelly, W. E. Geiger, *Chem. Rev.* **1996**, *96*, 877–910.

[29] R. Aasa, *J. Chem. Phys.* **1970**, *52*, 3919–3930.

[30] R. E. DeSimone, R. S. Drago, *J. Am. Chem. Soc.* **1970**, *92*, 2343–2352.

[31] L. Duelund, H. Toftlund, *Spectrochim. Acta Part A* **2000**, *56*, 331–340.

3.1 RESULTS AND DISCUSSION: A HETEROLEPTIC PUSH–PULL SUBSTITUTED
IRON(II) BIS(TRIDENTATE) COMPLEX WITH LOW-ENERGY CHARGE-
TRANSFER STATES

54

[32] C. Olea-Azar, B. Abarca, E. Norambuena, L. Opazo, C. Rigol, R. Balles-teros, M. Chadlaoui, *Spectrochim. Acta Part A* **2005**, *61*, 2261–2266.

[33] S. Schenker, P. C. Stein, J. A. Wolny, C. Brady, J. J. McGarvey, H. Toftlund, A. Hauser, *Inorg. Chem.* **2001**, *40*, 134–139.

[34] J. K. McCusker, H. Toftlund, A. L. Rheingold, D. N. Hendrickson, *J. Am. Chem. Soc.* **1993**, *115*, 1797–1804.

[35] J. J. McGarvey, I. Lawthers, K. Heremans, H. Toftlund, *J. Chem. Soc. Chem. Commun.* **1984**, 1575–1576.

[36] J. J. McGravey, I. Lawthers, *J. Chem. Soc. Chem. Commun.* **1982**, 906–907.

[37] K. A. Reeder, E. V. Dose, L. J. Wilson, *Inorg. Chem.* **1978**, *17*, 1071–1075.

[38] E. V. Dose, M. A. Hoselton, N. Sutin, M. F. Tweedle, L. J. Wilson, *J. Am. Chem. Soc.* **1978**, *100*, 1141–1147.

[39] J. K. Beattie, R. A. Binstead, R. J. West, *J. Am. Chem. Soc.* **1978**, *100*, 3044–3050.

[40] F. Neese, *Coord. Chem. Rev.* **2009**, *253*, 526–563.

[41] S. Ye, F. Neese, *Inorg. Chem.* **2010**, *49*, 772–774.

[42] C. R. Jacob, M. Reiher, *Int. J. Quantum Chem.* **2012**, *112*, 3661–3684.

[43] K. P. Kepp, *Coord. Chem. Rev.* **2013**, *257*, 196–209.

[44] Q. Sun, S. Mosquera-Vazquez, L. M. Lawson Daku, L. Guénée, H. A. Goodwin, E. Vauthey, A. Hauser, *J. Am. Chem. Soc.* **2013**, *135*, 13660–13663.

[45] S. Stoll, A. Schweiger, *J. Magn. Reson.* **2006**, *178*, 42–55.

[46] K. Lagarec, D. G. Rancourt, *Nucl. Instrum. Methods Phys. Res. Sect. B* **1997**, *129*, 266–280.

[47] *SMART Data Collection and SAINT-Plus Data Processing Software for the SMART System*, various versions, Bruker Analytical X-ray Instruments, Madison, WI, **2000**.

[48] R. H. Blessing, *Acta Crystallogr. A* **1995**, *51*, 33–38.

[49] G. M. Sheldrick, *SHELXTL*, version 5.1, Bruker AXS, Madison, WI, **1998**.

[50] G. M. Sheldrick, *SHELXL-97*; University of Göttingen: Göttingen, Germany, **1997**.

[51] Gaussian 09, Revision A.02, M. J. Frisch, G. W. Trucks, H. B. Schlegel, G. E. Scuseria, M. A. Robb, J. R. Cheeseman, G. Scalmani, V. Barone, B. Mennucci, G. A. Petersson, H. Nakatsuji, M. Caricato, X. Li, H. P. Hratchian, A. F. Izmaylov, J. Bloino, G. Zheng, J. L. Sonnenberg, M. Hada, M. Ehara, K. Toyota, R. Fukuda, J. Hasegawa, M. Ishida, T. Nakajima, Y. Honda, O. Kitao, H. Nakai, T. Vreven, J. A. Montgomery, Jr., J. E. Peralta, F. Ogliaro, M. Bearpark, J. J. Heyd, E. Brothers, K. N. Kudin, V. N. Staroverov, R. Kobayashi, J. Normand, K. Raghavachari, A. Rendell, J. C. Burant, S. S. Iyengar, J. Tomasi, M. Cossi, N. Rega, J. M. Millam, M. Klene, J. E. Knox, J. B. Cross, V. Bakken, C. Adamo, J. Jaramillo, R. Gomperts, R. E. Stratmann, O. Yazyev, A. J. Austin, R. Cammi, C. Pomelli, J. W. Ochterski, R. L. Martin, K. Morokuma, V. G. Zakrzewski, G. A. Voth, P. Salvador, J. J. Dannenberg, S. Dapprich, A. D. Daniels, Ö. Farkas, J. B. Foresman, J. V. Ortiz, J. Cioslowski, D. J. Fox, Gaussian, Inc., Wallingford CT, **2009**.

3.2 "Boosting Vis/NIR Charge Transfer Absorptions of Iron(II) Complexes by N-Alkylation

and N-Deprotonation in the Ligand Backbone"

Andreas K. C. Mengel, Christian Bissinger, Matthias Dorn, Oliver Back, Christoph

Förster and Katja Heinze

Chem. Eur J. **2017**, in press.
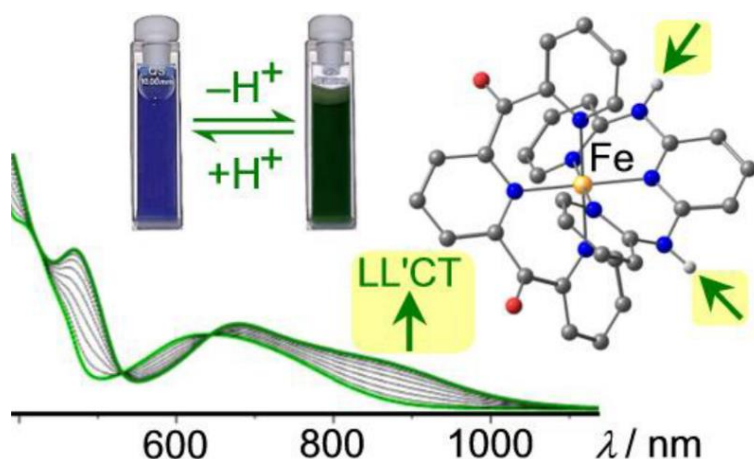
The heteroleptic $[Fe(H_2tpda)(dcpp)](PF_6)_2$ complex was synthesized and characterized by
▮▮▮▮▮▮▮ and the novel ligand hex_2tpda and homoleptic $[Fe(Hex_2tpda)_2](PF_6)_2$ was
synthesized by ▮▮▮▮▮▮▮▮ during their bachelor theses under the supervision of
Andreas K. C. Mengel. All remaining compounds were synthesized and characterized by
Andreas K. C. Mengel. The DFT calculations were carried out by Oliver Back (60 %) and
Andreas K. C. Mengel (40 %). The crystal structures were solved by Dr. Christoph Förster.
The manuscript was written by Prof. Dr. Katja Heinze based on a draft version of Andreas K.
C. Mengel.

Supporting information: page 129-160.

3.2 RESULTS AND DISCUSSION: BOOSTING VIS/NIR CHARGE TRANSFER ABSORPTIONS OF IRON(II) COMPLEXES BY N-ALKYLATION AND N-DEPROTONATION IN THE LIGAND BACKBONE

56

▌ **Luminescent Complexes**

Boosting Vis/NIR Charge-Transfer Absorptions of Iron(II) Complexes by N-Alkylation and N-Deprotonation in the Ligand Backbone

Andreas K. C. Mengel, Christian Bissinger, Matthias Dorn, Oliver Back, Christoph Förster, and Katja Heinze*[a]

◄◄ These are not the final page numbers!

3.2 RESULTS AND DISCUSSION: BOOSTING VIS/NIR CHARGE TRANSFER ABSORPTIONS OF IRON(II) COMPLEXES BY N-ALKYLATION AND N-DEPROTONATION IN THE LIGAND BACKBONE

57
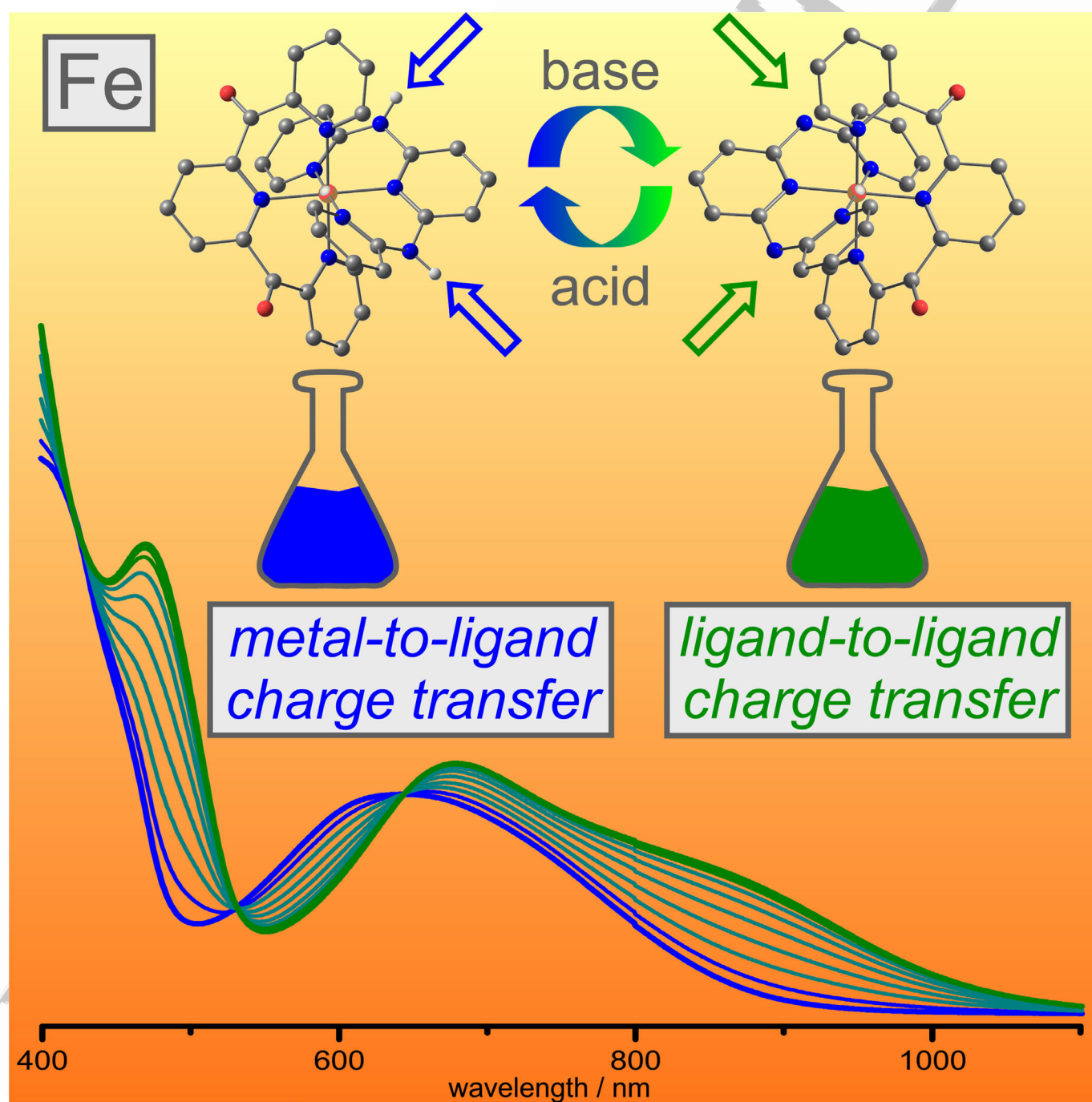
Abstract: Reversing the metal-to-ligand charge transfer (^{3}MLCT)/metal-centered (^{3}MC) excited state order in iron(II) complexes is a challenging objective, yet would finally result in long-sought luminescent transition-metal complexes with an earth-abundant central ion. One approach to achieve this goal is based on low-energy charge-transfer absorptions in combination with a strong ligand field. Coordinating electron-rich and electron-poor tridentate oligopyridine ligands with large bite angles at iron(II) enables both low-energy MLCT absorption bands around 590 nm and a strong ligand field. Variations of the electron-rich ligand by introducing longer alkyl substituents destabilizes the iron(II) complex towards ligand substitution reactions while hardly affecting the optical properties. On the other hand, N-deprotonation of the ligand backbone is feasible and reversible, yielding deep-green complexes with charge-transfer bands extending into the near-IR region. Time-dependent density functional theory calculations assign these absorption bands to transitions with dipole-allowed ligand-to-ligand charge transfer character. This unique geometric and electronic situation establishes a further regulating screw to increase the energy gap between potentially emitting charge-transfer states and the non-radiative ligand field states of iron(II) dyes.

Introduction

Six-coordinate ruthenium(II) polypyridine complexes are prototypical ingredients in photophysical and photochemical applications, including photocatalysis,[1] light-to-energy conversion such as dye-sensitized solar cells (DSSCs),[2] and display technologies.[3] Unfortunately, the usage of homologous earth-abundant iron(II) in these important fields is limited owing to the excited state ordering of iron(II) complexes with $E(^{1,3}\text{MLCT}) > E(^3\text{MC}) > E(^5\text{MC})$, leading to a rapid and efficient depopulation of the photophysically useful $^{1/3}$MLCT states (MLCT = metal-to-ligand charge transfer; MC = metal-centered). After excitation of the MLCT band, the prototypical low-spin iron(II) polypyridine complexes $[\text{Fe(bpy)}_3]^{2+}$ and $[\text{Fe(tpy)}_2]^{2+}$ relax through the $^1\text{MLCT} \rightarrow {}^3\text{MLCT} \rightarrow {}^3\text{MC} \rightarrow {}^5\text{MC} \rightarrow {}^1\text{GS}$ (ground state) cascade (bpy = 2,2'-bipyridine, tpy = 2,2':6',2''-terpyridine).[4, 5]

For $[\text{Fe(bpy)}_3]^{2+}$, $^1\text{MLCT} \rightarrow {}^3\text{MLCT}$ intersystem crossing (ISC) occurs in less than 20 fs,[6] the $^3\text{MLCT} \rightarrow {}^3\text{MC}$ internal conversion in around 150 ± 50 fs, and the $^3\text{MC} \rightarrow {}^5\text{MC}$ ISC in 70 ± 30 fs.[7] Hence, the ^5MC state is populated on the sub-picosecond timescale. The ^5MC high-spin states of $[\text{Fe(bpy)}_3]^{2+}$ and $[\text{Fe(tpy)}_2]^{2+}$ are long lived with lifetimes of 960 and 5350 ps, respectively.[8] For sensitizing purposes, MLCT lifetimes should significantly exceed 100 fs to allow efficient charge injection into a semiconductor as the injection occurs on this timescale.[9]

The obvious challenge is to reverse the energy between the ^{3}MLCT and the ^{3}MC (^{5}MC) states in low-spin iron(II) complexes. Recent ground-breaking approaches to increase the ^{3}MLCT lifetimes of iron(II) complexes are based on C^N^C pincer ligands or bidentate C^C ligands with N-heterocyclic carbene donors (NHCs, Scheme 1a)[10] or on tridentate N^N^N polypyridine ligands with large bite angles (Scheme 1b, dcpp = 2,6-bis(2-carboxypyridyl)pyridine, ddpd = N,N′-dimethyl-N,N′-dipyridine-2-yl-pyridine-2,6-diamine[11]).[8, 12] In both cases (Scheme 1b), the ligand field states ^{3}MC ($^3T_1$, $^3T_2$ in octahedral symmetry) and ^{5}MC ($^5T_2$) are shifted to higher energy relative to the $^1A_1$ ground state and the MLCT states. The strong field carbene ligands even increase the ^{3}MLCT lifetimes to the picosecond range (9–26 ps[10]). This is sufficiently long for charge injection into a TiO$_2$ semiconductor allowing for employment of these iron(II) carbene complexes as efficient sensitizers in DSSCs[13a,b] and as photosensitizer for proton reduction catalysts based on platinum nanoparticles.[13c]

The large bite angles of dcpp and ddpd (N-M-N ≈ 90°) induce a significantly enhanced metal–ligand orbital overlap and hence increase the ligand field strength compared to tpy (N-M-N ≈ 79°).[8, 11, 12] This strategy has been already successfully exploited for luminescent ruthenium(II)[11, 14–16] and Cr$^{\text{III}}$ complexes.[17] With iron(II) as the central ion, the ^{5}MC states are more destabilized than the ^{3}MC states at high ligand field strengths so that the energy of the ^{3}MC states is close to the

[a] A. K. C. Mengel, C. Bissinger, M. Dorn, O. Back, Dr. C. Förster, Prof. Dr. K. Heinze
Institute of Inorganic Chemistry and Analytical Chemistry
Johannes Gutenberg University of Mainz
Duesbergweg 10–14, 55128 Mainz (Germany)
Fax: (+ 49)6131-39-27-277
E-mail: katja.heinze@uni-mainz.de
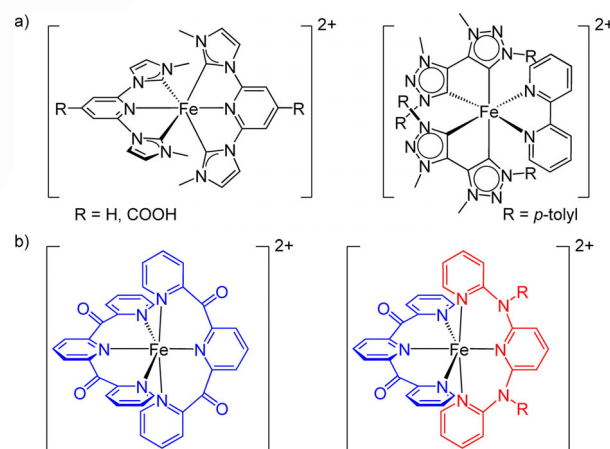
Scheme 1. Iron(II) complexes in strong ligand field environments by employing a) chelating N-heterocyclic carbene ligands[10] and b) polypyridine ligands dcpp and ddpd with large bite angles.[8, 12]

3.2 RESULTS AND DISCUSSION: BOOSTING VIS/NIR CHARGE TRANSFER ABSORPTIONS OF IRON(II) COMPLEXES BY N-ALKYLATION AND N-DEPROTONATION IN THE LIGAND BACKBONE

58

energy of the ^{5}MC states ($^5T_2/^3T_1$ crossing point in the d^6 Tanabe–Sugano diagram).[8,12] It has been suggested that the ^{5}MC states of [Fe(dcpp)$_2$]$^{2+}$ and [Fe(dcpp)(ddpd)]$^{2+}$ are not populated, resulting in a truncated relaxation cascade ^{1}MLCT→^{3}MLCT→^{3}MC→^{1}GS. Bypassing the long-lived ^{5}MC states could explain the observed faster ground state recovery with inverse rate constants of 280 and 548 ps for [Fe(dcpp)$_2$]$^{2+}$ and [Fe(dcpp)(ddpd)]$^{2+}$, respectively.[8,12] Furthermore, the electron-withdrawing dcpp ligand significantly lowers the energy of the $^{1/3}$MLCT states, giving deep-blue complexes with absorption bands around 600 nm tailing into the NIR region.[8,12] Harvesting of low-energy Vis/NIR photons is also beneficial for DSSC applications.[2,18,19] However, not every low-energy MLCT state is capable of injecting electrons efficiently.[20]

A similar situation is assumed for [Fe(bpy)(CN)$_4$]$^{2−}$, which incorporates strong field cyanido ligands and an electron-accepting bpy ligand.[21] This ligand combination gives rise to low-energy ^{1}MLCT absorption bands around 650 nm. The ^{3}MLCT, ^{3}MC, and ^{5}MC states are close in energy, yet their excited state distortions are distinctly different. The strong distortion of the ^{5}MC state prevents its efficient population. The lifetime of the ^{3}MLCT state amounts to 19 ps, although it remains unclear whether the ^{3}MLCT decays via an ultra-short-lived ^{3}MC state or directly to the ground state.[21]

Neither approach has yet succeeded in giving luminescent iron(II) complexes with sufficiently long ^{3}MLCT lifetimes. However, theoretical studies suggest that a suitably strong ligand field combined with low-energy charge-transfer states could possibly yield luminescent iron(II) complexes.[22,23]

In the present study, we target low-energy CT states in combination with high-energy ^{3}MC and ^{5}MC states in six-coordinate iron(II) complexes. To this end, we combine the electron-accepting dcpp ligand[14] with N^N^N ligands featuring large bite angles and varying electron-donating power. The employed electron-rich N^N^N ligands are derived from the known H$_2$tpda ligand (H$_2$tpda = 2,6-bis(2-pyridylamino)pyridine)[24] by alkylating the bridging nitrogen atoms with n-propyl or n-hexyl substituents (Pr$_2$tpda, Hex$_2$tpda). Alkylation of ruthenium(II)-based sensitizers boosts the performance of DSSCs, which provides a further motivation for the decoration with long alkyl chains.[25] Additionally, the electron-donating power of the H$_2$tpda ligand will be increased by N-deprotonation to give the anionic ligands [Htpda]$^−$ and [tpda]$^{2−}$ in the corresponding heteroleptic iron(II) complexes [Fe(dcpp)(Htpda)]$^+$ and Fe(dcpp)(tpda) with strong push–pull character. The mononuclear Fe(dcpp)(tpda) complex is fundamentally different from pentanuclear string complexes of the type M^{II}$_5$(tpda)$_4$X$_2$ involving the [tpda]$^{2−}$ ligand, which are prepared from MX$_2$, H$_2$tpda, and a base by self-assembly.[26]

The effects of N-alkylation and N-deprotonation on the optical properties and the stabilities of the homo- and heteroleptic complexes [Fe(R$_2$tpda)$_2$]$^{2+}$ and [Fe(dcpp)(R$_2$tpda)]$^{2+}$ will be explored and discussed in the following (R=H, Me, nPr, nHex; in this nomenclature, the ddpd ligand corresponds to Me$_2$tpda).

The results will form the basis for a new design principle towards long-lived CT states targeting new low-spin iron(II) complexes with sensitizing and hopefully luminescent properties.

Results and Discussion

Synthesis and characterization of ligands and iron(II) complexes

The known ligands H$_2$tpda,[24] Me$_2$tpda,[11] and dcpp[14,27] were prepared according to literature procedures. Deprotonation of H$_2$tpda by sodium hydride and treating the amide anions with n-propyl and n-hexyl iodide furnishes the N-alkylated ligands Pr$_2$tpda or Hex$_2$tdpa, respectively, in moderate yields as yellow oils after chromatographic workup (Figures S1–S6 in the Supporting Information).

The red-brown homoleptic iron(II) complexes [Fe(Pr$_2$tpda)$_2$][BF$_4$]$_2$ and [Fe(Hex$_2$tpda)$_2$][PF$_6$]$_2$ are prepared similar to the synthesis of [Fe(Me$_2$tpda)$_2$]$^{2+}$ from Fe[BF$_4$]$_2$·6H$_2$O and the respective ligand in an appropriate stoichiometric ratio (Scheme 2a).[12] The structure of [Fe(H$_2$tpda)$_2$]Cl$_2$ in the solid
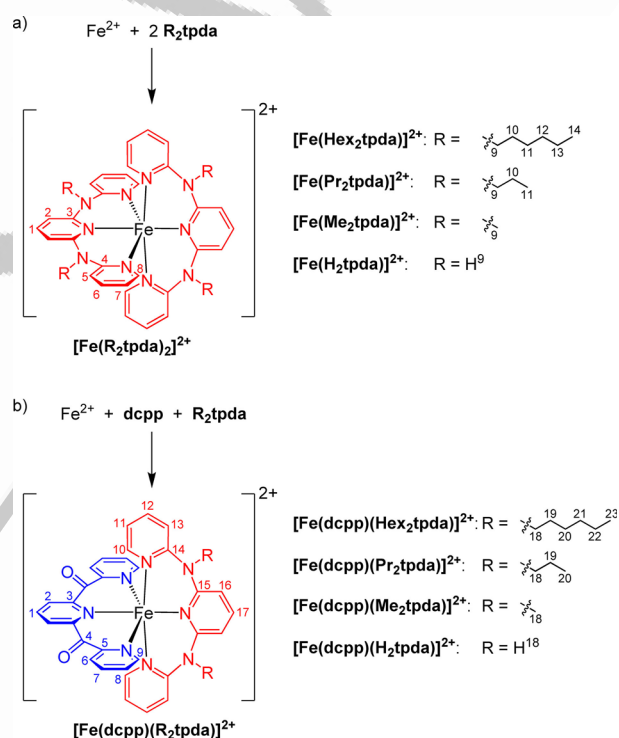
Scheme 2. Synthesis of [Fe(R$_2$tpda)$_2$]$^{2+}$ and [Fe(dcpp)(R$_2$tpda)$_2$]$^{2+}$ complexes and atom numbering used for NMR assignments.

state and its UV/Vis spectrum has been reported before,[28] yet for comparison reasons we prepared and fully characterized [Fe(H$_2$tpda)$_2$][BF$_4$]$_2$ as well. This furnishes the complete series of homoleptic complexes [Fe(R$_2$tpda)$_2$]$^{2+}$ with R=H, Me, nPr, nHex without the acceptor ligand.

The deep-blue heteroleptic complexes [Fe(dcpp)(R$_2$tpda)]$^{2+}$ (R=H, nPr, nHex) are obtained from an appropriate iron(II) salt and the two ligands in a 1:1:1 ratio, similar to the preparation of [Fe(dcpp)(Me$_2$tpda)]$^{2+}$ (Scheme 2b).[12] As found for [Fe(dcpp)(Me$_2$tpda)]$^{2+}$, the formation of heteroleptic complexes is favored over the homoleptic ones.[12] However, complexes featuring ligands with longer alkyl chains require signifi-

3.2 RESULTS AND DISCUSSION: BOOSTING VIS/NIR CHARGE TRANSFER ABSORPTIONS OF IRON(II) COMPLEXES BY N-ALKYLATION AND N-DEPROTONATION IN THE LIGAND BACKBONE

59

cantly increased reaction times and the use of dry solvents and molecular sieves for water removal and complete ligand coordination. This furnishes the complete series of heteroleptic complexes [Fe(dcpp)(R$_2$tpda)$_2$]$^{2+}$ with R=H, Me, nPr, nHex featuring the electron-accepting dcpp ligand.

ESI$^+$ mass spectra of all complexes show peaks at mass-to-charge ratios consistent with the dicationic nature of [Fe(R$_2$tpda)$_2$]$^{2+}$ and [Fe(dcpp)(R$_2$tpda)$_2$]$^{2+}$, respectively (Figures S7–S12 in the Supporting Information). Mass spectra of the homoleptic complexes show peaks for protonated [R$_2$tpda+H]$^+$ at $m/z=264$, 348, 432 (R=H, nPr, nHex), whereas the heteroleptic complexes additionally show peaks for protonated [dcpp+H]$^+$ at $m/z=290$, suggesting facile ligand decoordination under the ESI conditions. Fragments corresponding to [Fe(R$_2$tpda)F]$^+$ are observed in all cases as well, showing chelate ligand displacement by fluoride transfer from the [BF$_4$]$^-$ or [PF$_6$]$^-$ counter ions. The ease of ligand dissociation, especially concerning the alkylated ligands, is already reflected in the reluctant formation of the respective complexes (see above). The substitutional lability of Pr$_2$tpda and Hex$_2$tpda in iron(II) complexes will be discussed below.

Complexes of H$_2$tpda furthermore show fragments corresponding to proton loss at $m/z=318$, 581, and 607, corresponding to [Fe(Htpda)]$^+$, [Fe(Htpda)(H$_2$tpda)]$^+$, and [Fe(dcpp)(Htpda)]$^+$, respectively. This suggests that the complexes [Fe(H$_2$tpda)$_2$]$^{2+}$ and [Fe(dcpp)(H$_2$tpda)$_2$]$^{2+}$ are remarkably acidic. This will be further detailed and exploited below.

Sharp absorption bands are observed in the IR spectra (Figures S13–S20 in the Supporting Information) for the NH stretch of H$_2$tpda complexes at 3345 and 3380 cm^{-1} for [Fe(H$_2$tpda)$_2$]$^{2+}$ and [Fe(dcpp)(H$_2$tpda)$_2$]$^{2+}$ and for the C=O stretch of the dcpp complexes [Fe(dcpp)(R$_2$tpda)$_2$]$^{2+}$ around 1680 cm^{-1}, respectively. These values suggest a second sphere coordination of counter ions or solvents to the NH and CO groups (see below for selected solid-state structures). The counter ions cause characteristic absorption bands around 1060 cm^{-1} (BF) and 840 cm^{-1} (PF).

NMR spectra of the diamagnetic, low-spin iron(II) complexes feature ^{1}H and ^{13}C NMR resonances expected for the constituting ligands (Figures S21–S32 in the Supporting Information). The chemical shifts are unremarkable except for the CH$_2$ protons of the n-propyl and n-hexyl substituents close to the nitrogen atom. The CH$_2$ protons in the α and β positions relative to the nitrogen atom give rise to different chemical shifts at $\delta=3.8$–3.5 (H^a) and 3.4–3.3 (H^b) ppm for the α protons and at $\delta=1.1$–0.9 (H^b) and 0.2–0.7 (H^a) ppm for the β protons and are hence diastereotopic (Figures S23, S25, S29, and S31 in the Supporting Information). Clearly, the confined space within the ligand pocket of the complex hampers rotational averaging. The rigid geometry suggests steric interactions of the alkyl substituents with the coordinating pyridine rings and may be a driving force for the observed facile ligand displacement (see ESI mass spectrometry) and the retarded complex formation with Pr$_2$tpda and Hex$_2$tpda ligands (see synthesis). Indeed, in the presence of water, further proton resonances of [Fe(Pr$_2$tpda)$_2$]$^{2+}$ corresponding to freely rotating propyl groups around $\delta=4.01$, 1.78, and 0.99 ppm along with resonances for

a decoordinated pyridine ring at $\delta=7.97$, 7.88, 7.40, and 7.18 ppm appear (Figure S33 in the Supporting Information). Similar observations apply to [Fe(Hex$_2$tpda)$_2$]$^{2+}$ (Figure S34 in the Supporting Information). This is consistent with the initial substitution of a coordinated pyridine by water and released steric strain (Scheme 3). In the presence of excess water, R$_2$tpda (R=nPr, nHex) completely dissociates irreversibly from [Fe(R$_2$tpda)(dcpp)]$^{2+}$ (R=Pr, Hex; Figures S35 and S36 in the Supporting Information).
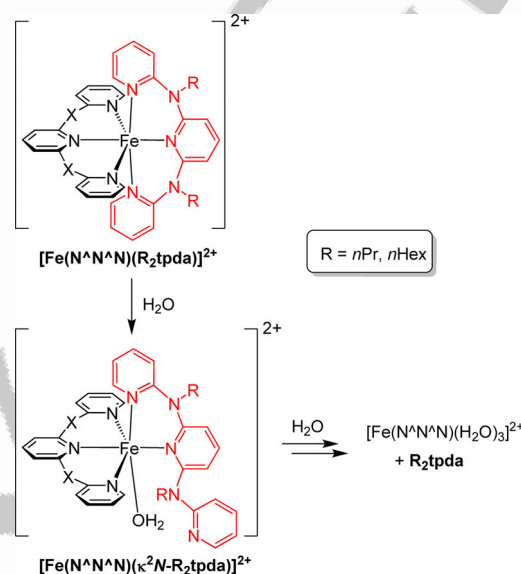
Scheme 3. Partial and complete R$_2$tpda ligand substitution of [Fe(N^N^N)(R$_2$tpda)]$^{2+}$ in the presence of water.

According to UV/Vis spectroscopic monitoring of the charge-transfer band of the blue heteroleptic complexes, [Fe(dcpp)(Pr$_2$tpda)]$^{2+}$ and [Fe(dcpp)(Hex$_2$tpda)]$^{2+}$ hydrolyze in a biphasic reaction with the Hex$_2$tpda ligand dissociating faster than the Pr$_2$tpda ligand in the presence of excess water (Figures S37 and S38 in the Supporting Information). Complexes with R=H and R=Me are stable in the presence of water. Larger steric strain in the periphery of complexes with longer alkyl chains clearly facilitates ligand substitution in homo- and heteroleptic iron(II) complexes of R$_2$tpda ligands.

In an associative ligand substitution mechanism, steric protection should retard the substitution, whereas for dissociative (D)/dissociative-interchange (I$_d$) substitution mechanisms, the reaction should be facilitated. As we observe a favored substitution, we assume a dissociative/intermediate–dissociative mechanism enabled by the release of ligand strain.[29] Hence, steric bulk—even from rather small linear alkyl groups—at the bridging atom destabilizes the iron(II) complexes with R$_2$tpda-based ligands.

Interestingly, the solubility of [Fe(Hex$_2$tpda)$_2$][PF$_6$]$_2$ is higher in CH$_3$CN (1.86 mol L^{-1}) than in CH$_2$Cl$_2$ (0.24 mol L^{-1}), whereas the reverse is found for [Fe(Me$_2$tpda)$_2$][PF$_6$]$_2$ (CH$_3$CN: 0.24 mol L^{-1}; CH$_2$Cl$_2$: 0.40 mol L^{-1}). This is probably associated with the different ion pairing properties[30] of the salts and solubilization power of the solvents. Tight ion pairs are also observed in the solid state.

3.2 RESULTS AND DISCUSSION: BOOSTING VIS/NIR CHARGE TRANSFER
ABSORPTIONS OF IRON(II) COMPLEXES BY N-ALKYLATION AND
N-DEPROTONATION IN THE LIGAND BACKBONE

60

Solid-state structures of selected iron(II) complexes

We report the solid-state structures of $[Fe(Hex_2tpda)_2][PF_6]_2$ and of $[Fe(dcpp)(H_2tpda)][PF_6]_2 \cdot 3.5\,H_2O$. The solid-state structures of $[Fe(H_2tpda)_2]Cl_2 \cdot 2\,MeOH$,[28] $[Fe(Me_2tpda)_2][PF_6]_2 \cdot CH_3CN$,[12] and $[Fe(dcpp)(Me_2tpda)][PF_6]_2 \cdot CH_3CN$[12] have been reported previously and are included here to discuss ion pairing and solvation in the solid state from a broader perspective (Figures 1 and 2; Figures S39 and S40 in the Supporting Information).

The H_2tpda complexes $[Fe(H_2tpda)_2]Cl_2 \cdot 2\,MeOH$ and $[Fe(dcpp)(H_2tpda)][PF_6]_2 \cdot 3.5\,H_2O$ feature hydrogen bonds from the NH groups of H_2tpda to counter ions (Cl^-, $[PF_6]^-$) or solvents ($MeOH$, H_2O) as suggested from the IR data. Water further solvates the carbonyl groups of dcpp by hydrogen bonds as exemplified in the solid state for $[Fe(dcpp)(H_2tpda)]$ $[PF_6]_2 \cdot 3.5\,H_2O$ (Figure S40 in the Supporting Information).

Hexafluorophosphate counter ions surround the cations with Fe···F distances of 4.5–7.6 Å with the counter ions bridging the cations in a μ_2 or μ_3 fashion. With an arbitrary cut-off of 6 Å, both $[Fe(Me_2tpda)_2][PF_6]_2 \cdot CH_3CN$ and $[Fe(Hex_2tpda)_2]$
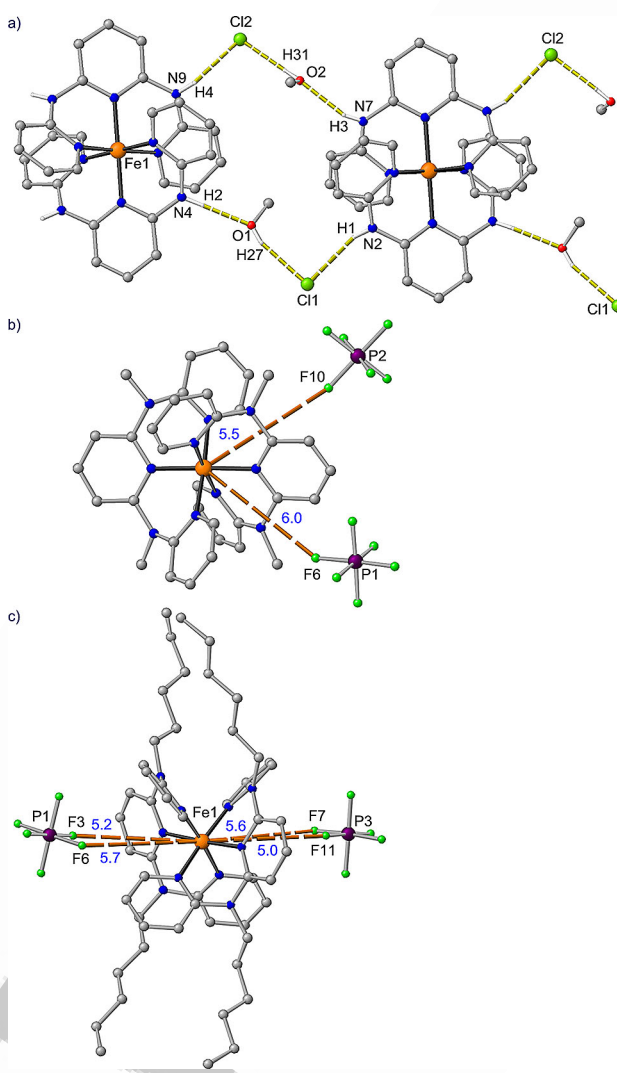
Figure 1. Illustration of the second coordination sphere of a) $[Fe(H_2tpda)_2]Cl_2$,[28] b) $[Fe(Me_2tpda)_2][PF_6]_2$[12] and c) $[Fe(Hex_2tpda)_2][PF_6]_2$ in the solid state; distances given in Å; CH hydrogen atoms omitted.

$[PF_6]_2$ feature a second-sphere coordination number of [2+6] counter ions. Figure 1 depicts the cations and the two closest counter ions and Figure S39 (in the Supporting Information) illustrates the [2+6] coordination.

The heteroleptic complexes $[Fe(dcpp)(H_2tpda)]^{2+}$ and $[Fe(dcpp)(Me_2tpda)]^{2+}$ realize [3+5] and [3+4] second-sphere coordination by the counter ions. Figure 2 shows the three closest contacts. Interestingly, a C=O group of a neighboring complex molecule approaches the iron center with Fe···O dis-
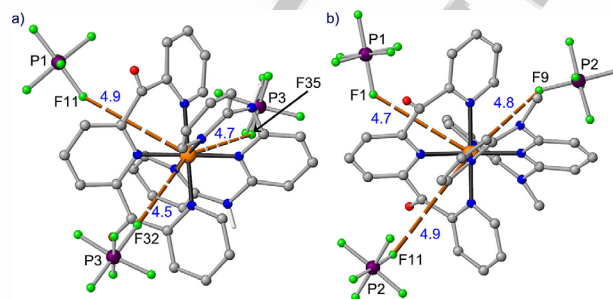
Figure 2. Illustration of the second coordination sphere of a) $[Fe(dcpp)(H_2tpda)][PF_6]_2$ and b) $[Fe(dcpp)(Me_2tpda)][PF_6]_2$[12] in the solid state; distances given in Å; CH hydrogen atoms omitted.

tances of 4.6–4.7 Å in both cases (Figure S40 in the Supporting Information). Two water molecules are additionally present in the pockets of $[Fe(dcpp)(H_2tpda)]^{2+}$ with Fe···O distances of 6.3–6.4 Å (Figure S40 in the Supporting Information). This second-sphere coordination suggests that nucleophiles (solvents, ions) can easily approach the iron(II) center in the six-coordinate complexes, which enables substitution reactions (I_d mechanism).

The steric strain as measured from the pyramidalization of the bridging nitrogen atoms of the R_2tpda ligand in $[Fe(H_2tpda)_2]^{2+}$,[28] $[Fe(Me_2tpda)_2]^{2+}$,[12] and $[Fe(Hex_2tpda)_2]^{2+}$ inversely correlates to the degree of planarization photoluminescence (PL) at the nitrogen atom ($PL = 100 \times [\Sigma(X\text{-}N\text{-}Y) - 3 \times 109.5°]/[3 \times 120.0° - 3 \times 109.5°] = 100, 88, 77\%$). A similar trend of the pyramidalization of the bridging nitrogen atoms is found for $[Fe(dcpp)(H_2tpda)]^{2+}$ and $[Fe(dcpp)(Me_2tpda)]^{2+}$ (PL = 100, 87%, respectively). The steric pressure might also affect the substitutional reactivity.

Fe–N distances, as well as N-Fe-N angles, allow the description of all $[FeN_6]$ coordination polyhedra as essentially octahedral. This has been suggested as an important prerequisite to achieve a large ligand field splitting in bis(tridentate) $[M(N^\wedge N^\wedge N)_2]^{n+}$ complexes.[12,14–17,31] The central pyridine rings are not oriented perpendicularly (90°), but are inclined by only $\approx 30°$ (Figures 1 and 2).

Optical properties of iron(II) complexes

The red-brown homoleptic complexes $[Fe(Pr_2tpda)_2]^{2+}$ and $[Fe(Hex_2tpda)_2]^{2+}$ possess absorption bands around 389–434 nm, which are assigned to mixed charge-transfer and ligand field transitions similar to the analogous band of $[Fe(Me_2tpda)_2]^{2+}$ (Figures S41 and S42 in the Supporting Informa-

↖↖ **These are not the final page numbers!**

3.2 RESULTS AND DISCUSSION: BOOSTING VIS/NIR CHARGE TRANSFER
ABSORPTIONS OF IRON(II) COMPLEXES BY N-ALKYLATION AND
N-DEPROTONATION IN THE LIGAND BACKBONE

61

tion).[12] Hence, R = Me, nPr, nHex bears no influence on the CT properties in the homoleptic complexes. Interestingly, the UV/Vis spectrum of [Fe(H$_2$tpda)$_2$]$^{2+}$ strongly differs from that of the alkyl derivatives (Figure S43 in the Supporting Information and Ref. [28]). It is conceivable that [Fe(H$_2$tpda)$_2$]$^{2+}$ partially deprotonates under these conditions (cf. ESI mass spectra and see below). However, addition of small amounts of trifluoroacetic acid to obtain fully protonated [Fe(H$_2$tpda)$_2$]$^{2+}$ resulted in decomposition.

All heteroleptic complexes [Fe(dcpp)(R$_2$tpda)]$^{2+}$ feature essentially identical charge-transfer bands around $\lambda_{max} = 592$ nm, irrespective of the substituent R at the nitrogen atom (Figure S44 in the Supporting Information). The charge-transfer character of these bands has been already demonstrated for [Fe(dcpp)(Me$_2$tpda)]$^{2+}$.[12] The independence from R demonstrates that the substituent bears no impact on the push–pull character and thus the charge-transfer properties of heteroleptic [Fe(dcpp)(R$_2$tpda)]$^{2+}$ complexes. Furthermore, [Fe(dcpp)(H$_2$tpda)]$^{2+}$ is not deprotonated under these conditions, unlike the homoleptic complex [Fe(H$_2$tpda)$_2$]$^{2+}$. Although the electronic influence of N-alkylation on the CT properties proved only marginal, selective deprotonation of [Fe(dcpp)(H$_2$tpda)]$^{2+}$ at the bridging nitrogen offers further opportunities (cf. ESI$^+$ mass spectrometry and see below).

Redox properties of iron(II) complexes

Redox potentials were measured by cyclic voltammetry in [nBu$_4$N][PF$_6$]/CH$_3$CN solution and the potentials are given relative to the ferrocene/ferrocenium couple. All R$_2$tpda ligands show only irreversible oxidation waves of the amine moieties (Figure S45 in the Supporting Information). However, the iron(II) complexes can be reversibly oxidized to their respective iron(III) counterparts, similar to the prototypic complexes [Fe(Me$_2$tpda)$_2$]$^{2+}$ and [Fe(dcpp)(Me$_2$tpda)]$^{2+}$ (Figures S46 and S47 in the Supporting Information).[12]

In the homoleptic series, the redox potential depends significantly on R (Figure S46 in the Supporting Information). The remarkably low potential of "[Fe(H$_2$tpda)$_2$]$^{2+}$" ($E_{1/2} = 0.17$ V) is probably caused by the already suggested deprotonation reaction to [Fe(Htpda)(H$_2$tpda)]$^+$ facilitating oxidation to iron(III). For R = Me, nPr, nHex, the Fe$^{III/II}$ potential increases from 0.33 V and 0.42 V to 0.44 V. This might be tentatively assigned to second-sphere coordination effects (Figure S39 in the Supporting Information).

In the heteroleptic series [Fe(dcpp)(R$_2$tpda)]$^{2+}$, the Fe$^{III/II}$ redox potential is independent of the substituent R (Figure S47 in the Supporting Information). This is in line with the optical properties (see above). Ligand (dcpp) centered reductions of the heteroleptic complexes [Fe(dcpp)(R$_2$tpda)]$^{2+}$ with R = nPr, nHex are irreversible, in contrast to the reversible dcpp/dcpp$^{\bullet-}$ reduction in [Fe(dcpp)(Me$_2$tpda)]$^{2+}$.[12] Scanning the potential below −0.8 V even produces new electrochemically active species from [Fe(dcpp)(R$_2$tpda)]$^{2+}$ (R = nPr, nHex) with re-oxidation waves appearing around 0.4 V (Figure S47 in the Supporting Information).

Acidity of [Fe(dcpp)(H$_2$tpda)]$^{2+}$ and optical properties of [Fe(dcpp)(Htpda)]$^+$ and Fe(dcpp)(tpda)

Counter ions and solvent water molecules coordinate to the NH groups of [Fe(dcpp)(H$_2$tpda)]$^{2+}$ (Figure S40a in the Supporting Information). ESI$^+$ mass spectrometry already suggested that the NH groups of [Fe(dcpp)(H$_2$tpda)]$^{2+}$ are acidic (see above). Hence, we hypothesized that selective deprotonation of [Fe(dcpp)(H$_2$tpda)]$^{2+}$ (instead of decoration with long alkyl groups R = nPr, nHex) might be feasible to give stable complexes with strong push–pull character and hence modified optical properties. Bases such as potassium $tert$-butoxide or potassium bis(trimethylsilyl)amide decomposed the complex, probably by ligand substitution instead of deprotonation. However, the non-nucleophilic Schwesinger base P$_1$-tBu [$tert$-butyliminotris(dimethylamino)phosphorane, pK_a(MeCN) = 26.98,[32] cleanly deprotonates [Fe(dcpp)(H$_2$tpda)]$^{2+}$ without decomposition (Scheme 4). With two equivalents of P$_1$-tBu, the green neutral complex Fe(dcpp)(tpda) forms, which is identified by its ^{1}H and ^{13}C NMR spectral signature in CD$_3$CN (Figures S48 and S49 in the Supporting Information). The NH proton resonance at $\delta = 8.56$ ppm (H^{18}) vanishes completely and the ^{1}H NMR resonances of the [tpda]$^{2-}$ ligands are strongly shifted to high fields with respect to those of H$_2$tpda. The resonances of the dcpp ligand are less affected.
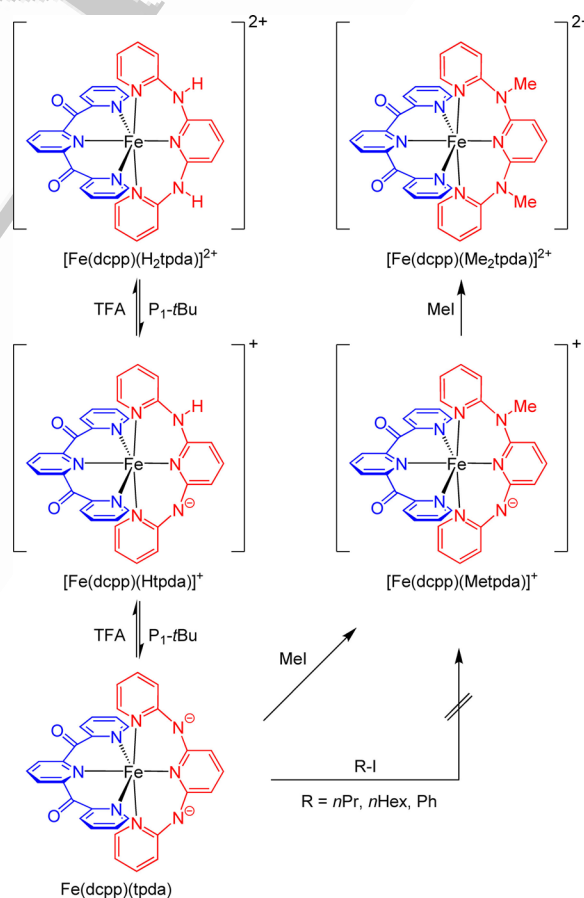
Scheme 4. Acid–base equilibria of [Fe(dcpp)(H$_2$tpda)]$^{2+}$, [Fe(dcpp)(Htpda)]$^+$, and Fe(dcpp)(tpda) and alkylation of Fe(dcpp)(tpda).

These are not the final page numbers! ↗↗

3.2 RESULTS AND DISCUSSION: BOOSTING VIS/NIR CHARGE TRANSFER
ABSORPTIONS OF IRON(II) COMPLEXES BY N-ALKYLATION AND
N-DEPROTONATION IN THE LIGAND BACKBONE

62

Titrating the diprotic acid [Fe(dcpp)(H$_2$tpda)]$^{2+}$ with P$_1$-tBu delivers two series of UV/Vis/NIR spectra in CH$_3$CN with individual isosbestic points at 315, 336, 488, 617, and 421, 532, 643 nm, respectively (Figure 3 a, b). Clearly, both corresponding green bases [Fe(dcpp)(Htpda)]$^+$ and Fe(dcpp)(tpda) are accessible. To re-protonate Fe(dcpp)(tpda) to [Fe(dcpp)(Htpda)]$^+$ 1300 equivalents of TFA are required, whereas full protonation requires an excess of 75 000 equivalents of TFA (Figure 3 c, d). This demonstrates the high acidity of [Fe(dcpp)(H$_2$tpda)]$^{2+}$ (Scheme 4).
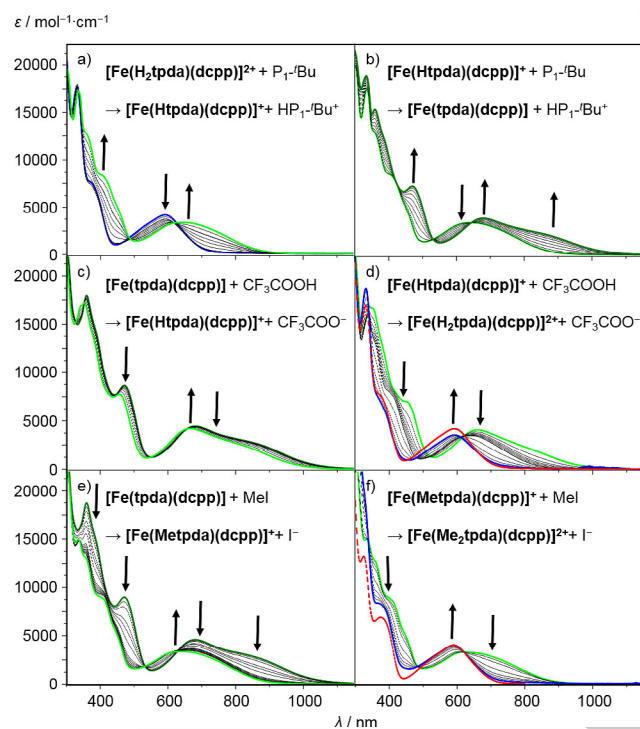
Figure 3. UV/Vis spectroscopic monitoring of a), b) the stepwise deprotonation of [Fe(dcpp)(H$_2$tpda)]$^{2+}$ to [Fe(dcpp)(Htpda)]$^+$ and Fe(dcpp)(tpda) by using P$_1$-tBu as base. c), d) The stepwise re-protonation of Fe(dcpp)(tpda) by TFA as acid (the red spectrum is that of [Fe(dcpp)(H$_2$tpda)]$^{2+}$). e), f) The stepwise alkylation of Fe(dcpp)(tpda) by MeI (the red spectrum is that of [Fe(dcpp)(Me$_2$tpda)]$^{2+}$) in CH$_3$CN.

The stability of Fe(dcpp)(tpda) prompted us to attempt alkylation/arylation reactions directly on the metal complex by using iodobenzene, n-hexyl iodide, n-propyl iodide, and methyl iodide, respectively (Scheme 4). Not too unexpectedly, this reaction only succeeds with the smallest electrophile, MeI (Figure 3 e, f). A large excess of MeI is required for the reaction to proceed at a useful rate. Similar to the protonation sequence, an intermediate monomethylated complex [Fe(dcpp)(Metpda)]$^+$ is identified by its UV/Vis/NIR characteristics (2500 equiv MeI). Formation of the final complex [Fe(dcpp)(Me$_2$tpda)]$^{2+}$ in a reasonable amount of time requires 18 000 equivalents of MeI. The thus-obtained [Fe(dcpp)(Me$_2$tpda)]$^{2+}$ complex is identified by comparing its ^{1}H NMR spectrum with that of an authentic sample (Figure S50 in the Supporting Information).[12]

Both [Fe(dcpp)(Htpda)]$^+$ and Fe(dcpp)(tpda) display irreversible oxidation waves around $E^p = 0.5$ V, which can be assigned to the oxidation of the deprotonated amino group(s) (Figure S51 in the Supporting Information). This irreversible behavior also blurs the Fe$^{II/III}$ redox wave.

The partially and fully deprotonated green complexes [Fe(dcpp)(Htpda)]$^+$ and Fe(dcpp)(tpda) feature low-energy charge-transfer absorption bands tailing into the NIR region above 1000 nm. The electronic spectra of [Fe(dcpp)(H$_2$tpda)]$^{2+}$, [Fe(dcpp)(Htpda)]$^+$, and Fe(dcpp)(tpda) suggest that the MLCT bands shift to lower energy from 592 to 613 to 682 nm, underscoring the increasing push–pull character of [Fe(dcpp)(Htpda)]$^+$ and Fe(dcpp)(tpda) (Figure S52 in the Supporting Information). Clearly, [Htpda]$^-$ and [tpda]$^{2-}$ are better π-donor ligands, which increases the energy of the filled metal t_{2g} orbitals, lowering the HOMO–LUMO gap. A desired effect of the higher t_{2g} orbitals is the lowering of the MLCT states; an unwanted consequence is the concomitant lowering of the MC states. Remarkably, further bands grow in with maxima around 724 and 872 nm for [Fe(dcpp)(Htpda)]$^+$ and Fe(dcpp)(tpda), respectively, according to Gaussian deconvolution (Figure S52 in the Supporting Information).

Time-dependent (TD)-DFT calculations (B3LYP, def2-TZVP, ZORA, COSMO CH$_3$CN, D3(BJ)) of [Fe(dcpp)(H$_2$tpda)]$^{2+}$, [Fe(dcpp)(Htpda)]$^+$, and Fe(dcpp)(tpda) find the MLCT transitions between 400 and 600 nm (Figure 4). [Fe(dcpp)(Htpda)]$^+$ features two additional transitions at 821 and 953 nm arising from CT transitions between the anionic amide of [Htpda]$^-$ (plus some small metal contribution) and a single CO moiety of the dcpp ligand (LL'CTs; ligand-to-ligand charge transfers). Figure 4 depicts the corresponding electron density difference maps (EDDMs). The oscillator strength of the former LL'CT transition (N([Htpda]$^-$)→cis-CO(dcpp)) is four times that of the latter (N([Htpda]$^-$)→$trans$-CO(dcpp)) transition (Figure 4). The corresponding LL'CT transitions in Fe(dcpp)(tpda) each involve both CO groups of the dcpp ligand and both nitrogen atoms
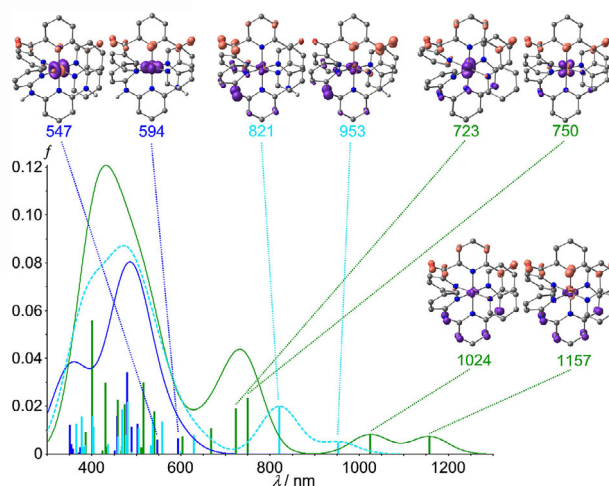
Figure 4. TD-DFT calculated electronic spectra and EDDMs of the MLCT and LL'CT transitions of [Fe(dcpp)(H$_2$tpda)]$^{2+}$ (blue solid line), [Fe(dcpp)(Htpda)]$^+$ (light-blue dotted line), and Fe(dcpp)(tpda) (green solid line). Contour value = 0.01 a.u.; purple = electron density depletion, orange = electron density gain; CH hydrogen atoms omitted.

↖↖ **These are not the final page numbers!**

3.2 RESULTS AND DISCUSSION: BOOSTING VIS/NIR CHARGE TRANSFER ABSORPTIONS OF IRON(II) COMPLEXES BY N-ALKYLATION AND N-DEPROTONATION IN THE LIGAND BACKBONE

63

of the [tpda]$^{2-}$ ligand. Their oscillator strengths are very similar and their energies are even lower than those of [Fe(dcpp)(Htpda)]$^+$ (Figure 4; 1024, 1157 nm). Fe(dcpp)(tpda) features further MLCT bands with some LL'CT character at 723 and 750 nm (Figure 4). The combined LL'CT transitions cover the spectral region from 600 to over 1000 nm. All trends are in qualitatively good agreement with the experimental data.

To conclude, longer alkyl groups than methyl at the bridging nitrogen atom do not significantly shift the MLCT absorption to lower energy. However, removal of the substituent (protons) from the nitrogen bridge induces the appearance of strong absorption bands with LL'CT character in the far red to the NIR spectral region.

In [M(tpyR^1)(tpyR^2)]$^{2+}$ and [M(tpy)(N^C^N)]$^+$ complexes with tridentate ligands with small bite angles, the two tridentate ligands are almost perfectly orthogonal including the central and the peripheral rings. Hence, all LL'CT transitions between these tridentate ligands are forbidden by symmetry.[33] Of course, this holds both for absorption and emission. The dark LL'CT states in these complexes provide non-radiative decay pathways and thus diminish the luminescence quantum yield as shown for [Ru(tpy)(N^C^N)]$^+$ complexes.[33]

In contrast, the LL'CT absorption bands in the iron(II) complexes [Fe(dcpp)(Htpda)]$^+$ and Fe(dcpp)(tpda) are clearly allowed according to their experimental extinction coefficients (Figure 3) and calculated oscillator strengths (Figure 4). Indeed, the DFT optimized geometries of the ground states as well as the X-ray diffraction analyses show that the central pyridine rings of dcpp and R$_2$tpda ligands are not orthogonal but are merely inclined by $\approx 30°$ dihedral angles. Hence, in a simplified view, transitions between a filled p-type orbital of the negatively charged nitrogen atom of the [Htpda]$^-$ ligand and the CO π^* orbital of the dcpp ligand are dipole-allowed in heteroleptic complexes with [Htpda]$^-$/[tpda]$^{2-}$ and dcpp ligands (Figure 4).

We therefore studied the possible luminescence of [Fe(dcpp)(Htpda)]$^+$ and Fe(dcpp)(tpda) in butyronitrile at 77 K with excitation wavelengths between 420 and 850 nm. Unfortunately, no luminescence could be detected up to 1200 nm. Clearly, the ligand field states ^{3}MC and ^{5}MC are too low in energy (lower than the ^{3}LL'CT states) because of the π-donating character of [Htpda]$^-$ and [tpda]$^{2-}$. This excited state ordering enables efficient non-radiative deactivation.

Nevertheless, we suggest that the combination of large ligand bite angles to increase the ligand field strength with a strong push–pull situation to enable low-energy dipole-allowed charge-transfer bands will pave the way for luminescent iron(II) complexes in the future.

Conclusion

The combination of electron-rich and electron-poor tridentate polypyridine ligands with large bite angles, R$_2$tpda and dcpp, induces a strong push–pull situation and a strong ligand field. Substituents R at R$_2$tpda larger than methyl lead to sterically induced destabilization and give no significant electronic effects in the optical spectra of the iron(II) complexes. However,

sequential deprotonation of the blue complex [Fe(dcpp)(H$_2$tpda)]$^{2+}$ yields the deep-green corresponding bases [Fe(dcpp)(Htpda)]$^+$ and Fe(dcpp)(tpda). These complexes absorb strongly in the red-NIR region (600–1000 nm) owing to low-energy dipole-allowed LL'CT transitions from the negatively charged nitrogen atoms of the [Htpda]$^-$ and [tpda]$^{2-}$ ligands to the carbonyl groups of the dcpp ligands. These LL'CT states might be suitable for charge injection into semiconductors and appropriately functionalized ligands for immobilization will be employed in the future. Furthermore, the dipole-allowed low-energy LL'CT transitions (instead of the commonly targeted MLCT transitions) might be a strategy for endowing luminescent properties (emission from ^{3}LL'CT states) to iron(II) complexes in strong ligand field environments. Attempts to design appropriate chelate ligands for iron(II) towards achieving this challenging goal are currently underway.

Experimental Section

General procedures

The ligands H$_2$tpda,[24] Me$_2$tpda,[11] and dcpp[14,27] and the complexes [Fe(Me$_2$tpda)$_2$][PF$_6$]$_2$[12] and [Fe(dcpp)(Me$_2$tpda)][PF$_6$]$_2$[12] were synthesized according to literature procedures. CH$_3$CN was distilled from CaH$_2$. THF, petroleum ether (PE, b.p. = 40–60 °C), and diethyl ether were distilled from sodium. All reagents were used as received from commercial suppliers (Acros, ABCR, Apollo Scientific, TCI, and Sigma–Aldrich). NMR spectra were recorded with a Bruker Avance DRX 400 spectrometer at 400.31 MHz (^{1}H) and 100.66 MHz (^{13}C{^{1}H}). All resonances are reported in ppm versus the solvent signal as an internal standard (CDCl$_3$: ^{1}H, δ = 7.28; ^{13}C, δ = 77.16 ppm; CD$_3$CN: ^{1}H, δ = 1.96; ^{13}C, δ = 1.24 ppm; s = singlet, d = doublet, t = triplet, m = multiplet, pt = pseudo-triplet, unresolved doublet of doublets, br = broad). IR spectra were recorded with a BioRad Excalibur FTS 3100 spectrometer as KBr or CsI disks. Electrochemical experiments were carried out with a BioLogic SP-50 voltammetric analyzer by using platinum wires as counter and working electrodes and 0.01 M Ag/AgNO$_3$ as the reference electrode. The measurements were carried out at a scan rate of 100 mV s^{-1} by using 0.1 M [nBu$_4$N][PF$_6$] as the supporting electrolyte in CH$_3$CN. Potentials are referenced against the ferrocene/ferrocenium couple. UV/Vis/near-IR spectra were recorded with a Varian Cary 5000 spectrometer by using 1.0 cm cells (Hellma, Suprasil). Emission spectra were recorded with a Varian Cary Eclipse spectrometer. ESI$^+$ mass spectra were recorded with a Micromass Q-TOF-Ultima spectrometer. FD mass spectra were recorded with a Thermo Fisher DFS mass spectrometer with a LIFDI upgrade (Linden CMS GmbH, Germany). Elemental analyses were performed by the microanalytical laboratory of the chemical institute of the University of Mainz.

Crystal structure determinations

Intensity data were collected with a Bruker AXS Smart1000 CCD diffractometer with an APEX II detector and an Oxford cooling system or with a STOE IPDS-2T diffractometer and corrected for absorption and other effects by using Mo$_{K\alpha}$ radiation (λ = 0.71073 Å) at 173(2) K. The diffraction frames were integrated by using the SAINT package or the STOE X-RED package.[34] Most were corrected for absorption with MULABS of the PLATON software package.[35] The structures were solved by direct methods and refined by the full-matrix method based on F^2 by using the SHELXTL software

These are not the final page numbers! ↗↗

3.2 RESULTS AND DISCUSSION: BOOSTING VIS/NIR CHARGE TRANSFER ABSORPTIONS OF IRON(II) COMPLEXES BY N-ALKYLATION AND N-DEPROTONATION IN THE LIGAND BACKBONE

64

package.[36,37] All non-hydrogen atoms, except some disordered solvent molecules, were refined anisotropically, whereas the positions of all hydrogen atoms were generated with appropriate geometric constraints and allowed to ride on their respective parent atoms with fixed isotropic thermal parameters. CCDC 1526745 ([Fe(-Hex$_2$tpda)$_2$][PF$_6$]$_2$) and 1526744 ([Fe(dcpp)(H$_2$tpda)][PF$_6$]$_2$) contain the supplementary crystallographic data for this paper. These data are provided free of charge by The Cambridge Crystallographic Data Centre.

Density functional theory calculations

DFT calculations were carried out by using the ORCA program package (version 3.0.2).[38] Tight convergence criteria were chosen for all calculations (Keywords TightSCF and TightOpt). Optimizations of geometries were done with the B3LYP functional.[39] All calculations employ the resolution of identity (Split-RI-J) approach for the Coulomb term in combination with the chain-of-spheres approximation for the exchange term (COSX).[40] TD calculations were performed by using the hybrid functional B3LYP as well.[39] In all calculations, Ahlrichs' split-valence triple-ξ basis set def2-TZVP, which comprises polarization functions for all non-hydrogen atoms, was employed.[41] Relativistic effects were calculated at the zeroth order regular approximation (ZORA) level.[42] The ZORA keyword automatically invokes relativistically adjusted basis sets.[41] To account for solvent effects, a conductor-like screening model (COSMO) modeling acetonitrile was used in all calculations.[43] Grimme's DFT dispersion correction with Becke–Johnson damping (DFT-D3(BJ)) was applied.[44] The presence of energy minima was checked by numerical frequency calculations. Explicit counter and/or solvent molecules were not taken into account in all cases.

Synthesis of Pr$_2$tpda

Under an argon atmosphere, 2,6-bis(2′-pyridylamino)pyridine H$_2$tpda (1.00 g, 3.82 mmol, 1.00 equiv) and sodium hydride (0.34 g, 14.1 mmol, 3.70 equiv) were dissolved in dry THF (60 mL) and stirred for 1 h at 40 °C. The reaction mixture turned from yellow to brown. n-Propyl iodide (0.89 mL, 1.56 g, 9.17 mmol, 2.40 equiv) was added slowly and the solution was heated at reflux for 3 d. The solution was cooled to room temperature and diluted with ethyl acetate (100 mL). The organic phase was washed with water (3× 100 mL) and brine (100 mL) and dried over MgSO$_4$. The solvent was removed under reduced pressure. The crude product (2.30 g) was purified by column chromatography (petroleum ether/ethyl acetate, 1:1, +5% NEt$_3$) to give the product as a yellow oil. Yield: 0.91 g (2.62 mmol, 69%). R_f = 0.78 (petroleum ether/ethyl acetate, 1:1, +5% NEt$_3$); ^{1}H NMR (CDCl$_3$, 400 MHz): δ = 8.38–8.30 (m, 2H, H^5), 7.53–7.45 (pt, 2H, H^6), 7.31 (t, 1H, $^3J_{HH}$ = 8.2 Hz, H^1), 7.18 (d, 2H, $^3J_{HH}$ = 8.2 Hz, H^2), 6.83 (pt, 2H, $^3J_{HH}$ = 7.3 Hz, H^7), 6.59 (d, 2H, $^3J_{HH}$ = 8.0 Hz, H^8), 4.11 (t, 4H, $^3J_{HH}$ = 7.5 Hz, H^9), 1.73 (m, 4H, $^3J_{HH}$ = 7.4 Hz, H^{10}), 0.91 ppm (t, 6H, $^3J_{HH}$ = 7.4 Hz, H^{11}); ^{13}C NMR (CDCl$_3$, 100 MHz): δ = 157.7 (C^4), 156.1 (C^3), 148.3 (C^8), 138.0 (C^1), 136.8 (C^6), 116.8 (C^7), 115.8 (C^5), 105.5 (C^2), 49.8 (C^9), 21.6 (C^{10}), 11.5 ppm (C^{11}); MS (FD, CH$_3$CN): m/z (rel. int. [%]) = 347.5 (100), [M$^+$]; CV ([nBu$_4$N][PF$_6$]/CH$_3$CN): $E_{1/2}$ = −1.52 (irrev.), −1.02 (irrev.), 0.27 (irrev.), 0.87 V (qrev.); elemental analysis calcd for C$_{21}$H$_{25}$N$_5$ (347.46): C 72.59, H 7.25, N 20.16; found: C 72.51, H 7.21, N 20.23.

Synthesis of Hex$_2$tpda

Under an argon atmosphere, 2,6-bis(2′-pyridylamino)pyridine H$_2$tpda (1.00 g, 3.82 mmol, 1.00 equiv) and sodium hydride (0.34 g, 14.1 mmol, 3.70 equiv) were dissolved in dry THF (60 mL) and stirred for 1 h at 40 °C. The reaction mixture turned from yellow to brown. n-Hexyl iodide (1.34 mL, 1.91 g, 9.00 mmol, 2.40 equiv) was added slowly and the solution was heated at reflux for 3 d. The solution was cooled to room temperature and diluted with ethyl acetate (100 mL). The organic phase was washed with water (3× 100 mL) and brine (100 mL) and dried over MgSO$_4$. The organic solvent was removed under reduced pressure. The crude product (1.20 g) was purified by column chromatography twice on SiO$_2$: (1) petroleum ether/ethyl acetate, 1:1, +5% NEt$_3$, (2) petroleum ether/ethyl acetate, 15:1, +10% NEt$_3$ to give the product as a yellow oil. Yield: 0.63 g (1.45 mmol, 38%). R_f = 0.83 (petroleum ether/ethyl acetate, 1:1, +5% NEt$_3$); R_f = 0.46 (petroleum ether/ethyl acetate, 15:1, +10% NEt$_3$); ^{1}H NMR (CDCl$_3$, 400 MHz): δ = 8.34 (d, 2H, $^3J_{HH}$ = 4.6 Hz, H^5), 7.48 (pt, 2H, $^3J_{HH}$ = 7.7 Hz, H^6), 7.31 (t, 1H, $^3J_{HH}$ = 8.2 Hz, H^1), 7.19 (d, 2H, $^3J_{HH}$ = 8.2 Hz, H^2), 6.82 (pt, 2H, $^3J_{HH}$ = 6.1 Hz, H^7), 6.60 (d, 2H, $^3J_{HH}$ = 7.9 Hz, H^8), 4.15 (t, 4H, J = ■■ Hz, H^9), 1.79–1.64 (m, 4H, H^{10}), 1.35–1.25 (m, 12H, H^{11}, H^{12}, H^{13}), 0.89–0.82 ppm (m, 6H, H^{14}); ^{13}C NMR (CDCl$_3$, 100 MHz): δ = 157.7 (C^4), 156.1 (C^3), 148.3 (C^8), 138.1 (C^1), 136.8 (C^6), 116.8 (C^7), 115.8 (C^5), 105.6 (C^2), 48.3 (C^9), 31.8 (C^{10}), 28.5 (C^{11}), 26.9 (C^{12}), 22.7 (C^{13}), 14.1 ppm (C^{14}); MS (FD, CH$_3$CN): m/z (rel. int. [%]) = 431.1 (100), [M$^+$]; CV ([nBu$_4$N][PF$_6$]/CH$_3$CN): $E_{1/2}$ = −1.64 (irrev.), −1.16 (irrev.), 0.16 (irrev.), 0.76 V (qrev.); elemental analysis calcd for C$_{27}$H$_{37}$N$_5$·0.25CH$_3$CN (431.62): C 74.75, H 8.61, N 16.64; found: C 74.51, H 8.46, N 16.65. For better handling, the oil was dissolved in CH$_3$CN and transferred into another flask. The solvent was removed under reduced pressure and the elemental analysis was measured.

Synthesis of [Fe(H$_2$tpda)$_2$][BF$_4$]$_2$

H$_2$tpda (300 mg, 1.14 mmol, 2.20 equiv) was dissolved in acetonitrile (20 mL) and Fe[BF$_4$]$_2$·6H$_2$O (180 mg, 0.53 equiv), dissolved in acetonitrile (10 mL), was added to the solution. The reaction mixture immediately turned from yellow to red-brown. After 1 d, the crude product was precipitated by addition of Et$_2$O (100 mL). The precipitate was filtered off, washed with Et$_2$O (200 mL), and dried under reduced pressure to give a brown powder. Yield 280 mg (0.37 mmol, 70%). ^{1}H NMR (CD$_3$CN, 400 MHz): δ = 9.40 (br.s, 4H, H^9), 7.77 (br.s, 4H), 7.66 (t, 2H, $^3J_{HH}$ = 7.9 Hz, H^1), 7.50 (pt, 4H, $^3J_{HH}$ = 7.6 Hz), 7.33 (d, 4H, $^3J_{HH}$ = 8.3 Hz), 7.27 (br.d, 4H, $^3J_{HH}$ = 8.3 Hz), 7.12 ppm (d, 4H, $^3J_{HH}$ = 7.9 Hz, H^2); ^{13}C NMR (CD$_3$CN, 100 MHz): δ = 160.8 (C^4), 153.8 (C^3), 151.3 (C^1), 140.6, 140.1, 121.9, 115.9 (C^5, C^6, C^7, C^8), 113.5 ppm (C^2); MS (ESI$^+$, CH$_3$CN): m/z (rel. int. [%]) = 187.14 (12), [C$_{10}$H$_{11}$N$_4$]$^+$, 264.19 (100), [C$_{15}$H$_{14}$N$_5$]$^+$, 291.12 (7), [C$_{30}$H$_{26}$FeN$_{10}$]$^{2+}$, 318.05 (27), [C$_{15}$H$_{12}$FeN$_5$]$^+$, 338.09 (22), [C$_{15}$H$_{13}$FFeN$_5$]$^+$, 581.24 (12), [C$_{30}$H$_{25}$FeN$_{10}$]$^+$; HR-MS (ESI$^+$, CH$_3$CN): calcd for [C$_{30}$H$_{26}$FeN$_{10}$]$^{2+}$: 291.0840; found: 291.0833; UV/Vis (CH$_3$CN): λ_{max} (ε) = 430 (3060), 375 (6170), 330 (32 920), 277 (34 360), 260 (31 000), 240 nm (26 500 M^{-1}cm^{-1}); IR (CsI): $\tilde{v}$ = 3355 (m, NH), 1655 (w), 1635 (vs.), 1630 (vs.), 1580 (vs.), 1540 (m), 1525 (m), 1510 (m), 1495 (s), 1480 (vs.), 1450 (vs.), 1340 (w) 1220 (w), 1180 (w), 1170 (m), 1060 (vs., BF), 875 (w), 805 (m), 775 (s), 770 (s), 755 (s), 525 cm^{-1} (w); CV ([nBu$_4$N][PF$_6$]/CH$_3$CN): $E_{1/2}$ = −2.52 (irrev.), 0.17 V (rev.); elemental analysis calcd for C$_{30}$H$_{26}$B$_2$F$_8$FeN$_{10}$ (756.18): C 47.66, H 3.47, N 18.53; found: C 47.79, H 3.42, N 18.42.

Synthesis of [Fe(Pr$_2$tpda)$_2$][BF$_4$]$_2$

Pr$_2$tpda (200 mg, 0.58 mmol, 2.00 equiv) was dissolved in acetonitrile (10 mL) and Fe[BF$_4$]$_2$·6H$_2$O (93 mg, 0.28 mmol, 1.00 equiv), dissolved in acetonitrile (10 mL), was added to the solution. The reaction mixture immediately turned from yellow to red-brown. After 4 h, the crude product was precipitated by addition of Et$_2$O (200 mL). The precipitate was filtered off, washed with Et$_2$O

3.2 RESULTS AND DISCUSSION: BOOSTING VIS/NIR CHARGE TRANSFER ABSORPTIONS OF IRON(II) COMPLEXES BY N-ALKYLATION AND N-DEPROTONATION IN THE LIGAND BACKBONE

65

(150 mL), and dried under reduced pressure to give 190 mg of the crude product. Under an argon atmosphere, the solid was dissolved in dry acetonitrile and was stirred with molecular sieve for 3 d. The product was precipitated with dry Et_2O (200 mL), filtered off, and dried under reduced pressure to give a brown-yellow powder. Yield: 110 mg (0.12 mmol, 43%). $R_f = 0.51$ (ethyl acetate); ^1H NMR (CD_3CN, 400 MHz): $\delta = 8.02$ (t, 2H, $^3J_{HH} = 7.9$ Hz, H^1), 7.77 (pt, 4H, $^3J_{HH} = 7.1$ Hz, H^6), 7.26 (d, 4H, $^3J_{HH} = 8.3$ Hz, H^5), 7.22 (d, 4H, $^3J_{HH} = 7.9$ Hz, H^2), 6.98–6.86 (br.d, 4H, $J = $ ■■ Hz, H^8), 6.73 (pt, 4H, $^3J_{HH} = 5.8$ Hz, H^7), 3.73 (m, 4H, H^{9a}), 3.41 (m, 4H, H^{9b}), 0.87 (m, 4H, H^{10b}), 0.79 (m, 6H, H^{11}), 0.31 ppm (m, 4H, H^{10a}); ^{13}C NMR (CD_3CN, 100 MHz): $\delta = 160.6$ (C^4), 159.9 (C^3), 154.4 (C^8), 140.4 (C^1), 138.8 (C^6), 121.2 (C^7), 115.8 (C^5), 111.9 (C^2), 52.7 (C^9), 19.7 (C^{10}), 10.2 ppm (C^{11}); MS (ESI$^+$, CH_3CN): m/z (rel. int. [%]) = 348.19 (67), $[C_{21}H_{26}N_5]^+$, 375.12 (100), $[C_{42}H_{50}FeN_{10}]^{2+}$, 390.23 (72), 422.11 (33), $[C_{21}H_{25}FFeN_5]^+$; HR-MS (ESI$^+$, CH_3CN): calcd for $[C_{42}H_{50}FeN_{10}]^{2+}$: 375.1779; found: 375.1776; UV/Vis (CH_3CN): λ_{max} (ε) = 201 (20800), 244 (14644), 292 (17450), 392 (4515), 414 (4180), 530 nm (200 $M^{-1} cm^{-1}$); IR (CsI): $\tilde{v} = 2970$ (w), 2935 (vw), 2875 (w), 1600 (s), 1580 (s), 1490 (s), 1445 (vs.), 1460 (m), 1345 (m), 1290 (m), 1245 (m), 1230 (m), 1140 (s), 1095 (vs., BF), 1060 (vs., BF), 810 (s), 785 (m), 755 (s), 520 cm^{-1} (w); CV ($[nBu_4N][PF_6]/CH_3CN$): $E_{1/2} = -2.26$ (irrev.), 0.46 V (rev.); elemental analysis calcd for $C_{42}H_{50}F_8FeN_{10}B_2 \cdot 3.5 H_2O$ (924.36): C 51.09, H 5.82, N 14.19; found: C 51.13, H 5.65, N 14.02.

Synthesis of [Fe(Hex$_2$tpda)$_2$][PF$_6$]$_2$

Hex$_2$tpda (200 mg, 0.46 mol, 2.00 equiv) was dissolved in acetonitrile (10 mL) and $Fe[BF_4]_2 \cdot 6 H_2O$ (78.0 mg, 0.23 mmol, 1.00 equiv), dissolved in acetonitrile (10 mL), was added to the solution. The reaction mixture immediately turned from yellow to red-brown. After 2 d, the crude product was precipitated by addition of Et_2O (200 mL). The precipitate was filtered off and washed with Et_2O (200 mL). The crude product was dissolved in acetonitrile (10 mL). Addition of a saturated aqueous solution of $[NH_4][PF_6]$ (20 mL) gave a brownish oily precipitate. The precipitate was filtered off and dried under reduced pressure. Recrystallization from ethanol (20 mL) gave brown crystals. Yield: 110 mg (0.12 mmol, 52%). $R_f = 0.60$ (ethyl acetate); ^1H NMR (CD_3CN, 400 MHz): $\delta = 8.01$ (t, 2H, $^3J_{HH} = 8.1$ Hz, H^1), 7.77 (pt, 4H, $^3J_{HH} = 7.6$ Hz, H^6), 7.30 (d, 4H, $^3J_{HH} = 8.4$ Hz, H^5), 7.25 (d, 4H, $^3J_{HH} = 8.1$ Hz, H^2), 6.99 (d, 4H, $^3J_{HH} = 5.2$ Hz, H^8), 6.74 (pt, 4H, $^3J_{HH} = 6.3$ Hz, H^7), 3.80 (m, 4H, H^{9a}), 3.42 (m, 4H, H^{9b}), 1.37–1.07 (m, 13H, H^{10b}, H^{13}, H^{14}), 0.90 (t, 8H, $^3J_{HH} = 7.0$ Hz, H^{11}, H^{12}), 0.23 ppm (m, 4H, H^{10a}); ^{13}C NMR (CD_3CN, 100 MHz): $\delta = 160.5$ (C^4), 160.0 (C^3), 154.5 (C^8), 140.5 (C^1), 138.9 (C^6), 121.2 (C^7), 116.0 (C^5), 111.9 (C^2), 51.3 (C^9), 31.0 (C^{13}), 26.4 (C^{10}), 26.0 (C^{11}), 22.2 (C^{12}), 13.2 ppm (C^{14}); MS (ESI$^+$, CH_3CN): m/z (rel. int. [%]) = 432.21 (28), $[C_{27}H_{38}N_5]^+$, 459.72 (82), $[C_{54}H_{74}FeN_{10}]^{2+}$, 506.22 (100), $[C_{27}H_{37}FFeN_5]^+$, 937.51 (92), $[C_{54}H_{74}FFeN_{10}]^+$, 1063.51 (16), $[C_{54}H_{74}F_6FeN_{10}P]^+$, 1668.21 (10), $[C_{162}H_{222}F_{24}Fe_3N_{30}P_4]^{2+}$, 2272.96 (12), $[C_{108}H_{148}F_{18}Fe_2N_{20}P_3]^+$; HR-MS (ESI$^+$, CH_3CN): calcd for $[C_{54}H_{74}F_6FeN_{10}P]^+$: 1063.5089; found: 1063.5093; UV/Vis (CH_3CN): λ_{max} (ε) = 208 (9945), 245 (10080), 295 (12540), 392 (4550), 417 (4150), 530 nm (255 $M^{-1} cm^{-1}$); CV ($[nBu_4N][PF_6]/CH_3CN$): $E_{1/2} = -2.12$ (irrev.), 0.46 V (rev.); IR (KBr): $\tilde{v} = 2955$ (m), 2930 (m), 2870 (m), 2860 (m), 1640 (w), 1600 (vs.), 1580 (s), 1570 (s), 1485 (vs.), 1445 (vs.), 1360 (m), 1340 (m), 1290 (m), 1230 (m), 1160 (m), 1140 (w), 1100 (w), 875 (s), 845 (vs., PF), 805 (s), 780 (m), 755 (m), 560 cm^{-1} (vs., PF$_{2,def}$); elemental analysis calcd for $C_{54}H_{74}F_{12}FeN_{10}P_2 \cdot 2 H_2O$ (1208.47): C 52.09, H 6.31, N 11.25; found: C 52.36, H 6.17, N 11.17.

Synthesis of [Fe(dcpp)(H$_2$tpda)][PF$_6$]$_2$

A solution of dcpp (200 mg, 0.69 mmol, 1.00 equiv) and H$_2$tpda (182 mg, 0.69 mmol, 1.00 equiv) in acetonitrile (20 mL) was added to a solution of $FeBr_2$ (136 mg, 0.63 mmol, 0.90 equiv) in acetonitrile (10 mL). The mixture turned black immediately. The solution was stirred at room temperature for 24 h. The mixture was diluted with Et_2O (100 mL) and a blue solid precipitated. The precipitate was filtered off, washed with Et_2O (100 mL), and dissolved in water (50 mL). The product was precipitated by addition of a saturated aqueous $[NH_4][PF_6]$ solution (20 mL). The dark-blue precipitate was filtered off and washed with water (200 mL). The blue product was collected by filtration and dried under reduced pressure to give a blue powder. Yield: 195 mg (2.17 mmol, 31%). $R_f = 0.68$ (KNO$_{3(aq)}$/CH_3CN, 4:1); ^1H NMR (CD_3CN, 400 MHz): $\delta = 8.56$ (s, 2H, H^{18}), 8.48 (t, 1H, $^3J_{HH} = 7.8$ Hz, H^1), 8.34 (d, 2H, $^3J_{HH} = 7.8$ Hz, H^2), 8.17 (d, 4H, $^3J_{HH} = 4.2$ Hz, H^6, H^7), 7.99 (m, 3H, H^9, H^{17}), 7.68 (pt, 2H, $^3J_{HH} = 7.8$ Hz, H^{12}), 7.26 (dd, 2H, $^3J_{HH} = 9.6$, 4.7 Hz, H^8), 7.03 (d, 2H, $^3J_{HH} = 7.8$ Hz, H^{13}), 6.81 (d, 2H, $^3J_{HH} = 8.3$ Hz, H^{16}), 6.61 (pt, 2H, $^3J_{HH} = 7.8$ Hz, H^{11}), 6.35 ppm (d, 2H, $^3J_{HH} = 5.8$ Hz, H^{10}); ^{13}C NMR (CD_3CN, 100 MHz): $\delta = 180.0$ (C^4), 161.3 (C^3), 159.8 (C^{14}), 159.2 (C^5), 158.3 (C^7), 155.0 (C^{15}), 153.5 (C^{13}), 141.2 (C^{17}), 140.4 (C^{12}), 139.4 (C^9), 139.0 (C^1), 130.7 (C^2), 127.4 (C^6), 126.6 (C^8), 120.3 (C^{10}), 112.6 (C^{11}), 110.0 ppm (C^{16}); UV/Vis (CH_3CN): λ_{max} (ε) = 330 (16290), 372 (7525), 592 nm (4195 $M^{-1} cm^{-1}$); IR (KBr): $\tilde{v} = 3380$ (m, NH), 1681 (vs., CO), 1625 (s), 1575 (s), 1490 (s), 1475 (s), 1450 (vs.), 1400 (m), 845 (vs., PF), 780 (m), 755 (s), 555 cm^{-1} (vs., PF$_{2,def}$); CV ($[nBu_4N][PF_6]/CH_3CN$): $E_{1/2} = -2.14$ (irrev.), -1.91 (irrev.), -1.21 (irrev.), 0.84 V (rev.); MS (ESI$^+$, CH_3CN): m/z (rel. int. [%]) = 264.23 (18), $[C_{15}H_{14}N_5]^+$, 290.10 (54), $[C_{17}H_{12}N_3O_2]^+$, 304.05 (22), $[C_{32}H_{24}FeN_8O_2]^{2+}$, 318.04 (4), $[C_{15}H_{12}FeN_5]^+$, 338.07 (31), $[C_{15}H_{13}FFeN_5]^+$, 607.09 (100), $[C_{32}H_{23}FeN_8O_2]^+$, 627.62 (29), $[C_{32}H_{24}FFeN_8O_2]^+$, 1203.07 (54), $[C_{96}H_{72}F_{24}Fe_3N_{24}O_6P_4]^{2+}$, 1652.42 (41), $[C_{64}H_{48}F_{18}Fe_2N_{16}O_4P_3]^+$, 2102.29 (9), $[C_{160}H_{120}F_{48}Fe_5N_{40}O_{10}P_8]^{2+}$, 2552.15 (12), $[C_{96}H_{72}F_{30}Fe_3N_{24}O_6P_5]^+$; HR-MS (ESI$^+$, CH_3CN): calcd for $[C_{32}H_{23}FeN_8O_2]^+$: 607.1288; found: 607.1313; elemental analysis calcd for $C_{32}H_{24}F_{12}FeN_8O_2P_2 \cdot 3 H_2O$ (898.07): C 40.36, H 3.17, N 11.77; found: C 40.04, H 2.68, N 11.47.

Deprotonation of [Fe(dcpp)(H$_2$tpda)][PF$_6$]$_2$

Under an argon atmosphere, [Fe(dcpp)(H$_2$tpda)][PF$_6$]$_2$ (20.0 mg, 22.3 μmol, 1.00 equiv) was dissolved in dry acetonitrile (5 mL) and stirred with molecular sieves for 1 h. The molecular sieves were filtered off, P$_1$-tBu (12.6 μL, 11.5 mg, 4.91 μmol, 2.20 equiv) was added and the color turned from blue to dark green. ^1H NMR (CD_3CN, 400 MHz): $\delta = 8.30–8.20$ (m, 5H, H^1, H^2, H^9), 8.08 (d, 2H, $^3J_{HH} = 7.8$ Hz, H^6), 7.95 (t, 2H, $^3J_{HH} = 7.5$ Hz, H^7), 7.40 (t, 1H, $^3J_{HH} = 7.7$ Hz, H^{17}), 7.04 (t, 2H, $^3J_{HH} = 6.5$ Hz, H^8), 6.77 (t, 2H, $^3J_{HH} = 7.1$ Hz, H^{12}), 6.36 (d, 2H, $^3J_{HH} = 7.7$ Hz, H^{16}), 5.79 (d, 2H, $^3J_{HH} = 8.6$ Hz, H^{13}), 5.54 (t, 2H, $^3J_{HH} = 6.3$ Hz, H^{11}), 5.13 ppm (d, 2H, $^3J_{HH} = 6.0$ Hz, H^{10}); ^{13}C NMR (CD_3CN, 100 MHz): $\delta = 177.6$ (C^4), 163.8 (C^3), 163.1 (C^{14}), 160.1 (C^5), 158.0 (C^{15}), 157.4 (C^7), 151.2 (C^{13}), 137.0 (C^1), 136.4 (C^{17}), 134.2 (C^9), 133.9 (C^{12}), 129.9 (C^2), 126.3 (C^8), 123.3 (C^6), 117.1 (C^{10}), 110.6 (C^{11}), 110.3 ppm (C^{16}); UV/Vis (CH_3CN): λ_{max} (ε) = 210 (2500), 260 (22800), 280 (23850), 335 (18700), 360 (15170), 470 (7200), 680 (3875), 830 nm (2500 $M^{-1} cm^{-1}$).

Synthesis of [Fe(dcpp)(Pr$_2$tpda)][PF$_6$]$_2$

A solution of dcpp (167 mg, 0.58 mmol, 1.00 equiv) and Pr$_2$tpda (200 mg, 0.58 mmol, 1.00 equiv) in acetonitrile (10 mL) was added to a solution of $Fe[BF_4]_2 \cdot 6 H_2O$ (195 mg, 0.58 mmol, 1.00 equiv) in acetonitrile (10 mL). The mixture turned dark blue. After 24 h, the

These are not the final page numbers! ↗↗

reaction mixture was diluted with dry Et_2O (100 mL) and the precipitate was filtered off and washed with dry Et_2O (100 mL). The dark-blue solid was dissolved in water (20 mL) and precipitated by addition of a saturated aqueous $[NH_4][PF_6]$ solution (20 mL). The dark-blue precipitate was filtered off and washed with water (200 mL). The blue solid was collected, dried under reduced pressure, and dissolved in dry acetonitrile (10 mL). The mixture was stirred under an argon atmosphere with molecular sieves for 3 d. The complex salt was precipitated by addition of dry Et_2O (200 mL). The precipitate was filtered off and dried under reduced pressure to give a blue powder. Yield: 80 mg (0.08 mmol, 14%). $R_f = 0.46$ ($KNO_{3(aq)}/CH_3CN$, 4:1); ^1H NMR (CD_3CN, 400 MHz): $\delta = 8.48$ (t, 1H, $^3J_{HH} = 7.8$ Hz, H^1), 8.29 (d, 2H, $^3J_{HH} = 7.8$ Hz, H^2), 8.18 (t, 1H, $^3J_{HH} = 8.2$ Hz, H^{17}), 8.11–8.04 (m, 4H, H^6, H^9), 7.84 (pt, 2H, $^3J_{HH} = 7.4$ Hz, H^{12}), 7.51 (m, 2H, H^7), 7.33 (d, 2H, $^3J_{HH} = 8.2$ Hz, H^{16}), 7.21 (pt, 2H, $^3J_{HH} = 6.4$ Hz, H^8), 7.13 (d, 2H, $^3J_{HH} = 8.2$ Hz, H^{13}), 6.71 (pt, 2H, $^3J_{HH} = 6.4$ Hz, H^{11}), 6.49 (br.d, 2H, $^3J_{HH} = 5.4$ Hz, H^{10}), 3.55–3.45 (m, 2H, H^{18a}), 3.35–3.25 (m, 2H, H^{18b}), 1.15–1.05 (m, 2H, H^{19b}), 0.84 (t, 3H, $^3J_{HH} = 7.0$ Hz, H^{20}), 0.75–0.65 ppm (m, 2H, H^{19a}); ^{13}C NMR (CD_3CN, 100 MHz): $\delta = 181.3$ (C^4), 161.1 (C^3), 160.3 (C^{14}), 158.3 (C^5), 157.7 (C^{15}), 157.2 (C^{10}), 156.4 (C^9), 141.3 (C^{17}), 140.5 (C^{12}), 139.4 (C^7), 139.3 (C^1), 130.4 (C^2), 127.8 (C^6), 127.6 (C^8), 121.0 (C^{11}), 114.8 (C^{13}), 113.1 (C^{16}), 53.2 (C^{18}), 19.8 (C^{19}), 10.3 ppm (C^{20}); MS (ESI$^+$, CH_3CN): m/z (rel. int. [%]) = 90.09 (3), $[C_{17}H_{12}N_3O_2]^+$, 317.04 (3), $[C_{34}H_{26}FeN_8O_2]^{2+}$, 346.11 (58), $[C_{38}H_{36}FeN_8O_2]^{2+}$, 348.21 (100), $[C_{21}H_{26}N_5]^+$, 422.14 (34), $[C_{21}H_{25}FFeN_5]^+$, 448.14 (15); HR-MS (ESI$^+$, CH_3CN): calcd for $[C_{38}H_{36}FeN_8O_2]^{2+}$: 346.1150; found: 346.1153; UV/Vis (CH_3CN): λ_{max} (ε) = 325 (18475), 372 (8840), 510 (2700), 590 nm (4150 M^{-1} cm^{-1}); IR (CsI): $\tilde{v} = 2965$ (w), 2930 (w), 1685 (s, CO), 1600 (m), 1580 (m), 1490 (m), 1440 (s), 1340 (m), 1330 (m), 1310 (m), 1290 (m), 1245 (m), 1225 (m), 985 (m), 840 (vs., PF), 805 (m), 780 (m), 760 (s), 670 (m), 555 cm^{-1} (vs., PF$_{2,def}$); CV ([nBu$_4$N][PF$_6$]/CH_3CN): $E_{1/2} = -2.29$ (irrev.), -1.98 (irrev.), -1.25 (irrev.), -0.97 (irrev.), 0.47 (irrev.), 0.84 V (rev.); elemental analysis calcd for $C_{38}H_{36}F_{12}FeN_8O_2P_2 \cdot 1.5H_2O$ (982.16): C 45.21, H 3.89, N 11.17; found. C 45.18, H 3.55, N 11.27.

Synthesis of [Fe(dcpp)(Hex$_2$tpda)][BF$_4$]$_2$

Under an argon atmosphere, Fe[BF$_4$]$_2 \cdot 6H_2O$ (155 mg, 0.46 mmol, 1.00 equiv) was dissolved in dry acetonitrile (10 mL) and stirred with molecular sieves for 3 h. Hex$_2$tpda (200 mg, 0.46 mmol, 1.00 equiv) and dcpp (134 mg, 0.46 mmol, 1.0 equiv) were dissolved in dry acetonitrile (10 mL) and added to the solution. After stirring for 24 h, the molar sieves were filtered off. The reaction mixture was diluted with dry Et_2O (400 mL) and the precipitate was filtered off, washed with dry Et_2O (100 mL), and dried under reduced pressure to give a blue powder. Yield: 83 mg (0.08 mmol, 17%). ^1H NMR (CD_3CN, 400 MHz): $\delta = 8.48$ (t, 1H, $^3J_{HH} = 7.8$ Hz, H^1), 8.29 (d, 2H, $^3J_{HH} = 7.8$ Hz, H^2), 8.18 (t, 1H, $^3J_{HH} = 8.2$ Hz, H^{17}), 8.11–8.04 (m, 4H, H^6, H^9), 7.84 (pt, 2H, $^3J_{HH} = 7.4$ Hz, H^{12}), 7.51 (d, 2H, $^3J_{HH} = 5.4$ Hz, H^7), 7.33 (d, 2H, $^3J_{HH} = 8.2$ Hz, H^{16}), 7.21 (pt, 2H, $^3J_{HH} = 6.4$ Hz, H^8), 7.13 (d, 2H, $^3J_{HH} = 8.2$ Hz, H^{13}), 6.71 (pt, 2H, $^3J_{HH} = 6.4$ Hz, H^{11}), 6.49 (d, 2H, $^3J_{HH} = 5.4$ Hz, H^{10}), 3.60–3.50 (m, 2H, H^{18a}), 3.38–3.28 (m, 2H, H^{18b}), 1.37–1.09 (m, 12H, H^{20}, H^{21}, H^{22}), 1.09–0.98 (m, 2H, H^{19b}), 0.97–0.87 (m, 6H, H^{23}), 0.65–0.51 ppm (m, 2H, H^{19a}); ^{13}C NMR (CD_3CN, 100 MHz): $\delta = 181.4$ (C^4), 161.1 (C^3), 160.3 (C^{14}), 158.4 (C^5), 157.7 (C^{15}), 157.2 (C^{10}), 156.4 (C^9), 141.3 (C^{17}), 140.5 (C^{12}), 139.5 (C^1), 139.4 (C^7), 130.4 (C^2), 127.8 (C^6), 127.6 (C^8), 121.0 (C^{11}), 115.0 (C^{13}), 113.2 (C^{16}), 51.7 (C^{18}), 30.9 (C^{22}), 26.4 (C^{19}), 26.2 (C^{20}), 22.2 (C^{21}), 13.3 ppm (C^{23}); MS (ESI$^+$, CH_3CN): m/z (rel. int. [%]) = 290.09 (8), $[C_{17}H_{12}N_3O_2]^+$, 388.13 (46), $[C_{44}H_{48}FeN_8O_2]^{2+}$, 432.28 (100), $[C_{27}H_{38}N_5]^+$, 506.22 (15), $[C_{27}H_{37}FFeN_5]^+$, 795.32 (2), $[C_{44}H_{48}FFeN_8O_2]^+$; HR-MS (ESI$^+$, CH_3CN): calcd for $[C_{44}H_{48}FeN_8O_2]^{2+}$:

388.1619; found: 388.1521; UV/Vis (CH_3CN): λ_{max} (ε) = 330 (16290), 372 (7525), 510 (2660), 592 nm (4195 M^{-1} cm^{-1}); IR (CsI): $\tilde{v} = 2960$ (w), 2930 (w), 2860 (w), 1720 (m), 1700 (m), 1685 (m, CO), 1655 (m), 1640 (m), 1600 (m), 1580 (m), 1560 (m), 1540 (m), 1520 (m), 1510 (m), 1490 (s), 1480 (m), 1460 (s), 1440 (s), 1290 (m), 1260 (s), 1095 (vs., BF), 1060 (vs., BF), 870 (m), 800 (vs.), 760 (m), 705 (w), 670 (w), 522 cm^{-1} (w); CV ([nBu$_4$N][PF$_6$]/CH_3CN): $E_{1/2} = -2.72$ (irrev.), -2.26 (irrev.), -1.18 (irrev.), 0.47 (irrev.), 0.84 V (rev.); elemental analysis calcd for $C_{44}H_{48}B_2F_8FeN_8O_2 \cdot H_2O$ (950.33): C 54.57, H 5.20, N 11.57; found: C 54.33, H 5.15, N 11.75.

Conflict of interest

The authors declare no conflict of interest.

[1] a) C. Stephenson, T. Yoon, Acc. Chem. Res. 2016, 49, 2059–2060; b) D. M. Schultz, T. P. Yoon, Science 2014, 343, 1239176; c) C. K. Prier, D. A. Rankic, D. W. C. MacMillan, Chem. Rev. 2013, 113, 5322–5363; d) J. M. R. Narayanama, C. R. J. Stephenson, Chem. Soc. Rev. 2011, 40, 102–113; e) T. P. Yoon, M. A. Ischay, J. Du, Nat. Chem. 2010, 2, 527–532; f) U. S. Schubert, A. Winter, G. R. Newkome, Terpyridine-Based Materials For Catalytic, Optoelectronic and Life Science Applications, Wiley-VCH, Weinheim, Germany, 2011.

[2] a) J.-F. Yin, M. Velayudham, D. Bhattacharya, H.-C. Lin, K.-L. Lu, Coord. Chem. Rev. 2012, 256, 3008–3035; b) A. Hagfeldt, G. Boschloo, L. Sun, L. Kloo, H. Pettersson, Chem. Rev. 2010, 110, 6595–6663; c) Md. K. Nazeeruddin, C. Klein, P. Liska, M. Grätzel, Coord. Chem. Rev. 2005, 249, 1460–1467; d) B. O'Regan, M. Grätzel, Nature 1991, 353, 737–740.

[3] a) R. D. Costa, E. Ortí, H. J. Bolink, F. Monti, G. Accorsi, N. Armaroli, Angew. Chem. Int. Ed. 2012, 51, 8178–8211; Angew. Chem. 2012, 124, 8300–8334; b) A. Breivogel, M. Park, D. Lee, S. Klassen, A. Kühnle, C. Lee, K. Char, K. Heinze, Eur. J. Inorg. Chem. 2014, 288–295; c) J. D. Slinker, J. A. DeFranco, M. J. Jaquith, W. R. Silveira, Y.-W. Zhong, J. M. Moran-Mirabal, H. G. Craighead, H. D. Abruña, J. A. Marohn, G. G. Malliaras, Nat. Mater. 2007, 6, 894–899; d) J. D. Slinker, J. Rivnay, J. S. Moskowitz, J. B. Parker, S. Bernhard, H. D. Abruña, G. G. Malliaras, J. Mater. Chem. 2007, 17, 2976–2988; e) K. Müllen, U. Scherf, Organic Light-Emitting Devices: Synthesis, Properties, and Applications, Wiley-VCH, Weinheim, Germany, 2006; f) H. J. Bolink, L. Cappelli, E. Coronado, M. Grätzel, M. K. Nazeeruddin, J. Am. Chem. Soc. 2006, 128, 46–47; g) H. Rudmann, S. Shimada, M. F. Rubner, J. Am. Chem. Soc. 2002, 124, 4918–4921; h) C. M. Elliott, F. Pichot, C. J. Bloom, L. S. Rider, J. Am. Chem. Soc. 1998, 120, 6781–6784.

[4] a) C. Bressler, C. Milne, V.-T. Pham, A. ElNahhas, R. M. van der Veen, W. Gawelda, S. Johnson, P. Beaud, D. Grolimund, M. Kaiser, C. N. Borca, G. Ingold, R. Abela, M. Chergui, Science 2009, 323, 489–492; b) M. Yang, D. W. Thompson, G. J. Meyer, Inorg. Chem. 2002, 41, 1254–1262; c) A. Hauser, Top. Curr. Chem. 2004, 234, 155–198; d) J. E. Monat, J. K.

↖↖ These are not the final page numbers!

3.2 RESULTS AND DISCUSSION: BOOSTING VIS/NIR CHARGE TRANSFER
ABSORPTIONS OF IRON(II) COMPLEXES BY N-ALKYLATION AND
N-DEPROTONATION IN THE LIGAND BACKBONE

67

McCusker, *J. Am. Chem. Soc.* **2000**, *122*, 4092–4097; e) W. Gawelda, A. Cannizzo, V.-T. Pham, F. van Mourik, C. Bressler, M. Chergui, *J. Am. Chem. Soc.* **2007**, *129*, 8199–8206.

[5] G. Vankó, A. Bordage, M. Pápai, K. Haldrup, P. Glatzel, A. M. March, G. Doumy, A. Britz, A. Galler, T. Assefa, D. Cabaret, A. Juhin, T. B. van Driel, K. S. Kjær, A. Dohn, K. B. Møller, H. T. Lemke, E. Gallo, M. Rovezzi, Z. Németh, E. Rozsályi, T. Rozgonyi, J. Uhlig, V. Sundström, M. M. Nielsen, L. Young, S. H. Southworth, C. Bressler, W. Gawelda, *J. Phys. Chem. C* **2015**, *119*, 5888–5902.

[6] W. Gawelda, A. Cannizzo, V.-T. Pham, F. van Mourik, C. Bressler, M. Chergui, *J. Am. Chem. Soc.* **2007**, *129*, 8199–8206■■duplicate with ref.[4e], please delete or replace one and renumber as appropriate■■.

[7] W. Zhang, R. Alonso-Mori, U. Bergmann, C. Bressler, M. Chollet, A. Galler, W. Gawelda, R. G. Hadt, R. W. Hartsock, T. Kroll, K. S. Kjær, K. Kubiček, H. T. Lemke, H. W. Liang, D. A. Meyer, M. M. Nielsen, C. Purser, J. S. Robinson, E. I. Solomon, Z. Sun, D. Sokaras, T. B. van Driel, G. Vankó, T.-C. Weng, D. Zhu, K. J. Gaffney, *Nature* **2014**, *509*, 345–348.

[8] L. L. Jamula, A. M. Brown, D. Guo, J. K. McCusker, *Inorg. Chem.* **2014**, *53*, 15–17.

[9] a) J. B. Asbury, R. J. Ellingson, H. N. Ghosh, S. Ferrere, A. J. Nozik, T. Q. Lian, *J. Phys. Chem. B* **1999**, *103*, 3110–3119; b) G. Ramakrishna, D. A. Jose, D. K. Kumar, A. Das, D. K. Palit, H. N. Ghosh, *J. Phys. Chem. B* **2005**, *109*, 15445–15453; c) G. Benkö, J. Kallioinen, J. E. I. Korppi-Tommola, A. P. Yartsev, V. Sundström, *J. Am. Chem. Soc.* **2002**, *124*, 489–493; d) D. Kuang, S. Ito, B. Wenger, C. Klein, J.-E. Moser, R. Humphry-Baker, S. M. Zakeeruddin, M. Grätzel, *J. Am. Chem. Soc.* **2006**, *128*, 4146–4154.

[10] a) L. Liu, T. Duchanois, T. Etienne, A. Monari, M. Beley, X. Assfeld, S. Haacke, P. C. Gros, *Phys. Chem. Chem. Phys.* **2016**, *18*, 12550–12556; b) Y. Liu, T. Harlang, S. E. Canton, P. Chábera, K. Suárez-Alcántara, A. Fleckhaus, D. A. Vithanage, E. Göransson, A. Corani, R. Lomoth, V. Sundström, K. Wärnmark, *Chem. Commun.* **2013**, *49*, 6412–6414; c) Y. Liu, K. S. Kjar, L. A. Fredin, P. Chábera, T. Harlang, S. E. Canton, S. Lidin, J. Zhang, R. Lomoth, K.-E. Bergquist, P. Persson, K. Wärnmark, V. Sundström, *Chem. Eur. J.* **2015**, *21*, 3628–3639; d) L. A. Fredin, M. Pápai, E. Rozsályi, G. Vankó, K. Wärnmark, V. Sundström, P. Persson, *J. Phys. Chem. Lett.* **2014**, *5*, 2066–2071.

[11] A. Breivogel, C. Förster, K. Heinze, *Inorg. Chem.* **2010**, *49*, 7052–7056.

[12] A. K. C. Mengel, C. Förster, A. Breivogel, K. Mack, J. R. Ochsmann, F. Laquai, V. Ksenofontov, K. Heinze, *Chem. Eur. J.* **2015**, *21*, 704–714.

[13] a) T. C. B. Harlang, Y. Liu, O. Gordivska, L. A. Fredin, C. S. Ponseca, Jr., P. Huang, P. Chábera, K. S. Kjaer, H. Mateos, J. Uhlig, R. Lomoth, R. Wallenberg, S. Styring, P. Persson, V. Sundström, K. Wärnmark, *Nat. Chem.* **2015**, *7*, 883–889; b) T. Duchanois, T. Etienne, C. Cebrián, L. Liu, A. Monari, M. Beley, X. Assfeld, S. Haacke, P. C. Gros, *Eur. J. Inorg. Chem.* **2015**, 2469–2477; c) P. Zimmer, P. Müller, L. Burkhardt, R. Schepper, A. Neuba, J. Steube, F. Dietrich, U. Flörke, S. Mangold, M. Gerhards, M. Bauer, *Eur. J. Inorg. Chem.* **2017**, 1504–1509.

[14] F. Schramm, V. Meded, H. Fliegl, K. Fink, O. Fuhr, Z. Qu, W. Klopper, S. Finn, T. E. Keyes, M. Ruben, *Inorg. Chem.* **2009**, *48*, 5677–5684.

[15] a) M. Abrahamsson, M. Jäger, T. Österman, L. Eriksson, P. Persson, H.-C. Becker, O. Johansson, L. Hammarström, *J. Am. Chem. Soc.* **2006**, *128*, 12616–12617; b) G. A. Parada, L. A. Fredin, M.-P. Santoni, M. Jäger, R. Lomoth, L. Hammarström, O. Johansson, P. Persson, S. Ott, *Inorg. Chem.* **2013**, *52*, 5128–5137; c) M. Abrahamsson, M. Jäger, R. J. Kumar, T. Österman, P. Persson, H.-C. Becker, O. Johansson, L. Hammarström, *J. Am. Chem. Soc.* **2008**, *130*, 15533–15542.

[16] a) A. Breivogel, M. Meister, C. Förster, F. Laquai, K. Heinze, *Chem. Eur. J.* **2013**, *19*, 13745–13760; b) A. Breivogel, S. Wooh, J. Dietrich, T. Y. Kim, Y. S. Kang, K. Char, K. Heinze, *Eur. J. Inorg. Chem.* **2014**, 2720–2734.

[17] S. Otto, M. Grabolle, C. Förster, C. Kreitner, U. Resch-Genger, K. Heinze, *Angew. Chem. Int. Ed.* **2015**, *54*, 11572–11576; *Angew. Chem.* **2015**, *127*, 11735–11739.

[18] a) S. Ferrere, B. A. Gregg, *J. Am. Chem. Soc.* **1998**, *120*, 843–844; b) S. Ferrere, *Chem. Mater.* **2000**, *12*, 1083–1089.

[19] M. Yang, D. W. Thompson, G. J. Meyer, *Inorg. Chem.* **2000**, *39*, 3738–3739.

[20] a) D. Bowman, J. H. Blew, T. Tsuchiya, E. Jakubikova, *Inorg. Chem.* **2013**, *52*, 8621–8628; b) E. Jakubikova, D. N. Bowman, *Acc. Chem. Res.* **2015**, *48*, 1441–1449.

[21] W. Zhang, K. S. Kjær, R. Alonso-Mori, U. Bergmann, M. Chollet, L. A. Fredin, R. G. Hadt, R. W. Hartsock, T. Harlang, T. Kroll, K. Kubiček, H. T. Lemke, H. W. Liang, Y. Liu, M. M. Nielsen, P. Persson, J. S. Robinson, E. I. Solomon, Z. Sun, D. Sokaras, T. B. van Driel, T.-C. Weng, D. Zhu, K. Wärnmark, V. Sundström, K. J. Gaffney, *Chem. Sci.* **2017**, *8*, 515–523.

[22] a) I. M. Dixon, G. Boissard, H. Whyte, F. Alary, J.-L. Heully, *Inorg. Chem.* **2016**, *55*, 5089–5091; b) I. M. Dixon, F. Alary, M. Boggio-Pasqua, J.-L. Heully, *Dalton Trans.* **2015**, *44*, 13498–13503; c) I. M. Dixon, S. Khan, F. Alary, M. Boggio-Pasqua, J.-L. Heully, *Dalton Trans.* **2014**, *43*, 15898–15905; d) I. M. Dixon, F. Alary, M. Boggio-Pasqua, J.-L. Heully, *Inorg. Chem.* **2013**, *52*, 13369–13374.

[23] D. N. Bowman, A. Bondarev, S. Mukherjee, E. Jakubikova, *Inorg. Chem.* **2015**, *54*, 8786–8793.

[24] K.-Y. Ho, W.-Y. Yu, K.-K. Cheung, C.-M. Che, *J. Chem. Soc. Dalton Trans.* **1999**, 1581–1586.

[25] a) J.-S. Ni, C.-Y. Hung, K.-Y. Liu, Y.-H. Chang, K.-C. Ho, K.-F. Lin, *J. Colloid Interface Sci.* **2012**, *386*, 359–365; b) S. N. Mori, W. Kubo, T. Kanzaki, N. Masaki, Y. Wada, S. Yanagida, *J. Phys. Chem. C* **2007**, *111*, 3522–3527.

[26] S.-A. Hua, M.-C. Cheng, C.-h. Chen, S.-M. Peng, *Eur. J. Inorg. Chem.* **2015**, 2510–2523.

[27] C. R. Goldsmith, T. D. P. Stack, *Inorg. Chem.* **2006**, *45*, 6048–6055.

[28] M.-H. Yang, T.-W. Lin, C.-C. Chou, H.-C. Lee, H.-C. Chang, G.-H. Lee, M.-K. Leung, S.-M. Peng, *Chem. Commun.* **1997**, 2279–2280.

[29] a) *Ligand Substitution Processes*, (Eds.: C. N. Langford, H. B. Gray), W. A. Benjamin, New York, **1966**; b) J. Burgess, M. V. Twigg, *J. Chem. Soc. Dalton Trans.* **1974**, 2032–2036; c) D. J. Farrington, J. G. Jones, M. V. Twigg, *J. Chem. Soc. Dalton Trans.* **1979**, 221–227; d) E. C. Constable, *Polyhedron* **1983**, *2*, 551–572; e) J. Maigut, R. Meier, A. Zahl, R. van Eldik, *Inorg. Chem.* **2007**, *46*, 5361–5371.

[30] a) N. Serpone, G. Ponterini, M. A. Jamieson, F. Bolleta, M. Maestri, *Coord. Chem. Rev.* **1983**, *50*, 209–302; b) L. Seiden, F. Basolo, H. M. Neumann, *J. Am. Chem. Soc.* **1959**, *81*, 3809–3813.

[31] K. Mack, A. Wünsche von Leupoldt, C. Förster, M. Ezhevskaya, D. Hinderberger, K. W. Klinkhammer, K. Heinze, *Inorg. Chem.* **2012**, *51*, 7851–7858.

[32] Y. Kondo, in *Superbases for Organic Synthesis* (Ed.: T. Ishikawa), Wiley, Chichester, UK, **2009**, pp. 145–185.

[33] a) C. Kreitner, K. Heinze, *Dalton Trans.* **2016**, *45*, 13631–13647; b) C. Kreitner, K. Heinze, *Dalton Trans.* **2016**, *45*, 5640–5658; c) C. Kreitner, E. Erdmann, W. W. Seidel, K. Heinze, *Inorg. Chem.* **2015**, *54*, 11088–11104.

[34] a) SMART Data Collection and SAINT-Plus Data Processing Software for the SMART System (various versions), Bruker Analytical X-Ray Instruments, Inc., Madison, WI, **2000**; b) Stoe & Cie, X-Red, Stoe & Cie, Darmstadt, Germany, **2002**.

[35] a) B. Blessing, *Acta Crystallogr. Sect. A* **1995**, *51*, 33–38; b) A. L. Spek, *Acta Crystallogr. D* **2009**, *65*, 148–155.

[36] G. M. Sheldrick, *Acta Crystallogr. Sect. A* **2015**, *71*, 3–8.

[37] G. M. Sheldrick, SHELXL-2014/7, University of Göttingen, Göttingen, Germany, **2014**.

[38] F. Neese, *WIREs Comput. Mol. Sci.* **2012**, *2*, 73–78.

[39] A. D. Becke, *J. Chem. Phys.* **1993**, *98*, 5648–5652.

[40] a) F. Neese, F. Wennmohs, A. Hansen, U. Becker, *Chem. Phys.* **2009**, *356*, 98–109; b) R. Izsák, F. Neese, *J. Chem. Phys.* **2011**, *135*, 144105.

[41] D. A. Pantazis, X. Y. Chen, C. R. Landis, F. Neese, *J. Chem. Theory Comput.* **2008**, *4*, 908–919.

[42] E. van Lenthe, E. J. Baerends, J. G. Snijders, *J. Chem. Phys.* **1993**, *99*, 4597–4610.

[43] S. Sinnecker, A. Rajendran, A. Klamt, M. Diedenhofen, F. Neese, *J. Phys. Chem. A* **2006**, *110*, 2235–2245.

[44] a) S. Grimme, S. Ehrlich, L. Goerigk, *J. Comput. Chem.* **2011**, *32*, 1456–1465; b) S. Grimme, J. Antony, S. Ehrlich, H. Krieg, *J. Chem. Phys.* **2010**, *132*, 154104.

3.2 RESULTS AND DISCUSSION: BOOSTING VIS/NIR CHARGE TRANSFER ABSORPTIONS OF IRON(II) COMPLEXES BY N-ALKYLATION AND N-DEPROTONATION IN THE LIGAND BACKBONE

68

FULL PAPER

A. K. C. Mengel, C. Bissinger, M. Dorn,
O. Back, C. Förster, K. Heinze*

■■ – ■■

Boosting Vis/NIR Charge-Transfer Absorptions of Iron(II) Complexes by N-Alkylation and N-Deprotonation in the Ligand Backbone
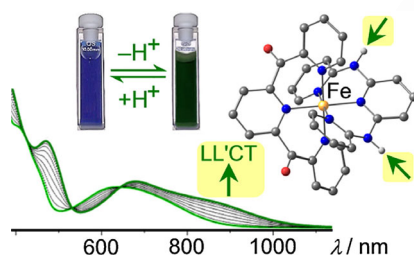
Making iron luminescent: N-deprotonation of the ligand backbone of electron-rich polypyridine ligands in push–pull substituted iron(II) complexes yields deep-green complexes with charge-transfer bands extending into the near-IR region. According to theoretical calculations, these absorption bands feature dipole-allowed ligand-to-ligand charge-transfer character (LL′CT).

Electron-rich and -poor tridentate ligands with large bite angles give blue iron(II) complexes with low energy MLCT states. The electron-donating power of the electron-rich ligand is further increased by deprotonation in the ligand's backbone, yielding intense green iron(II) complexes with absorption bands in the near-IR region. According to time-dependent DFT calculations, these bands are of dipole-allowed ligand-to-ligand CT character. Exploiting this low-energy CT state might be a novel strategy towards potentially luminescent iron(II) complexes. For more details, see the Full Paper by K. Heinze et al. on page ■ ■ ff.

Heinze et al. @uni mainz: boosting Vis/NIR charge-transfer absorptions of iron(II) complexes SPACE RESERVED FOR IMAGE AND LINK

Share your work on social media! *Chemistry - A European Journal* has added Twitter as a means to promote your article. Twitter is an online microblogging service that enables its users to send and read text-based messages of up to 140 characters, known as "tweets". Please check the pre-written tweet in the galley proofs for accuracy. Should you or your institute have a Twitter account, please let us know the appropriate username (i.e., @accountname), and we will do our best to include this information in the tweet. This tweet will be posted to the journal's Twitter account @ChemEurJ (follow us!) upon online publication of your article, and we recommended you to repost ("retweet") it to alert other researchers about your publication.

Please check that the ORCID identifiers listed below are correct. We encourage all authors to provide an ORCID identifier for each coauthor. ORCID is a registry that provides researchers with a unique digital identifier. Some funding agencies recommend or even require the inclusion of ORCID IDs in all published articles, and authors should consult their funding agency guidelines for details. Registration is easy and free; for further information, see http://orcid.org/.

Andreas K. C. Mengel
Christian Bissinger
Matthias Dorn
Oliver Back
Dr. Christoph Förster
Prof. Dr. Katja Heinze http://orcid.org/0000-0003-1483-4156

3.3"A Bis(tridentate)cobalt Polypyridine Complex as Mediator in Dye-Sensitized Solar Cells"

Andreas K. C. Mengel, Woohyung Cho, Aaron Breivogel, Kookheon Char, Yong S. Kang and Katja Heinze

Eur. J. Inorg. Chem. **2015**, 3299−3306.
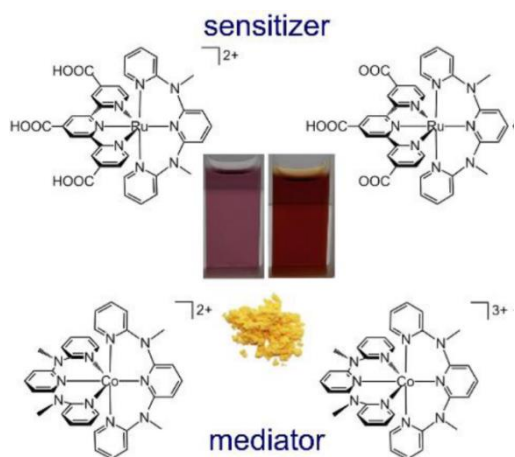
The synthesis and characterization of the deprotonated ruthenium(II) complex and the synthesis of the cobalt(II,III) redox couples were performed by Andreas K. C. Mengel. The development of the ruthenium(II) complexes and the [Co(ddpd)$_2$](BF$_4$)$_2$ was accomplished by ▮▮▮▮▮▮▮▮ during his PhD thesis. After instruction from ▮▮▮▮▮▮▮▮ (Hanyang University, Seoul) and ▮▮▮▮▮▮▮▮ (Seoul National Universtiy, Seoul) the DSSCs were built and characterized by Andreas K. C. Mengel and ▮▮▮▮▮▮▮▮ (Hanyang University, Seoul). The manuscript was written by ▮▮▮▮▮▮▮▮ (50 %) and Andreas K. C. Mengel (50 %).

Supporting information: page 161-166.

A Bis(tridentate)cobalt Polypyridine Complex as Mediator in Dye-Sensitized Solar Cells

Andreas K. C. Mengel,[a] Woohyung Cho,[b] Aaron Breivogel,[a]
Kookheon Char,[c] Yong Soo Kang,[b] and Katja Heinze*[a]

Dye-sensitized solar cells equipped with cationic and neutral Ru^{II}-based sensitizers $[Ru(ddpd)\{tpy(COOH)_3\}]^{2+}$ [1^{2+}; ddpd = N,N'-dimethyl-N,N'-di(pyridin-2-yl)pyridin-2,6-diamine, $tpy(COOH)_3$ = $2,2''6',2''$-terpyridine-4,4',4''-tricarboxylic acid] and $[Ru(ddpd)\{tpy(COOH)(COO)_2\}]$ (**2**) with and without the coadsorbent chenodeoxycholic acid were constructed with I_3^-/I^- or the $Co^{III/II}$-based redox mediators [Co(bpy)$_3$]$^{3+/2+}$ (**3**$^{3+/2+}$; bpy = 2,2'-bipyridine) and [Co(ddpd)$_2$]$^{3+/2+}$ (**4**$^{3+/2+}$) in the presence of $LiClO_4$ and 4-*tert*-butylpyridine. The best photovoltaic performance was achieved

by using the **4**$^{3+/2+}$ shuttle and the neutral sensitizer **2** without coadsorbent. The higher short-circuit photocurrent density and higher electron recombination lifetimes obtained with this combination suggest slow electron recombination kinetics at the TiO_2 surface with the Co^{III} complex **4**$^{3+}$. The slow electron transfer to **4**$^{3+}$ is tentatively ascribed to the high-lying $\pi^\star$ orbitals of the electron-rich ddpd ligands, which result in a weak electronic coupling. This contrasts with the faster recombination with **3**$^{3+}$, which features the low-energy $\pi^\star$ orbitals of the bpy ligands.

Introduction

Since Grätzel and O'Regan presented the first dye-sensitized solar cell (DSSC) in 1991, enormous efforts to improve photovoltaic efficiencies have been made worldwide.[1] From the variety of sensitizers based on inorganic and organic dyes, ruthenium(II) complexes provide stable and efficient solar cells.[2–6] One of the best-performing sensitizers in this class of dyes is the bis(tetra-*n*-butylammonio)[*cis*-di(isothiocyanato)bis(2,2'-bipyridyl-4,4'-dicarboxylato)]-ruthenium(II) complex known as N719. This dye features a broad absorption profile in the visible spectral region and delivers high efficiencies of up to $\eta = 11\%$.[7,8] However, monodentate or bidentate ligands, such as the SCN^- and 2,2'-bipyridine (bpy) ligands present in N719, have significant disadvantages with respect to the long-term stability of the cell owing to thermal or photoinduced isomerization or ligand exchange reactions. This lability reduces photo-

voltaic efficiencies.[9–16] To address this problem, we investigated a series of new bis(tridentate) heteroleptic ruthenium(II) complexes with N,N'-dimethyl-N,N'-di(pyridin-2-yl)pyridin-2,6-diamine (ddpd) as an electron-donating ligand and $2,2''6',2''$-terpyridine-4,4',4''-tricarboxylic acid [$tpy(COOH)_3$] as an electron-withdrawing ligand (Figure 1a for 1^{2+} as an example).[17,18] These dyes combine suitable optical properties with stability towards ligand dissociation.[19] Their photovoltaic performance was evaluated by using a standard DSSC setup with a triiodide/iodide (I_3^-/I^-) redox shuttle.[19]

Although these stable complexes absorb similarly to N719 in the visible spectral region, their cell performance was rather poor.[19] Indeed, efficient electron recombination with the oxidized electrolyte (I_3^-) at the TiO_2 electrode was assumed to be responsible for the low efficiency. The positive charge of 1^{2+} is assumed to attract the negatively charged I_3^- ions near to the TiO_2 surface and, thus, favors back electron transfer (back-ET) from TiO_2 to I_3^-.[20,21] Studies on the N719 sensitizer with different stages of protonation demonstrated the influence of the charge of the sensitizer on the optical properties as well as on the photovoltaic performance.[22]

In this study, we attempt to reduce the detrimental back-ET from TiO_2 to the oxidized mediator (1) by decreasing the charge of the sensitizers from +2 to zero through deprotonation (Figure 1, a), (2) by the addition of $LiClO_4$ and 4-*tert*-butylpyridine (TBP) to modify the TiO_2 surface and the TiO_2 acceptor states, (3) by coadsorption of chenodeoxycholic acid (CDCA, Figure 1, b) to protect the TiO_2

_____

[a] Institute of Inorganic Chemistry and Analytical Chemistry,
    Johannes Gutenberg University of Mainz,
    Duesbergweg 10–14, 55128 Mainz, Germany
    E-mail: katja.heinze@uni-mainz.de
    https://www.blogs.uni-mainz.de/fb09ak-heinze/
[b] The Departmet of Energy Engineering and Center for Next
    Generation Dye-Sensitized Solar Cells, Hanyang University,
    222 Wangsimni-ro, Seongdong-gu, Seoul 133-791, Korea
[c] The National Creative Research Initiative Center for Intelligent
    Hybrids, School of Chemical and Biological Engineering, Seoul
    National University,
    1 Gwanak-ro, Gwanak-gu, Seoul 151-744, Korea
    Supporting information for this article is available on the
    WWW under http://dx.doi.org/10.1002/ejic.201500252.
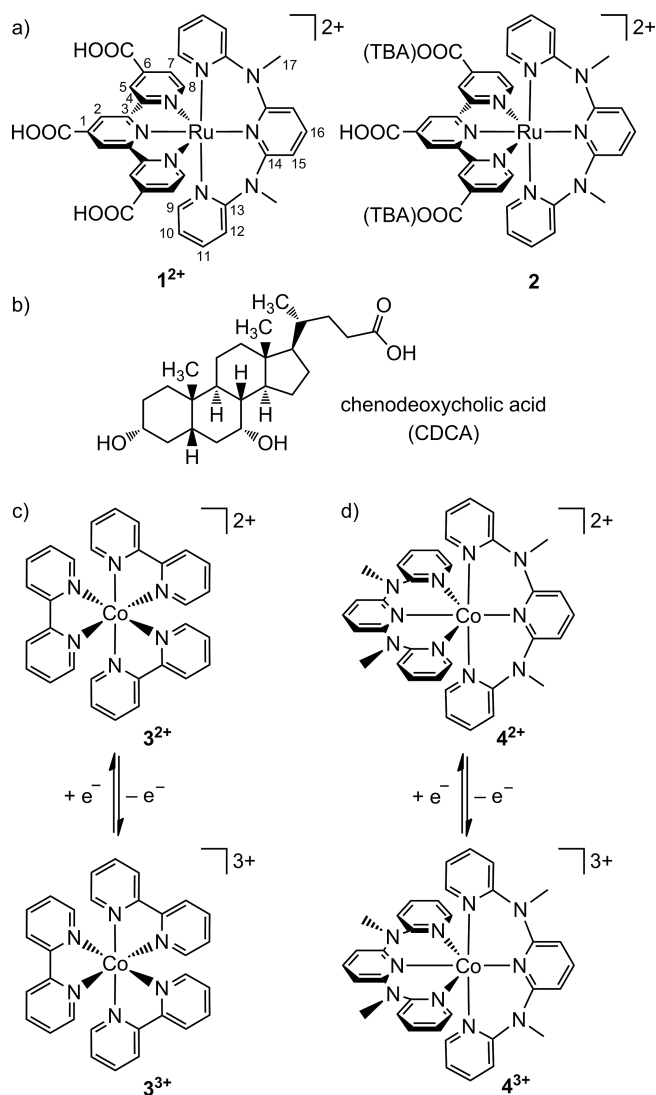
Figure 1. (a) Sensitizer **1**(PF$_6$)$_2$ and (*n*Bu$_4$N)$_2$**2**(PF$_6$)$_2$ (atom numbering for NMR assignments), (b) coadsorbent CDCA, (c) tris(bipyridine) complexes **3**$^{2+}$ and **3**$^{3+}$, and (d) bis(ddpd) complexes **4**$^{2+}$ and **4**$^{3+}$.

surface from the oxidized redox mediator,[23] and (4) by changing the redox mediator[24–35] from the negatively charged I$_3^-$/I$^-$ to the positively charged Co$^{III/II}$ couple. Specifically, the [Co(bpy)$_3$]$^{3+/2+}$ (**3**$^{3+}$/**3**$^{2+}$, Figure 1, c)[21,25–29,35] and the new [Co(ddpd)$_2$]$^{3+/2+}$ (**4**$^{3+}$/**4**$^{2+}$, Figure 1, d)[30] redox couples are employed.

The suitability of a redox couple as a mediator in DSSCs depends on several properties, namely, its ability to efficiently regenerate the oxidized dye with low driving forces, its resistance towards recombination with photoinjected electrons at the TiO$_2$ electrode, its efficient reduction at the counter electrode, its low absorbance in the visible spectral region, its ion mobility, and its stability. The I$_3^-$/I$^-$ couple fulfills several aspects but suffers from appreciable absorption in the visible spectral region, a rather low-lying redox potential, corrosive properties, and complicated redox

chemistry. One-electron redox mediators such as the Co$^{III/II}$ couple have attracted considerable interest in recent years owing to their favorable and tunable optical and redox properties[35] paired with their nonvolatility and noncorrosiveness. Indeed, they perform excellently in DSSCs with organic sensitizers[28,31,33] but usually give poorer results with ruthenium(II)-based sensitizers.[27,35g] As a prominent reason for the low efficiency with ruthenium(II)-based sensitizers, fast electron recombination with Co^{III} at the TiO$_2$ surface has been recently confirmed.[35g]

The facile reduction of Co^{III} species depends on the spin state of the Co^{II} species. The electron configuration of cobalt(III) ions in an octahedral ligand field is (t$_{2g}$)^6(e$_g$*)^0 (low-spin Co^{III}) in all relevant cases. Cobalt(II) complexes with pyridine donor ligands are close to the spin-crossover point.[36] Indeed, the ground-state electron configuration of the cobalt(II) center in [Co(bpy)$_3$]$^{2+}$ (**3**$^{2+}$) is (t$_{2g}$)^5(e$_g$*)^2 (high-spin Co^{II}), but the ground state is (t$_{2g}$)^6(e$_g$*)^1 for [Co(tpy)$_2$]$^{2+}$ (low-spin Co^{II}).[36] Electron transfer between Ru^{III} [(t$_{2g}$)^5] and low-spin Co^{II} (low-spin pathway) is reported to be faster than that for Ru^{III} and high-spin Co^{II} (high-spin pathway)[37] as much higher inner-sphere reorganization energy is associated with the high-spin Co^{II}/low-spin Co^{III} couple, specifically, appreciable Co–N bond length changes. Indeed, Ru^{III} dye regeneration seems to occur by the low-spin pathway involving a pre-equilibrium of high-spin and low-spin Co^{II} complexes (spin crossover).[27] Hence, cobalt-based mediators should preferably be close to the spin-crossover point[36] in the Co^{II} state to achieve high dye-regeneration rates.

The undesired interception of electrons at the TiO$_2$ surface by Co^{III} complexes is promoted by ion-pair formation with negatively charged sensitizers and retarded by bulky substituents.[27,35g] In this context, it is important to recognize that the initial ET product between the photoinjected electron and the Co^{III} complex is a low-spin Co^{II} complex. Hence, the excited low-spin state of **3**$^{2+}$ formed by the interfacial ET has to relax to the high-spin electronic ground state by spin crossover. Furthermore, Co$^{III/II}$ self-exchange reactions are slow for aliphatic amine ligands such as ethylenediamine (en) in [Co(en)$_3$]$^{3+/2+}$ ($k = 2 \times 10^{-5}$ M^{-1} s^{-1}) but are comparably fast for cobalt complexes with pyridine ligands [Co(phen)$_3$]$^{3+/2+}$ ($k = 40$ M^{-1} s^{-1}, phen = 1,10-phenanthroline).[38] Clearly, strong electronic coupling in the latter case is responsible for the fast ET, which might be ascribed to a feasible electron transfer pathway involving the π* orbitals of the pyridine ligands. Similarly, one-electron reduction of the chromium(III) complex [Cr^{III}(bpy)$_3$]$^{3+}$ occurs solely at the bpy ligand to afford [Cr^{III}(bpy$^{·-}$)(bpy)$_2$]$^{2+}$ instead of [Cr^{II}(bpy)$_3$]$^{2+}$.[39] In the present study, we suggest that pyridine ligands with high-energy π* orbitals could help to reduce the interfacial back electron transfer rate but still allow access to the low-spin and high-spin Co^{II} states required for dye regeneration. The latter process typically appears to be fast enough under working conditions.[35g]

The recently reported cobalt complexes **4**$^{3+}$/**4**$^{2+}$ possess high-energy π* orbitals of the coordinated electron-rich ddpd ligands (in contrast to **3**$^{3+}$/**3**$^{2+}$ with low-energy π* or-

bitals), and 4^{2+} has close-lying high-spin/low-spin states (similarly to 3^{2+}).[30] Indeed, the ddpd ligand in $4^{3+}/4^{2+}$ cannot be reduced at accessible potentials; therefore, an efficient electron transfer pathway through its π* orbitals can be excluded.[30] The same also holds for other $[M(ddpd)_2]^{2+/3+}$ complexes.[40] These features should allow for efficient dye regeneration but should retard the electron interception by Co^{III} species at the TiO_2 surface. The redox potential of $4^{3+}/4^{2+}$ (–0.17 V vs. ferrocene/ferrocenium) is between those of I_3^-/I^- (–0.38 V vs. ferrocene/ferrocenium) and $3^{3+}/3^{2+}$ (–0.04 V vs. ferrocene/ferrocenium).[29,30] Hence, the open-circuit voltages V_{OC} are expected to increase in the series $I_3^-/I^- < 4^{3+}/4^{2+} < 3^{3+}/3^{2+}$ as long as all ET processes show comparable rates, which is not necessarily the case.[35g]

Results and Discussion

The push–pull substituted Ru^{II}-based sensitizer 1^{2+} has been prepared according to a recently published procedure.[18,19] The double deprotonation of 1^{2+} to form the bis(tetra-n-butylammonium biscarboxylate) $(nBu_4N)_2\mathbf{2}$-$(PF_6)_2$ is accomplished with tetra-n-butylammonium hydroxide in aqueous solution (Figure 1, a, Exp. Sect.). The successful double deprotonation is confirmed by the correct integration ratio of the ^1H NMR resonances of the butyl protons of the ammonium cation and the dye protons (see Supporting Information, Figure S1). The most pronounced chemical shift differences are found for the resonances of 2-H, 5-H, and 8-H located in the vicinity of the COOH/COO$^-$ substituents (see Exp. Sect. and ref.[19]).

The high-spin cobalt(II) salts $3(BF_4)_2$[32] and $4(BF_4)_2$[30] were prepared according to literature procedures. The oxidation to the respective cobalt(III) salts $3(BF_4)_3$ and $4(BF_4)_3$ is achieved with silver tetrafluoroborate (Exp. Sect.). Both Co^{III} complexes 3^{3+} and 4^{3+} are diamagnetic [low-spin cobalt(III)] as expected (Figures S2 and S3).

The experimental UV/Vis spectra of the sensitizer $1(PF_6)_2$ and its conjugate base $(nBu_4N)_2\mathbf{2}(PF_6)_2$ in CH_3CN at room temperature are depicted in Figure 2. The spectrum of 1^{2+} shows the π→π* bands of the polypyridine ligands at $λ = 291$ and 340 nm and metal-to-ligand charge transfer (MLCT) bands in the visible region at $λ = 473, 537, 608,$ and 661 nm.[19] The low energies of the MLCT bands arise from the electron-withdrawing nature of the three carboxylic acid moieties of the tpy ligand, which lower the level of the lowest unoccupied molecular orbital (LUMO), and the electron-donating nature of the ddpd ligand, which increases the level of the ruthenium-based highest occupied molecular orbital (HOMO).[18,19] Deprotonation to the neutral dye $\mathbf{2}$ shifts all of the bands to higher energy owing to its higher LUMO energy (π–π* bands: $λ = 278, 323$ nm; MLCT bands: $λ = 455, 500, 550,$ and 611 nm; Figure 2, a).

The iodine/1-methyl-3-propylimidazolium iodide solution employed as the electrolyte absorbs appreciably in the $λ = 350–480$ nm region (Figure 2, b).[29] On the other hand, the Co^{II} and Co^{III} complexes feature only weak absorp-
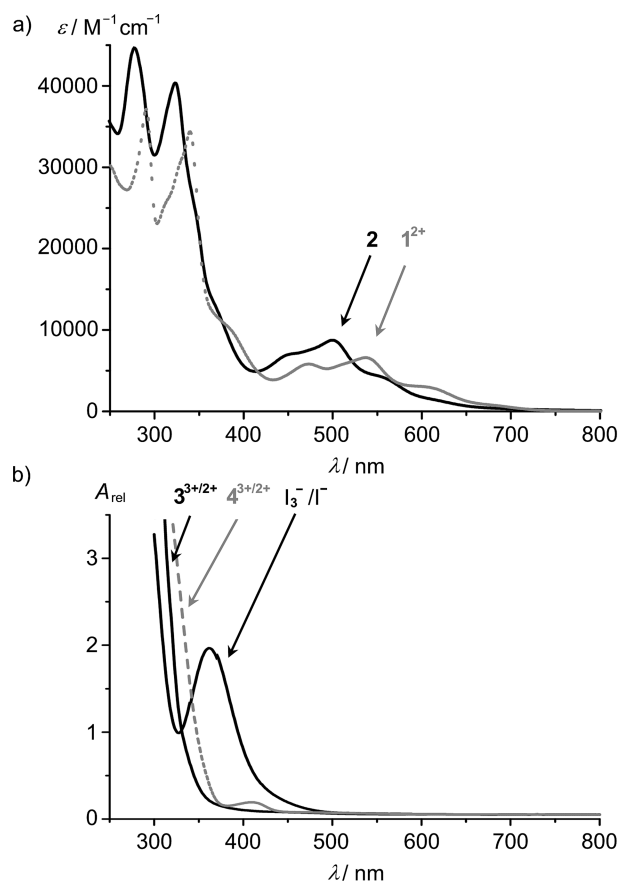
Figure 2. Experimental UV/Vis spectra of (a) sensitizers $1(PF_6)_2$ and $(nBu_4N)_2\mathbf{2}(PF_6)_2$ in CH_3CN and (b) electrolyte solutions as employed in the solar cells, diluted by a factor of 100.

tions, namely, Laporte forbidden ligand-field bands, in the visible spectral region.[30] Indeed, the employed electrolyte solutions $3^{3+/2+}$ and $4^{3+/2+}$ are much more transparent at $λ > 350$ nm (Figure 2, b), which should result in somewhat higher photocurrents.

The DSSCs were manufactured with a FTO/TiO$_2$/dye/electrolyte/Pt/FTO (FTO = fluorine-doped tin oxide) structure. The cationic sensitizer 1^{2+} and the neutral dye $\mathbf{2}$ were adsorbed onto the TiO_2 surface with and without the coadsorbent CDCA (Figure 1, b). Different electrolytes in combination with different additives were employed. The classical iodine (0.08 M)/1-methyl-3-propylimidazolium iodide (0.6 mM) redox shuttle was prepared in CH_3CN with and without $LiClO_4$ (0.1 M) and TBP additives (0.8 M). A Co^{III}/Co^{II} concentration ratio of 1:3.6 was adjusted in acetonitrile/succinonitrile (8:1 v/v) solution with $3^{2+}/3^{3+}$ (0.165/0.045 M) and with $4^{2+}/4^{3+}$ (0.083/0.023 M).

The effects of sensitizer charge ($1^{2+}/2$), coadsorbent (with/without CDCA), additives (Li$^+$/TBP), and electrolyte type (I_3^-/I^-; $3^{3+}/3^{2+}$, $4^{3+}/4^{2+}$) on the open-circuit voltage V_{OC} and the short-circuit photocurrent density I_{SC} will be presented next. The pertinent photovoltaic data of 16 different cells are compiled in Table 1.

Table 1. Photovoltaic data of DSSCs with different setups.

Dye	Relative amount of adsorbed dye	CDCA	Electrolyte	LiClO$_4$/TBP	V_{OC} [V]	I_{SC} [mA cm^{-2}]	Fill factor [%]	η [%]
1^{2+}	0.98	–	I$_3^-$/I$^-$	–	0.39	1.50	63.7	0.37
1^{2+}	0.93	+	I$_3^-$/I$^-$	–	0.38	1.49	64.8	0.36
1^{2+}	0.98	–	I$_3^-$/I$^-$	+	0.53	1.31	70.4	0.49
1^{2+}	0.93	+	I$_3^-$/I$^-$	+	0.53	1.58	73.8	0.61
1^{2+}	0.98	–	3^{3+}/3^{2+}	+	0.35	0.52	40.0	0.07
1^{2+}	0.93	+	3^{3+}/3^{2+}	+	0.26	0.35	46.3	0.04
1^{2+}	0.98	–	4^{3+}/4^{2+}	+	0.51	1.73	52.3	0.47
1^{2+}	0.93	+	4^{3+}/4^{2+}	+	0.55	2.29	57.1	0.71
2	1.00	–	I$_3^-$/I$^-$	–	0.57	0.58	50.0	0.16
2	1.00	+	I$_3^-$/I$^-$	–	0.57	0.93	63.8	0.34
2	1.00	–	I$_3^-$/I$^-$	+	0.50	1.13	69.7	0.39
2	1.00	+	I$_3^-$/I$^-$	+	0.49	1.10	69.8	0.38
2	1.00	–	3^{3+}/3^{2+}	+	0.21	0.65	61.6	0.08
2	1.00	+	3^{3+}/3^{2+}	+	0.59	0.85	38.9	0.19
2	1.00	–	4^{3+}/4^{2+}	+	0.54	2.46	57.1	0.76
2	1.00	+	4^{3+}/4^{2+}	+	0.54	2.24	58.6	0.71

From Table 1, it becomes clear that the dye loadings of the individual setups do not differ strongly. The cografted CDCA slightly diminishes the loading of dye 1^{2+}, which suggests that 1^{2+} competes with CDCA for binding sites at the TiO$_2$ surface. Apparently, CDCA does not displace **2** from the TiO$_2$ surface; this suggests that **2** binds more strongly to TiO$_2$ through its carboxylate groups. The stronger binding of **2** is also reflected in a slightly higher loading of **2** compared with that of 1^{2+}.

The standard triiodide/iodide redox mediator will be discussed first. Additives such as Li$^+$ shift the band edge of TiO$_2$ downward towards more positive potentials and reduce V_{OC},[41] whereas TBP results in an inverse band-edge movement and increases V_{OC}.[25] The relative strength of these effects is different for the different dyes 1^{2+} and **2** (Figures 3, a and S8, for I/V plots without Li$^+$/TBP additives). A beneficial effect of TBP on V_{OC} is clear for dye 1^{2+} but seems to be (over)compensated by the Li$^+$ effect for the carboxylate-substituted dye **2**. Possibly, this can be traced back to a predominant modification of the TiO$_2$/**2** surface by Li$^+$ ions and a predominant modification of the TiO$_2$/1^{2+} surface by TBP. The coadsorbent CDCA has no dramatic effect on V_{OC} for either dye (Figure 3, a). The I_{SC} values of cells with sensitizer **2** are improved either by the coadsorbent CDCA or by the Li$^+$/TBP additives from 0.58 to 0.93 and 1.13 mA cm^{-2}, respectively (Figure 3, a). Lithium ions lower the band edge for TiO$_2$/**2** and reduce V_{OC}. However, the lower band edge also enhances the charge-collection efficiency and, hence, increases I_{SC} for the cell with sensitizer **2** (Table 1, Figure 3 a and Supporting Information, Figure S8).

The employment of the well-known electrolyte mixture 3^{3+}/3^{2+} instead of the iodide-based couple significantly reduces I_{SC} for both dyes irrespective of the presence of CDCA (Figure 3, b). V_{OC} is also lowered for all cells with the 3^{3+}/3^{2+} electrolyte except for that with dye **2** cografted with CDCA. The low V_{OC} values match the literature

values of cells with the [Co(bpy)$_3$]$^{2+/3+}$ couple and the N3 sensitizer.[35g] The recombination reaction at the TiO$_2$ surface seems to be quite efficient for the bipyridine cobalt(III) complex 3^{3+} and results in the observed lower V_{OC}. Furthermore, a drop in I_{SC} is observed for the 3^{3+}/3^{2+} couple at approximately 0.15 V in the presence of CDCA under our conditions. This might be due to some chemical decomposition of the bpy complex. The feasible ligand loss in the ESI mass spectra of 3^{3+}/3^{2+} confirms a high reactivity of the bpy complexes {with m/z = 390 [Co(bpy)$_2$F]$^+$ as the strongest peak; see Figures S4 and S5}.

The replacement of 3^{3+}/3^{2+} with the new 4^{3+}/4^{2+} shuttle with tridentate ligands gives a different picture (Figure 3, c). The stability towards ligand substitution is enhanced, and the strongest peaks in the ESI mass spectra are found at m/z = 660, which corresponds to [Co(ddpd)$_2$F]$^+$ (see Figures S6 and S7). The V_{OC} values are comparable to or even slightly higher than those for cells with the I$_3^-$/I$^-$ mediator. Most encouragingly, the short-circuit photocurrent densities of cells with 4^{3+}/4^{2+} electrolytes are significantly enhanced with respect to those of cells with I$_3^-$/I$^-$ and 3^{3+}/3^{2+} shuttles. The 4^{3+}/4^{2+} redox mediator mixture outperforms both the 3^{3+}/3^{2+} and iodide-based couples (Figure 3). Even with the employed half absolute concentration of the 4^{3+}/4^{2+} couple (see Exp. Sect.), the I_{SC} reaches the highest values of I_{SC} = 1.73 (1^{2+}), 2.29 (1^{2+}/CDCA), 2.46 (**2**), and 2.24 A cm^{-2} (**2**/CDCA) in our setup. In summary, the mixed electrolyte 4^{3+}/4^{2+} enhances V_{OC} to 140%, I_{SC} to 164%, and efficiency to 200% with respect to those of the iodide-based couple without additives and coadsorbent (Figures 3c and S8).

The increases of the efficiency and cell performance are mirrored in the photocurrent action spectra of sensitizer 1^{2+} with the iodide-based electrolyte and the 4^{3+}/4^{2+} couple without CDCA and with CDCA (Figure 4, a, Table 1). The deprotonation of the sensitizer 1^{2+} to **2** further improves incident photon-to-current efficiency (IPCE) values and the efficiency (Figure 4, a, Table 1).
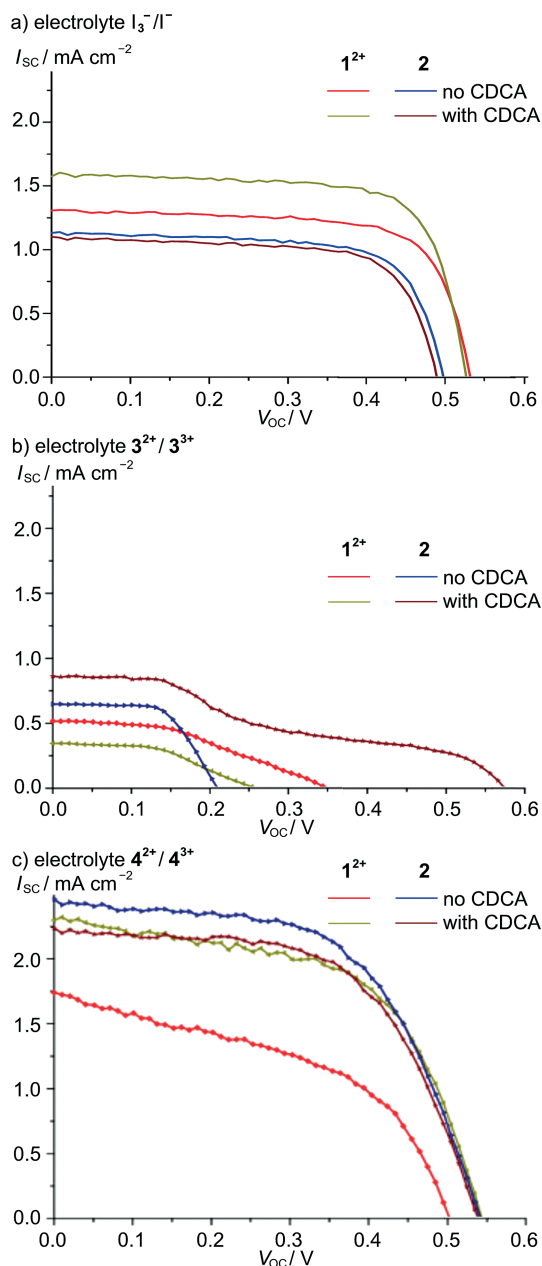
Figure 3. Photocurrent density versus voltage curves for DSSCs with sensitizers 1^{2+} and 2 and (a) I_3^-/I^-, (b) $3^{3+}/3^{2+}$, and (c) $4^{3+}/4^{2+}$ as redox mediators (with Li$^+$/TBP additives).

Figure 4. (a) Photocurrent action spectra of dyes 1^{2+} and 2 with the $4^{3+}/4^{2+}$ redox shuttle and 1^{2+} with the I_3^-/I^- couple (without Li$^+$/TBP); (b) electron lifetimes as a function of V_{OC} for DSSCs sensitized with 2 (with Li$^+$/TBP).

The electron recombination kinetics of DSSCs with sensitizer 2 and the I_3^-/I^- and $4^{3+}/4^{2+}$ electrolytes were probed by the photovoltage response of the cells to a small amplitude light modulation. The determined electron lifetimes as a function of V_{OC} are depicted in Figure 4 (b). At a given voltage, the electron lifetime in the DSSC with the $4^{3+}/4^{2+}$ shuttle (without CDCA) is 1.4 to 3.3 times higher than that in the DSSC with the I_3^-/I^- mediator (without CDCA). Thus, we suggest that electron capture from the TiO$_2$/2

surface by 4^{3+} is slower than electron interception by I_3^-. The comparably slow electron recombination with 4^{3+} might be associated with a higher ET barrier imposed by the high-energy π^* orbitals of the ddpd ligands.

To compare the heterogeneous electron transfer kinetics of the $4^{3+}/4^{2+}$ shuttle with those of the $3^{3+}/3^{2+}$ pair, cyclic voltammograms were recorded with platinum electrodes in acetonitrile with different electrolyte salts, namely, [TBA][PF$_6$] (TBA = tetrabutylammonium) and [TBA][B(C$_6$F$_5$)$_4$] (Figure 5). The ΔE versus scan rate plots are shown in Figure S9. All of the redox events are quasireversible, and the heterogeneous electron transfer of $4^{3+}/4^{2+}$ is substantially slower for both supporting electrolytes. Hence, the counterion is not responsible for the different electron transfer rates. The slow heterogeneous electron transfer of the $4^{3+}/4^{2+}$ couple on platinum compared with that of the $3^{3+}/3^{2+}$ pair fits the above suggestion of slow back-ET from TiO$_2$ to 4^{3+}. Again, this might be understood through the assumption that electron transfer to Co^{III} is mediated through the π^* orbitals of the ligand, which is hampered for ddpd.

FULL PAPER
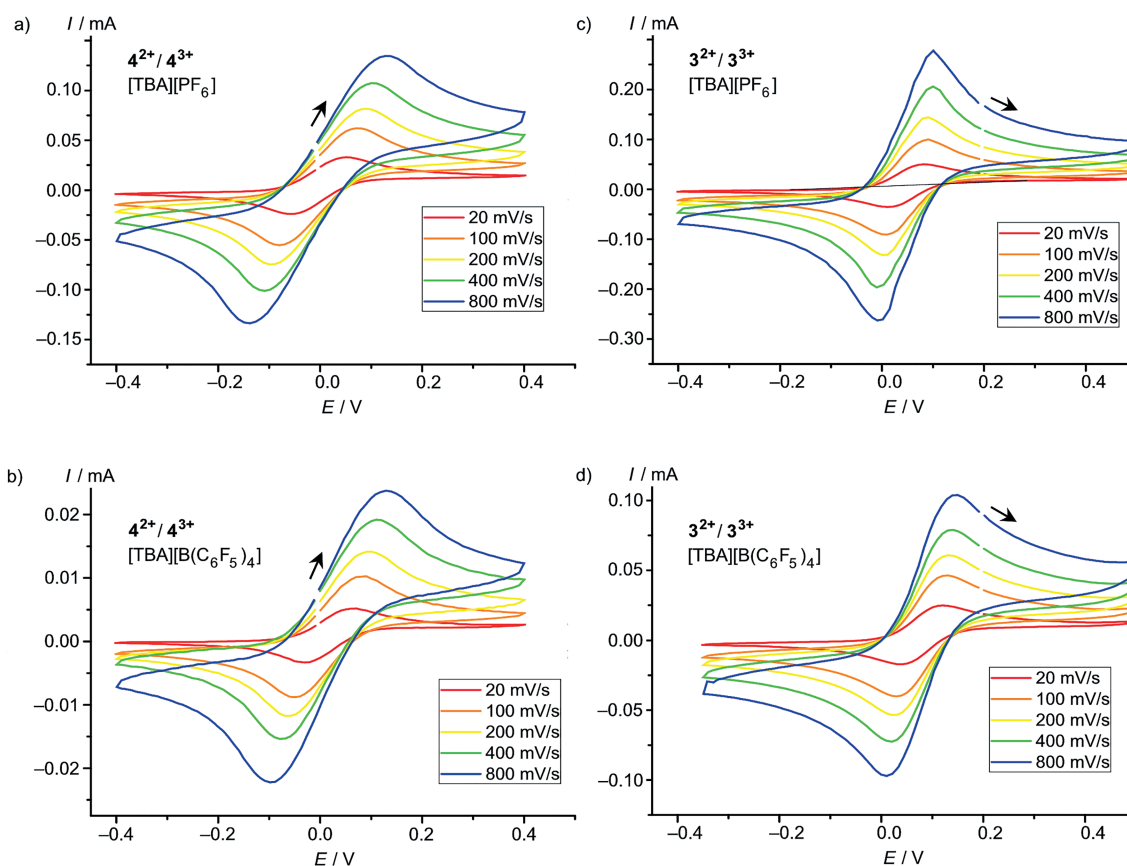
Figure 5. Cyclic voltammograms at varying scan rates for **4**(BF)$_2$ and **3**(BF$_4$)$_2$ in acetonitrile with [TBA][PF$_6$] and [TBA][B(C$_6$F$_5$)$_4$] as supporting electrolytes (potentials are given vs. ferrocene/ferrocenium).

Conclusions

With respect to those of the classical I$_3^-$/I$^-$ and well-known **3**$^{3+}$/**3**$^{2+}$ redox mediator mixtures, the **4**$^{3+}$/**4**$^{2+}$ shuttle considerably improves the short-circuit photocurrent density I_{SC} in DSSCs both with cationic and neutral Ru^{II}-based sensitizers **1**$^{2+}$ and **2** in the presence of 4-*tert*-butylpyridine and lithium cations. For the cationic dye **1**$^{2+}$, a further slight improvement is achieved by cografting the sensitizer with chenodeoxycholic acid, whereas no further beneficial effect is observed for the coadsorbent in combination with the neutral dye **2**. Electron recombination at the TiO$_2$ surface is retarded for **4**$^{3+}$ compared with electron recombination for **3**$^{3+}$ and I$_3^-$. Tentatively, we ascribe this slow recombination to the higher energy of the π* orbitals of the electron-rich ddpd ligands in **4**$^{3+}$ compared with the low-energy π* orbitals of bpy in **3**$^{3+}$. This results in a higher activation barrier for the electron recombination. At platinum electrodes, the heterogeneous electron transfer rates of **4**$^{3+}$/**4**$^{2+}$ are also lower than those of **3**$^{3+}$/**3**$^{2+}$. Further detailed studies of the **4**$^{3+}$/**4**$^{2+}$ mediator in comparison with the I$_3^-$/I$^-$ couple and other Co-based shuttles will serve to establish if this finding can be generalized to dye-sensitized solar cells with other types of sensitizers and setups, for example, with polymer gel electrolytes.[42]

Experimental Section

General Procedures: All reagents were used as received from commercial suppliers (Acros, Sigma–Aldrich, Solaronix SA, Wako, TCI). The syntheses of **1**(PF$_6$)$_2$,[19] **3**(BF$_4$)$_2$,[32] and **4**(BF$_4$)$_2$[30] have been reported previously. The NMR spectra were recorded with a Bruker Avance DRX 400 spectrometer at 400.31 MHz (^{1}H). All resonances are reported in ppm and were referenced to the solvent signal as internal standard {[D$_6$]dimethyl sulfoxide ([D$_6$]DMSO): ^{1}H, δ = 2.50 ppm; CD$_3$CN: ^{1}H, δ = 1.94 ppm}. The UV/Vis spectra were recorded with a Jasco V-670 UV/Vis/NIR spectrometer or a Varian Cary 5000 spectrometer. The electrochemical experiments were performed with a BioLogic SP-50 voltammetric analyzer, platinum wire working and counter electrodes, and a 0.01 M Ag/AgNO$_3$ reference electrode. The measurements were performed at varying scan rates of 20–800 mV s^{-1} for cyclic voltammetry experiments with 0.1 M [TBA][PF$_6$] or [TBA][B(C$_6$F$_5$)$_4$] as the supporting electrolytes in acetonitrile. The potentials are given relative to the ferrocene/ferrocenium couple. The current–voltage characteristics of the DSSCs were measured with a Keithley Model 2400 source meter and a solar simulator with a 300 W Xenon arc lamp (Newport) under 1 sun illumination (AM 1.5, 100 mW cm^{-2}). A light-shading mask, placed on the residual area of the front side of the fluorine-doped tin oxide substrate (except for the 0.25 cm^2 TiO$_2$ active area) was employed to prevent overestimation of the power conversion efficiency. The electron lifetimes were obtained by intensity-modulated photovoltage spectroscopy (IMVS) under open-circuit conditions as a function of light intensity by using a controlled

intensity-modulated photovoltage spectroscopy (CIMPS) system (Zahner).

TiO$_2$ Electrode Preparation: Fluorine-doped tin oxide (FTO) glass plates (Pilkington-TEC8) were cleaned with an ultrasonic bath with 2 vol-% Helmanex in deionized water and ethanol. A doctor-bladed layer of 20 nm TiO$_2$ particles (PST-18 NR, CCIC) was used as a photoelectrode. A 8 μm thick transparent film and an additional 4 μm scattering TiO$_2$ film (PST-400C, CCIC, particle size ca. 400 nm) were coated on top of the conducting glass electrode. The TiO$_2$ electrodes were heated at 450 °C for 30 min. The TiO$_2$ coated electrodes were treated with a 0.5 mM TiCl$_4$ solution for 20 min at 70 °C, followed by an annealing process for 30 min at 450 °C. Following the heat treatment, these electrodes were immersed in the sensitizer/coadsorbent solution [**1**(PF$_6$)$_2$: 3.05×10^{-4} M; (nBu$_4$N)$_2$**2**(PF$_6$)$_2$: 3.20×10^{-4} M. CDCA: 3.00×10^{-4} M in CH$_3$CN/ *tert*-butanol, 1:1 v/v] for 18 h at room temperature. The TiO$_2$ electrodes were rinsed with CH$_3$CN and dried.

Electrolyte Solutions: The triiodide/iodide electrolyte solutions were prepared from 1-methyl-3-propylimidazolium iodide (0.6 M) and iodine (0.08 M) in CH$_3$CN. 4-*tert*-Butylpyridine (0.8 M) and lithium perchlorate (0.1 M) were used when indicated. A Co^{III}/Co^{II} concentration ratio of 1:3.6 was achieved in acetonitrile/succinonitrile (4:1 v/v) with **3**$^{3+}$/**3**$^{2+}$ (0.045/0.165 M) and **4**$^{3+}$/**4**$^{2+}$ (0.023/0.083 M). Owing to the lower solubility of **4**$^{3+}$ and **4**$^{2+}$, this mediator was employed at lower concentration. 4-*tert*-Butylpyridine (0.8 M) and lithium perchlorate (0.1 M) were always employed with the cobalt-based redox couples.

Counter Electrode Preparation: The Pt electrode was prepared by the spin-coating of a 10 mM H$_2$PtCl$_6$ solution in 2-propanol and then sintered at 450 °C for 30 min. The cells were sealed with 60 μm Surlyn. The electrolyte was introduced through holes on the counter electrode.

Dye Loading: The TiO$_2$/FTO electrodes were immersed in a 0.1 M tetramethylammonium hydroxide H$_2$O/CH$_3$CN (1:1 v/v) solution for at least 120 min. From the UV/Vis absorption spectra of the resulting dye solutions, the concentrations of the attached dyes were calculated: **1**(PF$_6$)$_2$ without CDCA: 1.17×10^{-7} mol cm^{-2}, **1**(PF$_6$)$_2$ with CDCA: 1.11×10^{-7} mol cm^{-2}, (nBu$_4$N)$_2$**2**(PF$_6$)$_2$ without CDCA: 1.19×10^{-7} mol cm^{-2}, and (nBu$_4$N)$_2$**2**(PF$_6$)$_2$ with CDCA: 1.19×10^{-7} mol cm^{-2}.

Complex 3(BF$_4$)$_3$: **3**(BF$_4$)$_2$[32] (1.4 g, 2.0 mmol, 1.0 equiv.) was dissolved in CH$_3$CN (100 mL). AgBF$_4$ (1.0 g, 5.1 mmol, 2.6 equiv.) dissolved in CH$_3$CN (20 mL) was added. The solution was stirred for 2 h. The precipitated silver was removed by filtration, and the solvent was removed under reduced pressure. The greenish brown solid was washed with ethanol (100 mL). The solid was redissolved in CH$_3$CN (50 mL), the solution was filtered, and the solvent was removed under reduced pressure to give a greenish yellow solid (1.4 g, 1.8 mmol, 89%). C$_{30}$H$_{28}$N$_6$CoB$_3$F$_{12}$ (791.9). ^{1}H NMR (400 MHz, [D$_6$]DMSO): δ = 8.7–8.5 (br s, 6 H), 8.4–8.2 (br s, 6 H), 8.0–7.8 (br s, 6 H), 7.5–7.3 (br s, 6 H) ppm. ESI-MS: m/z (%) = 185.55 (29) [Co(bpy)$_2$]$^{2+}$, 390.09 (100) [Co(bpy)$_2$F]$^+$, 458.10 (49) [Co(bpy)$_2$BF$_4$]$^+$, 701.19 (42) [Co(bpy)$_3$(BF$_4$)$_2$]$^+$, 1489.38 (10) [Co$_2$(bpy)$_6$(BF$_4$)$_5$]$^+$.

Complex 4(BF$_4$)$_3$: **4**(BF$_4$)$_2$[30] (404 mg, 496 μmol, 1.0 equiv.) was dissolved in ethanol (25 mL). AgBF$_4$ (115 mg, 591 μmol, 1.5 equiv.) was added, and a brown precipitate appeared. The solid was removed by filtration, washed with ethanol (100 mL), dried, and dissolved in CH$_3$CN (100 mL). After filtration, the solvent was removed under reduced pressure to give a brown powder (330 mg, 366 μmol, 74%). C$_{34}$H$_{34}$N$_{10}$CoB$_3$F$_{12}$ (902.1). ^{1}H NMR (400 MHz,

[D$_6$]DMSO): δ = 8.24 (br s, 4 H), 7.59–7.57 (m, 4 H), 7.51–7.49 (m, 2 H), 7.24–7.23 (m, 4 H), 6.89–6.87 (m, 4 H), 6.70–6.68 (m, 4 H), 3.41 (s, 12 H, NCH$_3$) ppm. ESI-MS: m/z (%) = 320.61 (33) [Co(ddpd)$_2$]$^{2+}$, 369.09 (100) [Co(ddpd)F]$^+$, 660.21 (100) [Co-(ddpd)$_2$F]$^+$, 815.26 (31) [Co(ddpd)$_2$(BF$_4$)$_2$]$^+$, 1266.43 (2) [Co$_3$(ddpd)$_6$(BF$_4$)$_7$]$^{2+}$, 1630.55 (1) [Co$_2$(ddpd)$_4$(BF$_4$)$_4$]$^+$.

Complex (nBu$_4$N)$_2$2(PF$_6$)$_2$: **1**(PF$_6$)$_2$[19] (100 mg, 95.3 μmol, 1.0 equiv.) was dissolved in water (20 mL), and a 40% tetra-n-butyl-ammonium hydroxide solution (214 mg, 286 μmol, 3.0 equiv., 0.54 mL) was added. The solution was filtered, and the solvent was removed under reduced pressure. The dark residue was dissolved in methanol, and a solid was precipitated by the addition of diethyl ether. The solid was collected by filtration and dried under vacuum for 48 h to give a black powder (48.0 mg, 31.4 μmol, 33%). C$_{67}$H$_{98}$N$_{10}$O$_6$RuP$_2$F$_{12}$ (1530.6). ^{1}H NMR (400 MHz, CD$_3$CN): δ = 9.00 (s, 2 H, 2-H), 8.82–8.80 (m, 2 H, 5-H), 8.18 (t, J = 8 Hz, 1 H, 16-H), 8.04 (d, J = 6 Hz, 2 H, 8-H), 7.79 (dd, J = 6 Hz, 2 H, 7-H), 7.56 (pt, J = 8 Hz, 2 H, 11-H), 7.48 (d, J = 8 Hz, 2 H, 15-H), 7.11 (d, J = 8 Hz, 2 H, 12-H), 6.59–6.54 (m, 4 H, 9-H, 10-H), 3.47 (s, 6 H, NCH$_3$), 3.10–3.06 (m, 16 H, H$_{Bu}$), 1.60–1.58 (m, 16 H, H$_{Bu}$), 1.37–1.34 (m, 16 H, H$_{Bu}$), 0.98–0.94 (m, 24 H, H$_{Bu}$) ppm. UV/Vis (CH$_3$CN): λ_{max} (ε) = 610 (1570, sh), 550 (4380), 500 (8750), 455 (7080), 323 (40330), 278 (44640 M^{-1} cm^{-1}) nm.

[1] B. O'Regan, M. Grätzel, *Nature* **1991**, *353*, 737.
[2] A. Mishra, M. K. Fischer, P. Bäuerle, *Angew. Chem. Int. Ed.* **2009**, *48*, 2474.
[3] Z. Ning, H. Tian, *Chem. Commun.* **2009**, 5483.
[4] E. I. Mayo, K. Kilsa, T. Tirrell, P. I. Djurovich, A. Tamayo, M. E. Thompson, N. S. Lewis, H. B. Gray, *Photochem. Photobiol. Sci.* **2006**, *5*, 871.
[5] T. Bessho, E. C. Constable, M. Grätzel, A. Hernandez Redondo, C. E. Housecroft, W. Kylberg, M. K. Nazeeruddin, M. Neuburger, S. Schaffner, *Chem. Commun.* **2008**, 3717.
[6] H. Kisserwan, T. H. Ghaddar, *Inorg. Chim. Acta* **2010**, *363*, 2409.
[7] M. K. Nazeeruddin, F. De Angelis, S. Fantacci, A. Selloni, G. Viscardi, P. Liska, S. Ito, B. Takeru, M. Grätzel, *J. Am. Chem. Soc.* **2005**, *127*, 16835.
[8] M. K. Nazeeruddin, A. Kay, R. Humphry-Baker, E. Müller, P. Liska, N. Vlachopoulos, M. Grätzel, *J. Am. Chem. Soc.* **1993**, *115*, 6382.
[9] T. P. Brewster, W. Ding, N. D. Schley, N. Hazari, V. S. Batista, R. H. Crabtree, *Inorg. Chem.* **2011**, *50*, 11938.
[10] S. Betanzos-Lara, L. Salassa, A. Habtemariam, O. Novakova, A. M. Pizarro, G. J. Clarkson, B. Liskova, V. Brabec, P. J. Sadler, *Organometallics* **2012**, *31*, 3466.
[11] S. Kämper, A. Paretzki, J. Fiedler, S. Záliš, W. Kaim, *Inorg. Chem.* **2012**, *51*, 2097.
[12] G. Xue, Y. Guo, T. Yu, J. Guan, X. Yu, J. Zhang, J. Liu, Z. Zou, *Int. J. Electrochem. Sci.* **2012**, *7*, 1496.
[13] A. Bahreman, B. Limburg, M. A. Siegler, E. Bouwman, S. Bonnet, *Inorg. Chem.* **2013**, *52*, 9456.
[14] P. T. Nguyen, B. X. T. Lam, A. R. Andersen, P. E. Hansen, T. Lund, *Eur. J. Inorg. Chem.* **2011**, 2533.
[15] C. Dragonetti, A. Valore, A. Colombo, D. Roberto, V. Trifiletti, N. Manfredi, M. M. Salamone, R. Ruffo, A. Abbotto, *J. Organomet. Chem.* **2012**, *714*, 88.
[16] M. M. R. Choudhuri, R. J. Crutchley, *Inorg. Chem.* **2013**, *52*, 14404.

[17] A. Breivogel, C. Förster, K. Heinze, *Inorg. Chem.* **2010**, *49*, 7052.

[18] A. Breivogel, M. Meister, C. Förster, F. Laquai, K. Heinze, *Chem. Eur. J.* **2013**, *19*, 13745.

[19] A. Breivogel, S. Wooh, J. Dietrich, T. Y. Kim, Y. S. Kang, K. Char, K. Heinze, *Eur. J. Inorg. Chem.* **2014**, 2720.

[20] A. J. Frank, N. Kopidakis, J. van de Lagemaat, *Coord. Chem. Rev.* **2004**, *248*, 1165.

[21] S. Caramori, J. Husson, M. Beley, C. A. Bignozzi, R. Argazzi, P. C. Gros, *Chem. Eur. J.* **2010**, *16*, 2611.

[22] Md. K. Nazeeruddin, S. M. Zakeeruddin, R. Humphry-Baker, M. Jirousek, P. Liska, N. Vlachopoulos, V. Shklover, C.-H. Fischer, M. Grätzel, *Inorg. Chem.* **1999**, *38*, 6298.

[23] a) P. Salvatori, G. Marotta, A. Cinti, C. Anselmi, E. Mosconi, F. D. Angelis, *J. Phys. Chem. C* **2013**, *117*, 3874; b) N. R. Neale, N. Kopidakis, J. van de Lagemaat, M. Grätzel, A. J. Frank, *J. Phys. Chem. B* **2005**, *109*, 23183; c) J. H. Yum, S. J. Moon, R. Humphry-Baker, P. Walter, T. Geiger, F. Nüesch, M. Grätzel, Md. K. Nazeeruddin, *Nanotechnology* **2008**, *19*, 424005.

[24] G. Boschloo, A. Hagfeldt, *Acc. Chem. Res.* **2009**, *42*, 1819.

[25] a) H. Nusbaumer, S. M. Zakeeruddin, J.-E. Moser, M. Grätzel, *Chem. Eur. J.* **2003**, *9*, 3756; b) J. J. Nelson, T. J. Amick, C. M. Elliott, *J. Phys. Chem. C* **2008**, *112*, 18255; c) B. M. Klahr, T. W. Hamann, *J. Phys. Chem. C* **2009**, *113*, 14040.

[26] H. Nusbaumer, J.-E. Moser, S. M. Zakeeruddin, M. K. Nazeeruddin, M. Grätzel, *J. Phys. Chem. B* **2001**, *105*, 10461.

[27] E. Mosconi, J.-H. Yum, F. Kessler, C. J. G. García, C. Zuccaccia, A. Cinti, M. K. Nazeeruddin, M. Grätzel, F. D. Angelis, *J. Am. Chem. Soc.* **2012**, *134*, 19438.

[28] S. Mathew, A. Yella, P. Gao, R. Humphry-Baker, B. F. E. Curchod, N. Ashari-Astani, I. Tavernelli, U. Rothlisberger, Md. K. Nazeeruddin, M. Grätzel, *Nat. Chem.* **2014**, *6*, 242.

[29] a) T. W. Hamann, *Dalton Trans.* **2012**, *41*, 3111; b) J. W. Ondersma, T. W. Hamann, *Coord. Chem. Rev.* **2013**, *257*, 1533.

[30] a) C. Förster, K. Mack, L. M. Carrella, V. Ksenofontov, E. Rentschler, K. Heinze, *Polyhedron* **2013**, *52*, 576; b) C. Förster, T. E. Gorelik, U. Kolb, V. Ksenofontov, K. Heinze, *Eur. J. Inorg. Chem.* **2015**, 920.

[31] J.-H. Yum, E. Baranoff, F. Kessler, T. Moehl, S. Ahmad, T. Bessho, A. Marchioro, E. Ghadiri1, J.-E. Moser, C. Yi, Md. K. Nazeeruddin, M. Grätzel, *Nat. Commun.* **2012**, DOI: 10.1038/ncomms1655.

[32] S. A. Sapp, C. Elliott, C. Contado, S. Caramori, C. A. Bignozzi, *J. Am. Chem. Soc.* **2002**, *124*, 11215.

[33] A. Yella, H.-W. Lee, H. N. Tsao, C. Yi, A. K. Chandiran, Md. K. Nazeeruddin, E. W.-G. Diau, C.-Y. Yeh, S. M. Zakeeruddin, M. Grätzel, *Science* **2011**, *334*, 629.

[34] S. M. Feldt, E. A. Gibson, E. Gabrielsson, L. Sun, G. Boschloo, A. Hagfeldt, *J. Am. Chem. Soc.* **2010**, *132*, 16714.

[35] a) S. M. Feldt, G. Wang, G. Boschloo, A. Hagfeldt, *J. Phys. Chem. C* **2011**, *115*, 21500; b) S. M. Feldt, P. W. Lohse, F. Kessler, M. K. Nazeeruddin, M. Grätzel, G. Boschloo, A. Hagfeldt, *Phys. Chem. Chem. Phys.* **2013**, *15*, 7087; c) M. Wang, C. Grätzel, S. M. Zakeeruddin, M. Grätzel, *Energy Environ. Sci.* **2012**, *5*, 9394; d) M. Nasr-Esfahani, M. Zendehdel, N. Y. Nia, B. Jafaria, M. K. Babadi, *RSC Adv.* **2014**, *4*, 15961; e) M. K. Kashif, M. Nippe, N. W. Duffy, C. M. Forsyth, C. J. Chang, J. R. Long, L. Spiccia, U. Bach, *Angew. Chem. Int. Ed.* **2013**, *52*, 5527; *Angew. Chem.* **2013**, *127*, 3829; f) K. B. Aribia, T. Moehl, S. M. Zakeeruddin, M. Grätzel, *Chem. Sci.* **2013**, *4*, 454; g) K. Omata, S. Kuwahara, K. Katayama, S. Qing, T. Toyoda, K.-M. Lee, C.-G. Wu, *Phys. Chem. Chem. Phys.* **2015**, *17*, 10170.

[36] I. Krivokapic, M. Zerara, M. L. Dakua, A. Vargas, C. Enachescu, C. Ambrusc, P. Tregenna-Piggott, N. Amstutz, E. Krausz, A. Hauser, *Coord. Chem. Rev.* **2007**, *251*, 364.

[37] a) A. Yoshimura, M. J. Uddin, N. Amasaki, T. Ohno, *J. Phys. Chem. A* **2001**, *105*, 10846; b) H. Torieda, A. Yoshimura, K. Nozaki, S. Sakai, T. Ohno, *J. Phys. Chem. A* **2002**, *106*, 11034.

[38] M. Chou, C. Creutz, N. Sutin, *J. Am. Chem. Soc.* **1977**, *99*, 5615.

[39] C. C. Scarborough, S. Sproules, T. Weyhermüller, S. DeBeer, K. Wieghardt, *Inorg. Chem.* **2011**, *50*, 12446.

[40] a) K. Mack, A. Wünsche von Leupoldt, C. Förster, M. Ezhevskaya, D. Hinderberger, K. W. Klinkhammer, K. Heinze, *Inorg. Chem.* **2012**, *51*, 7851; b) A. K. C. Mengel, C. Förster, A. Breivogel, K. Mack, J. R. Ochsmann, F. Laquai, V. Ksenofontov, K. Heinze, *Chem. Eur. J.* **2015**, *21*, 704.

[41] B. Enright, C. Redmond, D. Fitzmaurice, *J. Phys. Chem.* **1994**, *98*, 6195.

[42] a) W. Xiang, W. Huang, U. Bach, L. Spiccia, *Chem. Commun.* **2013**, *49*, 8997; b) M. B. Achari, V. Elumalai, N. Vlachopoulos, M. Safdari, J. Gao, J. M. Gardner, L. Kloo, *Phys. Chem. Chem. Phys.* **2013**, *15*, 17419.

3.4 RESULTS AND DISCUSSION: STRONGLY COUPLED CYCLOMETALATED
RUTHENIUM TRIARYLAMINE CHROMOPHORES AS SENSITIZERS FOR DSSCS

79

3.4 "Strongly Coupled Cyclometalated Ruthenium Triarylamine Chromophores as Sensitizers

for DSSCs

Christoph Kreitner, Andreas K. C. Mengel, Tae K. Lee, Woohyung Cho, Kookheon

Char, Yong S. Kang and Katja Heinze

*Chem. Eur. J. **2016**, 22, 8915 – 8928.*
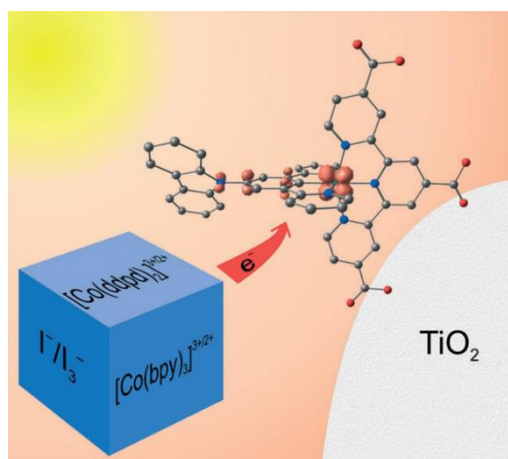
The synthesis and characterization of the ruthenium(II) complexes as well as all DFT calculations were performed by ███████████████. The cobalt(II,III) electrolytes were synthesized and characterized by Andreas K. C. Mengel. After instruction from ██████ ██████████ (Hanyang University, Seoul) and ███████████████ (Seoul National Universtiy, Seoul), the DSSCs were built and characterized by Andreas K. C. Mengel, ██ ██████████ (Hanyang University, Seoul) and ██████████ (Hanyang University, Seoul). The evaluation of the DSSC results and the experimental arrangements were performed by Andreas K. C. Mengel. The manuscript was written by ███████████████ (40 %) and Andreas K. C. Mengel (20 %) as well as ███████████████ (40 %).

■ **Cyclometalated Complexes**

Strongly Coupled Cyclometalated Ruthenium Triarylamine Chromophores as Sensitizers for DSSCs

Christoph Kreitner+,[a, d] Andreas K. C. Mengel+,[a] Tae Kyung Lee,[b] Woohyung Cho,[b] Kookheon Char,[c] Yong Soo Kang,[b] and Katja Heinze*[a]

Abstract: A series of anchor-functionalized cyclometalated bis(tridentate) ruthenium(II) triarylamine hybrids [Ru(dbp-X)(tctpy)]$^{2-}$ [$2a$]$^{2-}$–[$2c$]$^{2-}$ (H$_3$tctpy = 2,2′;6′,2′′-terpyridine-4,4′,4′′-tricarboxylic acid; dpbH = 1,3-dipyridylbenzene; X = N(4-C$_6$H$_4$OMe)$_2$ ([$2a$]$^{2-}$), NPh$_2$ ([$2b$]$^{2-}$), N-carbazolyl [$2c$]$^{2-}$) was synthesized and characterized. All complexes show broad absorption bands in the range 300–700 nm with a maximum at about 545 nm. Methyl esters [Ru(Me$_3$tctpy)(dpb-X)]$^+$ [$1a$]$^+$–[$1c$]$^+$ are oxidized to the strongly coupled mixed-valent species [$1a$]$^{2+}$–[$1c$]$^{2+}$ and the Ru^{III}(aminium) complexes [$1a$]$^{3+}$–[$1c$]$^{3+}$ at comparably low oxidation potentials. Theoretical calculations suggest an increasing spin delocalization between the metal center and the triarylamine unit in the order [$1a$]$^{2+}$ < [$1b$]$^{2+}$ < [$1c$]$^{2+}$. Solar cells were prepared with the saponified complexes [$2a$]$^{2-}$–[$2c$]$^{2-}$ and the reference dye **N719** as sensitizers using the I$_3^-$/I$^-$ couple and [Co(bpy)$_3$]$^{3+/2+}$ and [Co(ddpd)$_2$]$^{3+/2+}$ couples as [B(C$_6$F$_5$)$_4$]$^-$ salts as electrolytes (bpy = 2,2′-bipyridine; ddpd = N,N′-dimethyl-N,N′-dipyridin-2-yl-pyridine-2,6-diamine). Cells with [$2c$]$^{2-}$ and I$_3^-$/I$^-$ electrolyte perform similarly to cells with **N719**. In the presence of cobalt electrolytes, all efficiencies are reduced, yet under these conditions [$2c$]$^{2-}$ outperforms **N719**.

Introduction

Pioneered by O'Regan and Grätzel in 1991,[1] the dye-sensitized solar cell (DSSC) has emerged as a promising light-to-energy conversion device.[2, 3] Its setup has been optimized and standardized over the past 25 years. Typically, its central component is a molecular dye that is absorbed onto a mesoporous wide-bandgap semiconducting electrode, such as TiO$_2$ or ZnO.[3, 4] Upon excitation by visible light, electrons are injected from the excited state of the dye into the conduction band of the semiconductor. The oxidized dye is then regenerated by a redox mediator, which transports the positive charge to the counter electrode. The major advantages of dye sensitized solar cells over conventional silicon-based or inorganic thin film solar cells are lower costs and their modular architecture allowing for systematic optimization of all components (semiconductor, sensitizer, electrolyte) individually.[3–5]

Tremendous efforts have been put particularly into the development of new molecular dyes to optimize cell performance. An ideal sensitizer should be thermally and photochemically stable under working conditions, should rapidly inject electrons into the conduction band of the semiconductor after excitation and, most importantly, should efficiently absorb light between 400 and 900 nm. Among others, polypyridine complexes of iron,[6] copper,[7–9] platinum,[10, 11] iridium,[12, 13] and rhenium[14] as well as polyaromatic and conjugated organic compounds,[15, 16] porphyrins,[17–19] and quantum dots[20] have proven suitable for sensitization. Particularly, polypyridine complexes of ruthenium and osmium have emerged as a promising class of sensitizers due to their suitable photophysical properties.[21–24] The visible range of the electromagnetic spectrum of these complexes is dominated by characteristic metal-to-ligand charge transfer (MLCT) absorptions.[25–27] In these transitions, metal orbitals of the t$_{2g}$ set serve as electron donors, while the polypyridine π* orbitals function as electron acceptors.

The most prominent and well-established sensitizers are the complexes [nBu$_4$N]$_2$[Ru(Hdcbpy)$_2$(NCS)$_2$], **N719** (H$_2$dcbpy = 2,2′-bipyridine-4,4′-dicarboxylic acid, Scheme 1),[28, 29] and the so-called "black dye" [nBu$_4$N]$_3$[Ru(Htctpy)(NCS)$_3$] (H$_3$tctpy = 2,2′;6′,2′′-terpyridine-4,4′,4′′-tricarboxylic acid)[22] reaching power conversion efficiencies (PCE, η) of 10–11% under full air mass 1.5 (AM 1.5) irradiation. In these complexes, the carboxy

[a] C. Kreitner,+ A. K. C. Mengel,+ Prof. Dr. K. Heinze
     Institute of Inorganic Chemistry and Analytical Chemistry
     Johannes Gutenberg-University of Mainz
     Duesbergweg 10–14, 55128 Mainz (Germany)
     Fax: (+49) 6131-39-27-277
     E-mail: katja.heinze@uni-mainz.de

[b] T. K. Lee, W. Cho, Prof. Y. S. Kang
     The Department of Energy Engineering and Center for
     Next Generation Dye-Sensitized Solar Cells, Hanyang University
     222 Wangsimni-ro, Seongdong-gu, Seoul 133-791 (Korea)

[c] Prof. Dr. K. Char
     The National Creative Research Initiative Center for Intelligent
     Hybrids, School of Chemical and Biological Engineering, Seoul
     National University, 1 Gwanak-ro, Gwanak-gu, Seoul 151-744 (Korea)

[d] C. Kreitner+
     Graduate School Materials Science in Mainz
     Staudingerweg 9, 55128 Mainz (Germany)

[+] These authors contributed equally to the work.

⊡ Supporting information for this article is available on the WWW under
   http://dx.doi.org/10.1002/chem.201601001.

3.4 RESULTS AND DISCUSSION: STRONGLY COUPLED CYCLOMETALATED
RUTHENIUM TRIARYLAMINE CHROMOPHORES AS SENSITIZERS FOR DSSCS

81

Scheme 1. N719 reference dye and amine-substituted cyclometalated ruthenium(II) dyes (top) and cobalt-based electrolytes (bottom).

clometalating ligands as electron acceptors.[37,38,43–48] Additionally, cyclometalation substantially increases the energy of the polypyridine-centered lowest unoccupied molecular orbital (LUMO) compared to non-cyclometalated counterparts. This should potentially accelerate charge injection into the TiO$_2$ conduction band.[37,38,48] The highest occupied molecular orbital (HOMO) on the other side typically extends over the metal center and the anionic part of the cyclometalating ligand. This should facilitate dye regeneration after charge injection.[38,46,48] Furthermore, the high σ-donating strength destabilizes the inherently photochemically reactive metal-centered (^{3}MC) excited states.[38,48–52] The electron donating or withdrawing character of the cyclometalating ligands are easily tuned by further substitution (for example [A^{X,Me}]$^+$, Scheme 1) including hole-transport facilities (X = amines).[38,48–52] Indeed, several approaches have been developed to incorporate electron donors into the dye structure to rapidly detract the positive charge remaining on the sensitizer after electron injection away from the semiconductor surface.[53–56] Attaching the reversible triphenylamine radical cation/triphenylamine redox couple (TPA$^{+•}$/TPA^0) proved particularly successful in conjunction with several porphyrin dyes, for example, **YD2-o-C8**, yielding solar cells with $\eta > 12\,\%$.[19,57] Berlinguette and co-workers demonstrated that the overall cell performance can benefit from a TPA unit linked to a [Ru(pbpy)(tpy)]$^+$ complex via a thiophene spacer. This architecture yields cell efficiencies of up to 8.0 % (Scheme 1, [B^H]$^+$, [C^H]$^+$).[38] Through clever dye design and adjustment of relative oxidation potentials of Ru$^{III/II}$ and TPA$^{+•/0}$ an efficient transfer of the electron hole from the ruthenium center to the TPA unit is achieved after charge injection. This retards parasitic electron recombination processes with oxidized dyes in the DSSC.[38,58–60] The mixed-valent complexes [B^R]$^{2+}$ are valence-localized and assigned to Robin–Day class II with measurable electronic coupling between the metal center and the TPA unit.[60,61] Recently, Zhong and co-workers presented a structurally related series of complexes combining bis(tridentate) cyclometalated ruthenium complexes with TPA units (Scheme 1, [A^{X,Me}]$^{2+}$/[A^{X,Me}]$^+$) lacking the thiophene unit.[62,63] The mixed-valent state [A^{X,Me}]$^{2+}$ is valence-delocalized (Robin–Day class III) between the metal center and the amine moiety as evidenced by the shape and bandwidth of the near infrared absorption band and by density functional theoretical calculations.[62–65] The parent complex [A^{H,H}]$^+$ lacking the amine substituent (X = H) has been reported recently as well.[66]

In contrast to reported dyes [B^R]$^+$, featuring a valence-isomeric description of the [B^R]$^{2+}$ state (Robin–Day class II), potential DSSC sensitizers [A^{X,H}]$^+$ with X = amine that provide a means of detracting the electron hole away from the semiconductor surface in a resonant fashion ([A^{X,H}]$^{2+}$; Robin–Day class III) have not yet been reported. Saponifying the three methyl esters of [A^{X,Me}]$^+$ type complexes should provide suitable sensitizers [A^{X,H}]$^+$ with a class III mixed-valent state. Herein, we present a series of three complexes of the general structure [nBu$_4$N]$_2$[Ru(dpb-X)(tctpy)] (Hdpb-X = 5-substituted 1,3-di-(2-pyridyl)benzene) with different amine substituents X of increasing electron withdrawing power, namely N,N-bis(4-methoxy-phenyl)amine (X = N(4-C$_6$H$_4$OMe)$_2$; [nBu$_4$N]$_2$[**2a**]), N,N-diphenyl-

groups serve as anchors to the TiO$_2$ surface while the [NCS]$^-$ ligands are responsible for an efficient charge transfer from the redox mediator onto the dye after charge injection (dye regeneration).[29] However, a major drawback of complexes containing monodentate ligands is their high lability towards [NCS]$^-$ substitution in photoexcited or oxidized states hampering long-term application in photovoltaic devices.[30–33]

Recently, bi- and tridentate cyclometalating ligands emerged as viable and more robust alternatives for the labile [NCS]$^-$ ligands. In 2007, van Koten and co-workers reported the successful sensitization of TiO$_2$ by bis(tridentate) [Ru(pbpy)(tpy)]$^+$ complexes (tpy = 2,2′;6′,2′′-terpyridine, Hpbpy = 6-phenyl-2,2′-bipyridine).[34] Shortly thereafter, Grätzel and co-workers published a dye with record-breaking characteristics [Ru(H$_2$dcbpy)$_2$(ppy-F$_2$)]$^+$ ($\eta > 10\,\%$) based on a tris(bidentate) cyclometalating motif (Hppy-F$_2$ = 2-(2,4-difluorophenyl)pyridine).[35] Since then, much work has been dedicated towards the development of new cyclometalated ruthenium dyes both in the field of tris(bidentate) and bis(tridentate) complex architectures.[36–42] These studies indeed reveal several key benefits of the cyclometalating motif. The introduction of a Ru-C σ bond in the coordination environment reduces the local symmetry around the metal center. This yields a broad absorption band in the visible range resulting from multiple close-lying MLCT transitions involving both the polypyridine and cy-

amine (X = N(C$_6$H$_5$)$_2$; [nBu$_4$N]$_2$[**2b**]) and carbazole (X = N-carbazolyl; [nBu$_4$N]$_2$[**2c**]). We will discuss how the substituents at the dpb ligand affect the degree of valence-delocalization in the mixed-valent state [**2**]$^-$ and to what extent such delocalization is beneficial for the application of such sensitizers in DSSCs.

As outer-sphere cobalt-based electrolytes[67–80] should deliver higher open-circuit voltages V_{OC} due to their more positive redox potential as compared to the standard triiodide/iodide couple and as they perform extremely well in conjunction with TPA-appended porphyrin dyes (**YD2-o-C8**)[57] as well as with other potent TPA-appended dyes (**Y123**, **D35**),[72,73,74] we study the TPA-appended ruthenium(II) dyes [nBu$_4$N]$_2$[**2a**]–[nBu$_4$N]$_2$[**2c**] with cobalt-based electrolytes in addition to the commonly used triiodide/iodide couple. Specifically, we employ the [Co(bpy)$_3$]$^{3+/2+}$ [**3**]$^{3+/2+}$ and [Co(ddpd)$_2$]$^{3+/2+}$ [**4**]$^{3+/2+}$ redox mediators (bpy = 2,2′-bipyridine, ddpd = N,N'-dimethyl-N,N'-dipyridin-2-yl-pyridine-2,6-diamine,[80] Scheme 1).[81–83] The DSSCs are studied by incident photon-to-current conversion efficiency measurements, by current-voltage characteristics under AM 1.5 irradiation and in the dark as well as by electron lifetime measurements.

Results and Discussion

Synthesis and characterization of chromophores

The 5-substituted 1,3-di-(2-pyridyl)benzene ligands **L^a** (R = N(4-C$_6$H$_4$OMe)$_2$), **L^b** (R = N(C$_6$H$_5$)$_2$) and **L^c** (R = N-carbazolyl) were synthesized starting from the previously reported 1-bromo-3,5-di-(2-pyridyl)benzene under Buchwald–Hartwig cross-coupling reaction conditions similar to a method we,[48] as well Zhong and co-workers employed previously.[63a] In the present study, the dimeric palladium(II) precatalyst bis(μ-mesylate)bis[(2-(2′-aminophenyl-κN)phenyl-κC^1)palladium(II)] [**Pd**]$_2$[84] was used along with the phosphane ligand 2-dicyclohexylphosphano-2′,6′-diisopropoxybiphenyl[85] to provide a catalytically competent catalyst that afforded the ligands in yields of 82–98%. The identity of **L^a** was confirmed by comparison of its ^{1}H NMR spectrum with that reported before.[62,63a] The purity and integrity of the new ligands **L^b** and **L^c** were ascertained by ^{1}H and ^{13}C NMR spectroscopy, mass spectrometry, and elemental analyses (Experimental Section; Supporting Information, Figures S1–S4).

The heteroleptic ester-substituted [Ru(dpb)(tpy)]$^+$ complexes [**1a**]$^+$–[**1c**]$^+$ were prepared according to a previously employed synthetic method starting from RuCl$_3$(Me$_3$tctpy) (Scheme 2).[22,48] The two-step procedure includes chloride abstraction with silver tetrafluoroborate followed by complexation with the respective dipyridylbenzene ligand **L^a**–**L^c** under reducing conditions in n-butanol. Similar to observations made by Zhong and co-workers,[62,63a] we were not able to isolate the complexes [**1a**]$^+$–[**1c**]$^+$ with high purity. Despite the reducing conditions during their synthesis, substantial amounts of the open-shell Ru^{III} complexes [**1a**]$^{2+}$–[**1c**]$^{2+}$ were obtained, as evidenced from ESI mass spectra and the NMR silence of all three compounds (paramagnetic broadening).[62,63a] Additionally, the isolated products are black in solution and in the solid state instead of the dark purple color typically observed for
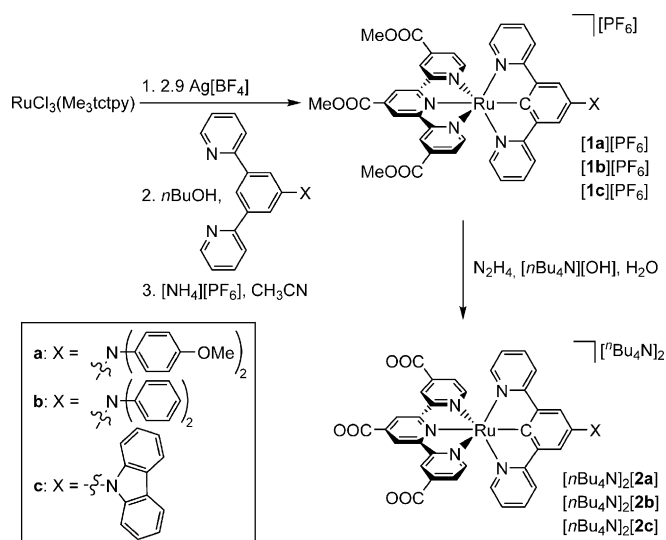
Scheme 2. Synthesis of [**1a**][PF$_6$]–[**1c**][PF$_6$] and [nBu$_4$N]$_2$[**2a**]–[nBu$_4$N]$_2$[**2c**].

[Ru(dpb)(tpy)]$^+$ complexes, suggesting the presence of a second colored species. Yet, cyclic voltammograms confirm the purity of the synthesized complexes by absence of redox waves in the range of −3.0 and 1.5 V other than the five expected reversible waves,[62,63a] namely for the [**1**]$^{3+/2+}$, [**1**]$^{2+/+}$, [**1**]$^{+/0}$, [**1**]$^{0/-}$ and [**1**]$^{-/2-}$ couples (Figure 1, Supporting Information, Figure S5).
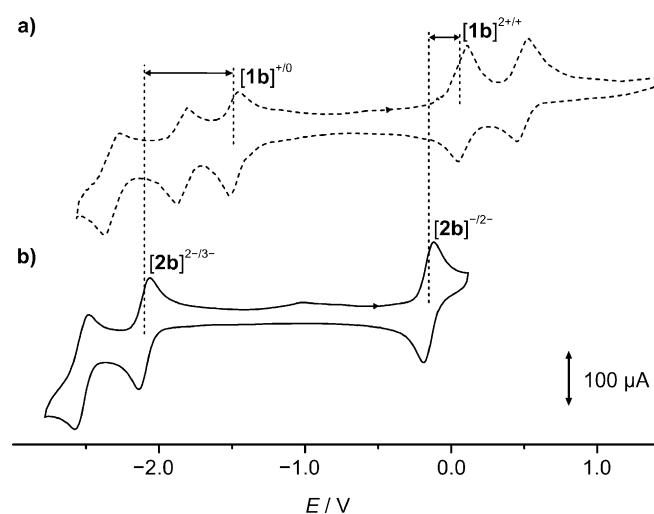
Figure 1. Cyclic voltammograms of a) [**1b**][PF$_6$] (- - - -) and b) [nBu$_4$N]$_2$[**2b**] (——) dyes in [nBu$_4$N][PF$_6$]/CH$_3$CN (E vs. FcH/FcH$^+$).

Subsequent saponification of the three methyl ester groups of [**1a**]$^+$–[**1c**]$^+$ in aqueous solution using [nBu$_4$N][OH] as base and hydrazine as reductant yielded the corresponding carboxylates as tetrabutylammonium salts [nBu$_4$N]$_2$[**2a**]–[nBu$_4$N]$_2$[**2c**]. This method affords the fully deprotonated complexes [**2a**]$^{2-}$–[**2c**]$^{2-}$, in contrast to Berlinguette's procedure,[38] which yields the complexes in their neutral zwitterionic form with two protonated carboxy groups. Owing to the high solubility of the

3.4 RESULTS AND DISCUSSION: STRONGLY COUPLED CYCLOMETALATED
RUTHENIUM TRIARYLAMINE CHROMOPHORES AS SENSITIZERS FOR DSSCS

83

tetrabutylammonium salts [nBu$_4$N]$_2$[**2a**]–[nBu$_4$N]$_2$[**2c**] in organic solvents, the products are isolated straight-forwardly by extraction of the aqueous phase with dichloromethane. Co-extracted [nBu$_4$N][PF$_6$] was removed by subsequent dissolution of the raw products in acetonitrile and addition of a diethylether/hexanes mixture that precipitates the desired complexes. The integrity of [nBu$_4$N]$_2$[**2a**]–[nBu$_4$N]$_2$[**2c**] was confirmed by ^{1}H NMR and ^{13}C NMR spectra as well as by ESI$^+$ and ESI$^-$ mass spectra (Supporting Information, Figures S6–S19). All NMR spectra lack paramagnetic shifts or broadening, substantiating the absence of Ru^{III} in the pristine samples. The ^{1}H NMR spectra confirm the presence of two equivalents of [nBu$_4$N]$^+$ cations per complex anion in all three cases corroborating the stoichiometry of the salt. IR spectra as KBr disk of the complexes [nBu$_4$N]$_2$[**2a**]–[nBu$_4$N]$_2$[**2c**] lack the characteristic vibrations of [PF$_6$]$^-$ ions at 843 cm^{-1} (asym. stretch) and 588 cm^{-1} (deformation) present in the parent complexes [**1a**][PF$_6$]–[**1c**][PF$_6$] underlining the quantitative [PF$_6$]$^-$ removal (Supporting Information, Figure S20). Additionally, ^{19}F NMR spectra of [nBu$_4$N]$_2$[**2a**]–[nBu$_4$N]$_2$[**2c**] confirm the absence of [PF$_6$]$^-$. Under the acidic and ionizing conditions of the ESI$^+$ mass spectrometry technique, the complexes are observed in their fully protonated form as monocations [**2**+3H]$^+$ with Ru^{II} metal sites or as dications [**2**+3H]$^{2+}$ with Ru^{III} centers (Supporting Information, Figure S18). The ESI$^-$ mass spectra (Supporting Information, Figure S19) show mass peaks at the expected m/z values for the dianions [**2**]$^{2-}$ (Ru^{II}) and anions [**2**]$^-$ (Ru^{III}) with typical ruthenium isotope patterns. Furthermore, several m/z peaks of decarboxylated complexes are found for all three complexes [nBu$_4$N]$_2$[**2a**]–[nBu$_4$N]$_2$[**2c**], confirming the presence of carboxylate substituents. The carboxylate groups are also evident from the characteristic IR CO stretching vibrations around 1617 cm^{-1} (Supporting Information, Figure S20).

Photophysical and electrochemical behavior

The absorption and emission spectra of the complexes [nBu$_4$N][**2a**]–[nBu$_4$N][**2c**] are depicted in Figure 2 and data are summarized in Table 1 (Supporting Information, Figure S21). In the spectral range between 300 and 800 nm all dyes exhibit very similar absorption features. The absorption maximum around 536–549 nm is accompanied by three additional bands around 500, 425, and 375 nm. These bands characteristic for cyclometalated [Ru(dpb)(tpy)]$^+$ complexes arise from metal-to-ligand charge transfer excitations involving both ligands as electron-
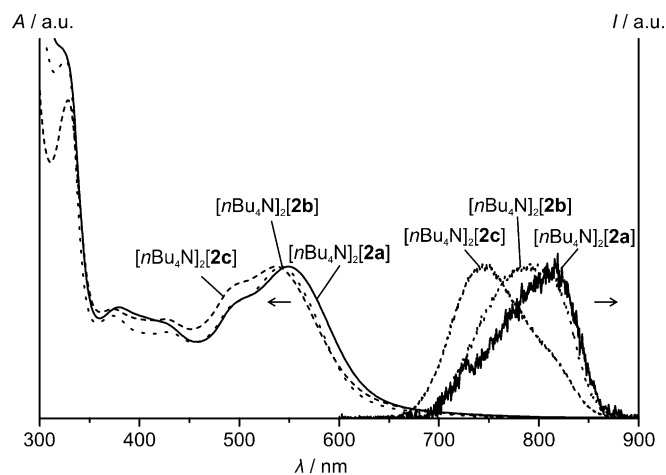
Figure 2. Normalized absorption and emission spectra of [nBu$_4$N]$_2$[**2a**] (——), [nBu$_4$N]$_2$[**2b**] (·····), and [nBu$_4$N]$_2$[**2c**] (----) in CH$_3$CN.

accepting sites ($d_{Ru}\rightarrow\pi^*_{tpy}$ and $d_{Ru}\rightarrow\pi^*_{dpb}$).[38,48] Owing to the low local symmetry around the metal center, the number of absorption bands is larger than for the more symmetric systems containing all-nitrogen donor ligands such as [Ru(tpy)$_2$]$^{2+}$ or [Ru(ddpd)(tpy)]$^{2+}$, for example.[38,46,47,86] The lower symmetry yields substantially broadened absorption spectra and a more efficient light harvesting throughout the visible range of the electromagnetic spectrum.

The tris(carboxylate) complexes [nBu$_4$N][**2a**]–[nBu$_4$N][**2c**] are very weakly emissive at room temperature (Figure 2, Table 1) with quantum yields below 5×10^{-6}. The wavelength of the emission maximum is shifted hypsochromically in the order [nBu$_4$N][**2a**] > [nBu$_4$N][**2b**] > [nBu$_4$N][**2c**] from 817 to 744 nm.

On the one hand, this trend is due to a more pronounced vibrational progression in [nBu$_4$N][**2a**] and [nBu$_4$N][**2b**] than in [nBu$_4$N][**2c**] similar to that observed for other [Ru(dpb)(tpy)]$^+$ complexes with a strong push–pull substitution.[48] On the other hand, the energy of the emissive ^{3}MLCT state increases with decreasing donor strength of the amine substituent, as this lowers the energy of the metal orbitals involved in the emission process while essentially maintaining the tctpy-centered LUMO energy (Figure 3; Supporting Information, Figure S22).[48]

Cyclovoltammetric studies of the ester-substituted complexes [**1a**][PF$_6$]–[**1c**][PF$_6$] reveal multiple reversible redox processes (Figure 1, Table 1, Supporting Information, Figure S5).

Table 1. Optical and electrochemical data of [**1a**][PF$_6$]–[**1c**][PF$_6$] and [nBu$_4$N]$_2$[**2a**]–[nBu$_4$N]$_2$[**2c**].

	UV/Vis (CH$_3$CN) λ_{max}/nm ($\varepsilon/10^3$ M^{-1}cm^{-1})	Emission (CH$_3$CN) λ_{em}/nm (λ_{exc}/nm)	Cyclic voltammetry E/V vs. FcH/FcH$^+$
[**1a**][PF$_6$][a]	323 (29), 339 (26), 420 (16), 507 (13), 583 (10)	–[b]	−1.87, −1.52, −0.05, +0.31
[**1b**][PF$_6$]	–[b]	–[b]	−1.85, −1.49, +0.09, +0.49
[**1c**][PF$_6$]	–[b]	–[b]	−1.83, −1.47, +0.34, +0.88
[nBu$_4$N]$_2$[**2a**]	549 (15.4), 503 (12.1), 424 (9.7), 379 (11.3), 323 (37.5), 289 (62.7)	817 (549)[c]	−2.52, −2.09, −0.21, –[d]
[nBu$_4$N]$_2$[**2b**]	543 (15.4), 501 (12.1), 428 (8.7), 374 (10.4), 325 (36.4), 288 (61.6)	791 (543)[c]	−2.54, −2.10, −0.15, –[d]
[nBu$_4$N]$_2$[**2c**]	536 (13.9), 499 (12.5), 426 (9.1), 373 (10.0), 328 (29.1), 283 (63.2)	744 (536)[c]	−2.51, −2.07, −0.06, –[d]

[a] From Ref. [63a]. [b] No optical data measured due to the presence of Ru^{III} species. [c] Quantum yield $<5\cdot10^{-6}$. [d] No second oxidation potential was obtained due to precipitation of the neutral dye on the electrode surface.

a)

b)
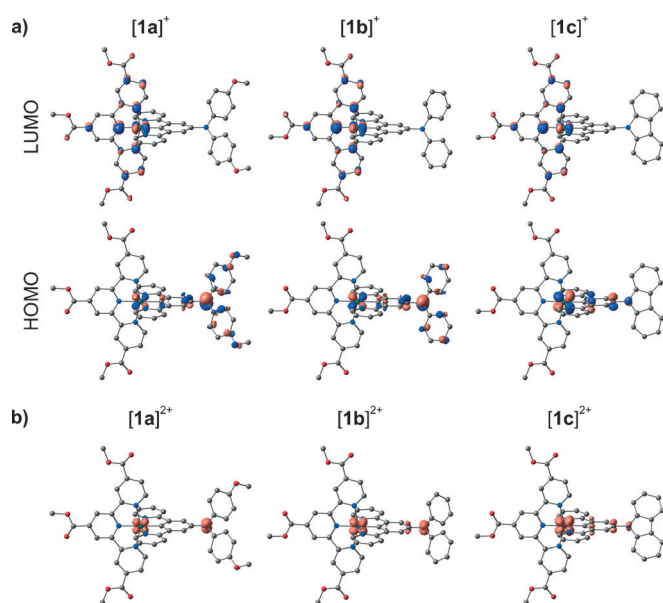
Figure 3. a) Frontier molecular orbitals of [1 a]+, [1 b]+, and [1 c]+ (contour value 0.06 a.u.) and b) spin densities of [1 a]2+, [1 b]2+, and [1 c]2+ (contour value 0.01 a.u.).

The complexes are oxidized at quite low potentials to the mixed-valent counterparts [1]2+ (-0.05 to 0.34 V vs. FcH/FcH+). A second oxidation step occurs at higher potentials yielding the Ru^{III}(aminium) complexes [1]3+ (0.31 to 0.88 V vs. FcH/FcH+).[62] The trend of the first and the second oxidation potentials towards higher values in the order N(4-$C_6H_4OCH_3)_2$ < N($C_6H_5)_2$ < N-carbazole is in agreement with the decreasing $+I$ effect of the respective amine substituent X. Additionally, the unpaired electron of the mixed-valent compounds [1]2+ is substantially delocalized between the metal center and the triarylamine fragment via the 1,4-phenylene bridge.[62,63a] The electron donor strength of the dpb substituent[62,63a] strongly affects degree of delocalization as evidenced by DFT calculations (Figure 3 b). Mulliken spin density analysis of [1 a]2+ indicates a balanced spin population of 0.26 and 0.25 at ruthenium and the amine nitrogen atom, respectively, while for [1 b]2+, values of 0.43 (Ru) and 0.20 (N) are obtained. In [1 c]2+, the spin density is further shifted towards the ruthenium atom with spin populations of 0.63 (Ru) and 0.07 (N). Thus, the degree of delocalization is reduced in this series from an essentially delocalized Robin–Day class III system in [1 a]2+ to a strongly coupled class II compound in [1 c]2+.[61,63a] As a consequence, the resonance stabilization within complex [1 a]2+ is the largest, yielding the most pronounced negative shift of the first oxidation potential followed by complexes [1 b]2+ and [1 c]2+. Additionally, two reversible reduction waves are observed for the ester-substituted complexes [1 a][PF6]–[1 c][PF6]. As these reductions are tpy-centered,[33b,46,48a,63a,87,88] their potentials are essentially independent from the substitution pattern at the dpb-X ligand with the first reduction occurring at -1.5 V and the second at -1.85 V vs. FcH/FcH+ for all three complexes.

Deprotection and deprotonation of the ester functionalities, however, shifts the first and second reduction potentials by

600 mV towards more negative values (Figure 1, Table 1; Supporting Information, Figure S5). This is consistent with the substantial increase of negative charge density on the tctpy^{3-} ligand in [2]2– and corroborates the tpy centered reduction. The oxidation waves shift to lower potentials as well, but to a lesser extent. This is mainly due to the fact, that the metal orbital involved with the oxidation process is orthogonal to the tpy ligand. However, a trend of the potential shifts is observed. While the first oxidation wave of [2 a]2– occurs 160 mV below that of [1 a]+, the first oxidation potentials of [2 c]2– and [1 c]+ differ by 400 mV. Consequently, the first oxidation potentials of complexes [2 a]2––[2 c]2– only differ by 150 mV as opposed to a difference of 390 mV between the esters [1 a]+–[1 c]+. This can be understood on the basis of the Mulliken spin populations of the metal center and the amine nitrogen atom in the mixed-valent anions [2 a]––[2 c]–: These amount to 0.49 (Ru)/0.17 (N) in [2 a]–, 0.57 (Ru)/0.13 (N) in [2 b]–, and 0.74 (Ru)/0.03 (N) in [2 c]–. Apparently, the charge delocalization over the triarylamine fragment is significantly reduced and the spin densities of the mixed-valent anions [2]– are more valence-localized at the electron-rich metal center than their ester counterparts. Consequently, the resonance stabilization of the mixed-valent species [2]– is not as pronounced as that of [1]2+ resulting in similar oxidation potentials for all three complexes. The strongest impact of deprotection and deprotonation is observed for [2 c]2–, since its spin density is basically metal-centered. Accordingly, oxidation occurs in the closest proximity to the negatively charged tctpy^{3-} ligand and is facilitated to the largest extent in the dye series [2]–.

Increasing the potential beyond 0.15 V vs FcH/FcH+ results in a multitude of irreversible redox waves. We ascribe this to the deposition of the neutral Ru^{III}(aminium) complexes [2]0 on the platinum electrode surface, which impeded an unambiguous determination of the second oxidation potentials.

Combining all electrochemical and spectroscopic data of the dyes [1 a]+–[1 c]+ and [2 a]2––[2 c]2– with the redox data of the electrolytes I$_3^-$/I$^-$, 3$^{3+/2+}$ and 4$^{3+/2+}$ and the conduction band edge of TiO$_2$ yields the redox potential diagram depicted in Figure 4. Cyclic voltammetry of the dyes (see above) highlighted the strong dependence of the ground state oxidation potentials of the dyes from the degree of protonation of the carboxylic acids of the tpy ligand. For the setup of the DSSCs, the tris(carboxylate) dyes [2 a]2––[2 c]2– were employed. Yet, under the given experimental conditions, partial protonation from water at the TiO$_2$ surface is conceivable. Additionally, the coadsorbent chenodeoxycholic acid (CDCA), as an organic acid, will modify the degree of protonation of the sensitizer. Hence, Figure 4 depicts redox potential ranges instead of distinct values for the redox potentials of the ruthenium dyes. An analogous range of ground state potentials is applied for **N719** owing to the conceivable variation of the protonation state.[28] In a similar manner, the excited state ^{1}MLCT and ^{3}MLCT redox potentials span ranges.

It is apparent from Figure 4 that, similar to the reference dye **N719**, all cyclometalated dyes are thermodynamically capable of injecting an electron from both excited states into the conduction band of TiO$_2$. Regeneration of the oxidized dyes by

3.4 RESULTS AND DISCUSSION: STRONGLY COUPLED CYCLOMETALATED
RUTHENIUM TRIARYLAMINE CHROMOPHORES AS SENSITIZERS FOR DSSCS

85
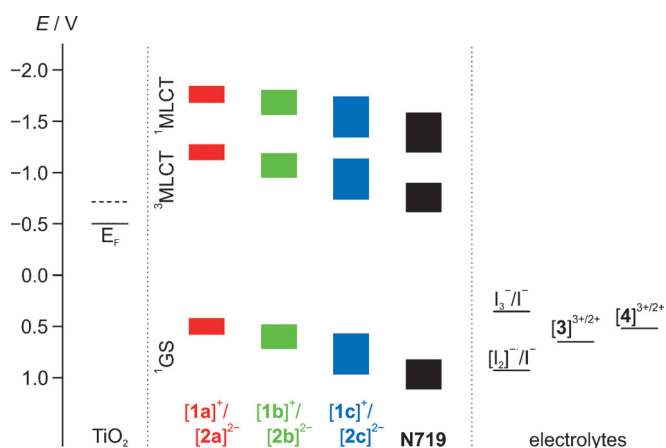
Figure 4. Diagram of the ground-state (^{1}GS) and excited-state (^{1}MLCT and ^{3}MLCT) redox potentials of $[1a]^+/[2a]^-$, $[1b]^+/[2b]^-$, $[1c]^+/[2c]^-$, and **N719**, the conduction band edge of TiO_2, and the redox potentials of the electrolytes.

Figure 5. Photocurrent action spectra of cells with $[nBu_4N]_2[2a]$, $[nBu_4N]_2[2b]$, $[nBu_4N]_2[2c]$, and N719. a) I_3^-/I^- redox mediator with/without CDCA (——/-----); b) $[3]^{3+/2+}$ (-----) and $[4]^{3+/2+}$ (——) electrolytes.

the employed electrolytes on the other hand is not generally possible. While the carbazole-substituted ruthenium(III) complex $[2c]^-$ is potentially regenerated by iodide even if the diiodide radical anion is formed as an intermediate,[89,90] this is not the case for the diarylamine-substituted dyes $[2a]^{2-}$ and $[2b]^{2-}$ in this simplified consideration of standard redox potentials. Hence, in a DSSC $[2c]^{2-}$ is expected to outperform $[2a]^{2-}$ and $[2b]^{2-}$. DSSC performances of all cyclometalated dyes in conjunction with the standard triiodide/iodide electrolyte and cobalt electrolytes will be discussed in the next section.

Solar cell performance

Dye-sensitized solar cells were prepared from the carboxylate substituted dyes $[nBu_4N]_2[2a]$–$[nBu_4N]_2[2c]$ and the benchmark dye **N719**. The coadsorbent CDCA was employed to protect the TiO_2 surface in several setups. Three different liquid electrolytes were utilized, namely the standard triiodide/iodide couple and two cobalt-based redox mediators.[67–69,82,83] The cobalt(III/II) complexes $[Co(bpy)_3]^{3+/2+}$ and $[Co(ddpd)_2]^{3+/2+}$ were prepared according to literature procedures.[74,78,82,91] Counter ion exchange was accomplished using $Li[B(C_6F_5)_4]$ giving the cobalt salts $[Co(bpy)_3][B(C_6F_5)_4]_2/[Co(bpy)_3][B(C_6F_5)_4]_3$ **[3]**$[B(C_6F_5)_4]_2/[3]$ $[B(C_6F_5)_4]_3$ and $[Co(ddpd)_2][B(C_6F_5)_4]_2/[Co(ddpd)_2][B(C_6F_5)_4]_3$ **[4]** $[B(C_6F_5)_4]_2/[4][B(C_6F_5)_4]_3$. NMR and mass spectrometric data confirm their compositions (Supporting Information, Figure S23–S31). The redox potential of $[4]^{3+/2+}$ ($E_{1/2} = 0.52$ V vs. NHE)[82] is intermediate of the I_3^-/I^- ($E_{1/2} = 0.32 \pm 0.03$ V vs. NHE)[89] and the $[3]^{3+/2+}$ ($E_{1/2} = 0.65$ V vs. NHE)[92–94] couples (Figure 4).

The incident photon-to-current conversion efficiency (IPCE, Figure 5) depends on several individual key steps, namely light-harvesting, electron injection, dye regeneration, and charge collection.[67] The extinction coefficients around the MLCT maxima of $[nBu_4N]_2[2a]$–$[nBu_4N]_2[2c]$ (Figure 2, Experimental Section) are close to that of **N719** ($\lambda = 535$ (14700), 395 (14300 $M^{-1} cm^{-1}$) nm.[28]). The achieved dye loadings of $[nBu_4N]_2[2a]$–$[nBu_4N]_2[2c]$ are consistently somewhat higher
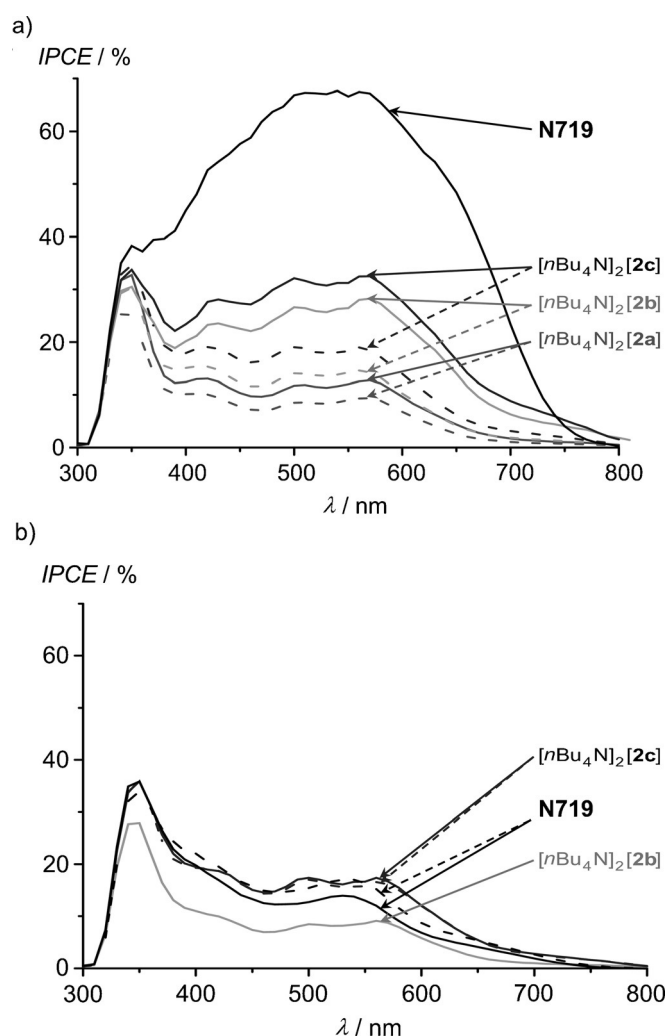
than that found with **N719** (Experimental Section). Hence, we assume that the light-harvesting efficiencies of $[nBu_4N]_2[2a]$–$[nBu_4N]_2[2c]$ in the cells prepared are in the same range as that of the reference dye **N719**.

Concerning the injection efficiency, all dyes feature ^{1}MLCT and ^{3}MLCT levels well above the Fermi level of TiO_2 (Figure 4). Hence, electron injection from the excited sensitizers should be feasible and fast for all dyes.[67] We assume rather similar injection efficiencies for all dyes.[67] Hence, the differences in DSSC performance in terms of power conversion efficiency η should predominantly relate to the dye regeneration efficiency, the charge collection efficiency (recombination losses) and the open-circuit voltage V_{OC}.

According to the electrochemical data of the dyes and the redox mediators, the Ru^{III} complex $[2b]^-$ cannot be efficiently regenerated by the bipyridine cobalt(II) complex $[3]^{2+}$, while $[2a]^-$ cannot be regenerated by both cobalt(II) complexes $[3]^{2+}$ and $[4]^{2+}$ (Figure 4). For all other dye/redox mediator combinations, dye regeneration is thermodynamically possible. In the electrolyte series, the highest driving force for dye re-

generation and hence the highest regeneration rate based on Marcus theory (Marcus normal region) is achieved with the I_3^-/I^- couple (although the $[I_2]^{-\bullet}/I^-$ couple with a higher potential is responsible for the dye regeneration; Figure 4[89,90]). As the regeneration rate furthermore depends on the concentration of the reduced mediator,[67] the regeneration rate should decrease in the series I^- (0.550 M), $[3]^{2+}$ (0.165 M), and $[4]^{2+}$ (0.080 M). All of these factors strongly favor the I_3^-/I^- couple over cobalt-based couples.

Electron recombination with oxidized dyes (driving forces around 1.0–1.5 eV;[67] Figure 4) is reported to occur in the Marcus inverted region. However, the rates better correlate with the inverse distance of the positive charge in the dye and the TiO_2 surface instead with the driving force.[67] In oxidized **N719** the positive charge is delocalized between Ru and the $[NCS]^-$ ligands. In $[1a]^{2+}$–$[1c]^{2+}$ the positive charge is efficiently delocalized onto the amine substituents of the dpb ligands (Robin–Day class III/class II behavior, see above). This is visualized in the DFT-calculated singly occupied molecular orbitals and corresponding spin densities of $[1a]^{2+}$–$[1c]^{2+}$ spreading over the metal center and the amine substituent (see Figure 3). In this respect, amine substituted sensitizers should be somewhat advantageous as compared to **N719**. On the other hand, electron recombination with oxidized dyes depends on the lifetime of the oxidized dye and hence on its regeneration efficiency in the specific cell. Dye regeneration is very efficient for SCN-based ruthenium dyes and iodide, but often slowed down with other dye/electrolyte combinations for various reasons (lower electrolyte concentration, lower driving force, smaller electronic coupling, inner/outer sphere electron transfer).[67–69] Considering the slower dye regeneration using $[2a]^{2-}$–$[2c]^{2-}$ sensitizers or cobalt redox mediators, the better performance of cells with the **N719**/I_3^-/I^- combination is quite expected (Figure 5a, Tables 2, Table 3). Interestingly, a lower electrolyte concentration decreases the efficiency of the **N719** cell to 5.8% but improves the efficiency of the cell with the $[nBu_4N]_2[2c]$ sensitizer to 3.3% (Table 2). Obviously, the effects of electrolyte concentration on dye regeneration

Table 3. Photovoltaic data of cells using the $[3]^{3+/2+}$ and $[4]^{3+/2+}$ redox mediators under AM1.5 light conditions.

Dye	Electrolyte	V_{OC} [V]	J_{SC} [mA cm^{-2}]	FF [%]	η [%]
$[nBu_4N]_2[2a]$	$[3]^{3+/2+}$	0.10	0.30	21	< 0.1
$[nBu_4N]_2[2a]$	$[4]^{3+/2+}$	0.59	1.07	66	0.4
$[nBu_4N]_2[2b]$	$[3]^{3+/2+}$	0.61	0.95	70	0.4
$[nBu_4N]_2[2b]$	$[4]^{3+/2+}$	0.66	1.90	73	0.9
$[nBu_4N]_2[2c]$	$[3]^{3+/2+}$	0.70	2.63	71	1.3
$[nBu_4N]_2[2c]$	$[4]^{3+/2+}$	0.66	3.06	71	1.4
N719	$[3]^{3+/2+}$	0.69	2.80	57	1.1
N719	$[4]^{3+/2+}$	0.64	2.68	62	1.1
N719[70a]	$[3]^{3+/2+}$	0.58	3.03	66	1.1
N719[92b]	$[3]^{3+/2+}$	0.62	3.80	76	1.8
N719[93c]	$[3]^{3+/2+}$	0.65	5.47	49	1.8

[a] $[Co(bpy)_3][B(CN)_4]_2$ (0.22 M); $[Co(bpy)_3][B(CN)_4]_3$ (0.05 M); 4-*tert*-butylpyridine (0.2 M) and lithium perchlorate (0.1 M) in CH_3CN; [b] $[Co(bpy)_3][PF_6]_2$ (0.2 M); $[Co(bpy)_3][PF_6]_3$ (0.02 M); 4-*tert*-butylpyridine (0.5 M) and lithium perchlorate (0.1 M) in CH_3CN; [c] $[Co(bpy)_3][PF_6]_2$ (0.2 M); $[Co(bpy)_3][PF_6]_3$ (0.02 M); 4-*tert*-butylpyridine (0.5 M) and lithium perchlorate (0.1 M) in CH_3CN.

and electron recombination kinetics differs for both dyes. This shows that the standard electrolyte concentration is optimized for **N719**, but the optimum electrolyte concentration needs to be determined for each dye individually. However, this is beyond the scope of this study.

Electron recombination of conduction band electrons with the oxidized mediator (I_3^-, $[3]^{3+}$, $[4]^{3+}$) is a complex function of the driving force (Marcus normal or inverted region), the electronic coupling, and the presence of surface protection.[89] Recombination kinetics with I_3^- is slow,[89] yet all cells with $[2]^{2-}/I_3^-/I^-$ combinations profit from the presence of CDCA as surface protecting agent and show higher short-circuit current densities (Table 2, Figure 5a, Figure 6a). With the I_3^-/I^- couple, the dark current for $[2a]^{2-}$–$[2c]^{2-}$ sensitizers is higher than that of **N719** (Figure 6b). However this observation reverses for the cobalt-based electrolytes (Figure 7b). Obviously, cells with the tridentate cyclometalated complexes $[2b]^{2-}$ and $[2c]^{2-}$ cope with the cobalt-based electrolytes, but the cell performance with **N719** dyes and cobalt-based electrolytes is severely reduced. The poor performance of **N719** in combination with cobalt-based electrolytes can be traced back to the higher dark current densities and consequently a strongly diminished short-circuit current density (Figure 6b, 7b; Table 1 and Table 2). As a working hypothesis, the **N719** dye better shields TiO_2 from I_2/I_3^-, but $[2b]^{2-}$ and $[2c]^{2-}$ better shield TiO_2 from cobalt-based electrolytes. This effect is certainly related to molecular structure, packing density (cf. dye loadings, Table 4) and protonation state of the dyes.[28]

Comparing the influence of the two cobalt-based electrolytes on the dark current densities of the **N719** and $[2c]^{2-}$ dyes, the bpy-based electrolyte $[3]^{3+/2+}$ shows the lower dark current density (Figure 7b). For cobalt-based electrolytes with potentials above about 0.55 V vs. NHE, recombination with electrons in the conduction band should be in the Marcus inverted region.[67] In accordance with this reported limiting value, recombination with $[3]^{3+}$ is hampered as compared to

Table 2. Photovoltaic data of cells using the I_3^-/I^- redox mediator with and without CDCA under AM1.5 light conditions (the data correspond to averaged values of several cells).

Dye	CDCA	V_{OC} [V]	J_{SC} [mA cm^{-2}]	FF [%]	η [%]
$[nBu_4N]_2[2a]$	–	0.50	1.77	63	0.6
$[nBu_4N]_2[2a]$	+	0.54	3.37	67	1.2
$[nBu_4N]_2[2b]$	–	0.53	2.91	67	1.1
$[nBu_4N]_2[2b]$	+	0.59	5.47	73	2.4
$[nBu_4N]_2[2c]$	–	0.57	5.06	72	2.1
$[nBu_4N]_2[2c]$	+	0.59	5.58	74	2.5
$[nBu_4N]_2[2c]$[b]	+	0.70	6.74	70	3.3
N719	+	0.74	13.4	75	7.3
N719[b]	+	0.78	10.97	68	5.8
$[A^{H,H}]^+$[66]	+	0.55	8.22	69	3.1
$[B^H]^+$[38,a]	–	0.54	8.49	73	3.4
$[C^H]^+$[38,a]	–	0.69	11.61	73	5.8

[a] Guanidinium thiocyanate was employed additionally in the electrolyte solution. [b] The electrolyte concentration was reduced to 0.100 M 1-methyl-3-propylimidazolium iodide and 0.020 M iodine in CH_3CN.

3.4 RESULTS AND DISCUSSION: STRONGLY COUPLED CYCLOMETALATED
RUTHENIUM TRIARYLAMINE CHROMOPHORES AS SENSITIZERS FOR DSSCS

87

Figure 6. a) Current density–voltage characteristics of cells with [nBu$_4$N]$_2$[2a], [nBu$_4$N]$_2$[2b], [nBu$_4$N]$_2$[2c], and N719 using the I$_3^-$/I$^-$ redox mediator with/without CDCA (——/-----) under illumination; b) corresponding dark current density–voltage measurements.

Figure 7. a) Current density–voltage characteristics of cells with [nBu$_4$N]$_2$[2b], [nBu$_4$N]$_2$[2c], and N719 using the [3]$^{3+/2+}$ (-----) and [4]$^{3+/2+}$ (——) redox mediators under illumination; b) corresponding dark current density–voltage measurements.

Table 4.	Dye loadings.	
Dye	CDCA	mol cm^{-2}
[nBu$_4$N]$_2$[2a]	–	1.39×10^{-7}
[nBu$_4$N]$_2$[2a]	+	1.24×10^{-7}
[nBu$_4$N]$_2$[2b]	–	1.08×10^{-7}
[nBu$_4$N]$_2$[2b]	+	0.84×10^{-7}
[nBu$_4$N]$_2$[2c]	–	1.81×10^{-7}
[nBu$_4$N]$_2$[2c]	+	1.42×10^{-7}
N719	+	0.55×10^{-7}

recombination with [4]$^{3+}$ accounting for the lower dark current density. For both low-spin cobalt(III) complexes [3]$^{3+}$ and [4]$^{3+}$ recombination with an electron initially yields low-spin cobalt(II) complexes corresponding to a metastable low-spin state which then undergoes spin crossover to the high spin state.[83,95] This effect might account for the favorable dark current densities of the cobalt-based electrolytes compared to the I$_3^-$/I$^-$ couple for [2b]$^{2-}$ and [2c]$^{2-}$ (Figure 6b,7b).

Electron lifetimes were determined by the photovoltage response to a small amplitude light modulation as a function of the quasi Fermi level of TiO$_2$ (Figure 8). All responses are linear in the semi-logarithmic plot, suggesting that recombination depends exponentially on the potential without participation of surface states.[68] As suggested above, CDCA retards recom-

bination with the iodine shuttle and increases the lifetime (Figure 8a). N719 displays the highest lifetime with the I$_3^-$/I$^-$ couple but performs poorly with the cobalt-based electrolytes (Figure 8). The slow dye regeneration kinetics of the cobalt-based electrolytes allowing for recombination with the oxidized dyes easily accounts for this observation. Slightly faster dye regeneration and/or better surface shielding with the dye/electrolyte combination [2c]$^{2-}$/[3]$^{3+/2+}$ yields a higher electron lifetime (Figure 8b).

Finally, the open-circuit voltages V_{OC} should increase in the electrolyte series I$_3^-$/I$^-$ < [3]$^{3+/2+}$ < [4]$^{3+/2+}$ according to the electrochemical data (Figure 4). Indeed, V_{OC} of the cobalt electrolytes is somewhat larger than that of the I$_3^-$/I$^-$ couple for [2a]$^{2-}$, [2b]$^{2-}$, and [2c]$^{2-}$ dyes, although the effect is less pronounced than expected from the redox potentials (Figure 4).

Overall, the combination of cobalt-based electrolytes with TPA-appended dyes, especially [2c]$^{2-}$ outperforms the standard dye N719 with cobalt-based electrolytes. The absolute performance of N719 and the I$_3^-$/I$^-$ couple with optimized concentration is still unrivaled with the systems under study.

Conclusion

The bis(tridentate) cylcometalated ruthenium complexes [1a][PF$_6$]–[1c][PF$_6$] as well as their saponified counterparts [nBu$_4$N]$_2$[2a]–[nBu$_4$N]$_2$[2c] were synthesized and characterized
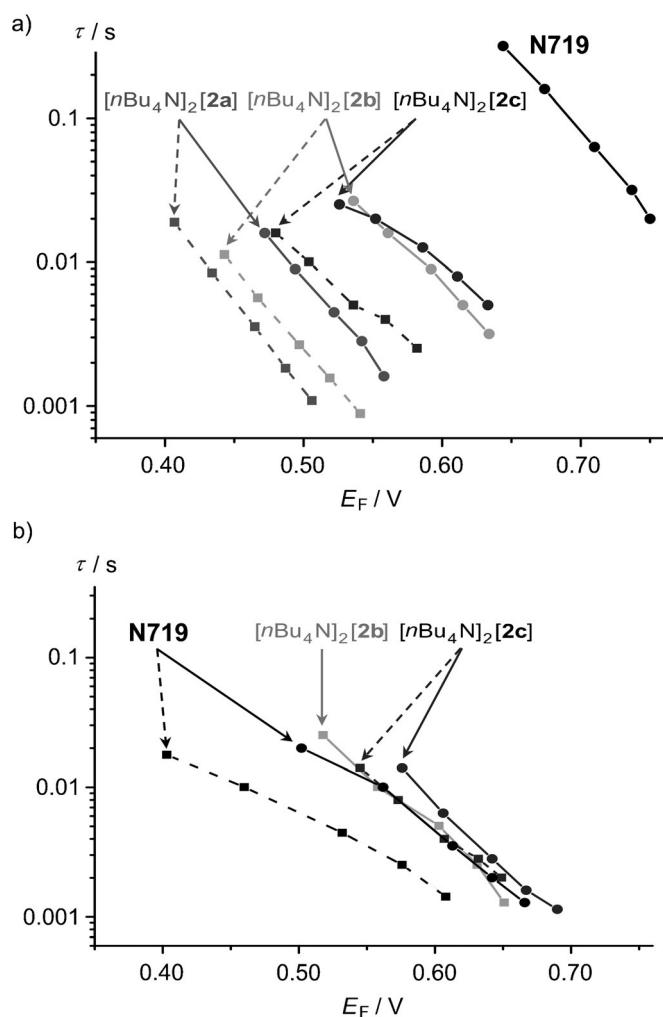
Figure 8. a) Electron recombination lifetimes (τ) of cells with [nBu$_4$N]$_2$[**2a**], [nBu$_4$N]$_2$[**2b**], [nBu$_4$N]$_2$[**2c**], and **N719** using a) the I$_3^-$/I$^-$ redox mediator with/without CDCA ($\circ$/$\square$) and b) using the [**3**]$^{3+/2+}$ ($\circ$) and [**4**]$^{3+/2+}$ ($\square$) redox mediators.

using mass spectrometry, UV/Vis and emission spectroscopy, and electrochemical methods. Oxidation of [**2a**]$^{2-}$–[**2c**]$^{2-}$ yields strongly coupled mixed valent species [**2a**]$^-$–[**2c**]$^-$ with substantial charge delocalization between the metal center and the triarylamine fragment as evidenced from TD-DFT calculations.[62,63] Yet, the degree of this delocalization is reduced in the saponified complexes [**2a**]$^-$–[**2c**]$^-$ as compared to the corresponding esters [**1a**]$^{2+}$–[**1c**]$^{2+}$ due to an increased charge density at the metal center. Concomitantly, all redox potentials shift to substantially lower values. Charge delocalization should be beneficial for applications in dye-sensitized solar cells as it hampers undesired recombination processes. However, the low redox potentials, which result from the large resonance stabilization, poses a challenge in the selection of a suitable redox electrolyte for efficient dye regeneration. As a consequence, dye [**2c**]$^{2-}$ with the highest oxidation potential yields the best cell performance of the cyclometalated complexes in this study in conjunction with triiodide/iodide ($\eta = 3.3\%$). The reference dye **N719**/triiodide/iodide combination remains un-

surpassed however ($\eta = 5.8\%$ under the same conditions). Compared to the triiodide/iodide cells, the efficiencies of the cells containing cobalt electrolytes are smaller by about a factor of three despite larger open-circuit voltages. We attribute this to the substantially slowed dye regeneration by the cobalt electrolytes which results in reduced short-circuit currents. In the presence of cobalt electrolytes, however, the cyclometalated dye with the carbazole substituent [**2c**]$^{2-}$ ($\eta = 1.4\%$) surpasses the thiocyanato-based dye **N719** ($\eta = 1.1\%$). This once again underlines the exceptional suitability of the triiodide/iodide electrolyte for thiocyanate-based sensitizers. We aim to dedicate further work to the understanding of the opposing trends of overall cell performances with the cobalt and iodide based electrolytes.

Experimental Section

Chemicals were obtained from commercial suppliers (Acros, Sigma-Aldrich, Solaronix SA, Wako, TCI, Boulder Scientific) and used without further purification. Air- or moisture-sensitive reactions were performed in dried glassware in an inert gas atmosphere (argon, quality 4.6). Acetonitrile was refluxed over CaH$_2$ and distilled under argon prior to use. Toluene was refluxed over sodium and distilled under argon prior to use. The ligands trimethyl-2,2′;6′,2″-terpyridine-4,4′,4″-tricarboxylate Me$_3$tctpy,[22] 1-bromo-3,5-di(2-pyridyl)-benzene,[96] ddpd[81] as well as the ruthenium(III) complex RuCl$_3$(Me$_3$tctpy)[22] and the palladium precatalyst [**Pd**]$_2$[84] were synthesized according to previously reported procedures. IR spectra were recorded on a Varian Excalibur Series 3100 FTIR spectrometer using KBr disks. IR absorption band intensities are classified as s (strong), m (medium), w (weak), and sh (shoulder). UV/Vis spectra were recorded on a Varian Cary 5000 spectrometer in 1 cm cuvettes. Emission spectra were recorded on a Varian Cary Eclipse spectrometer. Quantum yields were determined by comparing the areas under the emission spectra on an energy scale recorded for solutions of the samples and a reference with matching absorbances (Φ([Ru(bipy)$_3$]Cl$_2$) = 0.094 in deaerated MeCN).[97] Experimental uncertainty is estimated to be 15%. ESI$^+$ and high-resolution ESI$^+$ mass spectra were recorded on a Micromass QTof Ultima API mass spectrometer with analyte solutions in acetonitrile. FD mass spectra were recorded on a Thermo Fisher DFS mass spectrometer with a LIFDI upgrade. Elemental analyses were performed by the microanalytical laboratory of the chemical institutes of the University of Mainz. NMR spectra were obtained with a Bruker Avance II 400 spectrometer at 400.31 (^{1}H), 100.66 (^{13}C), 376.67 (^{19}F) at 25 °C. Chemical shifts δ [ppm] are reported with respect to residual solvent signals as internal standards (^{1}H, ^{13}C): CD$_3$CN δ(^{1}H) = 1.94 ppm, δ(^{13}C) = 1.32 and 118.26 ppm;[98] CD$_2$Cl$_2$ δ(^{1}H) = 5.32 ppm, δ(^{13}C) = 53.84 ppm[98] or external CFCl$_3$ (^{19}F: δ = 0 ppm). Electrochemical experiments were performed with a BioLogic SP-50 voltammetric analyzer at a sample concentration of 10^{-3} M using platinum wire working and counter electrodes and a 0.01 M Ag/AgNO$_3$ reference electrode. Measurements were carried out at a scan rate of 100 mV s^{-1} for cyclic voltammetry experiments and at 10 mV s^{-1} for square-wave voltammetry experiments using 0.1 M [nBu$_4$N][PF$_6$] as supporting electrolyte in acetonitrile. Potentials are given relative to the ferrocene/ferrocenium couple (0.40 V vs. SCE, $E_{1/2}$ = 0.09 ± 5 mV under the given conditions).[99]

Current–voltage characteristics of the DSSCs were measured with a Keithley Model 2400 source meter and a solar simulator with a 300 W Xenon arc-lamp (Newport) under 1 sun illumination

3.4 RESULTS AND DISCUSSION: STRONGLY COUPLED CYCLOMETALATED RUTHENIUM TRIARYLAMINE CHROMOPHORES AS SENSITIZERS FOR DSSCS

89

(AM 1.5, 100 mW cm^{-2}). A light shading mask, placed on the residual area of the front side of the FTO substrate (except for the 0.16 cm^2 TiO$_2$ active area), was employed to prevent overestimation of the power conversion efficiency. The quantum efficiencies of the DSSCs were measured by incident photon-to-current conversion efficiency (IPCE) measurements (PV Measurements, Inc.). UV/Vis spectra of the dye loading solutions were collected on a Jasco V-670 UV/Vis spectrometer. The electron lifetimes were obtained by intensity modulated photovoltage spectroscopy (IMVS) under open-circuit conditions as a function of light intensity using a controlled intensity modulated photo spectroscopy (CIMPS) system (Zahner).

Density functional theory calculations: DFT calculations were carried out using the ORCA program package (version 3.0.2).[100] Tight convergence criteria were chosen for all calculations (Keywords TightSCF and TightOpt). All calculations employ the resolution of identity (Split-RI-J) approach for the coulomb term in combination with the chain-of-spheres approximation for the exchange term (COSX).[101,102] All calculations were performed using the hybrid functional B3LYP[103] in combination with Ahlrichs' split-valence double-ζ basis set def2-SV(P), which comprises polarization functions for all non-hydrogen atoms.[104,105] Relativistic effects were calculated at the zeroth-order regular approximation (ZORA) niveau.[106] The ZORA keyword automatically invokes relativistically adjusted basis sets.[107] To account for solvent effects a conductor-like screening model (COSMO) modelling acetonitrile was used in all calculations.[108] Explicit counterions and/or solvent molecules were not taken into account in all cases.

Synthesis of *N*,*N*-bis-(4-methoxyphenyl)-3,5-(di-2-pyridyl)aniline (dpbH-N(4-C$_6$H$_4$OMe)$_2$) L^a: 2-Dicyclohexylphosphano-2′,6′-diisopropoxybiphenyl (12 mg, 0.026 mmol, 0.04 equiv) and the precatalyst **[Pd]$_2$** (8 mg, 0.011 mmol, 0.02 equiv) were suspended in dry toluene (10 mL) and stirred for 10 min followed by the addition of 1-bromo-3,5-di(2-pyridyl)benzene (200 mg, 0.643 mmol, 1 equiv), bis-(4-methoxyphenyl)amine (221 mg, 0.964 mmol, 1.50 equiv), sodium *tert*-butoxide (93 mg, 0.968 mmol, 1.51 equiv), and further dry toluene (40 mL). The resulting mixture was refluxed for 12 h. After cooling to room temperature, the solvent was removed under reduced pressure and the brown residue was purified by column chromatography on silica gel (eluent: dichloromethane/ethyl acetate 10:1→7:1), yielding **L^a** as slightly yellow solid. Yield: 241 mg (0.524 mmol, 82%). NMR and mass spectrometric data agree with reported values.[62]

Synthesis of *N*,*N*-diphenyl-3,5-(di-2-pyridyl)aniline (dpbH-NPh$_2$) L^b: 2-Dicyclohexylphosphano-2′,6′-diisopropoxybiphenyl (12 mg, 0.026 mmol, 0.04 equiv) and the precatalyst **[Pd]$_2$** (7 mg, 0.009 mmol, 0.01 equiv) were suspended in dry toluene (10 mL) and stirred for 10 min followed by the addition of 1-bromo-3,5-di(2-pyridyl)benzene (200 mg, 0.643 mmol, 1 equiv), diphenylamine (163 mg, 0.964 mmol, 1.50 equiv), sodium *tert*-butoxide (93 mg, 0.968 mmol, 1.51 equiv) and further dry toluene (40 mL). The resulting mixture was refluxed for 12 h. After cooling to room temperature, the solvent was removed under reduced pressure and the brown residue was purified by column chromatography on silica gel (eluent: dichloromethane/ethyl acetate 10:1) yielding **L^b** as slightly yellow solid. Yield: 222 mg (0.556 mmol, 86%). Anal. calcd. for C$_{28}$H$_{21}$N$_3$ (399.49): C 84.18, H 5.30, N 10.52; found: C 83.86, H 5.39, N 10.39. MS(FD$^+$): *m/z* (%) = 399.1 (100) [**L^b**]$^+$. ^{1}H NMR (CD$_2$Cl$_2$): δ [ppm] = 8.64 (d, $^3J_{HH}$ = 5 Hz, 2H, H^8), 8.32 (s, 1H, H^9), 7.80 (s, 2H, H^2), 7.76–7.71 (m, 4H, H^5, H^6), 7.29 (t, $^3J_{HH}$ = 8 Hz, 4H, H^{12}), 7.24 (dd, $^3J_{HH}$ = 9 Hz, 5 Hz, 2H, H^7), 7.17 (d, $^3J_{HH}$ = 8 Hz, 4H, H^{11}), 7.06 (t, $^3J_{HH}$ = 7 Hz, 2H, H^{13}). ^{13}C{^{1}H} NMR (CD$_2$Cl$_2$): δ [ppm] = 157.1 (C^4), 150.0 (C^8), 149.4 (C^1), 148.3 (C^{10}), 141.5 (C^3), 137.1 (C^6),

129.7 (C^{12}), 124.7 (C^{11}), 123.5 (C^2), 123.3 (C^{13}), 122.8 (C^7), 120.9 (C^5), 120.3 (C^9). IR (KBr disk): $\tilde{\nu}$ [cm^{-1}] = 3054 (w, aromatic C-H), 1584 (s, C=C), 1566 (s, C=C), 1492 (s), 1352 (s), 1255 (s), 779 (s), 749 (s), 700 (s).

Synthesis of 1-(*N*-carbazolyl)-3,5-(di-2-pyridyl)benzene (dpbH-*N*-carbazole) L^c: 2-Dicyclohexylphosphano-2′,6′-diisopropoxybiphenyl (12 mg, 0.026 mmol, 0.04 equiv) and the precatalyst **[Pd]$_2$** (7 mg, 0.009 mmol, 0.01 equiv) were suspended in dry toluene (10 mL) and stirred for 10 min followed by the addition of 1-bromo-3,5-di(2-pyridyl)benzene (200 mg, 0.643 mmol, 1 equiv), carbazole (161 mg, 0.964 mmol, 1.50 equiv), sodium *tert*-butoxide (93 mg, 0.968 mmol, 1.51 equiv), and further dry toluene (40 mL). The resulting mixture was refluxed for 12 h. After cooling to room temperature, the solvent was removed under reduced pressure and the brown residue was purified by column chromatography on silica gel (eluent: dichloromethane/ethyl acetate 20:1) yielding **L^c** as slightly yellow solid. Yield: 251 mg (0.556 mmol, 98%). Anal. calcd. for C$_{28}$H$_{19}$N$_3$ (397.47) ·0.5 H$_2$O: C 82.73, H 4.96, N 10.34; found: C 82.96, H 4.53, N 10.04. MS(FD$^+$): *m/z* (%) = 198.6 (1.5) [**L^c**]$^{2+}$, 397.1 (100) [**L^c**]$^+$. ^{1}H NMR (CD$_2$Cl$_2$): δ [ppm] = 8.85 (s, 1H, H^9), 8.73 (d, $^3J_{HH}$ = 4 Hz, 2H, H^8), 8.31 (s, 2H, H^2), 8.19 (d, *J* = 8 Hz, 2H, H^{14}), 7.92 (d, *J* = 8 Hz, 2H, H^5), 7.83 (t, $^3J_{HH}$ = 8 Hz, 2H, H^6), 7.54 (d, $^3J_{HH}$ = 8 Hz, 2H, H^{11}), 7.44 (t, $^3J_{HH}$ = 7 Hz, 2H, H^{12}), 7.29–7.35 (m, 4H, H^7, H^{13}). ^{13}C{^{1}H} NMR (CD$_2$Cl$_2$): δ [ppm] = 156.4 (C^4), 150.3 (C^8), 142.2 (C^3), 141.4 (C^{10}), 139.1 (C^1), 137.3 (C^6), 126.5 (C^{12}), 126.2 (C^2), 124.6 (C^9), 123.8 (C^{15}), 123.2 (C^7), 121.0 (C^5), 120.7 (C^{14}), 120.4 (C^{13}), 110.3 (C^{11}). IR (KBr disk): $\tilde{\nu}$ [cm^{-1}] = 3049 (w, aromatic C-H), 1587 (s, C=C), 1566 (s, C=C), 1448 (s), 1228 (s), 779 (s), 747 (s), 723 (s).

Synthesis of [Ru(L^a)(Me$_3$tctpy)][PF$_6$] [1a][PF$_6$]:[63a] RuCl$_3$(Me$_3$tctpy) (222 mg, 0.361 mmol, 1 equiv) and AgBF$_4$ (204 mg, 1.05 mmol, 2.9 equiv) were dissolved in dry acetonitrile (15 mL) and refluxed in the dark for 3 h. After cooling to room temperature, the mixture was filtered through a syringe filter (0.2 μm) and the solvent removed under reduced pressure. The dark residue was dissolved in deaerated *n*-butanol (20 mL) and **L^a** (200 mg, 0.435 mmol, 1.2 equiv) was added. The mixture was refluxed for 13 h followed by removal of the solvent under reduced pressure. The raw product was redissolved in MeCN (5 mL) and triturated by addition of a solution of [NH$_4$][PF$_6$] (177 mg, 1.08 mmol, 3 equiv) in H$_2$O (2 mL). The black precipitate was filtered off and washed with diethyl ether and hexanes. After purification via column chromatography on silica gel (eluent: chloroform/methanol 1:0→7:1), [**1a**][PF$_6$] was obtained as black powder. Yield: 364 mg (0.327 mmol, 91%). MS(ESI$^+$): *m/z* (%) = 967.1 (100) [**1a**]$^+$. Traces of the paramagnetic Ru^{III} complex [**1a**][PF$_6$]$_2$ broaden all NMR resonances of [**1a**][PF$_6$] due to the presence of a fast self-exchange reaction.[62,63a]

Synthesis of [*n*Bu$_4$N]$_2$[Ru(L^a)(H$_3$tctpy)] [*n*Bu$_4$N]$_2$[2a]: Complex [**1a**][PF$_6$] (360 mg, 0.324 mmol) was suspended in deaerated H$_2$O (35 mL) and *n*Bu$_4$NOH (1.5 M in H$_2$O, 5 mL) and hydrazine (1 mL) were added. After refluxing for 13 h, the mixture was extracted with dichloromethane (3×50 mL). The organic phases were combined, dried over MgSO$_4$, and the solvent was removed under reduced pressure. The purple residue was dissolved in MeCN (10 mL) and triturated by adding a 1:1 mixture of diethyl ether and hexanes (50 mL), yielding [*n*Bu$_4$N]$_2$[**2a**] as purple powder. Yield: 347 mg (0.247 mmol, 66%). Anal. calcd. for C$_{80}$H$_{104}$N$_8$O$_8$Ru (1406.8) ·8 H$_2$O: C 61.95, H 7.80, N 7.22; found: C 62.24, H 7.88, N 7.22. MS(ESI$^+$): *m/z* (%) = 242.3 (100) [*n*Bu$_4$N]$^+$, 462.6 (12) [**2a**+3H]$^{2+}$, 925.1 (48) [**2a**+3H]$^+$. HR-MS(ESI$^+$, *m/z*): Calcd. for C$_{48}$H$_{35}$N$_6$O$_8$^{96}Ru [**2a**+3H]$^+$: 919.1592; Found: 919.1578. MS(ESI$^-$): *m/z* (%) = 439.4 (85) [**2a**-CO$_2$]$^{2-}$, 461.4 (56) [**2a**]$^{2-}$, 834.9 (17) [**2a**-2CO$_2$]$^-$, 878.8 (100) [**2a**-CO$_2$]$^-$, 922.8 (19) [**2a**]$^-$, 1163.8 (77) ([*n*Bu$_4$N][**2a**])$^-$. ^{1}H NMR (CD$_3$CN): δ [ppm] = 9.25 (s, 2H, H^{2A}), 8.86 (s, 2H, H^{5A}), 8.03 (s, 2H,

90

3.4 RESULTS AND DISCUSSION: STRONGLY COUPLED CYCLOMETALATED RUTHENIUM TRIARYLAMINE CHROMOPHORES AS SENSITIZERS FOR DSSCS

H^{2B}), 7.90 (d, $^3J_{HH}$ = 8 Hz, 2 H, H^{5B}), 7.47 (t, $^3J_{HH}$ = 7 Hz, 2 H, H^{6B}), 7.37 (d, $^3J_{HH}$ = 6 Hz, 2 H, H^{7A}), 7.20 (d, $^3J_{HH}$ = 9 Hz, 4 H, H^{12A}), 7.07 (d, $^3J_{HH}$ = 6 Hz, 2 H, H^{8A}), 7.05 (d, $^3J_{HH}$ = 6 Hz, 2 H, H^{8B}), 6.92 (d, $^3J_{HH}$ = 9 Hz, 4 H, H^{12B}), 6.58 (t, $^3J_{HH}$ = 6 Hz, 2 H, H^{7B}), 3.79 (s, 6 H, H^{14B}), 3.19–3.00 (m, 16 H, H^1), 1.68–1.44 (m, 16 H, H^2), 1.38–1.21 (m, 16 H, H^3), 0.93 (t, $^3J_{HH}$ = 7 Hz, 24 H, H^4). ^{13}C{^{1}H} NMR (CD$_3$CN): δ [ppm] = 219.0 (C^{9B}), 169.1 (C^{4B}), 168.3 (C^{10A}), 167.1 (C^{11A}), 160.2 (C^{4A}), 155.7 (C^{13B}), 154.5 (C^{8A}), 153.7 (C^{3A}), 152.9 (C^{8B}), 147.9 (C^{6A}), 143.9 (C^{9B}), 143.5 (C^{3B}), 142.8 (C^{1B}), 136.0 (C^{6B}), 126.6 (C^{7A}), 124.8 (C^{11B}), 123.6 (C^{5A}), 123.4 (C^{2B}), 122.9 (C^{2A}), 122.4 (C^{7B}), 120.4 (C^{5B}), 115.6 (C^{12B}), 59.3 (C^1), 56.1 (C^{14B}), 24.3 (C^2), 20.3 (C^3), 13.8 (C^4). IR (KBr disk): $\tilde{\nu}$ [cm^{-1}] = 3440 (s, O-H crystal water), 3065 (w, aromatic C-H), 2960, 2873, 2843 (m, aliphatic C-H), 1620 (s, C=O carboxylate), 1598 (sh, C=C), 1465 (m, aliphatic C-N), 1341 (s, aromatic C-N), 1237 (s, C-O-C).

Synthesis of [Ru(L^b)(Me$_3$tctpy)][PF$_6$] [1 b][PF$_6$]: RuCl$_3$(Me$_3$tctpy) (263 mg, 0.429 mmol, 1 equiv) and AgBF$_4$ (243 mg, 1.25 mmol, 2.9 equiv) were dissolved in dry acetonitrile (15 mL) and refluxed in the dark for 3 h. After cooling to room temperature, the mixture was filtered through a syringe filter (0.2 µm) and the solvent removed under reduced pressure. The dark residue was dissolved in deaerated *n*-butanol (20 mL) and **L^b** (206 mg, 0.516 mmol, 1.2 equiv) was added. The mixture was refluxed for 13 h followed by removal of the solvent under reduced pressure. The raw product was redissolved in MeCN (5 mL) and triturated by addition of a solution of [NH$_4$][PF$_6$] (210 mg, 1.29 mmol, 3 equiv) in H$_2$O (2 mL). The black precipitate was filtered off and washed with diethyl ether and hexanes. After purification via column chromatography on silica gel (eluent: chloroform/methanol 1:0→7:1), [1 b][PF$_6$] was obtained as a black powder. Yield: 389 mg (0.370 mmol, 86 %). MS(ESI$^+$): *m/z* (%) = 453.6 (12) [1 b]$^{2+}$, 907.1 (100) [1 b]$^+$. HR-MS(ESI$^+$, *m/z*): Calcd. for C$_{49}$H$_{37}$N$_6$O$_6$^{96}Ru [1 b]$^+$: 901.1851; Found: 901.1857. Traces of the paramagnetic Ru^{III} complex [1 b][PF$_6$]$_2$ broaden all NMR resonances of [1 b][PF$_6$] due to the presence of a fast self-exchange reaction.[62,63a] IR (KBr disk): $\tilde{\nu}$ [cm^{-1}] = 3041 (w, aromatic C-H), 1725 (s, C=O ester), 1599 (m, C=C), 1243 (s), 843 (s, P-F), 588 (m, PF$_{def}$).

Synthesis of [*n*Bu$_4$N]$_2$[Ru(L^b)(H$_3$tctpy)] [*n*Bu$_4$N]$_2$[2 b]: Complex [1 b] [PF$_6$] (279 mg, 0.265 mmol) was suspended in deaerated H$_2$O (35 mL), and [*n*Bu$_4$N][OH] (1.5 M in H$_2$O, 5 mL) and hydrazine (1 mL) were added. After refluxing for 13 h, the mixture was extracted with dichloromethane (3×50 mL). The organic phases were combined, dried over MgSO$_4$, and the solvent was removed under reduced pressure. The purple residue was dissolved in MeCN (10 mL) and triturated by adding a 1:1 mixture of diethyl ether and hexanes (50 mL), yielding [*n*Bu$_4$N]$_2$[2 b] as purple powder. Yield: 312 mg (0.323 mmol, 87 %). Anal. calcd. for C$_{78}$H$_{100}$N$_8$O$_6$Ru (1346.8) ·6 H$_2$O: C 64.39, H 7.76, N 7.70; found: C 64.06, H 7.40, N 7.53. MS(ESI$^+$): *m/z* (%) = 242.3 (100) [*n*Bu$_4$N]$^+$, 432.6 (9) [2 b+3H]$^{2+}$, 865.2 (8) [2 b+3H]$^+$. HR-MS(ESI$^+$, *m/z*): Calcd. for C$_{46}$H$_{31}$N$_6$O$_6$^{96}Ru [2 b+3H]$^+$: 859.1381; Found: 859.1390. MS(ESI$^-$): *m/z* (%) = 387.5 (13) [2 b-2CO$_2$]$^{2-}$, 409.4 (47) [2 b-CO$_2$]$^{2-}$, 431.4 (15) [2 b]$^{2-}$, 775.0 (28) [2 b-2CO$_2$]$^-$, 818.9 (67) [2 b-CO$_2$]$^-$, 862.9 (13) [2 b]$^-$, 1103.7 (100) ([*n*Bu$_4$N][2 b])$^-$. ^{1}H NMR (CD$_3$CN): δ [ppm] = 9.20 (s, 2 H, H^{2A}), 8.80 (s, 2 H, H^{5A}), 8.10 (s, 2 H, H^{2B}), 7.96 (d, $^3J_{HH}$ = 8 Hz, 2 H, H^{5B}), 7.49 (t, $^3J_{HH}$ = 8 Hz, 2 H, H^{6B}), 7.40–7.26 (m, 10 H, H^{7A}, H^{11B}, H^{12B}), 7.11 (d, $^3J_{HH}$ = 5 Hz, 2 H, H^{8B}), 7.06–6.95 (m, 4 H, H^{8A}, H^{13B}), 6.61 (t, $^3J_{HH}$ = 6 Hz, 2 H, H^{7B}), 3.19–3.00 (m, 16 H, H^1), 1.67–1.49 (m, 16 H, H^2), 1.41–1.21 (m, 16 H, H^3), 0.94 (t, $^3J_{HH}$ = 7 Hz, 24 H, H^4). ^{13}C{^{1}H} NMR (CD$_3$CN): δ [ppm] = 218.8 (C^{9B}), 169.1 (C^{4B}), 167.6 (C^{9A}), 166.6 (C^{10A}), 160.2 (C^{4A}), 154.4 (C^{8A}), 153.6 (C^{3A}), 152.9 (C^{8B}), 149.9 (C^{6A}), 149.9 (C^{10B}), 149.4 (C^{1A}), 144.0 (C^{3B}), 141.0 (C^{1B}), 135.9 (C^{6B}), 130.3 (C^{11B}), 126.5 (C^{7A}), 124.7 (C^{2B}), 123.5 (C^{5A}), 123.1 (C^{12B}), 122.7 (C^{2A}), 122.5 (C^{7B}), 122.4 (C^{13B}), 120.4 (C^{5B}), 59.3 (C^1), 24.3 (C^2), 20.3 (C^3), 13.8 (C^4). IR (KBr

disk): $\tilde{\nu}$ [cm^{-1}] = 3440 (s, O-H crystal water), 3065 (w, aromatic C-H), 2960, 2873 (m, aliphatic C-H), 1617 (s, C=O carboxylate), 1598 (sh, C=C), 1465 (m, aliphatic C-N), 1351 (s, aromatic C-N).

Synthesis of [Ru(L^c)(Me$_3$tctpy)][PF$_6$] [1 c][PF$_6$]: RuCl$_3$(Me$_3$tctpy) (257 mg, 0.418 mmol, 1 equiv), and AgBF$_4$ (237 mg, 1.22 mmol, 2.9 equiv) were dissolved in dry acetonitrile (15 mL) and refluxed in the dark for 3 h. After cooling to room temperature, the mixture was filtered through a syringe filter (0.2 µm) and the solvent removed under reduced pressure. The dark residue was dissolved in deaerated *n*-butanol (20 mL) and **L^c** (200 mg, 0.503 mmol, 1.2 equiv) was added. The mixture was refluxed for 13 h followed by removal of the solvent under reduced pressure. The raw product was redissolved in MeCN (5 mL) and triturated by addition of a solution of [NH$_4$][PF$_6$] (204 mg, 1.25 mmol, 3 equiv) in H$_2$O (2 mL). The black precipitate was filtered off and washed with diethyl ether and hexanes. After purification via column chromatography on silica gel (eluent: chloroform/methanol 1:0→7:1) [1 c][PF$_6$] was obtained as black powder. Yield: 385 mg (0.366 mmol, 88 %). MS(ESI$^+$): *m/z* (%) = 905.1 (100) [1 c]$^+$. HR-MS(ESI$^+$, *m/z*): Calcd. for C$_{49}$H$_{35}$N$_6$O$_6$^{96}Ru [1 c]$^+$: 899.1694; Found: 899.1725. Traces of paramagnetic Ru^{III} complex [1 c][PF$_6$]$_2$ broaden all NMR resonances of [1 c][PF$_6$] due to the presence of a fast self-exchange reaction.[62,63a] IR (KBr disk): $\tilde{\nu}$ [cm^{-1}] = 3052 (w, aromatic C-H), 1725 (s, C=O ester), 1599 (m, C=C), 1249 (s), 842 (s, P-F), 588 (m, PF$_{def}$).

Synthesis of [*n*Bu$_4$N]$_2$[Ru(L^c)(H$_3$tctpy)] [*n*Bu$_4$N]$_2$[2 c]: Complex [1 c] [PF$_6$] (233 mg, 0.222 mmol) was suspended in deaerated H$_2$O (35 mL), and [*n*Bu$_4$N][OH] (1.5 M in H$_2$O, 5 mL) and hydrazine (1 mL) were added. After refluxing for 13 h, the mixture was extracted with dichloromethane (3×50 mL). The organic phases were combined, dried over MgSO$_4$, and the solvent was removed under reduced pressure. The purple residue was dissolved in MeCN (10 mL) and triturated by adding a 1:1 mixture of diethyl ether and hexanes (50 mL), yielding [*n*Bu$_4$N]$_2$[2 c] as purple powder. Yield: 159 mg (0.118 mmol, 53 %). Anal. calcd. for C$_{78}$H$_{98}$N$_8$O$_6$Ru (1344.7) ·8 H$_2$O: C 63.69, H 7.68, N 7.62; found: C 63.77, H 8.03, N 7.55. MS(ESI$^+$): *m/z* (%) = 242.3 (100) [*n*Bu$_4$N]$^+$, 431.6 (3) [2 a+3H]$^{2+}$, 863.1 (89) [2 a+3H]$^+$. HR-MS(ESI$^+$, *m/z*): Calcd. for C$_{46}$H$_{29}$N$_6$O$_6$^{96}Ru [2 c+3H]$^+$: 857.1225; Found: 857.1218. MS(ESI$^-$): *m/z* (%) = 386.5 (26) [2 c-2CO$_2$]$^{2-}$, 408.4 (74) [2 c-CO$_2$]$^{2-}$, 430.4 (20) [2 c]$^{2-}$, 773.0 (40) [2 c-2CO$_2$]$^-$, 816.9 (80) [2 c-CO$_2$]$^-$, 860.9 (13) [2 c]$^-$, 1101.7 (100) ([*n*Bu$_4$N][2 c])$^-$. ^{1}H NMR (CD$_3$CN): δ [ppm] = 9.25 (s, 2 H, H^{2A}), 8.85 (s, 2 H, H^{5A}), 8.39 (s, $^3J_{HH}$ = 9 Hz, 2 H, H^{2B}), 8.29 (d, $^3J_{HH}$ = 8 Hz, 2 H, H^{14B}), 8.11 (d, $^3J_{HH}$ = 8 Hz, 2 H, H^{5B}), 7.72 (d, $^3J_{HH}$ = 8 Hz, 2 H, H^{11B}), 7.60–7.50 (m, 4 H, H^{6B}, H^{12B}), 7.41–7.31 (m, 4 H, H^{7A}, H^{13B}), 7.21–7.12 (m, 4 H, H^{8A}, H^{8B}), 6.67 (t, $^3J_{HH}$ = 6 Hz, 2 H, H^{7B}), 3.16–3.00 (m, 16 H, H^1), 1.63–1.51 (m, 16 H, H^2), 1.40–1.24 (m, 16 H, H^3), 0.92 (t, $^3J_{HH}$ = 7 Hz, 24 H, H^4). ^{13}C{^{1}H} NMR (CD$_3$CN): δ [ppm] = 223.7 (C^{9B}), 169.0 (C^{4B}), 167.9 (C^{9A}), 166.9 (C^{10A}), 160.2 (C^{4A}), 154.7 (C^{8A}), 153.6 (C^{3A}), 153.0 (C^{8B}), 148.8 (C^{6A}), 146.8 (C^{1A}), 144.1 (C^{3B}), 143.2 (C^{10B}), 136.1 (C^{6B}), 130.3 (C^{1B}), 127.1 (C^{7A}), 126.5 (C^{15B}), 123.8 (C^{2B}), 123.6 (C^{5A}), 123.6 (C^{12B}), 122.8 (C^{2A}), 122.7 (C^{7B}), 121.3 (C^{14B}), 120.7 (C^{5B}), 120.6 (C^{13B}), 111.3 (C^{11B}), 59.2 (C^1), 24.3 (C^2), 20.3 (C^3), 13.8 (C^4). IR (KBr disk): $\tilde{\nu}$ [cm^{-1}] = 3440 (s, O-H crystal water), 3065 (w, aromatic C-H), 2960 (m, aliphatic C-H), 2873 (m, aliphatic C-H), 1614 (s, C=O carboxylate), 1598 (sh, C=C), 1465 (m, aliphatic C-N), 1353 (s, aromatic C-N).

Synthesis of [Co(bpy)$_3$][B(C$_6$F$_5$)$_4$]$_2$ [3][B(C$_6$F$_5$)$_4$]$_2$: The bpy ligand (2.27 g, 14.6 mmol, 3.2 equiv), dissolved in CH$_3$CN (50 mL) was added to a solution of Co(BF$_4$)$_2$·6 H$_2$O (1.55 g, 4.55 mmol, 1.0 equiv) in CH$_3$CN (50 mL) and the mixture was stirred for 6 h at room temperature. The complex was precipitated by addition of Et$_2$O (200 mL) and filtered off, washed with Et$_2$O (100 mL), and dried under reduced pressure. The yellow powder was dissolved in a minimum amount of CH$_3$CN and Li[B(C$_6$F$_5$)$_4$]·Et$_2$O (13.8 g, 18.2 mmol,

3.4 RESULTS AND DISCUSSION: STRONGLY COUPLED CYCLOMETALATED
RUTHENIUM TRIARYLAMINE CHROMOPHORES AS SENSITIZERS FOR DSSCS

91

4.0 equiv) was added. The volume of the solvent was reduced under reduced pressure and the product was precipitated by addition of water to give a yellow crystalline solid (6.52 g, 3.46 mmol, 76%). ^{1}H NMR (CD$_3$CN): δ [ppm] = 88.3 (bs, 1H), 85.0 (s, 1H), 46.5 (s, 1H), 14.7 (s, 1H). ^{19}F NMR (CD$_3$CN): δ [ppm] = −134.04 (bs, 2F), −164.20 (pt, 1F, $^3J_{FF}$ = 19.7 Hz), −168.68 (pt, 2F, $^3J_{FF}$ = 16.8 Hz). The ^{1}H NMR data match literature values of [Co(bpy)$_2$][PF$_6$]$_2$.[91] MS(ESI$^+$): m/z (%) = 185.6 (7) [Co(bpy)$_2$]$^{2+}$, 1206.2 (100) [Co(bpy)$_3$+ B(C$_6$F$_5$)$_4$]$^+$, 2149.3 (17) [3×(Co(bpy)$_3$)+4×(B(C$_6$F$_5$)$_4$)]$^{2+}$, 3092.44 (19) [4×(Co(bpy)$_3$)+6×(B(C$_6$F$_5$)$_4$)]$^{2+}$. HR-MS(ESI$^+$, m/z): Calcd. for C$_{54}$H$_{24}$^{10}BCoF$_{20}$N$_6$: 1205.1204; found: 1205.1224.

Synthesis of [Co(bpy)$_3$][B(C$_6$F$_5$)$_4$]$_3$ [3][B(C$_6$F$_5$)$_4$]$_3$: [Co(bpy)$_3$](BF$_4$)$_3$ (2.94 g, 4.20 mol, 1.0 equiv) was dissolved in CH$_3$CN (100 mL) and 2,3-dichloro-5,6-dicyano-1,4-benzoquinone (1.43 g, 6.30 mmol, 1.5 equiv) was added. The solution was stirred for 5 h at room temperature. Li[B(C$_6$F$_5$)$_4$]·Et$_2$O (12.8 g, 16.8 mol, 4.0 equiv) was added and the mixture was diluted with water (200 mL). The precipitate was filtered off, washed with water (200 mL), and dried under reduced pressure to give a slightly orange crystalline solid (7.65 g, 2.98 mmol, 71%). ^{1}H NMR (CD$_3$CN): δ [ppm] = 8.71 (d, 1H, $^3J_{HH}$ = 7.8 Hz), 8.49 (pt, 1H, $^3J_{HH}$ = 7.7 Hz), 7.76 (pt, 1H, $^3J_{HH}$ = 6.5 Hz), 7.31 (d, 1H, $^3J_{HH}$ = 5.5 Hz). ^{19}F NMR (CD$_3$CN): δ [ppm] = −134.07 (bs, 2F), −164.22 (pt, 1F, $^3J_{FF}$ = 19.7 Hz), −168.65 (bs, 2F). MS(ESI$^+$): m/z (%) = 185.6 (20) [Co(bpy)$_2$]$^{2+}$, 263.6 (6) [Co(bpy)$_3$]$^{2+}$, 371.1 (46) [Co(bpy)$_2$]$^+$, 423.1 (74), 1054.2 (14), 1206.2 (31) [Co(bpy)$_3$+ B(C$_6$F$_5$)$_4$]$^+$, 1885.2 (100) [Co(bpy)$_3$+2×(B(C$_6$F$_5$)$_4$)]$^+$, 2526.8 (6) [Co(bpy)$_3$+3×(B(C$_6$F$_5$)$_4$-2F)]$^+$, 2740.6 (7), 3168.3 (8) [3×(Co(bpy)$_3$)+ 7×(B(C$_6$F$_5$)$_4$)]$^{2+}$. HR-MS(ESI$^+$, m/z): Calcd. for C$_{78}$H$_{24}$^{10}B$_2$CoF$_{40}$N$_6$: 1883.1014; found: 1883.1052.

Synthesis of [Co(ddpd)$_2$][B(C$_6$F$_5$)$_4$]$_2$ [4][B(C$_6$F$_5$)$_4$]$_2$: The ddpd ligand (2.53 g, 8.68 mol, 2.2 equiv), dissolved in CH$_3$CN (50 mL), was added to a solution of Co(BF$_4$)$_2$·6H$_2$O (1.34 g, 3.95 mmol, 1.0 equiv) in CH$_3$CN (50 mL) and the mixture was stirred for 6 h at room temperature. The complex was precipitated by addition of Et$_2$O (400 mL) and filtered off, washed with Et$_2$O (100 mL), and dried under reduced pressure. The yellow powder was dissolved in a minimum amount of CH$_3$CN, and Li[B(C$_6$F$_5$)$_4$]·Et$_2$O (12.0 g, 15.7 mmol, 4.0 equiv) was added. The volume of the solvent was reduced under reduced pressure and the product was precipitated by addition of water to give a yellow crystalline solid (7.18 g, 3.51 mmol, 89%). ^{1}H NMR (CD$_3$CN): δ [ppm] = 75.0 (s, 2H), 69.0 (s, 2H), 34.6 (bs, 2H), 34.2 (s, 2H), 22.5 (s, 6H), 21.9 (s, 1H), 2.7 (s, 2H). ^{19}F NMR (CD$_3$CN): δ [ppm] = −134.07 (bs, 2F), −164.22 (pt, 1F, $^3J_{FF}$ = 19.7 Hz), −168.67 (pt, 2F, $^3J_{FF}$ = 16.8 Hz). The ^{1}H NMR data match reported values of [Co(ddpd)$_2$][BF$_4$]$_2$.[82] MS(ESI$^+$): m/z (%) = 292.1 (14) [ddpd+H]$^+$, 320.6 (18) [Co(ddpd)$_2$]$^{2+}$, 1320.1 (100) [Co(ddpd)$_2$+ B(C$_6$F$_5$)$_4$]$^+$, 2320.3 (13) [3×(Co(ddpd)$_2$)+4×(B(C$_6$F$_5$)$_4$)]$^{2+}$, 3320.3 (18) [4×(Co(dpdd)$_2$)+6×(B(C$_6$F$_5$)$_4$)]$^{2+}$. HR-MS(ESI$^+$, m/z): Calcd. for C$_{58}$H$_{34}$^{10}BCoF$_{20}$N$_{10}$: 1319.2110; found: 1319.2106.

Synthesis of [Co(ddpd)$_2$][B(C$_6$F$_5$)$_4$]$_3$ [4][B(C$_6$F$_5$)$_4$]$_3$: [Co(ddpd)$_2$](BF$_4$)$_2$ (3.24 g, 3.83 mmol, 1.0 equiv) was dissolved in CH$_3$CN (100 mL) and 2,3-dichloro-5,6-dicyano-1,4-benzoquinone (1.30 g, 5.75 mmol, 1.5 equiv) was added. The solution was stirred for 5 h at room temperature. Li[B(C$_6$F$_5$)$_4$]·Et$_2$O (11.6 g, 15.3 mmol, 4.0 equiv) was added and the mixture was diluted with water (200 mL). The precipitate was filtered off, washed with water (200 mL), and dried under reduced pressure to give a pinkish powder (8.32 g, 3.06 mmol, 86%). ^{1}H NMR (CD$_3$CN): δ [ppm] = 8.33 (pt, 1H, $^3J_{HH}$ = 8.1 Hz), 8.13 (pt, 2H, $^3J_{HH}$ = 7.8 Hz), 7.38–7.43 (m, 4H), 7.01 (pt, 2H, $^3J_{HH}$ = 6.7 Hz), 6.90 (d, 2H, $^3J_{HH}$ = 5.7 Hz), 3.12 (s, 6H). ^{19}F NMR (CD$_3$CN): δ [ppm] = −134.07 (s), −164.22 (pt), −168.68 (pt). The ^{1}H NMR data match reported values of [Co(ddpd)$_2$][BF$_4$]$_3$.[82] MS(ESI$^+$): m/z (%) = 175.1 (10) [Co(ddpd)]$^{2+}$, 184.1 (10) [Co(ddpd)+F]$^{2+}$, 291.2 (12) [ddpd]$^+$, 320.6

(56) [Co(ddpd)$_2$]$^{2+}$, 1320.2 (8) [Co(ddpd)$_2$+B(C$_6$F$_5$)$_4$]$^+$, 1999.2 (100) [Co(ddpd)$_2$+2×(B(C$_6$F$_5$)$_4$)]$^+$, 2535.5 (18), 2669.6 (20) [5× (Co(ddpd)$_2$)+11×(B(C$_6$F$_5$)$_4$)]$^{4+}$, 2892.8 (7) [4×(Co(ddpd)$_2$)+9× (B(C$_6$F$_5$)$_4$)]$^{3+}$, 3071.4 (12), 3339.4 (12) [3×(Co(ddpd)$_2$)+7× (B(C$_6$F$_5$)$_4$)]$^{2+}$. HR-MS(ESI$^+$, m/z): Calcd. for C$_{82}$H$_{34}$^{11}B$_2$CoF$_{40}$N$_{10}$: 1999.1847; found: 1999.1809.

TiO$_2$ electrode preparation: Fluorine-doped tin oxide (FTO) glass plates (Pilkington-TEC8) were cleaned using a ultrasonic bath with 2 vol% of Helmanex in deionized water and ethanol. A doctor-bladed layer of 35 nm TiO$_2$ particles (PST-35 NR, CCIC) was used as photoelectrode. A 8 µm thick transparent film and an additional 4 µm scattering TiO$_2$ film (PST-400C, CCIC, particle size ca. 400 nm) were coated on the top of the conducting glass electrode. The TiO$_2$ electrodes were heated to 450°C for 30 min, treated with a 0.5 mM TiCl$_4$ solution in deionized water for 20 min at 70°C, followed by an annealing process for 30 min at 450°C. Following the heat treatment, these electrodes were immersed into the sensitizer/CDCA solutions (2.95×10^{-4} M of [nBu$_4$N][2a], 3.01×10^{-4} M of [nBu$_4$N][2b], 3.01×10^{-4} M of [nBu$_4$N][2c], and 3.11×10^{-4} M of N719 solution (CH$_3$CN/tBuOH) (1:1, volume ratio) with or without 5.99× 10^{-4} M CDCA (Dyesol) and kept at room temperature for 6 h, 16 h or 24 h, respectively. The TiO$_2$ electrodes were rinsed with CH$_3$CN and dried.

Electrolyte solutions: The triiodide/iodide electrolyte solutions were prepared from 1-methyl-3-propylimidazolium iodide (0.600 M) and iodine (0.050 M) in CH$_3$CN. The Co$^{III/II}$ electrolytes were employed as 0.035/0.165 M and 0.020/0.080 M CH$_3$CN solutions of [3]$^{3+}$/[3]$^{2+}$ and [4]$^{3+}$/[4]$^{2+}$, respectively. Owing to the employed relative concentrations the redox potentials shift to lower values by 0.061, 0.039, and 0.036 V for I$_3^-$/I$^-$, [3]$^{3+}$/[3]$^{2+}$ and [4]$^{3+}$/[4]$^{2+}$, respectively. The absolute concentrations of the redox couples are 0.6 M, 0.2 M and 0.1 M for I$_3^-$/I$^-$, [3]$^{3+}$/[3]$^{2+}$ and [4]$^{3+}$/[4]$^{2+}$, respectively. 4-tert-Butylpyridine (0.8 M) and lithium perchlorate (0.1 M) were used in all cells.

Counter electrode preparation: The Pt electrode was prepared by spin-coating of 10 mM H$_2$PtCl$_6$ (Sigma-Aldrich) in 2-propanol and then sintered at 450°C for 30 min. The cells were sealed using 60 µm Surlyn. The electrolyte solutions were introduced through holes on the counter electrode.

Dye loading: TiO$_2$/FTO electrodes were immersed in a 0.1 M KOH H$_2$O/CH$_3$CN 1:1 solution for at least 5 min. From the UV/Vis absorption spectra of the resulting dye solutions, the concentrations of the attached dyes were calculated (Table 4).

Acknowledgements

[1]   B. O'Regan, M. Grätzel, *Nature* **1991**, *353*, 737–740.

[2]   M. A. Green, *Solar Energy* **2004**, *76*, 3–8.

[3]   M. Grätzel, *J. Photochem. Photobiol. C* **2003**, *4*, 145–153.

[4]   A. Hagfeldt, G. Boschloo, L. Sun, L. Kloo, H. Pettersson, *Chem. Rev.* **2010**, *110*, 6595–6663.

[5]   R. McConnell, *Renewable Sustainable Energy Rev.* **2002**, *6*, 271–293.

[6]   S. Ferrere, B. A. Gregg, *J. Am. Chem. Soc.* **1998**, *120*, 843–844.

[7]   N. Alonso-Vante, J.-F. Nierengarten, J.-P. Sauvage, *J. Chem. Soc. Dalton Trans.* **1994**, 1649–1654.

[8]   T. Bessho, E. C. Constable, M. Graetzel, A. Hernandez Redondo, C. E. Housecroft, W. Kylberg, M. K. Nazeeruddin, M. Neuburger, S. Schaffner, *Chem. Commun.* **2008**, 3717–3719.

[9]   C. E. Housecroft, E. C. Constable, *Chem. Soc. Rev.* **2015**, *44*, 8386–8398.

[10] E. A. M. Geary, N. Hirata, J. Clifford, J. R. Durrant, S. Parsons, A. Dawson, L. J. Yellowlees, N. Robertson, *Dalton Trans.* **2003**, 3757–3762.

[11] E. C.-H. Kwok, M.-Y. Chan, K. M.-C. Wong, W. H. Lam, V. W.-W. Yam, *Chem. Eur. J.* **2010**, *16*, 12244–12254.

[12] E. I. Mayo, K. Kilså, T. Tirrell, P. I. Djurovich, A. Tamayo, M. E. Thompson, N. S. Lewis, H. B. Gray, *Photochem. Photobiol. Sci.* **2006**, *5*, 871–873.

[13] E. Baranoff, J. Yum, I. Jung, R. Vulcano, M. Grätzel, M. K. Nazeeruddin, *Chem. Asian J.* **2010**, *5*, 496–499.

[14] J. B. Asbury, E. Hao, Y. Wang, T. Lian, *J. Phys. Chem. B* **2000**, *104*, 11957–11964.

[15] S. Kim, J. K. Lee, S. O. Kang, J. Ko, J.-H. Yum, S. Fantacci, F. de Angelis, D. Di Censo, M. K. Nazeeruddin, M. Grätzel, *J. Am. Chem. Soc.* **2006**, *128*, 16701–16707.

[16] A. Mishra, M. K. R. Fischer, P. Bäuerle, *Angew. Chem. Int. Ed.* **2009**, *48*, 2474–2499; *Angew. Chem.* **2009**, *121*, 2510–2536.

[17] W. M. Campbell, K. W. Jolley, P. Wagner, K. Wagner, P. J. Walsh, K. C. Gordon, L. Schmidt-Mende, M. K. Nazeeruddin, Q. Wang, M. Grätzel, D. L. Officer, *J. Phys. Chem. C* **2007**, *111*, 11760–11762.

[18] L.-L. Li, E. W.-G. Diau, *Chem. Soc. Rev.* **2013**, *42*, 291–304.

[19] S. Mathew, A. Yella, P. Gao, R. Humphry-Baker, B. F. E. Curchod, N. Ashari-Astani, I. Tavernelli, U. Rothlisberger, M. K. Nazeeruddin, M. Grätzel, *Nat. Chem.* **2014**, *6*, 242–247.

[20] S. Rühle, M. Shalom, A. Zaban, *ChemPhysChem* **2010**, *11*, 2290–2304.

[21] M. K. Nazeeruddin, A. Kay, I. Rodicio, R. Humphry-Baker, E. Mueller, P. Liska, N. Vlachopoulos, M. Graetzel, *J. Am. Chem. Soc.* **1993**, *115*, 6382–6390.

[22] M. K. Nazeeruddin, P. Péchy, T. Renouard, S. M. Zakeeruddin, R. Humphry-Baker, P. Comte, P. Liska, L. Cevey, E. Costa, V. Shklover, L. Spiccia, G. B. Deacon, C. A. Bignozzi, M. Grätzel, *J. Am. Chem. Soc.* **2001**, *123*, 1613–1624.

[23] S. Altobello, R. Argazzi, S. Caramori, C. Contado, S. Da Fré, P. Rubino, C. Choné, G. Larramona, C. A. Bignozzi, *J. Am. Chem. Soc.* **2005**, *127*, 15342–15343.

[24] T. W. Rees, E. Baranoff, *Polyhedron* **2014**, *82*, 37–49.

[25] G. A. Crosby, *Acc. Chem. Res.* **1975**, *8*, 231–238.

[26] M. L. Stone, G. A. Crosby, *Chem. Phys. Lett.* **1981**, *79*, 169–173.

[27] J. R. Winkler, T. L. Netzel, C. Creutz, N. Sutin, *J. Am. Chem. Soc.* **1987**, *109*, 2381–2392.

[28] M. K. Nazeeruddin, S. M. Zakeeruddin, R. Humphry-Baker, M. Jirousek, P. Liska, N. Vlachopoulos, V. Shklover, C.-H. Fischer, M. Grätzel, *Inorg. Chem.* **1999**, *38*, 6298–6305.

[29] M. K. Nazeeruddin, F. de Angelis, S. Fantacci, A. Selloni, G. Viscardi, P. Liska, S. Ito, B. Takeru, M. Grätzel, *J. Am. Chem. Soc.* **2005**, *127*, 16835–16847.

[30] M. Nazeeruddin, M. Grätzel, *J. Photochem. Photobiol. A* **2001**, *145*, 79–86.

[31] H. T. Nguyen, H. M. Ta, T. Lund, *Sol. Energy Mater. Sol. Cells* **2007**, *91*, 1934–1942.

[32] a) T. P. Brewster, W. Ding, N. D. Schley, N. Hazari, V. S. Batista, R. H. Crabtree, *Inorg. Chem.* **2011**, *50*, 11938–11946; b) S. Kämper, A. Paretzki, J. Fiedler, S. Záliš, W. Kaim, *Inorg. Chem.* **2012**, *51*, 2097–2104.

[33] a) A. Breivogel, S. Wooh, J. Dietrich, T. Y. Kim, Y. S. Kang, K. Char, K. Heinze, *Eur. J. Inorg. Chem.* **2014**, 2720–2734; b) A. Breivogel, C. Kreitner, K. Heinze, *Eur. J. Inorg. Chem.* **2014**, 5468–5490.

[34] S. H. Wadman, J. M. Kroon, K. Bakker, M. Lutz, A. L. Spek, G. P. M. van Klink, G. van Koten, *Chem. Commun.* **2007**, 1907–1909.

[35] T. Bessho, E. Yoneda, J.-H. Yum, M. Guglielmi, I. Tavernelli, H. Imai, U. Rothlisberger, M. K. Nazeeruddin, M. Grätzel, *J. Am. Chem. Soc.* **2009**, *131*, 5930–5934.

[36] B. D. Koivisto, K. C. D. Robson, C. P. Berlinguette, *Inorg. Chem.* **2009**, *48*, 9644–9652.

[37] S. H. Wadman, J. M. Kroon, K. Bakker, R. W. A. Havenith, G. P. M. van Klink, G. van Koten, *Organometallics* **2010**, *29*, 1569–1579.

[38] a) K. C. D. Robson, B. D. Koivisto, A. Yella, B. Sporinova, M. K. Nazeeruddin, T. Baumgartner, M. Grätzel, C. P. Berlinguette, *Inorg. Chem.* **2011**, *50*, 5494–5508; b) P. G. Bomben, T. J. Gordon, E. Schott, C. P. Berlinguette, *Angew. Chem. Int. Ed.* **2011**, *50*, 10682–10685; *Angew. Chem.* **2011**, *123*, 10870–10873.

[39] J.-J. Kim, H. Choi, S. Paek, C. Kim, K. Lim, M.-J. Ju, H. S. Kang, M.-S. Kang, J. Ko, *Inorg. Chem.* **2011**, *50*, 11340–11347.

[40] P. G. Bomben, K. C. Robson, B. D. Koivisto, C. P. Berlinguette, *Coord. Chem. Rev.* **2012**, *256*, 1438–1450.

[41] T. Funaki, H. Funakoshi, O. Kitao, N. Onozawa-Komatsuzaki, K. Kasuga, K. Sayama, H. Sugihara, *Angew. Chem. Int. Ed.* **2012**, *51*, 7528–7531; *Angew. Chem.* **2012**, *124*, 7646–7649.

[42] B. Schulze, D. G. Brown, K. C. D. Robson, C. Friebe, M. Jäger, E. Birckner, C. P. Berlinguette, U. S. Schubert, *Chem. Eur. J.* **2013**, *19*, 14171–14180.

[43] E. C. Constable, J. M. Holmes, *J. Organomet. Chem.* **1986**, *301*, 203–208.

[44] E. C. Constable, C. E. Housecroft, *Polyhedron* **1990**, *9*, 1939–1947.

[45] M. Beley, J. P. Collin, R. Louis, B. Metz, J. P. Sauvage, *J. Am. Chem. Soc.* **1991**, *113*, 8521–8522.

[46] S. H. Wadman, M. Lutz, D. M. Tooke, A. L. Spek, F. Hartl, R. W. A. Havenith, G. P. M. van Klink, G. van Koten, *Inorg. Chem.* **2009**, *48*, 1887–1900.

[47] P. G. Bomben, K. C. D. Robson, P. A. Sedach, C. P. Berlinguette, *Inorg. Chem.* **2009**, *48*, 9631–9643.

[48] a) C. Kreitner, E. Erdmann, W. W. Seidel, K. Heinze, *Inorg. Chem.* **2015**, *54*, 11088–11104; b) C. Kreitner, K. Heinze, *Dalton Trans.* **2016**, *45*, 5640–5658.

[49] B. Durham, J. V. Caspar, J. K. Nagle, T. J. Meyer, *J. Am. Chem. Soc.* **1982**, *104*, 4803–4810.

[50] K. Kalyanasundaram, *Coord. Chem. Rev.* **1982**, *46*, 159–244.

[51] M. Maestri, N. Armaroli, V. Balzani, E. C. Constable, A. M. W. C. Thompson, *Inorg. Chem.* **1995**, *34*, 2759–2767.

[52] V. Balzani, A. Juris, *Coord. Chem. Rev.* **2001**, *211*, 97–115.

[53] T. Edvinsson, C. Li, N. Pschirer, J. Schöneboom, F. Eickemeyer, R. Sens, G. Boschloo, A. Herrmann, K. Müllen, A. Hagfeldt, *J. Phys. Chem. C* **2007**, *111*, 15137–15140.

[54] A. Abbotto, C. Barolo, L. Bellotto, F. de Angelis, M. Grätzel, N. Manfredi, C. Marinzi, S. Fantacci, J.-H. Yum, M. K. Nazeeruddin, *Chem. Commun.* **2008**, 5318–5320.

[55] M. Ishida, S. W. Park, D. Hwang, Y. B. Koo, J. L. Sessler, D. Y. Kim, D. Kim, *J. Phys. Chem. C* **2011**, *115*, 19343–19354.

[56] J.-H. Yum, S.-J. Moon, C. S. Karthikeyan, H. Wietasch, M. Thelakkat, S. M. Zakeeruddin, M. Nazeeruddin, M. Grätzel, *Nano Energy* **2012**, *1*, 6–12.

[57] A. Yella, H.-W. Lee, H. N. Tsao, C. Yi, A. K. Chandiran, M. K. Nazeeruddin, E. W.-G. Diau, C.-Y. Yeh, S. M. Zakeeruddin, M. Grätzel, *Science* **2011**, *334*, 629–634.

[58] K. C. D. Robson, B. D. Koivisto, T. J. Gordon, T. Baumgartner, C. P. Berlinguette, *Inorg. Chem.* **2010**, *49*, 5335–5337.

[59] K. C. D. Robson, B. Sporinova, B. D. Koivisto, E. Schott, D. G. Brown, C. P. Berlinguette, *Inorg. Chem.* **2011**, *50*, 6019–6028.

[60] K. Hu, K. C. D. Robson, P. G. Johansson, C. P. Berlinguette, G. J. Meyer, *J. Am. Chem. Soc.* **2012**, *134*, 8352–8355.

[61] M. B. Robin, P. Day, *Adv. Inorg. Chem.* **1968**, *10*, 247–422.

[62] C.-J. Yao, R.-H. Zheng, Q. Shi, Y.-W. Zhong, J. Yao, *Chem. Commun.* **2012**, *48*, 5680–5682.

[63] a) C.-J. Yao, H.-J. Nie, W.-W. Yang, J.-Y. Shao, J. Yao, Y.-W. Zhong, *Chem. Eur. J.* **2014**, *20*, 17466–17477; b) B.-B. Cui, Y.-W. Zhong, J. Yao, *J. Am. Chem. Soc.* **2015**, *137*, 4058–4061.

[64] Y.-W. Zhong, Z.-L. Gong, J.-Y. Shao, J. Yao, *Coord. Chem. Rev.* **2016**, *312*, 22–40.

[65] B. S. Brunschwig, C. Creutz, N. Sutin, *Chem. Soc. Rev.* **2002**, *31*, 168–184.

3.4 RESULTS AND DISCUSSION: STRONGLY COUPLED CYCLOMETALATED
RUTHENIUM TRIARYLAMINE CHROMOPHORES AS SENSITIZERS FOR DSSCS

93

[66] R. K. Chitumalla, K. S. V. Gupta, C. Malapaka, R. Fallahpour, A. Islam, L. Han, B. Kotamarthi, S. P. Singh, *Phys. Chem. Chem. Phys.* **2014**, *16*, 2630–2640.

[67] S. M. Feldt, P. W. Lohse, F. Kessler, M. K. Nazeeruddin, M. Grätzel, G. Boschloo, A. Hagfeldt, *Phys. Chem. Chem. Phys.* **2013**, *15*, 7087–7097.

[68] J. W. Ondersma, T. W. Hamann, *Coord. Chem. Rev.* **2013**, *257*, 1533–1543.

[69] M. Wang, C. Grätzel, S. M. Zakeeruddin, M. Grätzel, *Energy Environ. Sci.* **2012**, *5*, 9394–9405.

[70] E. Mosconi, J.-H. Yum, F. Kessler, C. J. G. García, C. Zuccaccia, A. Cinti, M. K. Nazeeruddin, M. Grätzel, F. D. Angelis, *J. Am. Chem. Soc.* **2012**, *134*, 19438–19453.

[71] T. W. Hamann, *Dalton Trans.* **2012**, *41*, 3111–3115.

[72] J.-H. Yum, E. Baranoff, F. Kessler, T. Moehl, S. Ahmad, T. Bessho, A. Marchioro, E. Ghadiri, J.-E. Moser, C. Yi, M. K. Nazeeruddin, M. Grätzel, *Nat. Commun.* **2012**, *3*, 631; DOI: 10.1038/ncomms1655.

[73] S. M. Feldt, G. Wang, G. Boschloo, A. Hagfeldt, *J. Phys. Chem. C* **2011**, *115*, 21500–21507.

[74] S. M. Feldt, E. A. Gibson, E. Gabrielsson, L. Sun, G. Boschloo, A. Hagfeldt, *J. Am. Chem. Soc.* **2010**, *132*, 16714–16724.

[75] S. Caramori, J. Husson, M. Beley, C. A. Bignozzi, R. Argazzi, P. C. Gros, *Chem. Eur. J.* **2010**, *16*, 2611–2618.

[76] B. M. Klahr, T. W. Hamann, *J. Phys. Chem. C* **2009**, *113*, 14040–14045.

[77] J. J. Nelson, T. J. Amick, C. M. Elliott, *J. Phys. Chem. C* **2008**, *112*, 18255–18263.

[78] H. Nusbaumer, S. M. Zakeeruddin, J.-E. Moser, M. Grätzel, *Chem. Eur. J.* **2003**, *9*, 3756–3763.

[79] S. A. Sapp, C. Elliott, C. Contado, S. Caramori, C. A. Bignozzi, *J. Am. Chem. Soc.* **2002**, *124*, 11215–11222.

[80] H. Nusbaumer, J.-E. Moser, S. M. Zakeeruddin, M. K. Nazeeruddin, M. Grätzel, *J. Phys. Chem. B* **2001**, *105*, 10461–10464.

[81] A. Breivogel, C. Förster, K. Heinze, *Inorg. Chem.* **2010**, *49*, 7052–7056.

[82] C. Förster, K. Mack, L. M. Carrella, V. Ksenofontov, E. Rentschler, K. Heinze, *Polyhedron* **2013**, *52*, 576–581.

[83] A. K. C. Mengel, W. Cho, A. Breivogel, K. Char, Y. S. Kang, K. Heinze, *Eur. J. Inorg. Chem.* **2015**, 3299–3306.

[84] N. C. Bruno, M. T. Tudge, S. L. Buchwald, *Chem. Sci.* **2013**, *4*, 916–920.

[85] M. D. Charles, P. Schultz, S. L. Buchwald, *Org. Lett.* **2005**, *7*, 3965–3968.

[86] A. Breivogel, M. Meister, C. Förster, F. Laquai, K. Heinze, *Chem. Eur. J.* **2013**, *19*, 13745–13760.

[87] C. Kreitner, M. Grabolle, U. Resch-Genger, K. Heinze, *Inorg. Chem.* **2014**, *53*, 12947–12961.

[88] K. Heinze, K. Hempel, *Chem. Eur. J.* **2009**, *15*, 1346–1358.

[89] G. Boschloo, A. Hagfeldt, *Acc. Chem. Res.* **2009**, *42*, 1819–1826.

[90] X. Wang, D. M. Stanbury, *Inorg. Chem.* **2006**, *45*, 3415–3423.

[91] T. L. J. Huang, D. G. Brewer, *Can. J. Chem.* **1981**, *59*, 1689–1700.

[92] Y. Liu, J. R. Jennings, Y. Huang, Q. Wang, S. M. Zakeeruddin, M. Grätzel, *J. Phys. Chem. C* **2011**, *115*, 18847–18855.

[93] D. K. Lee, K.-S. Ahn, S. Thogiti, J. H. Kim, *Dyes Pigm.* **2015**, *117*, 83–91.

[94] V. V. Pavlishchuk, A. W. Addison, *Inorg. Chim. Acta* **2000**, *298*, 97–102.

[95] I. Krivokapic, M. Zerara, M. L. Dakua, A. Vargas, C. Enachescu, C. Ambrusc, P. Tregenna-Piggott, N. Amstutz, E. Krausz, A. Hauser, *Coord. Chem. Rev.* **2007**, *251*, 364–378.

[96] M. Chavarot, Z. Pikramenou, *Tetrahedron Lett.* **1999**, *40*, 6865–6868.

[97] K. Suzuki, A. Kobayashi, S. Kaneko, K. Takehira, T. Yoshihara, H. Ishida, Y. Shiina, S. Oishi, S. Tobita, *Phys. Chem. Chem. Phys.* **2009**, *11*, 9850–9860.

[98] G. R. Fulmer, A. J. M. Miller, N. H. Sherden, H. E. Gottlieb, A. Nudelman, B. M. Stoltz, J. E. Bercaw, K. I. Goldberg, *Organometallics* **2010**, *29*, 2176–2179.

[99] N. G. Connelly, W. E. Geiger, *Chem. Rev.* **1996**, *96*, 877–910.

[100] F. Neese, *WIREs Comput. Mol. Sci.* **2012**, *2*, 73–78.

[101] F. Neese, F. Wennmohs, A. Hansen, U. Becker, *Chem. Phys.* **2009**, *356*, 98–109.

[102] R. Izsák, F. Neese, *J. Chem. Phys.* **2011**, *135*, 144105.

[103] A. D. Becke, *J. Chem. Phys.* **1993**, *98*, 5648–5652.

[104] A. Schäfer, H. Horn, R. Ahlrichs, *J. Chem. Phys.* **1992**, *97*, 2571–2577.

[105] A. Schäfer, C. Huber, R. Ahlrichs, *J. Chem. Phys.* **1994**, *100*, 5829–5835.

[106] E. van Lenthe, E. J. Baerends, J. G. Snijders, *J. Chem. Phys.* **1993**, *99*, 4597–4610.

[107] D. A. Pantazis, X.-Y. Chen, C. R. Landis, F. Neese, *J. Chem. Theory Comput.* **2008**, *4*, 908–919.

[108] S. Sinnecker, A. Rajendran, A. Klamt, M. Diedenhofen, F. Neese, *J. Phys. Chem. A* **2006**, *110*, 2235–2245.

4 Summary and Outlook

In this work, the synthesis and characterization of a series of novel heteroleptic push-pull substituted tridentate oligopyridine iron(II) complexes with a broad absorption in the visible and NIR region are presented. These are distinguished by a perfect octahedral coordination of the iron(II) center due to their six-membered chelate coordination, whereby N-Fe-N bite angles of approximately 90° were achieved for all compounds. Due the low-lying π^*-orbital of the electron withdrawing **dcpp** ligand a low-energy MLCT absorption at $\lambda_{max} = 592$ nm is obtained resulting in a deep blue color. Thanks to the electron-donating **R_2tpda** scaffold, the absorptions extend into the near-infrared region owing to transitions with considerable LL'CT character from **R_2tpda** to **dcpp**. These structural properties improve a strong ligand field. However, only the methyl-substituted complex satisfies the expectations in terms of stability in presence of water, small nucleophiles and oxygen or in electrochemical processes. Substituents **R** at **R_2tpda** larger than methyl lead to sterically induced destabilization and give no significant electronic effects to the optical spectra of the iron(II) complexes. Overall, the concept of push-pull and bite angle optimization has been successful. The electronic geometry of the metal centre could be distorted within the push-pull system. The ligand field is stabilized so that the low spin state is maintained even during oxidation. Both charge-transfer excitations are highly directional. In the oxidized state, the system shows an important metal-centered electron process that stabilizes the low spin configuration of the Fe^{3+}. By one-electron reduction of the system, the electron is located on the **dcpp** ligand. This renders the system a perfect candidate in DSSC applications by appropriate anchoring functionalization (Scheme 14). The short lifetime of the excited state $\tau = 548$ ps suggests the $^5T_2$ state close in energy to the $^3T_1$ state. This situation is typically found in second- and third-row metal complexes and gives hints for further approaches towards luminescent iron(II) complexes.

The **[Fe(dcpp) (H$_2$tpda)]$^{2+}$** complex offers the possibility of stepwise deprotonation towards the green **[Fe(dcpp)(Htpda)]$^+$** and the deep green uncharged **Fe(dcpp)(tpda)** complexes. These complexes absorb strongly in the red-NIR region (600 – 1000 nm) due to low-energy dipole-allowed LL'CT transitions from the negatively charged nitrogen atoms of the **[Htpda]$^-$** and **[tpda]$^{2-}$** ligands to the carbonyl groups of the **dcpp** ligands. These transitions, responsible for the absorption, are mainly assigned to be LL'CT transitions, which are also suitable for possible charge injection into a semiconductor such as TiO_2. Finally, these findings provide two further strategies towards iron(II)-based chromophores. One is the optimization of such dipole-allowed low-energy LL'CT transitions towards emission through low-lying ^{3}LL'CT

states instead of targeting MLCT transitions. The second strategy is to reduce the electronical symmetry via half deprotonation which decreases the ^{3}MLCT energy towards the lowest excited state. In the future, the combination of all the before mentioned strategies like *push-pull* concept, bite angel tuning, reduced geometry, carbene bonds and tridentate coordination will be the subject of the research for iron(II) chromophores (Scheme 14).

R^1 = H, Me
R^2 = H, Me
R^3 = H, Me
R^4 = H, CO$_2$H, SO$_3$H
R^5 = H, CO$_2$H, SO$_3$H
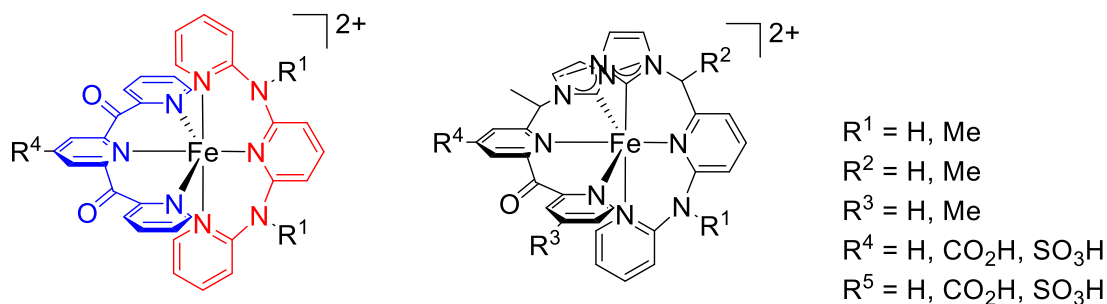
Scheme 14. Possible design concepts for iron(II) complexes with long-lived ^{3}MLCT states and usable for DSSC applications.

The concepts effecting on the structure shown here are a large bite angle of nearly 90° for an optimal orbital overlap with the coordinating atoms. Furthermore, the complex follows the *push-pull*-concept stabilizing the MLCT states by strong electron-withdrawing substitutents lowering the π*-orbitals of the acceptor ligands. The electron *push* into the metal-centre is given by an electron rich **Me$_2$tpda** ligand in combination with a strong σ-electron donating *N*-heterocyclic carbene (NHC). Additionally, the NHC ring is connected without having an electronic coupling to the acceptor ligand. The combination of the amine bridged pyridine and the two imidazole units should stabilize a MLCT and destabilize ^{3}MC states. The recently developed emitting completely by carbene coordinated iron(III) complex by Wärnmark, Persson and Sundström undersores this desing principle for earth-abundant metal emitters.

The homoleptic complexes **[Fe(R$_2$tpda)$_2$]$^{2+}$** give insights in terms of solvent-free crystallisation and structural influence at the redox potential. Although the complexes themselves should not be useful for application, the new ligands could provide an improvement to the redox mediator reported in this work. Contrary to expectations, the redox potential increased with the extension of the side chains. Actually, enhancing the +I-effect increases the electron density of the metal centre and should thereby reduce its redox potential. The attributes of boosting the redox potential and a higher solubility renders this ligand as an interesting candidate in cobalt(II,III) redox mediators in DSSC applications. Furthermore, in applications with chromium(III) metal centre the sterically demanding groups

R = nPr, nHex can shield this complex against quenching processes through oxygen and allow elongation of the NIR emission lifetimes (Scheme 15).[166]

The results of DSSC applications present several approaches to achieve improved DSSC performance. Strategies for reducing the interactions between TiO$_2$ surface and electrolyte are state of the art like finding a perfect matching dye/redox mediator/additive system.

With dye **[32]$^{2+}$** of Breivogel the positive effects of deprotonation, additives like **TBP** or LiClO$_4$ and addition of **CDCA** are demonstrated. **TBP** and LiClO$_4$ in DSSCs delivered better results in terms of efficiency and fill factor. While the addition of **CDCA** impacts positively to the cationic dye, the neutral dye delivers nearly the same performance without **CDCA**. The well-known **[Co(bpy)$_3$]$^{2+/3+}$** and the cobalt(II,III) redox mediator **[Co(Me$_2$tpda)$_2$]$^{2+/3+}$** in combination with **TBP** and Li$^+$-salt improved the open-circuit voltage and photo current as well. Lower concentration of I$^-$/I$_3^-$, addition of other additives like guanidine thiocyanate and high concentration of **CDCA** or in combination with the more sterically demanding redox mediator mentioned here, the performance of **32** dye may be increased further.
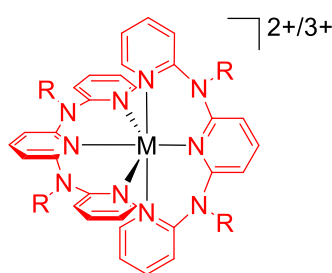
R = nPr, nHex
M = Co, Cr

Scheme 15. **[Co(Me$_2$tpda)$_2$]$^{2+/3+}$** and its possible analogue structures.

The cobalt(II,III) redox couple based on the **Me$_2$tpda** ligand used in conjunction with Breivogel dye **[32]$^{2+}$** evidenced the best performance in the series. This is suggested by the slower recombination of the **[Co(Me$_2$tpda)$_2$]$^{3+}$** complex compared to the **[Co(bpy)$_3$]$^{3+}$** and the I$_3^-$ redox mediator at the TiO$_2$ surface. The slower recombination is ascribed to the higher energy of the π*-orbitals caused by the high electron density of the **Me$_2$tpda** ligands in the Co^{3+} complex in contrast to the low energy π*-orbitals of the **bpy** ligands, which results in a higher recombination barrier for the electron recombination for **[Co(Me$_2$tpda)$_2$]$^{3+}$**. The better efficiencies imposed by cobalt(II,III) complex are due to the higher I_{SC} values which result from the higher electron density in this system. CV measurements showed lower electron transfer rates of **[Co(Me$_2$tpda)$_2$]$^{2+/3+}$** at platinum electrodes compared to the **[Co(bpy)$_3$]$^{2+/3+}$** complex. The disadvantage of the lower solubility of the **Me$_2$tpda** complex could be reduced by anion exchange of BF$_4^-$ to the weakly coordinating **BARF$^-$** anions in the test series with cyclometalated ruthenium(II) dyes. Nevertheless, the solubility of the cobalt(II,III) redox couple (0.080 M) was only less than 50 % of the **[Co(bpy)$_3$]$^{2+/3+}$** redox couple (0.165 M). Here, ligand exchange by **Pr$_2$tpda** or the **Hex$_2$tpda** might be an option. These findings will

pave the way for further developments of novel redox mediators up to setups with polymer gels or solid state devices with the redox couple as part of a conducting polymers. [167]

Finally, a series of three cyclometallated dyes as well as their saponified counterparts based on a **[Ru(dbp-X)(tctpy)]$^{2-}$** (**H$_3$tctpy** = 2,2';6',2''-terpyridine-4,4',4''-tricarboxylic acid; **dpbH** = 1,3-dipyridylbenzene; X = N(4-C$_6$H$_4$OMe)$_2$, NPh$_2$, N-carbazolyl) scaffold synthesized by Dr. C. Kreitner are presented in DSSC applications. The saponification of the dyes affects the redox potentials and the absorption as the degree of delocalization is reduced compared to the ester functionalized complexes, which have a higher electron density at the metal centre. Concomitantly, all redox potentials shift to substantially lower values. Here, the principle of a strong charge delocalization should be beneficial for applications in DSSC which shall prevent fast charge recombination.

With respect to the DSSC performance, the dyes deliver the opposite of the expected order. The strongest donor N(4-C$_6$H$_4$OMe)$_2$ substituted dye achieves the lowest performance in the best setup with I$^-$/I$_3^-$ redox couple by addition of **CDCA** and additives with $\eta = 1.2$ %, followed by the NPh$_2$ substituted with $\eta = 2.4$ % and ending with the carbazolyl one with up $\eta = 2.5$ %, but still not reaching the reference dye **N719** with up to $\eta = 7.3$ %. Reducing the concentration of the I$^-$/I$_3^-$ redox couple down to 0.1 M **MPII** and 0.02 M iodide, the carbazolyl dye gives the highest efficiency of all tested dyes with $\eta = 3.3$ %, coming closer to the result of **N719** with $\eta = 5.8$ %. The reason for the poor performance of the dyes is most likely due to the low redox potentials, which result from the large resonance stabilization. This poses a challenge in the selection of a suitable redox electrolyte for efficient dye regeneration. These findings can be seen in the order of the DSSC performance.

In contrast to the cells containing the I$^-$/I$_3^-$ electrolyte, cells employing the cobalt(II,III) electrolyte **[45]$^{2+/3+}$** deliver all lower efficiencies. Here, the efficiencies are between $\eta = <0.1$ % for the N(4-C$_6$H$_4$OMe)$_2$ substituted one, $\eta = 0.9$ % for the NPh$_2$ and $\eta = 1.4$ % by the cabarzolyl-substituted dye. The cabarzolyl-substituted dye exceeds **N719** ($\eta = 1.1$ %) in the terms of efficiency and fill factor under these conditions. As for the I$^-$/I$_3^-$ electrolyte the cells suffer from the low redox potentials of the dyes. For **N719**, the slow recombination of the cobalt redox couples is responsible for the weak performance. Despite the high V_{OC}, the low I_{SC} through the slow recombination reduces the overall efficiency.

This result confirms that in the case of SCN-based sensitizers, iodide is still the best redox partner since they perform well by rapid recombination. Cobalt(II,III) electrolytes offer an interesting alternative for the thiocyanate-free dyes. Nevertheless, not always high

concentrations of redox mediator deliver the best performance in a DSSC, which should be taken into account for future studies.

5 Appendix

The Supporting Information of all publications is inset on the following pages.

CHEMISTRY

A European Journal

Supporting Information

A Heteroleptic Push–Pull Substituted Iron(II) Bis(tridentate) Complex with Low-Energy Charge-Transfer States

Andreas K. C. Mengel,[a] Christoph Förster,[a] Aaron Breivogel,[a] Katharina Mack,[a] Julian R. Ochsmann,[b] Frédéric Laquai,[b] Vadim Ksenofontov,[a] and Katja Heinze*[a]

chem_201404955_sm_miscellaneous_information.pdf

Supporting Information

Table S1. ^{1}H, ^{13}C and ^{15}N NMR data of **1(PF$_6$)$_2$**, **2(PF$_6$)$_2$** and **3(PF$_6$)$_2$**.

	1$^{2+[a]}$	**2$^{2+[a]}$**	**3$^{2+[a]}$**
H1		8.48 (t, $^3J_{HH}$ = 7.7 Hz, 1H)	8.58 (t, $^3J_{HH}$ = 8.0 Hz, 2H)
H2		8.32 (d, $^3J_{HH}$ = 7.7 Hz, 2H)	8.35 (d, $^3J_{HH}$ = 8.0 Hz, 4H)
H6		8.13 (m, 2H)	8.07 (m, 4H)
H7		8.15 (m, 2H)	8.20 (m,4H)
H8		7.27 (m, 2H)	7.33 (m, 4H)
H9		7.67 (d, $^3J_{HH}$ = 5.7 Hz, 2H)	7.51 (d, $^3J_{HH}$ = 5.6 Hz, 4H)
H10	7.08 (m, 4H)	6.57 (d, $^3J_{HH}$ = 6.0 Hz, 2H)	
H11	6.75 (m, 4H)	6.75 (dd, $^3J_{HH}$ = 7.0/6.0 Hz, 2H)	
H12	7.80 (m, 4H)	7.86 (dd, $^3J_{HH}$ = 8.6/7.0 Hz, 2H)	
H13	7.11 (m, 4H)	7.08 (d, $^3J_{HH}$ = 8.6 Hz, 2H)	
H15	2.98 (s, 12H)	2.90 (s, 6H)	
H17	7.12 (d, $^3J_{HH}$ = 8.0 Hz, 4H)	7.31 (d, $^3J_{HH}$ = 8.1 Hz, 2H)	
H18	7.96 (t, $^3J_{HH}$ = 8.0 Hz, 2H)	8.20 (t, $^3J_{HH}$ = 8.1 Hz, 1H)	
C1		138.64 [b]	141.44 [b]
C2		130.09 [b]	131.32 [b]
C3		160.28 [b]	158.78 [b]
C4		180.02 [b]	181.08 [b]
C5		158.50 [b]	159.17 [b]
C6		126.64 [b]	128.00 [b]
C7		139.01 [b]	140.86 [b]
C8		126.60 [b]	128.83 [b]
C9		157.38 [b]	161.38 [b]
C10	155.60	156.12 [b]	
C11	120.80	120.58 [b]	
C12	140.20	140.39 [b]	
C13	113.10	112.76 [b]	
C14	162.40	160.03 [b]	
C15	39.80	39.39 [b]	
C16	159.30	156.13 [b]	
C17	112.20	112.08 [b]	
C18	140.90	141.20 [b]	
Na	222.9	210.9 [b]	
Nb	100.3	102.7 [b]	
Nc	229.2	214.8 [b]	
Nd		261.5 [b]	247.9
Ne		272.2 [b]	256.2

[a] in CD$_3$CN. [b] in d$_6$-DMSO.

Table S2. Crystal and structure refinement data for **$1(PF_6)_2 \times CH_3CN$** and **$1(BF_4)_2 \times 2CH_3CN$**.

	$1(PF_6)_2 \times CH_3CN$	**$1(BF_4)_2 \times 2CH_3CN$**
Empirical formula	$C_{36}H_{37}F_{12}FeN_{11}P_2$	$C_{38}H_{40}B_2F_8FeN_{12}$
Formula weight	969.56	894.29
Crystal color, habit	brown block	red block
Crystal dimensions / mm	$0.36 \times 0.34 \times 0.12$	$0.31 \times 0.29 \times 0.25$
Crystal system	monoclinic	orthorhombic
Space group	$P2_1/c$	Fddd
a / Å	14.7922(5)	13.9995(4)
b / Å	19.6954(7)	21.2940(6)
c / Å	15.9366(4)	26.4582(7)
α / °	90	90
β / °	122.534(2)	90
γ / °	90	90
V / Å^3	3914.3(2)	7887.3(4)
Z	4	8
$F(000)$	1976	3680
Density (calcd) / g cm^{-3}	1.645	1.506
Absorption coefficient μ / mm^{-1}	0.570 (MULABS)	0.468 (MULABS)
Theta range / °	2.56 – 27.89	2.46 – 27.99
Index ranges	$-19 \leq h \leq 19$	$-18 \leq h \leq 18$
	$-25 \leq k \leq 25$	$-28 \leq k \leq 28$
	$-20 \leq l \leq 20$	$-34 \leq l \leq 34$
Reflections collected	77490	27331
Independent reflections	9314 ($R_{int} = 0.0872$)	2390 ($R_{int} = 0.0615$)
Observed reflections	9314	2390
Parameters	617	166
Max. / min. transmission	0.9347 / 0.8210	0.8920 / 0.8685
Goodness-of-fit on F^2	0.887	1.059
Largest difference peak and hole / e Å^{-3}	0.670 / –0.849	0.543 / –0.732
R_1 ($I>2\sigma(I)$)	0.0383	0.0451
R_1 (all data)	0.0785	0.0555
wR_2 ($I>2\sigma(I)$)	0.0854	0.1133
wR_2 (all data)	0.0970	0.1202

2

Table S3. Crystal and structure refinement data for **2(PF₆)₂×CH₃CN** and **3(PF₆)₂×½CH₃CN**.

	2(PF₆)₂×CH₃CN	**3(PF₆)₂×½CH₃CN**
Empirical formula	$C_{36}H_{31}F_{12}FeN_9O_2P_2$	$C_{35}H_{23.5}F_{12}FeN_{6.5}O_4P_2$
Formula weight	967.49	944.89
Crystal color, habit	brown needle	brown needle
Crystal dimensions / mm	$0.36 \times 0.34 \times 0.12$	$0.78 \times 0.07 \times 0.06$
Crystal system	orthorhombic	orthorhombic
Space group	$Pbca$	$Pbcn$
a / Å	22.170(16)	21.1443(18)
b / Å	15.285(11)	21.5947(19)
c / Å	22.317(17)	15.5538(14)
α / °	90	90
β / °	90	90
γ / °	90	90
V / Å³	7563(10)	7101.9(11)
Z	8	8
$F(000)$	3920	3800
Density (calcd) / g cm⁻³	1.699	1.767
Absorption coefficient μ / mm⁻¹	0.593 (MULABS)	0.631 (MULABS)
Theta range / °	1.83 – 28.29	2.30 – 27.99
Index ranges	$-25 \leq h \leq 29$	$-27 \leq h \leq 27$
	$-19 \leq k \leq 20$	$-28 \leq k \leq 28$
	$-29 \leq l \leq 29$	$-20 \leq l \leq 20$
Reflections collected	38083	67623
Independent reflections	9220 ($R_{int} = 0.1687$)	8554 ($R_{int} = 0.1515$)
Observed reflections	9220	8554
Parameters	739	545
Max. / min. transmission	0.9060 / 0.7287	0.9631 / 0.6388
Goodness-of-fit on F^2	0.990	0.981
Largest difference peak and hole / e Å⁻³	0.718 / −1.047	1.121 / −1.678
R_1 ($I>2\sigma(I)$)	0.0888	0.0904
R_1 (all data)	0.1648	0.1740
wR_2 ($I>2\sigma(I)$)	0.2361	0.2533
wR_2 (all data)	0.2768	0.3006

Figure S1. ^{1}H NMR spectrum of the reaction mixture of dcpp, ddpd and FeBr$_2$ after precipitating with Et$_2$O and redissolving in CD$_3$CN.
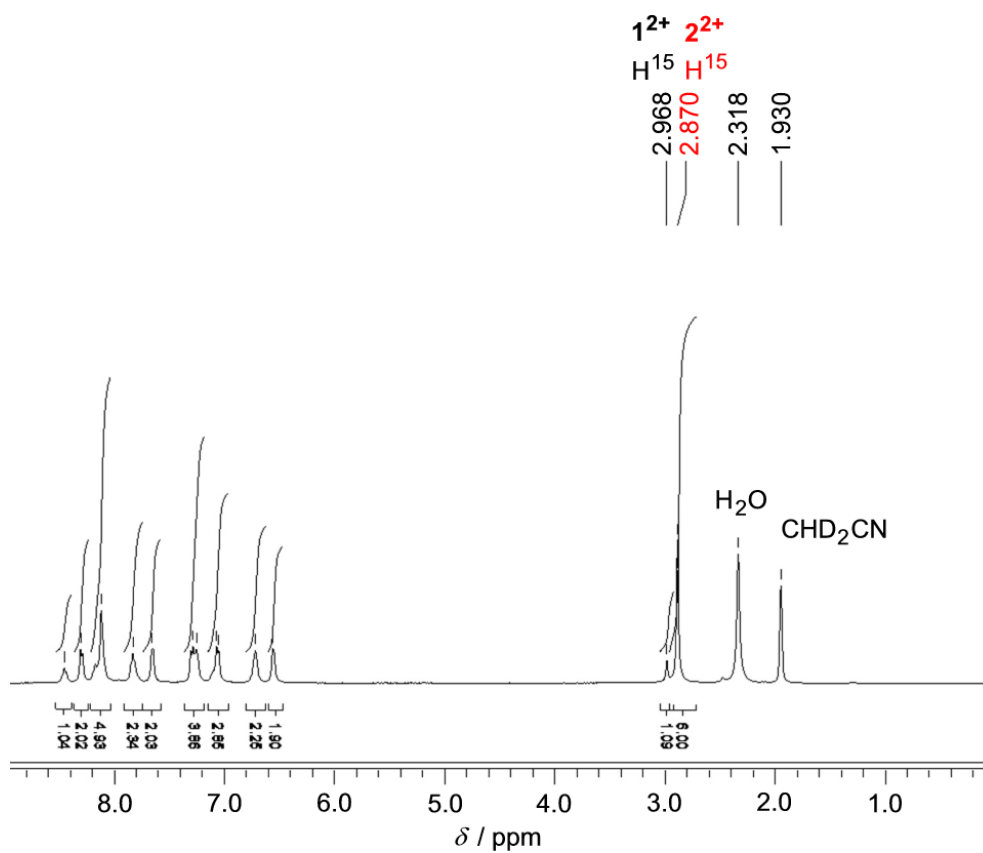
Figure S2. DFT (B3LYP, LANL2DZ, IEFPCM CH$_3$CN) calculated geometries of **1^{2+} – 3^{2+}** in their singlet ground states; Fe-N bond distances indicated in Å.
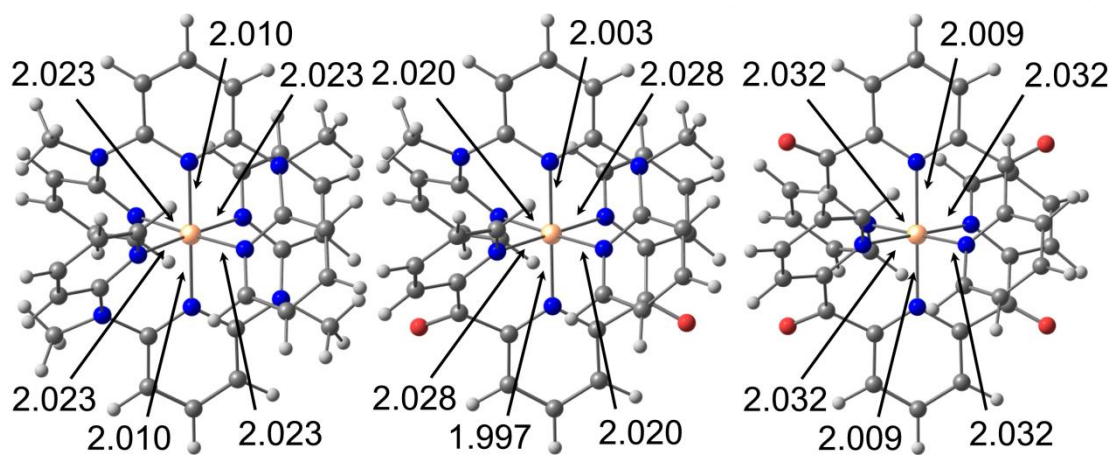
Figure S3. Mößbauer spectra of **1(PF$_6$)$_2$** − **3(PF$_6$)$_2$** at 295 K.
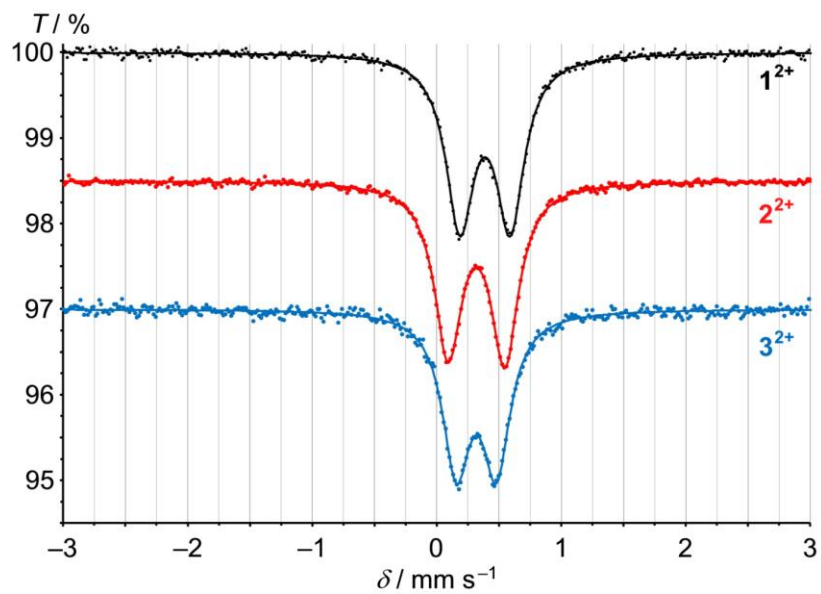
Figure S4. DFT calculated spin densities of **1³⁺**, **2³⁺** and **3³⁺** (B3LYP, LANL2DZ, IEFPCM CH₃CN, isosurface value 0.002 a.u.).
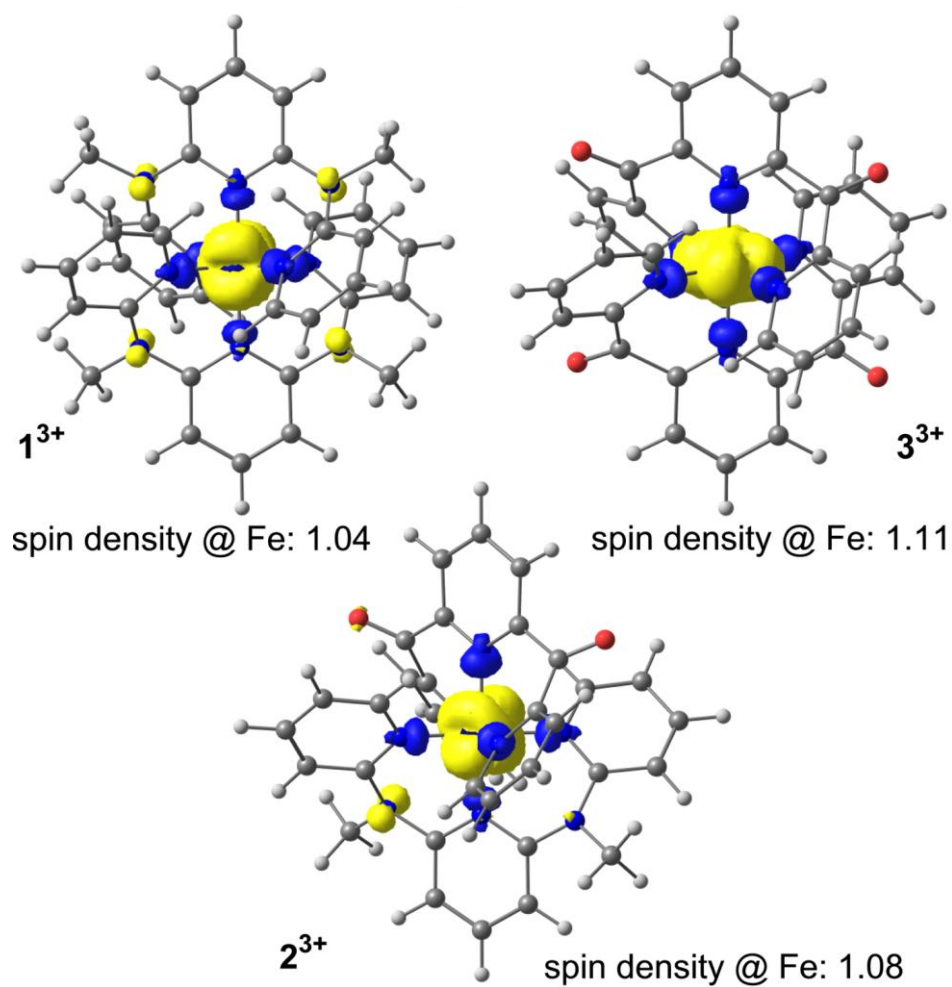
Figure S5. Mößbauer spectra of **1**$^{3+}$ and **2**$^{3+}$ at 295 K.
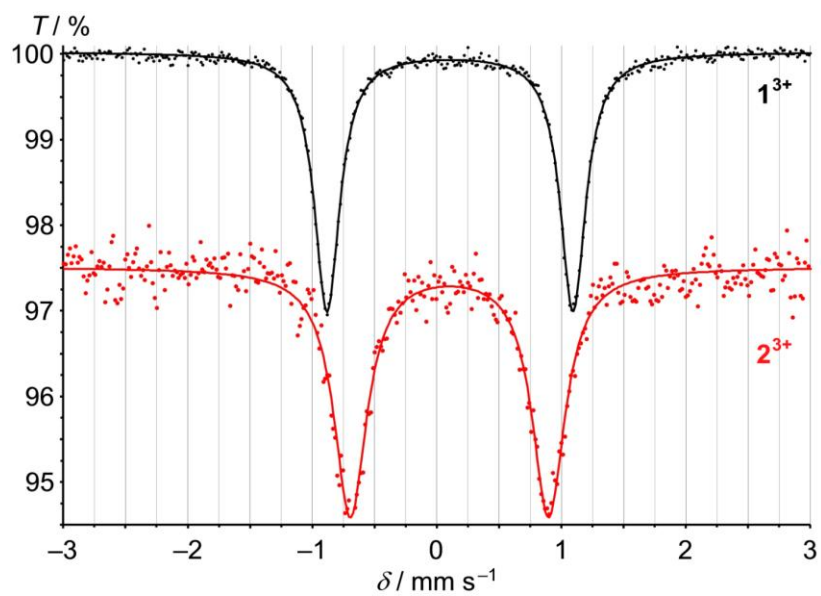
Figure S6. UV/Vis spectrum of $\mathbf{1}^{3+}$ in H_2O.
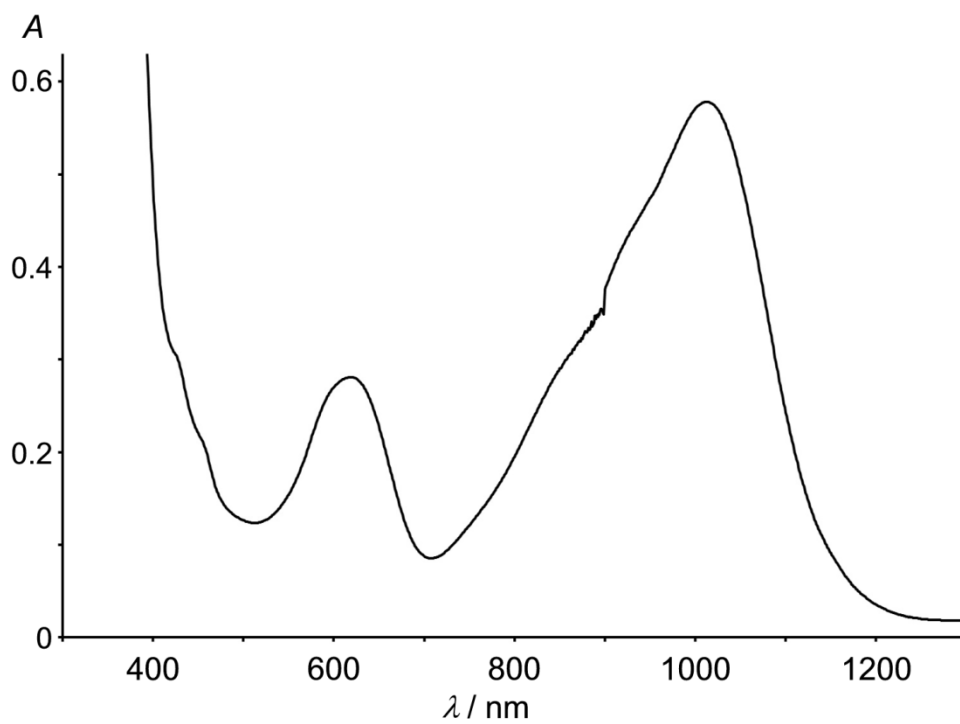
Figure S7. UV/Vis spectroscopic monitoring of the oxidation of **2**$^{2+}$ with CAN in TFA/CH$_3$CN.
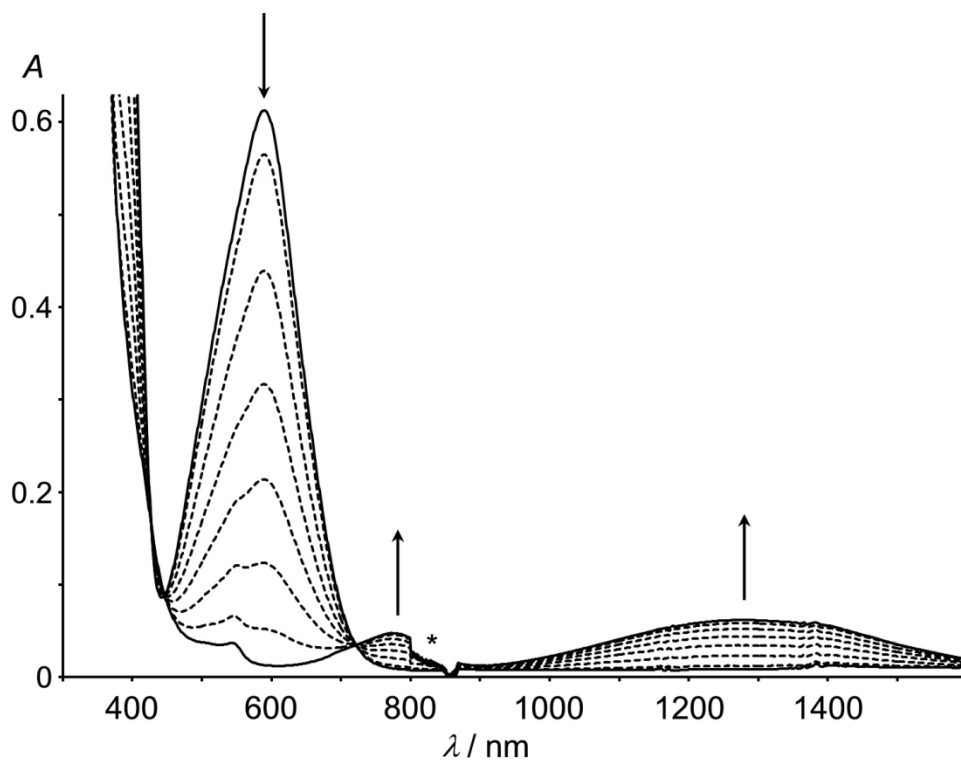
* denotes an artifact from the spectrometer/detector.

Figure S8. TD-DFT derived UV/Vis stick spectrum of **1**[3+] and relevant molecular orbitals (isosurface value 0.07 a.u.).
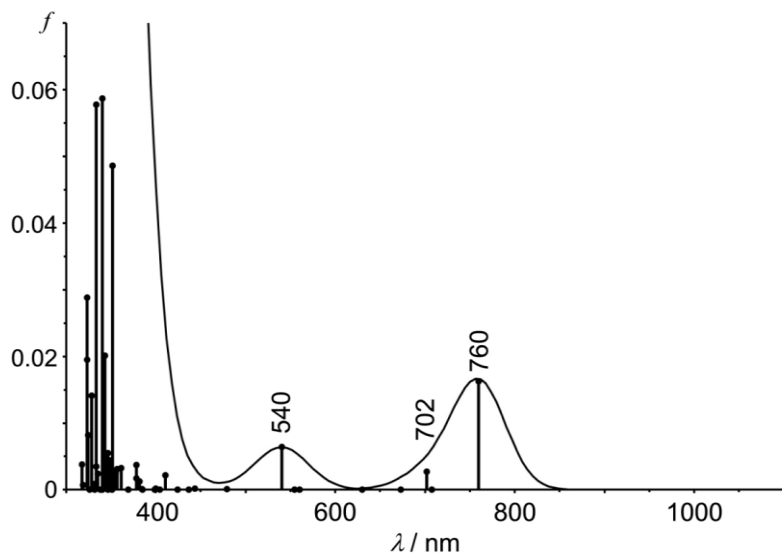

```
Excited State   3:  2.142-A      1.6322 eV  759.61 nm  f=0.0163  <S**2>=0.897
    146B ->161B         0.12783
    155B ->161B         0.24878
    160B ->161B         0.95126
Excited State   5:  2.139-A      1.7665 eV  701.86 nm  f=0.0027  <S**2>=0.894
    159B ->161B         0.99581
Excited State  10:  2.130-A      2.2953 eV  540.16 nm  f=0.0064  <S**2>=0.885
    158B ->161B         0.98803
```


158B	159B	160B
161B		
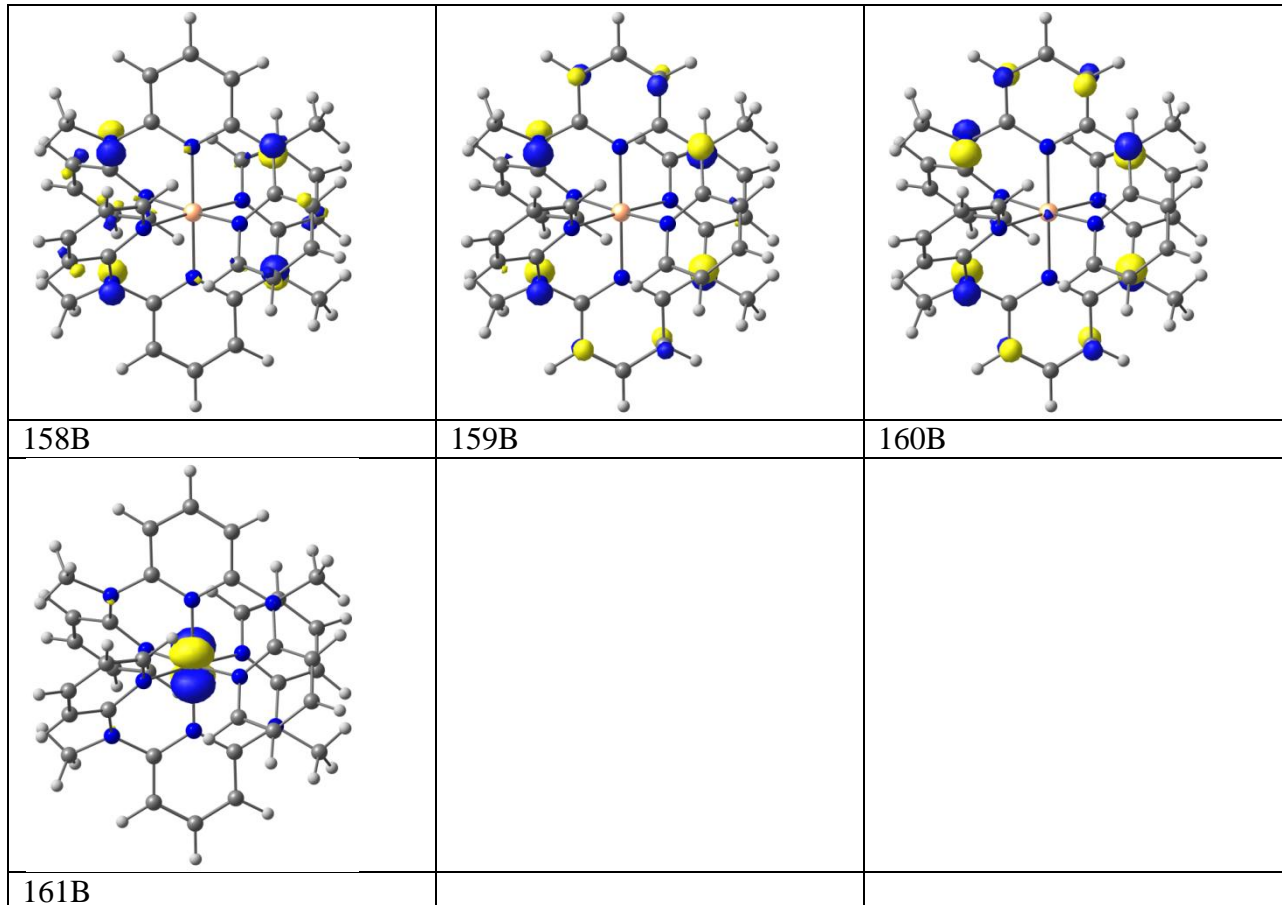
Figure S9. TD-DFT derived UV/Vis stick spectrum of **2^{3+}** and relevant molecular orbitals (isosurface value 0.07 a.u.).


```
Excited State   3:  2.212-A      1.2928 eV  959.02 nm  f=0.0075  <S**2>=0.973
    152B ->159B        0.11169
    158B ->159B        0.96991
Excited State   5:  2.358-A      1.8603 eV  666.46 nm  f=0.0024  <S**2>=1.141
    152B ->162B       -0.14132
    157B ->159B        0.92225
```


| 157B | 158B | 159B |
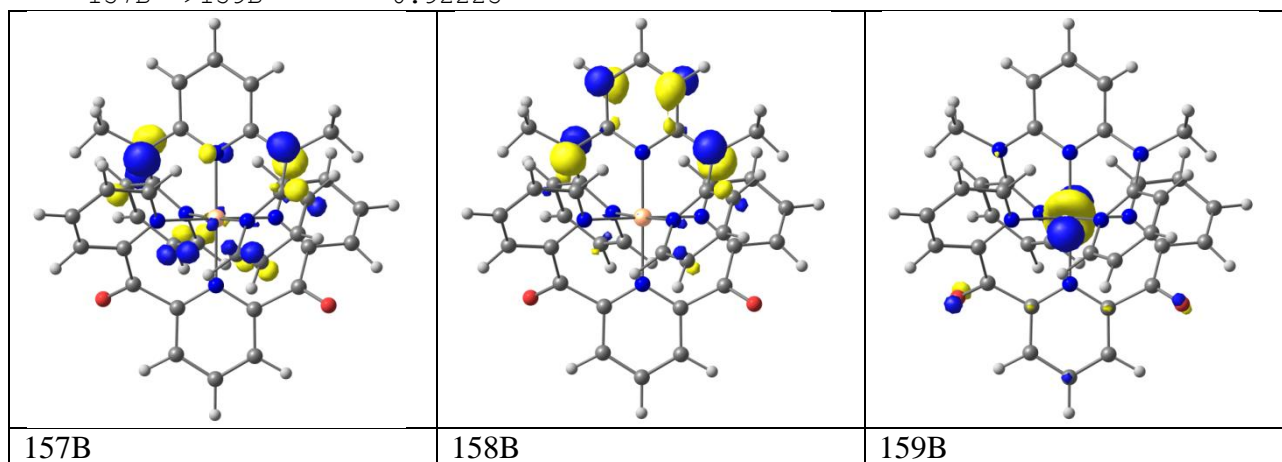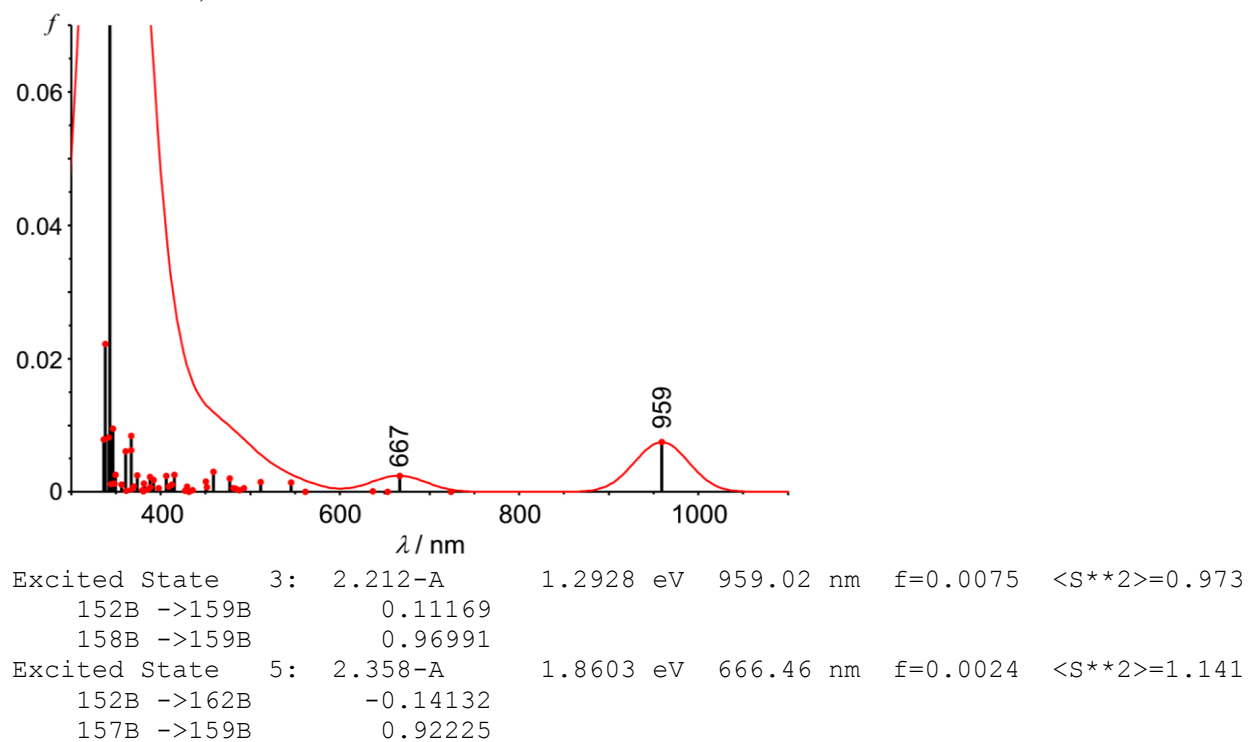
Figure S10. DFT calculated spin densities of **2⁺** and **3⁺** (B3LYP, LANL2DZ, IEFPCM CH$_3$CN, isosurface value 0.008 a.u.).
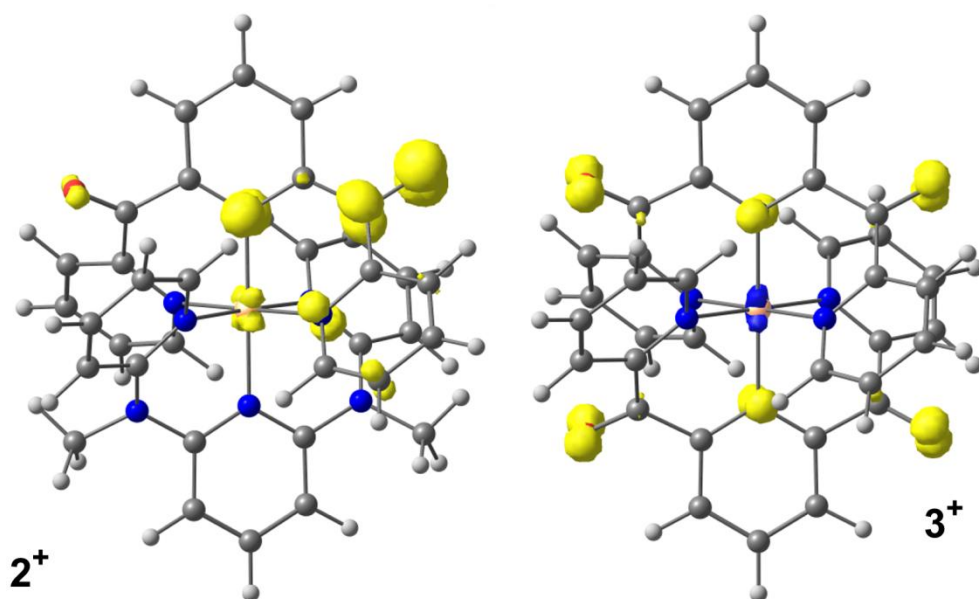
Cartesian Coordinates of optimized geometries

1^{2+} (singlet)

```
6     -1.155845000    -2.712171000     0.241512000
6     -1.182498000    -4.122267000     0.243360000
6     -0.000076000    -4.827514000    -0.000819000
6      1.182369000    -4.122223000    -0.244766000
6      1.155761000    -2.712127000    -0.242452000
7     -0.000031000    -2.010335000    -0.000353000
1     -2.099470000    -4.650570000     0.465520000
1      2.099326000    -4.650481000    -0.467095000
6     -1.408989000     0.908768000     2.433396000
6     -2.444294000     1.055155000     3.355065000
6     -3.538140000     0.168738000     3.276138000
6     -3.524035000    -0.844706000     2.314270000
6     -2.424427000    -0.949254000     1.424203000
7     -1.405068000    -0.044516000     1.454072000
1     -4.370711000     0.248724000     3.968358000
1     -0.556845000     1.573491000     2.451586000
1     -2.396231000     1.838436000     4.102844000
1     -4.328941000    -1.566690000     2.276096000
6      2.424403000    -0.948843000    -1.424533000
6      3.524018000    -0.844017000    -2.314558000
6      3.538146000     0.169750000    -3.276085000
6      2.444318000     1.056214000    -3.354720000
6      1.409008000     0.909541000    -2.433102000
7      1.405067000    -0.044067000    -1.454093000
1      4.370722000     0.249952000    -3.968274000
1      4.328909000    -1.566031000    -2.276621000
1      2.396272000     1.839743000    -4.102239000
1      0.556877000     1.574287000    -2.451076000
6     -1.155745000     2.712213000    -0.241511000
6     -1.182340000     4.122309000    -0.243394000
6      0.000118000     4.827514000     0.000739000
6      1.182538000     4.122181000     0.244679000
6      1.155872000     2.712085000     0.242403000
7      0.000046000     2.010334000     0.000343000
1     -2.099296000     4.650643000    -0.465547000
1      2.099520000     4.650407000     0.466976000
6     -1.409085000    -0.908718000    -2.433363000
6     -2.444433000    -1.055085000    -3.354988000
6     -3.538256000    -0.168644000    -3.276014000
6     -3.524088000     0.844804000    -2.314152000
6     -2.424438000     0.949333000    -1.424135000
7     -1.405102000     0.044569000    -1.454042000
1     -4.370861000    -0.248617000    -3.968196000
1     -0.556957000    -1.573461000    -2.451586000
1     -2.396419000    -1.838368000    -4.102767000
1     -4.328977000     1.566804000    -2.275945000
6      2.424456000     0.948763000     1.424492000
6      3.524069000     0.843917000     2.314518000
6      3.538175000    -0.169845000     3.276051000
6      2.444327000    -1.056284000     3.354690000
6      1.409019000    -0.909590000     2.433074000
7      1.405097000     0.044014000     1.454062000
1      4.370749000    -0.250062000     3.968241000
1      4.328976000     1.565913000     2.276577000
1      2.396264000    -1.839809000     4.102213000
1      0.556871000    -1.574314000     2.451055000
7     -2.360487000     2.015598000    -0.504481000
6     -3.631520000     2.678491000    -0.125685000
1     -3.989271000     3.390510000    -0.881316000
1     -4.397333000     1.914621000     0.029145000
1     -3.488270000     3.208037000     0.818290000
```

14

```
7        2.360574000       2.015336000       0.505186000
6        3.631645000       2.678295000       0.126630000
1        3.989386000       3.390090000       0.882475000
1        4.397439000       1.914444000      -0.028388000
1        3.488447000       3.208111000      -0.817201000
7       -2.360550000      -2.015512000       0.504533000
7        2.360489000      -2.015423000      -0.505239000
6       -3.631623000      -2.678347000       0.125769000
1       -3.989372000      -3.390372000       0.881394000
1       -4.397412000      -1.914444000      -0.029012000
1       -3.488428000      -3.207873000      -0.818226000
6        3.631537000      -2.678436000      -0.126702000
1        3.989249000      -3.390229000      -0.882562000
1        4.397360000      -1.914617000       0.028329000
1        3.488324000      -3.208266000       0.817119000
1       -0.000092000      -5.912792000      -0.000994000
1        0.000147000       5.912792000       0.000885000
26       0.000005000       0.000000000      -0.000001000
```

2^{2+} (singlet)

```
6        1.159755000      -2.654028000      -0.224258000
6        1.185170000      -4.062912000      -0.225271000
6       -0.001503000      -4.766847000       0.001046000
6       -1.187688000      -4.062032000       0.227159000
6       -1.161309000      -2.653157000       0.225745000
7       -0.000537000      -1.952994000       0.000629000
1        2.104104000      -4.592986000      -0.433251000
1       -2.106981000      -4.591431000       0.435263000
6        1.428406000       0.957321000      -2.427163000
6        2.466191000       1.092441000      -3.344613000
6        3.562962000       0.210086000      -3.247575000
6        3.546690000      -0.794061000      -2.276965000
6        2.443280000      -0.894488000      -1.392362000
7        1.425211000       0.015964000      -1.430576000
1        4.399219000       0.285909000      -3.935412000
1        0.573343000       1.617835000      -2.462446000
1        2.420222000       1.865148000      -4.102958000
1        4.353076000      -1.513303000      -2.228776000
6       -2.443608000      -0.892136000       1.392992000
6       -3.546813000      -0.790619000       2.277725000
6       -3.562449000       0.214171000       3.247685000
6       -2.465271000       1.096103000       3.343922000
6       -1.427692000       0.959878000       2.426400000
7       -1.425076000       0.017818000       1.430475000
1       -4.398547000       0.290832000       3.935621000
1       -4.353538000      -1.509519000       2.230154000
1       -2.418831000       1.869320000       4.101719000
1       -0.572335000       1.620041000       2.461081000
6        1.157502000       2.753790000       0.176635000
6        1.194257000       4.161495000       0.151350000
6        0.001225000       4.881134000      -0.001724000
6       -1.192149000       4.161952000      -0.154299000
6       -1.156069000       2.754210000      -0.178657000
7        0.000551000       2.046636000      -0.000765000
1        2.147117000       4.662271000       0.273211000
1       -2.144766000       4.663103000      -0.276504000
6        1.358500000      -0.876136000       2.465509000
6        2.377263000      -1.007060000       3.419999000
6        3.497706000      -0.161522000       3.348886000
6        3.532856000       0.814584000       2.340937000
6        2.457823000       0.909839000       1.437233000
7        1.392648000       0.054596000       1.473681000
1        4.309808000      -0.249218000       4.062859000
1        0.500634000      -1.532354000       2.488582000
```

15

```
1       2.286950000    -1.763858000    4.191156000
1       4.357128000     1.512874000    2.254453000
6      -2.457421000     0.909822000   -1.437766000
6      -3.532701000     0.814120000   -2.341121000
6      -3.498060000    -0.162807000   -3.348297000
6      -2.377866000    -1.008705000   -3.419007000
6      -1.358865000    -0.877330000   -2.464830000
7      -1.392540000     0.054187000   -1.473729000
1      -4.310354000    -0.250845000   -4.062011000
1      -4.356736000     1.512738000   -2.255033000
1      -2.287949000    -1.766150000   -4.189575000
1      -0.501230000    -1.533866000   -2.487517000
7       2.368433000    -1.954644000   -0.469161000
7      -2.369495000    -1.952836000    0.470326000
6       3.635841000    -2.628935000   -0.089916000
1       3.986092000    -3.341816000   -0.847420000
1       4.406999000    -1.871353000    0.066503000
1       3.487346000    -3.158877000    0.852848000
6      -3.637383000    -2.626346000    0.091295000
1      -3.988200000    -3.338670000    0.849059000
1      -4.407968000    -1.868255000   -0.065459000
1      -3.489239000    -3.156760000   -0.851262000
1      -0.001881000    -5.851913000    0.001189000
1       0.001480000     5.965429000   -0.002103000
26      0.000067000     0.049715000   -0.000050000
6      -2.455259000     2.059779000   -0.483328000
6       2.456321000     2.058892000    0.481715000
8       3.535328000     2.567737000    0.093251000
8      -3.533941000     2.568392000   -0.093666000
```

3²⁺ (singlet)

3^{2+} (singlet)

```
6       1.159755000    -2.654028000   -0.224258000
6       1.185170000    -4.062912000   -0.225271000
6      -0.001503000    -4.766847000    0.001046000
6      -1.187688000    -4.062032000    0.227159000
6      -1.161309000    -2.653157000    0.225745000
7      -0.000537000    -1.952994000    0.000629000
1       2.104104000    -4.592986000   -0.433251000
1      -2.106981000    -4.591431000    0.435263000
6       1.428406000     0.957321000   -2.427163000
6       2.466191000     1.092441000   -3.344613000
6       3.562962000     0.210086000   -3.247575000
6       3.546690000    -0.794061000   -2.276965000
6       2.443280000    -0.894488000   -1.392362000
7       1.425211000     0.015964000   -1.430576000
1       4.399219000     0.285909000   -3.935412000
1       0.573343000     1.617835000   -2.462446000
1       2.420222000     1.865148000   -4.102958000
1       4.353076000    -1.513303000   -2.228776000
6      -2.443608000    -0.892136000    1.392992000
6      -3.546813000    -0.790619000    2.277725000
6      -3.562449000     0.214171000    3.247685000
6      -2.465271000     1.096103000    3.343922000
6      -1.427692000     0.959878000    2.426400000
7      -1.425076000     0.017818000    1.430475000
1      -4.398547000     0.290832000    3.935621000
1      -4.353538000    -1.509519000    2.230154000
1      -2.418831000     1.869320000    4.101719000
1      -0.572335000     1.620041000    2.461081000
6       1.157502000     2.753790000    0.176635000
6       1.194257000     4.161495000    0.151350000
6       0.001225000     4.881134000   -0.001724000
6      -1.192149000     4.161952000   -0.154299000
6      -1.156069000     2.754210000   -0.178657000
```

```
7       0.000551000      2.046636000     -0.000765000
1       2.147117000      4.662271000      0.273211000
1      -2.144766000      4.663103000     -0.276504000
6       1.358500000     -0.876136000      2.465509000
6       2.377263000     -1.007060000      3.419999000
6       3.497706000     -0.161522000      3.348886000
6       3.532856000      0.814584000      2.340937000
6       2.457823000      0.909839000      1.437233000
7       1.392648000      0.054596000      1.473681000
1       4.309808000     -0.249218000      4.062859000
1       0.500634000     -1.532354000      2.488582000
1       2.286950000     -1.763858000      4.191156000
1       4.357128000      1.512874000      2.254453000
6      -2.457421000      0.909822000     -1.437766000
6      -3.532701000      0.814120000     -2.341121000
6      -3.498060000     -0.162807000     -3.348297000
6      -2.377866000     -1.008705000     -3.419007000
6      -1.358865000     -0.877330000     -2.464830000
7      -1.392540000      0.054187000     -1.473729000
1      -4.310354000     -0.250845000     -4.062011000
1      -4.356736000      1.512738000     -2.255033000
1      -2.287949000     -1.766150000     -4.189575000
1      -0.501230000     -1.533866000     -2.487517000
7       2.368433000     -1.954644000     -0.469161000
7      -2.369495000     -1.952836000      0.470326000
6       3.635841000     -2.628935000     -0.089916000
1       3.986092000     -3.341816000     -0.847420000
1       4.406999000     -1.871353000      0.066503000
1       3.487346000     -3.158877000      0.852848000
6      -3.637383000     -2.626346000      0.091295000
1      -3.988200000     -3.338670000      0.849059000
1      -4.407968000     -1.868255000     -0.065459000
1      -3.489239000     -3.156760000     -0.851262000
1      -0.001881000     -5.851913000      0.001189000
1       0.001480000      5.965429000     -0.002103000
26      0.000067000      0.049715000     -0.000050000
6      -2.455259000      2.059779000     -0.483328000
6       2.456321000      2.058892000      0.481715000
8       3.535328000      2.567737000      0.093251000
8      -3.533941000      2.568392000     -0.093666000
```

1^{3+} (doublet)

```
6       1.171563000      2.687327000      0.206609000
6       1.191491000      4.093545000      0.197435000
6       0.000089000      4.796109000     -0.000829000
6      -1.191344000      4.093530000     -0.198862000
6      -1.171476000      2.687309000     -0.207555000
7       0.000027000      1.983594000     -0.000346000
1       2.112832000      4.624924000      0.387644000
1      -2.112664000      4.624882000     -0.389248000
6       1.379500000     -0.885082000      2.431579000
6       2.417005000     -1.033103000      3.343750000
6       3.534588000     -0.177508000      3.235341000
6       3.543261000      0.815135000      2.254879000
6       2.439639000      0.936387000      1.374164000
7       1.399572000      0.055304000      1.432702000
1       4.368964000     -0.266119000      3.923427000
1       0.513154000     -1.528110000      2.475163000
1       2.354310000     -1.797011000      4.109259000
1       4.366954000      1.513059000      2.196831000
6      -2.439602000      0.936019000     -1.374527000
6      -3.543177000      0.814547000     -2.255272000
6      -3.534535000     -0.178461000     -3.235363000
6      -2.417022000     -1.034193000     -3.343389000
```

```
6      -1.379547000     -0.885913000     -2.431225000
7      -1.399593000      0.054842000     -1.432699000
1      -4.368877000     -0.267254000     -3.923465000
1      -4.366813000      1.512565000     -2.197525000
1      -2.354352000     -1.798393000     -4.108608000
1      -0.513256000     -1.529034000     -2.474529000
6       1.171451000     -2.687379000     -0.206613000
6       1.191308000     -4.093597000     -0.197495000
6      -0.000134000     -4.796108000      0.000716000
6      -1.191535000     -4.093478000      0.198749000
6      -1.171597000     -2.687258000      0.207498000
7      -0.000054000     -1.983594000      0.000346000
1       2.112627000     -4.625014000     -0.387710000
1      -2.112886000     -4.624793000      0.389091000
6       1.379600000      0.885061000     -2.431498000
6       2.417141000      1.033066000     -3.343631000
6       3.534687000      0.177425000     -3.235208000
6       3.543290000     -0.815243000     -2.254770000
6       2.439639000     -0.936470000     -1.374089000
7       1.399606000     -0.055347000     -1.432641000
1       4.369089000      0.266021000     -3.923264000
1       0.513282000      1.528127000     -2.475092000
1       2.354500000      1.796995000     -4.109123000
1       4.366954000     -1.513201000     -2.196713000
6      -2.439662000     -0.935936000      1.374496000
6      -3.543246000     -0.814439000      2.255226000
6      -3.534576000      0.178542000      3.235343000
6      -2.417031000      1.034227000      3.343406000
6      -1.379552000      0.885932000      2.431249000
7      -1.399621000     -0.054800000      1.432701000
1      -4.368925000      0.267351000      3.923437000
1      -4.366910000     -1.512421000      2.197451000
1      -2.354340000      1.798405000      4.108646000
1      -0.513233000      1.529014000      2.474585000
7       2.375781000     -1.996113000     -0.453799000
6       3.647840000     -2.675156000     -0.087370000
1       3.987604000     -3.380370000     -0.855291000
1       4.418500000     -1.918124000      0.069977000
1       3.504939000     -3.209353000      0.853051000
7      -2.375882000     -1.995852000      0.454509000
6      -3.647986000     -2.674908000      0.088270000
1      -3.987739000     -3.379977000      0.856330000
1      -4.418623000     -1.917872000     -0.069161000
1      -3.505155000     -3.209275000     -0.852068000
7       2.375852000      1.996005000      0.453838000
7      -2.375792000      1.995961000     -0.454575000
6       3.647954000      2.674950000      0.087381000
1       3.987758000      3.380185000      0.855265000
1       4.418568000      1.917862000     -0.069921000
1       3.505093000      3.209103000     -0.853072000
6      -3.647867000      2.675119000     -0.088423000
1      -3.987541000      3.380171000     -0.856531000
1      -4.418562000      1.918141000      0.069012000
1      -3.505040000      3.209524000      0.851894000
1       0.000112000      5.880811000     -0.001009000
1      -0.000166000     -5.880811000      0.000849000
26     -0.000015000      0.000000000      0.000013000
```

2^{3+} (doublet)

```
6       1.125444000     -2.664402000     -0.190294000
6       1.117955000     -4.068965000     -0.189193000
6      -0.084769000     -4.750934000      0.017905000
6      -1.261217000     -4.029067000      0.232019000
6      -1.217040000     -2.623631000      0.243682000
```

```
7      -0.034493000    -1.942071000     0.025663000
1       2.027693000    -4.616716000    -0.388679000
1      -2.188471000    -4.546345000     0.430551000
6       1.396267000     0.883935000    -2.441383000
6       2.437825000     1.005506000    -3.351333000
6       3.546967000     0.140914000    -3.224492000
6       3.540639000    -0.840915000    -2.233098000
6       2.432997000    -0.942252000    -1.356856000
7       1.407432000    -0.041400000    -1.423750000
1       4.386185000     0.213904000    -3.908213000
1       0.535662000     1.533759000    -2.502729000
1       2.385924000     1.758137000    -4.128463000
1       4.357291000    -1.545778000    -2.163348000
6      -2.441374000    -0.835688000     1.405618000
6      -3.528381000    -0.680735000     2.301321000
6      -3.487123000     0.323827000     3.267223000
6      -2.352395000     1.162240000     3.350631000
6      -1.332817000     0.988832000     2.427036000
7      -1.387439000     0.038175000     1.431794000
1      -4.308679000     0.435408000     3.966948000
1      -4.364444000    -1.364949000     2.268158000
1      -2.266194000     1.932349000     4.107244000
1      -0.453598000     1.614701000     2.454061000
6       1.181404000     2.745027000     0.114729000
6       1.223279000     4.149881000     0.065234000
6       0.029443000     4.871662000    -0.072362000
6      -1.172554000     4.158856000    -0.189285000
6      -1.145246000     2.753518000    -0.193018000
7       0.013835000     2.048951000    -0.025504000
1       2.180886000     4.647447000     0.157089000
1      -2.124116000     4.663976000    -0.300871000
6       1.385465000    -0.849345000     2.454122000
6       2.411288000    -0.961049000     3.403499000
6       3.532207000    -0.121805000     3.306511000
6       3.565453000     0.834608000     2.277833000
6       2.488783000     0.917174000     1.379961000
7       1.421057000     0.066935000     1.448227000
1       4.349065000    -0.197647000     4.015783000
1       0.529354000    -1.505761000     2.503380000
1       2.321314000    -1.701408000     4.189674000
1       4.390768000     1.528958000     2.173405000
6      -2.464288000     0.904163000    -1.417824000
6      -3.533994000     0.812621000    -2.321751000
6      -3.503957000    -0.170388000    -3.326332000
6      -2.392767000    -1.025138000    -3.394651000
6      -1.373511000    -0.902547000    -2.439841000
7      -1.406686000     0.037476000    -1.455937000
1      -4.316337000    -0.254101000    -4.039896000
1      -4.351893000     1.518923000    -2.242465000
1      -2.306118000    -1.785308000    -4.161986000
1      -0.524238000    -1.568484000    -2.465475000
7       2.344159000    -1.990797000    -0.427910000
7      -2.406705000    -1.909555000     0.504968000
6       3.602487000    -2.696286000    -0.057458000
1       3.930582000    -3.404682000    -0.827055000
1       4.386793000    -1.954769000     0.105670000
1       3.445459000    -3.232144000     0.879630000
6      -3.696820000    -2.581065000     0.178488000
1      -4.020009000    -3.271981000     0.965361000
1      -4.463318000    -1.818565000     0.030836000
1      -3.583192000    -3.128274000    -0.758270000
1      -0.104051000    -5.835291000     0.013954000
1       0.035335000     5.955563000    -0.089607000
26     -0.006908000     0.029253000     0.002890000
6      -2.453257000     2.061839000    -0.472308000
6       2.484723000     2.049600000     0.406521000
```

```
8        3.554028000      2.540678000     -0.013167000
8       -3.520638000      2.571141000     -0.070307000
```

3^{3+} (doublet)

```
6       -1.157754000     -2.719460000      0.195036000
6       -1.193551000     -4.125779000      0.171213000
6       -0.002434000     -4.844127000     -0.001768000
6        1.189443000     -4.126846000     -0.173905000
6        1.155082000     -2.720463000     -0.196267000
7       -0.000970000     -2.018419000     -0.000308000
1       -2.144176000     -4.626425000      0.308419000
1        2.139552000     -4.628343000     -0.311574000
6       -1.351981000      0.977271000      2.426506000
6       -2.363857000      1.113940000      3.384789000
6       -3.478378000      0.262033000      3.332726000
6       -3.514839000     -0.738448000      2.345407000
6       -2.450792000     -0.852434000      1.438494000
7       -1.393574000      0.020257000      1.454248000
1       -4.289001000      0.361515000      4.046073000
1       -0.500162000      1.639926000      2.442545000
1       -2.270751000      1.884552000      4.140615000
1       -4.336295000     -1.441913000      2.280272000
6        2.450280000     -0.854114000     -1.438349000
6        3.514746000     -0.740582000     -2.344817000
6        3.479365000      0.260258000     -3.331818000
6        2.365402000      1.112882000     -3.384098000
6        1.353075000      0.976621000     -2.426226000
7        1.393681000      0.019334000     -1.454203000
1        4.290354000      0.359437000     -4.044791000
1        4.335678000     -1.444656000     -2.279606000
1        2.273076000      1.883752000     -4.139758000
1        0.501658000      1.639796000     -2.442430000
6       -1.155163000      2.720515000     -0.195426000
6       -1.189569000      4.126888000     -0.172619000
6        0.002295000      4.844156000     -0.000343000
6        1.193450000      4.125795000      0.172318000
6        1.157704000      2.719466000      0.195708000
7        0.000927000      2.018448000      0.000243000
1       -2.139703000      4.628398000     -0.310070000
1        2.144066000      4.626431000      0.309616000
6       -1.353173000     -0.975970000     -2.426403000
6       -2.365558000     -1.112017000     -3.384244000
6       -3.479548000     -0.259446000     -3.331663000
6       -3.514902000      0.741128000     -2.344389000
6       -2.450378000      0.854466000     -1.437966000
7       -1.393749000     -0.018940000     -1.454125000
1       -4.290582000     -0.358462000     -4.044608000
1       -0.501735000     -1.639117000     -2.442827000
1       -2.273255000     -1.882687000     -4.140111000
1       -4.335858000      1.445152000     -2.278937000
6        2.450927000      0.852093000      1.438493000
6        3.515070000      0.737851000      2.345261000
6        3.478726000     -0.262921000      3.332289000
6        2.364214000     -1.114847000      3.384228000
6        1.352235000     -0.977908000      2.426093000
7        1.393722000     -0.020619000      1.454103000
1        4.289427000     -0.362605000      4.045519000
1        4.336507000      1.441351000      2.280252000
1        2.271194000     -1.885678000      4.139841000
1        0.500426000     -1.640578000      2.442032000
1       -0.003004000     -5.928052000     -0.002370000
1        0.002828000      5.928082000     -0.000606000
26       0.000004000      0.000013000      0.000023000
6        2.456106000      2.025774000      0.509534000
```

```
6      -2.454313000      2.027951000     -0.508780000
8      -3.532029000      2.539301000     -0.140650000
8       3.534410000      2.536316000      0.141968000
8      -3.534463000     -2.536294000      0.141671000
8       3.531959000     -2.539460000     -0.141730000
6      -2.456104000     -2.025808000      0.509149000
6       2.454236000     -2.027843000     -0.509472000
```

2$^+$ (doublet)

```
6      -1.243415000     -2.633411000      0.183722000
6      -1.317340000     -4.040879000      0.145336000
6      -0.160027000     -4.776763000     -0.129492000
6       1.043339000     -4.104375000     -0.362573000
6       1.064062000     -2.694428000     -0.319468000
7      -0.066934000     -1.963934000     -0.048149000
1      -2.248893000     -4.546377000      0.359519000
1       1.940631000     -4.656025000     -0.607528000
6      -1.358232000      0.946316000      2.464114000
6      -2.366756000      1.086976000      3.415084000
6      -3.482519000      0.227437000      3.338968000
6      -3.516370000     -0.759754000      2.350232000
6      -2.442835000     -0.863125000      1.429876000
7      -1.404076000      0.021557000      1.456004000
1      -4.295747000      0.307262000      4.053828000
1      -0.488879000      1.588384000      2.472688000
1      -2.283784000      1.847419000      4.183008000
1      -4.338329000     -1.462384000      2.313711000
6       2.391447000     -0.932712000     -1.443846000
6       3.498737000     -0.825504000     -2.323919000
6       3.544728000      0.221087000     -3.248548000
6       2.474201000      1.137522000     -3.303432000
6       1.431746000      0.988254000     -2.390880000
7       1.399444000      0.002686000     -1.443959000
1       4.384283000      0.304659000     -3.931923000
1       4.285453000     -1.567886000     -2.306858000
1       2.451826000      1.947488000     -4.023428000
1       0.598290000      1.676545000     -2.384142000
6      -1.087704000      2.792831000     -0.133692000
6      -1.091606000      4.193536000     -0.170708000
6       0.137082000      4.887883000     -0.078753000
6       1.299206000      4.147935000      0.111103000
6       1.252976000      2.728195000      0.235885000
7       0.055021000      2.045775000      0.053369000
1      -2.030995000      4.715645000     -0.307394000
1       2.268755000      4.621567000      0.207080000
6      -1.420700000     -0.792854000     -2.459845000
6      -2.454255000     -0.883126000     -3.401105000
6      -3.553665000     -0.010620000     -3.297409000
6      -3.546691000      0.948220000     -2.274430000
6      -2.455164000      1.005100000     -1.383827000
7      -1.415828000      0.119772000     -1.448222000
1      -4.378725000     -0.065785000     -4.000208000
1      -0.578517000     -1.468266000     -2.506559000
1      -2.394205000     -1.627997000     -4.187101000
1      -4.350295000      1.666814000     -2.162582000
6       2.492591000      0.842772000      1.433393000
6       3.607083000      0.609585000      2.289371000
6       3.580886000     -0.433856000      3.213802000
```

21

```
6          2.423953000       -1.245730000        3.286899000
6          1.383699000       -1.003584000        2.388203000
7          1.411720000       -0.012638000        1.449379000
1          4.422833000       -0.606045000        3.878175000
1          4.448680000        1.287545000        2.214204000
1          2.335992000       -2.051188000        4.007973000
1          0.499566000       -1.626314000        2.401756000
7         -2.422566000       -1.902534000        0.477780000
7          2.290303000       -2.032632000       -0.569715000
6         -3.719224000       -2.517916000        0.103773000
1         -4.080728000       -3.245679000        0.842182000
1         -4.466361000       -1.728598000       -0.007730000
1         -3.610129000       -3.018622000       -0.860582000
6          3.539293000       -2.746470000       -0.210544000
1          3.876622000       -3.443569000       -0.989044000
1          4.327127000       -2.011684000       -0.028511000
1          3.377463000       -3.301456000        0.715616000
1         -0.195925000       -5.861013000       -0.160971000
1          0.167511000        5.970793000       -0.144404000
26        -0.004933000        0.045155000        0.007152000
6          2.503980000        2.068956000        0.619401000
6         -2.405570000        2.145186000       -0.418800000
8         -3.479800000        2.675508000       -0.018117000
8          3.638992000        2.694276000        0.435683000
```

3^+ (doublet)

```
6          1.167262000        2.698999000        0.166732000
6          1.196715000        4.107437000        0.133181000
6          0.001943000        4.828474000       -0.001537000
6         -1.193443000        4.108308000       -0.135579000
6         -1.165136000        2.699826000       -0.167937000
7          0.000767000        1.987625000       -0.000361000
1          2.151676000        4.607205000        0.243141000
1         -2.147987000        4.608786000       -0.245917000
6          1.386288000       -0.934937000        2.443808000
6          2.407277000       -1.067625000        3.390970000
6          3.529303000       -0.219236000        3.311505000
6          3.555217000        0.760695000        2.310813000
6          2.473841000        0.866968000        1.410251000
7          1.416558000       -0.004881000        1.445270000
1          4.347216000       -0.309789000        4.018878000
1          0.526616000       -1.589544000        2.469639000
1          2.323559000       -1.826602000        4.160713000
1          4.376081000        1.462499000        2.222073000
6         -2.473450000        0.868244000       -1.410230000
6         -3.555170000        0.762272000       -2.310399000
6         -3.530082000       -0.217978000       -3.310809000
6         -2.408508000       -1.066945000       -3.390406000
6         -1.387152000       -0.934522000       -2.443592000
7         -1.416645000       -0.004187000       -1.445302000
1         -4.348280000       -0.308333000       -4.017878000
1         -4.375633000        1.464542000       -2.221626000
1         -2.325413000       -1.826169000       -4.159973000
1         -0.527829000       -1.589586000       -2.469500000
6          1.165141000       -2.699880000       -0.167084000
6          1.193441000       -4.108350000       -0.134321000
6         -0.001962000       -4.828473000       -0.000171000
6         -1.196739000       -4.107392000        0.134246000
6         -1.167283000       -2.698943000        0.167392000
7         -0.000770000       -1.987625000        0.000199000
1          2.147990000       -4.608867000       -0.244444000
```

```
1     -2.151712000   -4.607124000    0.244265000
6      1.387349000    0.933862000   -2.443719000
6      2.408796000    1.066048000   -3.390469000
6      3.530373000    0.217117000   -3.310540000
6      3.555373000   -0.762870000   -2.309867000
6      2.473566000   -0.868622000   -1.409781000
7      1.416755000    0.003789000   -1.445183000
1      4.348639000    0.307293000   -4.017552000
1      0.528025000    1.588915000   -2.469879000
1      2.325768000    1.825072000   -4.160241000
1      4.375834000   -1.465110000   -2.220835000
6     -2.473958000   -0.866584000    1.410286000
6     -3.555391000   -0.760097000    2.310755000
6     -3.529549000    0.220089000    3.311200000
6     -2.407536000    1.068508000    3.390521000
6     -1.386484000    0.935589000    2.443460000
7     -1.416682000    0.005280000    1.445156000
1     -4.347507000    0.310812000    4.018498000
1     -4.376245000   -1.461930000    2.222140000
1     -2.323872000    1.827676000    4.160082000
1     -0.526813000    1.590202000    2.469188000
1      0.002392000    5.912996000   -0.002023000
1     -0.002417000   -5.912994000   -0.000356000
26    -0.000003000    0.000001000   -0.000031000
6     -2.462693000   -2.025610000    0.476222000
6      2.461194000   -2.027564000   -0.475621000
8      3.552066000   -2.569276000   -0.120826000
8     -3.554107000   -2.566949000    0.122435000
8      3.554095000    2.566844000    0.121816000
8     -3.552062000    2.569389000   -0.122041000
6      2.462649000    2.025768000    0.475900000
6     -2.461160000    2.027416000   -0.476364000
```

2^{2+} (triplet)

```
6     -1.167884000   -2.763453000    0.179310000
6     -1.195983000   -4.173974000    0.182114000
6      0.000286000   -4.876516000   -0.000898000
6      1.196421000   -4.173724000   -0.183770000
6      1.168072000   -2.763201000   -0.180700000
7      0.000027000   -2.070541000   -0.000647000
1     -2.121485000   -4.706107000    0.354195000
1      2.122020000   -4.705659000   -0.355942000
6     -1.684688000    0.849982000    2.435863000
6     -2.795211000    0.947636000    3.272287000
6     -3.843830000    0.020655000    3.091446000
6     -3.723767000   -0.974740000    2.117349000
6     -2.556189000   -1.026913000    1.311763000
7     -1.575523000   -0.089417000    1.448542000
1     -4.729625000    0.058368000    3.717979000
1     -0.855822000    1.541182000    2.530549000
1     -2.840279000    1.720253000    4.030953000
1     -4.502316000   -1.717744000    2.008144000
6      2.556050000   -1.025987000   -1.312521000
6      3.723607000   -0.973240000   -2.118106000
6      3.843427000    0.022580000   -3.091797000
6      2.794593000    0.949401000   -3.272247000
6      1.684121000    0.851177000   -2.435820000
7      1.575198000   -0.088636000   -1.448872000
1      4.729199000    0.060745000   -3.718335000
1      4.502317000   -1.716122000   -2.009222000
1      2.839469000    1.722317000   -4.030620000
1      0.855093000    1.542222000   -2.530197000
6     -1.148805000    2.920525000   -0.223448000
6     -1.190718000    4.328587000   -0.198409000
```

```
6        0.000889000        5.042822000        0.001123000
6        1.192180000        4.327974000        0.200361000
6        1.149634000        2.919924000        0.224815000
7        0.000262000        2.227805000        0.000535000
1       -2.136090000        4.834089000       -0.354369000
1        2.137779000        4.832990000        0.356528000
6       -1.301841000       -0.800656000       -2.475735000
6       -2.293513000       -0.922281000       -3.459410000
6       -3.397692000       -0.054547000       -3.430328000
6       -3.442239000        0.934687000       -2.435200000
6       -2.393120000        1.024738000       -1.500575000
7       -1.345454000        0.143924000       -1.497255000
1       -4.191441000       -0.134785000       -4.165508000
1       -0.457309000       -1.473466000       -2.460465000
1       -2.195892000       -1.690480000       -4.218186000
1       -4.256269000        1.647976000       -2.382131000
6        2.393043000        1.023159000        1.501330000
6        3.441938000        0.932495000        2.436146000
6        3.396925000       -0.057107000        3.430884000
6        2.292551000       -0.924616000        3.459360000
6        1.301114000       -0.802353000        2.475535000
7        1.345145000        0.142630000        1.497452000
1        4.190485000       -0.137819000        4.166216000
1        4.256169000        1.645586000        2.383513000
1        2.194598000       -1.693113000        4.217790000
1        0.456447000       -1.474982000        2.459806000
7       -2.392542000       -2.060259000        0.363217000
7        2.392609000       -2.059788000       -0.364447000
6       -3.627054000       -2.730714000       -0.121373000
1       -4.034109000       -3.456024000        0.595240000
1       -4.385732000       -1.971175000       -0.324806000
1       -3.406832000       -3.247492000       -1.057378000
6        3.627247000       -2.730213000        0.119859000
1        4.034377000       -3.455215000       -0.597022000
1        4.385815000       -1.970626000        0.323519000
1        3.407150000       -3.247324000        1.055705000
1        0.000386000       -5.961811000       -0.000999000
1        0.001129000        6.127300000        0.001342000
26      -0.000130000        0.104613000        0.000089000
6        2.424893000        2.193835000        0.564239000
6       -2.424404000        2.195149000       -0.563137000
8       -3.520846000        2.689654000       -0.208763000
8        3.521571000        2.687897000        0.209994000
```

2^{2+} (quintet)

```
6        1.152266000       -2.824016000       -0.260144000
6        1.180846000       -4.234161000       -0.265524000
6       -0.000617000       -4.936265000        0.000063000
6       -1.181890000       -4.233857000        0.265683000
6       -1.152936000       -2.823716000        0.260361000
7       -0.000243000       -2.132596000        0.000117000
1        2.092722000       -4.766094000       -0.500546000
1       -2.093903000       -4.765559000        0.500692000
6        1.518950000        0.781190000       -2.568666000
6        2.591799000        0.894727000       -3.450329000
6        3.661418000       -0.016518000       -3.311199000
6        3.599589000       -1.013079000       -2.333128000
6        2.465436000       -1.086385000       -1.481968000
7        1.465476000       -0.164154000       -1.582194000
1        4.520726000        0.035876000       -3.972715000
1        0.675078000        1.459180000       -2.622939000
1        2.595701000        1.667850000       -4.209659000
1        4.395568000       -1.741230000       -2.255137000
6       -2.465581000       -1.085695000        1.482198000
```

```
6      -3.599598000    -1.012149000     2.333517000
6      -3.661133000    -0.015501000     3.311520000
6      -2.591351000     0.895586000     3.450422000
6      -1.518640000     0.781805000     2.568622000
7      -1.465453000    -0.163627000     1.582220000
1      -4.520337000     0.037079000     3.973157000
1      -4.395698000    -1.740187000     2.255693000
1      -2.595024000     1.668773000     4.209688000
1      -0.674651000     1.459663000     2.622725000
6       1.155422000     2.951652000     0.190170000
6       1.194713000     4.361395000     0.170446000
6       0.000371000     5.076546000    -0.000328000
6      -1.194069000     4.361535000    -0.171010000
6      -1.154972000     2.951785000    -0.190551000
7       0.000177000     2.254576000    -0.000141000
1       2.142488000     4.868790000     0.302850000
1      -2.141773000     4.869043000    -0.303487000
6       1.683018000    -0.742262000     2.511820000
6       2.802499000    -0.850460000     3.353674000
6       3.866223000     0.053506000     3.188116000
6       3.760153000     1.050587000     2.203453000
6       2.591127000     1.117286000     1.419930000
7       1.573782000     0.219795000     1.561483000
1       4.751423000    -0.009916000     3.812437000
1       0.856325000    -1.437448000     2.593009000
1       2.833847000    -1.628847000     4.107857000
1       4.548280000     1.777807000     2.047920000
6      -2.590934000     1.117461000    -1.420101000
6      -3.759989000     1.050789000    -2.203582000
6      -3.866173000     0.053630000    -3.188153000
6      -2.802532000    -0.850442000    -3.353664000
6      -1.683021000    -0.742270000    -2.511846000
7      -1.573680000     0.219856000    -1.561592000
1      -4.751395000    -0.009768000    -3.812446000
1      -4.548042000     1.778102000    -2.048102000
1      -2.833967000    -1.628890000    -4.107780000
1      -0.856391000    -1.437536000    -2.592994000
7       2.360337000    -2.117654000    -0.524291000
7      -2.360805000    -2.117040000     0.524559000
6       3.623306000    -2.777023000    -0.100348000
1       3.997692000    -3.503138000    -0.833521000
1       4.385982000    -2.011438000     0.060503000
1       3.453910000    -3.289619000     0.848393000
6      -3.623977000    -2.776098000     0.100732000
1      -3.998463000    -3.502141000     0.833924000
1      -4.386483000    -2.010324000    -0.060019000
1      -3.454801000    -3.288711000    -0.848039000
1      -0.000762000    -6.021572000     0.000042000
1       0.000446000     6.161111000    -0.000402000
26      0.000011000     0.036112000    -0.000024000
6      -2.472991000     2.255866000    -0.447781000
6       2.473343000     2.255574000     0.447455000
8       3.513765000     2.757988000    -0.042282000
8      -3.513314000     2.758263000     0.042185000
```

25

Supporting Information

Figure S1. FD mass spectrum of **Pr₂tpda** in CH₃CN.
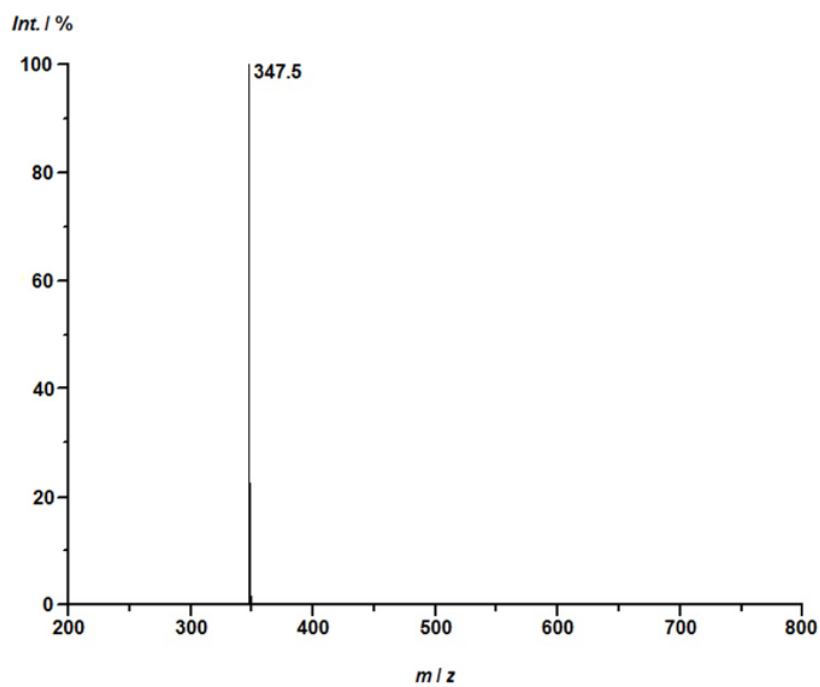
Figure S2. FD mass spectrum of **Hex₂tpda** in CH₃CN.
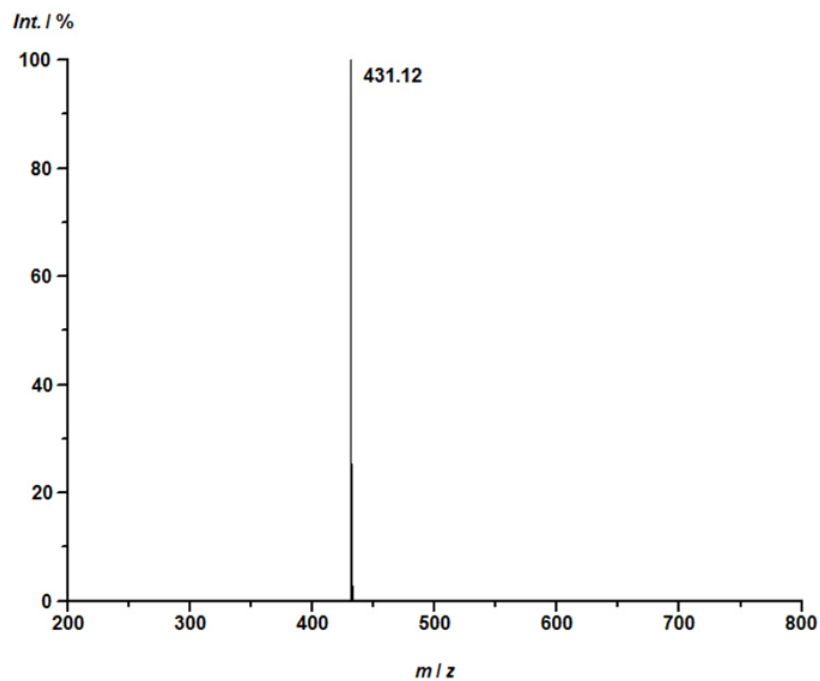
Figure S3. ^{1}H NMR spectrum of **Pr₂tpda** in CDCl₃. Asterisk denotes solvent resonance. # denote resonances of residual ethyl acetate.
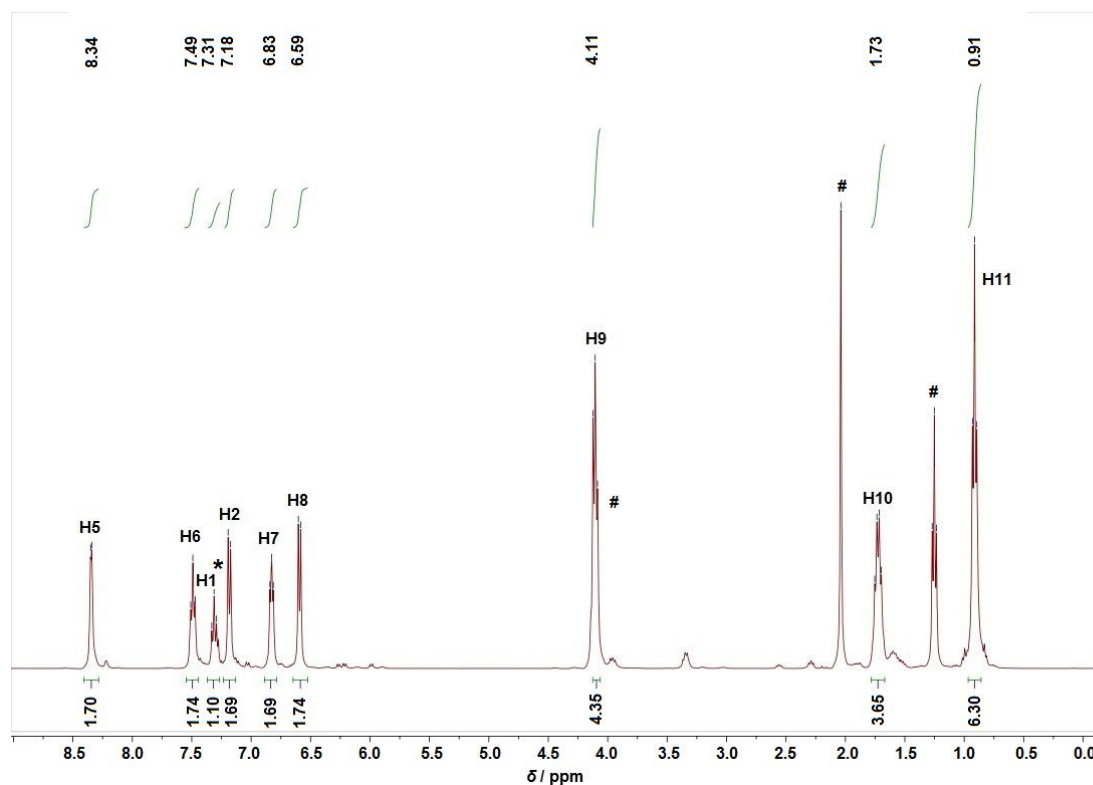
Figure S4. ^{13}C{^{1}H} NMR spectrum of **Pr₂tpda** in CDCl₃. Asterisk denotes solvent resonance. # denote resonances of residual ethyl acetate.

2
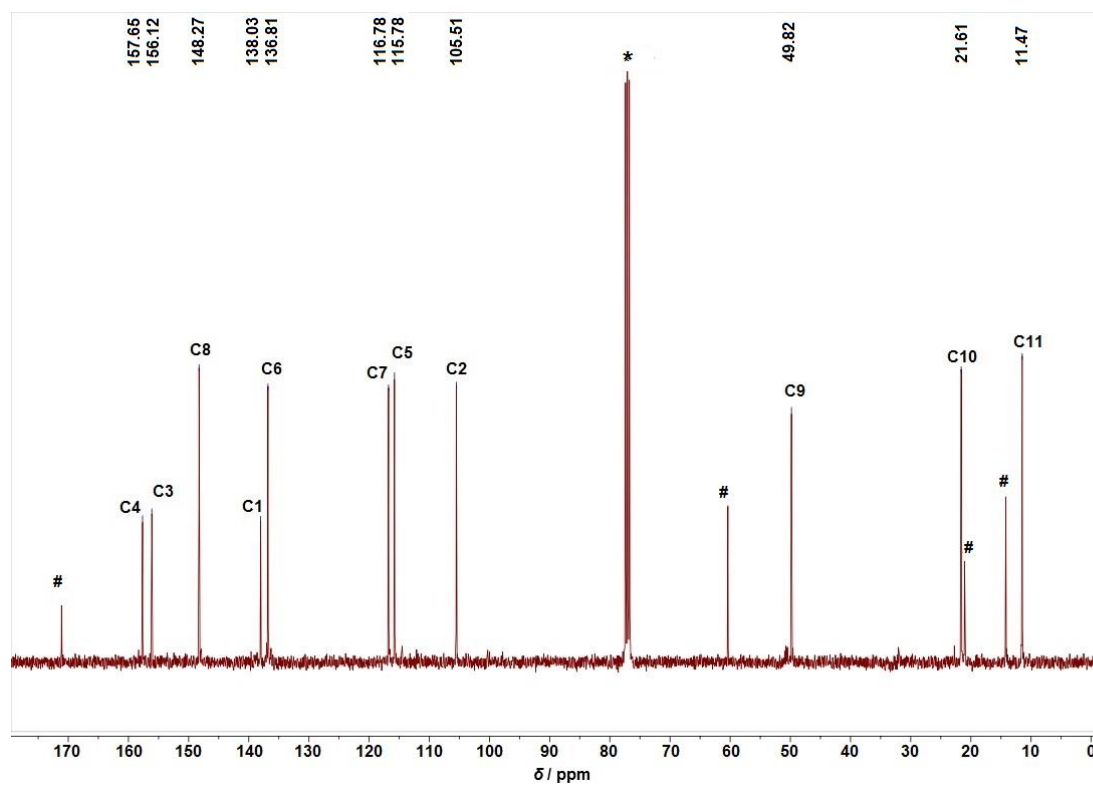
Figure S5. ^{1}H NMR spectrum of **Hex$_2$tpda** in CDCl$_3$. Asterisk denotes solvent resonance.
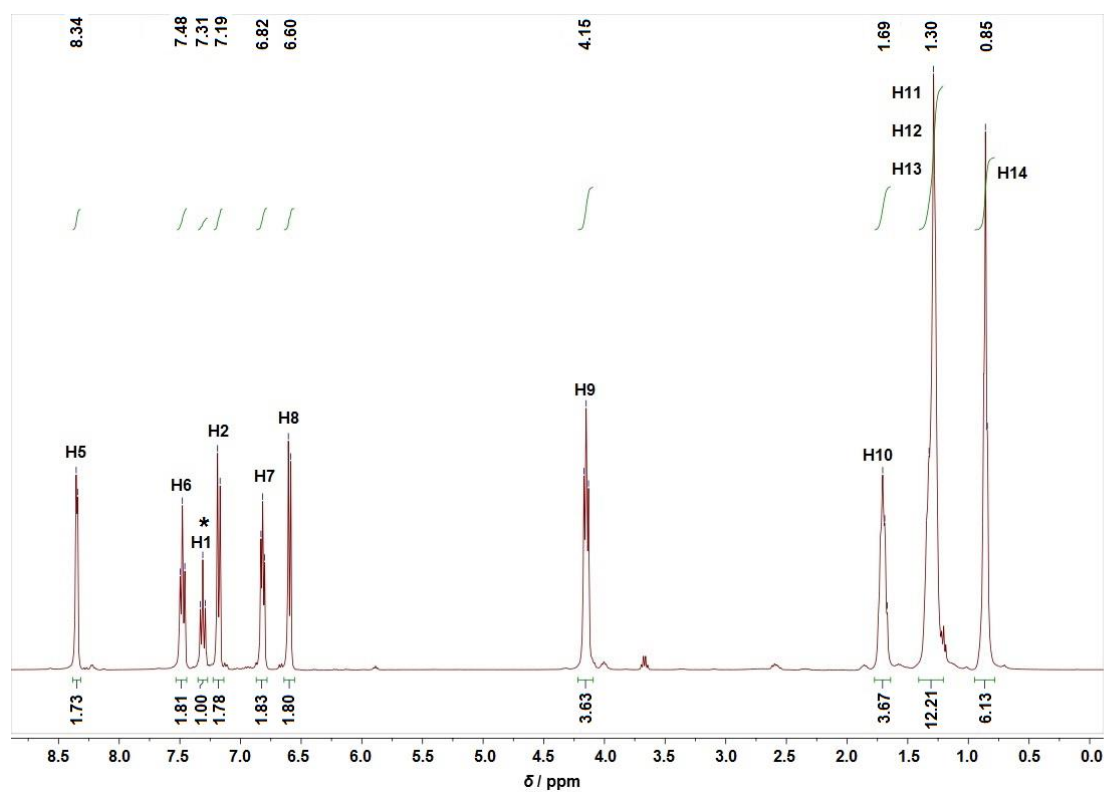
Figure S6. ^{13}C{^{1}H} NMR spectrum of **Hex$_2$tpda** in CDCl$_3$. Asterisk denotes solvent resonance.

3
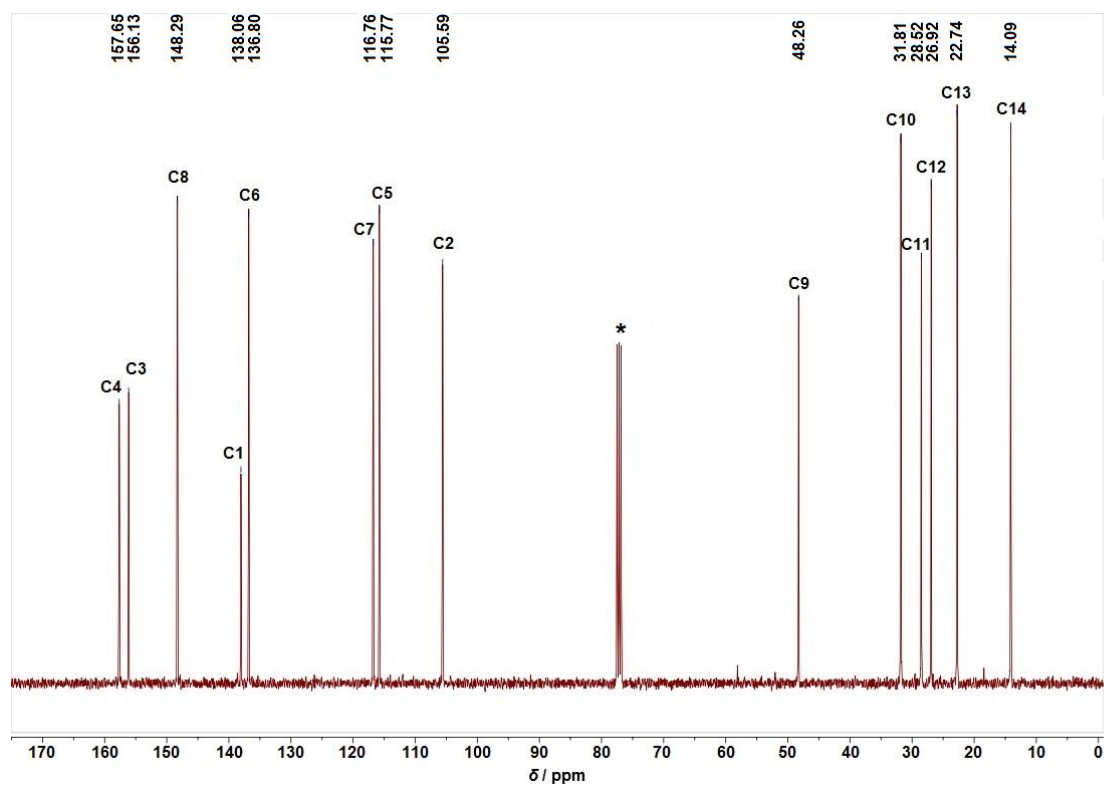
Figure S7. ESI$^+$ mass spectrum of **[Fe(H$_2$tpda)$_2$][BF$_4$]$_2$** in CH$_3$CN.
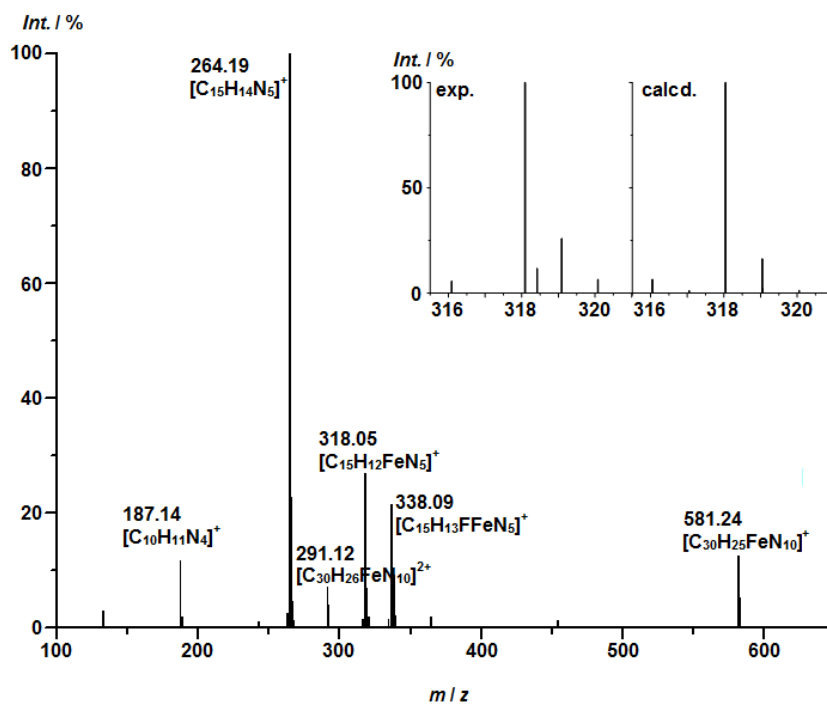
Figure S8. ESI$^+$ mass spectrum of **[Fe(Pr$_2$tpda)$_2$][BF$_4$]$_2$** in CH$_3$CN.
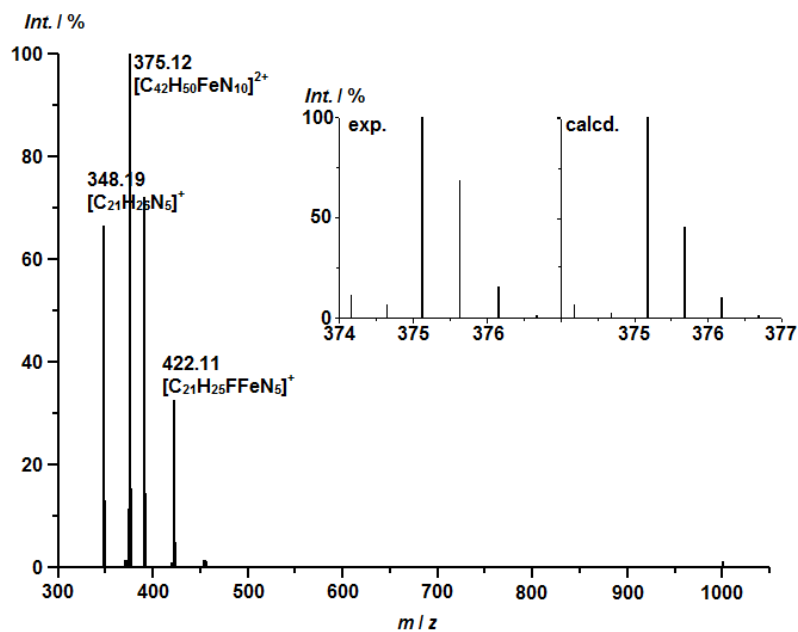
Figure S9. ESI$^+$ mass spectrum of **[Fe(Hex$_2$tpda)$_2$][PF$_6$]$_2$** in CH$_3$CN.
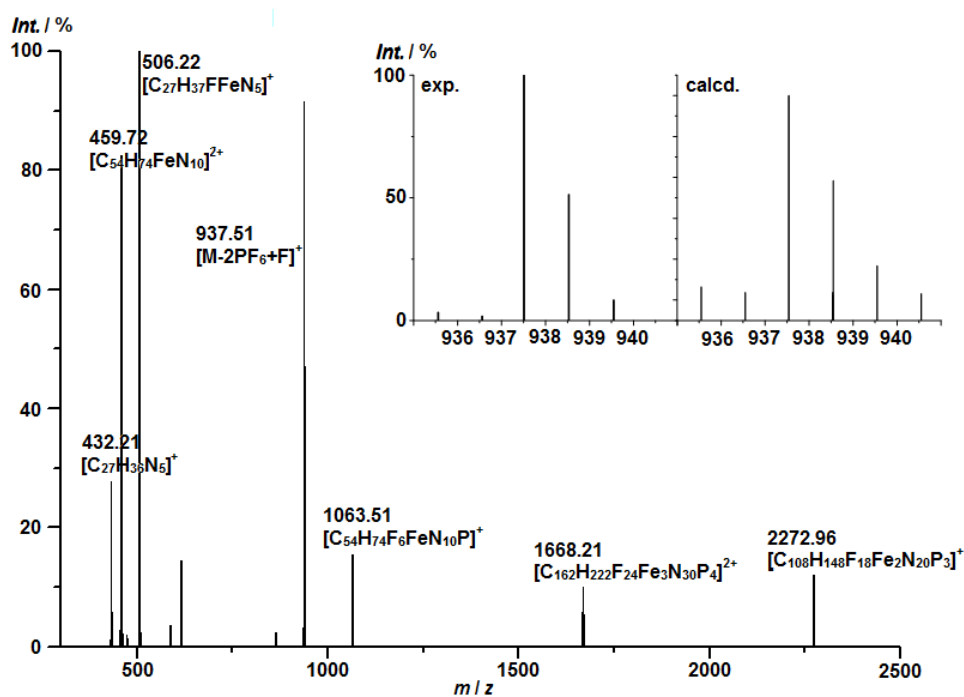
Figure S10. ESI$^+$ mass spectrum of **[Fe(dcpp)(H$_2$tpda)][PF$_6$]$_2$** in CH$_3$CN.
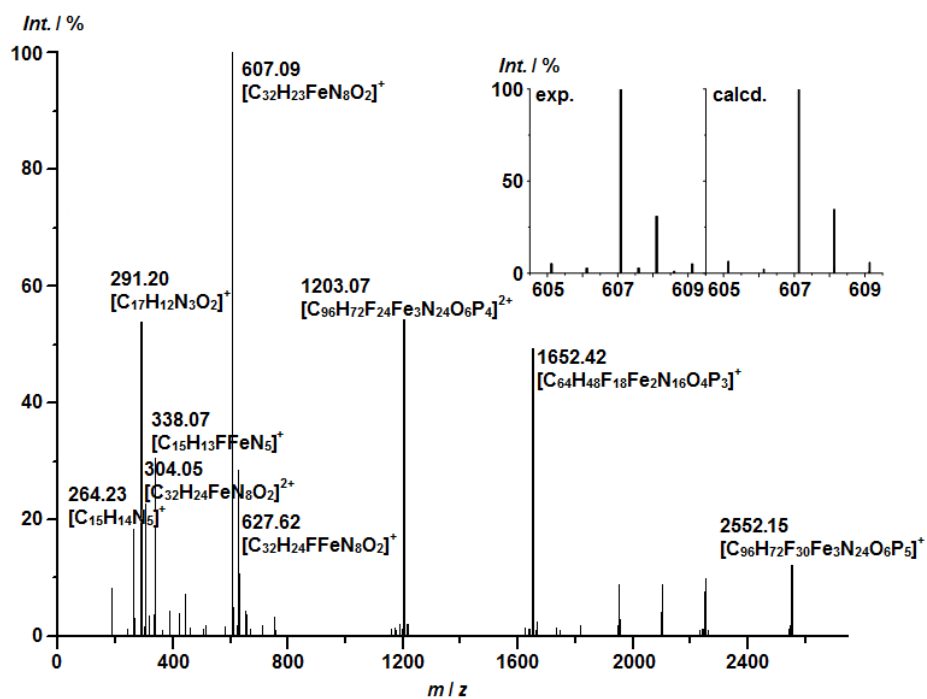
Figure S11. ESI$^+$ mass spectrum of **[Fe(dcpp)(Pr$_2$tpda)][PF$_6$]$_2$** in CH$_3$CN.
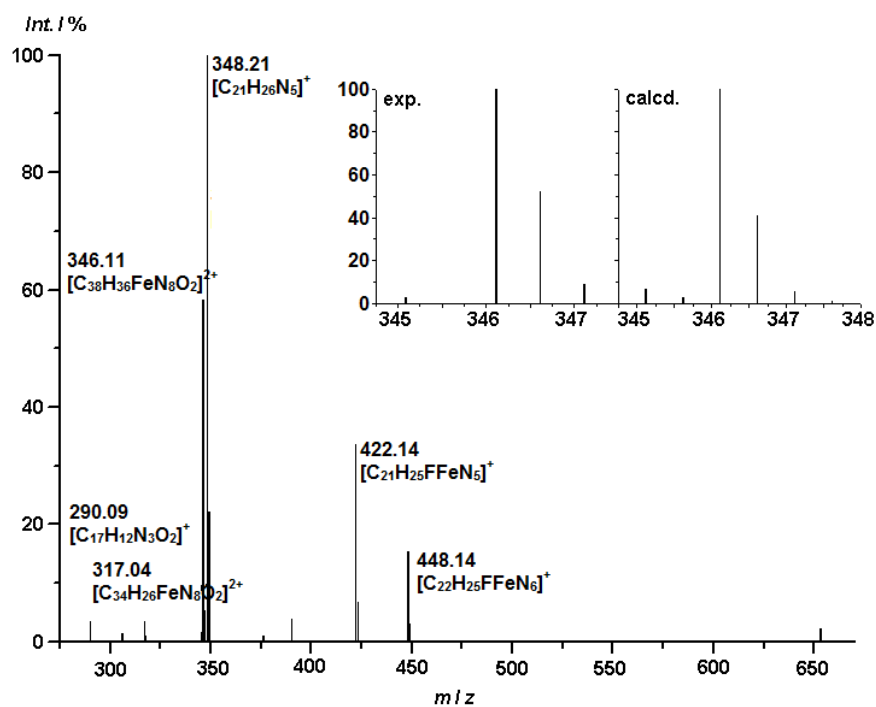
Figure S12. ESI$^+$ mass spectrum of **[Fe(dcpp)(Hex$_2$tpda)][BF$_4$]$_2$** in CH$_3$CN.
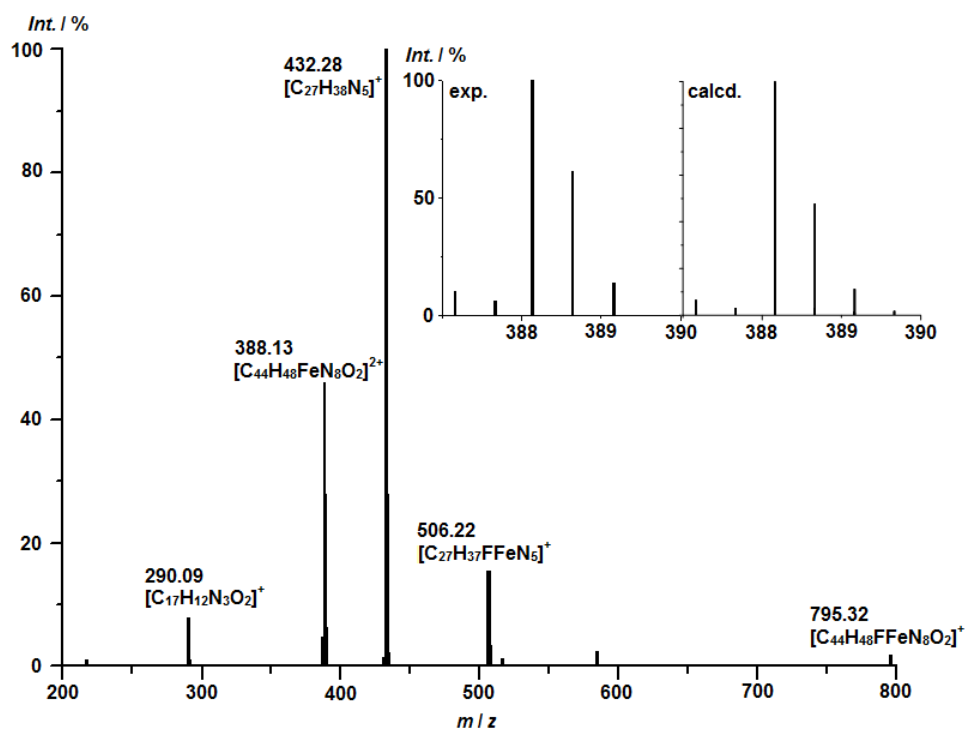
Figure S13. IR spectrum of **[Fe(H₂tpda)₂][BF₄]₂** in CsI.
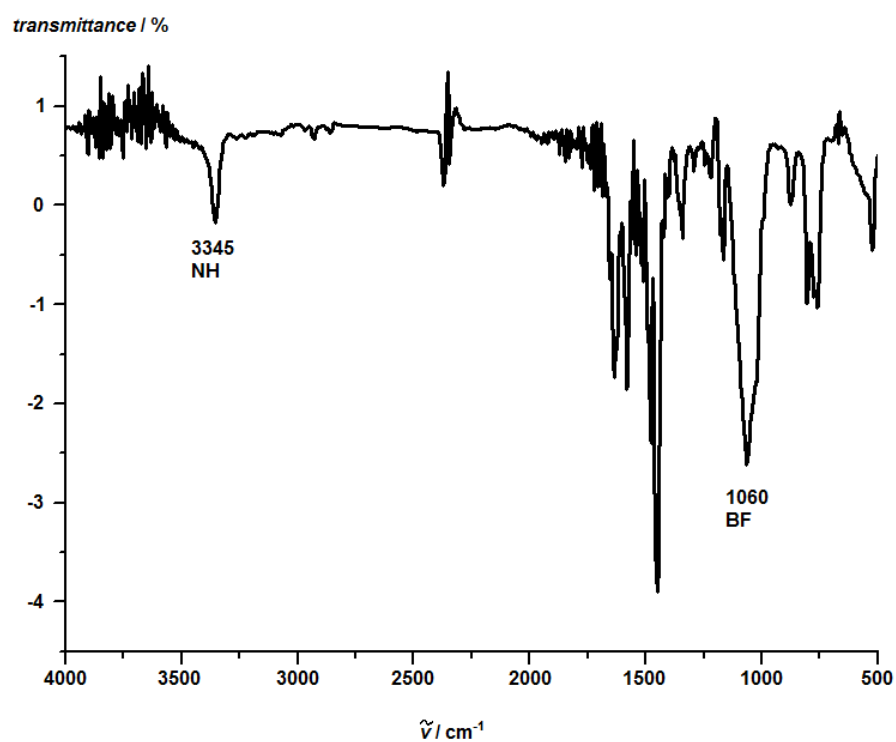
Figure S14. IR spectrum of **[Fe(Me₂tpda)₂][PF₆]₂** in CsI.
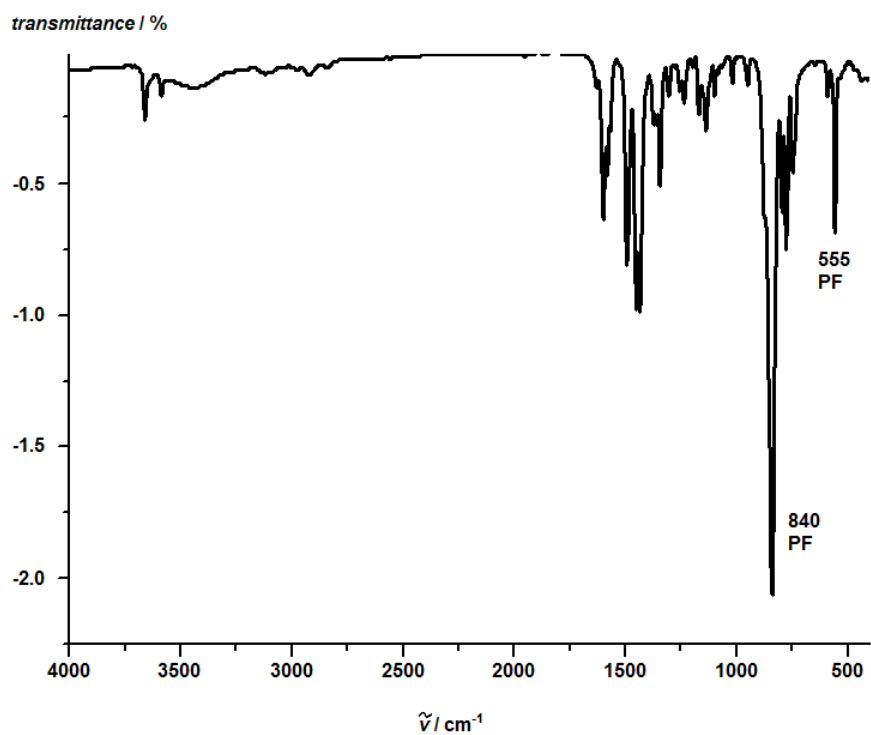
Figure S15. IR spectrum of **[Fe(Pr₂tpda)₂][BF₄]₂** in CsI.
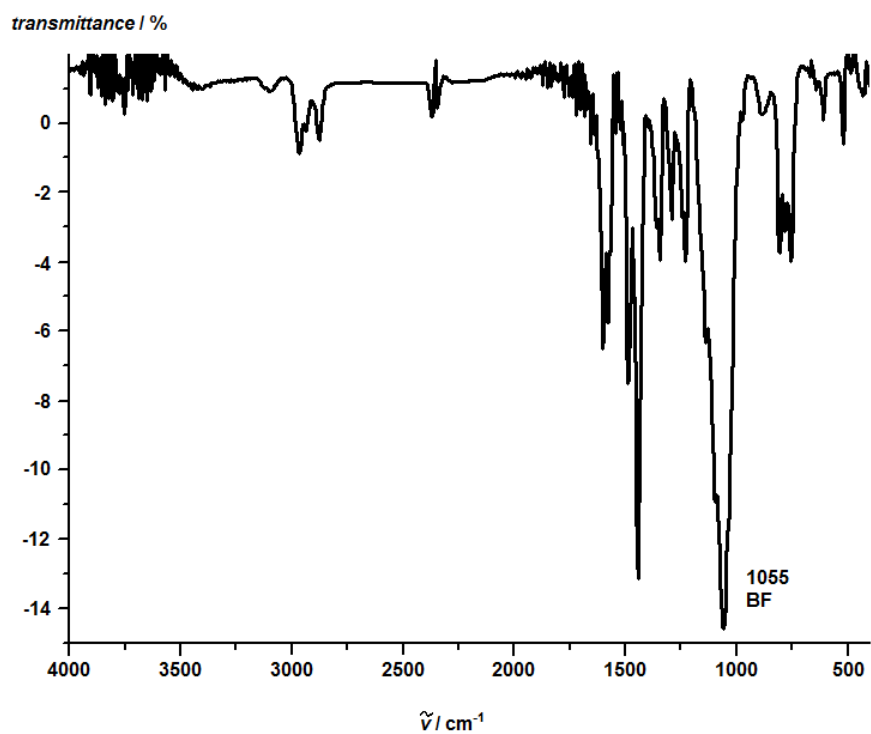
Figure S16. IR spectrum of **[Fe(Hex₂tpda)₂][PF₆]₂** in KBr.
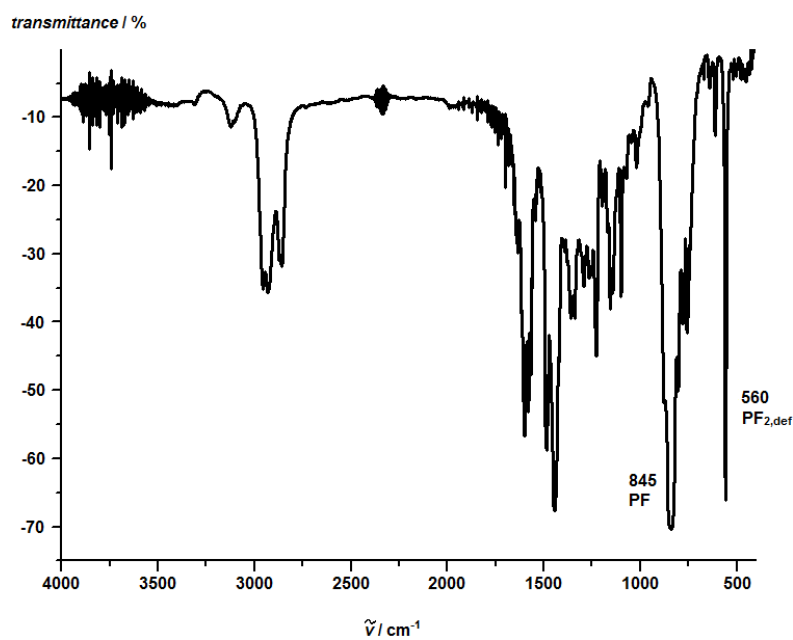
Figure S17. IR spectrum of **[Fe(dcpp)(H₂tpda)][PF₆]₂** in KBr.
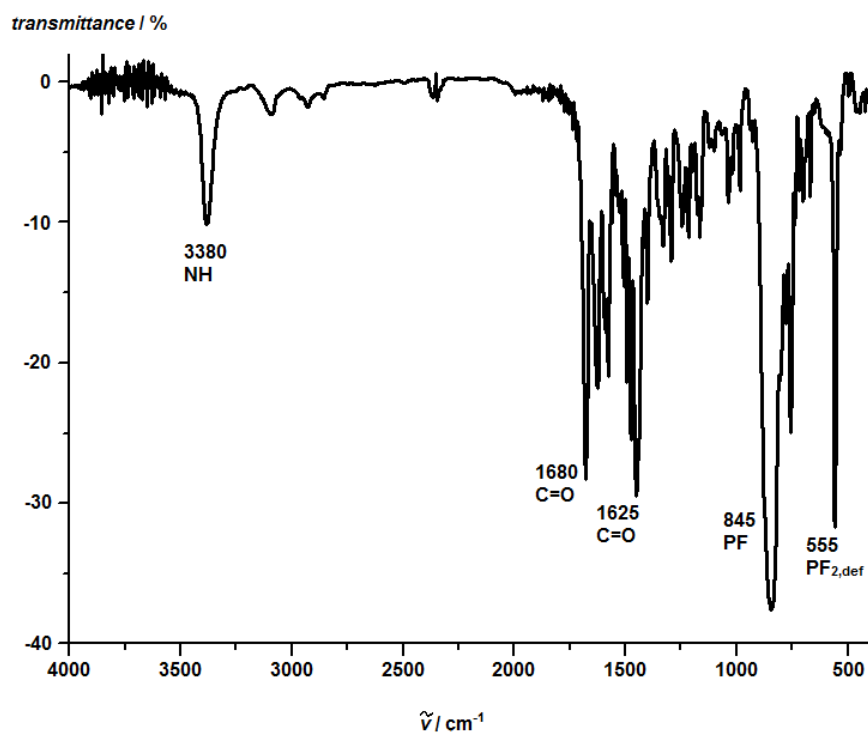
Figure S18. IR spectrum of **[Fe(dcpp)(Me₂tpda)][PF₆]₂** in CsI.
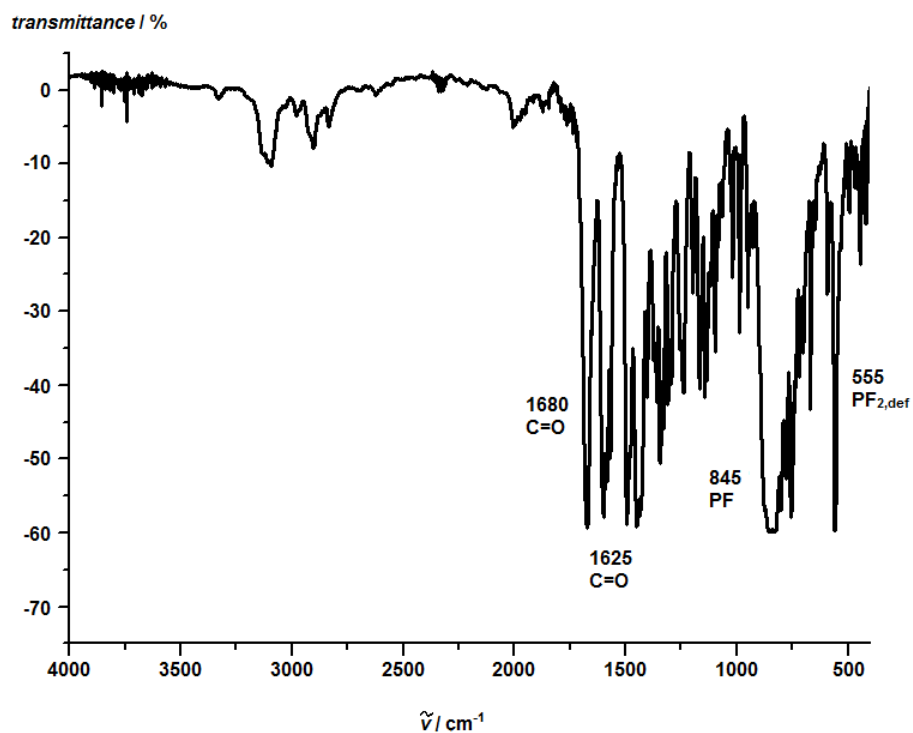
Figure S19. IR spectrum of **[Fe(dcpp)(Pr$_2$tpda)][PF$_6$]$_2$** in CsI.
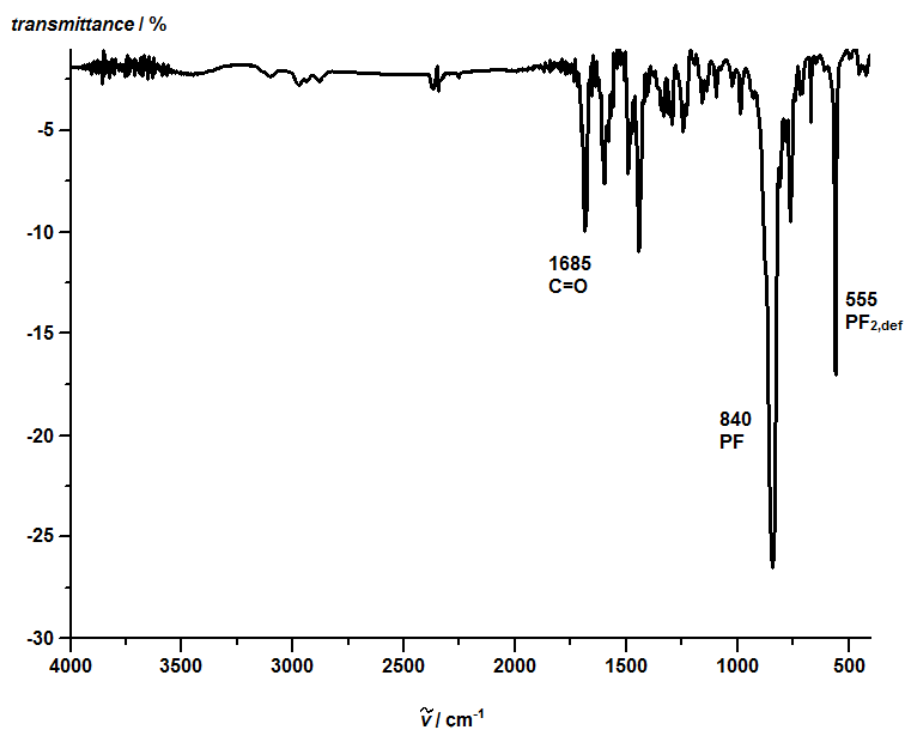
Figure S20. IR spectrum of **[Fe(dcpp)(Hex$_2$tpda)][BF$_4$]$_2$** in CsI.
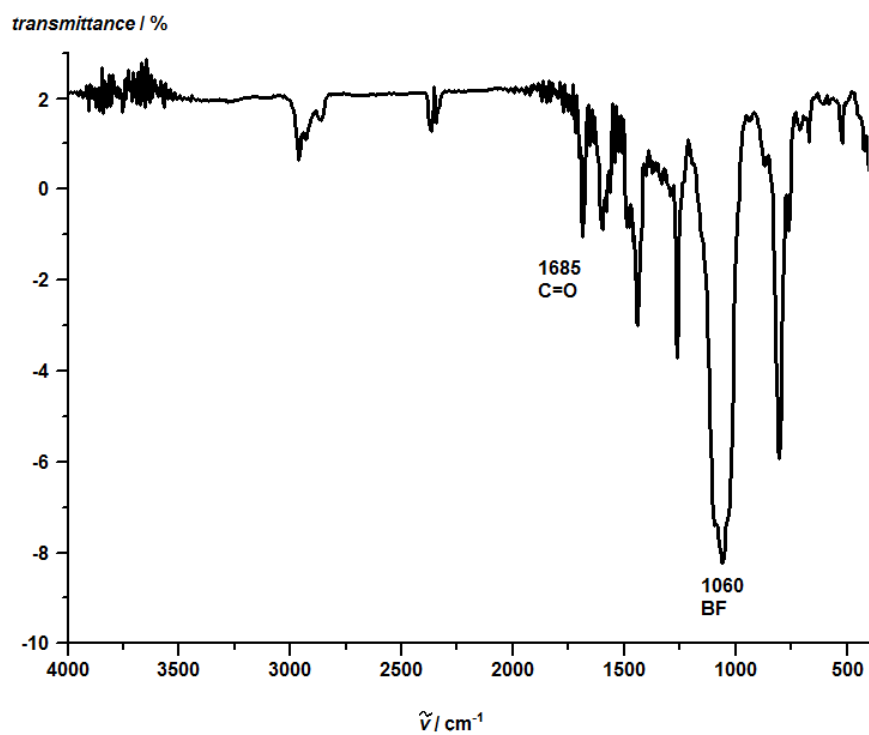
Figure S21. ^{1}H NMR spectrum of **[Fe(H$_2$tpda)$_2$][BF$_4$]$_2$** in CD$_3$CN. Asterisk denotes solvent resonance. # denotes resonance of residual water.
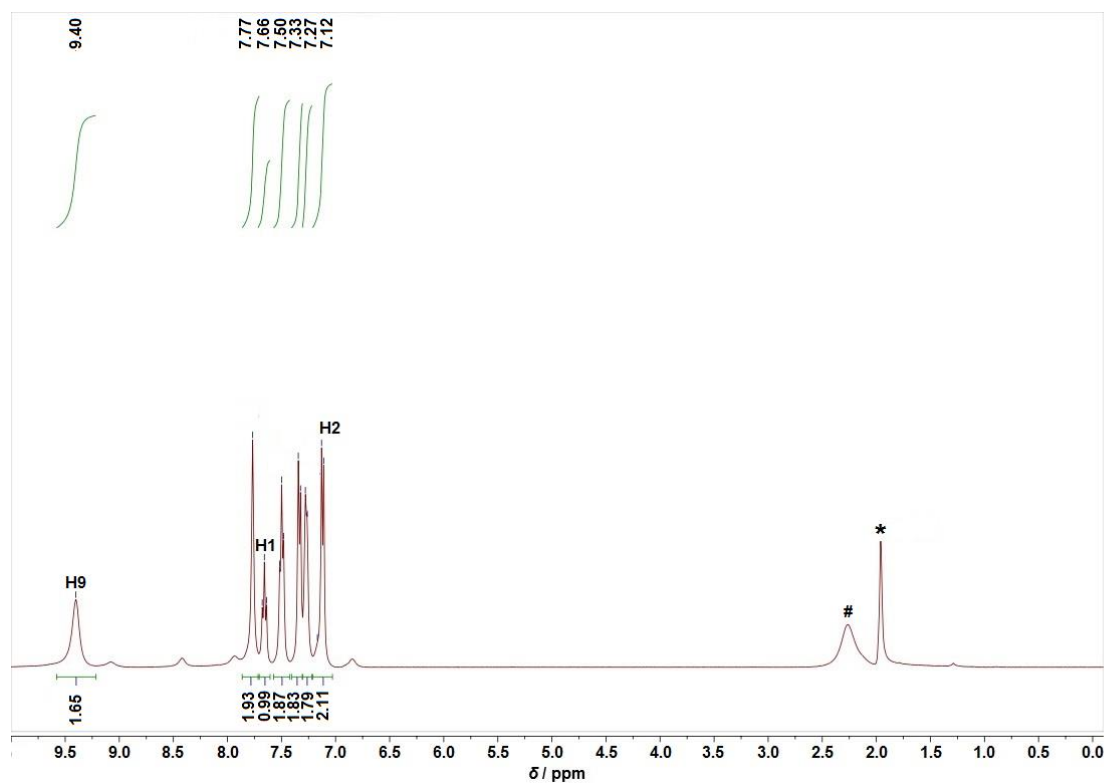
Figure S22. ^{13}C{^{1}H} NMR spectrum of **[Fe(H$_2$tpda)$_2$][BF$_4$]$_2$** in CD$_3$CN. Asterisk denotes solvent resonance.

11
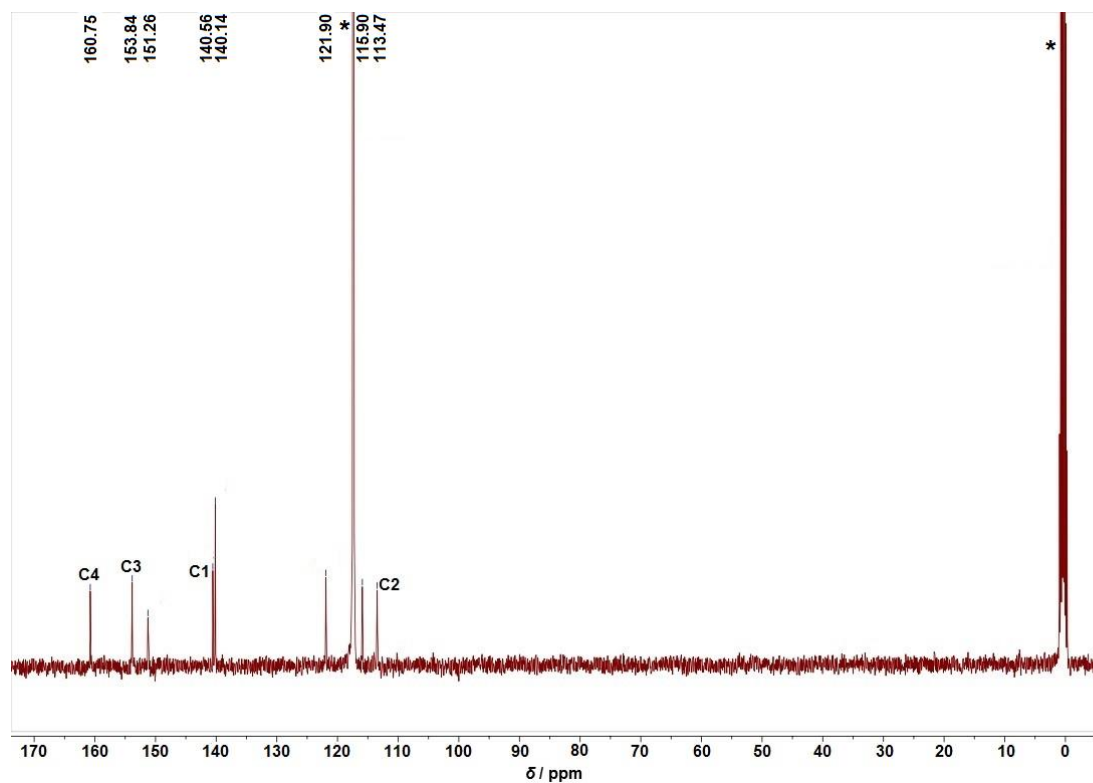
Figure S23. ^{1}H NMR spectrum of **[Fe(Pr$_2$tpda)$_2$][BF$_4$]$_2$** in CD$_3$CN. Asterisk denotes solvent resonance.
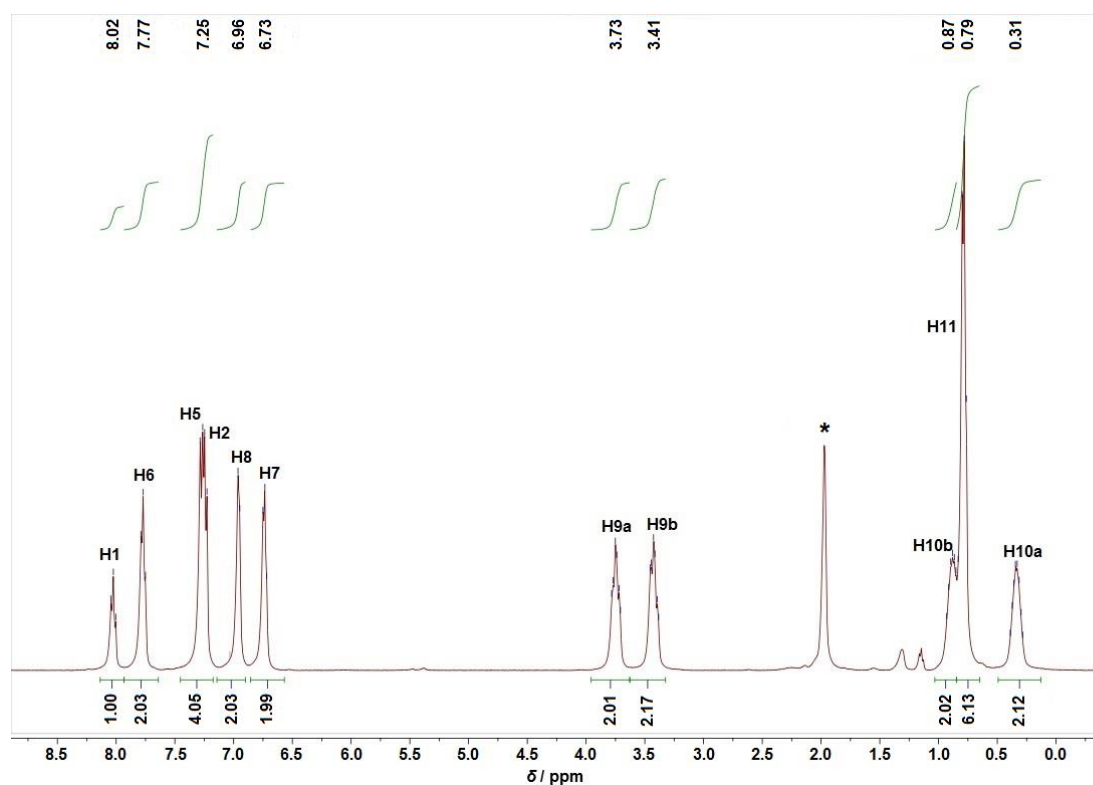
Figure S24. ^{13}C{^{1}H} NMR spectrum of **[Fe(Pr$_2$tpda)$_2$][BF$_4$]$_2$** in CD$_3$CN. Asterisk denotes solvent resonance.
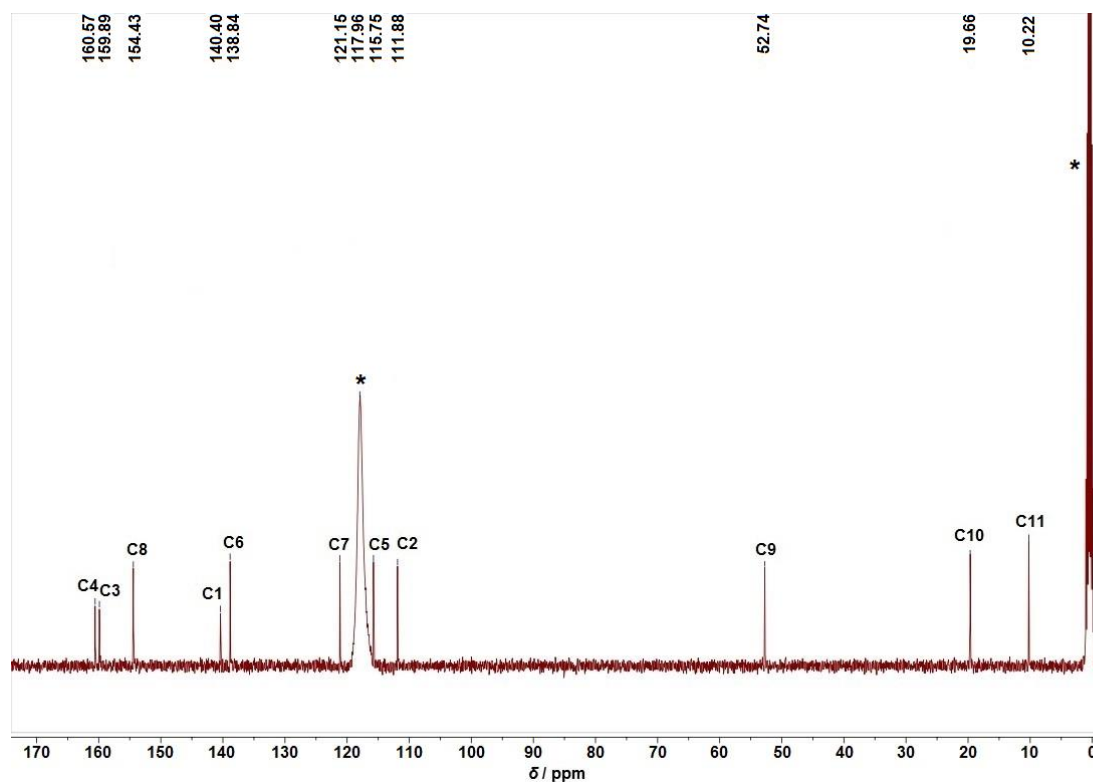
Figure S25. ^{1}H NMR spectrum of **[Fe(Hex$_2$tpda)$_2$][PF$_6$]$_2$** in CD$_3$CN. Asterisk denotes solvent resonance. # denotes resonance of residual water.
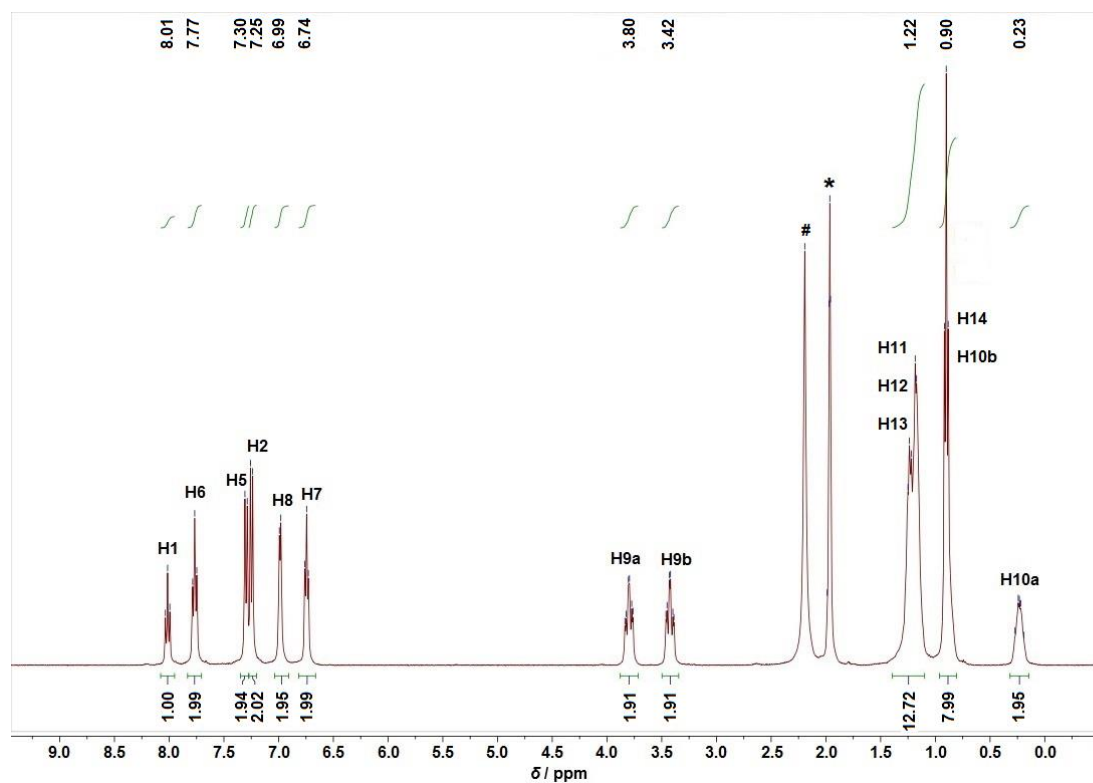
Figure S26. ^{13}C{^{1}H} NMR spectrum of **[Fe(Hex$_2$tpda)$_2$][PF$_6$]$_2$** in CD$_3$CN. Asterisk denotes solvent resonance.
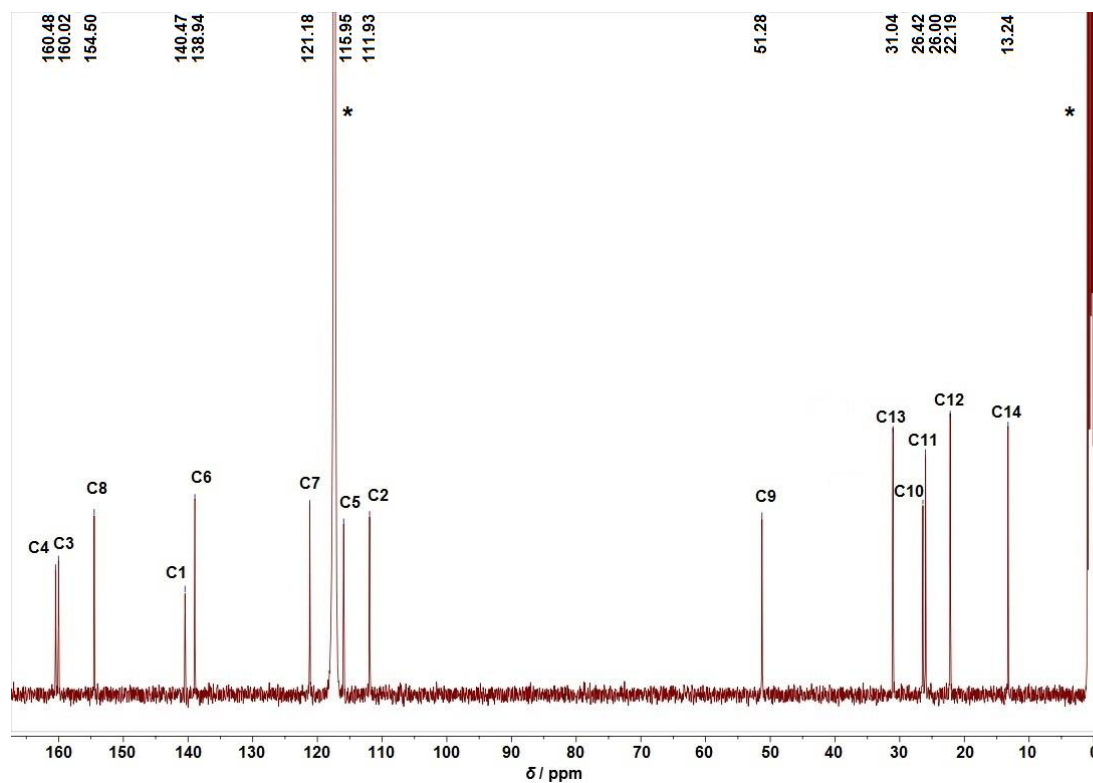
Figure S27. ^{1}H NMR spectrum of **[Fe(dcpp)(H$_2$tpda)][PF$_6$]$_2$** in CD$_3$CN. Asterisk denotes solvent resonance. # denotes resonance of residual water.
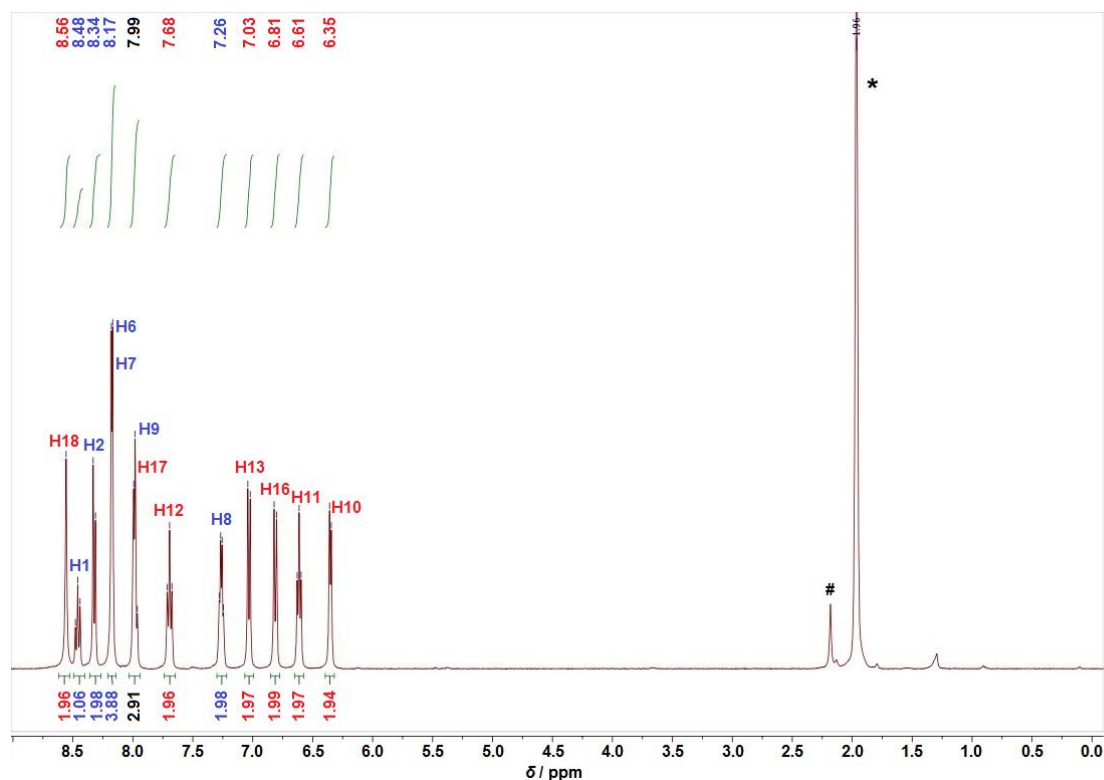
Figure S28. ^{13}C{^{1}H} NMR spectrum of **[Fe(dcpp)(H$_2$tpda)][PF$_6$]$_2$** in CD$_3$CN. Asterisk denotes solvent resonance.

14
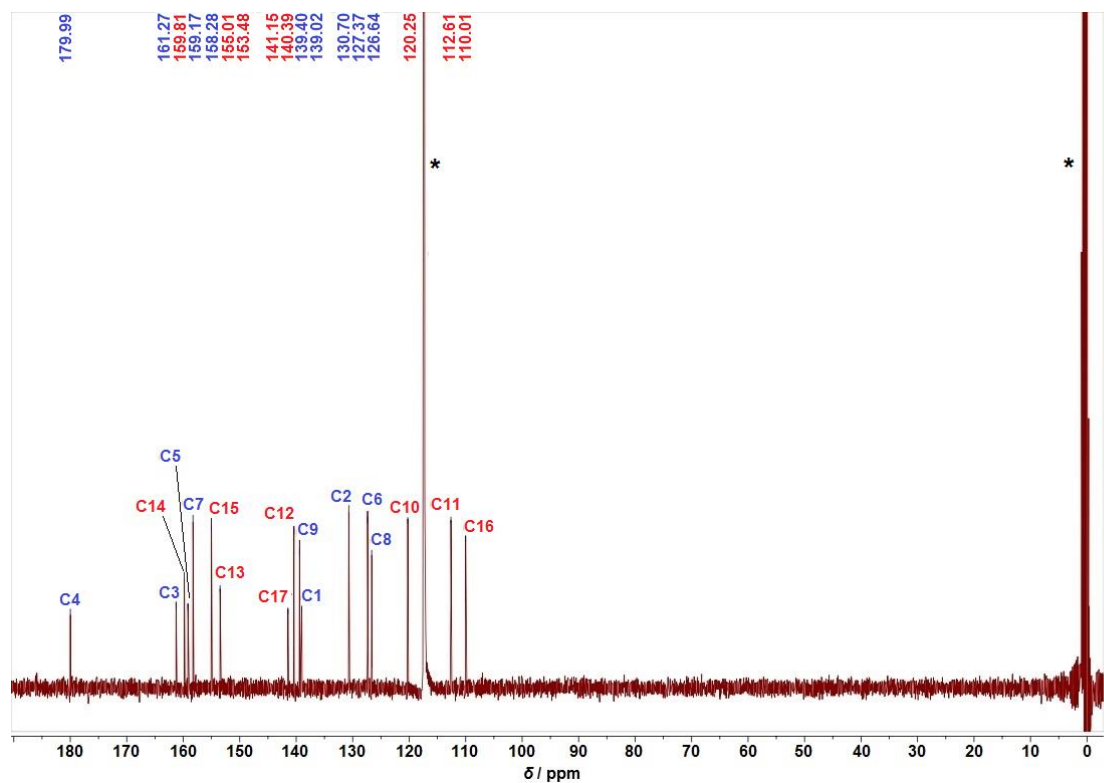
Figure S29. ^{1}H NMR spectrum of **[Fe(dcpp)(Pr$_2$tpda)][PF$_6$]$_2$** in CD$_3$CN. Asterisk denotes solvent resonance.
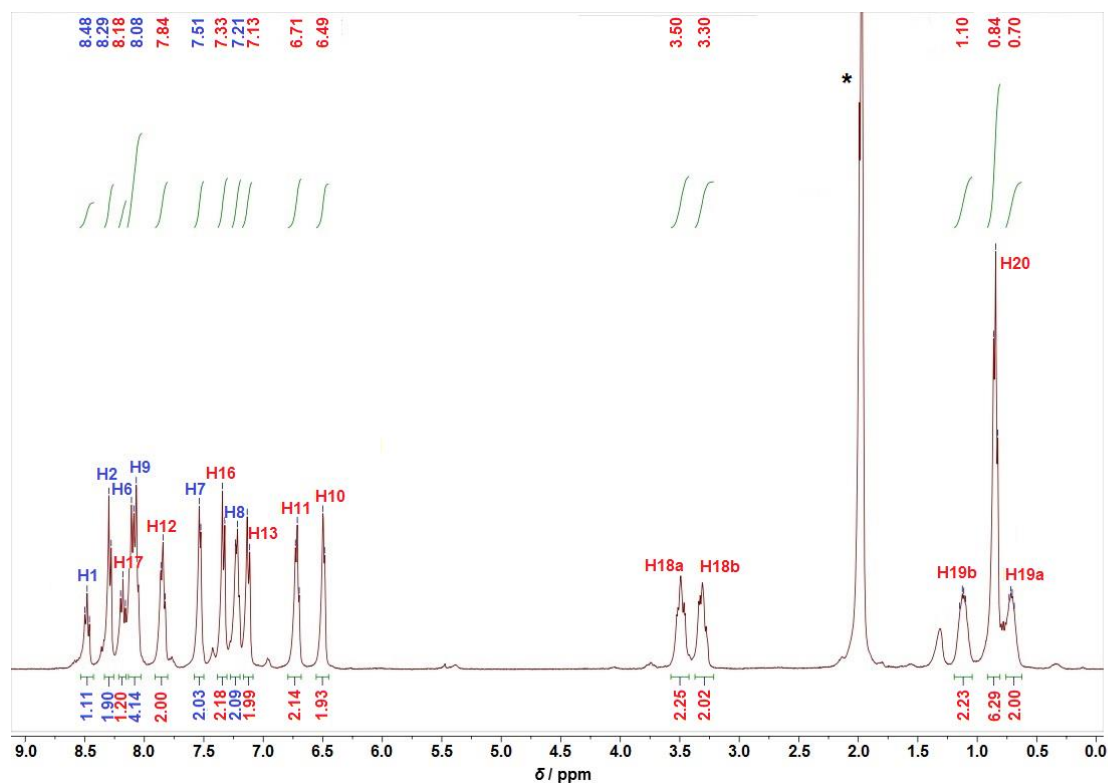
Figure S30. ^{13}C{^{1}H} NMR spectrum of **[Fe(dcpp)(Pr$_2$tpda)][PF$_6$]$_2$** in CD$_3$CN. Asterisk denotes solvent resonance.
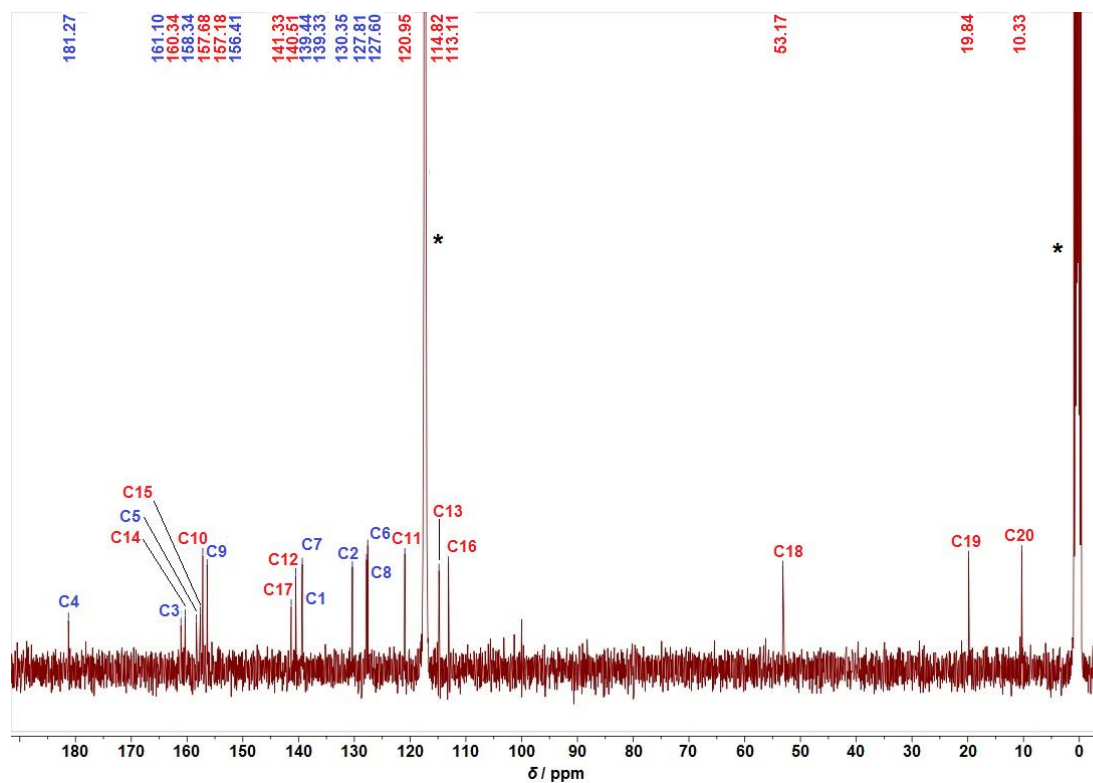
Figure S31. ^{1}H NMR spectrum of **[Fe(dcpp)(Hex$_2$tpda)][BF$_4$]$_2$** in CD$_3$CN. Asterisk denotes solvent resonance. # denote resonances of residual diethyl ether.
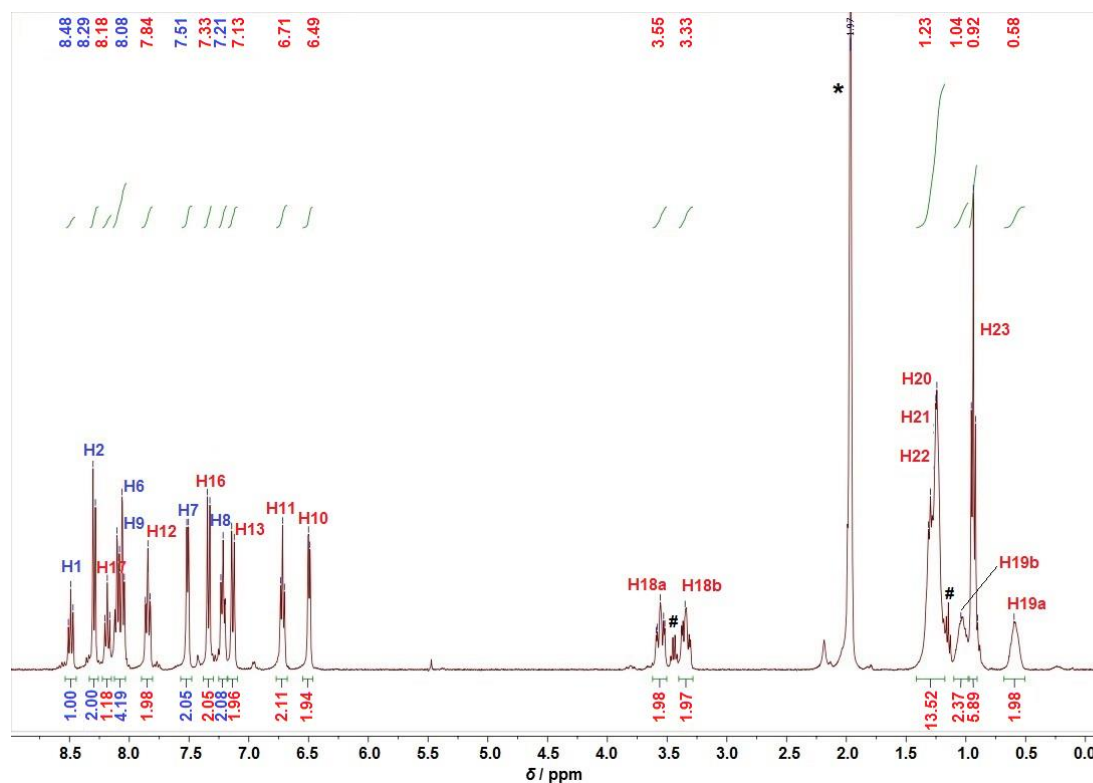
Figure S32. ^{13}C{^{1}H} NMR spectrum of **[Fe(dcpp)(Hex$_2$tpda)][BF$_4$]$_2$** in CD$_3$CN. Asterisk denotes solvent resonance.
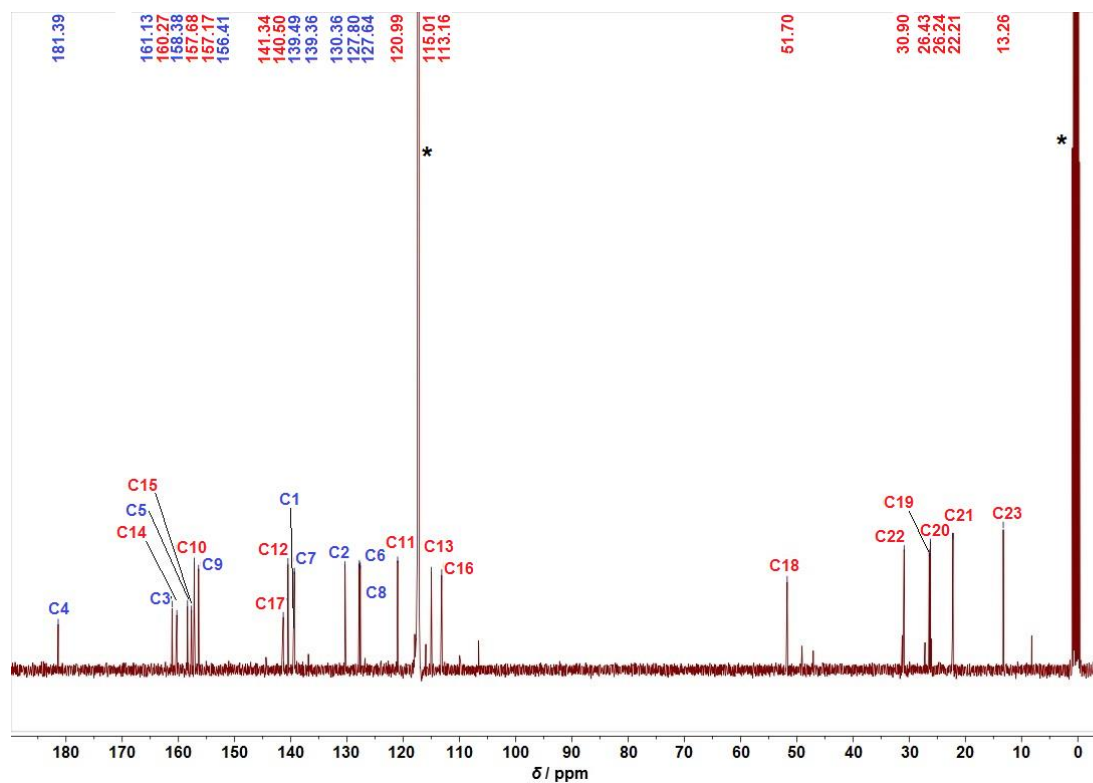
Figure S33. ^{1}H NMR spectra of **[Fe(Pr₂tpda)₂][BF₄]₂** in CD$_3$CN after addition of 2 µl H$_2$O over 15 d at room temperature. Asterisk denotes solvent resonance. # denotes resonance of water.
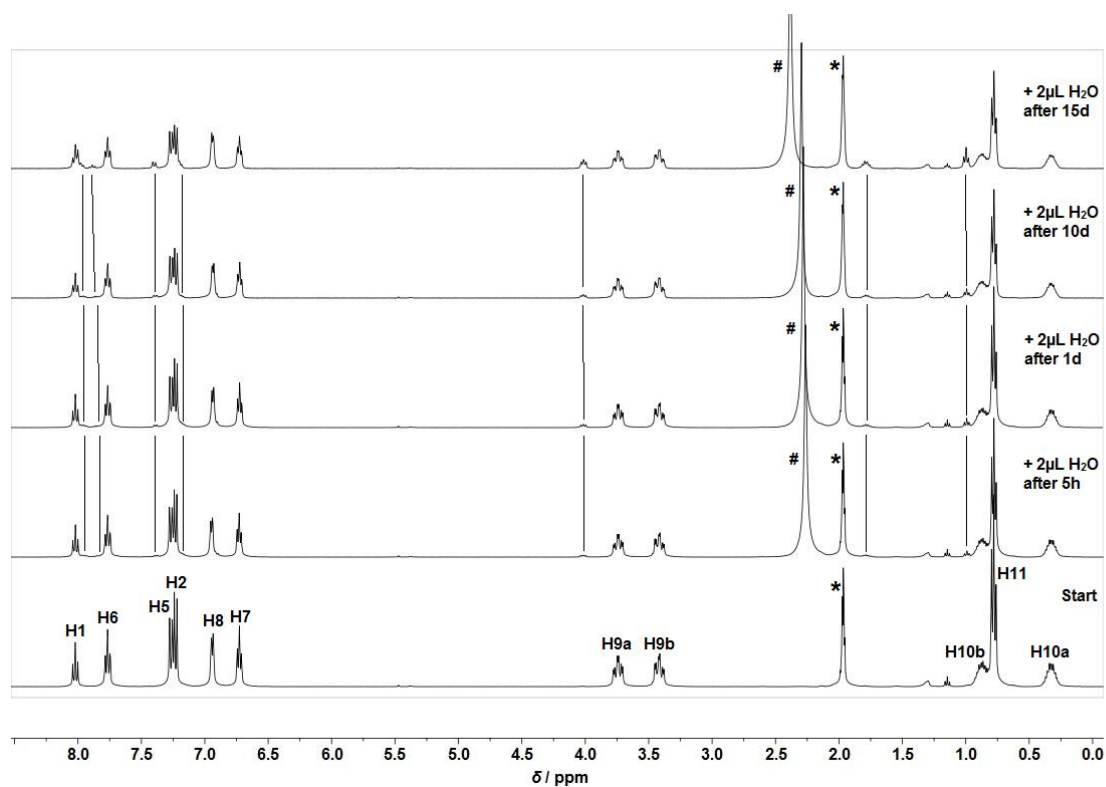
Figure S34. ^{1}H NMR spectra of **[Fe(Hex₂tpda)₂][PF₆]₂** in CD$_3$CN after addition of 5 µl H$_2$O over 20 d at room temperature. Asterisk denotes solvent resonance. # denotes resonance of water.
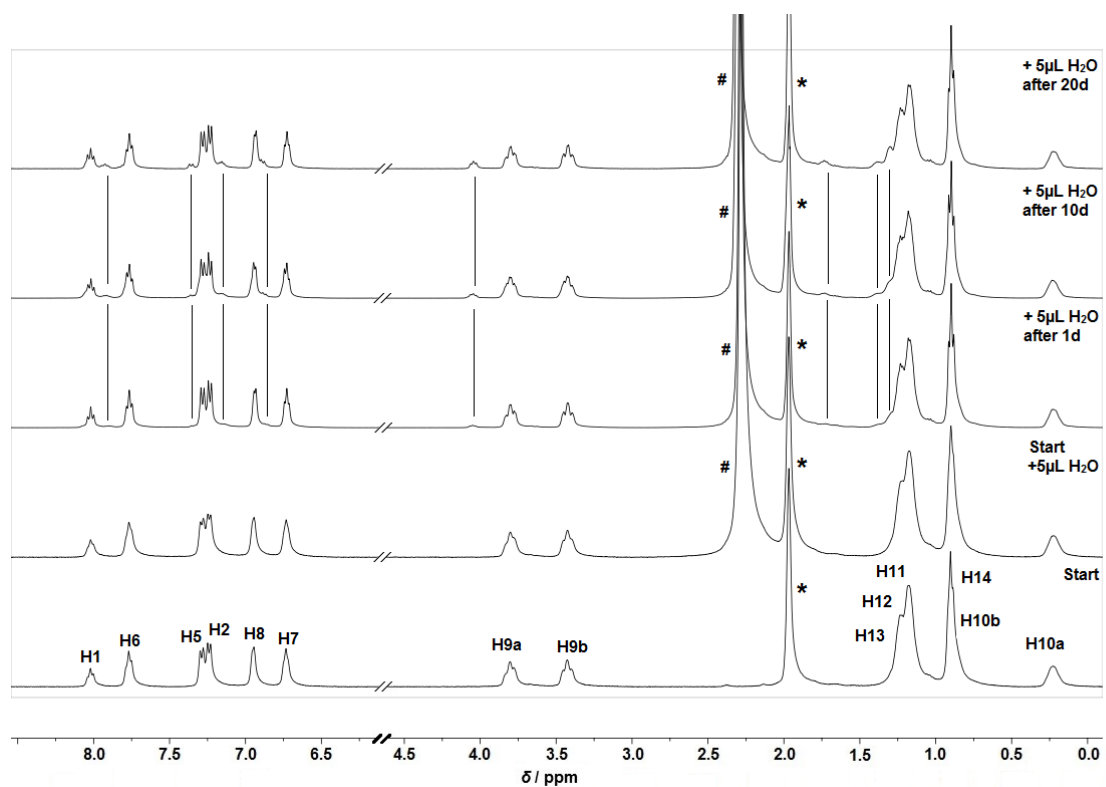
Figure S35. ^{1}H NMR spectra of **[Fe(dcpp)(Pr₂tpda)][PF₆]₂** in CD₃CN after addition of 2 µl H₂O over 15 d and after further addition of molecular sieve after 2d at room temperature. Top ^{1}H NMR spectrum corresponds to **Pr₂tpda** in CD₃CN. Asterisk denotes solvent resonance. # denotes resonance of water.
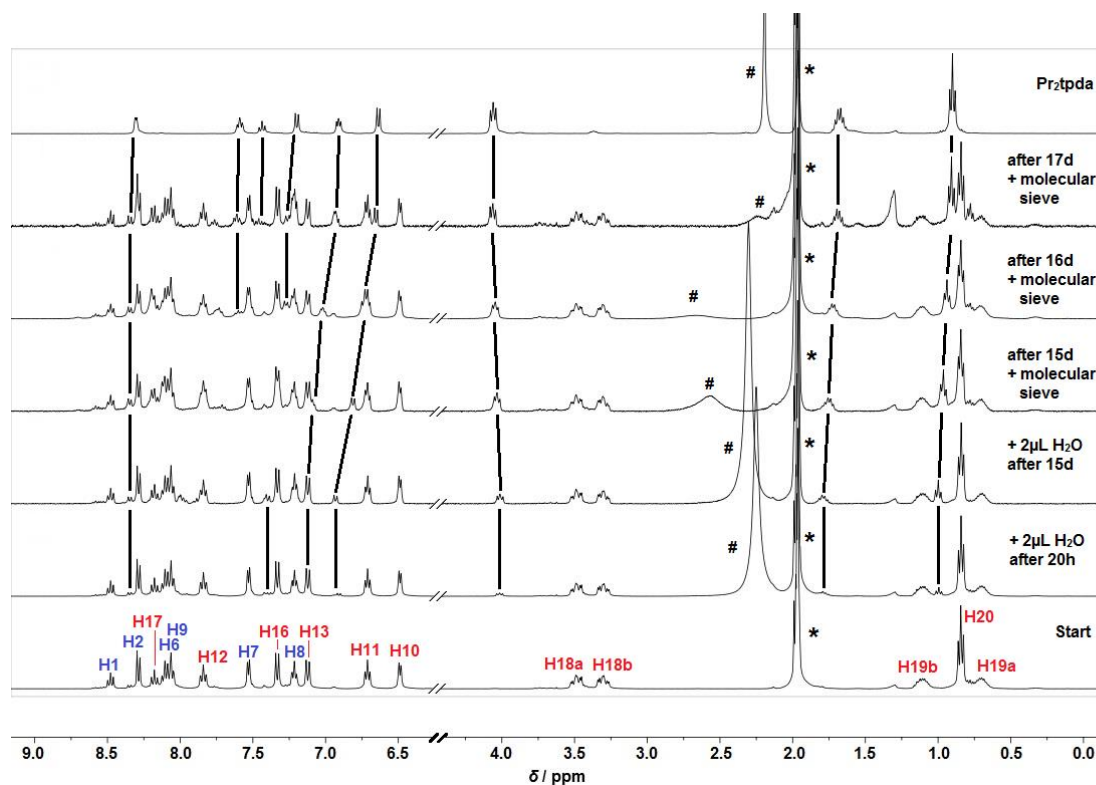
Figure S36. ^{1}H NMR spectra of **[Fe(dcpp)(Hex₂tpda)][BF₄]₂** in CD₃CN after addition of 1 µl and 50 µl H₂O over 12 d and after further addition of molecular sieve after 2d at room temperature. Top ^{1}H NMR spectrum corresponds to **Hex₂tpda** in CD₃CN. Asterisk denotes solvent resonance. # denotes resonance of water.

18
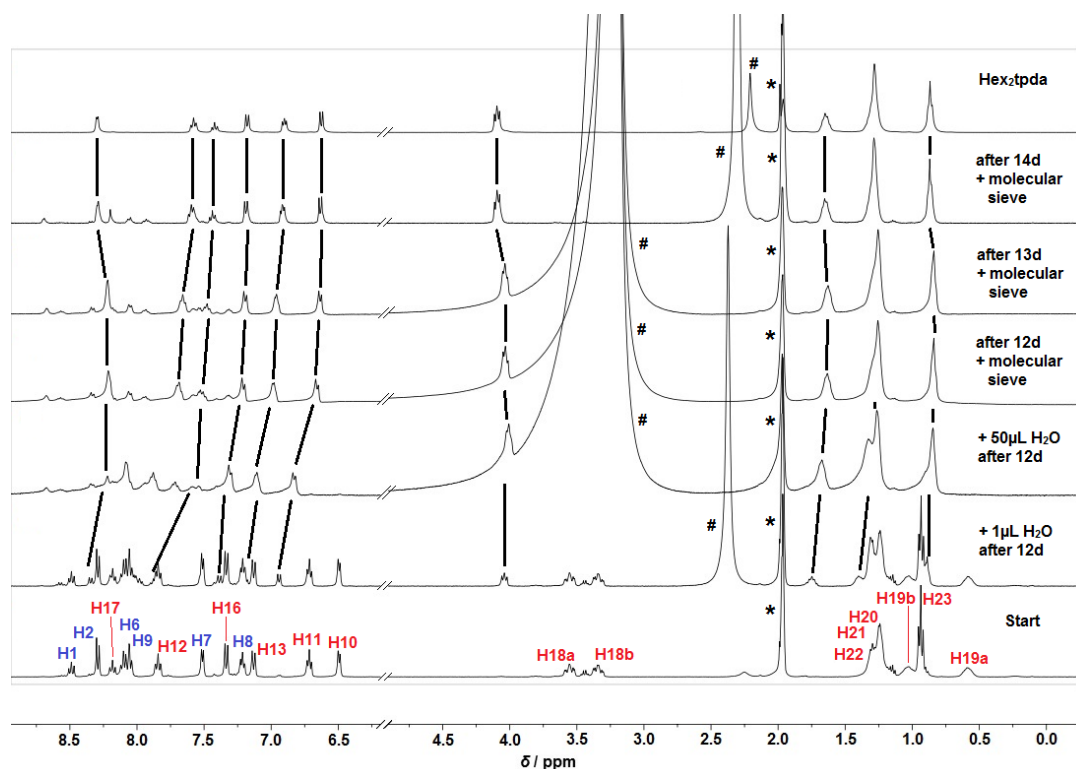
Figure S37. a) UV/Vis spectra of **[Fe(dcpp)(Pr₂tpda)][PF₆]₂** in CH₃CN after addition of > 8500 eq H₂O over time and b) UV/Vis spectra of **[Fe(dcpp)(Hex₂tpda)][BF₄]₂** in CH₃CN after addition of > 8500 eq H₂O over time.
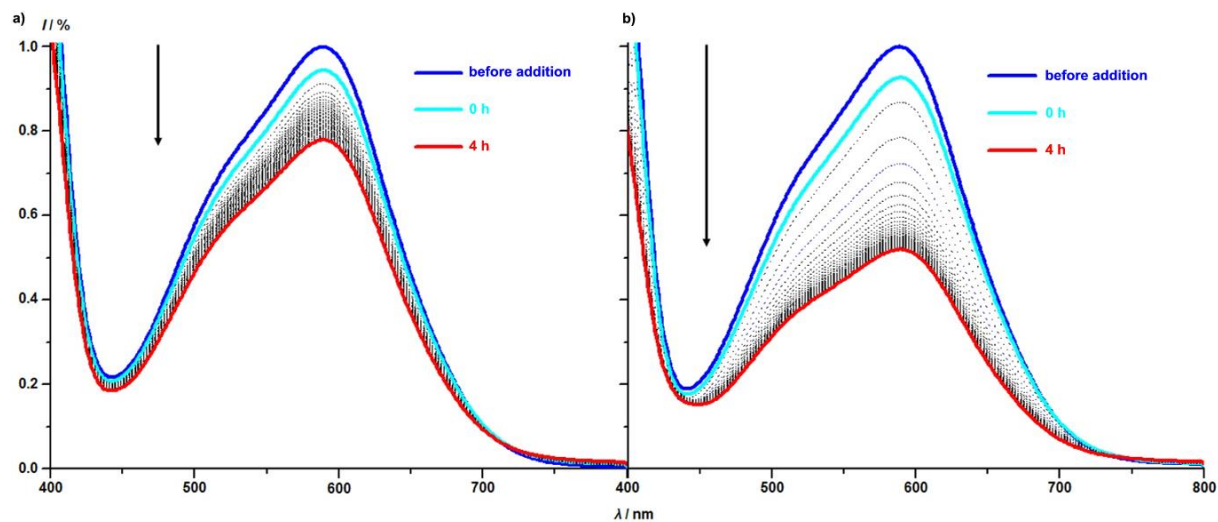
Figure S38. Plot of normalized absorption A_{592} vs. time for **[Fe(dcpp)(Pr₂tpda)][PF₆]₂** / > 8500 eq H₂O and **[Fe(dcpp)(Hex₂tpda)][BF₄]₂** / > 8500 eq H₂O.
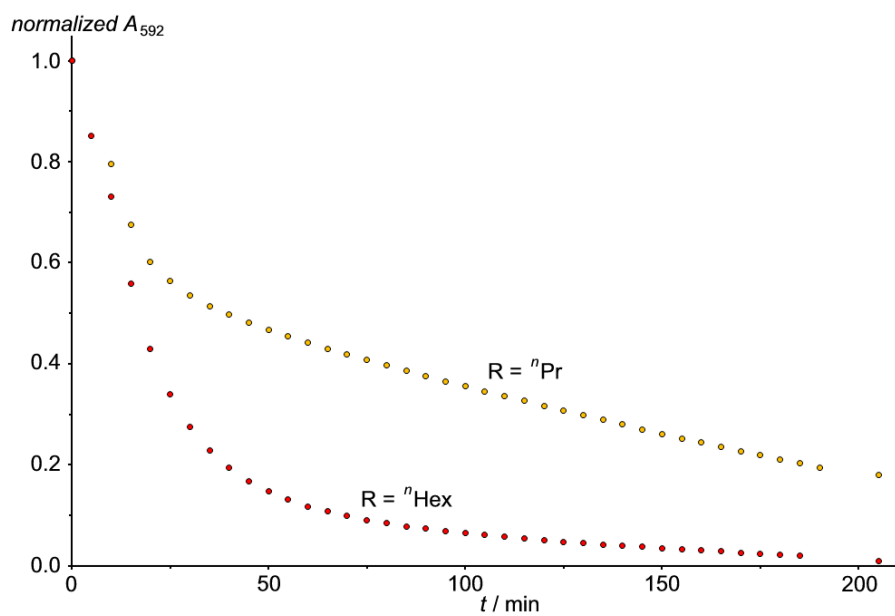
Figure S39. Illustration of the complete second coordination sphere of a) **[Fe(Me₂tpda)₂][PF₆]₂×CH₃CN** and b) **[Fe(Hex₂tpda)₂][PF₆]₂** in the solid state; distances given in Å; CH hydrogen atoms omitted.
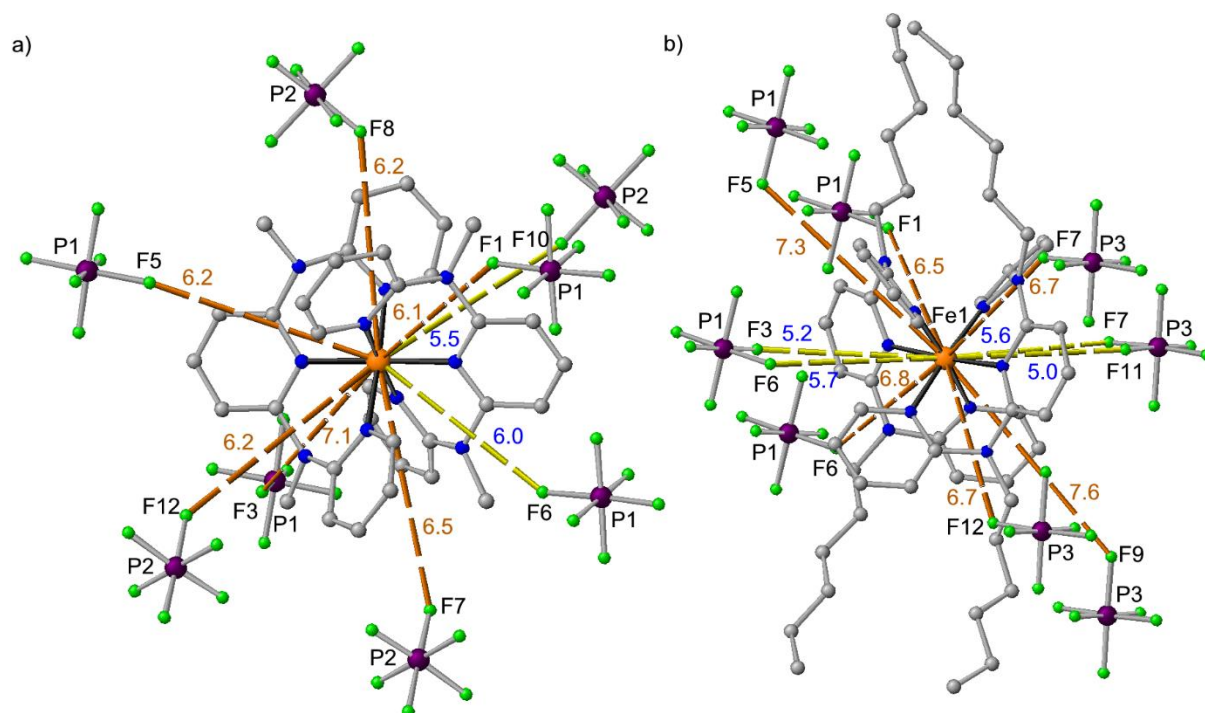
Figure S40. Illustration of the complete second coordination sphere of a) **[Fe(dcpp)(H₂tpda)][PF₆]₂×3.5H₂O** and b) **[Fe(dcpp)(Me₂tpda)][PF₆]₂×CH₃CN**[12] in the solid state; distances given in Å; CH hydrogen atoms omitted.
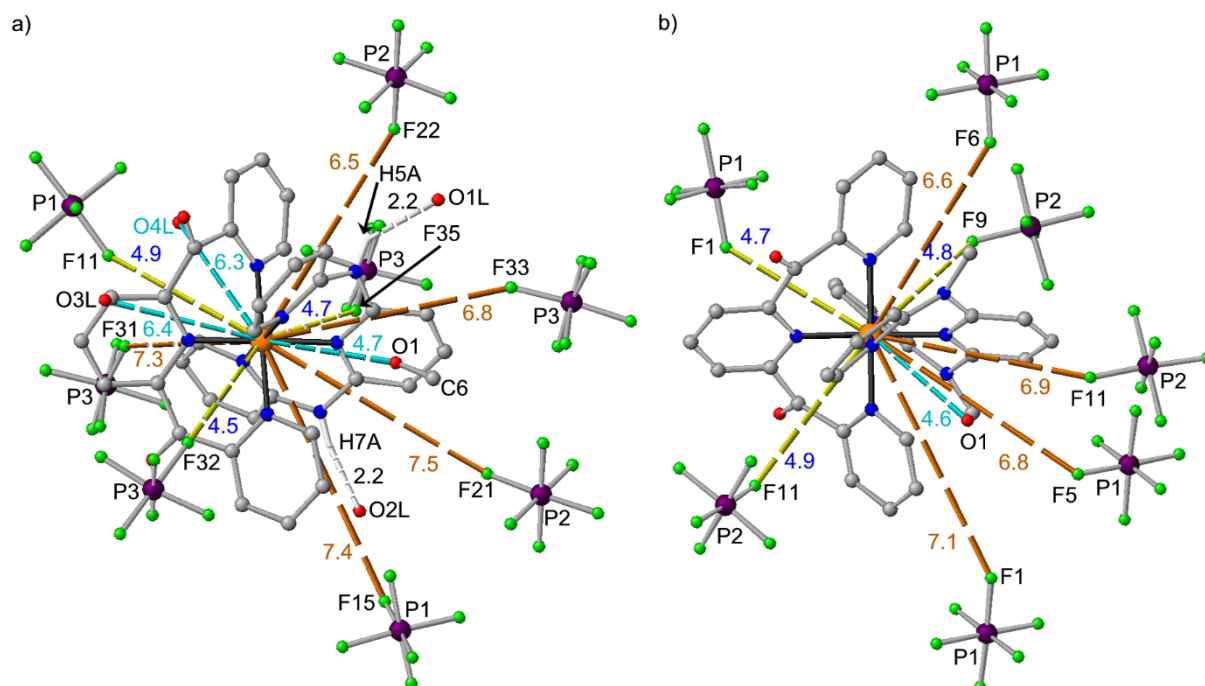
Figure S41. UV/Vis spectrum of **[Fe(Pr₂tpda)₂][BF₄]₂** in CH₃CN and Gaussian deconvolution of the MLCT/MC bands.
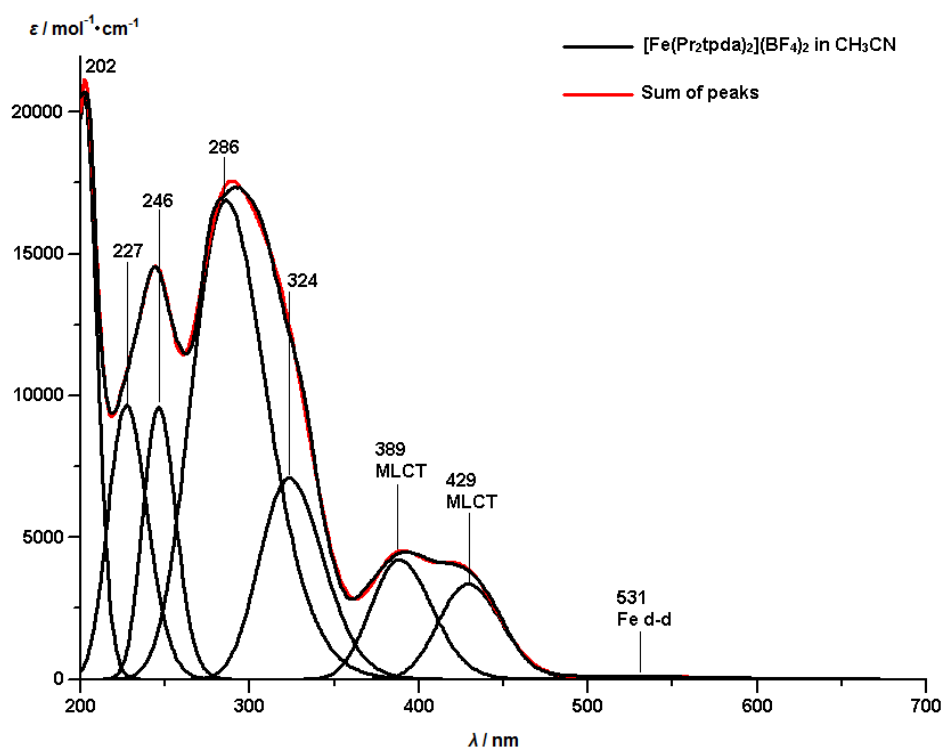
Figure S42. UV/Vis spectrum of **[Fe(Hex₂tpda)₂][PF₆]₂** in CH₃CN and Gaussian deconvolution of the MLCT/MC bands.

21
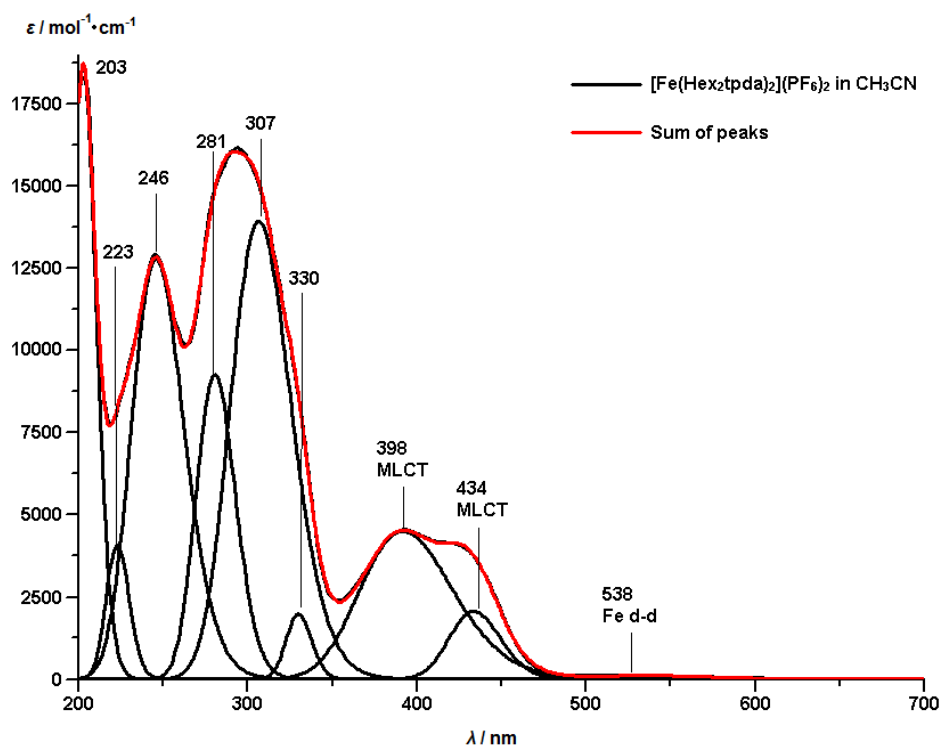
Figure S43. UV/Vis spectrum of "[Fe(H₂tpda)₂][BF₄]₂" in CH₃CN.
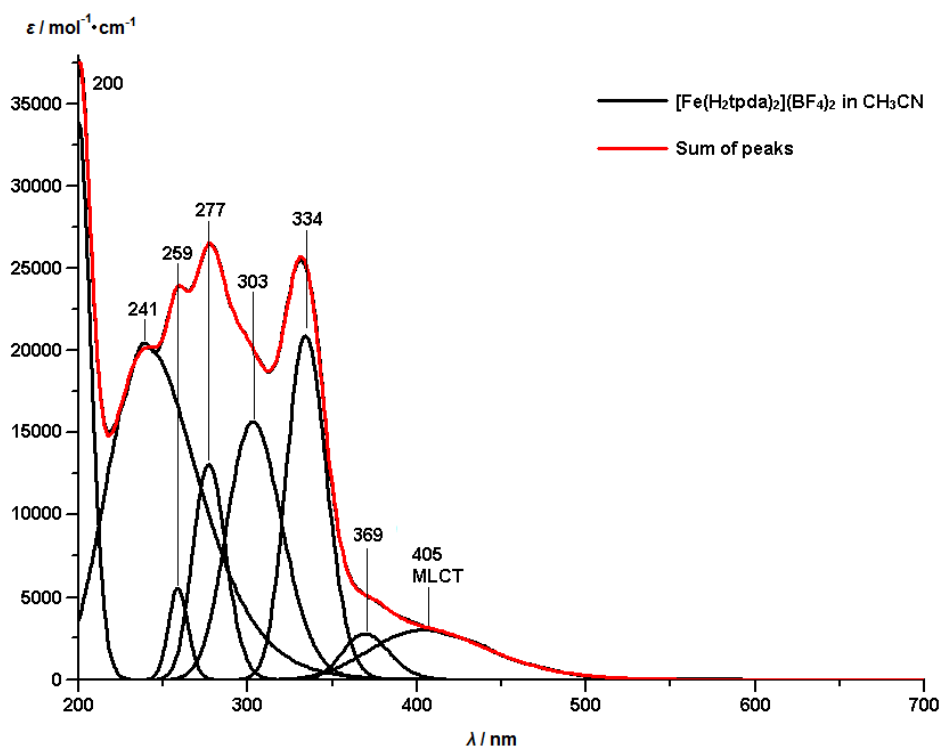
Figure S44. UV/Vis spectra of **[Fe(dcpp)(H₂tpda)][PF₆]₂, [Fe(dcpp)(Me₂tpda)][PF₆]₂, [Fe(dcpp)(Pr₂tpda)][PF₆]₂** and **[Fe(dcpp)(Hex₂tpda)][BF₄]₂** in CH₃CN.
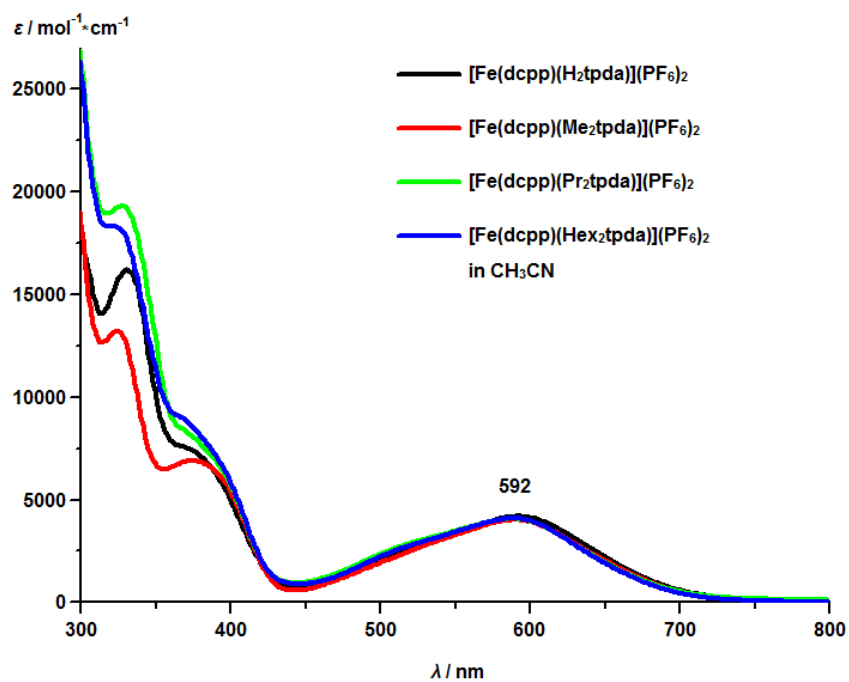
Figure S45. Cyclic voltammograms of a) **H₂tpda**, b) **Me₂tpda**, c) **Pr₂tpda** and d) **Hex₂tpda** in [ⁿBu₄N][PF₆]/CH₃CN solution, potentials vs. ferrocene/ferrocenium.

23
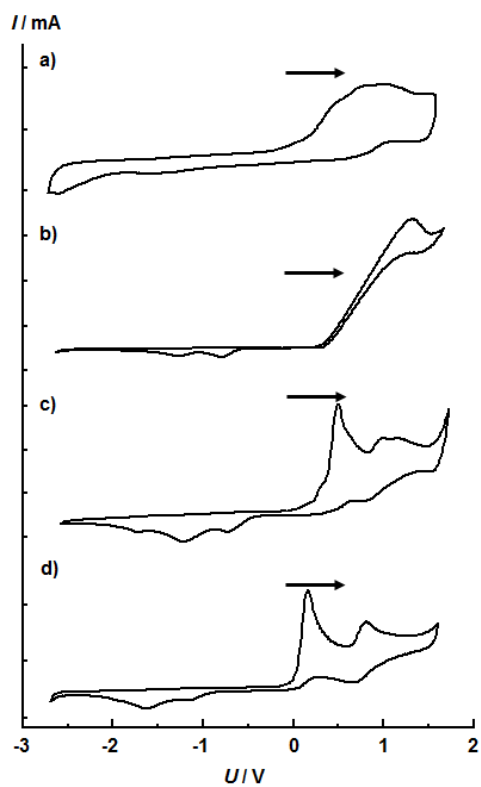
Figure S46. Cyclic voltammograms of a) **[Fe(H$_2$tpda)$_2$][BF$_4$]$_2$**, b) **[Fe(Me$_2$tpda)$_2$][PF$_6$]$_2$**, c) **[Fe(Pr$_2$tpda)$_2$][BF$_4$]$_2$** and d) **[Fe(Hex$_2$tpda)$_2$][PF$_6$]$_2$** in [^{n}Bu$_4$N][PF$_6$]/CH$_3$CN solution, potentials vs. ferrocene/ferrocenium.
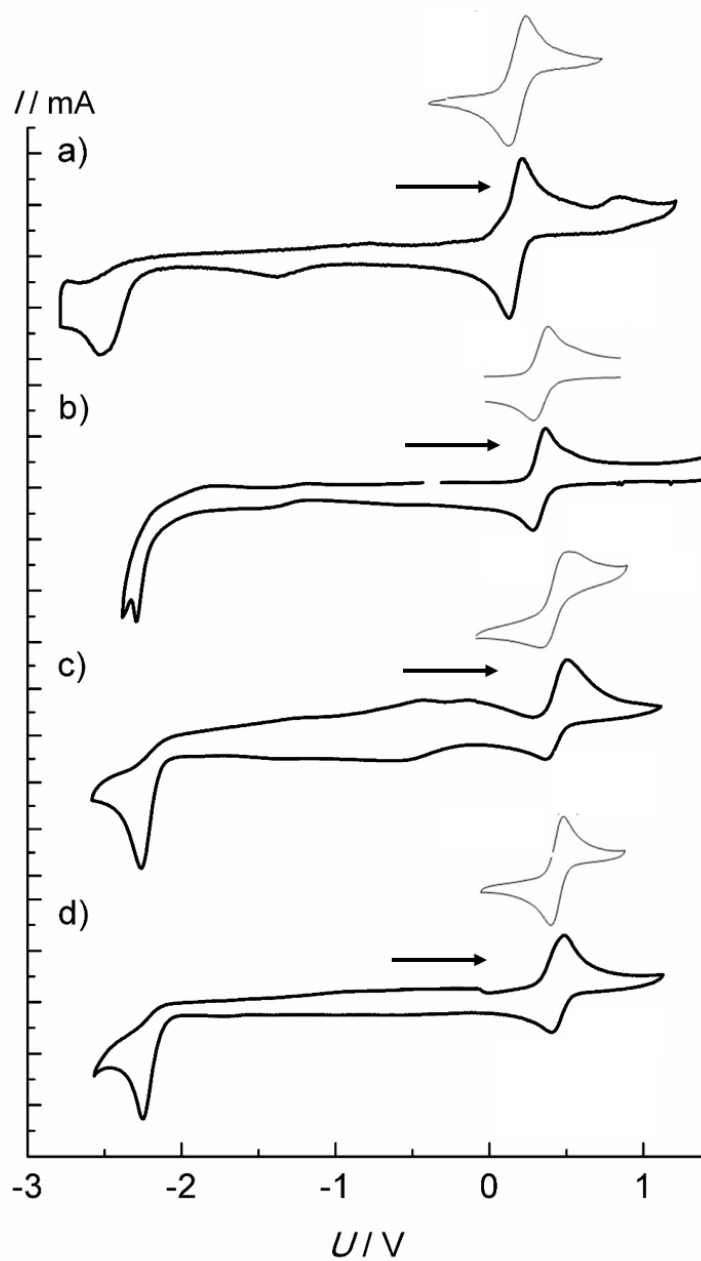
Figure S47. Cyclic voltammograms of a) **[Fe(dcpp)(H₂tpda)][PF₆]₂**, b) **[Fe(dcpp)(Me₂tpda)][PF₆]₂**, c) **[Fe(dcpp)(Pr₂tpda)][PF₆]₂** and d) **[Fe(dcpp)(Hex₂tpda)][BF₄]₂** in [^{n}Bu₄N][PF₆]/CH₃CN solution, potentials vs. ferrocene/ferrocenium. The extra waves around 0.4 V appear only after scanning to negative potentials and hence belong to a follow-up product after the irreversible reduction.
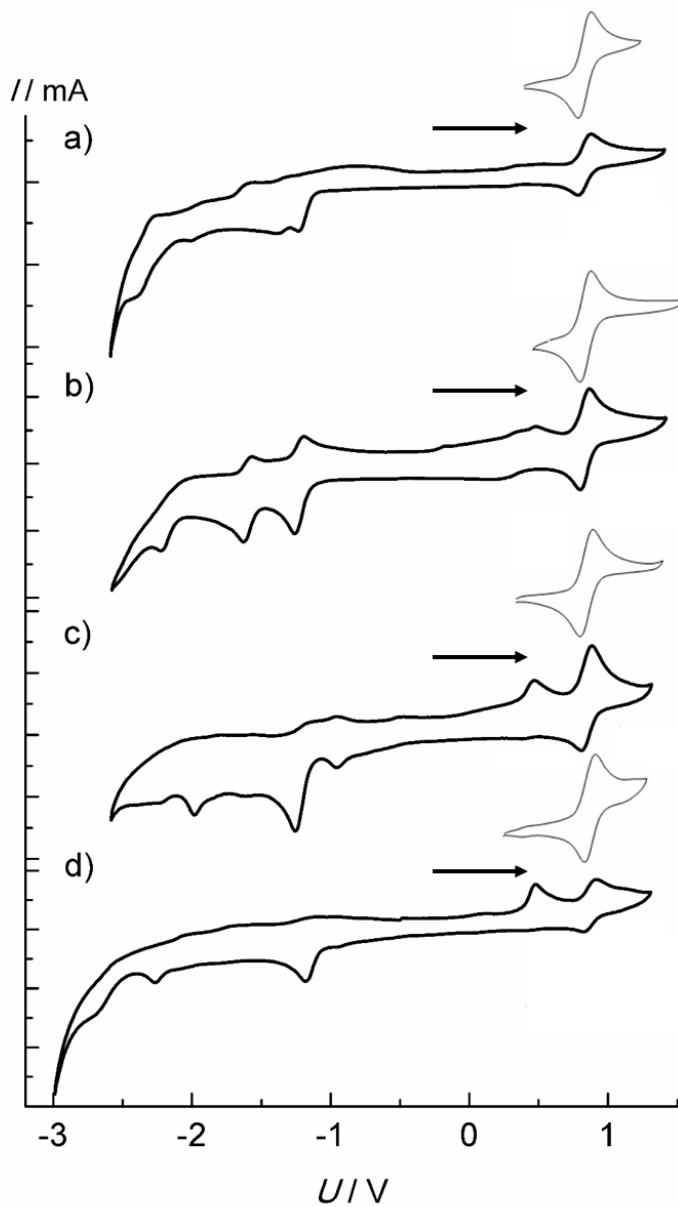
Figure S48. ^{1}H NMR spectra of a) **[Fe(dcpp)(H₂tpda)][PF₆]₂** and b) **[Fe(dcpp)(H₂tpda)][PF₆]₂** in the presence of 2.2 eq P₁-^{t}Bu in CD₃CN. Asterisk denotes solvent resonance. # denote resonances of protonated P₁-^{t}Bu.
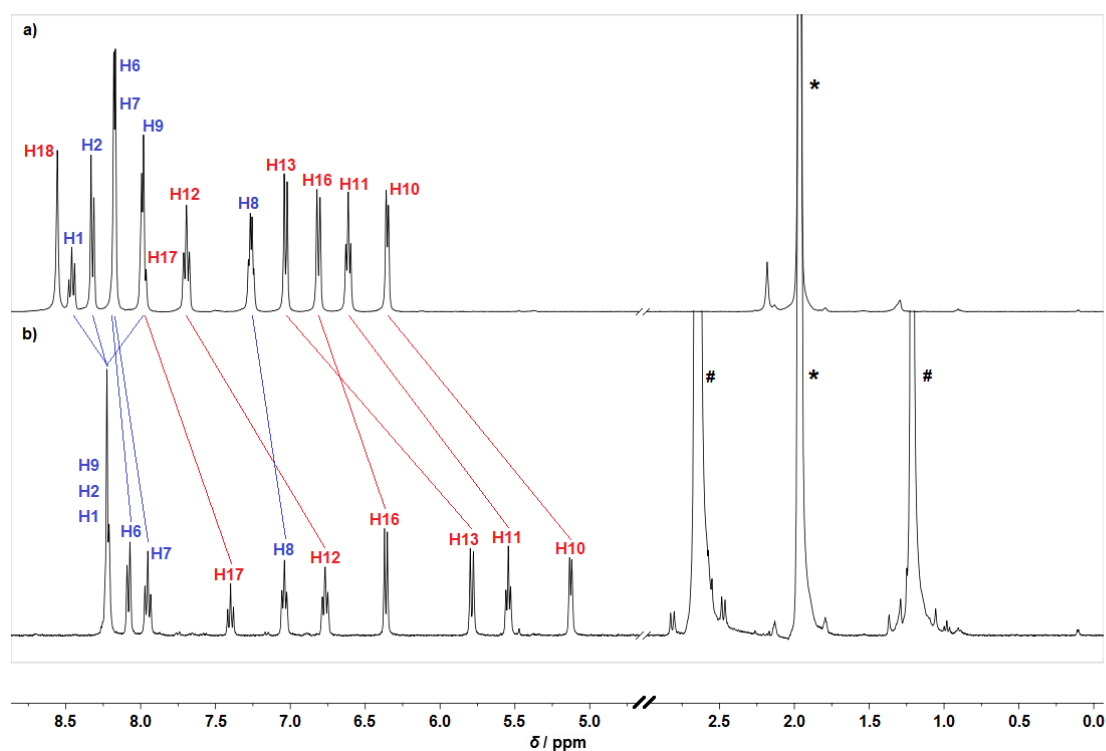
Figure S49. ^{13}C{^{1}H} NMR spectra of a) **[Fe(dcpp)(H₂tpda)][PF₆]₂** and b) **[Fe(dcpp)(H₂tpda)][PF₆]₂** in the presence of 2.2 eq P₁-^{t}Bu in CD₃CN. Asterisk denotes solvent resonance. # denote resonances of protonated P₁-^{t}Bu.

26
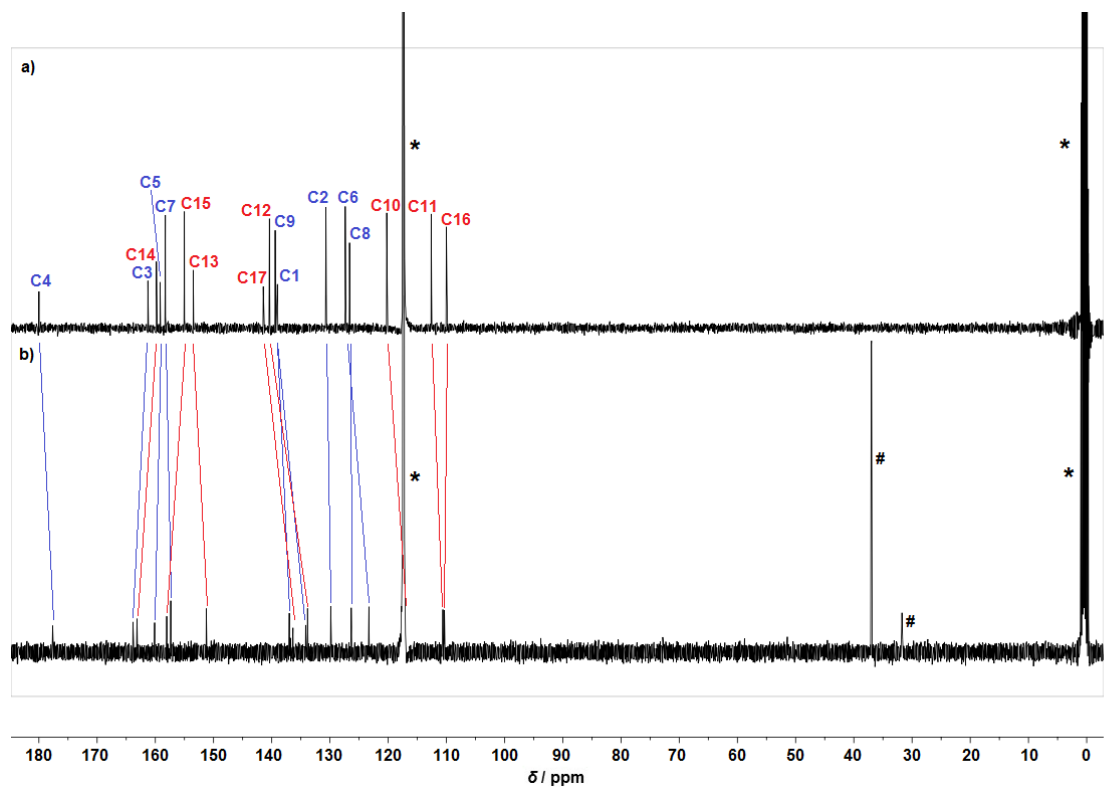
Figure S50. ^{1}H NMR spectra of a) **[Fe(dcpp)(Me₂tpda)][PF₆]₂** and b) **[Fe(dcpp)(Me₂tpda)][PF₆]₂** prepared from **[Fe(dcpp)(Me₂tpda)][PF₆]₂** / 2.2 eq P₁-[t]Bu / excess MeI in CD₃CN. Asterisk denotes solvent resonance. # denote resonances of protonated P₁-[t]Bu.
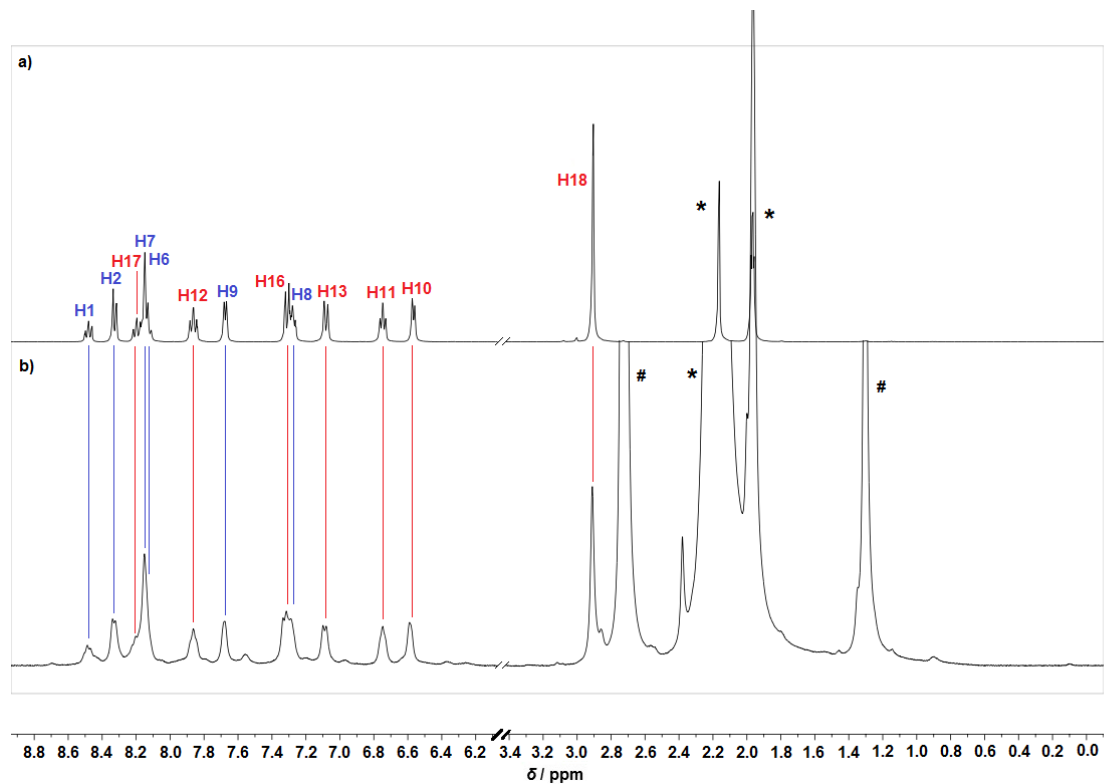
Figure S51. Cyclic voltammograms of a) **[Fe(dcpp)(H$_2$tpda)][PF$_6$]$_2$** in the absence of P$_1$-^{t}Bu, b) in the presence of 1 eq P$_1$-^{t}Bu and c) in the presence of 2 eq P$_1$-^{t}Bu in [^{n}Bu$_4$N][PF$_6$]/CH$_3$CN solution, potentials vs. ferrocene/ferrocenium.
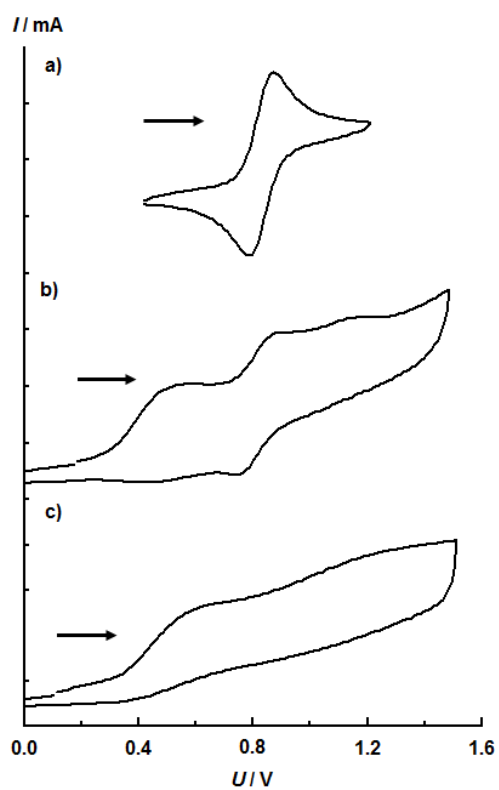
Figure S52. UV/Vis spectra of **[Fe(dcpp)(H₂tpda)][PF₆]₂** a) in the presence of 1 eq P₁-*t*Bu and b) in the presence of 2 eq P₁-*t*Bu in CH₃CN and Gaussian deconvolutions of the MLCT/LL'CT bands.
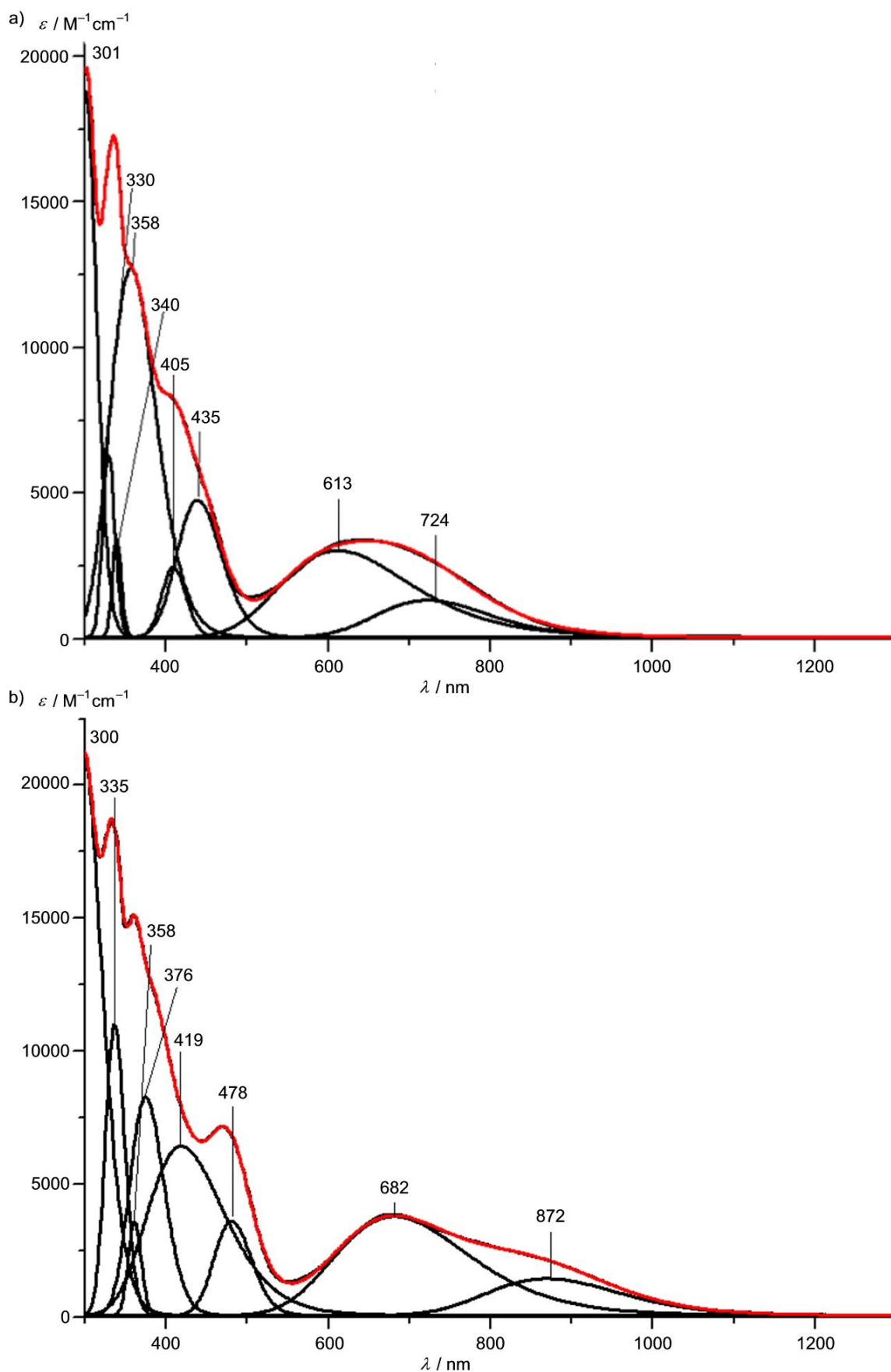
Cartesian coordinates of DFT calculated geometries

[Fe(dcpp)(H$_2$tpda)]$^{2+}$

```
6        1.119250000      -2.633421000      -0.288762000
6        1.160951000      -4.023111000      -0.277709000
6       -0.000349000      -4.720383000       0.000347000
6       -1.161564000      -4.022903000       0.278273000
6       -1.119679000      -2.633223000       0.289040000
7       -0.000171000      -1.937511000       0.000067000
1        2.081424000      -4.532970000      -0.522584000
1       -2.082084000      -4.532560000       0.523362000
6        1.394839000       0.999788000      -2.420550000
6        2.437165000       1.163895000      -3.298260000
6        3.527186000       0.296100000      -3.203751000
6        3.487935000      -0.730223000      -2.287545000
6        2.368165000      -0.857020000      -1.458217000
7        1.372635000       0.040391000      -1.465916000
1        4.380275000       0.405756000      -3.859246000
1        0.542285000       1.659334000      -2.443587000
1        2.405743000       1.958462000      -4.028918000
1        4.285437000      -1.457100000      -2.218713000
6       -2.368324000      -0.856551000       1.458332000
6       -3.488034000      -0.729580000       2.287721000
6       -3.527150000       0.296854000       3.203794000
6       -2.437048000       1.164560000       3.298156000
6       -1.394742000       1.000236000       2.420466000
7       -1.372673000       0.040730000       1.465936000
1       -4.380192000       0.406725000       3.859319000
1       -4.285598000      -1.456405000       2.219014000
1       -2.405489000       1.959215000       4.028711000
1       -0.542129000       1.659713000       2.443396000
6        1.147692000       2.720548000       0.122862000
6        1.184945000       4.109861000       0.099957000
6        0.000517000       4.819411000      -0.000642000
6       -1.184078000       4.110081000      -0.100879000
6       -1.147124000       2.720752000      -0.123170000
7        0.000207000       2.026023000      -0.000054000
1        2.138092000       4.610151000       0.181940000
1       -2.137103000       4.610577000      -0.183058000
6        1.444535000      -0.864401000       2.377127000
6        2.513174000      -1.030370000       3.241566000
6        3.632889000      -0.225417000       3.092793000
6        3.619928000       0.745880000       2.104541000
6        2.498202000       0.871421000       1.294778000
7        1.433405000       0.055056000       1.402685000
1        4.490988000      -0.339487000       3.740521000
1        0.574746000      -1.496724000       2.453053000
1        2.460650000      -1.788998000       4.009227000
1        4.449619000       1.422283000       1.963392000
6       -2.498089000       0.871799000      -1.294710000
6       -3.619841000       0.746493000      -2.104462000
6       -3.633003000      -0.224765000      -3.092752000
6       -2.513446000      -1.029936000      -3.241537000
6       -1.444764000      -0.864195000      -2.377103000
7       -1.433444000       0.055249000      -1.402651000
1       -4.491126000      -0.338613000      -3.740474000
1       -4.449462000       1.422988000      -1.963312000
1       -2.461031000      -1.788571000      -4.009196000
1       -0.575095000      -1.496680000      -2.453063000
7        2.282928000      -1.946197000      -0.611424000
7       -2.283265000      -1.945771000       0.611581000
1       -0.000485000      -5.801698000       0.000518000
1        0.000625000       5.900264000      -0.001011000
26      -0.000007000       0.058510000       0.000013000
6       -2.452639000       2.014248000      -0.339921000
6        2.453056000       2.013868000       0.339959000
8        3.472611000       2.479302000      -0.126125000
8       -3.472066000       2.480093000       0.126018000
1        3.086141000      -2.553999000      -0.671859000
1       -3.086576000      -2.553438000       0.672044000
```

[Fe(dcpp)(Htpda)]⁺

6	1.156200000	-2.611692000	-0.317614000
6	1.192581000	-4.016028000	-0.138967000
6	0.057426000	-4.707638000	0.199022000
6	-1.131976000	-4.012287000	0.412448000
6	-1.106892000	-2.633091000	0.305694000
7	-0.007950000	-1.933052000	-0.041594000
1	2.129097000	-4.517910000	-0.332030000
1	-2.041920000	-4.516069000	0.704878000
6	1.373918000	1.013797000	-2.425503000
6	2.434872000	1.222749000	-3.265776000
6	3.558434000	0.390588000	-3.122990000
6	3.512949000	-0.644019000	-2.229122000
6	2.344028000	-0.886578000	-1.455131000
7	1.342037000	0.043676000	-1.480117000
1	4.440221000	0.548852000	-3.730820000
1	0.507021000	1.656192000	-2.467912000
1	2.404091000	2.023456000	-3.990242000
1	4.331735000	-1.342014000	-2.125195000
6	-2.390148000	-0.858318000	1.427917000
6	-3.519725000	-0.716186000	2.245041000
6	-3.553912000	0.306035000	3.165142000
6	-2.451831000	1.157942000	3.277449000
6	-1.403775000	0.983708000	2.408198000
7	-1.385135000	0.029959000	1.448946000
1	-4.412648000	0.425073000	3.811920000
1	-4.327372000	-1.430710000	2.163787000
1	-2.417021000	1.947377000	4.013621000
1	-0.542335000	1.631920000	2.441223000
6	1.144503000	2.694419000	0.105892000
6	1.188632000	4.084544000	0.101786000
6	0.008539000	4.803417000	0.024745000
6	-1.181832000	4.102746000	-0.074404000
6	-1.154092000	2.713871000	-0.115420000
7	-0.009454000	2.009156000	-0.011156000
1	2.146160000	4.577069000	0.179300000
1	-2.132373000	4.610087000	-0.142604000
6	1.446555000	-0.913403000	2.313770000
6	2.525751000	-1.098041000	3.160014000
6	3.651954000	-0.302824000	3.000653000
6	3.633055000	0.677630000	2.022748000
6	2.500077000	0.822994000	1.230398000
7	1.430370000	0.014540000	1.346728000
1	4.518924000	-0.431699000	3.633909000
1	0.571612000	-1.537576000	2.394224000
1	2.478337000	-1.864101000	3.920773000
1	4.466770000	1.347628000	1.874860000
6	-2.515544000	0.886364000	-1.305600000
6	-3.637850000	0.773899000	-2.118009000
6	-3.654519000	-0.188707000	-3.114069000
6	-2.538855000	-0.999663000	-3.267123000
6	-1.470397000	-0.848197000	-2.399927000
7	-1.456494000	0.064353000	-1.419020000
1	-4.511941000	-0.292338000	-3.764668000
1	-4.463934000	1.453766000	-1.972154000
1	-2.491019000	-1.752744000	-4.040743000
1	-0.602805000	-1.483599000	-2.472275000
7	2.281825000	-2.042181000	-0.782084000
7	-2.296353000	-1.939589000	0.580629000
1	0.080977000	-5.784619000	0.304543000
1	0.015610000	5.884230000	0.040250000
26	-0.017959000	0.048286000	-0.032931000
6	-2.463786000	2.020390000	-0.341387000
6	2.448929000	1.979897000	0.295818000
8	3.467603000	2.465979000	-0.156448000
8	-3.483367000	2.492947000	0.121483000
1	-3.090856000	-2.557989000	0.646342000

Fe(dcpp)(tpda)

```
6        1.140714000      -2.617424000      -0.334160000
6        1.160599000      -4.023489000      -0.276035000
6       -0.000253000      -4.719460000       0.000502000
6       -1.161038000      -4.023311000       0.276838000
6       -1.141040000      -2.617236000       0.334555000
7       -0.000135000      -1.932874000       0.000103000
1        2.085132000      -4.524883000      -0.521528000
1       -2.085604000      -4.524557000       0.522491000
6        1.379336000       0.996974000      -2.416752000
6        2.452586000       1.223857000      -3.236546000
6        3.596712000       0.422859000      -3.053276000
6        3.557434000      -0.604331000      -2.153317000
6        2.366983000      -0.882062000      -1.415581000
7        1.350053000       0.036552000      -1.462229000
1        4.490842000       0.602928000      -3.637231000
1        0.498923000       1.620428000      -2.479730000
1        2.420001000       2.015891000      -3.970587000
1        4.394026000      -1.276430000      -2.020229000
6       -2.367157000      -0.881567000       1.415620000
6       -3.557659000      -0.603541000       2.153157000
6       -3.596899000       0.423799000       3.052941000
6       -2.452679000       1.224664000       3.236224000
6       -1.379357000       0.997496000       2.416796000
7       -1.350091000       0.036908000       1.462241000
1       -4.491085000       0.604082000       3.636742000
1       -4.394337000      -1.275530000       2.020062000
1       -2.420120000       2.016814000       3.970142000
1       -0.498867000       1.620847000       2.479573000
6        1.152210000       2.684727000       0.093766000
6        1.186573000       4.074711000       0.070965000
6        0.000521000       4.785219000      -0.000377000
6       -1.185690000       4.074953000      -0.071511000
6       -1.151631000       2.684957000      -0.093954000
7        0.000213000       1.989415000      -0.000035000
1        2.141921000       4.573866000       0.131252000
1       -2.140918000       4.574325000      -0.131927000
6        1.477393000      -0.898545000       2.330636000
6        2.560432000      -1.073085000       3.173437000
6        3.685047000      -0.275971000       3.002935000
6        3.659843000       0.696479000       2.018103000
6        2.522372000       0.833700000       1.228751000
7        1.456751000       0.021892000       1.355989000
1        4.554795000      -0.397819000       3.634049000
1        0.601502000      -1.520800000       2.413454000
1        2.519208000      -1.833309000       3.940620000
1        4.491221000       1.367494000       1.861577000
6       -2.522198000       0.834143000      -1.228742000
6       -3.659679000       0.697167000      -2.018116000
6       -3.685062000      -0.275268000      -3.002959000
6       -2.560616000      -1.072619000      -3.173437000
6       -1.477566000      -0.898328000      -2.330592000
7       -1.356749000       0.022109000      -1.355951000
1       -4.554810000      -0.396894000      -3.634108000
1       -4.490901000       1.368376000      -1.861611000
1       -2.519506000      -1.832877000      -3.940591000
1       -0.601807000      -1.520772000      -2.413394000
7        2.294402000      -2.036405000      -0.760491000
7       -2.294685000      -2.036005000       0.760703000
1       -0.000336000      -5.803040000       0.000683000
1        0.000622000       5.866310000      -0.000602000
26       0.000007000       0.038380000       0.000024000
6       -2.461181000       1.984459000      -0.287944000
6        2.461608000       1.983988000       0.287903000
8        3.479466000       2.482807000      -0.158409000
8       -3.478929000       2.483593000       0.158263000
```

Eur. J. Inorg. Chem. **2015** · ISSN 1099–0682

SUPPORTING INFORMATION

Author(s): Andreas K. C. Mengel, Woohyung Cho, Aaron Breivogel, Kookheon Char, Yong Soo Kang, Katja Heinze*

Figure S1. ^{1}H NMR spectra of **1(PF6)2** (blue) and **(nBu4N)2(PF6)2** (red) in CD3CN recorded at 400 MHz.
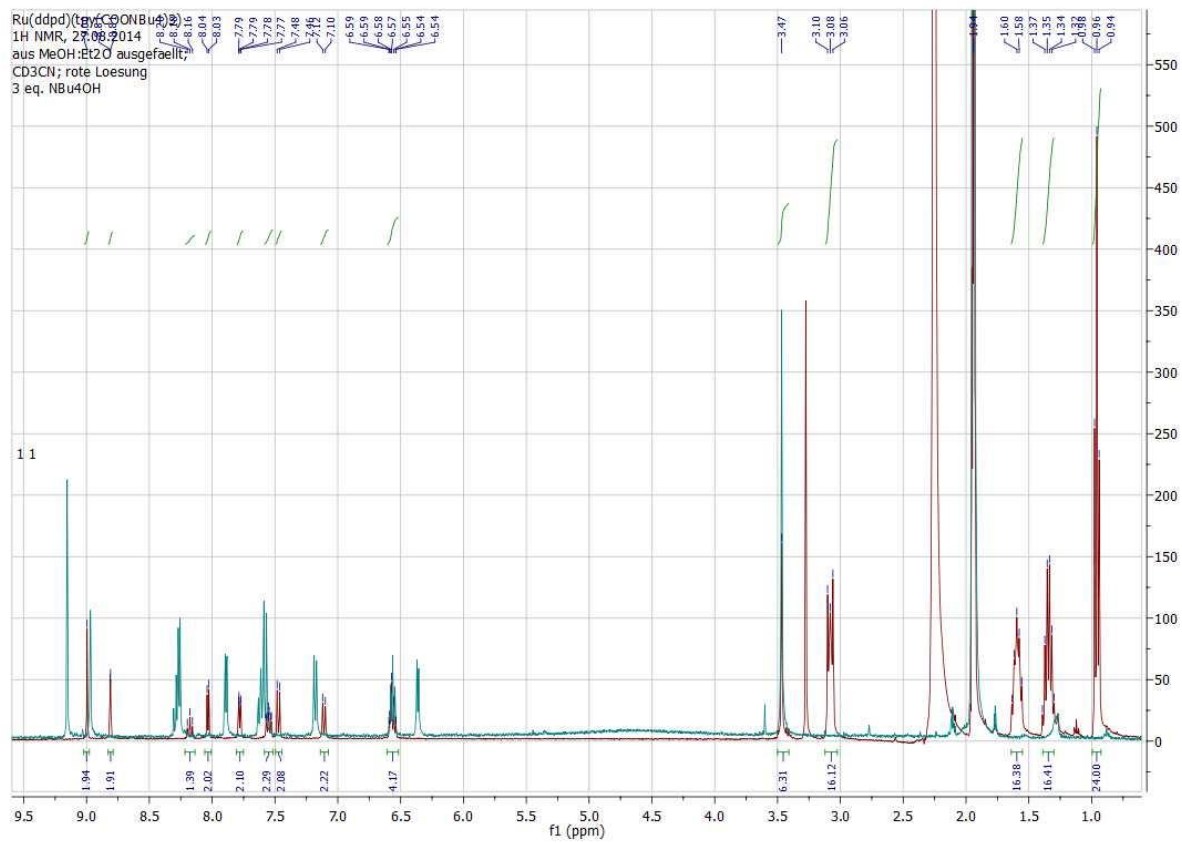
Figure S2. ^{1}H-NMR spectrum of **3**(BF$_4$)$_3$ in DMSO-d_6 recorded at 400 MHz.
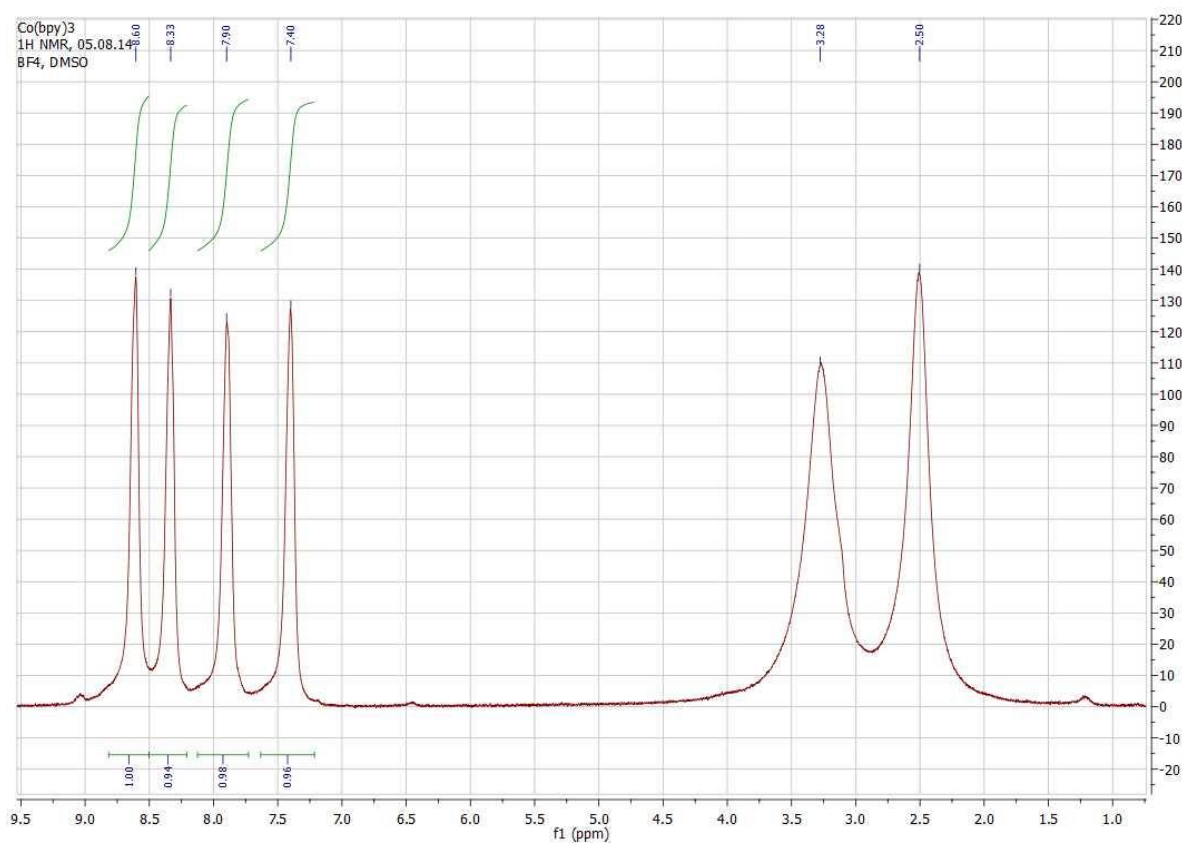
Figure S3. ^{1}H-NMR spectrum of **4**(BF$_4$)$_3$ in DMSO-d_6 recorded at 400 MHz.
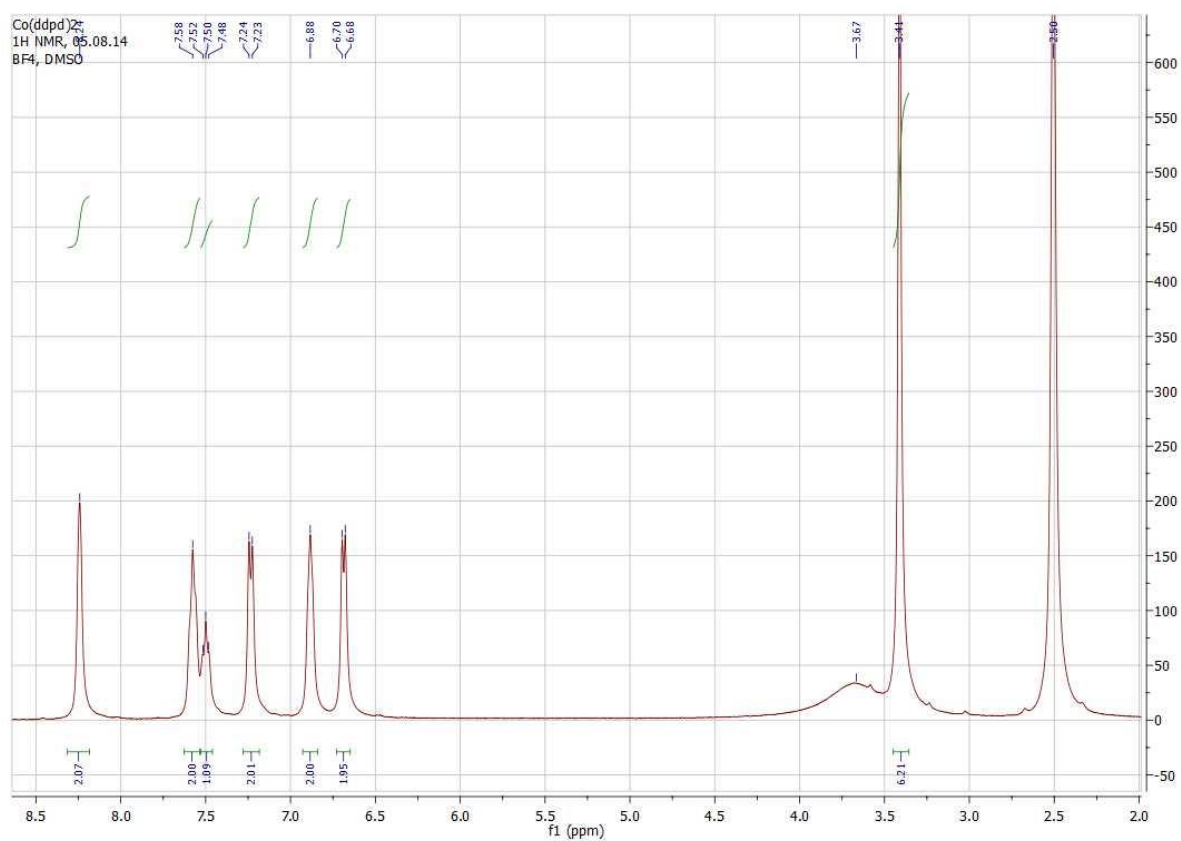
Figure S4. ESI mass spectrum of **3**(BF$_4$)$_2$ in CH$_3$CN.
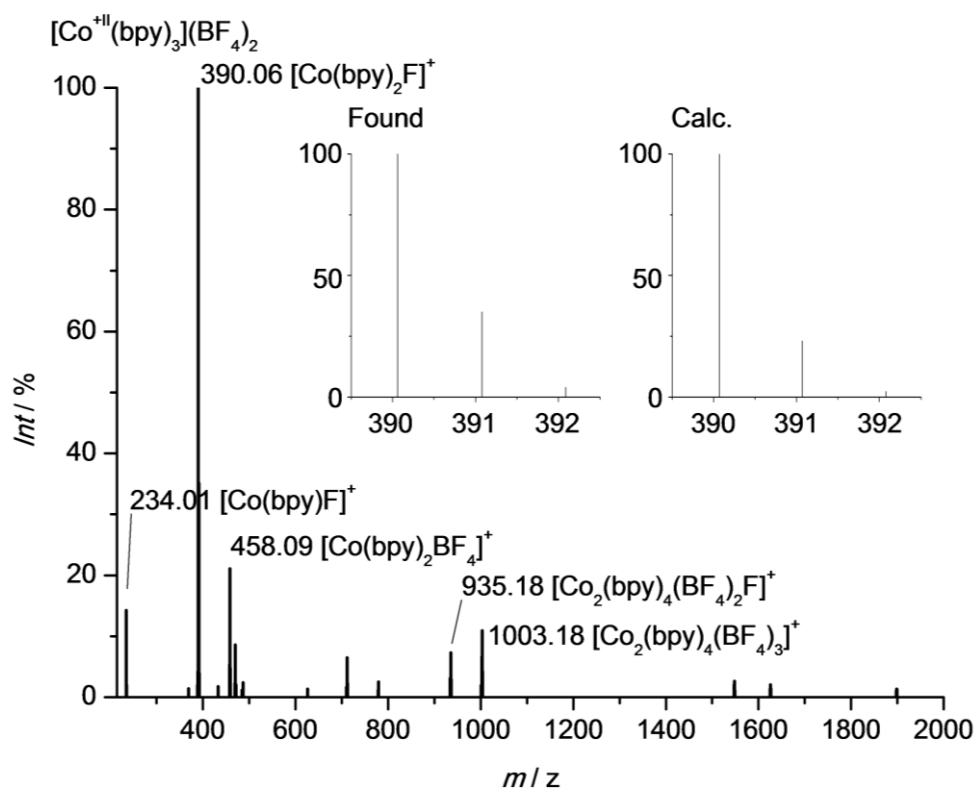
Figure S5. ESI mass spectrum of **3**(BF$_4$)$_3$ in CH$_3$CN..
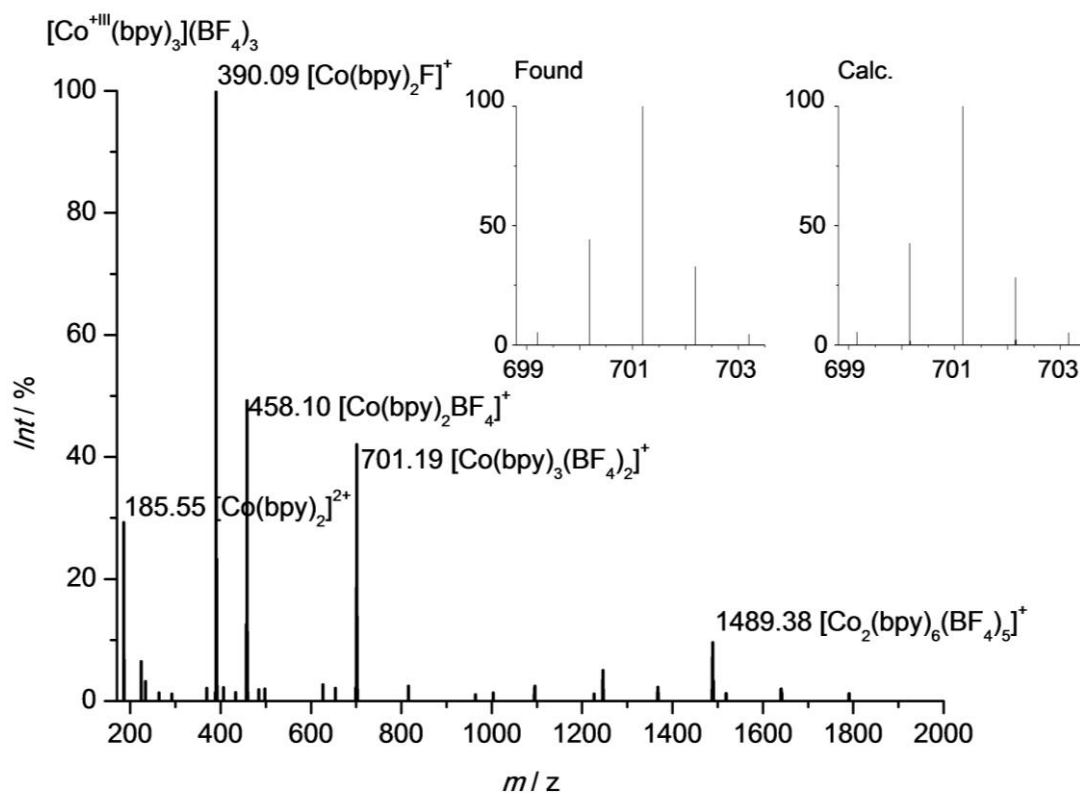
Figure S6. ESI mass spectrum of **4**(BF$_4$)$_2$ in CH$_3$CN..
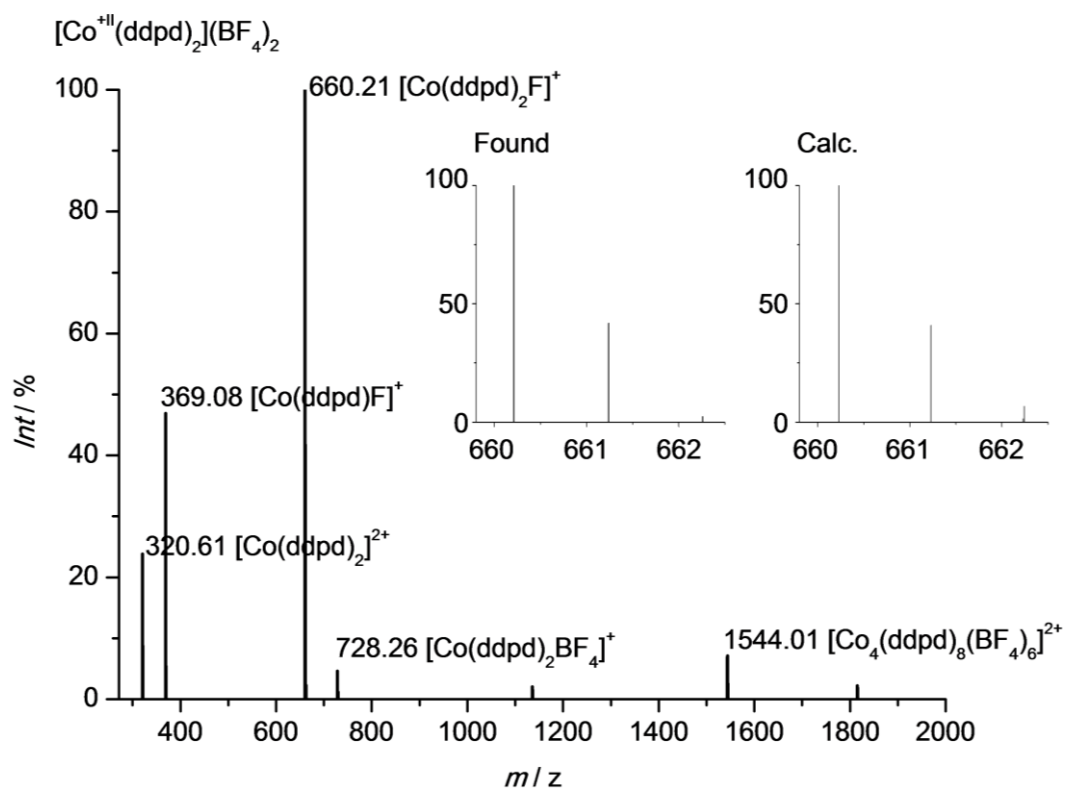
Figure S7. ESI mass spectrum of **4**(BF$_4$)$_3$ in CH$_3$CN..
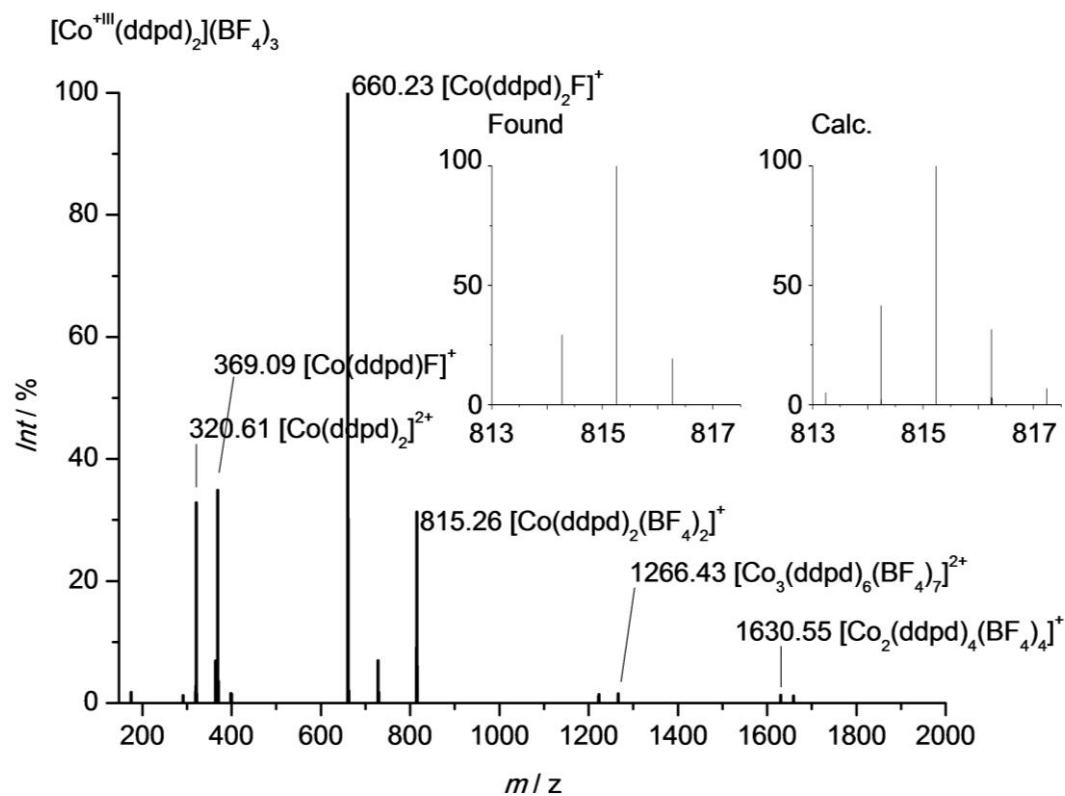
Figure S8. Photocurrent density – voltage curves for DSSCs with sensitizers $\mathbf{1^{2+}}$ and $\mathbf{2}$ using the I_3^-/I^- redox mediator without Li^+/TBP additives.
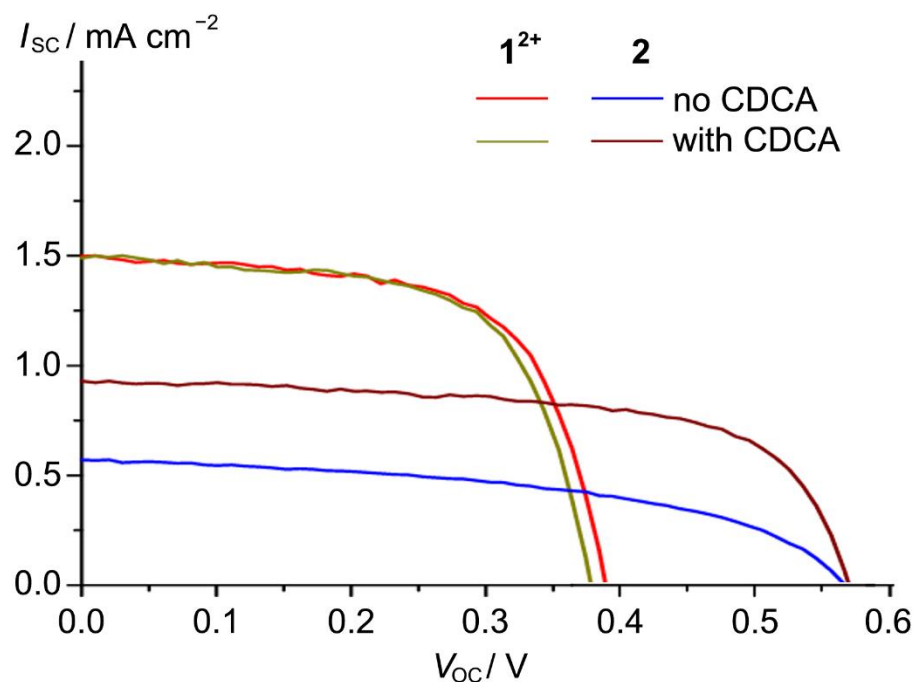
Figure S9. ΔE_p vs. scan rate plots for $\mathbf{4(BF)_2}$ and $\mathbf{3(BF_4)_2}$ in acetonitrile with [TBA][PF$_6$] and [TBA][B(C$_6$F$_5$)$_4$] supporting electrolytes.

5
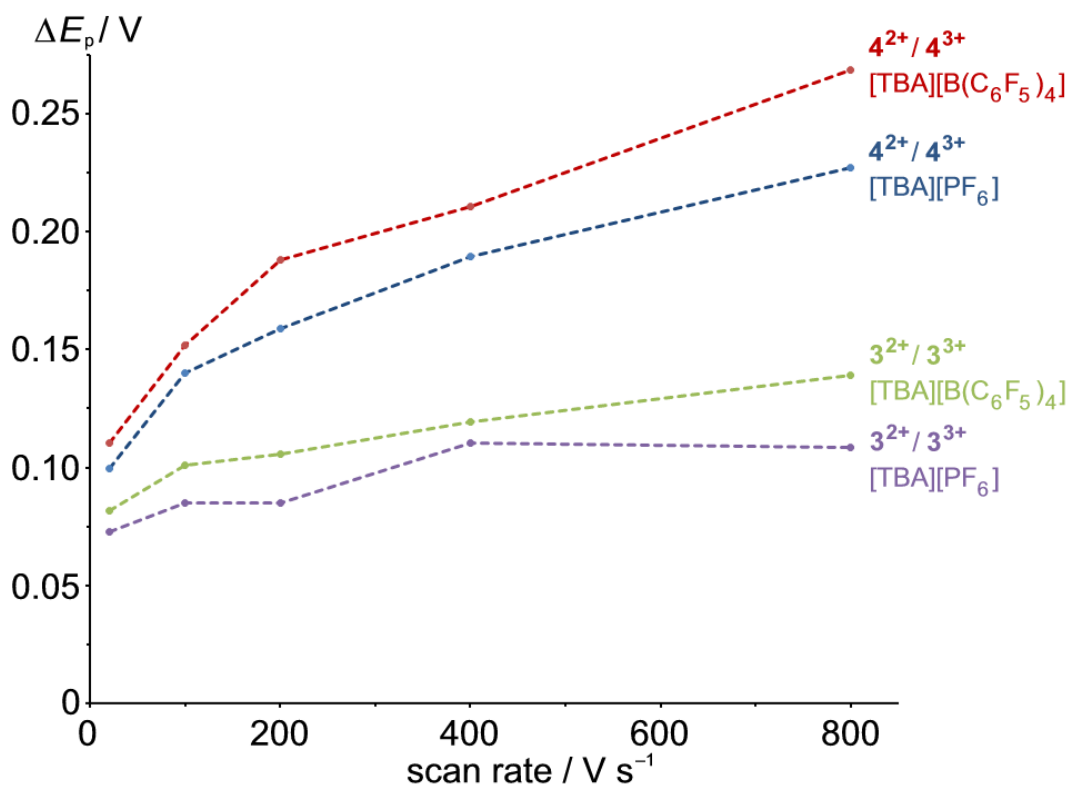
CHEMISTRY

A European Journal

Supporting Information

Strongly Coupled Cyclometalated Ruthenium Triarylamine Chromophores as Sensitizers for DSSCs

Christoph Kreitner[+],[a, d] Andreas K. C. Mengel[+],[a] Tae Kyung Lee,[b] Woohyung Cho,[b] Kookheon Char,[c] Yong Soo Kang,[b] and Katja Heinze*[a]

chem_201601001_sm_miscellaneous_information.pdf
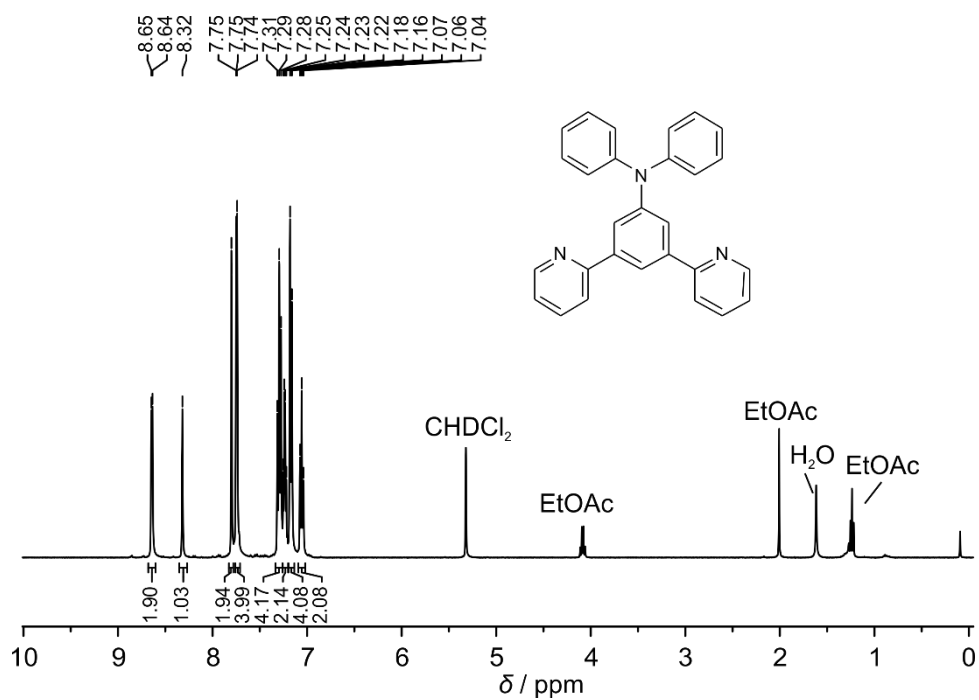
Figure S1 ^{1}H NMR spectrum (400 MHz) of ligand **L^b** in CD$_2$Cl$_2$.
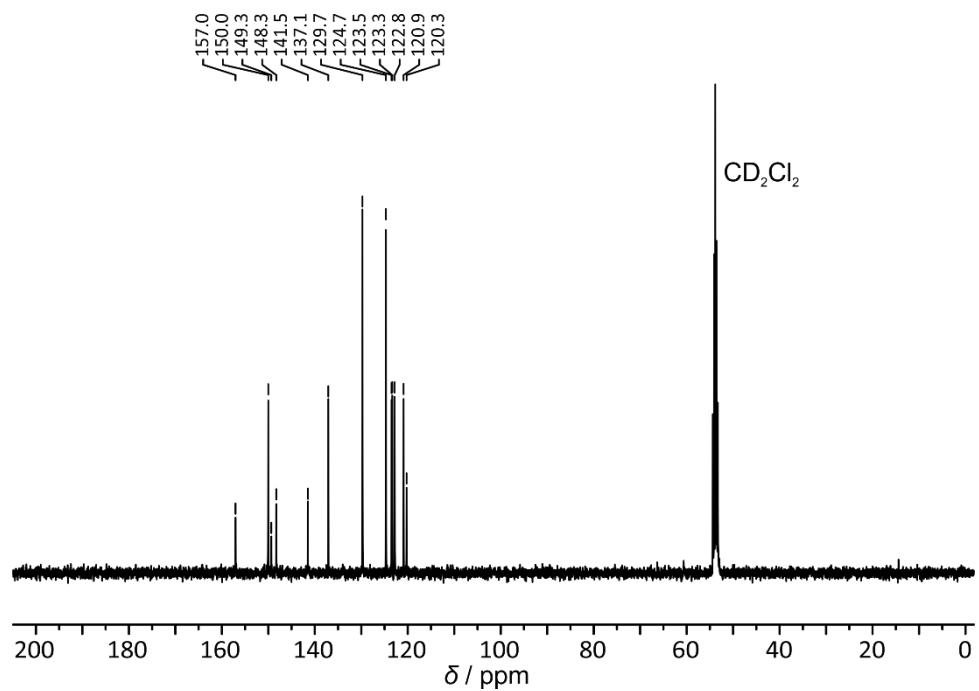
Figure S2 ^{13}C NMR spectrum (100 MHz) of ligand **L^b** in CD$_2$Cl$_2$.
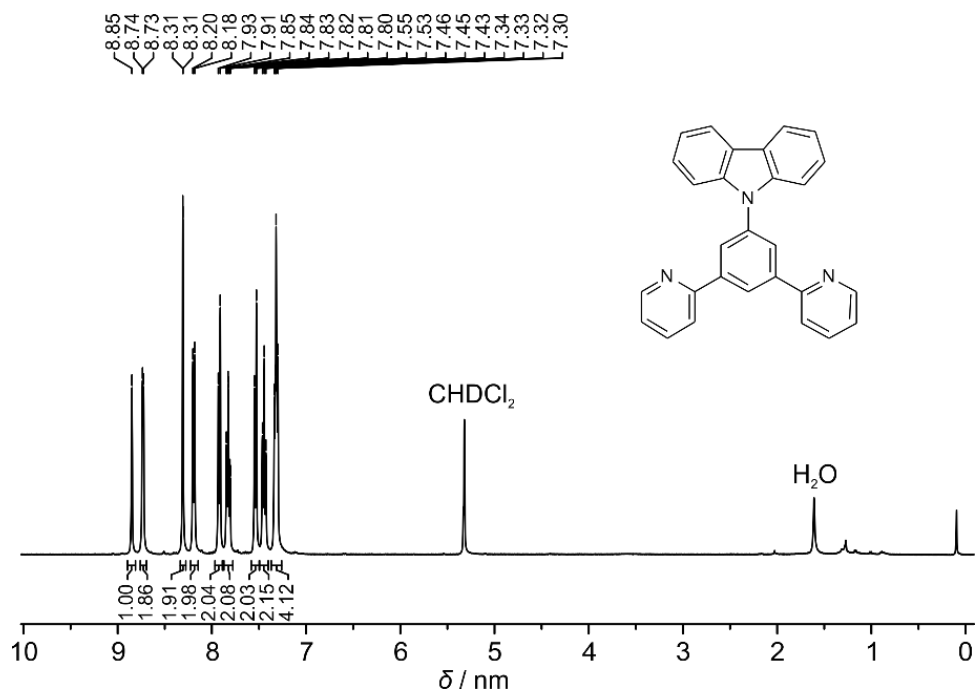
Figure S3 ^{1}H NMR spectrum (400 MHz) of ligand **L^{c}** in CD$_2$Cl$_2$.
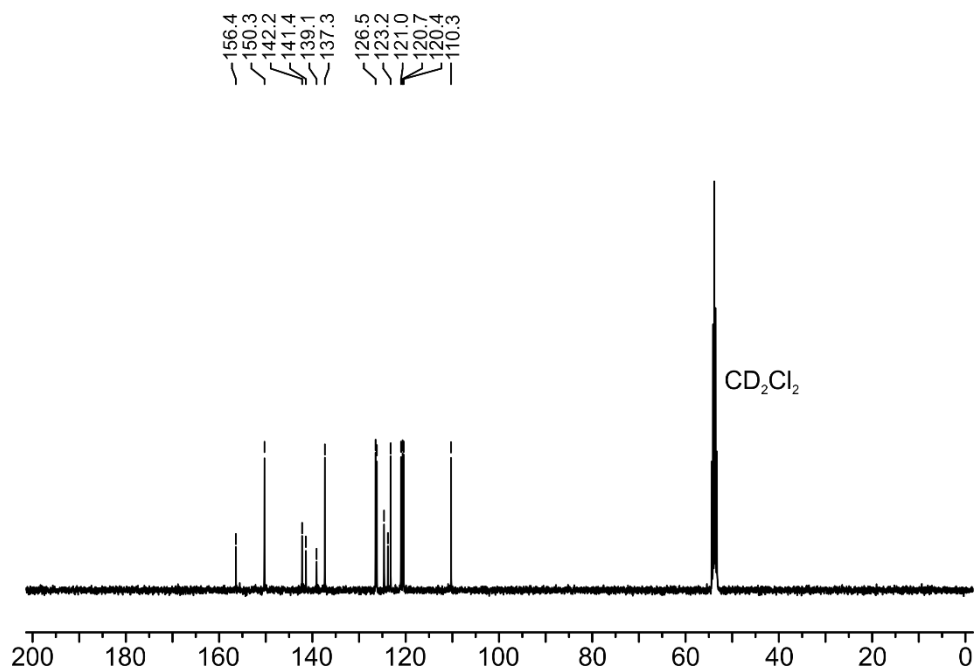
Figure S4 ^{13}C NMR spectrum (100 MHz) of ligand **L^{c}** in CD$_2$Cl$_2$.
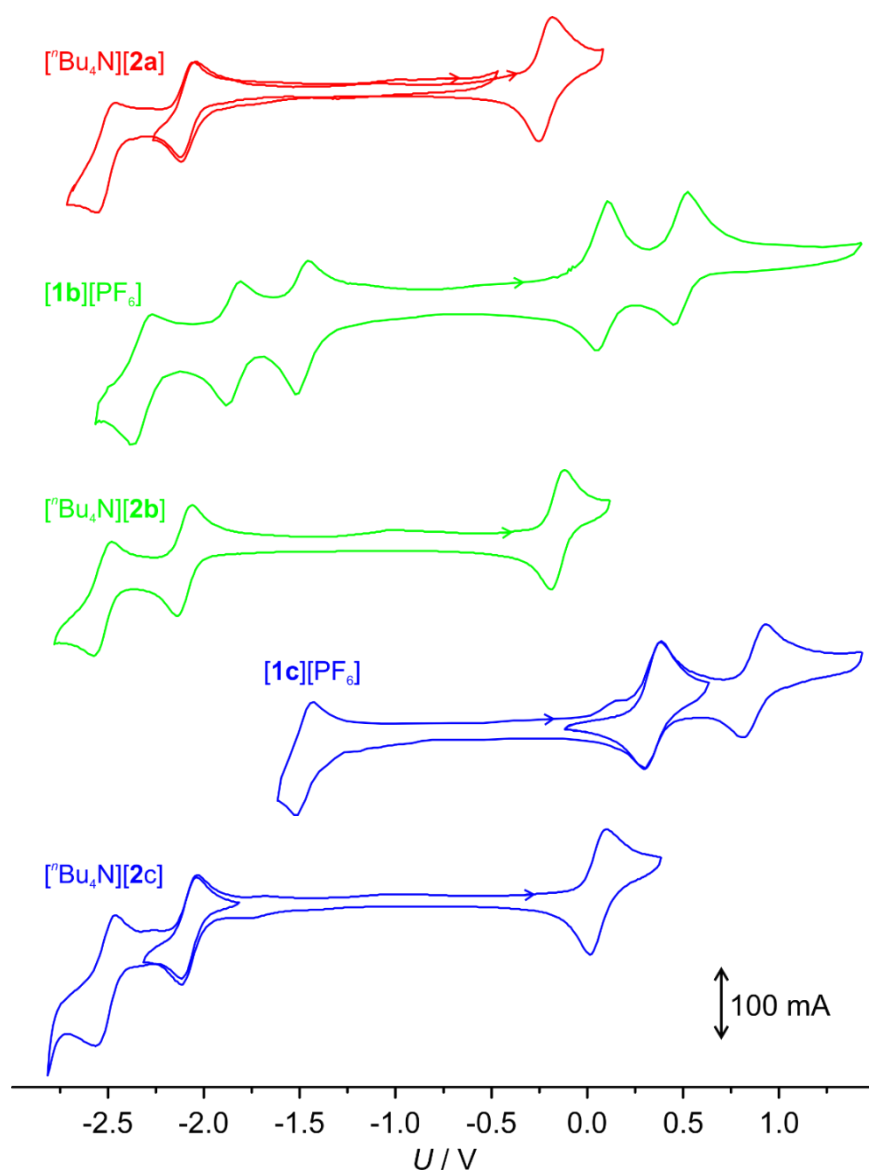
Figure S5 Cyclic voltammograms of dyes [nBu$_4$N]$_2$[**2a**], [**1b**][PF$_6$], [nBu$_4$N]$_2$[**2b**], [**1c**][PF$_6$] and [nBu$_4$N]$_2$[**2c**] in CH$_3$CN (c = 0.1 M; supporting electrolyte: [nBu$_4$N][PF$_6$], c = 10^{-3} M; E vs. FcH/FcH$^+$).
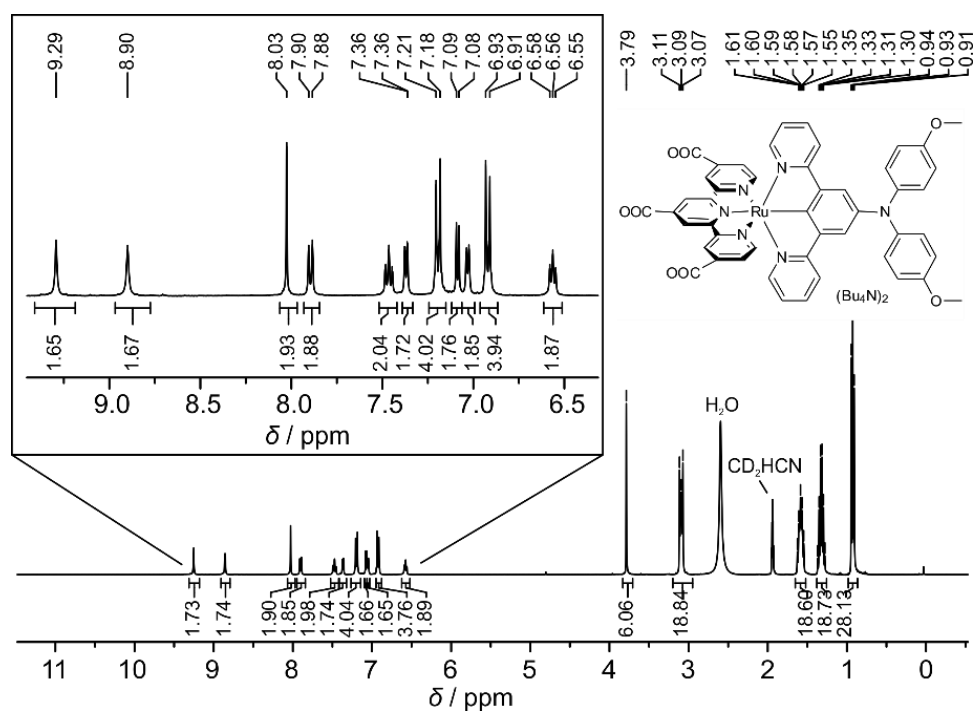
Figure S6 ^{1}H NMR spectrum (400 MHz) of dye [nBu$_4$N]$_2$[**2a**] in CD$_3$CN.
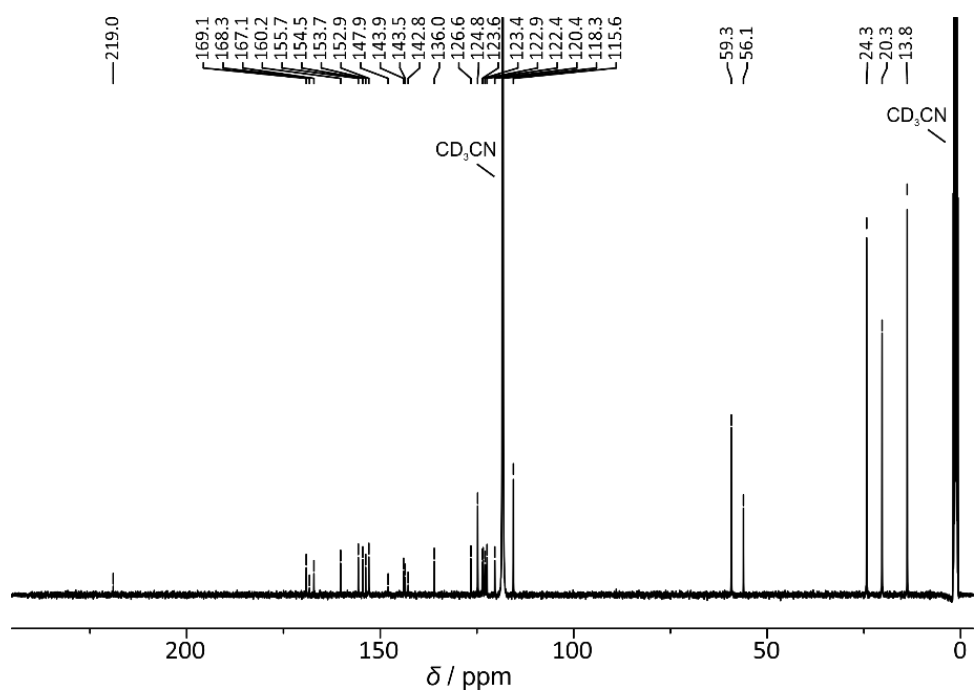
Figure S7 ^{13}C NMR spectrum (100 MHz) of dye [nBu$_4$N]$_2$[**2a**] in CD$_3$CN.
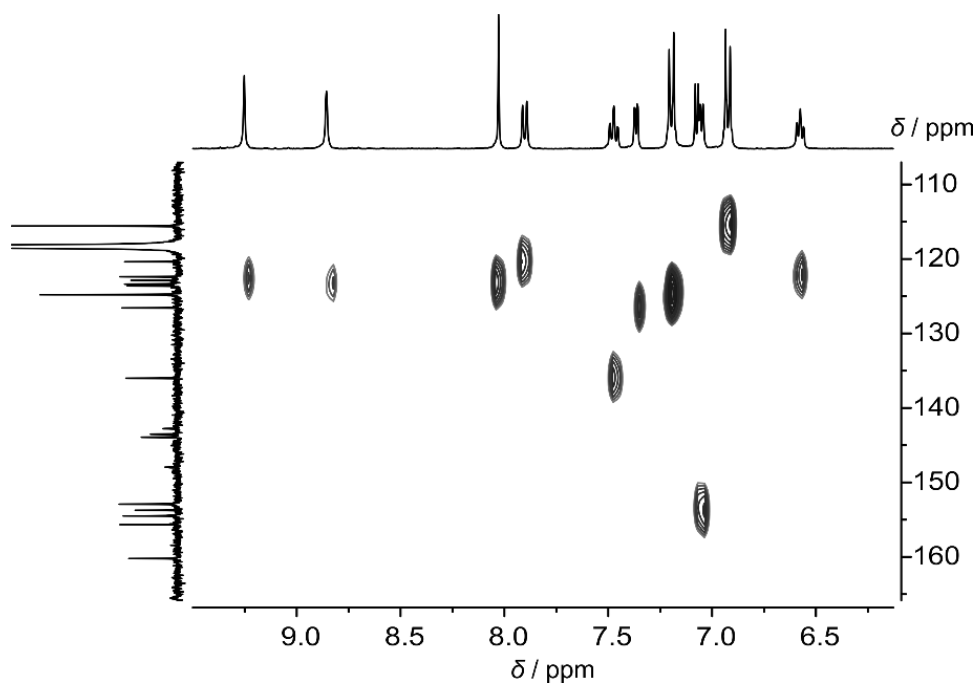
Figure S8 ^{1}H-^{13}C HSQC NMR spectrum of the aromatic region of dye [nBu$_4$N]$_2$[**2a**] in CD$_3$CN.
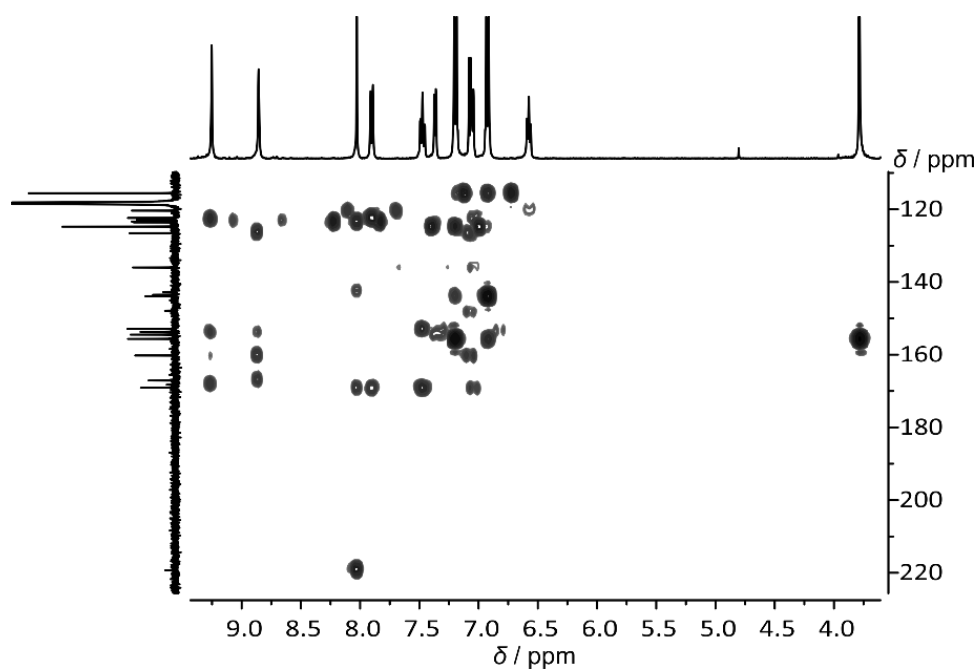
Figure S9 ^{1}H-^{13}C HMBC NMR spectrum of the aromatic region of dye [nBu$_4$N]$_2$[**2a**] in CD$_3$CN.
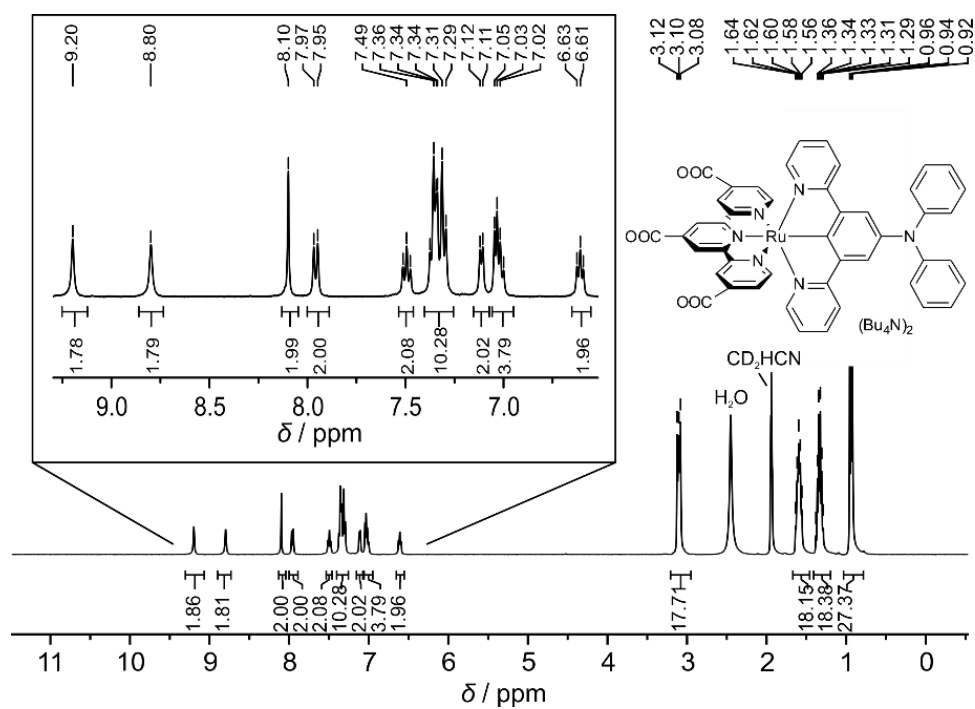
Figure S10 ¹H NMR spectrum (400 MHz) of dye [*n*Bu₄N]₂[**2b**] in CD₃CN.
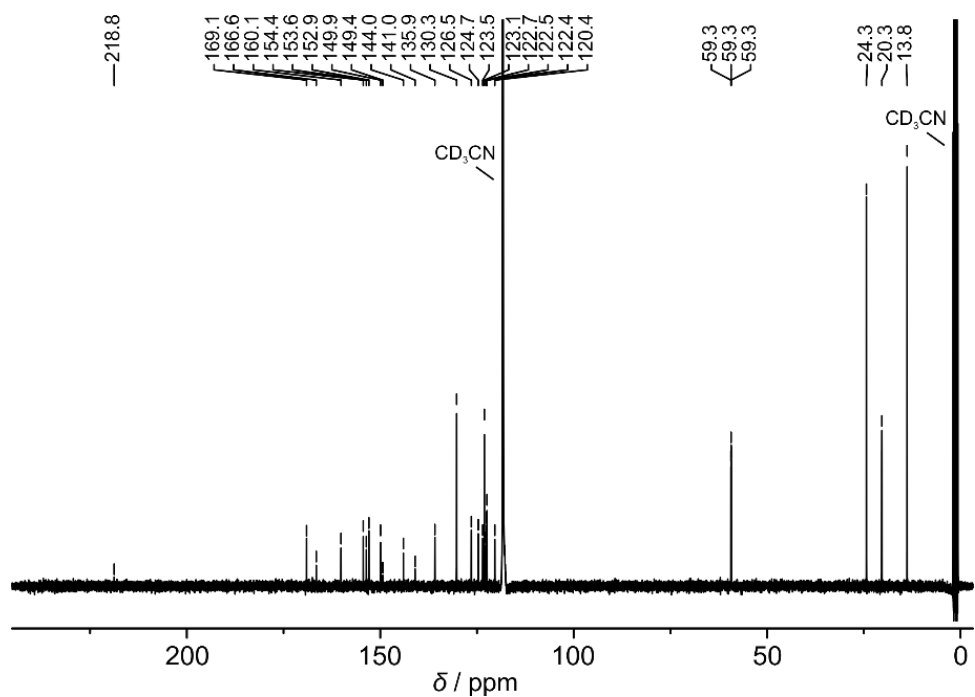
Figure S11 ¹³C NMR spectrum (100 MHz) of dye [*n*Bu₄N]₂[**2b**] in CD₃CN.
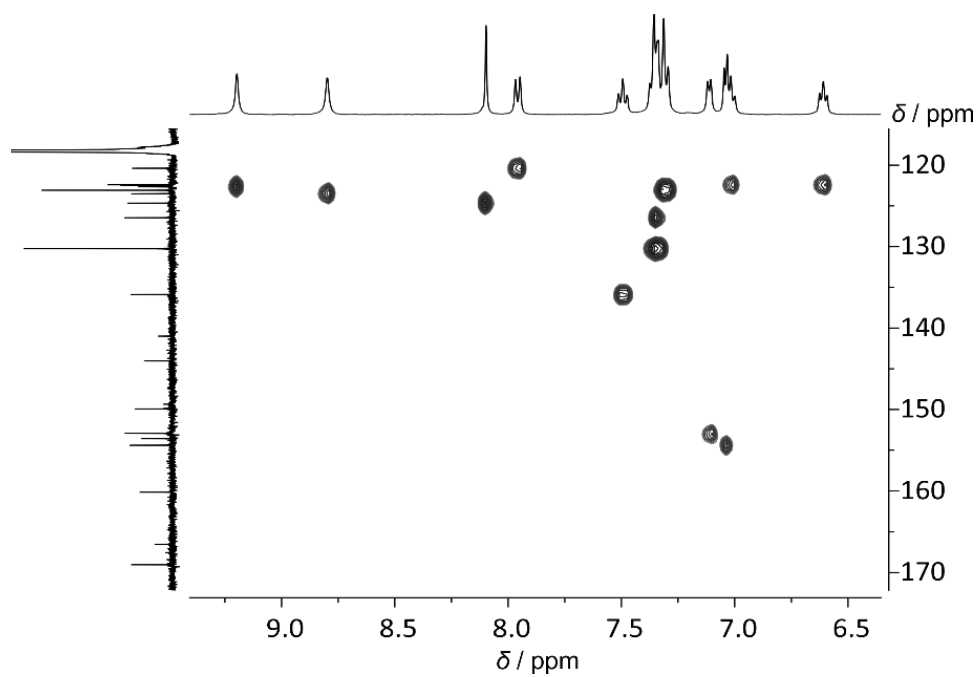
Figure S12 ^{1}H-^{13}C HSQC NMR spectrum of the aromatic region of dye [nBu$_4$N]$_2$[**2b**] in CD$_3$CN.
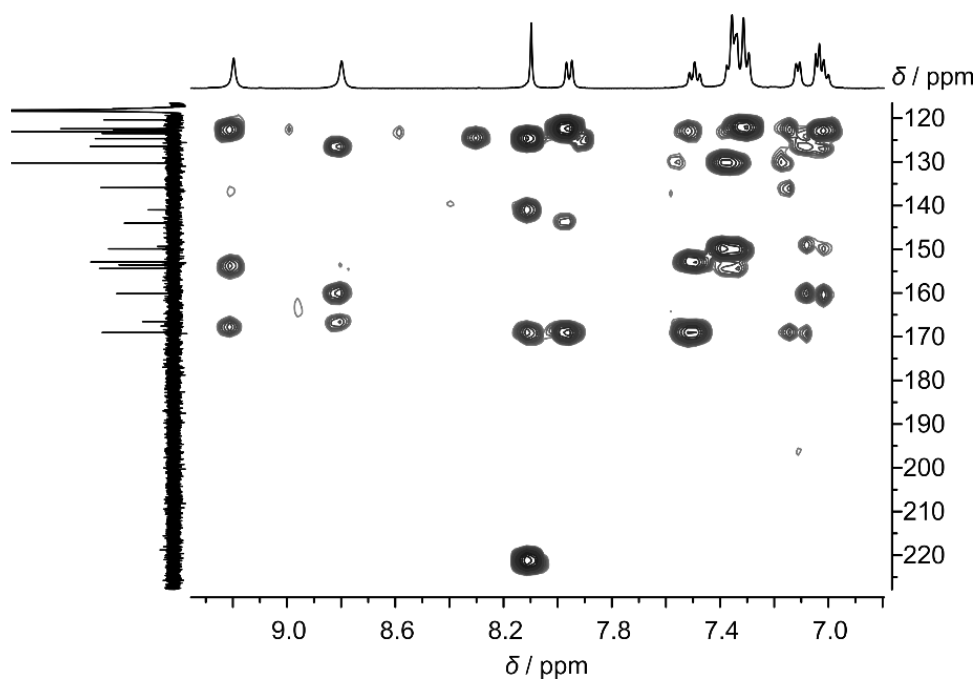
Figure S13 ^{1}H-^{13}C HMBC NMR spectrum of the aromatic region of dye [nBu$_4$N]$_2$[**2b**] in CD$_3$CN.
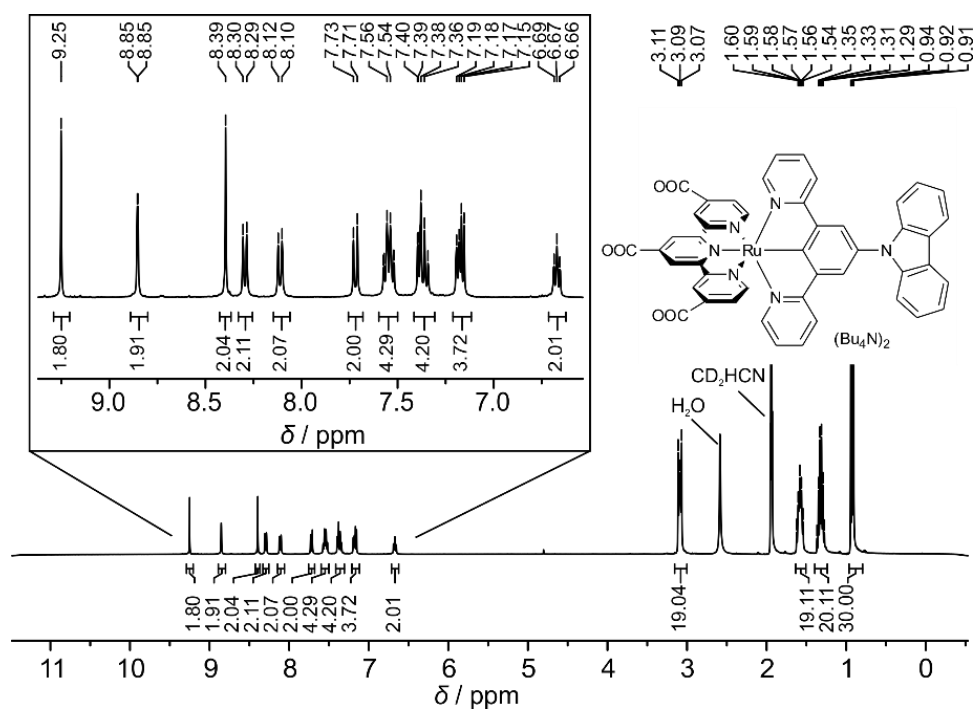
Figure S14 ^{1}H NMR spectrum (400 MHz) of dye [nBu$_4$N]$_2$[**2c**] in CD$_3$CN.
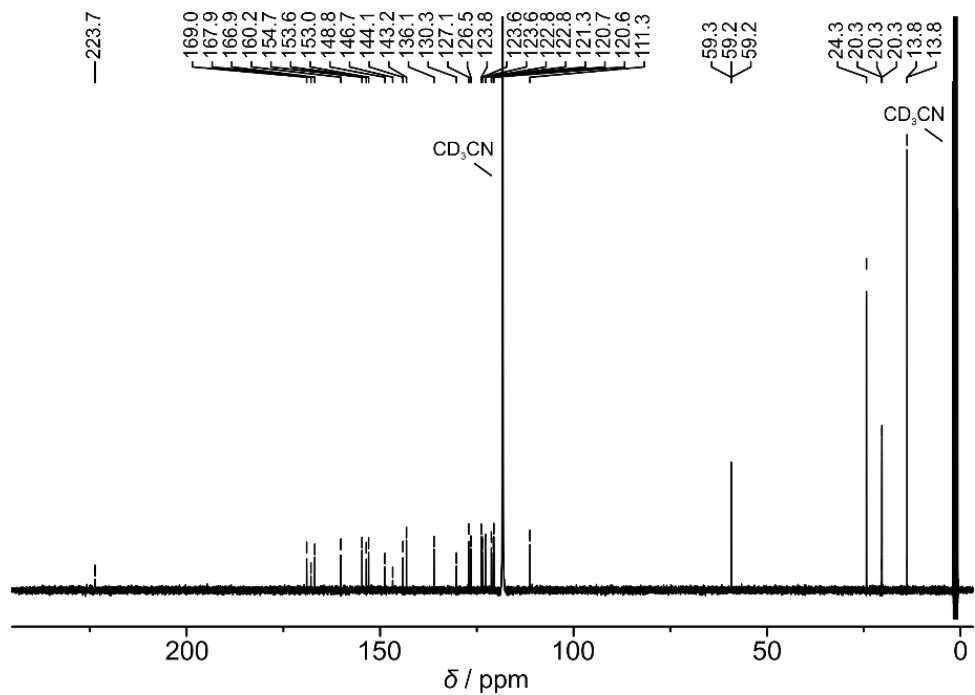
Figure S15 ^{13}C NMR spectrum (100 MHz) of dye [nBu$_4$N]$_2$[**2c**] in CD$_3$CN.
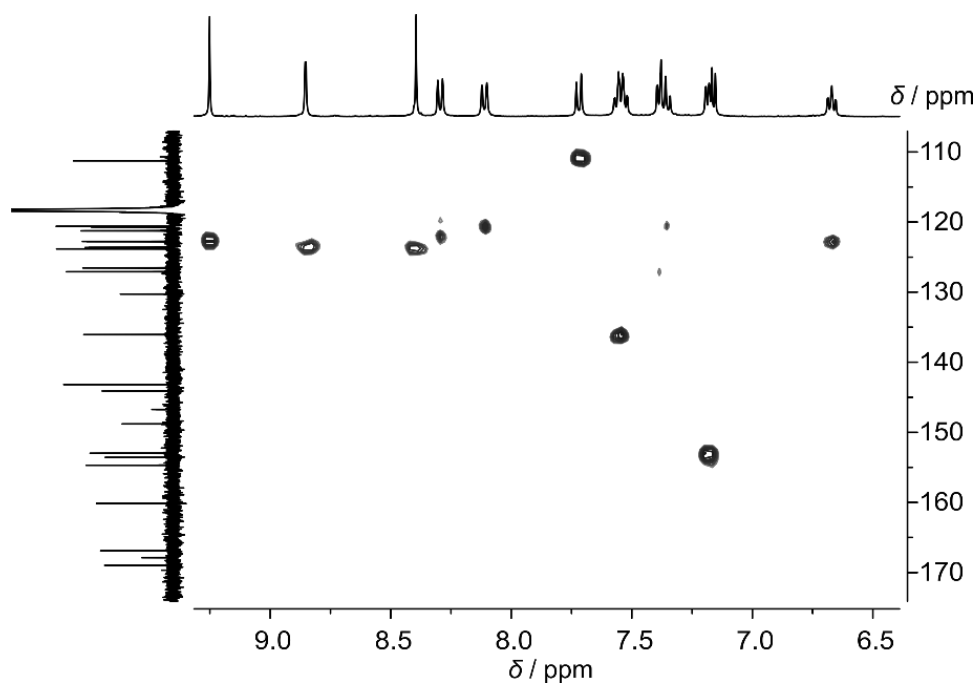
Figure S16 ^{1}H-^{13}C HSQC NMR spectrum of the aromatic region of dye [nBu4N]2[**2c**] in CD3CN.
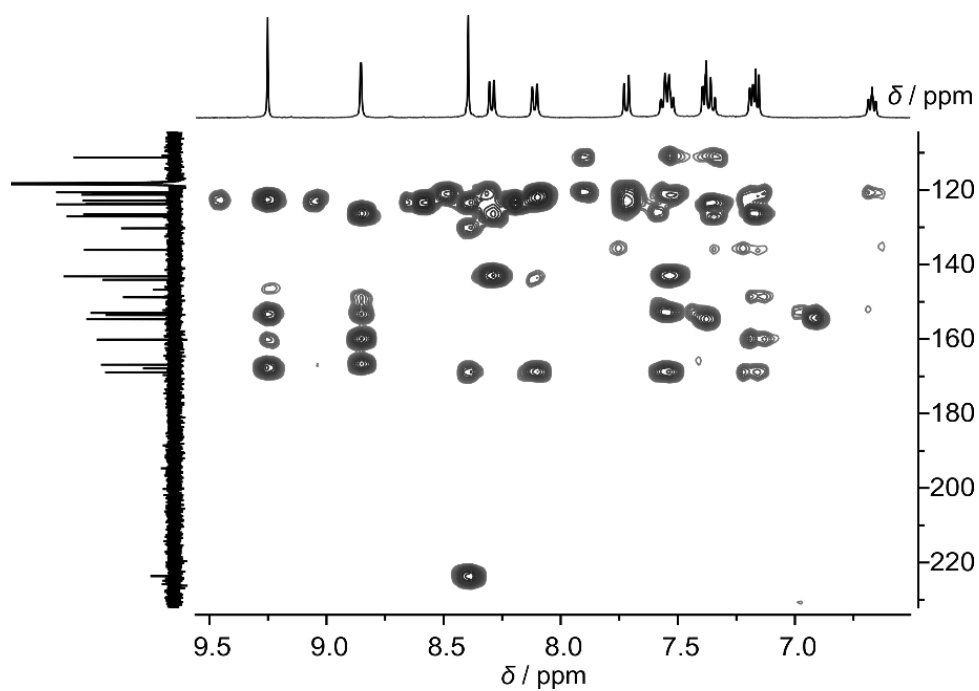
Figure S17 ^{1}H-^{13}C HMBC NMR spectrum of the aromatic region of dye [nBu4N]2[**2c**] in CD3CN.
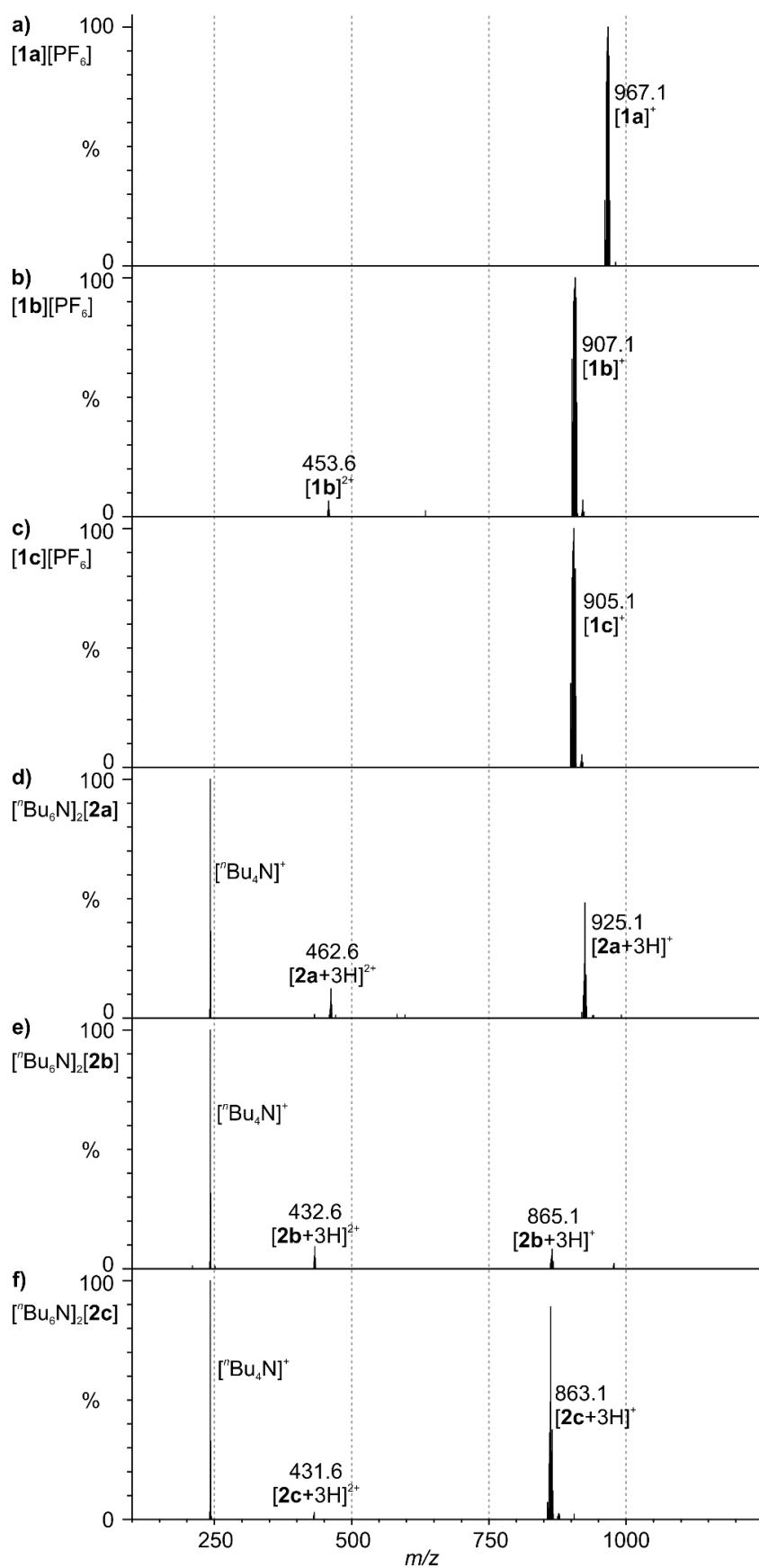
Figure S18 ESI+ mass spectra of dyes **a)** [**1a**][PF6], **b)** [**1b**][PF6], **c)** [**1c**][PF6], **d)** [*n*Bu4N]2[**2a**], **e)** [*n*Bu4N]2[**2b**] and **f)** [*n*Bu4N]2[**2c**] from CH3CN solution.
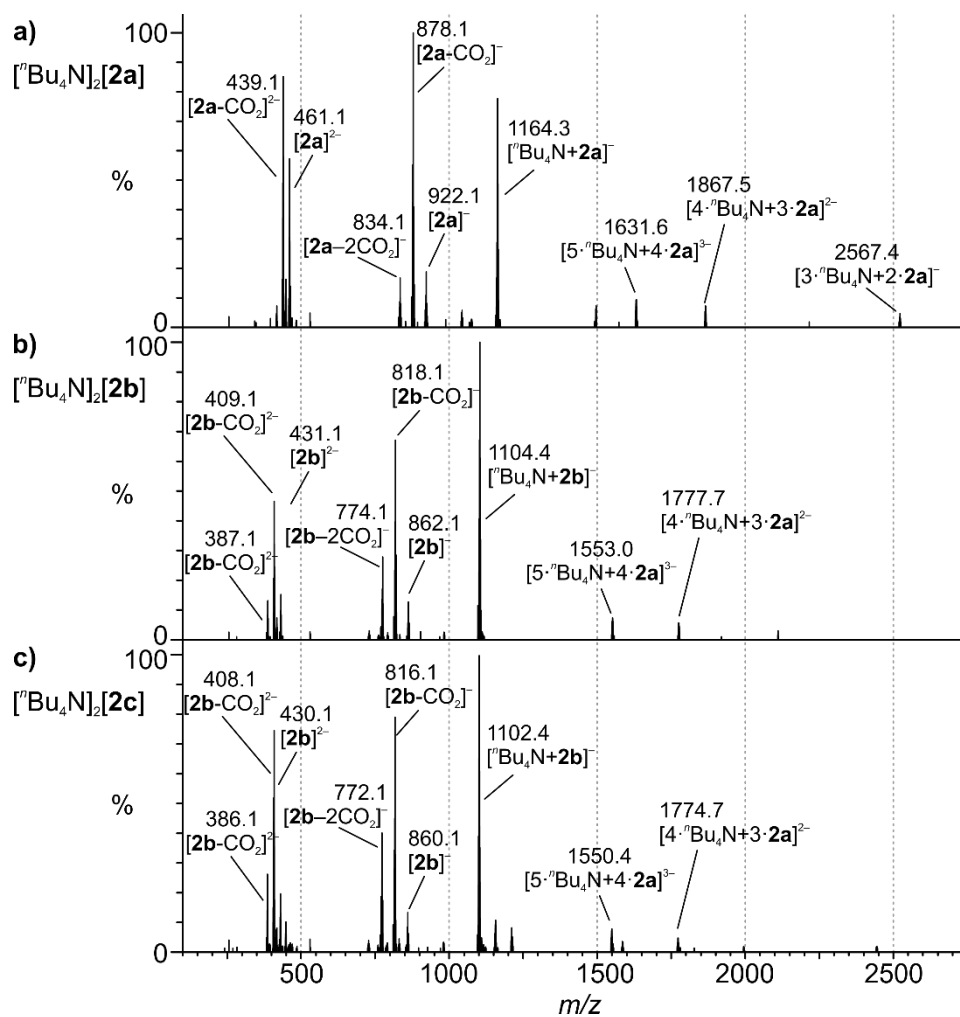
Figure S19 ESI⁻ mass spectra of dyes **a)** [*n*Bu₄N]₂[**2a**], **b)** [*n*Bu₄N]₂[**2b**] and **c)** [*n*Bu₄N]₂[**2c**] from CH₃CN solution.

T / a.u.
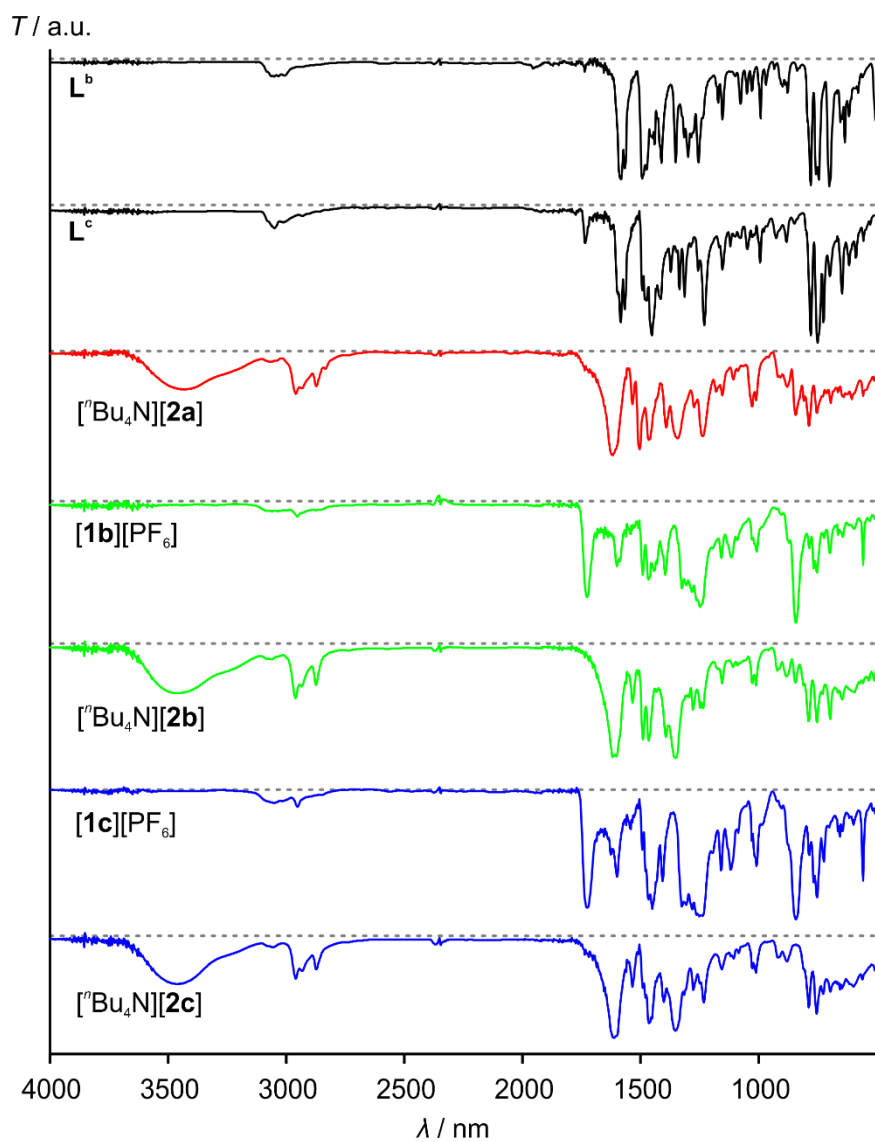
Figure S20 Solid state IR spectra (KBr disk) of ligands **L**^{b} and **L**^{c} and dyes [*n*Bu$_4$N]$_2$[**2a**], [**1b**][PF$_6$], [*n*Bu$_4$N]$_2$[**2b**], [**1c**][PF$_6$] and [*n*Bu$_4$N]$_2$[**2c**].
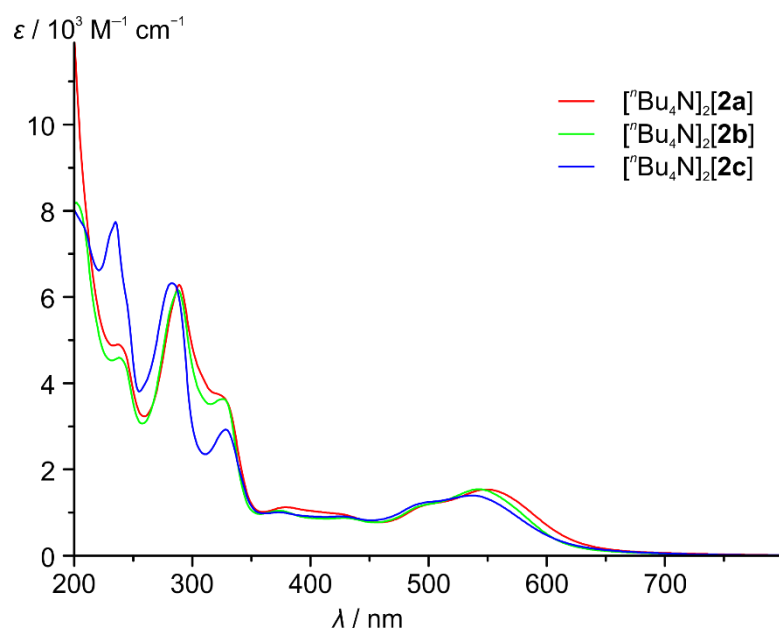
Figure S21 UV-Vis spectra (200-800 nm) of dyes [nBu$_4$N]$_2$[**2a**], [nBu$_4$N]$_2$[**2b**] and [nBu$_4$N]$_2$[**2c**] in CH$_3$CN solution.
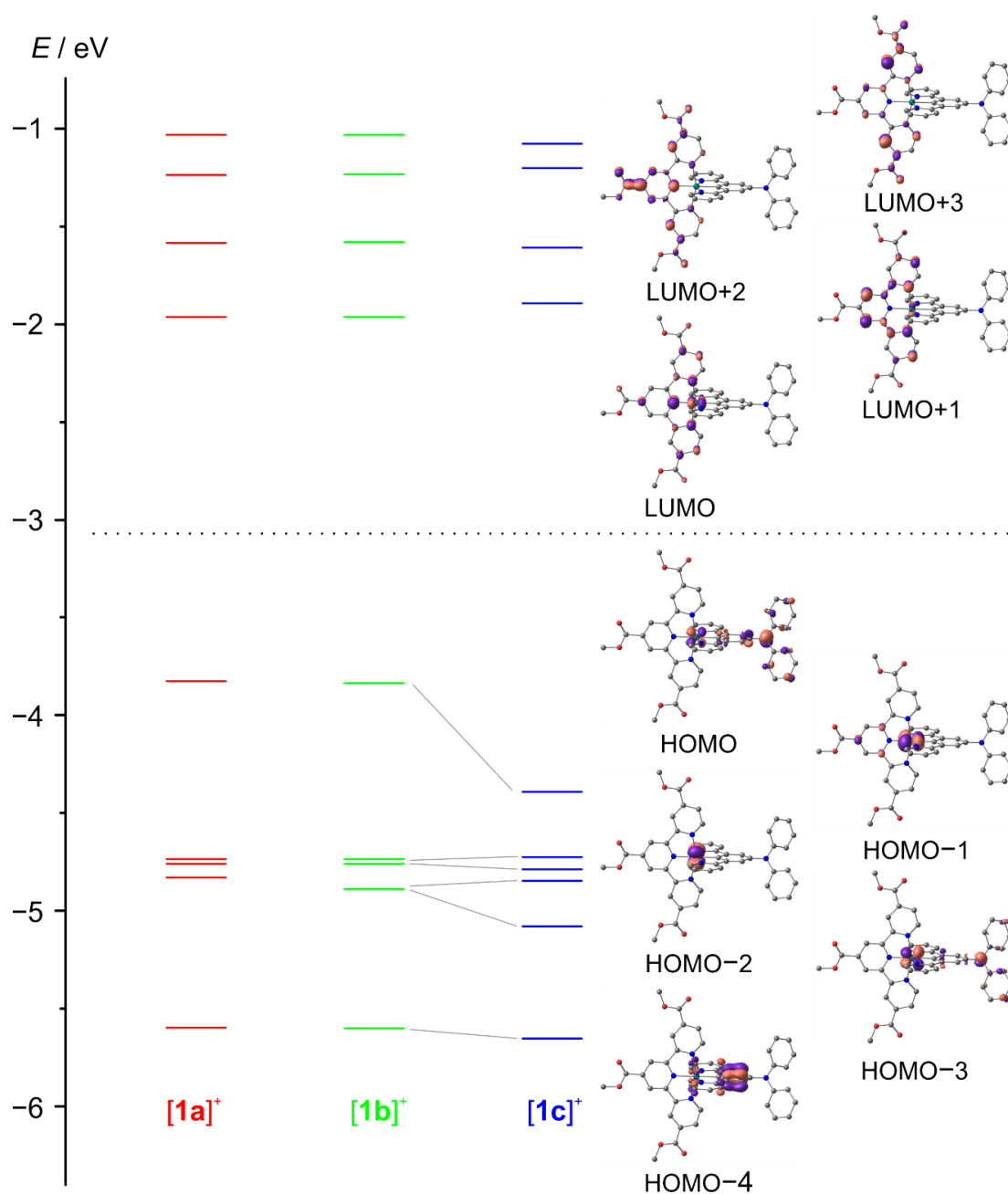
Figure S22 DFT calculated MO diagram of ester complexes [1a]⁺, [1b]⁺ and [1c]⁺ and frontier orbitals of [1b]⁺ (contour value: 0.06).
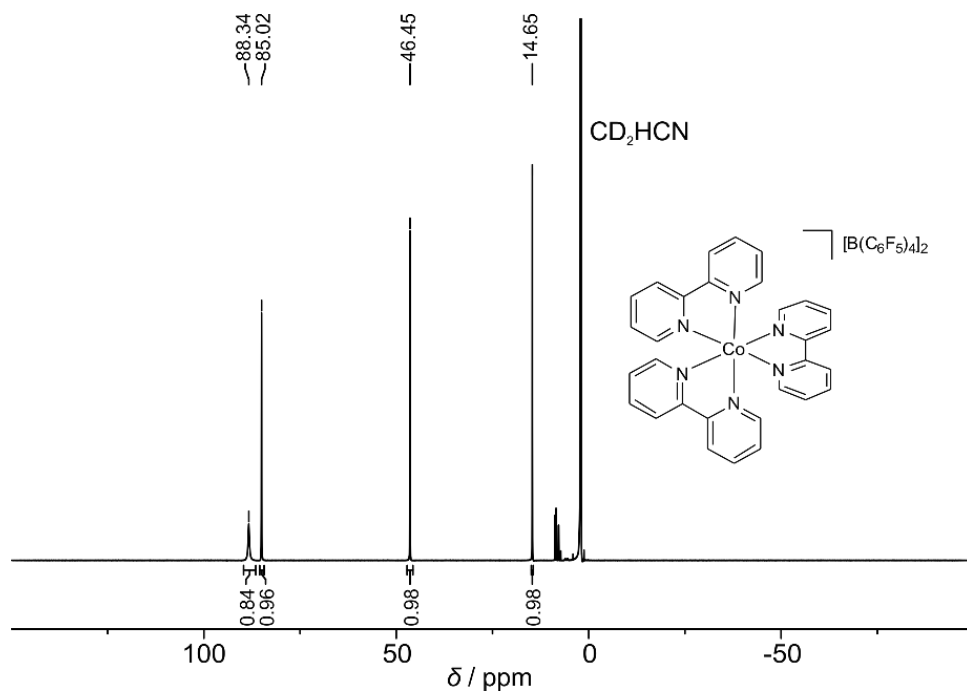
Figure S23 Paramagnetic ^{1}H NMR spectrum (400 MHz) of electrolyte [**3**][B(C$_6$F$_5$)$_4$]$_2$ in CD$_3$CN.
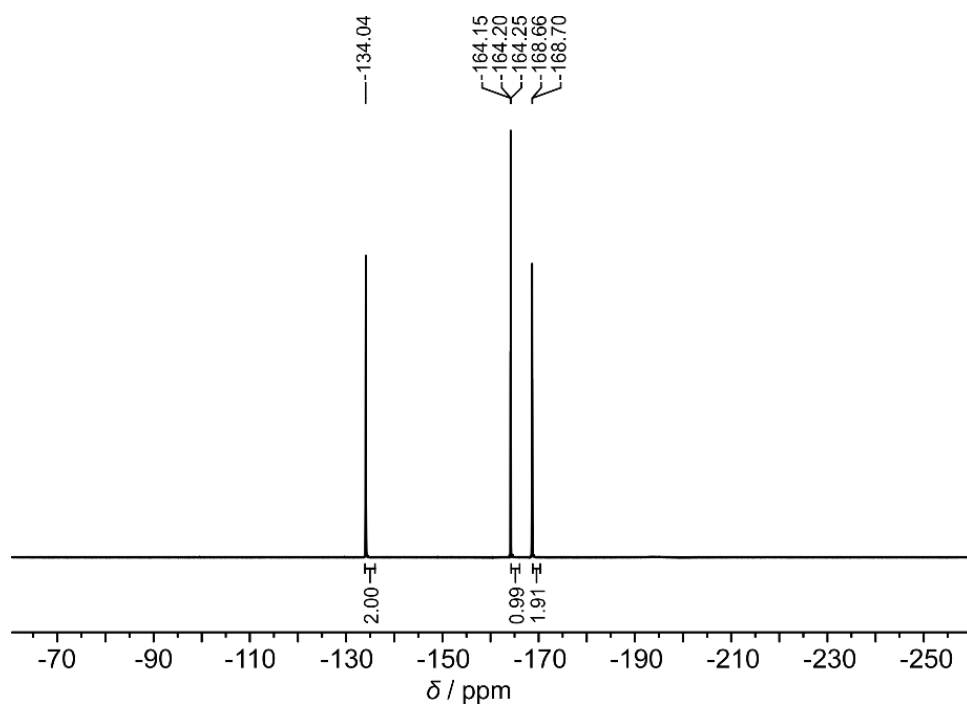
Figure S24 ^{19}F NMR spectrum (377 MHz) of electrolyte [**3**][B(C$_6$F$_5$)$_4$]$_2$ in CD$_3$CN.
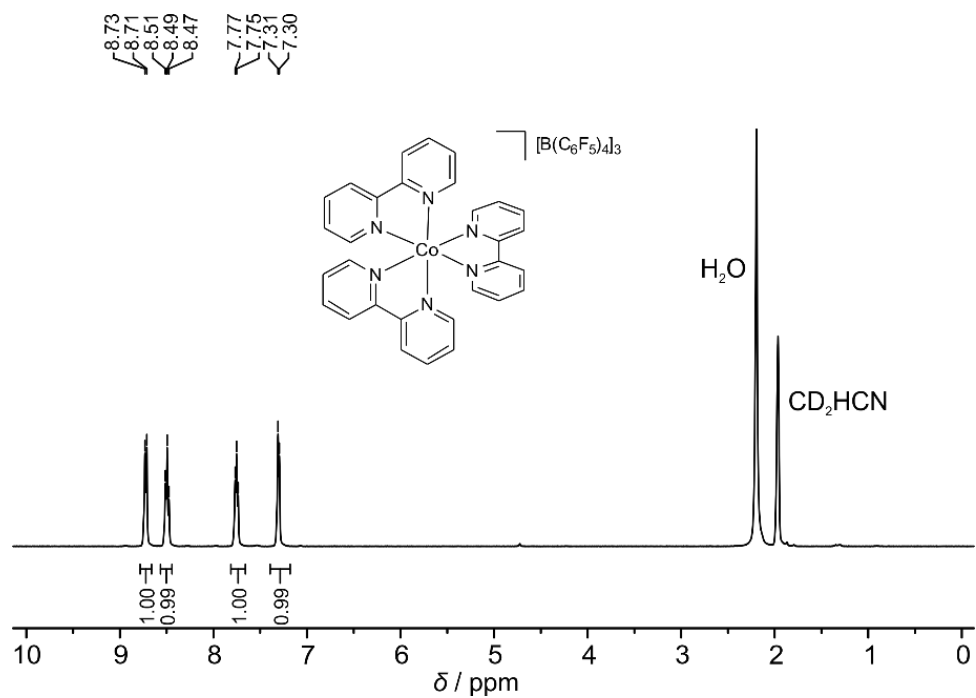
Figure S25 ^{1}H NMR spectrum (400 MHz) of electrolyte [**3**][B(C$_6$F$_5$)$_4$]$_3$ in CD$_3$CN.
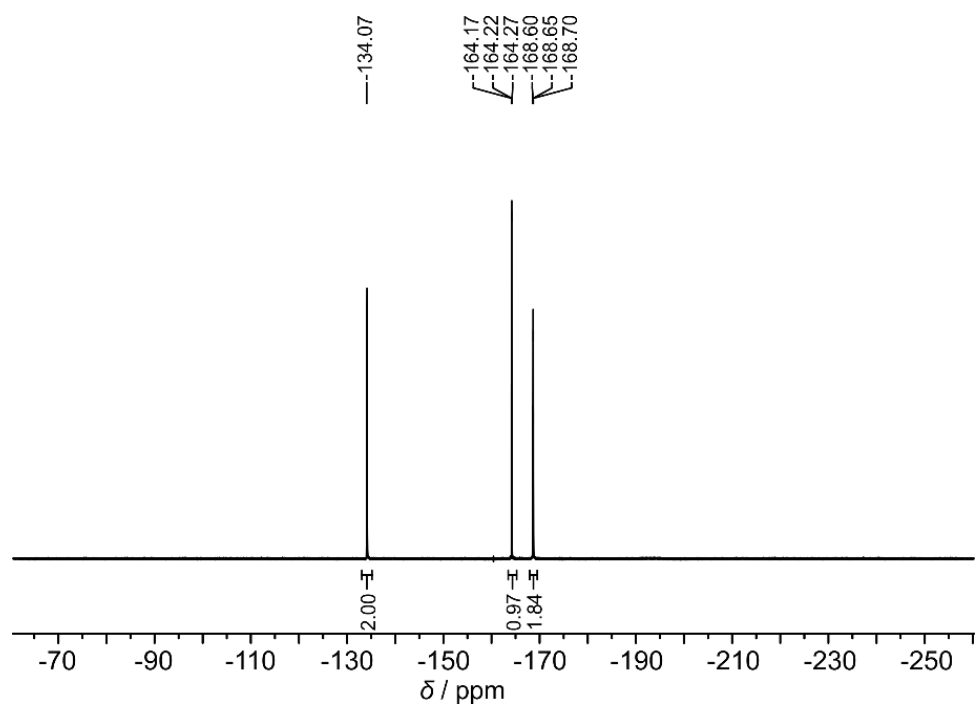
Figure S26 ^{19}F NMR spectrum (377 MHz) of electrolyte [**3**][B(C$_6$F$_5$)$_4$]$_3$ in CD$_3$CN.
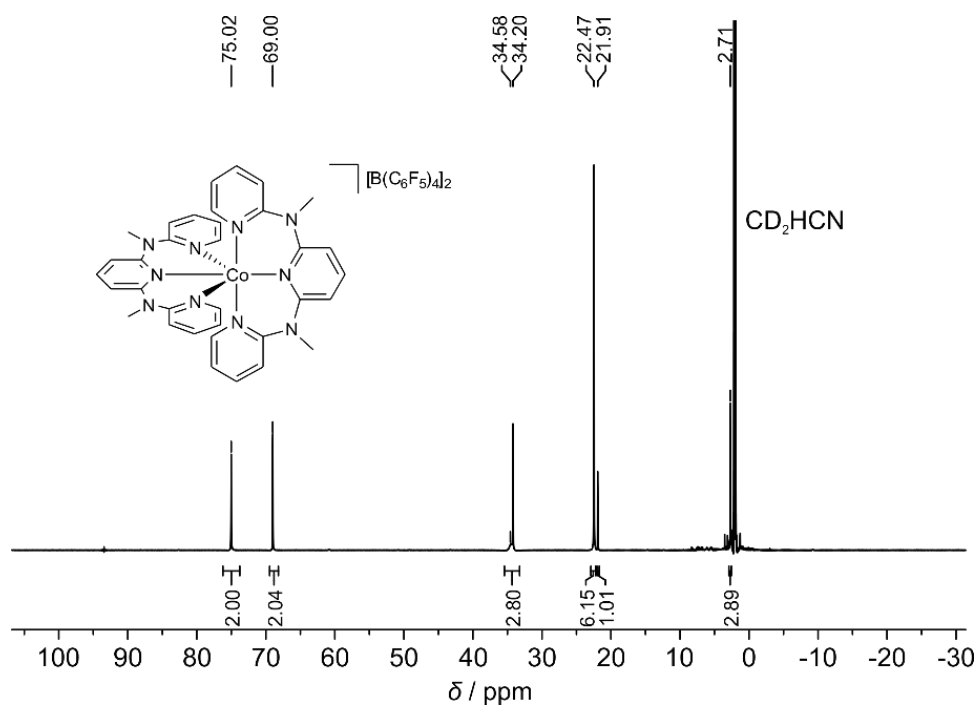
Figure S27 Paramagnetic ^{1}H NMR spectrum (400 MHz) of electrolyte [**4**][B(C$_6$F$_5$)$_4$]$_2$ in CD$_3$CN.
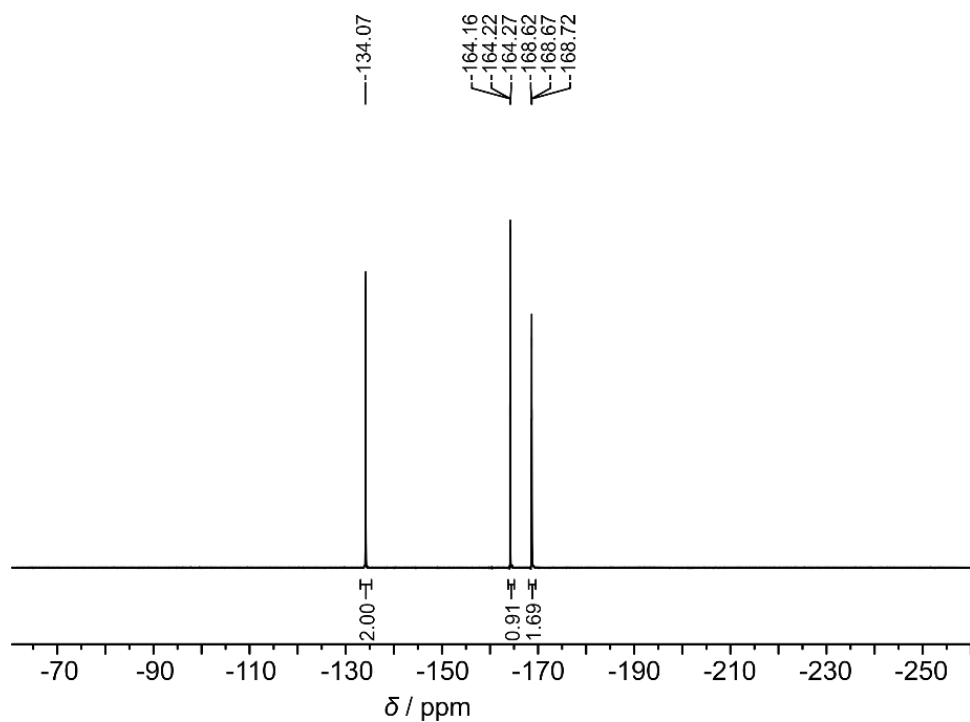
Figure S28 ^{19}F NMR spectrum (377 MHz) of electrolyte [**4**][B(C$_6$F$_5$)$_4$]$_2$ in CD$_3$CN.
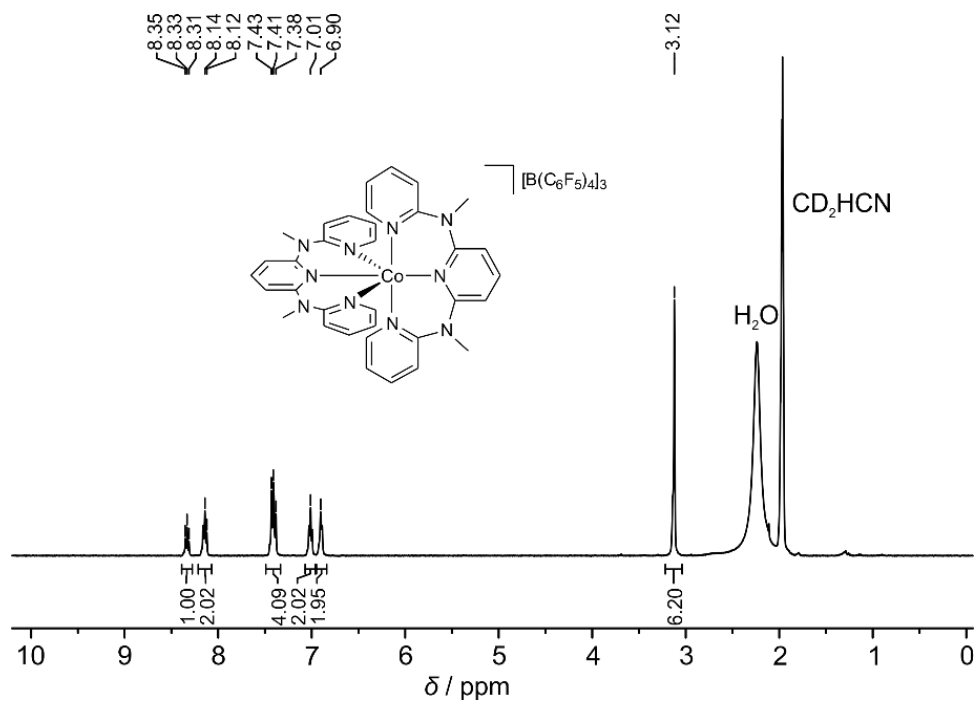
Figure S29 ^{1}H NMR spectrum (400 MHz) of electrolyte [**4**][B(C$_6$F$_5$)$_4$]$_3$ in CD$_3$CN.
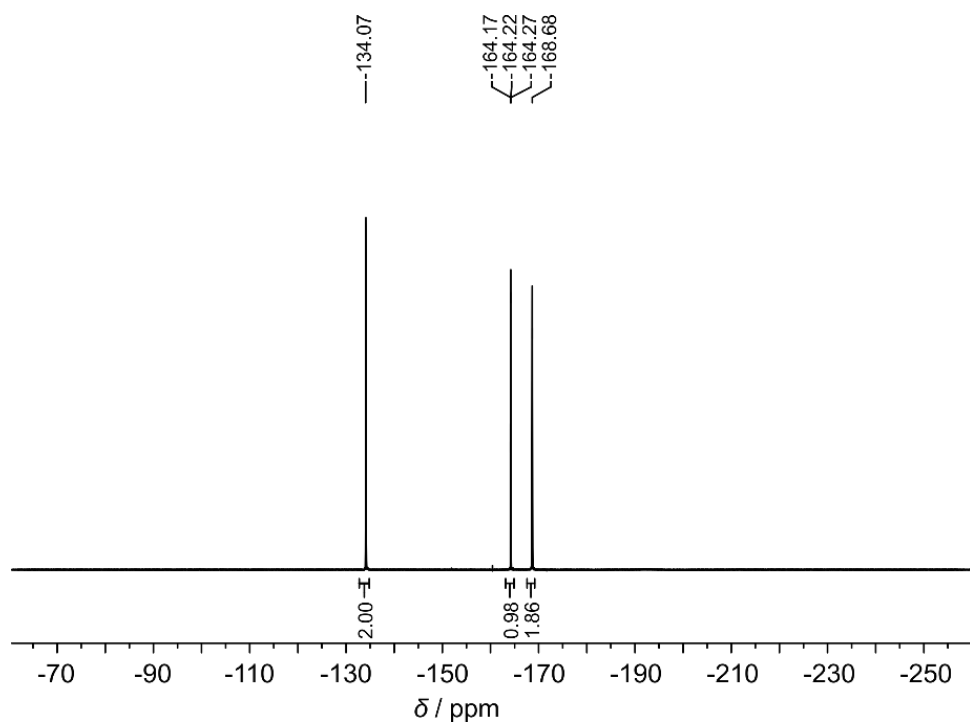
Figure S30 ^{19}F NMR spectrum (377 MHz) of electrolyte [**4**][B(C$_6$F$_5$)$_4$]$_3$ in CD$_3$CN.
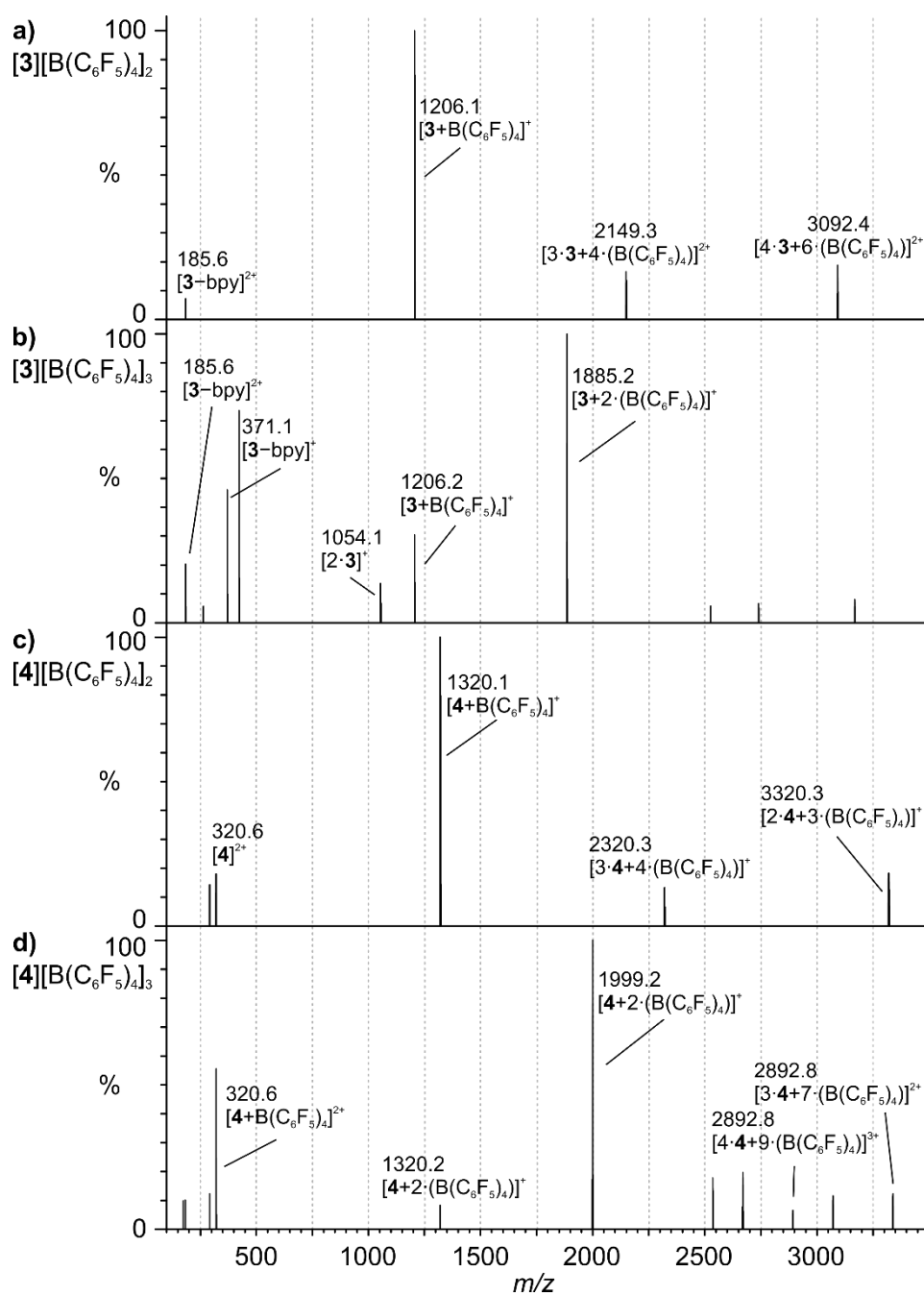
Figure S31 ESI$^+$ mass spectra of electrolytes **a)** [**3**][B(C$_6$F$_5$)$_4$]$_2$, **b)** [**3**][B(C$_6$F$_5$)$_4$]$_3$, **c)** [**4**][B(C$_6$F$_5$)$_4$]$_2$ and **d)** [**4**][B(C$_6$F$_5$)$_4$]$_3$ from CH$_3$CN solution.

Table S1. Photovoltaic data of cells using the I_3^-/I^- redox mediator without CDCA under AM1.5 light conditions.

dye	V_{OC} [V]	J_{SC} [mA cm^{-2}]	FF [%]	η [%]
[^{n}Bu$_4$N]$_2$[**2a**]	0.49	1.43	64	0.45
[^{n}Bu$_4$N]$_2$[**2a**]	0.51	1.43	62	0.46
[^{n}Bu$_4$N]$_2$[**2a**]	0.52	1.33	61	0.42
[^{n}Bu$_4$N]$_2$[**2a**]	0.48	2.90	66	0.91
[^{n}Bu$_4$N]$_2$[**2b**]	0.51	2.42	67	0.83
[^{n}Bu$_4$N]$_2$[**2b**]	0.52	2.25	67	0.78
[^{n}Bu$_4$N]$_2$[**2b**]	0.54	2.52	65	0.88
[^{n}Bu$_4$N]$_2$[**2b**]	0.54	2.45	65	0.87
[^{n}Bu$_4$N]$_2$[**2b**]	0.55	3.68	70	1.50
[^{n}Bu$_4$N]$_2$[**2b**]	0.52	4.16	69	1.41
[^{n}Bu$_4$N]$_2$[**2c**]	0.56	4.14	72	1.68
[^{n}Bu$_4$N]$_2$[**2c**]	0.56	4.15	73	1.69
[^{n}Bu$_4$N]$_2$[**2c**]	0.59	4.32	71	1.81
[^{n}Bu$_4$N]$_2$[**2c**]	0.57	4.84	72	1.98
[^{n}Bu$_4$N]$_2$[**2c**]	0.57	6.69	73	2.77
[^{n}Bu$_4$N]$_2$[**2c**]	0.57	6.21	73	2.60

Table S2. Photovoltaic data of cells using the I_3^-/I^- redox mediator with CDCA under AM1.5 light conditions.

dye	V_{OC} [V]	J_{SC} [mA cm^{-2}]	FF [%]	η [%]
[^{n}Bu$_4$N]$_2$[**2a**]	0.54	3.12	71	1.21
[^{n}Bu$_4$N]$_2$[**2a**]	0.53	2.60	65	0.89
[^{n}Bu$_4$N]$_2$[**2a**]	0.54	2.31	63	0.78
[^{n}Bu$_4$N]$_2$[**2a**]	0.55	4.61	69	1.74
[^{n}Bu$_4$N]$_2$[**2a**]	0.55	4.20	68	1.56
[^{n}Bu$_4$N]$_2$[**2b**]	0.59	5.25	75	2.31
[^{n}Bu$_4$N]$_2$[**2b**]	0.61	5.15	76	2.37
[^{n}Bu$_4$N]$_2$[**2b**]	0.57	4.54	68	1.76
[^{n}Bu$_4$N]$_2$[**2b**]	0.59	6.27	73	2.70
[^{n}Bu$_4$N]$_2$[**2b**]	0.60	6.16	72	2.63
[^{n}Bu$_4$N]$_2$[**2c**]	0.59	6.18	74	2.72
[^{n}Bu$_4$N]$_2$[**2c**]	0.60	5.49	75	2.48
[^{n}Bu$_4$N]$_2$[**2c**]	0.60	4.91	74	2.17
[^{n}Bu$_4$N]$_2$[**2c**]	0.60	4.75	74	2.11
[^{n}Bu$_4$N]$_2$[**2c**]	0.58	6.02	74	2.61
[^{n}Bu$_4$N]$_2$[**2c**]	0.58	6.11	73	2.58
N719	0.74	13.54	74	7.34
N719	0.74	13.52	74	7.46
N719	0.73	14.85	74	8.10
N719	0.74	11.29	76	6.30
N719	0.73	13.65	75	7.49
N719	0.73	13.55	74	7.34

DFT optimized coordinates of **1a**⁺

```
* xyz 1 1
  C      15.379885     -0.875761      4.667278
  C      14.863025     -1.745718      5.640707
  C      15.737715     -2.502760      6.450132
  C      17.134090     -2.373626      6.283909
  C      17.649976     -1.476918      5.334719
  C      16.774089     -0.731424      4.519624
  H      13.788906     -1.850893      5.792222
  H      17.791239     -2.977467      6.909631
  C      14.811282      1.566877      2.020979
  C      13.428033      1.664097      1.886429
  C      12.618981      0.879209      2.717499
  C      13.224656      0.033513      3.644934
  C      14.624398     -0.025326      3.737958
  N      15.405317      0.753349      2.913208
  H      11.532600      0.925531      2.642975
  H      15.471287      2.161440      1.391728
  H      13.003189      2.339757      1.146047
  H      12.617755     -0.587276      4.301543
  C      19.062794     -1.194018      5.048183
  C      20.158831     -1.783934      5.698024
  C      21.458645     -1.431122      5.339750
  C      21.649248     -0.483692      4.325991
  C      20.526848      0.070396      3.714834
  N      19.268094     -0.263594      4.054024
  H      22.310805     -1.887293      5.843002
  H      19.984533     -2.517564      6.483303
  H      22.644311     -0.175112      4.010400
  H      20.636366      0.810320      2.923558
  C      18.514527      1.399829      0.566405
  C      19.034579      2.277058     -0.386563
  C      19.281216      3.610471     -0.020470
  C      19.008945      4.039946      1.289108
  C      18.491540      3.119515      2.204282
  H      19.253464      1.957620     -1.402427
  H      19.202366      5.070427      1.572560
  C      17.369715     -1.979913      1.382638
  C      17.538903     -2.706090      0.208463
  C      18.058975     -2.062045     -0.922717
  C      18.386134     -0.706257     -0.825897
  C      18.192028     -0.029151      0.382384
  N      17.685180     -0.673719      1.485531
  H      16.969913     -2.449417      2.278332
  H      17.272287     -3.759879      0.172195
  H      18.791249     -0.181275     -1.686461
  C      18.149561      3.367558      3.619100
  C      18.327773      4.607035      4.242177
  C      17.987161      4.763246      5.589037
  C      17.466870      3.659339      6.278622
  C      17.312863      2.452223      5.605157
  N      17.644352      2.291169      4.308832
  H      18.732526      5.445951      3.683060
  H      17.189309      3.741692      7.326929
  H      16.914358      1.576096      6.111275
  Ru     17.501884      0.534015      3.183362
  N      18.256538      1.841355      1.821601
  C      19.836772      4.531943     -1.060090
  O      20.099797      4.183879     -2.192406
  O      20.007978      5.773445     -0.605036
  C      20.534412      6.742323     -1.525497
  H      19.867830      6.847728     -2.390193
  H      20.590435      7.682174     -0.969812
  H      21.531813      6.440148     -1.867502
  N      15.216967     -3.385071      7.434812
  C      14.068819     -4.172856      7.150008
  C      13.955718     -4.876600      5.932701
```

```
C      13.014408     -4.275819      8.071753
C      12.827028     -5.642550      5.651320
C      11.885894     -5.061539      7.806189
C      11.779681     -5.749996      6.586602
H      14.762156     -4.820101      5.201860
H      13.072920     -3.737738      9.017171
H      12.743208     -6.184341      4.709150
H      11.095766     -5.115517      8.552257
C      15.799225     -3.432822      8.730105
C      15.990261     -4.657664      9.390499
C      16.192616     -2.253766      9.397539
C      16.538050     -4.716378     10.678266
C      16.758354     -2.305266     10.669274
C      16.933529     -3.536304     11.329714
H      15.701133     -5.584439      8.896013
H      16.051080     -1.287845      8.913788
H      16.661147     -5.687936     11.152279
H      17.059237     -1.390868     11.180937
O      17.481464     -3.484673     12.572945
C      17.671663     -4.689182     13.296496
H      16.716795     -5.207757     13.475904
H      18.358982     -5.371631     12.772449
H      18.112239     -4.405800     14.258427
O      10.725687     -6.530032      6.229406
C       9.638067     -6.678410      7.127187
H       9.957374     -7.135746      8.076712
H       9.152398     -5.712669      7.337550
H       8.918716     -7.341192      6.634103
C      18.245192     -2.851697     -2.183059
O      17.973061     -4.029518     -2.277052
O      18.741093     -2.118029     -3.178577
C      18.161732      6.058428      6.322905
O      17.878197      6.204415      7.492718
O      18.661991      7.021372      5.549653
C      18.880296      8.304969      6.157988
H      17.935203      8.712486      6.536793
H      19.597707      8.217386      6.983104
H      19.282797      8.944703      5.368092
C      18.972672     -2.783099     -4.431265
H      19.697732     -3.595884     -4.301462
H      18.033758     -3.190115     -4.825620
H      19.370948     -2.019772     -5.104981
*
```

DFT optimized coordinates of **1a**$^{2+}$

```
* xyz 2 2
C   15.36149337709779     -0.87663461439730      4.65862105535094
C   14.84701432746700     -1.74763923602776      5.61123495140605
C   15.73263628018902     -2.45766030699596      6.47221843816773
C   17.14166032124838     -2.27937764323695      6.35874834351625
C   17.65120622486677     -1.40261570036824      5.40822263375299
C   16.76675341504912     -0.69393379083405      4.55040774696339
H   13.77462562453188     -1.87946324649541      5.74095368007884
H   17.79607324229896     -2.85984564183073      7.00620370972053
C   14.80466705901615      1.50808498910760      1.96131842827129
C   13.42146020573642      1.56864017595486      1.79083122694663
C   12.60985608283012      0.78111600087930      2.61303323376252
C   13.21068326683822     -0.03519138858361      3.57250011307659
C   14.60516538886579     -0.05495122872912      3.69743442700024
N   15.38988836814001      0.72502184181195      2.88263698211194
H   11.52534970062257      0.80024818139294      2.50973997387495
H   15.46613673291492      2.10691245689260      1.33801532508707
H   13.00045105783886      2.22059847223054      1.02758777027336
H   12.60025468361030     -0.65801525719276      4.22360703202874
C   19.06793614178136     -1.09380104331080      5.14466064883848
C   20.15747467222822     -1.64410386077754      5.83093394038468
```

```
C    21.45689888752802    -1.26333665644909     5.49223948284883
C    21.64374973895034    -0.33219953029061     4.46593008442119
C    20.52088361576681     0.18183897216833     3.81755666341352
N    19.26748838484944    -0.18028391223260     4.13767363239490
H    22.30906111818948    -1.68715069469439     6.02233581084022
H    19.98666337448326    -2.36662511857198     6.62696089300087
H    22.63706429466311    -0.00363254176382     4.16590991142374
H    20.62939011459762     0.90850378169662     3.01428108729811
C    18.54115011111107     1.37817036884833     0.60213059417145
C    19.06815008989743     2.24128910032638    -0.36177018395554
C    19.28192260901669     3.58495813562507    -0.01947482722202
C    18.97225273554815     4.04100802952651     1.27085854999369
C    18.44960849357181     3.12961611432240     2.19403147820072
H    19.31647200253787     1.90264399479348    -1.36436782178391
H    19.14112530456567     5.08081688438626     1.53456144223437
C    17.44002777592279    -2.00477519878211     1.46689593710908
C    17.64069084806919    -2.75050268811115     0.30876389633348
C    18.16854521162657    -2.12010408263753    -0.82365553425452
C    18.47332660348779    -0.75737797031865    -0.74825429304676
C    18.24747121486196    -0.06176914115323     0.44259709402875
N    17.73277384019972    -0.69311399615010     1.54693346071939
H    17.03258852258563    -2.46801826066769     2.36179171519265
H    17.39113077251794    -3.80884263740368     0.28985541953026
H    18.88420188254692    -0.24263826747946    -1.61213422501496
C    18.07234325729741     3.40518196065080     3.59661075674458
C    18.21818800031529     4.66152500840795     4.19101065487566
C    17.84932750468611     4.84371443630377     5.52744291223339
C    17.33429202792274     3.75060808921517     6.23320232293319
C    17.21241054976839     2.52395016302380     5.58645699269338
N    17.57177235464647     2.33990001335390     4.30212301417716
H    18.61984036686807     5.49332309808073     3.61949537021989
H    17.03471862248427     3.85213849682362     7.27360779482813
H    16.81781002751728     1.65720310783030     6.11028982521573
Ru   17.47969801603427     0.53356247968021     3.23314619454335
N    18.24917878550307     1.84519050561628     1.83424443537648
C    19.84886469695201     4.49492771500691    -1.06949976023433
O    20.14430438539761     4.12098523849283    -2.18400580331185
O    19.98587053990238     5.74570558082190    -0.63736803257336
C    20.51988203408798     6.70670063355122    -1.56389297272628
H    19.87583940326327     6.77887519581271    -2.44859910035598
H    20.54063118086528     7.65838207782129    -1.02663890639926
H    21.53242244162564     6.41649954585706    -1.86922600734025
N    15.21404567159808    -3.32908451659436     7.43222171349825
C    14.01045362103881    -4.04217199969023     7.17931571485102
C    13.80860367775834    -4.68847645373423     5.94028562270116
C    13.01020778186064    -4.12247979694003     8.16412726611954
C    12.63422040941415    -5.38593834527481     5.69756538949292
C    11.82830147287045    -4.82356263546655     7.92544536545617
C    11.62689146919383    -5.46169868454850     6.68499647611159
H    14.58656974354759    -4.65872670116151     5.17861707772512
H    13.14829170172152    -3.61757926262238     9.11882939196366
H    12.47635157471504    -5.89908613921899     4.74997122311327
H    11.06909065343517    -4.85678603622013     8.70315686738838
C    15.87046992587533    -3.51503612365315     8.67738324809527
C    15.99040833811135    -4.80241130040348     9.23172637842657
C    16.39464134707767    -2.41183992346133     9.38725420360860
C    16.61936129501469    -4.99558315618830    10.46116738072856
C    17.02368202524479    -2.59951127905236    10.60921155571630
C    17.14560703103679    -3.89302818069099    11.16404705598657
H    15.60344119523203    -5.66341901215984     8.68930474733596
H    16.28538488172186    -1.40504304334625     8.98700036782446
H    16.70464008229031    -6.00511251115371    10.85577089059886
H    17.41637798685199    -1.75207480380216    11.16945339042024
O    17.76650074111145    -3.97418551834083    12.35409849222639
C    17.89772826889410    -5.23617056585230    13.00120575454713
H    16.91278244000311    -5.67841085037507    13.21070226811017
H    18.49363645600486    -5.93399691148111    12.39501609389408
H    18.41677071198752    -5.04140914158322    13.94478842910404
O    10.52480635451102    -6.15893926168271     6.35752460511373
```

```
C     9.46895180400573      -6.30536243208746      7.30182227879811
H     9.81600523983270      -6.82204744051156      8.20851958777147
H     9.04071420729284      -5.32956850263624      7.57388609416358
H     8.70293373246114      -6.91219493922904      6.80907502929729
C    18.38722169586125      -2.93184328145755     -2.06753063097074
O    18.13510972008460      -4.11488844770440     -2.13890440518818
O    18.88483861814128      -2.20812089231810     -3.06679106071427
C    17.98944997630310       6.16131946439289      6.23337274000793
O    17.67289942233071       6.32958145141949      7.39083013622783
O    18.49780721228195       7.10707414124381      5.44769454518794
C    18.68294693062639       8.41191598830892      6.02327315457233
H    17.72233354472832       8.81567717529571      6.36488710294216
H    19.37982906571871       8.35770692151991      6.86841999484055
H    19.09708542967109       9.03330682399960      5.22500329338772
C    19.14931862526569      -2.89103164235742     -4.30439316400332
H    19.88720175131239      -3.68709560841366     -4.14706800222366
H    18.22423825337295      -3.32227197706478     -4.70524968947219
H    19.54414548318161      -2.13206262552882     -4.98477396317296
*
```

DFT optimized coordinates of **1b**[+]

```
* xyz 1 1
  C     15.346649     -0.780540      4.758388
  C     14.804497     -1.630220      5.734872
  C     15.659230     -2.340373      6.601229
  C     17.057141     -2.190532      6.502118
  C     17.599666     -1.316672      5.546279
  C     16.744675     -0.616332      4.669333
  H     13.727606     -1.761020      5.843396
  H     17.692047     -2.762440      7.179273
  C     14.853342      1.541030      1.991904
  C     13.475746      1.607547      1.795000
  C     12.644457      0.842358      2.622349
  C     13.223113      0.046954      3.609706
  C     14.618126      0.018281      3.764137
  N     15.421281      0.775567      2.941806
  H     11.561825      0.865141      2.499072
  H     15.529903      2.120774      1.366374
  H     13.072305      2.244277      1.009549
  H     12.599010     -0.557776      4.265207
  C     19.018782     -1.021479      5.305310
  C     20.095654     -1.561235      6.026413
  C     21.403320     -1.200189      5.706508
  C     21.620466     -0.296106      4.659200
  C     20.515820      0.208591      3.976788
  N     19.249765     -0.133676      4.278536
  H     22.241011     -1.616766      6.265235
  H     19.900576     -2.261538      6.836774
  H     22.622687      0.016603      4.371565
  H     20.646106      0.913445      3.157232
  C     18.570883      1.332554      0.668651
  C     19.094305      2.167104     -0.320370
  C     19.313876      3.521688     -0.020626
  C     19.011475      4.014760      1.259599
  C     18.492268      3.134876      2.213017
  H     19.334713      1.798905     -1.314664
  H     19.181639      5.062242      1.490871
  C     17.450415     -2.014307      1.640361
  C     17.640245     -2.796521      0.506061
  C     18.165990     -2.204241     -0.650256
  C     18.482015     -0.842665     -0.617207
  C     18.267039     -0.107913      0.553178
  N     17.749962     -0.701054      1.680150
  H     17.043656     -2.442629      2.553397
  H     17.383502     -3.853332      0.519320
  H     18.892462     -0.357458     -1.498370
```

```
C       18.116451      3.451808       3.605509
C       18.273262      4.722342       4.168488
C       17.903734      4.943498       5.498493
C       17.375335      3.872393       6.231881
C       17.242960      2.631691       5.617121
N       17.603002      2.408180       4.337964
H       18.685233      5.534734       3.576547
H       17.075360      4.005301       7.268725
H       16.839279      1.779537       6.158762
Ru      17.507519      0.592697       3.304119
N       18.285503      1.834869       1.894457
C       19.870418      4.397879      -1.098634
O       20.156582      3.996469      -2.207370
O       20.013169      5.663972      -0.706153
C       20.536967      6.593392      -1.668169
H       19.885442      6.636945      -2.549460
H       20.562220      7.562738      -1.163371
H       21.547088      6.295198      -1.974481
N       15.099170     -3.218375       7.580498
C       14.166445     -4.201379       7.157596
C       14.391312     -4.929955       5.972582
C       12.989000     -4.451911       7.890523
C       13.462693     -5.878636       5.533217
C       12.071311     -5.411644       7.452805
C       12.298508     -6.130360       6.271196
H       15.298576     -4.748944       5.397375
H       12.792285     -3.889199       8.802271
H       13.657637     -6.431659       4.613384
H       11.165056     -5.587305       8.034046
C       15.441287     -3.063759       8.943640
C       15.505790     -4.178446       9.807066
C       15.742704     -1.790380       9.472163
C       15.844005     -4.018410      11.153716
C       16.094673     -1.641682      10.817234
C       16.144089     -2.750905      11.671573
H       15.292470     -5.173379       9.419069
H       15.696658     -0.914721       8.826320
H       15.885779     -4.897114      11.799112
H       16.320102     -0.645433      11.200797
C       18.366128     -3.052549      -1.869672
O       18.100502     -4.234915      -1.908820
O       18.864695     -2.364652      -2.895781
C       18.056591      6.275371       6.168977
O       17.736906      6.482010       7.320111
O       18.582059      7.196190       5.362150
C       18.780329      8.511275       5.906969
H       17.823698      8.935798       6.234613
H       19.472625      8.469973       6.756779
H       19.205804      9.108756       5.096327
C       19.107991     -3.088218      -4.113359
H       19.834857     -3.891005      -3.939210
H       18.173403     -3.517214      -4.494458
H       19.508539     -2.356566      -4.820022
H       11.577813     -6.873965       5.930077
H       16.412601     -2.630567      12.721291
*
```

DFT optimized coordinates of **1b**[2+]

```
* xyz 2 2
  C   15.31629230334688     -0.80763313949540      4.69752130966704
  C   14.77896992952266     -1.66219557076606      5.64941176922460
  C   15.63830834083025     -2.31933786438642      6.58199280709700
  C   17.04864785912020     -2.09658427235718      6.53433244182842
  C   17.58120310043288     -1.23923716905896      5.58184920785498
  C   16.72060548534381     -0.58683087527306      4.65643931663193
  H   13.70615683750796     -1.82484744343425      5.72433848592580
```

```
H    17.68601051275976     -2.63288083984007      7.23372940325439
C    14.83442526102118      1.45579195271770      1.88295382788200
C    13.45970921687053      1.46972496438046      1.64150398645343
C    12.62938720438573      0.69044973940077      2.45129361047002
C    13.20180259547960     -0.07134921193519      3.47229994656908
C    14.58698114390364     -0.04471213173575      3.66691864416752
N    15.39041447704324      0.72535099213248      2.86207108469108
H    11.55167945016752      0.67353065317290      2.29248929458517
H    15.51065479981822      2.04882048829799      1.26996414502710
H    13.06090926167720      2.07978870881291      0.83315121788866
H    12.57559877567719     -0.68648773939453      4.11556112820426
C    19.00302410546901     -0.90321052789833      5.37545415114010
C    20.06765884032115     -1.39212057339307      6.14038570431897
C    21.37331252670268     -0.98986388487662      5.85005600742315
C    21.58892821622660     -0.10106826100722      4.79357231924771
C    20.48779900068343      0.35226789243913      4.06548150447629
N    19.23098923095149     -0.03080035505254      4.33924856216214
H    22.20726865793976     -1.36549903152308      6.44167438317076
H    19.87484957939424     -2.08262881113915      6.95922738626912
H    22.58755349213500      0.24173769856596      4.52953157921412
H    20.61936224534004      1.04515350663631      3.23631110341222
C    18.64050836228676      1.32320378442287      0.69451190565358
C    19.20785331474110      2.14112499543487     -0.28658124971925
C    19.39437461198707      3.50197508212110     -0.00273048889948
C    19.01497948422976      4.02037739316308      1.24420543283719
C    18.45194495673193      3.15116677069301      2.18464496235492
H    19.50858575331336      1.75395624607429     -1.25671773979988
H    19.16160538664768      5.07406844079808      1.46222606822451
C    17.53119365385937     -2.02329499883723      1.68274768266605
C    17.78134515761812     -2.82285160189462      0.57076004201897
C    18.35018231593378     -2.24447158976119     -0.56858838238197
C    18.64497990482150     -0.87754188298630     -0.54897025831060
C    18.36684211360617     -0.12635612181468      0.59551479423982
N    17.81229205283234     -0.70724657934422      1.70709153949156
H    17.09215798321197     -2.44644361061501      2.58232928244467
H    17.53804584653440     -3.88255506122180      0.59427820016902
H    19.08696136824254     -0.40267620464260     -1.42027171375437
C    17.99688632824832      3.49587890211966      3.54844716152015
C    18.08229770980709      4.78674285545268      4.07525503311240
C    17.63928098179732      5.03444856767873      5.37815513861773
C    17.11557033597298      3.97051798885527      6.11974021251361
C    17.05486102234034      2.70586235644525      5.53982082733011
N    17.48232253045967      2.46151289828253      4.28715999013908
H    18.49354346528688      5.59492785969934      3.47759535183451
H    16.76026440270022      4.12236069036385      7.13614141107387
H    16.65355152550951      1.86088623179524      6.09291294069337
Ru   17.46458051500210      0.59071307680921      3.32492169302042
N    18.28415689704712      1.84925349324068      1.88306139844287
C    20.00957746830038      4.36486139770929     -1.06767481036826
O    20.34475147028412      3.94209119173024     -2.15263407622410
O    20.13913186104490      5.63026463946172     -0.68088424806961
C    20.71945934215086      6.55054208213619     -1.62151109651077
H    20.11563842187956      6.58860054620923     -2.53606347988668
H    20.72190725030593      7.52314963115965     -1.12295365846277
H    21.74281754787548      6.24338399004035     -1.86838799865590
N    15.10062283501541     -3.17543285694158      7.53223083334340
C    13.87437948229811     -3.86965478545112      7.28523692671689
C    13.69963798193729     -4.59064741185073      6.09065932513829
C    12.85287511309929     -3.85085432216302      8.25042454842682
C    12.50400436518717     -5.27735852637573      5.86210022477403
C    11.66288510023463     -4.54460083610456      8.01540979232134
C    11.48330374716091     -5.25768942951321      6.82205159834513
H    14.50279750534166     -4.62537893597712      5.35528481380792
H    12.98889197923415     -3.28767433052080      9.17259813080424
H    12.37679179514015     -5.84035454053582      4.93746666613303
H    10.87079530028516     -4.52140397295999      8.76412197077258
C    15.75185010082514     -3.39404671160161      8.78567127538636
C    15.92288683534938     -4.70430562983316      9.26614703908045
C    16.19737953963477     -2.30193451588170      9.55188325230370
```

```
C    16.54159648788204     -4.91629386760223     10.50081002063754
C    16.81958161578662     -2.52417064851168     10.78326482981594
C    16.99353141034443     -3.82963853021894     11.26223301054889
H    15.58118202728579     -5.54899391500949      8.66980233327927
H    16.04123786202489     -1.28587456766411      9.19133756954075
H    16.67712944545749     -5.93471887255251     10.86528710266313
H    17.15618802444205     -1.67335768166365     11.37545546194055
C    18.62026553276518     -3.11364991906670     -1.76343348605186
O    18.36177225371474     -4.29680507186578     -1.79231044895683
O    19.16977890761106     -2.43775499418024     -2.76788736196926
C    17.70679508755530      6.39625844257739      6.00870997184331
O    17.32048537073065      6.62404505209670      7.13397494866120
O    18.23526043075321      7.30512181750679      5.19439466627641
C    18.35266146077766      8.64887831492047      5.69370047598834
H    17.36289669752031      9.04558371461363      5.94948602711165
H    18.99709560511922      8.66798126095972      6.58082830740354
H    18.79997807674109      9.22958472541193      4.88292550253024
C    19.48480015956206     -3.17448642807184     -3.96232985143669
H    20.20492776111518     -3.97026295600893     -3.73654855910211
H    18.57450792579268     -3.61259507705556     -4.38864618699086
H    19.92034263582812     -2.44839988976285     -4.65359944757423
H    10.55395669004973     -5.79828000775486      6.64299506285101
H    17.47483443271463     -3.99914297515567     12.22519455202393
*
```

DFT optimized coordinates of **1c**[+]

```
* xyz 1 1
C      17.674160     -4.483491      9.155635
C      16.870412     -3.635653      8.377549
C      15.509870     -3.945659      8.196593
C      14.938208     -5.085760      8.791113
C      15.738792     -5.928446      9.577424
C      17.107444     -5.629867      9.754400
H      17.268833     -2.739036      7.901913
H      13.882024     -5.292062      8.615351
C      20.935635     -5.308394     10.558640
C      21.796854     -4.298766     10.134659
C      21.281249     -3.273932      9.331851
C      19.930155     -3.299960      8.989574
C      19.107802     -4.341449      9.446254
N      19.630732     -5.342881     10.232107
H      21.922737     -2.467408      8.977872
H      21.301962     -6.122040     11.182186
H      22.844258     -4.322742     10.429948
H      19.505506     -2.514795      8.366609
C      15.334002     -7.161727     10.266382
C      14.033037     -7.687316     10.292533
C      13.769927     -8.868320     10.984485
C      14.821422     -9.515071     11.645246
C      16.092804     -8.948275     11.587645
N      16.355826     -7.807175     10.924529
H      12.760613     -9.278316     11.008824
H      13.232810     -7.164377      9.772007
H      14.667072    -10.440040     12.197877
H      16.933465     -9.422220     12.091404
C      20.095826     -9.097940     11.212326
C      20.927037     -9.972132     11.914764
C      21.073200     -9.804620     13.301281
C      20.390345     -8.767434     13.957714
C      19.569550     -7.922271     13.205428
H      21.462502    -10.778296     11.419509
H      20.504804     -8.637658     15.030148
C      18.633136     -8.108715      8.006541
C      19.162463     -9.004262      7.082701
C      20.061780     -9.984836      7.522505
C      20.382690    -10.032084      8.882103
```

```
C      19.811825     -9.108948      9.763589
N      18.941809     -8.143478      9.317649
H      17.938783     -7.331686      7.695513
H      18.883745     -8.937910      6.033431
H      21.074525    -10.783703      9.251528
C      18.765830     -6.787781     13.703401
C      18.710966     -6.428702     15.053397
C      17.910084     -5.356132     15.455620
C      17.186569     -4.659916     14.478137
C      17.286729     -5.059993     13.149156
N      18.049121     -6.098586     12.754246
H      19.282201     -6.985884     15.790400
H      16.552104     -3.819508     14.750981
H      16.737100     -4.540978     12.367377
Ru     18.248291     -6.848891     10.808882
N      19.444978     -8.109114     11.870496
C      21.963940    -10.760494     14.032271
O      22.552972    -11.672804     13.491073
O      22.034292    -10.498849     15.337231
C      22.861204    -11.359960     16.136159
H      23.901558    -11.315863     15.791987
H      22.781979    -10.984568     17.159790
H      22.501013    -12.394290     16.078886
N      14.696963     -3.097314      7.382118
C      14.703454     -3.063997      5.988826
C      15.479515     -3.807005      5.087541
C      13.739775     -2.116909      5.538646
C      15.282098     -3.586284      3.721445
C      13.561419     -1.912856      4.159960
C      14.334341     -2.648562      3.257976
H      16.212268     -4.532662      5.438846
H      15.873627     -4.152391      3.000892
H      12.827687     -1.191350      3.797638
C      13.743908     -2.190768      7.842506
C      13.124596     -1.556338      6.727657
C      13.385396     -1.872797      9.160482
C      12.126563     -0.591722      6.946271
C      12.389989     -0.909883      9.350825
C      11.763532     -0.273942      8.257469
H      13.865786     -2.359636     10.008512
H      11.641314     -0.096269      6.104167
H      12.093389     -0.645894     10.366698
C      20.643579    -10.938391      6.522695
O      20.346869    -10.934311      5.347327
O      21.519387    -11.779936      7.070308
C      17.788388     -4.937665     16.889983
O      17.068292     -4.037056     17.263792
O      18.554288     -5.668365     17.699115
C      18.511397     -5.359170     19.101594
H      18.826121     -4.322392     19.272215
H      17.495934     -5.501671     19.490880
H      19.205691     -6.053298     19.581835
C      22.142292    -12.738488      6.199657
H      21.383912    -13.383065      5.739102
H      22.711547    -12.225142      5.415114
H      22.810540    -13.327650      6.833187
H      14.205166     -2.500026      2.185471
H      10.990021      0.472576      8.440688
*
```

DFT optimized coordinates of **1c**$^{2+}$

```
* xyz 2 2
  C   17.70161985487928     -4.54629332665026      9.05872484225734
  C   16.89950915311120     -3.68818276003568      8.30997816815546
  C   15.51272020407095     -3.96021059485416      8.18378925993847
  C   14.92747987935765     -5.09011443819835      8.81082823973804
```

```
C    15.72682650963613      -5.94400712552150       9.56807166770725
C    17.11291138238472      -5.67208391637663       9.68785173844310
H    17.30154925265153      -2.78790124643966       7.84983220894017
H    13.86902239325658      -5.28772431553227       8.65348122390894
C    20.97973283598782      -5.42271778464753      10.38901215263692
C    21.85304304734096      -4.44086582551176       9.91616113485423
C    21.34063737007547      -3.42182576536317       9.11059775023409
C    19.97619306589057      -3.41868500922777       8.80739744137435
C    19.15131935310891      -4.42887560253100       9.31055048873671
N    19.67030891886646      -5.42509599852997      10.10027364252039
H    21.99035977869363      -2.63909706330792       8.72127722496156
H    21.34555612093753      -6.23191989281276      11.01820070040926
H    22.90779929047800      -4.48615167100728      10.18016798080368
H    19.55437014056079      -2.63459153575257       8.18179764146573
C    15.31007653516860      -7.16347694520785      10.28753822156603
C    14.00302677281790      -7.65599882518043      10.34606846739757
C    13.73241232982130      -8.82002628198203      11.07054329027461
C    14.78140331878589      -9.47034992890962      11.72384081792605
C    16.06598304838567      -8.93045271779300      11.63042549992906
N    16.33093561726740      -7.81317699318208      10.93751702880248
H    12.71655468896432      -9.20978228577821      11.12206677690590
H    13.20197583255887      -7.13134620050054       9.82929090197731
H    14.62050739198370     -10.37955977263596      12.29978955265248
H    16.90616817411144      -9.40982867884830      12.12934473987427
C    20.06283555285634      -9.16001954379504      11.22833186759366
C    20.90434296193346     -10.01441568193879      11.94591236949771
C    21.08993567861307      -9.78015072682823      13.31558009372962
C    20.43749233742559      -8.70913522457940      13.94267062343036
C    19.60678857002848      -7.89078482794094      13.16904244946344
H    21.41645543903501     -10.84930616736007      11.47457561584381
H    20.58256449703820      -8.52998934875507      15.00394490932549
C    18.53779996028392      -8.28761504179834       8.01723004373887
C    19.01479705172571      -9.24596968689805       7.12602696265052
C    19.89300862312199     -10.22933243942506       7.59101515727411
C    20.25504479189194     -10.21956991718836       8.94162843216906
C    19.73924489061188      -9.23646945644031       9.78830413256591
N    18.88671871235559      -8.27352950817743       9.31657186187325
H    17.85789863732142      -7.50902912788929       7.68174631980021
H    18.70587171885882      -9.22229309168361       6.08362548026284
H    20.93370460111015     -10.97379601699354       9.32918614957293
C    18.83323159899656      -6.72065846610835      13.63555662897423
C    18.81391545412466      -6.30085466754949      14.96690572151340
C    18.04724793387155      -5.18964115535752      15.33146491446455
C    17.32326183581779      -4.52130560103573      14.33977656777197
C    17.38138894063159      -4.98703232043099      13.02829814170127
N    18.11203805798976      -6.06050699528799      12.67551791694760
H    19.38634398372983      -6.83709208201065      15.71820148654915
H    16.71708070114649      -3.65167148402857      14.58282221187536
H    16.82449477081311      -4.48945484016377      12.23875346442644
Ru   18.22454974291343      -6.86064666253967      10.73049195546446
N    19.45010822998754      -8.13892620963253      11.85602836262246
C    22.00115023177072     -10.71016702291097      14.06845084099056
O    22.56713865451260     -11.64507639262275      13.54619453647872
O    22.10616195666313     -10.38572323391729      15.35226214405900
C    22.95249336123779     -11.20928754771896      16.17420911815430
H    23.98248651549037     -11.18557246097483      15.79918053942053
H    22.90031924403925     -10.78045070450649      17.17801687976025
H    22.58571367273218     -12.24259313292161      16.17809060658835
N    14.70682209414810      -3.09700088603071       7.42684433366148
C    15.01398285472434      -2.58873287840964       6.14940374993764
C    16.11475463196242      -2.84922859316954       5.32203052684999
C    13.94742599864805      -1.75766576269087       5.71722425372557
C    16.14949859719271      -2.23295539406799       4.06625634784505
C    14.00036161822337      -1.15218513800326       4.45424017911081
C    15.10913302374352      -1.38757604784358       3.63549336852454
H    16.91825719678155      -3.51734544393461       5.62415222924805
H    16.99903103943145      -2.41961696350239       3.40918334301393
H    13.18545608745746      -0.51382128788240       4.11214181683945
C    13.45008222168619      -2.59057546640560       7.81274963651570
```

```
C    12.95402769224192     -1.75530377588770      6.77764812251463
C    12.75012002339429     -2.75121520673352      9.01618953709556
C    11.72396710552308     -1.10224179252114      6.93500429240135
C    11.52374399896514     -2.09164421892397      9.15264761654735
C    11.00797904471477     -1.28208634907412      8.12242712243298
H    13.13952426223164     -3.35344359307807      9.83414238171063
H    11.33502595465655     -0.45765289371779      6.14645549826395
H    10.96244868083172     -2.20616082433520     10.08010997253448
C    20.41241121790260    -11.25622422228218      6.62391821861337
O    20.08317980831804    -11.29213537336594      5.45921824721097
O    21.26336344434637    -12.10197822661467      7.19550894614026
C    17.96568660961708     -4.69709341842949     16.74930888618817
O    17.31489124087763     -3.72973705206592     17.07647016253593
O    18.67832694364877     -5.44695437877551     17.58389714678506
C    18.66724633366702     -5.07946761296637     18.97442431782985
H    19.06290940055711     -4.06457072785069     19.10078618819601
H    17.64532495321317     -5.12769222195153     19.36916996759244
H    19.30816654385159     -5.80618996708010     19.47958156321848
C    21.82932498337130    -13.13127722519216      6.36514859082643
H    21.03471164366649    -13.76602868145385      5.95534513911778
H    22.40146552477701    -12.68212630235903      5.54451972315310
H    22.48604876569863    -13.71259295186643      7.01734714078557
H    15.16444844110801     -0.92254342303517      2.65144586501215
H    10.04882856698752     -0.78262129177079      8.25779693207532
*
```

DFT optimized coordinates of **2a**[+]

```
* xyz 1 1
C    15.37788393196535     -0.80084724559981      4.76577876048181
C    14.85646290947366     -1.66632639547173      5.74024124494875
C    15.72003045818354     -2.50500819397953      6.47748371432664
C    17.11203149251093     -2.46123257205948      6.24453404837695
C    17.63908956744843     -1.56655241395766      5.29962208772324
C    16.77283534101324     -0.73963761415387      4.54920967250869
H    13.78675640482745     -1.70945887206873      5.94663922576114
H    17.75711306856653     -3.12701269569413      6.81861838806247
C    14.84062186042151      1.75536509109628      2.22253324916537
C    13.46152102638908      1.94548954713256      2.16229850907423
C    12.64428404012574      1.18857622503779      3.01223647340864
C    13.23964832360093      0.27703155337776      3.88201526226495
C    14.63623318352658      0.12486555819491      3.90065542606833
N    15.42674321707343      0.87824847957474      3.05826122238997
H    11.56082911074295      1.30740394511049      2.99627438982908
H    15.50755726620500      2.32556566380796      1.57780953574133
H    13.04534890110425      2.67022938553592      1.46432422185591
H    12.62703834565624     -0.32392909451583      4.55207307627462
C    19.05062864219030     -1.35807368206806      4.95238595283589
C    20.13819320130992     -2.04013710053690      5.52337529479853
C    21.43934780655830     -1.75551492979069      5.11322267395373
C    21.63986376457023     -0.78150404789934      4.12602318786281
C    20.52623809368762     -0.13516891111698      3.59388489390949
N    19.26538692712640     -0.40124020674247      3.98257110367990
H    22.28402996628729     -2.28392524750132      5.55500534520489
H    19.95529500601306     -2.79268517660247      6.28889209664161
H    22.63626384419515     -0.52293914993810      3.77143590722443
H    20.64271475972771      0.62811336307366      2.82577342011605
C    18.49905654401261      1.43645348350702      0.60607482300907
C    19.04385589284402      2.31957342839670     -0.33260927979953
C    19.37621166939616      3.62422863266121      0.06061677984637
C    19.15628908955468      4.01278850880271      1.39045818910952
C    18.60915262373186      3.09437831968969      2.29351172873350
H    19.22230971358364      2.02949424576237     -1.36538699595116
H    19.42114508356044      5.02583691828949      1.68399990941767
C    17.19824256439666     -1.91180863461527      1.31894590135239
C    17.31228738424542     -2.59837622650201      0.11221274106288
C    17.84501432723307     -1.94587951947644     -1.00708931460582
```

```
C    18.23649719009761    -0.61356979408093    -0.85216834191392
C    18.09819456065657     0.03118235761824     0.38084291841195
N    17.57901812145903    -0.62796759216603     1.46952292557019
H    16.79172348158718    -2.39410848522099     2.20574617681401
H    16.99462972452299    -3.63581082757222     0.03049306860545
H    18.65275859665861    -0.09269486543704    -1.71158102840633
C    18.31321810675523     3.31789207873800     3.72487777042365
C    18.54659189628245     4.53476477865301     4.37326626022930
C    18.23980432533952     4.69063534629635     5.72766919561952
C    17.69786349387396     3.58744581861865     6.39974482583785
C    17.48922643976702     2.39607768987932     5.70921483727669
N    17.78373864844935     2.24573677648817     4.40284711555637
H    18.96810660172265     5.38194686218262     3.83668227433624
H    17.44530499875140     3.67023860738906     7.45487985725590
H    17.07127965356706     1.52270882682221     6.20619433731149
Ru   17.50982489517990     0.51967724228079     3.23273271191117
N    18.29593136186447     1.84669615901929     1.87789099357966
C    19.97879087831123     4.61558655619068    -0.95523160739447
O    20.13122195412068     4.18344772048559    -2.12098045339505
O    20.25623030729238     5.75466640659170    -0.51452735622497
N    15.18726489425358    -3.39152654449582     7.45818407853775
C    14.00203536328226    -4.12250587243157     7.17850247010966
C    13.82587931441648    -4.76983087063658     5.93728502682953
C    12.96726987613405    -4.21945937459129     8.12358833508689
C    12.65830511748117    -5.47508855477309     5.65612303124325
C    11.79892006440702    -4.94487599821357     7.85709291658514
C    11.63091436303322    -5.57594262467468     6.61369945377168
H    14.61408337073327    -4.71551113010258     5.18680845822075
H    13.07261907478256    -3.72367665221642     9.08789722043342
H    12.52716181884502    -5.97240562028399     4.69498070249083
H    11.02607362404931    -4.99543246807240     8.62144123966034
C    15.80827554907439    -3.50771614047060     8.72860671903949
C    15.92609658798669    -4.75523554102436     9.36510690408209
C    16.32643326761757    -2.37707966175115     9.39610700996064
C    16.52121318881535    -4.88068898404927    10.62692627818006
C    16.93819379628612    -2.49701747613250    10.64180322377426
C    17.03962741729568    -3.74902626946525    11.27729867588627
H    15.54266882341238    -5.64767180992626     8.87174835932677
H    16.24856059651739    -1.39481505447844     8.93150376539214
H    16.58483396352967    -5.86770771682475    11.08046215882140
H    17.33561714886553    -1.61903861888587    11.15145953792131
O    17.64282895906213    -3.76441084763588    12.49718201328951
C    17.76554188203368    -4.99464128643331    13.19042232083273
H    16.78030288403979    -5.43832030670382    13.40427667277013
H    18.37080068466457    -5.72008892177442    12.62426962545747
H    18.26984000616537    -4.76843049363014    14.13618464826407
O    10.53324351245803    -6.29283985300325     6.25210149483318
C     9.46281355604568    -6.43126753621882     7.17101698018302
H     9.78373029287027    -6.94293216237707     8.09201809618648
H     9.02672784344324    -5.45490369017502     7.43465180608223
H     8.70185780182343    -7.03945289694295     6.66990874247820
C    17.99820432482332    -2.66315718061578    -2.36304039795124
O    17.59707195697300    -3.84812843326640    -2.40443456001035
O    18.50840294514812    -1.98784468610206    -3.28615557873553
C    18.48721673106851     6.03115917257372     6.44770412666108
O    18.16884448834902     6.06988967613775     7.65779552134107
O    18.98017090589431     6.94626881213097     5.74912670089523
*
```

DFT optimized coordinates of **2a**[2+]

```
* xyz 2 2
C    15.35617597373604    -0.83581546190268     4.70502345241694
C    14.82480642413321    -1.70935515211576     5.64539776526104
C    15.69454267390070    -2.45976821302199     6.49270582552781
C    17.10931906641856    -2.30771370577051     6.37432761431369
C    17.63596750626609    -1.42458911881978     5.44003647010673
```

```
C     16.76471445456810      -0.68385414456153       4.59670796981304
H     13.74998856809891      -1.82136062096345       5.77151978332212
H     17.75395653940732      -2.91028220699771       7.01066128975533
C     14.84558565348077       1.59152049431013       2.03386243396880
C     13.46235550407993       1.68830984852097       1.87127155914893
C     12.63626626943471       0.91285779649485       2.68933990671397
C     13.22192049405154       0.07087209767352       3.63729971531423
C     14.61552582778850       0.01581380786669       3.75405251277013
N     15.41476277047787       0.78532635933593       2.94300077725816
H     11.55194505483156       0.96027213109523       2.59277271067744
H     15.52025245350596       2.17970655087818       1.41440433222283
H     13.05363834808784       2.35881934929927       1.11741407551482
H     12.59972949155367      -0.54334537059714       4.28546111284297
C     19.06094288327816      -1.13986417138361       5.17964305032486
C     20.13777831213146      -1.72056375668525       5.85958377861456
C     21.44580094419787      -1.36180592917105       5.52608244409447
C     21.65220910554046      -0.42225661403415       4.51222380494049
C     20.53939952433558       0.12304320124837       3.86962100427858
N     19.28029121415417      -0.21767815978293       4.18452936232276
H     22.28863622262651      -1.80975127791831       6.05138148387809
H     19.95172831501094      -2.44896744523801       6.64681493185978
H     22.65225860494084      -0.11019532958287       4.21681958149798
H     20.66098972509687       0.85786599703156       3.07554916509470
C     18.59178160481495       1.39136927646336       0.65502114822935
C     19.13770219108705       2.25205369392922      -0.30380930445019
C     19.37837843127189       3.59043669671582       0.03688330627085
C     19.06904222888447       4.03522415433653       1.32967144667317
C     18.52637260917624       3.13221851578507       2.25052616685337
H     19.38472388568032       1.91992467707811      -1.30920478998836
H     19.26249401675520       5.07530937379764       1.58043031210609
C     17.42189933206381      -1.97792756365312       1.48784616329808
C     17.61653050885419      -2.71610227386554       0.32263693685609
C     18.16429148886192      -2.09531983992178      -0.80511724253574
C     18.49103545597352      -0.73965345738415      -0.70540410476331
C     18.27256495713386      -0.04315698037883       0.48504897258014
N     17.73921052634712      -0.67226444947303       1.58134240013878
H     16.99993836035683      -2.43808243764268       2.37832510300311
H     17.34857982934796      -3.76966950035227       0.28288469313220
H     18.91734473584002      -0.24325908344685      -1.57420889401437
C     18.14664040141287       3.41209253530795       3.65258092887040
C     18.29596287967508       4.66595135940503       4.24842462969745
C     17.92126083296966       4.86885435449104       5.57982170276087
C     17.39753441937692       3.77708647250682       6.28042483035109
C     17.26981120686897       2.54609834124475       5.64061842373936
N     17.63230065511874       2.35368441384559       4.35774188109943
H     18.70546760642616       5.50520496646429       3.69097921834679
H     17.09426320001378       3.89588052626522       7.31830737430905
H     16.86611026843344       1.68240145265350       6.16383533499336
Ru    17.49801769953873       0.53302715523356       3.29769076764958
N     18.30498699960539       1.85510121579229       1.88624449087708
C     19.98213588145729       4.56504164581439      -0.99960815782517
O     20.23388685057501       4.07747383674096      -2.12386309959682
O     20.15648314558797       5.73942342662510      -0.60551300136963
N     15.16292611491466      -3.33638744668079       7.43218409761023
C     13.88685499081461      -3.94514009014064       7.22781671563043
C     13.58793407458309      -4.59290504060229       6.01230928389062
C     12.91963312541729      -3.92724804082813       8.24350535362778
C     12.34758552759892      -5.19000792777355       5.81874666543856
C     11.67323637081717      -4.53350290532690       8.05905487238303
C     11.37371046881347      -5.16719075985039       6.83862045933378
H     14.33666872837252      -4.63554050232814       5.22199666784485
H     13.13641543277666      -3.42840388284517       9.18726184878630
H     12.11334856436197      -5.69699795563212       4.88333067896450
H     10.94484587266011      -4.49595830002694       8.86585721018284
C     15.87834218524095      -3.65899918486824       8.62495086260902
C     16.02539157869741      -4.99555605820613       9.02509795384834
C     16.42998437973770      -2.64157308264861       9.42952024387235
C     16.71483028073745      -5.32275357990090      10.19636145508794
C     17.12544618120448      -2.96041555907069      10.59021250861532
```

```
C   17.27914524928942     -4.30502667794115     10.98740701303612
H   15.60511565238135     -5.79217639192865      8.41266901799047
H   16.30380401465132     -1.59726217239989      9.14603209645470
H   16.81515963572074     -6.36961275267476     10.47307011952955
H   17.55018591325864     -2.17786048784606     11.21798942339030
O   17.97070624027539     -4.51742616882126     12.12814664902008
C   18.14720872883539     -5.84488807962518     12.60534091530972
H   17.18034471308722     -6.32409319450348     12.82083378747296
H   18.70640374044765     -6.45936167337346     11.88379496401380
H   18.72418684481698     -5.76260755170563     13.53225617088032
O   10.20016951807078     -5.77486308611806      6.55882345816093
C    9.17109008192639     -5.80174749454676      7.53904975924646
H    9.49677351405176     -6.33047619083357      8.44746104514705
H    8.84483822394535     -4.78490660165147      7.80465172210030
H    8.33299635063493     -6.34288197242294      7.08800961255947
C   18.39981075095597     -2.87322667990900     -2.11757468727893
O   18.06171465946621     -4.07720181386425     -2.10331030019605
O   18.90253371457938     -2.21706933484143     -3.05684575611644
C   18.08130220733122      6.25321218627610      6.24408946449262
O   17.70927672428168      6.33084853654798      7.43556760707312
O   18.56499609560014      7.15112692332661      5.51932861484020
*
```

DFT optimized coordinates of **2b**[+]

```
* xyz 1 1
C   15.33426066828234     -0.74400373282529      4.81833453237494
C   14.78408327099952     -1.56822454881689      5.81166757706314
C   15.62990265324506     -2.35109733087183      6.62242235927650
C   17.02817569085828     -2.30394591694810      6.45162413095430
C   17.58412260109453     -1.45735127013583      5.47982371402552
C   16.73756295468350     -0.67992483153261      4.65533617070320
H   13.70765199337762     -1.62185418260759      5.97962032138360
H   17.65204283319197     -2.92836709289773      7.09238496648740
C   14.87556940439989      1.68592768568914      2.14060493031824
C   13.49817438983404      1.85572132907773      2.01573281819988
C   12.65451917853408      1.12776225019317      2.86499167461907
C   13.22307658549234      0.26435831616071      3.79959752896432
C   14.61907051349606      0.13178963450300      3.88192662251750
N   15.43579111075582      0.85526571086589      3.03923730242226
H   11.57146294036084      1.23152790587284      2.79876812525584
H   15.56222960648964      2.23448874648282      1.49790569213859
H   13.10348352036663      2.54265692609584      1.26878050100334
H   12.59028953882133     -0.31400303203785      4.47077716762338
C   19.00576863563869     -1.25287751861726      5.17370193411370
C   20.07691324612698     -1.89251690967880      5.81937407286284
C   21.38965453136960     -1.61736898814504      5.44064629494359
C   21.61750352455157     -0.69656520063580      4.40943736219757
C   20.51872593145382     -0.09026993826497      3.80429914722511
N   19.24693480520654     -0.34738604725433      4.16244485126893
H   22.22220124598175     -2.11257323992182      5.94010091333992
H   19.87237566952439     -2.60419805990123      6.61777293081867
H   22.62388896243429     -0.44822684622640      4.07636815624655
H   20.65644744288431      0.63146135184488      3.00046577755410
C   18.56186921839878      1.33918976730018      0.67288105129796
C   19.11630569740321      2.19071154942673     -0.28919967887794
C   19.42255292524458      3.51476163480122      0.05763991984702
C   19.16734366567295      3.95417859109826      1.36506539124578
C   18.61293052410995      3.06544674202539      2.29294299324708
H   19.32099246619694      1.86153719895603     -1.30526187601278
H   19.41070225394223      4.98246077007227      1.62177979959569
C   17.27283934338263     -1.98959164930900      1.49068563925146
C   17.41490629281044     -2.72147280203596      0.31397584614067
C   17.96578381629178     -2.10900077707052     -0.81898277102171
C   18.34664353035691     -0.76921061821985     -0.70815679396671
C   18.17888267892545     -0.07798997037041      0.49563572359446
N   17.64199703819697     -0.69814011953644      1.59845234511496
```

```
H    16.85108596365999      -2.44015731449629       2.38701154817776
H    17.10469406297658      -3.76326610325161       0.26606437065883
H    18.77667696560197      -0.27920286011644      -1.57888914019551
C    18.28106165064030       3.34378511899683       3.70679193542784
C    18.49377840084637       4.58654676665223       4.31142332889056
C    18.15870393289434       4.79313443312580       5.65227379883964
C    17.60879743031667       3.71383438282440       6.35566221917428
C    17.41936342800101       2.49564507704851       5.70764791817890
N    17.74179072998477       2.29620433120950       4.41462949770943
H    18.92223834078457       5.41447373918570       3.75088402198605
H    17.33493271847594       3.83555653601258       7.40161904164719
H    16.99536239194068       1.64023594092919       6.22998430293087
Ru   17.51217146022094       0.52128229611728       3.30990715951816
N    18.32646490185531       1.79768675808871       1.92221969882268
C    20.03412751884394       4.47364071143396      -0.98387172269592
O    20.22478982906792       3.99603357257571      -2.12589780447107
O    20.27939519132743       5.63502261910151      -0.58437717737683
N    15.05833904472047      -3.19755030101313       7.62753353157968
C    14.08293376109776      -4.14939179153619       7.23513867316301
C    14.24764036610550      -4.88345891760173       6.04316342708409
C    12.91851774070019      -4.36235284812369       8.00124934048279
C    13.27691062263513      -5.80204060863431       5.63200102182600
C    11.95789612822822      -5.29143051224322       7.59053530564303
C    12.12717586357943      -6.01733743717972       6.40351606008141
H    15.14145644993635      -4.72929801434103       5.43985494746158
H    12.76578411038100      -3.79362379606561       8.91768051644781
H    13.42708499748067      -6.35951561366925       4.70641306633947
H    11.06332016971134      -5.43701843979697       8.19783796552933
C    15.44067236199787      -3.03888631790072       8.97776581602751
C    15.45996576726353      -4.13755154286696       9.86490397486192
C    15.83740337977498      -1.77699733802449       9.47171483293296
C    15.84456626973556      -3.97209891704536      11.19834346134753
C    16.23377798943087      -1.62390967351581      10.80378724846104
C    16.23688687340059      -2.71603063693540      11.68137474519700
H    15.17636962952454      -5.12547162459356       9.50519486973502
H    15.83247388020185      -0.91400809498233       8.80768021934562
H    15.84990378058015      -4.83920589599062      11.86076459083020
H    16.53311443335614      -0.63645417608677      11.15861015763751
C    18.14837069726923      -2.87725008426180      -2.14305636413601
O    17.75204711860048      -4.06446388038927      -2.14615214277218
O    18.67470000286077      -2.23601904546897      -3.08124886324221
C    18.38634004498316       6.16186739426129       6.32433649560781
O    18.04921136975827       6.24437688824514       7.52712937102547
O    18.88410976026308       7.05286346063848       5.59864498118935
H    11.37316066062802      -6.73699303853108       6.08360846673895
H    16.54170138196775      -2.59182396238898      12.72069670999358
*
```

DFT optimized coordinates of **2b**[2+]

```
* xyz 2 2
C    15.32493826463101      -0.77746981039493       4.74075069066196
C    14.76925387735406      -1.61456850322202       5.70084320517456
C    15.61610978920604      -2.32021235665247       6.60649938405330
C    17.03208584987332      -2.15973315568696       6.53047043749543
C    17.58337927818228      -1.31107387888117       5.57736242194705
C    16.73372175436006      -0.61779248046647       4.67631177764038
H    13.69189154886464      -1.73193677983041       5.79460522625617
H    17.65992222061248      -2.72736550729720       7.21377960934812
C    14.88417793241189       1.52391717861858       1.94740400126090
C    13.50661512735762       1.59280871533752       1.72912309651350
C    12.66086191719377       0.84125703235897       2.54865492749519
C    13.22101389852309       0.05077125765150       3.55519968578723
C    14.60923765052180       0.02236834133414       3.72635055559247
N    15.42786346703679       0.76691653978335       2.91196868819390
H    11.58061121515546       0.86715971020644       2.40875998329245
H    15.57399610859509       2.09391534588375       1.32757569395243
```

```
H    13.11813827867716      2.22316564949662      0.93127910102047
H    12.58262258463218     -0.54397127364930      4.20566041115902
C    19.01484140384778     -1.02369399880869      5.35229189929015
C    20.07193450585679     -1.56400150826641      6.09264236999949
C    21.38787808923810     -1.20736117621559      5.78731505601744
C    21.62113717439938     -0.31146487892539      4.74093855444579
C    20.52619320953703      0.19490191125457      4.03766656609359
N    19.26077297500483     -0.14413870823930      4.32545971479064
H    22.21586221909718     -1.62406189059974      6.35970948058267
H    19.86547993539861     -2.25925434423918      6.90425565708846
H    22.62807837936662     -0.00328248546852      4.46572643855677
H    20.66884984347158      0.89520658897329      3.21642322522800
C    18.66470050715782      1.30575933079667      0.70103847723587
C    19.22798731346350      2.13002169190366     -0.27946495555718
C    19.44694211806178      3.48412964481387      0.00980577425580
C    19.09899002408797      3.98079912052817      1.27356678868883
C    18.53962872621559      3.11250602219231      2.21739518076742
H    19.50430455083992      1.75775473758317     -1.26294533772198
H    19.27514620808324      5.03287914751304      1.48391531711547
C    17.49801971010986     -2.03354507907990      1.65044036499034
C    17.72859913417037     -2.82048423472390      0.52453865134889
C    18.30223804897919     -2.24578974783148     -0.61452808778578
C    18.61674623192841     -0.88420986587889     -0.56743288960020
C    18.36172594181033     -0.13757605964109      0.58459675462340
N    17.80381904106345     -0.72250038691378      1.69262241305541
H    17.05608161653739     -2.45753980633319      2.54905022585172
H    17.46948235713146     -3.87700319834038      0.52454811279626
H    19.06308768861521     -0.42342603428449     -1.44577141010160
C    18.11673316962698      3.44849811326708      3.59451609768211
C    18.23719627184540      4.72693251806393      4.14246171295549
C    17.82422869418780      4.97894692616929      5.45421428236667
C    17.29123675011329      3.91138747227440      6.18412953166913
C    17.19129346175671      2.65457374392178      5.59171124632178
N    17.59120359486613      2.41563027029976      4.32800064475246
H    18.65448478839189      5.54709586321444      3.56283996731264
H    16.95923746465778      4.06865883798663      7.20793305556847
H    16.78054025224294      1.80898095777624      6.13826044815781
Ru   17.50023700490171      0.54901091162556      3.34936048448949
N    18.34103753782059      1.81876469750359      1.90292867926875
C    20.06667537181150      4.42086335260353     -1.05245446759937
O    20.34729155204970      3.88936770128827     -2.14938526086620
O    20.22189070398844      5.61168656207750     -0.70282713205410
N    15.05832125961393     -3.16508728742018      7.56147055483188
C    13.78880142325458     -3.78754069384135      7.34074006025130
C    13.54358669241024     -4.49690599889137      6.15195300354188
C    12.78916153882476     -3.71047996321007      8.32535575506926
C    12.30404560977066     -5.11055885883211      5.94792887734991
C    11.55544569380478     -4.33499204983704      8.11825280238010
C    11.30682068063093     -5.03412917197337      6.92944782597513
H    14.32532009199319     -4.57397064997739      5.39685898971550
H    12.97816473444802     -3.15787225002027      9.24484235415414
H    12.12364062659028     -5.66155733000511      5.02466026409768
H    10.78344862460650     -4.26665986123929      8.88526799369012
C    15.73167853065137     -3.44279642866184      8.79173642532888
C    15.86281595373664     -4.77051953145045      9.23445750642473
C    16.24202032106288     -2.39361467819490      9.57677217506505
C    16.50095804005711     -5.04268313642668     10.44818647419616
C    16.88728026262066     -2.67467674223976     10.78468697300380
C    17.01815185630823     -3.99822204046833     11.22620202699248
H    15.47057322675294     -5.58398689401578      8.62554285163751
H    16.12359292259989     -1.36239242462147      9.24573025491214
H    16.60133001365676     -6.07592806805176     10.78171095751600
H    17.27632730593117     -1.85442198330338     11.38818479578549
C    18.58009897533262     -3.08103689711659     -1.88315300347377
O    18.24846873092892     -4.28529702285556     -1.82293826136930
O    19.10697282530195     -2.46461128418968     -2.83571866316551
C    17.95523956825398      6.38975006821064      6.06825174700195
O    17.55569496596416      6.50788635315239      7.24737123353344
O    18.44670858138273      7.26384659157452      5.32034513367979
```

```
   H    10.34335110376616      -5.51845993634465       6.77021531147825
   H    17.51662797882081      -4.21379384817994      12.17125564047064
*
```

DFT optimized coordinates of **2c**[+]

```
* xyz 1 1
   C    17.67727361486725      -4.50555894913873       9.12913499851713
   C    16.87246763738274      -3.63686630727625       8.37671451270893
   C    15.51116681948380      -3.94256584063853       8.18649362115000
   C    14.93953379625844      -5.09880310955188       8.75149933423589
   C    15.73637413416601      -5.95612749012129       9.52468903857176
   C    17.10934486106991      -5.66567978930143       9.70797241921756
   H    17.26939851712134      -2.72364963602896       7.93179247552669
   H    13.88397239872230      -5.30213401043355       8.56688655684862
   C    20.93436713494932      -5.36184564070005      10.52289309118584
   C    21.79861641627503      -4.34629656037224      10.11914411750568
   C    21.28648888626983      -3.30501683509110       9.33427694827314
   C    19.93618762022913      -3.32401893265074       8.98884389202490
   C    19.11002946363792      -4.37257655746944       9.42492101988619
   N    19.62927324005830      -5.39040066449327      10.19555319180227
   H    21.92982600826469      -2.49256878770186       8.99712407998315
   H    21.29659755299301      -6.18794993776759      11.13267348682680
   H    22.84553302633486      -4.37731907201572      10.41625743185605
   H    19.51371385976647      -2.52696250925405       8.37918169199656
   C    15.32854518758074      -7.19454122482170      10.20111334310282
   C    14.02942147438819      -7.72778883305121      10.20454283074856
   C    13.76109396567230      -8.91523971423244      10.88308120434756
   C    14.80670439731294      -9.56076757243658      11.55568030974505
   C    16.07556288295342      -8.98591771168218      11.52207496890419
   N    16.34575318613660      -7.83903207671942      10.87147599659908
   H    12.75391203065685      -9.33154119646835      10.88774463433549
   H    13.23462796932819      -7.20601507281443       9.67404731348612
   H    14.64903312401352     -10.49105662625177      12.09875600140057
   H    16.91207810581320      -9.45741497081316      12.03539880315158
   C    20.06480195907533      -9.15013062322530      11.22462514160495
   C    20.89842086371619     -10.01101619675538      11.94740133071391
   C    21.06358852020672      -9.81343162807618      13.32627424564146
   C    20.38789986253028      -8.75386143560018      13.94966987385436
   C    19.56400519213075      -7.91965955342658      13.18537444518157
   H    21.42919569825761     -10.83483979972161      11.47577358658882
   H    20.52646354322833      -8.61090368200304      15.01896620082883
   C    18.61442980682938      -8.22705928486987       7.99100389940749
   C    19.11222039983770      -9.17207797749464       7.09722783154543
   C    19.98087122173206     -10.16932656264516       7.55826309609536
   C    20.30448655081571     -10.16642535299383       8.91778945431797
   C    19.77108635908170      -9.19903911674503       9.77547441382224
   N    18.92464674605864      -8.22542862225199       9.30201794601061
   H    17.94119686254101      -7.43887724944055       7.65959174208996
   H    18.83448371997500      -9.14323258414981       6.04555563378706
   H    20.97811991586579     -10.93448224236380       9.29140688943626
   C    18.77990831134429      -6.75874401393411      13.66152992371266
   C    18.76232050559593      -6.34311661809946      14.99651189774003
   C    18.00383935800485      -5.23659212117245      15.38822593439302
   C    17.26827812428663      -4.57244647937996      14.39863893014982
   C    17.31858411268858      -5.02718501353256      13.08313224493160
   N    18.05264636627265      -6.09165304241396      12.70472084966012
   H    19.33733623606399      -6.87100906300692      15.75410336652445
   H    16.66450993426509      -3.70722522286655      14.66516430621979
   H    16.75655944341863      -4.53073037581852      12.29446051617850
   Ru   18.23238882695804      -6.87950676974617      10.76235646592556
   N    19.42757209944271      -8.14109739025428      11.85919248263245
   C    21.97768020175956     -10.74734694404389      14.14629992298179
   O    22.53836762315817     -11.66761177898493      13.50822365091329
   O    22.06888539707559     -10.49267372912002      15.36904887261028
   N    14.69524660357739      -3.06802635309634       7.40362280754803
   C    14.81573273761921      -2.85192862366508       6.03187516744384
```

```
   C    15.72598922284896      -3.40812410924861       5.12055725148150
   C    13.81060283503505      -1.93457589615496       5.61117228446359
   C    15.62417877791554      -3.02627050734708       3.77995072727988
   C    13.73072824453135      -1.56490417189823       4.25801720904264
   C    14.63973926113659      -2.11113363862748       3.34853793140030
   H    16.48756349555288      -4.11592702977836       5.44518617293875
   H    16.32142080350159      -3.44611475411683       3.05391787479871
   H    12.96697466318944      -0.86254405248031       3.92096390366749
   C    13.62645399432876      -2.30906718212118       7.87729791577283
   C    13.04612135348382      -1.58834997232116       6.79444991009843
   C    13.13072107633961      -2.19038134158818       9.18444034036697
   C    11.94598175508020      -0.74685259397127       7.03102376809296
   C    12.03646490615788      -1.34652200520257       9.39370512954322
   C    11.44468998200106      -0.63166586131998       8.32990081523901
   H    13.58190182339309      -2.73868180320318      10.01032330260569
   H    11.48964886743965      -0.18932693867482       6.21185229582671
   H    11.63293261401852      -1.24051176008283      10.40144487684853
   C    20.55997192936584     -11.23493460188617       6.60604826400331
   O    20.18581902493901     -11.16426467001487       5.41359512859107
   O    21.34502547622490     -12.06331605623386       7.12123004679935
   C    17.98339421234980      -4.77008506226010      16.85743611835273
   O    17.27915121285458      -3.76487776568324      17.10368757293710
   O    18.67440848166798      -5.44366886983938      17.65552492007410
   H    14.58870709441339      -1.83206247296909       2.29573147464230
   H    10.59023062911067       0.01667442421982       8.52653765070303
*
```

DFT optimized coordinates of **2c**[2+]

```
* xyz 2 2
   C    17.68835359790308      -4.54502605567130       9.06612681887159
   C    16.88594527517546      -3.67900434470788       8.32091103194076
   C    15.50537471116022      -3.96010774488944       8.17744519209971
   C    14.91923383716210      -5.09592195970067       8.78529589872732
   C    15.71602149784483      -5.94946374684711       9.55218415442903
   C    17.09557795035287      -5.67150645071810       9.68031956087108
   H    17.28698253113246      -2.77442442477014       7.86754871049196
   H    13.86188131863977      -5.29366438974968       8.61850268327738
   C    20.96918543001374      -5.43370784500421      10.39198929260219
   C    21.84165401297304      -4.44386054788033       9.93324317424809
   C    21.32774549796821      -3.41582951679358       9.14051416461219
   C    19.96350047997272      -3.41251659121931       8.83440501350381
   C    19.13985423740402      -4.43070332775658       9.32309399001118
   N    19.66071327453101      -5.43513810352638      10.10178136322862
   H    21.97587551026540      -2.62583860729944       8.76312210554480
   H    21.33357128106082      -6.25099255699271      11.01167404120200
   H    22.89607740355627      -4.48975484455037      10.19868133377789
   H    19.54089943429955      -2.62115370850845       8.21844509973837
   C    15.29818784557236      -7.16980781749523      10.27246826485665
   C    13.99259748573010      -7.66830822425484      10.31767587770650
   C    13.71874853756262      -8.83198369497288      11.04162761640715
   C    14.76293883083112      -9.47588631209812      11.70893098248686
   C    16.04621163400908      -8.93026378627526      11.62872414088687
   N    16.31458997306325      -7.81424342324826      10.93571674478150
   H    12.70418789550403      -9.22665678086676      11.08177919808945
   H    13.19539808132878      -7.14856637508340       9.78991392087988
   H    14.59928552005093     -10.38457496990729      12.28505506571097
   H    16.88420574726026      -9.40299176682013      12.13774640514008
   C    20.03881168855694      -9.18374640597690      11.24916072429494
   C    20.88355858671766     -10.03235830289230      11.97253664496355
   C    21.09604247755867      -9.78485592323264      13.33571861121787
   C    20.45641677961349      -8.69555519238026      13.94295982143895
   C    19.62072552937763      -7.87978896398493      13.17254222375025
   H    21.38517186225469     -10.88117424059899      11.51414323238717
   H    20.63012390063490      -8.51579037205070      15.00122692557253
   C    18.48669647052576      -8.34488641280101       8.04121114581615
   C    18.93118313993469      -9.33229198540307       7.16515719201489
```

```
C    19.79353754442671      -10.33073159829386       7.62957993131586
C    20.17270824344352      -10.28986780332432       8.97481228981650
C    19.69502928489998       -9.28250104274754       9.81448263478205
N    18.85341450716297       -8.31204339894235       9.33660038933660
H    17.81780713549386       -7.55681289379527       7.70345625263356
H    18.61227710686068       -9.33313807444285       6.12522626036164
H    20.84323874482958      -11.06002644403781       9.34918894704583
C    18.86566264158915       -6.69430966036563      13.63168928075968
C    18.88939705239171       -6.22835573297010      14.94687286405463
C    18.14879209058148       -5.10017165858822      15.31306314498440
C    17.38918200051132       -4.46998285705799      14.32213595045481
C    17.39699553909808       -4.97454541401190      13.02380506067378
N    18.11754712271266       -6.05782672433491      12.67545431069206
H    19.48144732804214       -6.73059126342491      15.70854192874574
H    16.79824082815118       -3.59092268928104      14.57001569456431
H    16.81407553952344       -4.50223241554306      12.23655973034545
Ru   18.20837161382883       -6.86713755061929      10.72992265131947
N    19.44138557377228       -8.14692199421012      11.86561507598397
C    22.02666244598782      -10.70394559856521      14.16182655291703
O    22.55119722733779      -11.64980554524651      13.53446440277493
O    22.15543024089073      -10.40269535352505      15.36847108865727
N    14.69892095486806       -3.09051763793488       7.41478376863525
C    14.99593666942648       -2.60810896573880       6.12870147081460
C    16.08799451205535       -2.88893629629630       5.29550467049710
C    13.93718807706849       -1.76520391879050       5.69651225372348
C    16.11949324949205       -2.28840586053302       4.03261440533040
C    13.98869904514300       -1.17447210727139       4.42479478050365
C    15.08568028563452       -1.43449299867955       3.59939817515307
H    16.88802698860555       -3.55898727817858       5.60360663225860
H    16.96205384178091       -2.49195982091538       3.37127141903855
H    13.18074555004900       -0.52645592848997       4.08363240984907
C    13.45855999760510       -2.56030088885370       7.80934397099527
C    12.95873274494368       -1.73269512042346       6.76832238907519
C    12.76653596941112       -2.70269906344040       9.02031687674883
C    11.73575592815437       -1.06478331018556       6.93233945390944
C    11.54966589966367       -2.02797629237824       9.16220381807433
C    11.03138911161525       -1.22247908719613       8.12858458914240
H    13.15641938470391       -3.30665094558391       9.83715916473065
H    11.34369335095968       -0.42748140697778       6.13911850241382
H    10.99553051604256       -2.12806941932059      10.09585659308328
C    20.30967297821977      -11.44690144250073       6.69446620707223
O    19.88555516195912      -11.40694209261476       5.51926493934351
O    21.09444622675124      -12.27057079364788       7.21391373642384
C    18.17542318016500       -4.57438436862969      16.76538213057449
O    17.48149344248754       -3.55848076082572      16.98709178750314
O    18.88981135350046       -5.22174874119591      17.56211260116694
H    15.13963375032674       -0.98111832047838       2.60969474095739
H    10.07850490232886       -0.71209547566212       8.26866897318159
*
```

6 ACKNOWLEDGEMENTS

LIST OF PUBLICATIONS

A. K. C. Mengel, B. He, O. S. Wenger, A Triarylamine–Triarylborane Dyad with a Photochromic Dithienylethene Bridge, *J. Org. Chem.* **2012**, *77*, 6545–6552.

A. K. C. Mengel, C. Förster, A. Breivogel, K. Mack, J. R. Ochsmann, F. Laquai, V. Ksenofontov, K. Heinze, A Heteroleptic Push–Pull Substituted Iron(II) Bis(tridentate) Complex with Low-Energy Charge-Transfer States, *Chem. Eur J.* **2015**, *21*, 704–714.

A. K. C. Mengel, W. Cho, A. Breivogel, K. Char, Y. S. Kang, K. Heinze, A Bis(tridentate)cobalt Polypyridine Complex as Mediator in Dye-Sensitized Solar Cells, *Eur. J. Inorg. Chem.* **2015**, 3299−3306.

A. K. C. Mengel, C. Bissinger, M. Dorn, O. Back, C. Förster, K. Heinze, Boosting Vis/NIR Charge Transfer Absorptions of Iron(II) Complexes by *N*-Alkylation and *N*-Deprotonation in the Ligand Backbone, *Chem. Eur. J.* **2017**, in press, DOI: 10.1002/chem.201700959.

C. Kreitner, A. K. C. Mengel, T. K. Lee, W. Cho, K. Char, Y. S. Kang, K. Heinze, Strongly Coupled Cyclometalated Ruthenium Triarylamine Chromophores as Sensitizers for DSSCs. *Chem. Eur. J.* **2016**, *22*, 8915−8928.

[1] G. Smestad, C. Bignozzi, R. Argazzi, *Solar Energy Materials and Solar Cells* **1994**, *32*, 259−272.

[2] M. A. Green, K. Emery, Y. Hishikawa, W. Warta, E. D. Dunlop, *Prog. Photovolt: Res. Appl.* **2015**, *23*, 1–9.

[3] https://commons.wikimedia.org/wiki/File:Best_Research-Cell_Efficiencies.png (status: 2017/04/10). License: "This file has been identified as being free of known restrictions under copyright law, including all related and neighboring rights."

[4] B. O'Regan, M. Grätzel, *Nature* **1991**, *353*, 737−740.

[5] R. D. Costa, E. Ortí, H. J. Bolink, F. Monti, G. Accorsi, N. Armaroli, *Angew. Chem.* **2012**, *124*, 8300−8334; *Angew. Chem. Int. Ed.* **2012**, *51*, 8178−8211.

[6] T. Bleith, H. Wadepohl, L. H. Gade, *J. Am. Chem. Soc.* **2015**, *137*, 2456−2459.

[7] T. G. Gopakumar, M. Bernien, H. Naggert, F. Matino, C. F. Hermanns, A. Bannwarth, S. Mühlenberend, A. Krüger, D. Krüger, F. Nickel, W. Walter, R. Berndt, W. Kuch, F. Tuczek, *Chem. Eur. J.* **2013**, *19*, 15702–15709.

[8] M. K. Nazeeruddin, A. Key, L. Rodicio, R. Humphrey-Baker, E. Müller, P. Liska, N. Vlachopoulos, M. Grätzel, *J. Am. Chem. Soc.* **1993**, *115*, 6382–6390.

[9] S. Ferrere, B. A. Gregg, *J. Am. Chem. Soc.* **1998,** *120,* 843−844.

[10] S. Ferrere, *Chem. Mater.* **2000**, *12*, 1083−1089.

[11] A. Sepehrifard, S. Chen, A. Stublla, P. G. Potvin, S. Morin, *Electrochimica Acta* **2013**, *87*, 236– 244.

[12] T. Duchanois, T. Etienne, C. Cebrián, L. Liu, A. Monari, M. Beley, X. Assfeld, S. Haacke, P. C. Gros, *Eur. J. Inorg. Chem.* **2015**, 2469–2477.

[13] S. Campagna, F. Puntoriero, F. Nastasi, G. Bergamini, V. Balzani, *Top. Curr. Chem.* **2007**, *280*, 117–214.

[14] A. Inagaki, M. Akita, *Coord. Chem. Rev.* **2010**, *254*, 1220–1239.

[15] C. K. Prier, D. A. Rankic, D. W. C. MacMillan, *Chem. Rev.* **2013**, *113*, 5322–5363.

[16] A. Juris, V. Balzani, F. Barigelletti, S. Campagna, P. Belser, A. von Zelewsky, *Coord. Chem. Rev.* **1988**, *84*, 85–277.

[17] J.-P. Sauvage, J.-P. Collin, J.-C. Chambron, S. Guillerez, C. Coudret, V. Balzani, F. Barigelletti, L. D. Cola, L. Flamigni, *Chem. Rev.* **1994**, *94*, 993–1019.

[18] Y. Liu, R. Hammitt, D. A. Lutterman, R. P. Thummel, C. Turro, *Inorg. Chem.* **2007**, *46*, 6011–6021.

[19] L. Hammarström, O. Johansson, *Coord. Chem. Rev.* **2010**, *254*, 2546–2559.

[20] D. N. Bowman, A. Bondarev, S. Mukherjee, E. Jakubikova, *Inorg. Chem.* **2015**, *54*, 8786−8793.

[21] C. Bressler, C. Milne, V.-T. Pham, A. ElNahhas, R. M. van der Veen, W. Gawelda, S. Johnson, P. Beaud, D. Grolimund, M. Kaiser, C. N. Borca, G. Ingold, R. Abela, M. Chergui, *Science* **2009**, *323*, 489−492.

[22] W. Gawelda, A. Cannizzo, V.-T. Pham, F. van Mourik, C. Bressler, M. Chergui, *J. Am. Chem. Soc.* **2007**, *129*, 8199−8206.

[23] R.-A. Fallahpour, *Synthesis* **2000**, *8*, 1138−1142.

[24] R.-A. Fallahpour, *Eur. J. Inorg. Chem.* **1998**, 1205−1207.

[25] R.-A. Fallahpour, M. Neuburger, M. Zehnder, *New J. Chem.* **1999**, *23*, 53−61.

[26] J. A. Moss, J. C. Yang, J. M. Stipkala, X. Wen, C. A. Bignozzi, G. J. Meyer, T. J. Meyer, *Inorg. Chem.* **2004**, *43*, 1784–1792.

[27] C. N. Langford, H. B. Gray, W. A. Benjamin (Eds.): *Ligand Substitution Processes*, New York, **1966**.

[28] J. Burgess, M. V. Twigg, *J. Chem. Soc.*, *Dalton Trans.* **1974**, 2032–2036.

[29] D. J. Farrington, J. G. Jones, M. V. Twigg, *Dalton Trans.* **1979**, 221–227.

[30] E. C. Constable, *Polyhedron* **1983**, *2*, 551–572.

[31] J. Maigut, R. Meier, A. Zahl, R. van Eldik, *Inorg. Chem.* **2007**, *46*, 5361–5371.

[32] N. Serpone, G. Ponterini, M. A. Jamieson, F. Bolleta, M. Maestri, *Coord. Chem. Rev.* **1983**, *50*, 209–302.

[33] L. Seiden, F. Basolo, H. M. Neumann, *J. Am. Chem. Soc.* **1959**, *91*, 3809–3813.

[34] Harry H. Binder: *Lexikon der chemischen Elemente*, S. Hirzel Verlag, Stuttgart **1999**, ISBN 3-7776-0736-3 David R. Lide (Hrsg.): *CRC Handbook of Chemistry and Physics.* 90.

Auflage. CRC, Boca Raton **2009**, ISBN 978-1-4200-9084-0 (Section 14, Geophysics, Astronomy, and Acoustics; Abundance of Elements in the Earth's Crust and in the Sea).

[35] Y. Liu, T. Harlang, S. E. Canton, P. Chábera, K. Suárez-Alcántara, A. Fleckhaus, D. A. Vithanage, E. Göransson, Al. Corani, R. Lomoth, V. Sundström, K. Wärnmark, *Chem. Commun.* **2013**, *49*, 6412–6414.

[36] L. A. Fredin, M. Pápai, E. Rozsályi, G. Vankó, K. Wärnmark, V. Sundström, P. Persson, *J. Phys. Chem. Lett.* **2014**, *5*, 2066–2071.

[37] T. C. B. Harlang, Y. Liu, O. Gordivska, L. A. Fredin, C. S. Ponseca Jr, P. Huang, P. Chábera, K. S. Kjaer, H. Mateos, J. Uhlig, R. Lomoth, R. Wallenberg, S. Styring, P. Persson, V. Sundström, K. Wärnmark, *Nature Chemistry* **2015**, 7, 883–889.

[38] T. Duchanois, T. Etienne, C. Cebrián, L. Liu, A. Monari, M. Beley, X. Assfeld, S. Haacke, P. C. Gros, *Eur. J. Inorg. Chem.* **2015**, 2469–2477.

[39] L. Liu, T. Duchanois, T. Etienne, A. Monari, M. Beley, X. Assfeld, S. Haacke, P. C. Gros, *Phys. Chem. Chem. Phys.* **2016**, *18*, 12550−12556.

[40] L. Cambi, L. Szegö, *Ber. Dtsch. Chem. Ges.* **1931**, *64*, 2591–2598.

[41] W. A. J. Baker, H. M. Bobonich, *Inorg. Chem.* **1964**, *3*, 1184–1188.

[42] E. König, G. Ritter, S. Kulshreshtha, *Chem. Rev.* **1985**, *85*, 219–234.

[43] H. Toftlund, *Coord. Chem. Rev.* **1989**, *94*, 67−108.

[44] H. A. Goodwin, *Coord. Chem. Rev.* **1976**, *18*, 293–325.

[45] J. A. Real, A. B. Gaspar, M. C. Muñoz, *Dalton Trans.* **2005**, 2062 – 2079.

[46] P. Gütlich, Y. Garcia, H. A. Goodwin, *Chem. Soc. Rev.* **2000**, *29*, 419–427.

[47] G. A. Renovitch, W. A. Baker, *J. Am. Chem. Soc.* **1967**, *89*, 6377−6378.

[48] J. J. McGravey, I. Lawthers, *J. Chem. Soc. Chem. Commun.* **1982**, 906−907.

[49] S. Decurtins, P. Gütlich, C. P. Köhler, H. Spiering, A. Hauser, *Chem. Phys. Lett.* **1984**, *105*, 1–4.

[50] S. Decurtins, P. Gütlich, K. M. Hasselbach, A. Hauser, H. Spiering, *Inorg. Chem.* **1985**, *24*, 2174–2178.

[51] J.-F. Létard, P. Guionneau, O. Nguyen, J. S. Costa, S. Marcén, G. Chastanet, M. Marchivie, L. Goux-Capes, *Chem. Eur. J.* **2005**, *11*, 4582–4589.

[52] A. Hauser, *Coord. Chem. Rev.* **1991**, *111*, 275–290.

[53] A. Hauser, *Comments Inorg. Chem.* **1995**, *17*, 17–40.

[54] W. Zhang, R. Alonso-Mori, U. Bergmann, C. Bressler, M. Chollet, A. Galler, W. Gawelda, R. G. Hadt, R. W. Hartsock, T. Kroll, K. S. Kjær, K. Kubiček, H. T. Lemke, H. W. Liang, D. A. Meyer, M. M. Nielsen, C. Purser, J. S. Robinson, E. I. Solomon, Z. Sun, D. Sokaras, T. B. van Driel, G. Vankó, T.-C. Weng, D. Zhu, K. J. Gaffney, *Nature* **2014**, *509*, 345–348.

[55] G. Vankó, A. Bordage, M. Pápai, K. Haldrup, P. Glatzel, A. M. March, G. Doumy, A. Britz, A. Galler, T. Assefa, D. Cabaret, A. Juhin, T. B. van Driel, K. S. Kjær, A. Dohn, K. B. Møller, H. T. Lemke, E. Gallo, M. Rovezzi, Z. Németh, E. Rozsályi, T. Rozgonyi, J. Uhlig, V. Sundström, M. M. Nielsen, L. Young, S. H. Southworth, C. Bressler, W. Gawelda, *J. Phys. Chem. C* **2015**, *119*, 5888–5902.

[56] L. L. Jamula, A. M. Brown, D. Guo, J. K. McCusker, *Inorg. Chem.* **2014**, *53*, 15−17.

[57] C. R. Goldsmith, T. D. P. Stack, *Inorg. Chem.* **2006**, *45*, 6048−6055.

[58] P. G. Bomben, K. C. D. Robson, B. D. Koivisto, C. P. Berlinguette, *Coord. Chem. Rev.* **2012**, *256*, 1438−1450.

[59] T. Bessho, E. Yoneda, J.-H. Yum, M. Guglielmi, I. Tavernelli, H. Imai, U. Rothlisberger, M. K. Nazeeruddin, M. Grätzel, *J. Am. Chem. Soc.* **2009**, *131*, 5930−5934.

[60] D. G. Brown, N. Sanguantrakun, B. Schulze, U. S. Schubert, C. P. Berlinguette, *J. Am. Chem. Soc.* **2012**, *134*, 12354−12357.

[61] W. Zhang, K. S. Kjær, R. Alonso-Mori, U. Bergmann, M. Chollet, L. A. Fredin, R. G. Hadt, R. W. Hartsock, T. Harlang, T. Kroll, K. Kubiček, H. T. Lemke, H. W. Liang, Y. Liu, M. M. Nielsen, P. Persson, J. S. Robinson, E. I. Solomon, Z. Sun, D. Sokaras, T. B. van Driel, T.-C. Weng, D. Zhu, K. Wärnmark, V. Sundström, K J. Gaffney, *Chem. Sci.* **2017**, *8*, 515–523.

[62] M. Grätzel, *J. Photochem. Photobiol. C*, **2003**, *4*, 145–153.

[63] J.-F. Yin, M. Velayudhama, D. Bhattacharyaa, H.-C. Lin, K.-L. Lu, *Coord. Chem. Rev.* **2012**, *256*, 3008–3035.

[64] O. K. Varghese, C. A. Grimes, *Sol. Energy Mater. Sol. Cells* **2008**, *92*, 374–384.

[65] L. Zhang, J. M. Cole, *Appl. Mater. Interfaces* **2015**, *7*, 3427−3455.

[66] B. E. Hardin, H. J. Snaith, M. D. McGehee, *Nature Photonics* **2012**, *6*, 162–169.

[67] J. B. Asbury, R. J. Ellingson, H. N. Ghosh, S. Ferrere, A. J. Nozik, T. Q. Lian, *J. Phys. Chem. B* **1999**, *103*, 3110–3119.

[68] G. Ramakrishna, D. A. Jose, D. K. Kumar, A. Das, D. K. Palit, H. N. Ghosh, *J. Phys. Chem. B* **2005**, *109*, 15445–15453.

[69] G. Benkö, J. Kallioinen, J. E. I. Korppi-Tommola, A. P. Yartsev, V. Sundström, *J. Am. Chem. Soc.* **2002**, *124*, 489–493.

[70] Z.-S. Wang, N. Koumura, Y. Cui, M. Takahashi, H. Sekiguchi, A. Mori, T. Kubo, A. Furube, K. Hara, *Chem. Mater.* **2008**, *20*, 3993−4003.

[71] W. Zeng, Y. Cao, Y. Bai, Y. Wang, Y. Shi, M. Zhang, F. Wang, C. Pan, P. Wang, *Chem. Mater.* **2010**, *22*, 1915–1925.

[72] A. Yella, H.-W. Lee, H. N. Tsao, C. Yi, A. K. Chandiran, M. K. Nazeeruddin, E. W.-G. Diau, C.-Y. Yeh, S. M. Zakeeruddin, M. Grätzel, *Science* **2011**, *334*, 629–634.

[73] S. Mathew, A. Yella, P. Gao, R. Humphry-Baker, B. F. E. Curchod, N. Ashari-Astani, I. Tavernelli, U. Rothlisberger, M. K. Nazeeruddin, M. Grätzel, *Nat. Chem.* **2014**, *6*, 242–247.

[74] A. Mishra, M. K. Fischer, P. Bauerle, *Angew. Chem.* **2009**, *48*, 2474–2499.

[75] E. I. Mayo, K. Kilsa, T. Tirrell, P.I. Djurovich, A. Tamayo, M.E. Thompson, N.S. Lewis, H. B. Gray, *Photochem. Photobiol. Sci.* **2006**, *5*, 871–873.

[76] Z. Ning, H. Tian, *Chem. Commun.* **2009**, *37*, 5483–5495.

[77] T. Bessho, E. C. Constable, M. Grätzel, A. Hernandez Redondo, C. E. Housecroft, W. Kylberg, M. K. Nazeeruddin, M. Neuburger, S. Schaffner, *Chem. Commun.* **2008**, 3717–3719.

[78] H. Kisserwan, T. H. Ghaddar, *Inorg. Chim. Acta* **2010**, *363*, 2409–2415.

[79] M. K. Nazeeruddin, F. De Angelis, S. Fantacci, A. Selloni, G. Viscardi, P. Liska, S. Ito, B. Takeru, M. Grätzel, *J. Am. Chem. Soc.* **2005**, *127*, 16835–16847.

[80] M. K. Nazeeruddin, S. M. Zakeeruddin, R. Humphry-Baker, M. Jirousek, P. Liska, N. Vlachopoulos, V. Shklover, C.-H. Fischer, M. Grätzel, *Inorg. Chem.* **1999**, *38*, 6298–6305.

[81] Y. Cao, Y. Bai, Q. Yu, Y. Cheng, S. Liu, D. Shi, F. Gao, P. Wang, *J. Phys. Chem. C* **2009**, *113*, 6290–6297.

[82] X. Li, K. Hou, X. Duan, F. Li, C. Huang, *Inorg. Chem. Commun.* **2006**, *9*, 394–396.

[83] M. K. Nazeeruddin, P. Péchy, T. Renouard, S. M. Zakeeruddin, R. Humphry-Baker, P. Comte, P. Liska, Le Cevey, E. Costa, V. Shklover, L. Spiccia, G. B. Deacon, C. A. Bignozzi, M. Grätzel, *J. Am. Chem. Soc.* **2001**, *123*, 1613–1624.

[84] T. P. Brewster, W. Ding, N. D. Schley, N. Hazari, V. S. Batista, R. H. Crabtree, *Inorg. Chem.* **2011**, *50*, 11938–11946.

[85] S. Betanzos-Lara, L. Salassa, A. Habtemariam, O. Novakova, A. M. Pizarro, G. J. Clarkson, B. Liskova, V. Brabec, P. J. Sadler, *Organometallics* **2012**, *31*, 3466–3479.

[86] S. Kämper, A. Paretzki, J. Fiedler, S. Záliš, W. Kaim, *Inorg. Chem.* **2012**, *51*, 2097–2104.

[87] G. Xue, Y. Guo, T. Yu, J. Guan, X. Yu, J. Zhang, J. Liu, Z. Zou, *Int. J. Electrochem. Sci.* **2012**, *7*, 1496–1511.

[88] A. Bahreman, B. Limburg, M. A. Siegler, E. Bouwman, S. Bonnet, *Inorg. Chem.* **2013**, *52*, 9456–9469.

[89] P. T. Nguyen, B. X. T. Lam, A. R. Andersen, P. E. Hansen, T. Lund, *Eur. J. Inorg. Chem.* **2011**, 2533–2539.

[90] C. Dragonetti, A. Valore, A. Colombo, D. Roberto, V. Trifiletti, N. Manfredi, M. M. Salamone, R. Ruffo, A. Abbotto, *J. Organomet. Chem.* **2012**, *714*, 88–93.

[91] M. M. R. Choudhuri, R. J. Crutchley, *Inorg. Chem.* **2013**, *52*, 14404–14410.

[92] A. Breivogel, S. Wooh, J. Dietrich, T. Y. Kim, Y. S. Kang, K. Char, K. Heinze, *Eur. J. Inorg. Chem.* **2014**, *2014*, 2720–2734.

[93] A. Breivogel, C. Förster, K. Heinze, *Inorg. Chem.* **2010**, *49*, 7052–7056.

[94] A. J. Frank, N. Kopidakis, J. van de Lagemaat, *Coord. Chem. Rev.* **2004**, *248*, 1165–1179.

[95] S. Caramori, J. Husson, M. Beley, C. A. Bignozzi, R. Argazzi, P. C. Gros, *Chem. Eur. J.* **2010**, *16*, 2611–2618.

[96] A. K. C. Mengel, W. Cho, A. Breivogel, K. Char, Y. S. Kang, K. Heinze, *Eur. J. Inorg. Chem.* **2015**, 3299−3306.

[97] P. Salvatori, G. Marotta, A. Cinti, C. Anselmi, E. Mosconi, F. D. Angelis, *J. Phys. Chem. C* **2013**, *117*, 3874−3887.

[98] D. Song, H. An, J. H. Lee, J. Lee, H. Choi, I. S. Park, J.-M. Kim, Y. S. Kang, *ACS Appl. Mater. Interfaces*, **2014**, *6*, 12422–12428.

[99] K. C. D. Robson, B. D. Koivisto, A. Yella, B. Sporinova, M. K. Nazeeruddin, T. Baumgartner, M. Grätzel, C. P. Berlinguette, *Inorg. Chem.* **2011**, *50*, 5494–5508.

[100] R. K. Chitumalla, K. S. V. Gupta, C. Malapaka, R. Fallahpour, A. Islam, L. Han, B. Kotamarthi, S. P. Singh, *Phys.Chem.Chem.Phys.* **2014**, *16*, 2630−2640.

[101] B.-B. Cui, Y.-W. Zhong, J. Yao, *J. Am. Chem. Soc.* **2015**, *137*, 4058−4061.

[102] C. Kreitner, A. K. C. Mengel, T. K. Lee, W. Cho, K. Char, Y. S. Kang, K. Heinze, *Chem. Eur. J.* **2016**, *22*, 8915–8928.

[103] J. E. Monat, J. K. McCusker, *J. Am. Chem. Soc.* **2000**, *122*, 4092–4097.

[104] E. Jakubikova, D. N. Bowman, *Acc. Chem. Res.* **2015**, *48*, 1441–1449.

[105] L. A. Fredin, K. Wärnmark, V. Sundström, P. Persson, *ChemSusChem.* **2016**, *9*, 667–675.

[106] K. R. Siefermann, C. D. Pemmaraju, S. Neppl, A. Shavorskiy, A. A. Cordones, J. Vura-Weis, D. S. Slaughter, F. P. Sturm, F. Weise, H. Bluhm, M. L. Strader, H. Cho, M.-F. Lin, C. Bacellar, C. Khurmi, J. Guo, G. Coslovich, J. S. Robinson, R. A. Kaindl, R. W. Schoenlein, A. Belkacem, D. M. Neumark, S. R. Leone, D. Nordlund, H. Ogasawara, O. Krupin, J. J. Turner, W. F. Schlotter, M. R. Holmes, M. Messerschmidt, M. P. Minitti, S. Gul, J. Z. Zhang, N. Huse, D. Prendergast, O. Gessner, *J. Phys. Chem. Lett.* **2014**, *5*, 2753–2759.

[107] M. Yang, D. W. Thompson, G. J. Meyer, *Inorg. Chem.* **2000**, *39*, 3738–3739.

[108] M. Yang, D. W. Thompson, G. J. Meyer, *Inorg. Chem.* **2002**, *41*, 1254–1262.

[109] T. C. B. Harlang, Y. Liu, O. Gordivska, L. A. Fredin, C. S. Ponseca Jr, P. Huang, P. Chábera, K. S. Kjaer, H. Mateos, J. Uhlig, R. Lomoth, R. Wallenberg, S. Styring, P. Persson, V. Sundström, K. Wärnmark, *Nat. Chem.* **2015**, 7, 883–889.

[110] D. N. Bowman, J. H. Blew, T. Tsuchiya, E. Jakubikova, *Inorg. Chem.* **2013**, *52*, 8621−8628.

[111] E. Jakubikova, D. N. Bowman, *Acc. Chem. Res.* **2015**, *48*, 1441−1449.

[112] G. Boschloo, A. Hagfeldt, *Acc. Chem. Res.* **2009**, *42*, 1819−1826.

[113] T. W. Hamann, J. W. Ondersma, *Energy Environ. Sci.* **2011**, *4*, 370−381.

[114] T. W. Hamann, *Dalton Trans.* **2012**, *41*, 3111–3115.

[115] E. Mosconi, J.-H. Yum, F. Kessler, C. J. G. García, C. Zuccaccia, A. Cinti, M. K. Nazeeruddin, M. Grätzel, F. D. Angelis, *J. Am. Chem. Soc.* **2012**, *134*, 19438–19453.

[116] J.-H. Yum, E. Baranoff, F. Kessler, T. Moehl, S. Ahmad, T. Bessho, A. Marchioro, E. Ghadiri, J.-E. Moser, C. Yi, M. K. Nazeeruddin, M. Grätzel, *Nat. Commun.* **2012**, *3*, 631–639.

[117] M. D. Newton, *Coord. Chem. Rev*. **2003**, *238*, 167−185.

[118] S. A. Sapp, C. M. Elliott, C. Contado, S. Caramori, C. A. Bignozzi, *J. Am. Chem. Soc*. **2002**, *124*, 11215–11222.

[119] H. Nusbaumer, J.-E. Moser, S. M. Zakeeruddin, M. K. Nazeeruddin, M. Grätzel, *J. Phys. Chem. B* **2001**, *105*, 10461–10464.

[120] Y. Liu, J. R. Jennings, Y. Huang, Q. Wang, S. M. Zakeeruddin, M. Grätzel, *J. Phys. Chem. C* **2011**, *115*, 18847−18855.

[121] D.K. Lee, K.-S. Ahn, S. Thogiti, J. H. Kim, *Dyes and Pigments* **2015**, *117*, 83−91.

[122] Z.-S. Wang, K. Sayama, H. Sugihara, *J. Phys. Chem. B* **2005,** *109,* 22449-22455.

[123] G. Oskam, B. V. Bergeron, G. J. Meyer, P. C. Searson, *J. Phys. Chem. B* **2001**, *105*, 6867–6873.

[124] P. Wang, S. M. Zakeeruddin, J.-E. Moser, R. Humphry-Baker, M. Grätzel, *J. Am. Chem. Soc*. **2004**, *126*, 7164–7165.

[125] S. Hattori, Y. Wada, S. Yanagida, S. Fukuzumi, *J. Am. Chem. Soc.* **2005**, *127*, 9648–9654.

[126] Z. Zhang, P. Chen, T. N. Murakami, S. M. Zakeeruddin, M. Grätzel, *Adv. Funct. Mater.* **2008**, *18*, 341–346.

[127] B. A. Gregg, F. Pichot, S. Ferrere, C. L. Fields, *J. Phys. Chem. B* **2001**, *105*, 1422–1429.

[128] B. Bozic-Weber, E. C. Constable, C. E. Housecroft, *Coord. Chem. Rev.* **2013**, *257*, 3089–3106.

[129] U. Bach, D. Lupo, P. Comte, J. E. Moser, F. Weissortel, J. Salbeck, H. Spreitzer, M. Grätzel, *Nature* **1998**, *395*, 583–585.

[130] Q. Pei, G. Yu, C. Zhang, Y. Yang, A. J. Heeger, *Science* **1995**, *269*, 1086–1088.

[131] G. Yu, Y. Cao, M. Andersson, J. Gao, A. J. Heeger, *Adv. Mater.* **1998**, *10*, 385–388.

[132] Q. Pei, Y. Yang, G. Yu, C. Zhang, A. J. Heeger, *J. Am. Chem. Soc*. **1996**, *118*, 3922–3929.

[133] S. Reineke, F. Lindner, G. Schwartz, N. Seidler, K. Walzer, B. Lussem, K. Leo, *Nature* **2009**, *459*, 234−238.

[134] R. D. Costa, E. Ortí, H. J. Bolink, *Pure Appl. Chem.* **2011**, *83*, 2115–2128.

[135] I. D. Parker, *J. Appl. Phys.* **1994**, *75*, 1656−1666.

[136] L. Chen, L. Zhu, Z. Shuai, *J. Phys. Chem. A* **2006**, *110*, 13349−13354.

[137] A. Köhler, H. Bässler, *Mater. Sci. Eng.* *2009*, R *66*, 71–109.

[138] C. Adachi, M. A. Baldo, M. E. Thompson, S. R. Forrest, *J. App. Phys.* **2001**, *90*, 5048–5051.

[139] F. *Träger, Handbook of Lasers and Optics.* 2nd edition. Springer-Verlag Berlin Heidelberg **2012**.: p 556. ISBN 978-3-642-19408-5.

[140] J. Slinker, D. Bernards, P. L. Houston, H. D. Abruña, S. Bernhard, G. G. Malliaras, *Chem. Commun.* **2003**, *19*, 2392–2399.

[141] M. S. Lowry, S. Bernhard, *Chem. Eur. J.* **2006**, *12*, 7970 – 7977.

[142] P. Chábera, Y. Liu, O. Prakash, E. Thyrhaug, A. E. Nahhas, A. Honarfar, S. Essén, L. A. Fredin, T. C. B. Harlang, K. S. Kjær, K. Handrup, F. Ericson, H. Tatsuno, K. Morgan, J. Schnadt, L. Häggström, T. Ericsson, A. Sobkowiak, S. Lidin, P. Huang, S. Styring, J. Uhlig, J. Bendix, R. Lomoth, V. Sundström, P. Persson, K. Wärnmark, *Nature* **2017**, 543, 695−699.

[143] Y. F. Lee, J. R. Kirchoff, *J. Am. Chem. Soc.* **1994**, *116*, 3599–3600.

[144] A. S. Del Negro, C. J. Seliskar, W. R. Heineman, S. E. Hightower, S. A. Bryan, B. P. Sullivan, *J. Am. Chem. Soc.* **2006**, *128*, 16494–16495.

[145] R. Hogg, R. G. Wilkins, *J. Chem. Soc.* **1962**, 341–350.

[146] R. H. Holyer, C. D. Hubbard, S. F. A. Kettle, R. G. Wilkins, *Inorg. Chem.* **1966**, *5*, 622–625.

[147] K. Suzuki, A. Kobayashi, S. Kaneko, K. Takehira, T. Yoshihara, H. Ishida, Y. Shiina, S. Oishi, S. Tobita, *Phys. Chem. Chem. Phys.* **2009**, *11*, 9850−9860.

[148] J. D. Slinker, J. Rivnay, J. S. Moskowitz, J. B. Parker, S. Bernhard, H. D. Abruña, G. G. Malliaras, *J. Mater. Chem.* **2007**, *17*, 2976−2988.

[149] M. Maestri, N. Armaroli, V. Balzani, E. C. Constable, A. M. W. Cargill Thompson, *Inorg. Chem.* **1995**, *34*, 2759–2767.

[150] Y. Liu, R. Hammitt, D. A. Lutterman, R. P. Thummel, C. Turro, *Inorg. Chem.* **2007**, *46*, 6011–6021.

[151] M. Abrahamsson, M. Jäger, T. Österman, L. Eriksson, P. Persson, H.-C. Becker, O. Johansson, L. Hammarström, *J. Am. Chem. Soc.* **2006**, *128*, 12616−12617.

[152] M. Abrahamsson, H. Wolpher, O. Johansson, J. Larsson, M. Kritikos, L. Eriksson, P.O. Norrby, J. Bergquist, L. Sun, B. Åkermark, L. Hammarström, *Inorg. Chem.* **2005**, *44*, 3215−3225.

[153] M. Jäger, A. Smeigh, F. Lombeck, H. Görls, J.-P. Collin, J.-P. Sauvage, L Hammarström, O. Johansson, *Inorg. Chem.* **2010**, *49*, 374−376.

[154] F. Schramm, V. Meded, H. Fliegl, K. Fink, O. Fuhr, Z. Qu, W. Klopper, S. Finn, T. E. Keyes, M. Ruben, *Inorg. Chem.* **2009**, *48*, 5677–5684.

[155] M. Abrahamsson, M. Jäger, R. J. Kumar, T. Österman, P. Persson, H.-C. Becker, O. Johansson, L. Hammarström, *J. Am. Chem. Soc.* **2008**, *130*, 15533–15542.

[156] M. Jäger, R. J. Kumar, H. Görls J. Bergquist, O. Johansson, *Inorg. Chem.* **2009**, *48*, 3228−3238.

[157] H. J. Bolink, L. Cappelli, E. Coronado, P. Gaviña, *Inorg. Chem.* **2005**, *44*, 5966−5968.

[158] K. Heinze, K. Hempel, M. Beckmann, *Eur. J. Inorg. Chem.* **2006**, 2040–2050.

[159] K. Heinze, K. Hempel, S. Tschierlei, M. Schmitt, J. Popp, S. Rau, *Eur. J. Inorg. Chem.* **2009**, 3119–3126.

[160] A. Breivogel, M. Meister, C. Förster, F. Laquai, K. Heinze, *Chem. Eur. J.* **2013**, *19*, 13745–13760.

[161] A. K. C. Mengel, C. Förster, A. Breivogel, K. Mack, J. R. Ochsmann, F. Laquai, V. Ksenofontov, K. Heinze, *Chem. Eur. J.* **2015**, *21*, 704 – 714.

[162] I. M. Dixon, F. Alary, M. Boggio-Pasqua, J.-L. Heully, *Inorg. Chem.* **2013**, *52*, 13369−13374.

[163] I. M. Dixon, S. Khan, F. Alary, M. Boggio-Pasqua, J.-L. Heully, *Dalton Trans.* **2014**, *43*, 15898–15905.

[164] I. M. Dixon, G. Boissard, H. Whyte, F. Alary, J.-L. Heully, *Inorg. Chem.* **2016**, *55*, 5089–5091.

[165] I. M. Dixon, F. Alary, M. Boggio-Pasqua, J.-L. Heully, *Dalton Trans.* **2015**, *44*, 13498–13503.

[166] S. Otto, M. Grabolle, C. Förster, C. Kreitner, U. Resch-Genger, K. Heinze, *Angew. Chem.* **2015**, *127*, 11735-11739; *Angew. Chem. Int. Ed.* **2015**, *54*, 11572–11576.

[167] A.F. Nogueira, C. Longo, M.-A. De Paoli, *Coord. Chem. Rev.* **2004**, *248*, 1455–1468.

[168] J. van Houton, *J. Chem. Educ.* **2002**, *79*, 548–550.

[169] A. E. Bragg, D. M. Neumark, *Chem. Rev.* **2004,** *104,* 1719–1757.

CURRICULUM VITAE

Andreas K. C. Mengel

Date of birth: 01.08.1983
Place of birth: Witzenhausen, Germany
Nationality: German

Doctorate

01/2013 – 07/2017	**Doctorate** at the Johannes Gutenberg-University of Mainz
	Institute of Inorganic Chemistry and Analytical Chemistry, in the workgroup of █████████████████
	„Bis(tridentate) Polypyridyl Transition Metal Complexes for DSSC and LEC Applications"
01/2013 – 06/2016	**Scholarship** of the International Research Training Group (IRTG) 1404 *„Self-organized Materials for Optoelectronics"*
08/2014 – 12/2014 08/2015 – 12/2015	**Stays abroad** in the the workgroup of ██████████████████ in the Seoul National University and of ███████████████████ in the Hanyang University in Seoul, South Korea

Education

09/2004 – 08/2012	**Studies of chemistry** at the Georg-August-University of Göttingen
	Degree: Diploma
	„Electron-transfer of a photo switchable donor-bridge-acceptor system"
09/2001 – 07/2004	"Berufliches Gymnasium" (major economics) in Eschwege
09/1994 – 08/2001	Friedrich-Wilhelm-Gymnasium in Eschwege
	Completion: General university entrance qualification

Sprachen

German (first language)

English (fluent)

Korean (basics)

Latein (basics)

Conferences

06/2015	IRTG meeting Berlin (poster)
03/2015	„Koordinationschemikertagung" Paderborn (poster)
01/2015	IRTG meeting Gonjiam, South Korea (poster)
06/2014	IRTG meeting Mainz (poster)
02/2014	IRTG meeting Daejeon, South Korea (talk)
10/2013	Sommerschool "Self-Organized Materials for Optoelectronics" Oppenheim
08/2013	8th German Korean Polymer Symposium Hamburg (poster)

Publications

A. K. C. Mengel, B. He, O. S. Wenger, *Org. Chem.* **2012**, *77*, 6545.

A. K. C. Mengel, C. Förster, A. Breivogel, K. Mack, J. R. Ochsmann, F. Laquai, V. Ksenofontov, K. Heinze, *Chem. Eur J.* **2015**, *21*, 704.

A. K. C. Mengel, W. Cho, A. Breivogel, K. Char, Y. S. Kang, K. Heinze, *Eur. J. Inorg. Chem.* **2015**, 3299.

C. Kreitner, A. K. C. Mengel, T. K. Lee, W. Cho, K. Char, Y. S. Kang, K. Heinze, *Chem. Eur. J.* **2016**, *22*, 8915.

A. K. C. Mengel, C. Bissinger, M. Dorn, C. Förster, K. Heinze, *Chem. Eur. J.* **2017**, in press.

Mainz, 18th of May 2017